HORT PAPERS IN—

nalytical techniques

artography

conomic geology

ngineering geology

eochemical exploration

eochemistry

eomorphology

eophysics

lacial geology

round water

larine geology

lineralogy

re deposits

aleontology

etrology

uality of water

edimentation

tratigraphy

tructural geology

urface water

heoretical hydrology

GEOLOGICAL SURVEY RESEARCH 1964

Chapter D

Special Instructions

GEOLOGICAL SURVEY PROFESSIONAL PAPER 501-D

GEOLOGICAL SURVEY RESEARCH 1964

Chapter D

GEOLOGICAL SURVEY PROFFESSIONAL PAPER 501-D

Scientific notes and summaries of investigations prepared by members of the Geologic, Conservation, Water Resources, and Topographic Divisions in geology, hydrology, topographic mapping, and related fields

UNITED STATES GOVERNMENT PRINTING OFFICE, WASHINGTON: 1964

UNITED STATES DEPARTMENT OF THE INTERIOR

STEWART L. UDALL, Secretary

GEOLOGICAL SURVEY

Thomas B. Nolan, Director

For sale by the Superintendent of Documents, U.S. Government Printing Office,
Washington, D. C., 20402

FOREWORD

This collection of 43 short papers is the last of the chapters of Geological Survey Research 1964. The papers report on scientific and economic results of current work by members of the Geologic, Conservation, Water Resources, and Topographic Divisions of the U.S. Geological Survey. Some of the papers present results of completed parts of continuing investigations; others announce new discoveries or preliminary results of investigations that will be discussed in greater detail in reports to be published in the future. Still others are scientific notes of limited scope, and short papers on techniques and instrumentation.

Chapter A of this series presents a summary of results of work done during the present fiscal year.

Thomas B. Nolan,
Director.

CONTENTS

TEMPERATURES IN THE CRUST AND MELT OF ALAE LAVA LAKE, HAWAII, AFTER THE AUGUST 1963 ERUPTION OF KILAUEA VOLCANO—A PRELIMINARY REPORT

By DALLAS L. PECK,[1] JAMES G. MOORE,[2] and GEORGE KOJIMA,[1]
[1] Hawaiian Volcano Observatory, Hawaii, [2] Menlo Park, Calif.

Abstract.—The August 1963 eruption of Kilauea Volcano produced a lake of basaltic lava as much as 50 feet deep in Alae pit crater. Repeated drilling and temperature measurements in the crust and underlying melt of the lake during a 6-month period beginning 6 days after the eruption have identified the base of the crust as the 1,067°C isotherm and have followed the growth of the crust as it increased from 3.4 to 19 feet in thickness.

An eruption of Kilauea Volcano in August 1963 created a pond of lava in the bottom of Alae pit crater, Hawaii (fig. 1). The lava contains rare olivine phenocrysts and has the composition of silica-saturated tholeiitic basalt. On August 28, five days after the end of the eruption, an aerial tram was completed for lowering equipment and water into the crater, and on the following day a hole (DH 1 of fig. 2) was drilled 34 inches into the crust of the lake, an estimated 3 inches less than the thickness of the crust. During the following 6 months the drill hole was extended in the thickening crust, and 4 other holes were drilled (see accompanying table). The base of the crust was penetrated 6 times between September 6 and November 27. On December 3 a ceramic probe 7½ feet long was pushed into the underlying melt. Temperature gradients were measured on 27 days during the 6 months following the eruption.

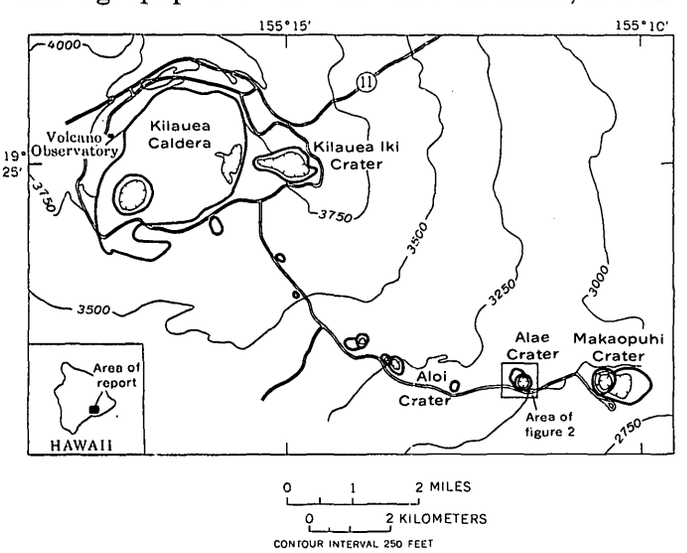

FIGURE 1.—Index map of the summit and the upper east rift zone of Kilauea Volcano, Hawaii. Boundaries of craters and Kilauea caldera are shown by heavy lines.

The temperature measurements of the cooling lava lake are part of a continuing program of study that includes continuous recording of rainfall at the rim of the crater, detailed mapping, leveling, and magnetic studies of the lake, and chemical, petrographic, and density studies of drill core and of selected samples from the crust. Alae lava lake offers an excellent opportunity to supplement the data on cooling of basaltic lava in the nearby Kilauea Iki lava lake formed in 1959. The absence of continuing eruptions, the availability of equipment, and the experience gained from Kilauea Iki allowed us to obtain temperature data in a shorter time after the eruption of Alae Crater. Moreover the shallower depth of the lake will result in complete solidification of the lava in a much shorter period of time, about 1 year for Alae compared with more than 50 years for Kilauea Iki.

We gratefully acknowledge the assistance and advice of Drs. T. Minakami and Shigeo Aramaki of the University of Tokyo, and of the staff of the Hawaiian Volcano Observatory, in the study described in this paper.

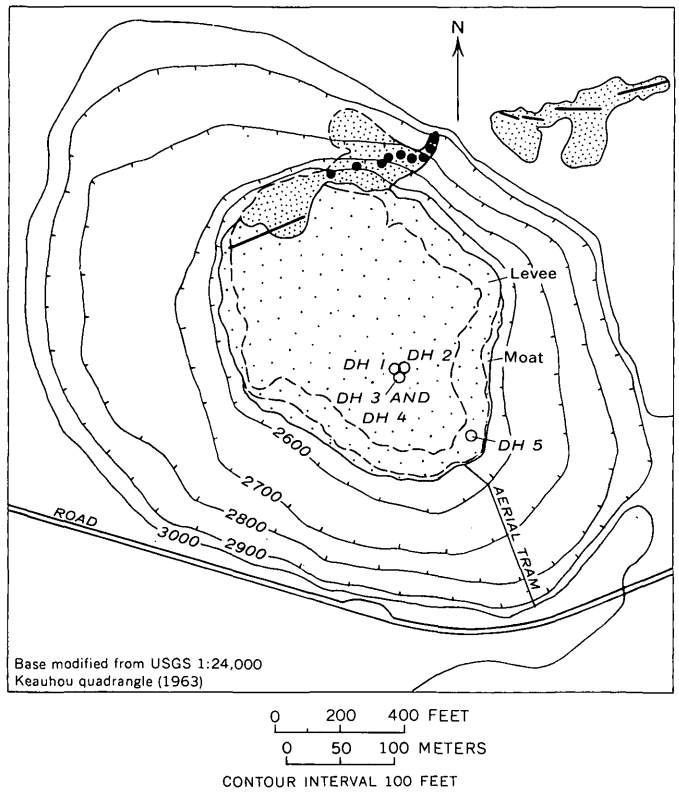

FIGURE 2.—Map of Alae Crater, showing distribution of volcanic rocks from the August 1963 eruption, and location of numbered drill holes (DH 1 to 5) in the crust of Alae lava lake. Lava lake, coarse stipple; spatter, thin flows, and pumice, fine stipple. Eruptive vents are shown by heavy lines and dots. Location of crater is shown on figure 1.

Drilling data in Alae lava lake

Date	Drill-hole No.	Depth of interval drilled (feet)	Remarks
1963:			
Aug. 29	[1] 1	0 – 2.83	
Sept. 3	1	2.67– 3.75	
Sept. 6	1	3.62– 4.6	To base of crust.
	[2] 2	0 – 2.15	Do.
Sept. 17	1	4.2 – 5.58	Do.
Oct. 1–2	[3] 3	0 – 9.33	Do.
Oct. 24	3	7.80–11.40	Do.
Nov. 7	3	9.9 –13.35	Do.
Nov. 20	[4] 4	0 –15.8	Do.
Nov. 27	4	11.3 –15.3	Do.
Dec. 16	[5] 5	0 –29.2	To near base of lake.
1964:			
Jan. 29	5	17.5 –21.0	Plug of ooze.

[1] Near the major axis of the lava lake on the opposite side from the vents, 165 feet S. 44° E. of the center of the lake (fig. 2).
[2] 16 feet N. 75° E. of drill hole 1.
[3] 20 feet S. 15° E. of drill hole 1.
[4] 1 foot N. 75° E. of drill hole 3.
[5] 305 feet S. 49° E. of drill hole 1.

THE ERUPTION

On August 21–23, 1963, a small but spectacular flank eruption occurred in and near Alae Crater, a small pit crater on the upper east rift zone of Kilauea Volcano. Alae Crater is ¾ of a mile east of Aloi Crater, the site of the December 1962 eruption, and 5 miles southeast of the summit caldera (fig. 1). The eruption was preceded by three epochs of subsurface magma migration (on May 9, July 1, and August 3) that were marked by seismic activity, detumescence of the summit, and tumescence and surface cracking along the upper east rift zone. The first indication of the impending eruption, however, was the onset at 13^{h}46^m [1] August 21 of nearly continuous earthquakes and tremors that recorded stronger on a seismograph near the Makaopuhi Crater than on seismographs near Kilauea Caldera. At 13^{h}50^m, displacement of the Press-Ewing instruments in the Uwekahuna vault near the Hawaiian Volcano Observatory indicated the beginning of a distinct southeastward tilt (detumescence of the summit region). Earthquake and tremor died to a low level after 15^{h}00^m, but at 18^{h}00^m they began to increase again.

The eruption was first observed between 18^{h}15^m and 18^{h}30^m by an employee of the National Park Service; at that time an en echelon line of active lava fountains extended for 0.3 mile across the floor and north wall of Alae Crater and in the forest on the north rim. At 19^{h}20^m, when scientists of the Hawaiian Volcano Observatory arrived at the crater, the fountains on the floor formed an almost continuous curtain 20 to 30 feet high and 265 feet long (long eruptive vent, fig. 2). Lava from 11 vents on the north wall cascaded down the cliff and plunged beneath the surface of the growing lava lake, the dark crust of which was broken by glowing cracks that splayed outward from the curtain of fire and the base of the lava cascades. Maximum temperature measurements of the fountains, using 2 optical pyrometers of incandescent filament type, ranged from 1,090°C to 1,100°C. The line of fountains in the forest on the north rim died by 19^{h}45^m, after sending thin flows of shelly pahoehoe over an area of about 8,000 square yards.

During the night, activity on the north wall consolidated into two main fountains, the length of the curtain of fire on the floor shortened to 125 feet, and the rate of extrusion decreased from 150×10^3 cubic yards an hour at 20^{h}00^m August 21 to 35×10^3 cu yd an hour at 03^{h}00^m August 22. Comparison of photographs of the lake taken at 10-minute intervals between 01^{h}40^m and 02^{h}10^m, August 22, show that the crust of the lake was being rafted outward on lava flowing from the vents at a rate of about 600 feet an hour, to be piled in a narrow slabby levee at the edge of the far end of the lake. By 06^{h}00^m the lava lake had

[1] All times given are in hours and minutes, Hawaiian standard time.

reached its maximum thickness (about 62 feet); thereafter it slowly subsided at a rate of 5×10^3 cu yd an hour. The vents on the floor of the crater began to fountain erratically, spewing bursts of spatter to heights of 20 to 150 feet. The two remaining fountains on the north wall were spattering weakly and sending two sluggish rivers of aa down to a low delta on the lake.

The eruption continued at a diminished rate during daytime of August 22. At 18^h30^m, a party of observers reached the edge of the lava lake and found that it was impounded by a slabby levee that stood 15 to 20 feet above the adjacent talus at the foot of the crater walls. At this time the surface of the lake was broken by widely spaced, glowing, radial and transverse cracks. At 21^h20^m, optical-pyrometer measurements of the fountains gave maximum temperatures of 1,130°C to 1,140°C. During the evening the glowing cracks began to darken, beginning at the end of the lake farthest from the vents, and by 00^h03^m August 23, the lake was dark except for scattered spots. The fountains became progressively fewer in number and less active, and by 07^h00^m only one small fountain about 10 feet in diameter was bubbling at intervals of 5 to 7 seconds. The surface of the lake near the fountain appeared to have sunk several feet as the result of drainback into the vent. All activity at the fountain stopped at 08^h10^m, and the eruption was over.

On August 24, vertical-angle transit sights from the rim of the crater showed that drainback and degassing had lowered the surface of the lava lake about 10 feet since 19^h00^m August 22, leaving about 800×10^3 cu yd of lava in the lake, and 30×10^3 cu yd in the spatter cones and in the flows in the forest on the north rim.

The lava lake formed by the eruption in Alae Crater is a lens 1,000 feet long, 800 feet wide, and as much as 50 feet deep, covered and bordered on the northwest side by a low spatter ridge that continues as coalescing spatter cones on the north wall of the crater. A 100-foot wide levee of discontinuous pressure ridges and uptilted slabs borders all but the northwest end of the lake, and is bounded for most of its length by a moat 10 to 15 feet deep and 50 to 100 feet wide (fig. 2). The lake within the levee has a hummocky surface that slopes almost imperceptibly toward the vent. Sharp pressure ridges and linear squeezeups that stand as much as 3 feet above the lake surface trace the position of glowing cracks during the later phase of the eruption, and a row of blocky pressure domes 5 to 10 feet high cross the northern side of the lake. Jagged tension cracks, formed during drainback of lava near the end of the eruption, radiate outward from the center of the lake. Secondary contraction cracks are growing in the intervening areas as the crust thickens and cools.

TEMPERATURE DATA

Temperature measurements were made with thermocouples of chromel-alumel and platinum-platinum plus 10 percent rhodium, using a portable millivolt potentiometer and a 0°C reference junction in an ice-filled vacuum bottle. Holes in the solidified lava were drilled with tungsten carbide bits in a portable 1⅛-inch diameter core drill powered by a 9-horsepower gasoline engine. The drilling in August and September was done by holding the drill and pouring cooling water into the hole by hand. After the first of October the drill was mounted on a portable mast anchored in the crust, and cooling water was pumped through the drill pipe by a 3¼-hp gasoline engine.

The coolant water drastically lowered the temperatures in the drill holes, particularly in those drilled after October 1, when 150 to 200 gallons of water were used in each operation. In each of the 5 drilling operations of October and November, the base of the crust was depressed 1.75 to 3.2 feet. Temperatures in the lower part of the crust recovered to near predrilling levels within a few days, but those in the upper part required many weeks; as much as 32 days after the November 27 drilling, the 300°C isotherm was still rising.

Three temperature profiles are shown on figure 3: one measured August 30, 7 days after the end of the eruption; another measured December 30, 129 days after the eruption; and a third, which includes the highest temperature measured in Alae and Kilauea Iki lava lakes, measured November 5 and 8. During the 6 months following the eruption, the solid crust of Alae lava lake at the main drilling site increased in thickness from 1 to 19 feet. Temperatures in the lake measured during this period ranged from 45°C at the surface on December 30, to 1,135°C at a depth of 18 feet in molten lava 7.6 feet below the base of the crust on November 8. Extrapolation from this value 5 feet downward to the center of the lake suggests a maximum temperature of about 1,140°C, in good agreement with the maximum temperature measured during the eruption of 1,140°C.

The temperature at the base of the crust was determined to be $1,067°\pm2°$C during 4 penetrations, using the method described by Ault and others (1962). This is the temperature at which a pointed mullite probe 1 inch in diameter with walls 0.1 inch thick can be pushed slowly under a load of about 200 pounds

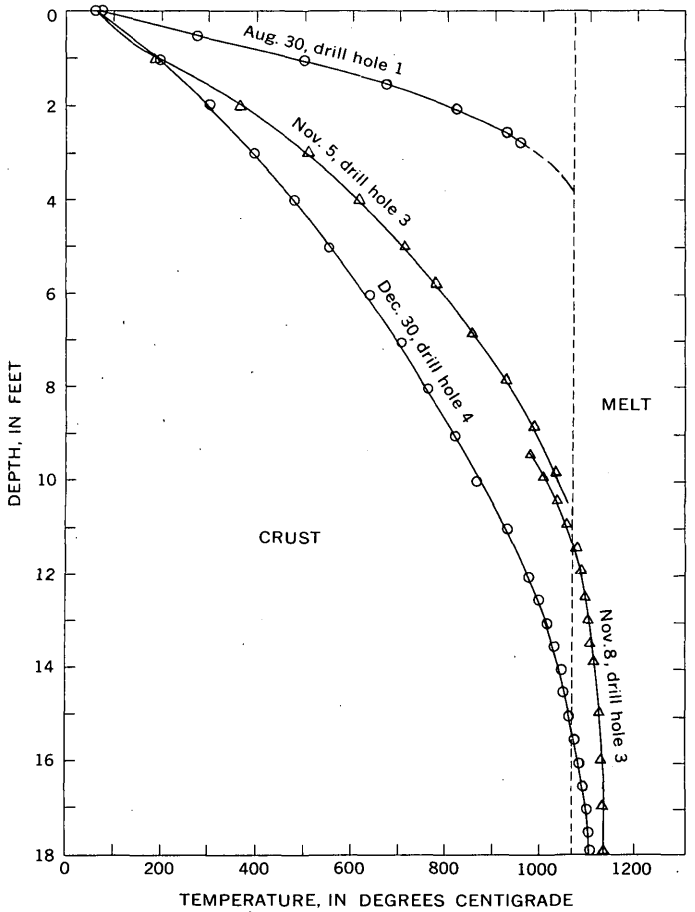

FIGURE 3.—Graph showing temperature gradients in Alae lava lake on August 30, November 5 and 8, and December 30, 1963. The gradient of November 5 was measured immediately before drilling; that of November 8 was measured soon after drilling.

through the chilled lava after drilling, and corresponds to the yielding temperature of the basaltic glass under these conditions. Actually the base of the crust is a zone several feet thick in which the abundance of the solid material and the strength gradually increase upward; at 1,067°C the lava consists of equally abundant melt and crystalline material.

The depth of the 500°C isotherm, the 800°C isotherm, and the 1,067°C isotherm (the base of the crust) are plotted against the square-root of time on figure 4. The data from measured gradients are supplemented by depths to the base of the crust where penetrated in drilling, and estimated thicknesses of the crust during the eruption. Thickness *a* (fig. 4) of 3 to 4 inches is based on the average thickness of pahoehoe slabs in the lava levee at the edge of the lake; the slabs are from crust that was rafted across the lake in about 1½ hours during the night of August 21–22. Thickness *b* of 6 to 9 inches was estimated during a trip to the edge of the lava lake at 18^h30^m August 22; at that time the crust was barely thick enough to walk upon with caution. Thickness *c* of 10 to 12 inches is based on the thickness of slabby crust in tumuli on the lake that were formed during drainback of molten lava into the vent at about 06^h00^m August 23.

The rate of depression of the isotherms has markedly decreased since the formation of the lava lake; for example, the thickness of the crust increased at the rate of 25 feet per month after 0.01 month (7.3 hours), 3.5 feet per month after 1 month, and 2.0 feet per month after 6 months. With respect to the square root of time, however, the rate of depression of the isotherms has been constant over extended periods. Thus for the 6-month interval shown on figure 4, each isotherm can be represented by 3 straight line segments, each of which differs in slope from the adjacent segments. These differences are small, however, and not readily apparent where the data from Alae and Kilauea Iki lava lakes are compared over a 36-month period on the smaller scale of figure 6. The isotherms of figure 4 were temporarily displaced by rainfall (as in mid-September) or by drilling water (as in November), but they recovered over periods of several days or weeks in the absence of rain and of drilling.

A linear relation between the depth of an isotherm and the square root of time follows from the equations for the conductive cooling of a body, such as that of Carslaw and Jaeger (1959, equation 7, section 2.4) for a semi-infinite body initially a uniform temperature, V, by reducing its surface temperature to zero at time, $t=0$:[2]

$$\frac{v}{V} = \text{erf}\,\frac{x}{2\sqrt{kt}},$$

where

v = temperature at depth x at time t,
k = diffusivity, and
erf = the tabulated error function.

Comparing the depths, x_1 and x_2 of an isotherm, v, at times t_1 and t_2,

$$\frac{v}{V} = \text{erf}\,\frac{x_1}{2\sqrt{kt_1}} = \text{erf}\,\frac{x_2}{2\sqrt{kt_2}}.$$

Thus

$$\frac{x_1}{2\sqrt{kt_1}} = \frac{x_2}{2\sqrt{kt_2}}$$

and

$$\frac{x_1}{x_2} = \frac{\sqrt{t_1}}{\sqrt{t_2}}.$$

[2] Note that the equation is an idealization, assuming heat loss by conduction only, and neglecting heat loss by convection, radiation, and volatile transfer, and heat gain from the latent heat of fusion of the lava.

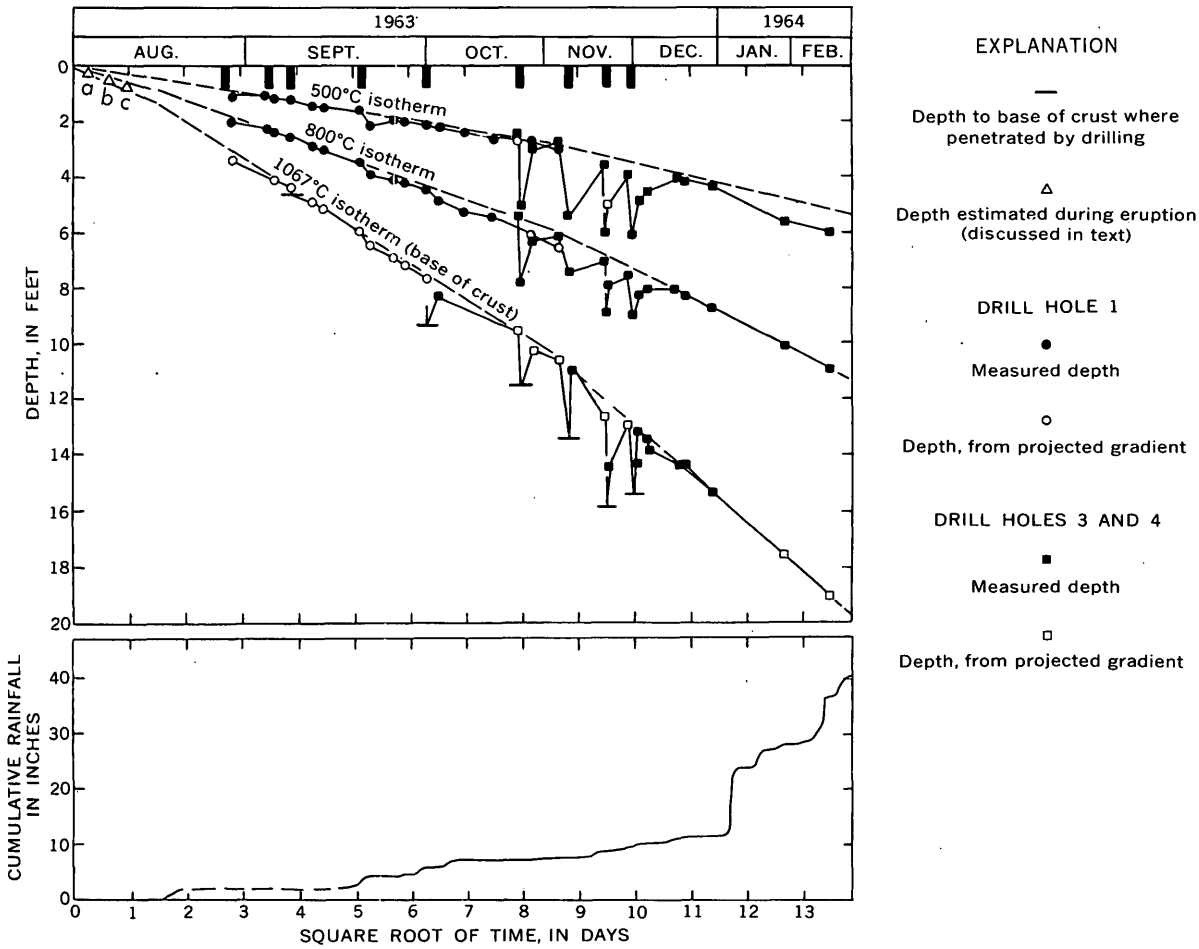

FIGURE 4.—Depth of 500°C isotherm, 800°C isotherm, and 1,067°C isotherm (base of crust) in Alae lava lake, and cumulative rainfall as a function of the square root of time. Dashed lines are idealized isotherms fitted to the points least affected by rainfall and drilling water. Vertical bars at top of figure represent drilling dates.

The rate of depression of isotherms at the main drilling site (drill holes 1, 2, 3, and 4) has not remained constant with respect to the square root of time during the 6 months following the eruption. The rate of depression of the base of the crust, dx/dt, has changed from $2.5/\sqrt{t}$ (with time t in months of 30.4 days) during the later part of the eruption, to $3.5/\sqrt{t}$ during September, to $5.0/\sqrt{t}$ during January and February. The reason for the change is obscured by the drastic effect at the main drilling site of cooling water used during the drilling. Possibly the change took place only at this site as the result of the abundant use of water during repeated drilling. The change probably is not the result of heavy rainfall, as can be seen by comparing the major inflection points on the cumulative rainfall curve with the discontinuities in the isothermal curves on figure 4. However, it may be caused by a progressive increase with time in the diffusivity of the lava solidifying at the base of the crust. The vesicularity of the crust of Alae lava lake decreases with depth from an average of 30 to 40 percent in the upper 1 foot to about 10 percent below 10 feet. The vesicularity-depth curve breaks sharply between 1 and 2 feet and between 8 and 10 feet—depths that correspond approximately to the discontinuities in the 1,067°C isothermal curve. If the thermal conductivity of the crust increases with decreasing vesicularity more rapidly than does density, then diffusivity will also increase, since

$$k=\frac{K}{\rho c},$$

where k=diffusivity,
K=conductivity,
c=specific heat, and
ρ=density.

On December 16, a hole (drill hole 5 in the table) was drilled 29 feet to near the base of the lava lake at

a site 50 feet from the southeast edge of the lake. Microscopic study of the core indicates that the drill hole did not reach the base of the lake, but the increasing vesicularity of core from the lower 3 feet suggests that the base is close. Comparison of the location of the hole with a special 1:2400 scale map of the pre-eruption topography of the bottom of the crater (prepared photogrammetrically with 5-foot contour intervals by the Topographic Division of the Geological Survey) indicates a lake thickness of 25±5 feet. Thus the lake is about 30 feet thick at the site. Temperature profiles (fig. 5) during the period December 18 to February 26 show maxima between 18 and 20 feet, 60 to 70 percent of the depth to the base of the lake. These depths are comparable to those that would be anticipated from theoretical analysis of cooling at the center or edge of a sheet, such as that of Jaeger (1961, figs. 1, 2, and 11).

COMPARISON WITH KILAUEA IKI LAVA LAKE

The thickness of the crust of Alae lava lake as a function of the square root of time is compared with that of Kilauea Iki lava lake on figure 6. Estimates of thickness based on gradients strongly affected by drilling water or rainfall have been omitted. The dashed line on figure 6 is a theoretical curve for Kilauea Iki lava lake (Ault and others, 1962, fig. 3) during the first 4 months after the formation of the lake, a period when no temperature data were obtained from the cooling lake; the curve is based on calculations from 2 temperature profiles obtained 6 and 8 months after the formation of the lake (Ault and others, 1961, p. 793). These calculations led to the suggestion that the crust of Kilauea Iki lava lake was 2.4 feet thick after 1 month (Ault and others, 1961, p. 793; 1962, p. 2811). However, later data from Kilauea Iki shown on figure 6 (J. G. Moore and D. H. Richter, written communication, Jan. 1964) and data from Alae show that the calculated rate of increase in thickness of the crust of Kilauea Iki lava lake for the period from 1 to 4 months was too great, and that

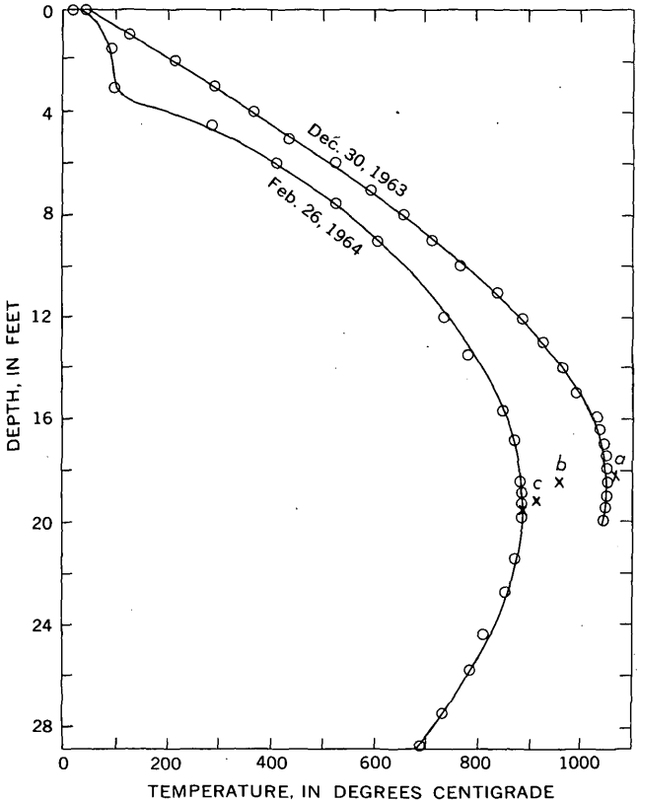

FIGURE 5.—Temperature gradients in the thin edge of Alae lava lake on December 30, 1963, and February 26, 1964, and depth of maximum temperatures on December 18 and 30, 1963 (*a*); January 29, 1964 (*b*), and February 17 and 26, 1964 (*c*).

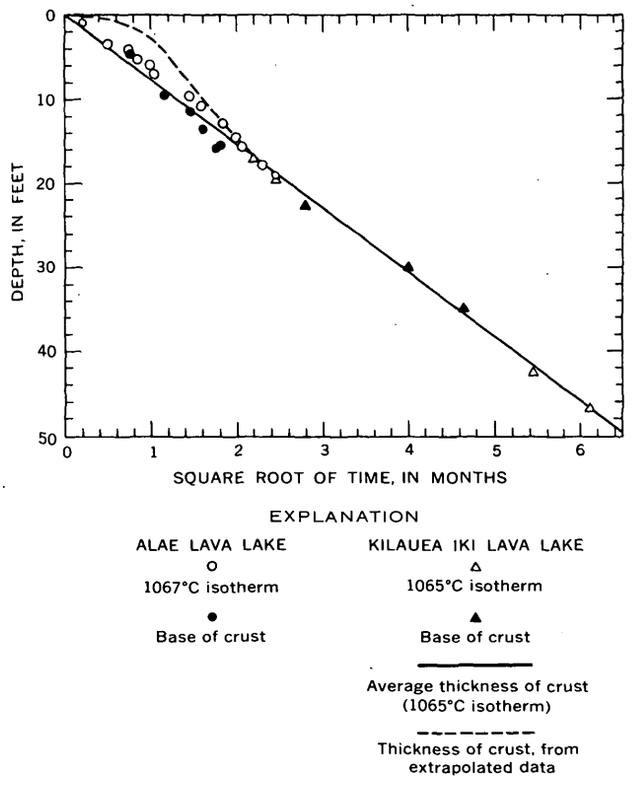

FIGURE 6.—Selected thicknesses of crust in Alae and Kilauea Iki lava lakes as a function of the square root of time. Depths of the 1,067°C isotherm in Alae lava lake and the 1,065°C isotherm in Kilauea Iki lava lake are based on (1) measured or extrapolated gradients least affected by drilling water or rainfall, and (2) an estimated thickness of the crust during the August 1963 eruption. The extrapolated curve for the thickness of the crust of Kilauea Iki lava lake during the first 4 months is from Ault and others (1962, fig. 3). Time for Alae lava lake is measured from 06^{h}00^{m} August 22, 1963; time for Kilauea Iki lava lake is measured from December 23, 1959. Data on Kilauea Iki is from Ault and others (1961, 1962) and J. G. Moore and D. H. Richter (written communication, Jan. 1964).

the suggested crustal thickness of 2.4 feet after 1 month was too small. The crust of Alae lava lake was 6.5 feet thick after 1 month.

Comparison of the data from the two lakes (fig. 6) indicates that the crusts of both grew at about the same rate; both had about 19 feet of crust 6 months after they formed. Since both lakes had similar initial temperatures, the similarity of their cooling rates indicates that the lava in both lakes had about the same thermal diffusivity.

REFERENCES

Ault, W. U., Eaton, J. P., and Richter, D. H., 1961, Lava temperatures in the 1959 Kilauea eruption and cooling lake: Geol. Soc. America Bull., v. 72, p. 791–794.

Ault, W. U., Richter, D. H., and Stewart, D. B., 1962, A temperature probe into the melt of the Kilauea Iki lava lake in Hawaii: Jour. Geophys. Research, v. 67, p. 2809–2812.

Carslaw, H. S., and Jaeger, J. C., 1959, Conduction of heat in solids: London, Oxford Univ. Press, 510 p.

Jaeger, J. C., 1961, The cooling of irregularly shaped igneous bodies: Am. Jour. Sci., v. 259, p. 721–734.

VARIATION IN MODES AND NORMS OF AN "HOMOGENEOUS" PLUTON OF THE BOULDER BATHOLITH, MONTANA

By ROBERT I. TILLING, Washington, D.C.

Abstract.—In outcrop and in hand sample, the granodiorite of Rader Creek is one of the most homogeneous-appearing plutons in the composite Boulder batholith. However, detailed study of 36 chemically analyzed specimens of the granodiorite shows significant variations in mode and norm which indicate that the apparently "homogeneous" pluton is actually zoned compositionally.

The Boulder batholith is a composite intrusive mass which ranges in composition from syenogabbro to alaskite and is exposed over an area of approximately 1,200 square miles in southwestern Montana. Field relations demonstrate that the syenogabbroic plutons (too small to be shown on fig. 1) are earliest in the intrusive sequence. Next in sequence in the southern part of the batholith is the granodiorite of Rader Creek. The Butte Quartz Monzonite, which is coextensive with the Clancy Granodiorite of Knopf (1957), cuts the granodiorite of Rader Creek and is in turn cut by younger plutons of leucogranodiorite and alaskite. In the northern part of the batholith, the Unionville Granodiorite of Knopf (1957) is younger than the syenogabbroic bodies and older than the Butte-Clancy rocks. As the Unionville Granodiorite and the granodiorite of Rader Creek occupy similar positions in the intrusive sequence, they are perhaps correlative.

The Boulder batholith intrudes rocks ranging from Precambrian to Late Cretaceous in age and is unconformably overlain and locally injected by the Eocene Lowland Creek Volcanics (Smedes and Thomas, 1964). Thus, the emplacement of the batholith was post-Late Cretaceous and pre-Eocene. K–Ar radiometric ages of biotite (70–76 million years) of the batholith rocks are consistent with the age of the batholith inferred from stratigraphic and structural relations (M. R. Klepper and W. H. Smedes, oral communications, 1963).

This study is a progress report of a recently initiated systematic investigation of the petrology and chemistry of the Boulder batholith. The 36 specimens studied in this report were collected in the summer of 1962 from the best exposed portions of the granodiorite pluton of Rader Creek along two east-west traverses and from quarry pits (fig. 2). The modal and normative data presented here not only serve to test the homogeneity of the pluton but also to provide a valuable and necessary adjunct to the detailed mineralogic and chemical investigation currently underway on the individual mineral phases in the granodiorite and other batholith rocks.

MACROSCOPIC AND MICROSCOPIC DESCRIPTION

Where not exposed in roadcuts and quarry pits, the granodiorite of Rader Creek crops out as round bouldery masses with grayish-brown weathered surfaces. Freshly fractured surfaces always have a distinctive bluish-gray color. In hand sample, the rock is medium grained and typically displays equigranular granitoid texture, spotted by small clots of mafic minerals which are generally at least several inches apart. The characteristically equigranular granodiorite, however, grades imperceptibly into porphyritic varieties(with plagioclase phenocrysts up to 1 cm in length) at the easternmost margin of the outcrop area adjacent to Tertiary valley fill. It should be emphasized that all specimens, with the exception of porphyritic variants collected from the two easternmost localities (fig. 2), are remarkably uniform macroscopically. In fact, it was because of this monotonously homogeneous appearance in outcrop and hand sample that the granodiorite of Rader Creek was selected as the most suitable unit of the batholith to test the homogeneity of a mappable unit.

U.S. GEOL. SURVEY PROF. PAPER 501-D, PAGES D8–D13

Under the microscope, the granodiorite, with the exception of the macroscopically porphyritic specimens, has a hypidiomorphic-granular texture composed of grains which range from 0.5 mm to 3.5 mm across and average 1.5 mm. A specimen from the westernmost locality near the contact with the Butte Quartz Monzonite (fig. 2), however, exhibits an atypical microporphyritic texture which is not detectable in hand sample. The principal constituents of all samples are plagioclase, K-feldspar, quartz, hornblende, and biotite; accessory minerals include opaque minerals, apatite, sphene, zircon, tourmaline, and, probably, monazite. Subhedral plagioclase crystals, generally with myrmekitic borders, show moderate to strong normal zoning from calcic andesine to oligoclase, and weaker oscillatory zoning. Reconnaissance of plagioclase composition by flat-stage methods indicates that the anorthite content ranges from An_{63-46} in the core to An_{32-20} at the margins. The cores of some plagioclase grains are sericitized and (or) slightly epidotized. The K-feldspar is orthoclase microperthite which forms large poikilitic optically continuous plates. In any given thin section, the microperthite grains show extreme variability in the extent of grid twinning, ranging from completely untwinned grains to distinctly microclinic grains; moreover, portions of a single grain may exhibit varying degrees of grid twinning. Anhedral quartz characteristically occupies interstices and commonly displays undulatory or patchy extinction. Green hornblende, some of which contains ragged relict cores of augite, occurs as slightly biotitized and (or) chloritized subhedral prisms. Subhedral biotite flakes, pleochroic from pale yellow to dark brown or greenish brown, are generally associated with irregular aggregates of sphene. The opaque minerals are concentrated in the mafic minerals, particularly in areas where the mafic minerals themselves are clustered to form clots which give the granodiorite its distinctive sparsely spotted appearance in hand sample.

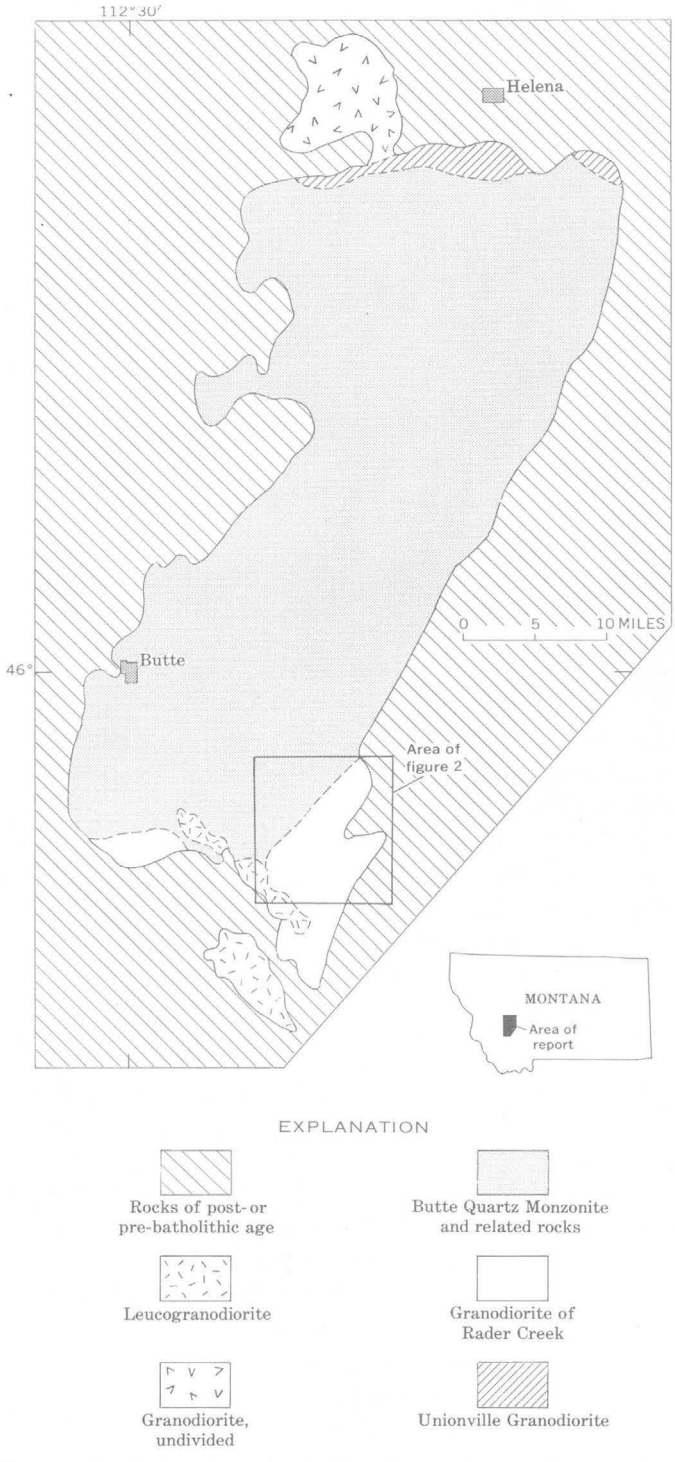

FIGURE 1.—Index map of the Boulder batholith, showing distribution of major intrusive units and location of area studied in detail (shown on fig. 2).

VARIATIONS IN MODAL AND NORMATIVE COMPOSITION

At least two standard-size thin sections were cut from each hand specimen, which, on the average, weighed close to 10 pounds. All modes, determined by means of a Chayes click stage, are based on at least 1,000 point counts per thin section. To facilitate determination of K-feldspar, all thin sections were stained with sodium cobaltinitrite. The accompanying table (p. D11) shows the reproducibility of the mode of a given thin section. There is excellent agreement between the modes, regardless of the number of point counts and the bias of the various operators.

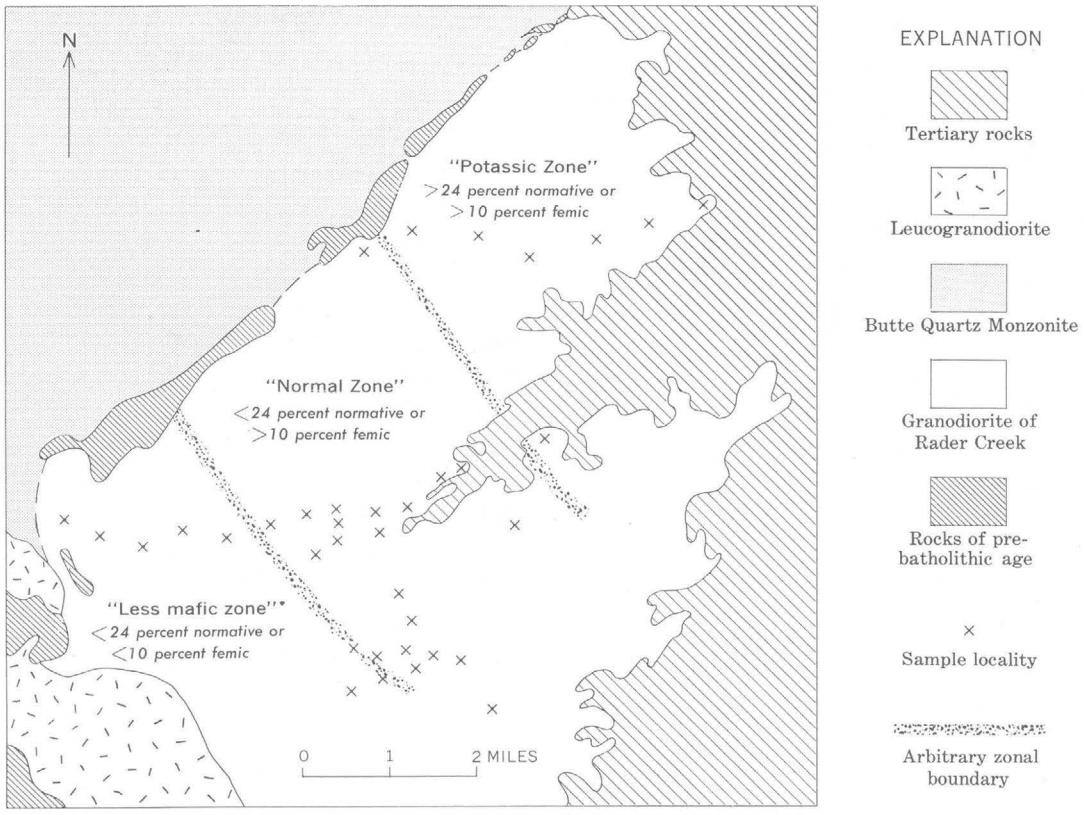

FIGURE 2.—Map showing sample localities and compositional zonation in the granodiorite of Rader Creek, about 15 miles southeast of Butte, Mont.

Modal compositions of the granodiorite of Rader Creek are plotted on figure 3*A*. It is important to note that modes determined from several thin sections of the same hand specimen often exhibit a greater range than do the modes of single samples of rocks from separate localities. Thus, from even casual examination of figure 3*A*, it is apparent that the mode based on a single thin section is rarely representative of the modal composition of the hand specimen, let alone the entire rock unit.

To test the possibility that some unrecognized linear or planar fabric might cause the often wide range in mode, modes were determined for three randomly selected specimens, each represented by three mutually perpendicular thin sections. These specimens showed smaller range in mode than the range observed in most of the other rocks represented by only two sections cut at random. This suggests that the variations in mode do not reflect any subtle planar or linear fabric, because if the modes did, in fact, reflect rock fabric, then the differences in mode in the specimens represented by three mutually perpendicular sections should be as great as, or greater than, those in specimens with only two random sections. Rather, the modal differences between thin sections cut from the same specimen can generally be accounted for by the differing proportions of the characteristically poikilitic, blebby K-feldspar and quartz in the sections.

Figure 3*B* is a plot of CIPW normative minerals computed from rapid rock chemical analyses, each of which is based on several pounds of chips from the same large specimen from which thin sections were cut. Although the range in normative quartz is approximately the same as that in modal quartz, the scatter in the ratio plagioclase/K-feldspar, represented by the width of fields 1 and 3 on figure 3 (excluding points bounded by the dashed line), is only about half as wide for the normative as for the modal plots, if averages of at least two modal determinations (open circles) are used. The scatter is only a third as wide if single modal determinations (ends of bars) are used. In other words, the variation in modal quartz cannot be "averaged out" by chemical analysis, but the scatter in plagioclase/K-feldspar is significantly reduced.

The data plotted on figure 3 have spatial significance. On figure 3*B*, the field enclosed by a solid line contains points which represent rocks collected from the area west of the arbitrarily drawn stippled line (shown on fig. 2), all of which have less than 10 percent of normative femic minerals (in terms of quartz–

femic minerals–total feldspar). Those points enclosed by the dashed line represent rocks collected from the area east of another arbitrarily drawn stippled line (fig. 2); these rocks contain more than 24 percent of normative K-feldspar (in terms of quartz-plagioclase–K-feldspar) and are distinctively more potassic than rocks from the rest of the sampled area. These arbitrary zones—less mafic, normal, and potassic—based on normative compositions can likewise be established by modal compositions; the zones based on modal data, however, are not as sharply defined (fig. 3*A*). The plot of the specimen with the lowest normative quartz content (collected at the western end of the northern east-west traverse) is anomalous and may indicate contamination by Paleozoic carbonate rocks present in the nearby screen of prebatholithic rocks (see fig. 2).

The variations in modal and normative compositions of the grandodiorite of Rader Creek are summarized on figure 4, on which the plotted data of figure 3 have been contoured and superimposed. There can be no question that the clearly defined maxima of the normative data have their counterparts in the somewhat more diffuse maxima of the modal data. The normative and modal maxima are slightly offset in the manner to be expected from a comparison between mode and norm. These discrepancies are inherent in the calculation of the CIPW norm, in which orthoclase is computed as Or_{100}; in determination of the mode the composition of the K-feldspar (orthoclase microperthite) is approximately $Or_{75\text{-}80}$. Also, in calculation of the norm, certain oxides may be assigned to a specific mineral and no other; for example, K_2O is assigned solely to K-feldspar even though it is present in other modal minerals, mainly biotite. Discrepancy between the normative and modal maxima caused by the use of inconsistent units—weight percent (norm) versus volume percent (mode)—is probably insignificant. This is because of the quartz—total feldspar—mafic (femic) minerals plot (fig. 4*B*), where such discrepancy would be greatest due to the large differences in specific gravities of the minerals plotted, the conversion of modal data into weight percent would shift the modal maximum toward the mafic minerals corner, thus increasing, rather than decreasing the discrepancy.

The petrologic significance of the variations in modes and norms observed in the granodiorite of Rader Creek is unknown at present and can better be evaluated when the other units of the Boulder batholith also are studied in detail. Nonetheless, it is perhaps petrologically and (or) structurally significant that the arbitrarily delimited zones here described are very crudely parallel to the contact between the grandodiorite and the younger leucogranodioritic plutons to the west and, at the same time, are roughly perpendicular to the trend of the screen of prebatholithic rocks which separates the granodiorite from the Butte Quartz Monzonite (figs. 1 and 2).

Moreover, the data presented here clearly demonstrate that even an exceedingly homogeneous-appearing mappable unit such as the granodiorite of Rader Creek may not be mineralogically or chemically homogeneous. To be sure, differences in the proportion of dark minerals from locality to locality within the unit were noted during the course of fieldwork but were interpreted as minor random departures from the overall homogeneity of the unit. However, with the accumulation of more detailed data, it became evident that the apparently homogeneous Rader Creek pluton is actually compositionally zoned. Obviously then, the assessment of "homogeneity" must be tempered by the degree of detail required or desired in a particular study, by the amount of data available, and by the reservation that a certain amount of variation may exist. What are considered as systematic and, possibly, significant departures from "homogeneity" in this study—approximately 10 percent K-feldspar relative to a gross average of the other leucocratic constituents and 5 percent mafic minerals relative to a gross average in the total rock—perhaps might only be considered as expectable variations within the

Reproducibility of the mode of a single thin section of granodiorite of Rader Creek [1]

[Results in volume percent]

	2,000 point counts		1,000 point counts							Average	Mean deviation
	1	2	3	4	5	6	7	8	9		
Plagioclase	51.3	51.0	51.3	50.7	53.0	50.2	50.3	47.3	50.7	50.7	0.8
K-feldspar	14.7	16.6	13.2	14.7	13.3	15.3	16.2	16.2	14.0	14.9	1.0
Quartz	20.3	19.7	20.1	19.1	20.3	20.5	18.2	22.1	20.4	20.1	.7
Hornblende	6.8	5.7	6.9	7.0	6.1	7.0	6.3	6.4	7.2	6.6	.4
Biotite	5.6	5.1	6.6	6.5	5.1	4.8	7.5	7.2	5.8	6.0	.8
Opaque accessory minerals	.9	1.2	1.4	1.3	1.6	1.4	1.0	.6	.8	1.1	.3
Non-opaque accessory minerals	.4	.7	.5	.7	.6	.8	.5	.2	1.1	.6	.2

[1] Modes 1–6 are by the writer, mode 7 by M. R. Klepper, mode 8 by H. W. Smedes, and mode 9 by T. L. Wright.

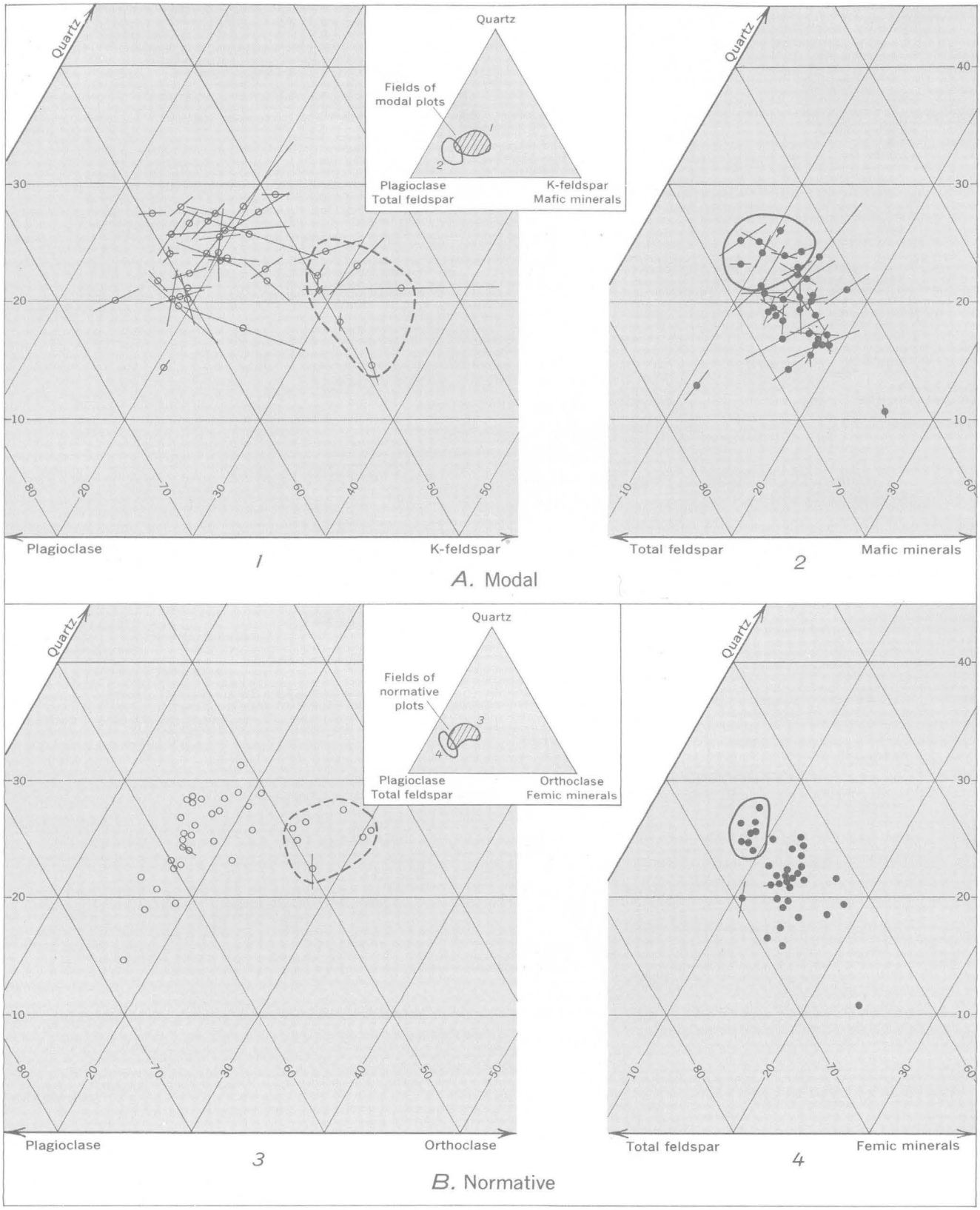
Quartz
Fields of modal plots
1
2
Plagioclase
Total feldspar
K-feldspar
Mafic minerals
Quartz
40
30
20
10
80
20
70
30
60
40
50
50
Plagioclase
K-feldspar
1
Quartz
40
30
20
10
10
80
20
70
30
60
Total feldspar
Mafic minerals
2
A. Modal
Quartz
Fields of normative plots
3
4
Plagioclase
Total feldspar
Orthoclase
Femic minerals
Quartz
40
30
20
10
80
20
70
30
60
50
50
Plagioclase
Orthoclase
3
Quartz
40
30
20
10
10
80
20
70
30
60
Total feldspar
Femic minerals
4
B. Normative

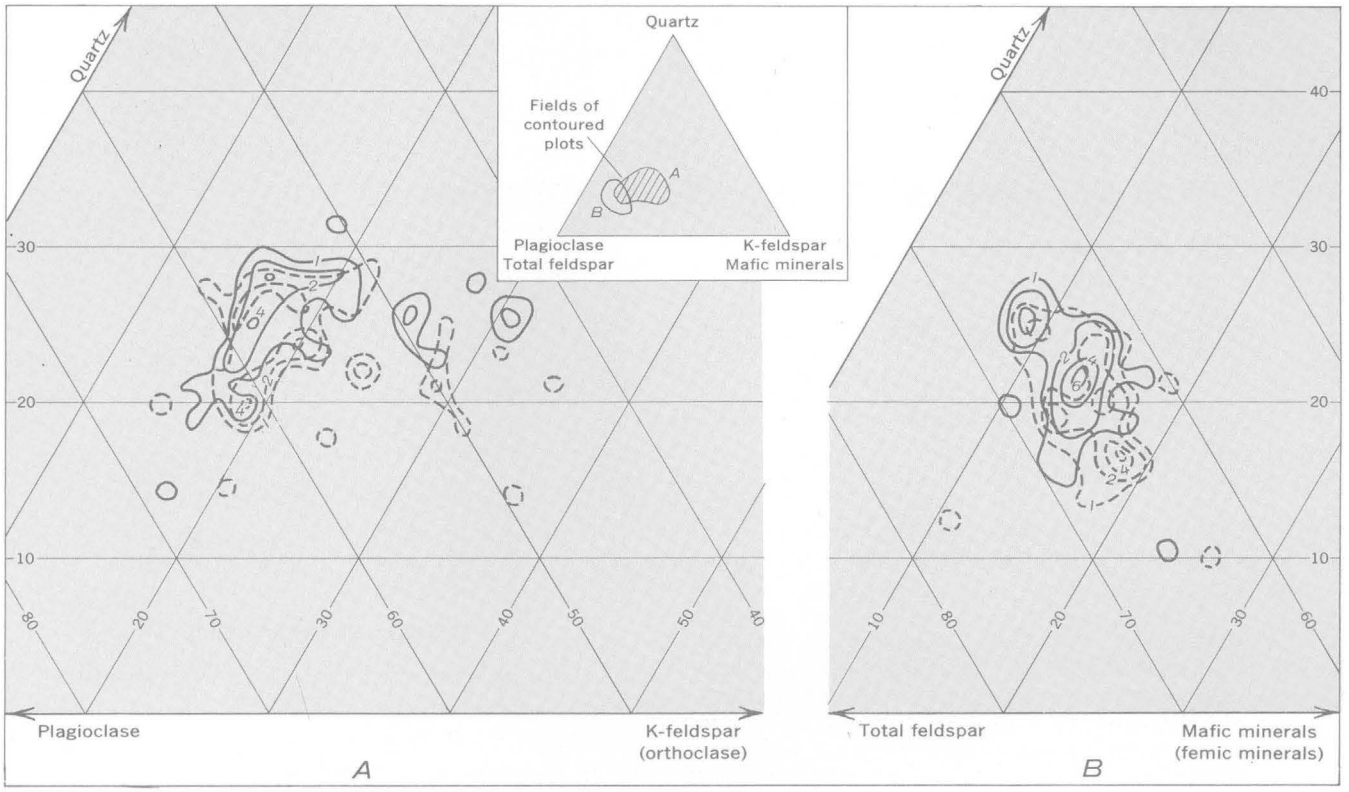

FIGURE 4.—Contour diagram showing proportions of normative (solid contours) and modal (dashed contours) minerals in the granodiorite of Rader Creek. Data compiled from the plotted circles on figure 3; modal data in volume percent and normative data in weight percent. Contours shown represent 1, 2, 4, and 6 points per 0.06 percent of area of compositional triangle (inset).

limits of "homogeneity" in other petrologic applications. If so, then the variations representative of the unit could be determined merely by the study of 3 or 4 properly spaced hand specimens. In any event, this preliminary investigation emphasizes the commonly neglected fact that selection of supposedly "representative" samples for purposes of comparing modal and (or) chemical compositions of different rock units must be done with great caution to avoid erroneous conclusions from misleading comparisons.

REFERENCES

Knopf, Adolph, 1957, The Boulder bathylith of Montana: Am. Jour. Sci., v. 255, p. 81–103.

Smedes, H. W., and Thomas, H. H., 1964, Re-assignment of the Lowland Creek volcanics to Eocene age: Jour. Geology. [in press]

FIGURE 3.—Relative proportions of modal (*A*) and CIPW normative (*B*) minerals in the granodiorite of Rader Creek. Fields of modal plots (*1, 2*) in volume percent and normative plots (*3, 4*) in weight percent, with reference to the complete compositional triangles, are outlined in insets. Open circles are plots in the quartz-plagioclase-K-feldspar (or orthoclase) triangle; filled circles are plots in the quartz-total feldspar-mafic (or femic) minerals triangle. Ends of bars indicate compositions of different thin sections (or analyses) from the same hand specimen, whose average composition is marked by the position of the circle. Fields enclosed by a solid line represent rocks from the less mafic zone; fields enclosed by a dashed line represent rocks from the potassic zone (see text and fig. 2).

MAFIC LAVAS OF DOME MOUNTAIN, TIMBER MOUNTAIN CALDERA, SOUTHERN NEVADA

By STANLEY J. LUFT, Washington, D.C.

Work done in cooperation with the U.S. Atomic Energy Commission

Abstract.—Eleven or more mafic flows of Dome Mountain were erupted in Pliocene time within the moat of the Timber Mountain caldera of southern Nevada. They consist of a lower group of trachybasalt, basalt, and andesite flows; a middle group of trachyandesite flows; and an upper group of trachyandesite to latite flows. Differentiation toward the upper flows is clearly indicated by decreasing abundance of mafic minerals, color index, and content of normative anorthite, and by increasing content of alkalies and silica, K/Ca ratio, and differentiation index. The rocks are silica saturated. A Peacock index slightly below 56 puts the suite near the boundary of the alkali-calcic and calc-alkalic fields. The normal calc-alkalic differentiation trend shows marked chemical variation for eruptions of limited extent and duration.

A sequence of mafic lava flows forms a subarcuate outcrop area of about 25 square miles on the southeast flank of Timber Mountain on the Nevada Test Site in southern Nye County, Nev. (fig. 1). Dome Mountain, 6,195 feet high, is the most conspicuous landmark in this area. Eleven or more flows having a maximum stratigraphic thickness of more than 900 feet are present on the northeast slope of the mountain where it is cut by Chukar Canyon. The sequence thins abruptly away from Dome Mountain and is represented by a single flow near, and north of, Cat Canyon. Dome Mountain itself is an erosionally truncated pile of mafic to intermediate lava flows which in general appearance can be described as a miniature shield volcano.

These flows were first noted by Ball (1907, p. 153), who along with later workers considered them basalts. The chemical and petrographic data obtained during the present study show them to be primarily trachybasalt and trachyandesite. The flows are of particular interest because they show a considerable degree of magmatic differentiation for rocks erupted during a short time span.

GEOLOGIC RELATIONS

The mafic lavas of Dome Mountain are part of a volcanic sequence that includes bedded and massive tuff, welded tuff, rhyolitic and mafic lava flows, and poorly consolidated tuffaceous sand and gravel deposited in the structural depression or moat of the Timber Mountain caldera (Byers and others, 1963). The attitude of the sequence varies from horizontal to gently dipping away from Timber Mountain. The Dome Mountain lavas flank the faulted and eroded welded tuffs of Cat Canyon, but generally rest unconformably upon the younger rhyolitic lava flows and tuffs of Fortymile Canyon. Locally the Dome Mountain flows overlie scoriaceous basaltic andesite older than the rhyolite of Fortymile Canyon. Rhyolite lava flows of Shoshone Mountain overlie the Dome Mountain lavas east of Fortymile Canyon, and two thin flows of olivine-andesine trachybasalt overlie the Dome Mountain lavas on the west and north slopes of Dome Mountain. The Dome Mountain and younger lavas are overlain conformably by the Spearhead Member of the Thirsty Canyon Tuff (Noble and others, 1964) at Buckboard Mesa and along Beatty Wash. Tuffaceous sand and gravel, locally indurated, are interlayered with the Dome Mountain lavas and with the overlying volcanic rocks.

Source vents clearly related to the Dome Mountain lava flows were not recognized in the field. The upper flows on Dome Mountain dip away from the summit, suggesting that this area was the major source for the upper flows. One or perhaps two thin and discontinu-

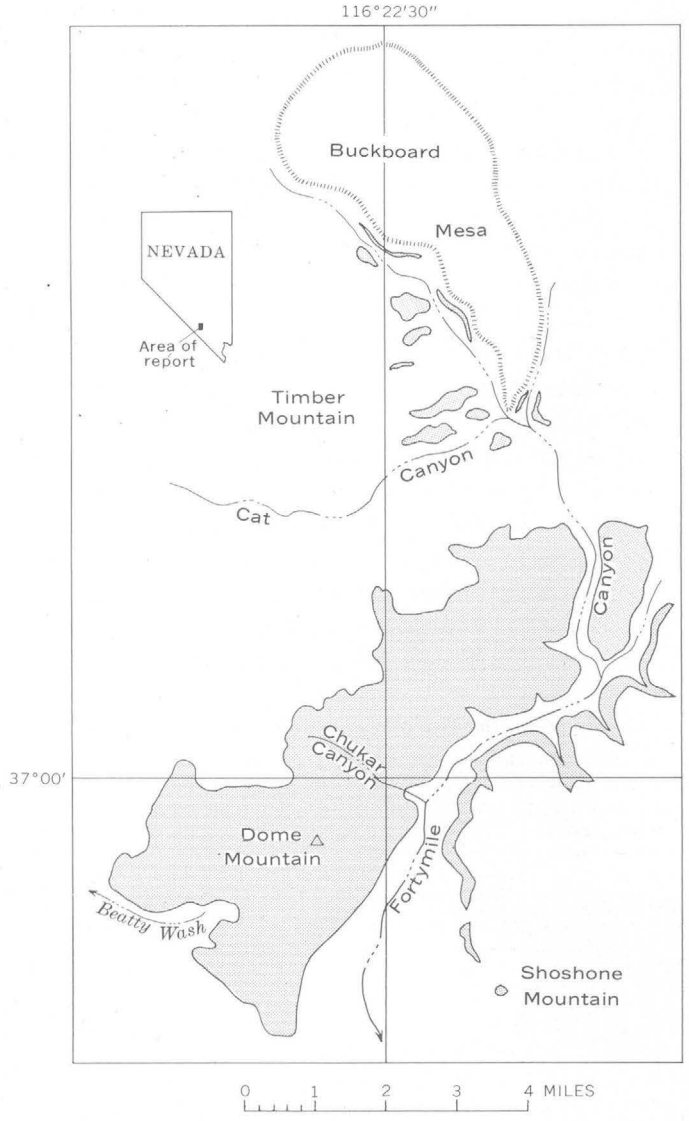

FIGURE 1.—Map of a portion of the Nevada Test Site, Nye County, Nev., showing principal topographic features and general distribution of the mafic lavas (stippled) of Dome Mountain.

ous dikes of olivine trachyandesite, which chemically and mineralogically resemble the lower Dome Mountain flows, are present along a north-northwest-trending normal fault of minor displacement in tuff north of Cat Canyon and west of Buckboard Mesa, outside the principal outcrop area of the Dome Mountain lavas. Although a dike is known to be a feeder for a very small flow, most of the lavas probably issued from fissures which now are buried beneath and near Dome Mountain. A small extinct fumarole occurs below the summit of the mountain. Spatter cones near the bottom of Fortymile Canyon appear to be related to the scoriaceous basaltic andesite that underlies the rhyolite of Fortymile Canyon.

Rocks above, and below, the mafic lavas of Dome Mountain have been dated by the K–Ar method by R. W. Kistler of the U.S. Geological Survey. The overlying Spearhead Member of the Thirtsy Canyon Tuff is about 7.5 million years old (Noble and others, 1964), and the underlying tuffs of Cat Canyon are about 10.9 million years old (F. A. McKeown, written communication, 1963). The age of the Dome Mountain lavas is bracketed as Pliocene and, on the basis of field relations with the overlying and underlying volcanic rocks, is probably not more than 8 million years.

Individual flows range in thickness from 0 to about 170 feet; the average thickness is about 70 feet. A typical flow has a reddish, glassy, scoriaceous, and rubbly basal zone, less than 5 feet thick. The basal zone grades upward through a few feet of transitional rock, characterized by closely spaced horizontal jointing or sheeting, into a massive central zone that forms the thickest part of the flow. Fractures and joints in this zone are widely spaced and usually broadly curving. The central zone grades upward into a zone of variable thickness, usually less than 25 feet, of scoriaceous rock at the top of the flow. The top few feet of this upper zone are reddish. Distal ends of flows are contorted, blocky, scoriaceous, and rubbly. The rubble and scoria commonly are mixed with sediment of the caldera moat.

Vesicles, which may be completely absent from the main part of the central zone, form as much as 40 percent of the lower and upper zones of a flow. Most of the vesicles are less than ½ inch long, but a few are as much as 3 inches long. Length-to-height ratios are greatest in the lower part of the flow and may reach 10:1 or more. The ratios are generally less than 2:1 in the central and upper zones.

The lavas in most places are fresh, and are dark to medium gray and rarely medium light gray (Rock-color chart, Goddard, 1948). Weathering colors vary, but are chiefly pale and moderate yellowish brown, grayish orange, and yellowish gray.

PETROGRAPHY

Petrographically, the mafic lavas of Dome Mountain are similar to andesitic rocks described in standard works such as those of Johannsen (1937, p. 162–166) and Williams and others (1954, p. 93–95). The rocks generally have a fine-grained matrix set with poorly discernible phenocrysts, giving the rocks a uniform megascopic appearance. Textures are generally seriate, and intersertal or intergranular to subophitic. Pilotaxitic texture characterizes the matrix of about

half the specimens studied, but true trachytic texture is rare. Phenocrysts commonly tend to form glomeroporphyritic clusters. Many of the upper flows are diktytaxitic, but few of the lower flows are.

The flows are divisible chemically and mineralogically into three groups. The lower flows are characterized by phenocrysts of iddingsite after olivine and are the most mafic rocks of the sequence. They are chiefly trachybasalt, but also include basalt and andesite. The lower flows are present in the topographically lower parts of Fortymile and Chukar Canyons and are the only flows present near and north of Cat Canyon. Two flows overlying the lower flows in the measured section are only slightly less mafic than those below but are almost indistinguishable in the field from the upper flows and have generally been mapped with them. These middle flows are trachyandesite. The upper flows form an uninterrupted pile within the major area that includes Dome Mountain and lies between Cat Canyon and Beatty Wash. These flows are characterized by ragged and cloudy plagioclase phenocrysts and are also trachyandesite. Chemically, however, the highest flow on Dome Mountain is close to latite in composition.

The primary minerals of the mafic flows and the products of magmatic or deuteric alteration, together with the modal composition of chemically analyzed flows, are given in table 1. The modes were determined by counting 2,000 or more points per thin section. An arbitrary minimum size limit of 0.2 mm for microphenocrysts was empirically found to be useful in accentuating the modal differences between the lower and upper flows. Secondary minerals and voids, never more than 5 percent, were excluded from the modes. Phenocrysts appear to be more abundant in the more mafic of the lower flows than in the rest of the sequence. Although the frequencies of some minerals show progressive increases or decreases that are related to the sequence of eruption, preliminary optical studies do not indicate large variations in the

TABLE 1.—*Modal composition of chemically analyzed mafic lavas of Dome Mountain*

[Modes recalculated to 100 percent after excluding secondary minerals and voids. All data in volume percent. Chemical analyses given in table 2]

	Lower flows—basalt, trachybasalt, and andesite							Middle flows—trachyandesite		Upper flows—trachyandesite and latite						
Sample No.	1	2	3	4	5	6	7	8	9	10	11	12	13	14	15	16	17
Laboratory No.	161242	161018	161017	161693	161129	161016	161128	161019	161694	161021	161024	161022	161696	161025	161695	161023	161020
Field No.	TM-9724a	SL-62-85	SL-62-84	SL-62-83	SL-62-102	SL-62-82	SL-62-99	SL-62-86	SL-62-88	SL-62-89	SL-62-95	SL-62-92	SL-63-52	SL-62-96	SL-63-50	SL-62-94	SL-62-87
Phenocrysts:																	
Plagioclase, ragged phenocrysts	0	0	0	0	0	0	0	0	2.6	6.3	6.0	6.9	7.4	5.2	5.0	6.3	1.6
Plagioclase, laths	19.7	25.0	19.8	17.7	21.9	5.5	7.4	12.2	1.4	2.2	5.2	3.9	6.0	6.4	7.5	5.3	4.2
Clinopyroxene	1.2	1.4	1.0	4.1	1.2	.8	.5	1.2	.1	.4	2.1	.9	.8	1.3	.7	.8	1.4
Orthopyroxene	0	0	0	0	0	Tr.	Tr.	0	.2	0	.2	.2	.2	Tr.	.1	0	0
Olivine and iddingsite	8.0	5.8	3.0	4.4	7.5	1.2	.3	Tr.	Tr.	.2	.4	.1	Tr.	.4	.9	.2	.1
Magnetite	0	0	0	0	0	0	0	.4	0	0	.1	.1	0	.1	.1	Tr.	Tr.
Total phenocrysts	28.9	32.2	23.8	26.2	30.6	7.5	8.2	13.8	4.3	9.1	[1]14.0	12.1	14.4	13.4	15.1	[2]12.7	7.3
Matrix:																	
Plagioclase [3]	32.9	27.5	32.1	37.1	34.1	34.8	50.0	8.0	53.7	40.4	40.8	48.7	47.1	50.0	31.9	45.1	36.5
Clinopyroxene	16.3	17.2	16.0	8.3	14.5	10.5	14.2	2.2	16.2	11.2	7.8	9.0	6.5	6.9	3.3	6.8	7.3
Orthopyroxene	0	0	0	0	0		Tr.	0		0	1.0		.2	.6	0	0	0
Olivine	3.2	0	5.9	0	11.8	8.2	0	3.4	10.9	8.9	1.6	7.6	2.9	3.7	5.7	6.2	0
Iddingsite	7.3	7.1		10.9			9.0				3.1		3.6	1.7	0		6.1
Opaque minerals	7.3	7.4	10.8	9.2	6.7	17.0	7.8	2.7	6.4	3.4	4.2	4.1	2.6	3.6	2.2	2.3	6.2
Glass and cryptocrystalline material	4.1	8.6	11.4	8.3	2.3	22.0	10.8	69.9	8.5	27.0	27.5	18.5	22.7	20.1	41.8	26.9	36.6
Total matrix	71.1	67.8	76.2	73.8	69.4	92.5	91.8	86.2	95.7	90.9	86.0	87.9	85.6	86.6	84.9	87.3	92.7
Total lava	100.0	100.0	100.0	100.0	100.0	100.0	100.0	100.0	100.0	100.0	100.0	100.0	100.0	100.0	100.0	100.0	100.0
Estimated maximum anorthite content of plagioclase laths	An_{58}	An_{57}	An_{53}	An_{57}	An_{60}	An_{55}	An_{55}	An_{47}	An_{47}	An_{53}	An_{53}	-----	An_{54}	An_{60}	An_{60}	An_{58}	An_{43}
Sum of mafic minerals (volume percent)	43	39	37	37	42	38	32	[4]	34	24	20½	22	17	18	[4]	16	21

[1] Includes trace of hornblende(?).
[2] Includes 0.1 percent of hornblende (?).
[3] May include minor amounts of alkali feldspar and silica minerals.
[4] Sum of mafic minerals is anomalously low due to the high content of glass and cryptocrystalline material.

composition of these minerals. The maximum crystal size remains relatively constant throughout the sequence.

DESCRIPTIVE MINERALOGY

The ragged and cloudy plagioclase phenocrysts (to 10 mm) of the upper flows and of one middle flow, best seen on weathered surfaces, closely resemble those described by Kuno (1950, p. 967–968, and figs. 5 and 6) from Hakone Volcano, Japan. They commonly are zoned and twinned and are filled with zonally concentrated "dust" inclusions and microlites of mafic minerals. Borders commonly are embayed and corroded, and resorption borders may be alkalic. Some of these crystals appear to be more sodic than the labradorite to andesine laths. Their appearance and textural relations suggest an intratelluric origin. Similar crystals, described by G. A. Macdonald as inclusion-filled and "moth-eaten," are considered by him to be characteristic of calc-alkaline andesite provinces (*in* Stark, 1963, p. C5). Plagioclase laths (to 3.5 mm) are subhedral to euhedral and irregularly terminated. Larger ones, particularly in the lower flows, show pronounced oscillatory zoning and albite twinning; carlsbad, pericline, and baveno twin laws are also represented. Phenocryst-size laths are sodic labradorite to calcic andesine, whereas those of the matrix are chiefly andesine. Differentiation of the laths toward the sodic end was not observed in the preliminary optical study of the sequence of flows (table 1). Minor amounts of alkali feldspar and silica minerals are also present but were counted together with the plagioclase laths.

Quartz xenocrysts (to 1 mm) are present in trace quantities in one specimen from a lower flow. The grains are rounded and fractured, and surrounded by reaction rims of radiating acicular clinopyroxene intermixed with fine-grained quartz, feldspar, and magnetite. Similar xenocrysts may constitute as much as 0.5 percent of the later olivine-andesine trachybasalt flows.

Clinopyroxene (to 2.3 mm) forms stubby to elongate (axial ratios as high as 5:1) euhedral to anhedral prisms. Simple twins and indistinct zones are present, and mafic inclusions, chiefly magnetite, are common. Phenocryst compositions lie within the diopside and augite fields (colorless or very pale green, pleochroism absent or faint, $2V_z$=45° to 70°, estimated birefringence as much as 0.03). Pigeonite (colorless, length-slow, $2V_z \approx 15°$, estimated birefringence as much as 0.01) rarely forms phenocrysts. Subequal amounts of high- and low-calcium pyroxene are present in the matrix. Clinopyroxene commonly jackets orthopyroxene phenocrysts, locally forms overgrowths on olivine, and may in turn be jacketed by hornblende(?).

Orthopyroxene (to 1.6 mm) forms stubby to elongate (axial ratios 2:1 to 10:1) subhedral to euhedral prisms. Most crystals are near enstatite in composition (colorless, $2V_z$ = 60° to 70°, birefringence estimated as up to 0.012), but some hypersthene is also present. Minute crystals are difficult to distinguish from clinopyroxene and olivine. Orthopyroxene, present in trace quantities only in a few specimens from lower flows, is found in most specimens of the upper flows where it may form more than 1 percent of the rock. It is absent, however, in the most silicic upper flows. No explanation is ventured here for the relative abundance of this early precipitate mineral in the later differentiates of the Dome Mountain sequence, and for the apparent reversal of the usual calc-alkalic trend of diminishing orthopyroxene : clinopyroxene ratios.

Olivine (to 2.2 mm) forms stubby to elongate (axial ratios as high as 4:1) euhedral to subhedral dipyramids and dipyramidal prisms that are most abundant in the lower flows. The optic sign ranges from (+) to (−), with a very large $2V$. Magnetite inclusions are abundant except in large, probably intratelluric crystals that commonly are resorbed and enclose cryptocrystalline matrix material. Olivine generally is largely to entirely replaced by iddingsite or similar minerals inward from borders and fractures. Matrix-size grains of upper flows tend to be less altered than those of lower flows. Olivine commonly is found in glomeroporphyritic clusters with large later forming plagioclase laths.

Magnetite (to 0.6 mm) is the principal opaque mineral of the lavas, and has a trend similar to that of olivine. Phenocrysts, absent in lower flows, are rounded and embayed or ragged and were probably late forming. Matrix-size grains are euhedral to subhedral octahedrons, fresh or partly to completely altered to hematite. Rods, also present, probably include some ilmenite. Apatite and zircon(?), present in trace quantities throughout the flows, form slender minute prisms in plagioclase and in the glassy matrix.

Glass is colorless or red- and gray-brown to black, according to the state of oxidation and quantity of contained magnetite "dust." Colorless and brown glasses are typical of the upper flows. Cryptocrystalline material includes all matrix material too fine to be identified at 250× magnification. The norms indicate that it probably consists mainly of K-feldspar and silica, probably as tridymite or cristobalite.

TABLE 2.—*Chemical composition and norms of mafic lavas of Dome Mountain*

[Analyses by rapid methods and listed in order of increasing SiO_2 content. Analysts: P. L. D. Elmore, S. D. Botts, Gillison Chloe, H. Smith, and Lowell Artis; norms and other calculations by author; analyses recalculated to 100-percent volatile-free constituents]

	Lower flows—basalt, trachybasalt, and andesite							Middle flows—trachyandesite		Upper flows—trachyandesite and latite								Average of lower flows	Average of middle flows	Average of upper flows
Sample No.	1	2	3	4	5	6	7	8	9	10	11	12	13	14	15	16	17	1–7	8 and 9	10–17
Laboratory No.	161242	161018	161017	161693	161129	161016	161128	161019	161694	161021	161024	161022	161696	161025	161695	161023	161020			
Field No.	TM-9724a	SL-62-85	SL-62-84	SL-62-83	SL-62-102	SL-62-82	SL-62-99	SL-62-86	SL-62-88	SL-62-89	SL-62-95	SL-62-92	SL-63-52	SL-62-96	SL-63-50	SL-62-94	SL-62-87			
Composition (weight percent):																				
SiO_2	50.0	50.2	50.3	50.8	51.0	51.3	51.9	52.8	53.0	57.4	56.6	59.0	59.1	59.2	59.4	59.6	60.0	50.8	52.9	59.0
Al_2O_3	17.4	16.6	16.8	16.6	16.8	17.1	17.4	16.9	16.7	16.9	16.8	16.7	16.7	16.7	16.6	16.7	16.3	16.9	16.8	16.1
Fe_2O_3	9.3	6.6	5.7	7.8	5.8	4.1	8.1	5.6	4.0	3.8	2.3	3.8	3.7	2.6	1.7	3.9	3.8	6.8	4.8	3.2
FeO	1.5	4.0	4.7	2.4	4.1	5.7	2.5	4.4	5.3	3.5	4.6	3.6	3.0	4.2	4.7	3.4	3.0	3.6	4.9	3.8
(Sum as FeO) [1]	(9.9)	(9.9)	(9.8)	(9.4)	(9.3)	(9.4)	(9.8)	(9.4)	(8.9)	(6.9)	(6.7)	(7.0)	(6.3)	(6.6)	(6.2)	(6.9)	(6.4)	(9.7)	(9.2)	(6.7)
MgO	5.3	6.0	5.9	5.9	6.7	5.2	3.9	4.3	4.4	3.5	3.0	2.6	2.4	2.9	2.7	1.8	2.4	5.5	4.4	2.7
CaO	9.1	8.4	8.4	9.0	8.8	8.3	8.0	7.8	7.9	6.1	5.1	5.2	5.0	5.3	5.3	5.0	4.5	8.6	7.8	5.1
Na_2O	3.3	3.3	3.4	3.3	3.2	3.3	3.5	3.6	4.1	4.1	4.4	4.2	4.9	4.2	4.3	4.4	4.6	3.3	3.8	4.4
K_2O	1.4	1.7	1.6	1.7	1.3	2.0	1.7	1.9	2.2	2.8	3.0	2.8	3.3	3.2	3.4	3.1	3.2	1.6	2.0	3.1
TiO_2	1.8	2.2	2.1	1.6	1.4	2.0	2.0	1.9	1.7	1.3	1.4	1.4	1.3	1.3	1.3	1.4	1.5	1.9	1.8	1.4
P_2O_5	.76	.93	.94	.76	.74	.87	.89	.76	.61	.47	.58	.46	.61	.60	.58	.59	.62	.84	.69	.56
MnO	.17	.12	.13	.16	.17	.12	.16	.12	.13	.09	.10	.11	.13	.10	.07	.09	.10	.15	.12	.10
Total	100.0	100.0	100.0	100.0	100.0	100.0	100.0	100.1	100.0	100.0	99.9	100.0	100.1	100.0	100.1	100.0	100.0	100.0	100.0	100.0
Volatile material (weight percent):																				
H_2O^-	1.5	.86	.69	2.0	.98	.23	1.6	.80	.56	.45	.06	.47	.38	.12	.17	.27	.66	1.1	.68	.39
H_2O^+	1.7	1.6	1.7	1.8	1.2	.72	1.2	1.1	.72	.83	.63	.79	.65	.92	.85	.73	.94	1.4	.9	.79
CO_2	.10	.16	.16	1.7	.32	<.05	.09	<.05	<.05	<.05	.14	<.05	.17	.08	<.05	.17	<.05	.36	<.05	------
Weight norms:																				
Quartz	2.6	2.5	2.0	2.3	2.5	1.9	6.2	5.5	0.4	6.9	6.6	10.3	6.6	7.7	6.7	10.9	10.4	3.5	2.9	8.3
Orthoclase	8.3	10.0	9.5	10.0	7.8	11.7	10.0	11.1	12.8	16.7	17.8	16.7	19.5	18.9	20.0	18.4	18.9	9.5	12.0	18.3
Albite	27.8	27.8	28.8	27.8	27.3	27.8	29.3	30.6	34.6	34.6	37.2	35.6	41.4	35.6	36.2	37.2	38.8	27.8	32.6	37.2
Anorthite	28.6	25.6	25.9	25.6	27.5	25.9	27.0	24.5	20.9	19.4	17.2	18.4	13.9	17.2	16.1	16.7	14.5	26.7	22.7	16.7
Magnetite	------	7.0	8.4	3.5	8.4	6.0	2.8	8.1	5.8	5.6	3.3	5.6	5.3	3.7	2.6	5.6	5.6	6.5	6.9	4.6
Hematite	9.3	1.8	------	5.4	------	------	6.2	------	------	------	------	------	------	------	------	------	------	2.2	------	------
Ilmenite	3.4	4.3	4.0	3.0	2.7	3.8	3.8	3.7	3.2	2.4	2.7	2.7	2.4	2.4	2.4	2.7	2.9	3.7	3.4	2.7
Apatite	1.7	2.4	2.4	1.7	1.7	2.0	2.0	1.7	1.3	1.0	1.3	1.0	1.3	1.3	1.3	1.3	1.3	2.0	1.5	1.3
Wollastonite	4.9	3.9	3.9	6.0	4.8	4.1	3.0	3.9	6.2	3.4	1.9	2.2	3.0	1.6	2.8	1.9	1.7	4.4	5.0	2.1
Enstatite	13.3	15.0	14.7	14.7	16.8	13.0	9.8	10.7	11.0	8.7	7.5	6.5	6.0	7.3	6.8	4.5	6.0	13.8	10.9	6.7
Ferrosilite	------	------	.7	------	.7	4.0	------	.5	4.0	1.3	4.4	1.3	.7	3.6	5.1	.8	------	------	2.2	2.1
Total	99.9	100.1	100.3	100.0	100.2	100.2	100.1	100.3	100.2	100.0	99.9	100.3	100.1	99.3	100.0	100.0	100.1	100.1	100.1	100.0

Normative feldspar (weight percent):																				
Orthoclase	13	16	15	16	12	18	15	17	19	24	25	24	26	26	28	25	26	15	18	25
Albite	43	44	45	44	44	42	44	46	51	49	51	50	55	50	50	52	54	43	48	52
Anorthite	44	40	40	40	44	40	41	37	30	27	24	26	19	24	22	23	20	42	34	23
Normative anorthite $\times 100$ / Normative albite+anorthite (weight percent)	51	48	47	48	50	48	48	44	38	36	32	34	25	33	31	31	27	49	41	31
Differentiation index	39	40	40	40	38	41	46	47	48	58	62	63	67	62	63	66	68	41	48	64
Color index	33	34	34	34	35	33	28	29	31	22	21	19	19	20	21	17	18	33	30	20
K : Ca (ionic ratio)	.22	.30	.28	.28	.22	.36	.31	.36	.42	.68	.88	.79	.99	.96	.96	.93	1.06	.28	.39	.91
Proportions (molecular percent):																				
Total iron as FeO [1]	41	38	39	38	36	39	44	41	38	35	34	37.5	33.5	34.0	33	39	35	39	39.5	35
K_2O+Na_2O	20	20	20	20	18	22	24	25	28	34	38	37.5	43.5	38.5	41	43	42	21	26.5	40
MgO	39	42	41	42	46	39	32	34	34	31	28	25.0	23.0	27.5	26	18	23	40	34.0	25

[1] Equal to $FeO+0.9\ Fe_2O_3$.

Secondary minerals include calcite and zeolite, and are found principally in vesicles. Calcite also fills fine fractures and rarely occurs as a replacement of plagioclase phenocrysts. Potassium-bearing clay minerals line voids and fractures and also locally replace cryptocrystalline matrix.

PETROCHEMISTRY

Chemical composition, norms, and other petrochemical parameters of the Dome Mountain rocks are given in table 2. Normative color indices (sum of normative femic constituents) are between 17 and 35, thus falling within the andesite range of Kuno (1950, p. 958) and Stark (1963, p. C3). The chemical analyses and norms of the lower and middle flows lie between the values of average basalt and average andesite of Nockolds (1954, tables 6 and 7) and between the average Columbia River Basalt and the average andesite complex of the Cascade Range (Waters, 1955, table 1). Values for SiO_2, total iron plus MgO, and TiO_2 are closer to those for basalt, whereas values for Al_2O_3 and alkalies are nearer those for andesite. P_2O_5 content is unusually high in all analyses of Dome Mountain rocks. The average composition of the lower flows lies between the fields of trachybasalt and basalt, in the classification of Rittmann (1952). The slightly more salic middle flows are olivine trachyandesite by Rittmann's classification, but the low modal olivine content and the absence of normative olivine make trachyandesite a better term for these middle flows. The upper flows are higher in SiO_2 and alkali content, and lower in MgO and CaO than the average doreite of Nockolds (1954, table 5), and are trachyandesite to latite by Rittmann's classification. All the rocks are silica saturated.

The analyses are plotted on a Harker variation diagram (fig. 2) which, together with a triangular FeO-MgO-alkali diagram (fig. 3), shows a normal calc-alkaline differentiation trend for the Dome Mountain lavas. The threefold stratigraphic division of the Dome Mountain sequence follows this trend, but the succession within these divisions is random. The high degree of differentiation of the lavas is further emphasized by variations in the differentiation index of Thornton and Tuttle (1960), the proportion of normative anorthite, and the K:Ca ratios summarized in table 2.

Rittmann's suite index, *s*, (1962, p. 110–111) averages 3.1 for the trachybasalt and allied lavas of the lower flows and 3.5 for the trachyandesite and latite of the middle and upper flows, defining a weakly calc-alkaline suite. The Peacock alkali-lime index (1931, p. 55–56) taken from figure 2 is slightly less than 56, defining the suite as alkali-calcic but near the calcalkalic field.

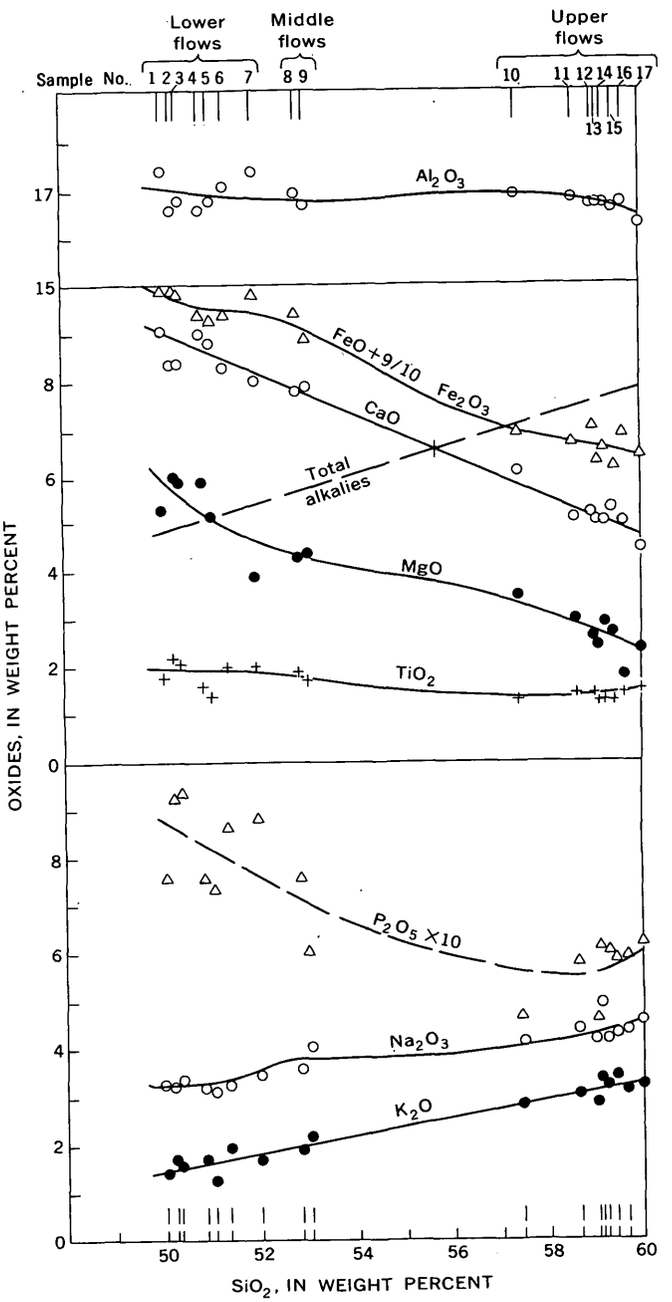

FIGURE 2.—Variation diagram for chemically analyzed rocks of the mafic lavas of Dome Mountain. Data from table 2.

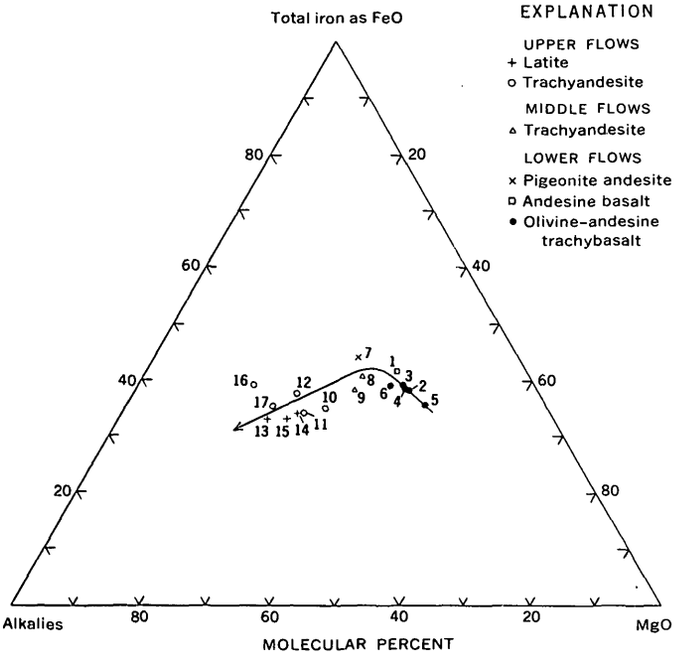

FIGURE 3.—FeO-MgO-alkali diagram, showing trend of differentiation for the mafic lavas of Dome Mountain. Data from table 2.

REFERENCES

Ball, S. H., 1907, A geologic reconnaissance in southwestern Nevada and eastern California: U.S. Geol. Survey Bull. 308, p. 153.

Byers, F. M., Jr., Orkild, P. P., Carr, W. J., and Christiansen, R. L., 1963, Timber Mountain caldera, Nevada Test Site and vicinity—a progress report: Am. Geophys. Union Trans., v. 44, p. 113.

Goddard, E N., chm., and others, 1948, Rock-color chart: Washington, D.C., Natl. Research Council.

Johannsen, Albert, 1937, A descriptive petrography of the igneous rocks, v. III. The intermediate rocks: Univ. Chicago Press, 360 p.

Kuno, Hisashi, 1950, Petrology of Hakone Volcano and the adjacent areas, Japan: Geol. Soc. America Bull., v. 61, p. 957–1020.

Noble, D. C., Anderson, R. E., Ekren, E. B., and O'Connor, J. T., 1964, Thirsty Canyon Tuff of Nye and Esmeralda Counties, Nevada: Art. 126 *in* U.S. Geol. Survey Prof. Paper 475–D, p. D124–D127.

Nockolds, S. R., 1954, Average chemical compositions of some igneous rocks: Geol. Soc. America Bull., v. 65, p. 1007–1032.

Peacock, M. A., 1931, Classification of igneous rock series: Jour. Geology, v. 39, p. 54–67.

Rittmann, A., 1952, Nomenclature of volcanic rocks: Bull. Volcanology, ser. II, v. XII, p. 75–102.

———(E. A. Vincent, translator), 1962, Volcanoes and their activity: New York, Interscience, 305 p.

Stark, J. T., 1963, Petrology of the volcanic rocks of Guam: U.S. Geol. Survey Prof. Paper 403–C, p. C1–C32.

Thornton, C. P., and Tuttle, O. F., 1960, Chemistry of igneous rocks, I. Differentiation index: Am. Jour. Sci., v. 258, p. 664–684.

Waters, A. C., 1955, Volcanic rocks and the tectonic cycle, *in* Poldervaart, Arie, ed., Crust of the Earth: Geol. Soc. America Spec. Paper 62, p. 703–722.

Williams, Howel, Turner, F. J., and Gilbert, C. M., 1954, Petrography: San Francisco, W. H. Freeman, 407 p.

PRELIMINARY REPORT ON THE STRUCTURE OF THE SOUTHEAST GROS VENTRE MOUNTAINS, WYOMING

By WILLIAM R. KEEFER, Denver, Colo.

Abstract.—The Gros Ventre Mountains are an asymmetric anticlinal uplift, steep and faulted along the southwest margin. The range lies between structures typical of Laramide deformation (Late Cretaceous and early Tertiary) in central Wyoming and those of late Tertiary deformation (post-Early Pliocene) in northwestern Wyoming. Tentative interpretations are that the Gros Ventre Mountains and adjacent Hoback Basin were formed during the Laramide and were modified by later movements.

The Gros Ventre Mountains of northwestern Wyoming (fig. 1) lie amidst large, diverse, complex tectonic features formed at different times. The southwest edge of the range is within a mile of the easternmost thrust sheets of the overthrust belt. Farther south the range is bounded by the synclinal Hoback Basin, which forms the northern extension of the Green River Basin and is one of the deepest structural depressions in Wyoming. Structural elements to the east, in central Wyoming, were formed in latest Cretaceous and early Tertiary times, whereas others, to the west and northwest in Jackson Hole and the Teton Mountains, were formed in late Cenozoic time. The time of maximum Gros Ventre uplift has, therefore, been a problem of some interest. Although much is already known about the geology of the region (Nelson and Church, 1943; Richmond, 1945; Baker, 1946; Horberg and others, 1949; Love and others, 1951; Eardley, 1951, p. 320–325; Love, 1956a, 1956b; Dorr, 1956, 1958; Berg, 1961), critical data are still too meager to permit recognition of each tectonic event.

The present paper is based on the detailed field study of approximately 125 square miles of the southeast end of the range and an adjacent narrow strip of the Hoback and Green River Basins (figs. 1 and 2).

STRATIGRAPHY

Strata exposed in the southeastern Gros Ventre Mountains range in age from Ordovician to Late Cretaceous (fig. 2) and are about 7,500 feet thick. Cambrian rocks underlie the area and crop out to the northwest, where they are 1,250 feet thick. The formations are described by Blackwelder (1918), Rich-

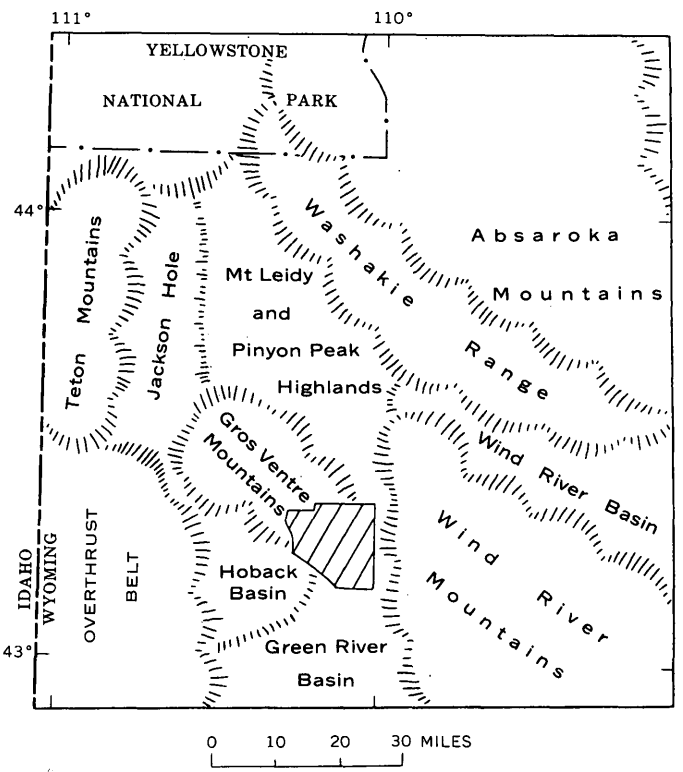

FIGURE 1.—Index map showing location of mapped area (diagonal pattern) with respect to major physiographic and structural features in northwestern Wyoming. The overthrust belt includes the Wyoming, Salt River, and Hoback Ranges.

mond (1945), Love and others (1948, 1951), Horberg and others (1949), Wanless and others (1955), and Love (1956a).

Cretaceous rocks younger than the Frontier Formation are extensively exposed along the northeast flank of the range, where they are about 8,300 feet thick (Love and others, 1948, p. 25–41; Love, 1956a, p. 79–83). Along the southwest flank, about 20 miles northwest of the map area, the post-Frontier Cretaceous sequence may be nearly 10,000 feet thick (J. D. Love, oral communication, 1963). Comparable thicknesses of these strata probably are present in the deep part of the Hoback Basin along the southwest edge of the map area (fig. 2).

Tertiary rocks in the Hoback Basin include the Hoback Formation of Paleocene and early Eocene age, and the Pass Peak Formation of probable middle Eocene age, both formations of Horberg and others (1949). The Hoback Formation is exposed across the central part of the basin, where it is more than 15,000 feet thick and consists chiefly of fine-grained sandstone, siltstone, and shale (Dorr, 1956, p. 102). The Pass Peak Formation crops out along the southwest edge of the map area (fig. 2); it is about 1,500 feet thick and composed of massive conglomerate beds with minor amounts of sandstone and shale (Dorr, 1956, p. 106). The conglomerate consists almost entirely of rounded boulders of Precambrian quartzite resembling, and undoubtedly derived from, those in the Pinyon Conglomerate of Paleocene age now exposed along the north side of the Gros Ventre Mountains (Love, 1956a, p. 84).

STRUCTURE

The Gros Ventre Mountains were formed primarily from a broad asymmetric anticline that is steep and faulted along its southwest flank. The major boundary fault is the Cache thrust fault which has been traced from the southwest corner of the range southeastward along the entire mountain front (Dorr, 1958, p. 1218; Love, 1956b, p. 141). Within the range proper, extensive vertical faults, trending partly west and partly northwest, divide the uplift into three major structural segments (Nelson and Church, 1943, fig. 7). This report concerns the easternmost of these segments.

At its southeast end the main anticlinal structure of the Gros Ventre Mountains plunges 10° to 15° east and southeast, and is separated from the north end of the adjacent Wind River Mountains, along the east slope of the Green River valley, by a series of shallow north-trending folds (Richmond, 1945; Skinner, 1960). The crest of the uplift is remarkably flat over broad areas, although subsidiary folds are evident (fig. 2). Strata along the northeast flank dip 5° to 10° northeast.

Normal faults cut the crest of the uplift in the central part of the map area (fig. 2). The dominant trend of the faults is northeast, but a secondary set trends northwest at an oblique angle of about 120°, nearly parallel to the major structural trend of the range. Displacements range from less than 100 feet to as much as 1,250 feet; there is no consistent pattern regarding which sides were upthrown or downthrown.

Whether the Pass Peak Formation is involved in the faulting along the Cache fault has been a matter of controversy. Horberg and others (1949, p. 198, pl. 2) show the fault terminating before it reaches the southeast margin of the Gros Ventre Mountains, whereas Dorr (1958, p. 1218) and Eardley (1951, figs. 182 and 183) indicate that the Pass Peak was overridden in this region. Though the fault surface was not observed during the present investigation, the following field relations suggest strongly that the contact between the Pass Peak Formation and older rocks is tectonic rather than sedimentary: (1) the contact appears to be very sharp and linear in most places, showing little irregularity suggestive of overlap; (2) residual debris from the highly conglomeratic Pass Peak strata was not found on adjacent slopes of the older rocks examined north of the contact; (3) conversely, there appears to be little debris locally derived from these older rocks in the Pass Peak; and (4) in places, strata of the Pass Peak are turned up sharply near the contact.

There is little doubt that the next older Hoback Formation was overridden by the upper plate of the Cache fault. Approximately 15,000 feet of Hoback beds exposed on the southwest limb of the Hoback Basin syncline dip toward the Gros Ventre Mountains, but do not emerge at the surface on the opposing (northeast) limb.

Maximum structural displacement between the trough of the Hoback Basin and the crest of the Gros Ventre uplift is about 35,000 feet, much of it having taken place along the Cache fault (fig. 2). The fault surface dips about 45° northeast where observed by J. D. Love (oral communication, 1963) northwest of the map area.

The Elbow Mountain fault (Nelson and Church, 1943, p. 158) is a major fracture which extends west-northwest through the central part of the area, nearly parallel to and 1 to 3 miles north of the Cache fault; at the

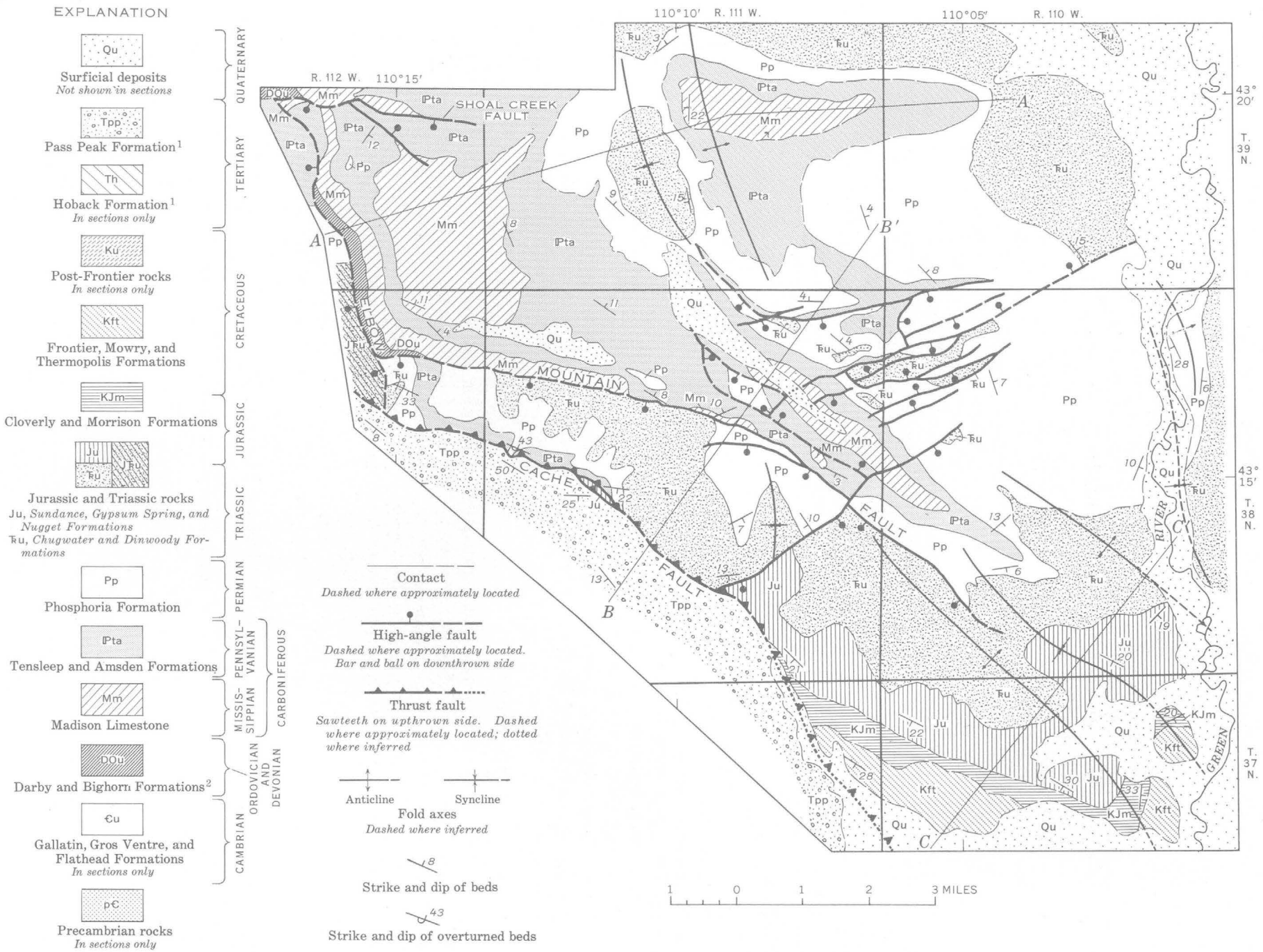
EXPLANATION
Qu
Surficial deposits
Not shown in sections
Tpp
Pass Peak Formation[1]
Th
Hoback Formation[1]
In sections only
Ku
Post-Frontier rocks
In sections only
Kft
Frontier, Mowry, and Thermopolis Formations
KJm
Cloverly and Morrison Formations
Ju
Jru
Jurassic and Triassic rocks
Ju, Sundance, Gypsum Spring, and Nugget Formations
Tru, Chugwater and Dinwoody Formations
Pp
Phosphoria Formation
IPta
Tensleep and Amsden Formations
Mm
Madison Limestone
DOu
Darby and Bighorn Formations[2]
€u
Gallatin, Gros Ventre, and Flathead Formations
In sections only
p€
Precambrian rocks
In sections only
[1] Of Horberg and others (1949)
[2] Without pattern in sections
QUATERNARY
TERTIARY
CRETACEOUS
JURASSIC
TRIASSIC
PERMIAN
PENNSYLVANIAN
MISSISSIPPIAN
CARBONIFEROUS
ORDOVICIAN AND DEVONIAN
CAMBRIAN
Contact
Dashed where approximately located
High-angle fault
Dashed where approximately located. Bar and ball on downthrown side
Thrust fault
Sawteeth on upthrown side. Dashed where approximately located; dotted where inferred
Anticline
Syncline
Fold axes
Dashed where inferred
Strike and dip of beds
Strike and dip of overturned beds
R. 112 W.
110°15′
110°10′
R. 111 W.
110°05′
R. 110 W.
43° 20′
43° 15′
T. 39 N.
T. 38 N.
T. 37 N.
SHOAL CREEK FAULT
MOUNTAIN
CACHE
FAULT
FAULT
RIVER
GREEN
A
A′
B
B′
C
1 0 1 2 3 MILES

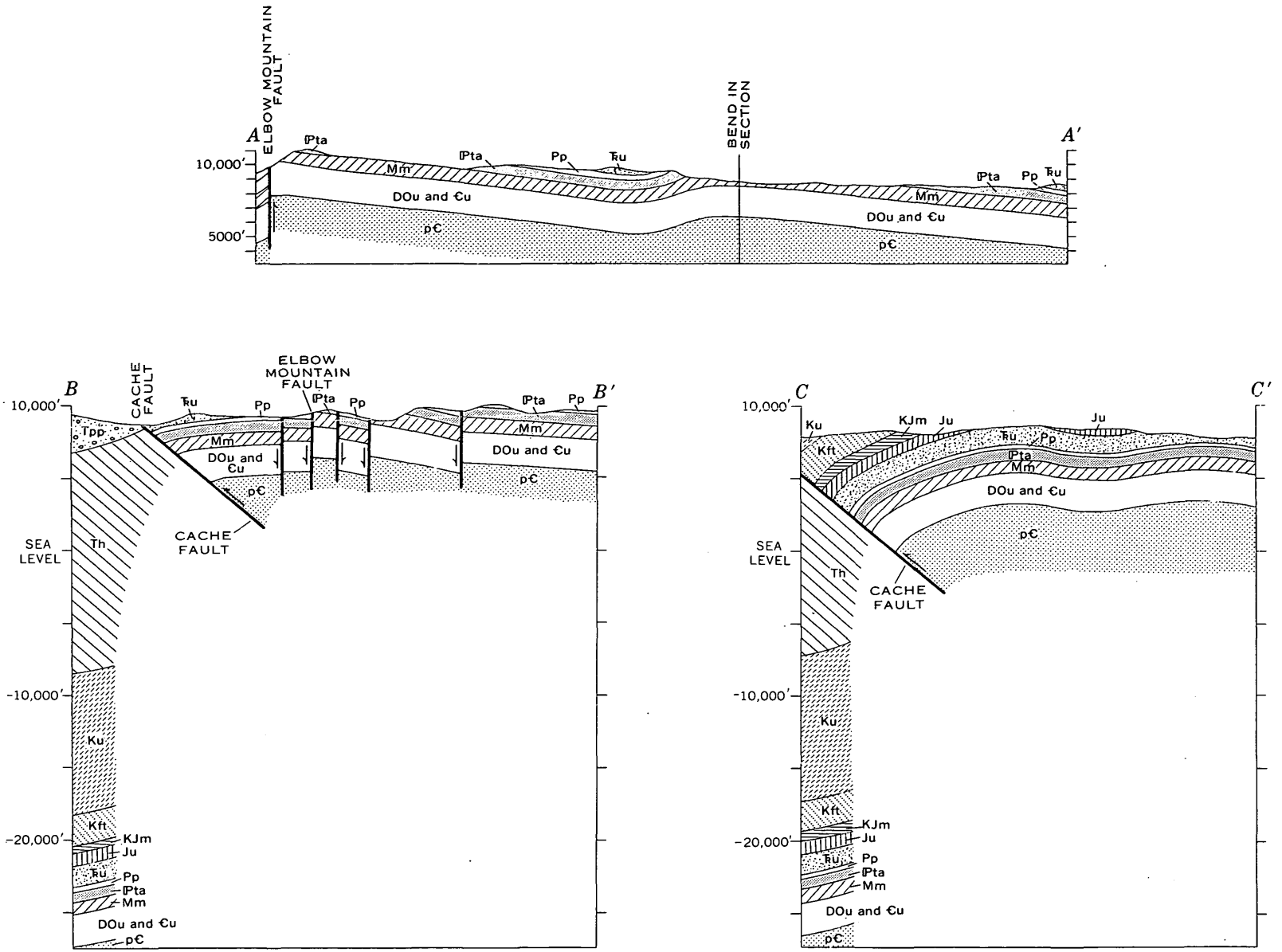

FIGURE 2.—Geologic map and structure sections of the southeastern Gros Ventre Mountains. Geologic mapping by W. R. Keefer and D. B. Andretta, 1955–57, with additions from unpublished maps by Eliot Blackwelder; base from U.S. Geological Survey orthophotograph.

west edge of the area, however, it turns abruptly northward. This feature bounds the south and west sides of the easternmost structural segment of the Gros Ventre Mountains. Spectacular scarps rise 1,500 to 2,000 feet in the upthrown block north and east of the fault and form a prominent "sawtooth" ridge. One segment of the fault extends from the southwest corner of the upthrown block south to the Cache fault. Strata in the upthrown block turn down sharply against the Elbow Mountain fault in places along the west edge of the map area, but toward the southeast little or no drag folding is evident. Maximum structural displacement is about 3,000 feet. Reliable dips were not observed along the fault plane, but it may be nearly vertical. Horberg and others (1949, pl. 2) considered it to be a high-angle reverse fault, although they measured a 65° southward dip on slickensided surfaces along the trace of the fault near its southeast end. The pattern of faulting and the steepness of the scarps suggest, but do not prove, that the Elbow Mountain is a normal fault.

The fault shown at the northwest corner of the map (fig. 2) is the eastern extension of the Shoal Creek fault which forms the south side of the central structural segment of the Gros Ventre Mountains. This fault extends westward for about 6 miles beyond the area shown on figure 2, thence it swings sharply north for another 6 miles, thus resembling the trace of the Elbow Mountain fault (Nelson and Church, 1943, fig. 7). The Shoal Creek fault may also be nearly vertical, and undoubtedly is genetically related to the Elbow Mountain fault.

INTERPRETATION OF STRUCTURE AND GEOLOGIC HISTORY

Major diastrophism in the Gros Ventre Mountains has been variously dated as Late Cretaceous to late Tertiary. Horberg and others (1949, p. 207–208), for example, conclude that uplift must have begun in Late Cretaceous time because the range appears to have formed a buttress against which the eastward-moving thrust sheets of the overthrust belt impinged (fig. 1). Dorr (1958, p. 1239) interprets the initial movements to have been in post-early Eocene time, based on relations observed in the Hoback and Pass Peak Formations. Eardley (1951, p. 325) places the major uplift in post-middle or late Eocene time, because the Pass Peak was overridden by the Cache fault. In the western part of the range, Love (1956b, p. 145; oral communication, 1963) has found that significant movements took place in early Eocene time and again in post-early Pliocene time. Pre-Paleocene folding is indicated in some places along the northeast margin of the Gros Ventre Mountains by an angular discordance between the Pinyon Conglomerate and older rocks (Love and others, 1951).

Major structures in central Wyoming are interpreted by Keefer and Love (1963) to have formed by (1) basin subsidence in Late Cretaceous time, continuing through all of Paleocene and early Eocene time; and (2) progressive folding of the mountain ranges during or at the close of the Cretaceous, culminating in pronounced uplift along high-angle reverse faults at the end of Paleocene time or during earliest Eocene time. Basin sinking was as important tectonically as mountain uplift; in large segments of some basins, subsidence equalled, or exceeded, uplift of the adjacent mountains.

Events in the mapped area were analogous in part to those in central Wyoming. The Hoback Basin began to sink in Late Cretaceous time, and subsidence was virtually continuous through all of Paleocene, early Eocene, and possibly middle Eocene times. The actual downward movements probably exceeded 20,000 feet in the deepest parts of the basin.

The Gros Ventre Mountains probably were folded early in Tertiary time, but it is doubtful that the range stood very high with respect to the Hoback Basin before major uplift in probable middle Eocene time; Pinyon strata (Paleocene) were then stripped off the area now occupied by the mountains and redeposited in the Pass Peak Formation. After deposition and lithification, perhaps as late as post-early Pliocene time, the Pass Peak was overridden by the upper plate of the Cache fault. Though there is no direct evidence, it seems likely that considerable movement must also have taken place along this major boundary fault during uplift of the range at the beginning of Pass Peak time.

Whether the Elbow Mountain and Shoal Creek faults originated in early Tertiary time is likewise conjectural. The steepness and fresh appearance of the fault-line scarps, however, suggest that the most significant movements along these faults may have taken place in late Tertiary time, concomitant with extensive faulting in Jackson Hole and the Teton Mountains to the west.

Available data thus suggest that the Gros Ventre Mountains and Hoback Basin were well outlined as positive and negative tectonic units, respectively, during Laramide deformation, but that the mountains may have been modified considerably by late Tertiary movement.

REFERENCES

Baker, C. L., 1946, Geology of the northwestern Wind River Mountains, Wyo.: Geol. Soc. America Bull., v. 57, p. 565–596.

Berg, R. R., 1961, Laramide tectonics of the Wind River Mountains, *in* Wyoming Geol. Assoc. Guidebook 16th Ann. Field Conf., 1961: p. 70–80.

Blackwelder, Eliot, 1918, New geologic formations in western Wyoming: Washington Acad. Sci. Jour., v. 8, p. 417–426.

Dorr, J. A., Jr., 1956, Post-Cretaceous geologic history of the Hoback Basin area, central western Wyoming, *in* Wyoming Geol. Assoc. Guidebook 11th Ann. Field Conf., 1956: p. 99–108.

——— 1958, Early Cenozoic vertebrate paleontology, sedimentation, and orogeny in central western Wyoming: Geol. Soc. America Bull., v. 69, p. 1217–1243.

Eardley, A. J., 1951, Structural geology of North America: New York, Harper and Bros., 624 p.

Horberg, C. L., Nelson, V. E., and Church, Victor, 1949, Structural trends in central western Wyoming: Geol. Soc. America Bull., v. 60, no. 1, p. 183–215.

Keefer, W. R., and Love, J. D., 1963, Laramide vertical movements in central Wyoming: Wyoming Univ. Contr. to Geology, v. 2, p. 47–54.

Love, J. D., 1956a, Cretaceous and Tertiary stratigraphy of the Jackson Hole area, northwestern Wyoming, *in* Wyoming Geol. Assoc. Guidebook 11th Ann. Field Conf., 1956: p. 76–94.

Love, J. D., 1956b, Summary of geologic history of Teton County, Wyoming, during Late Cretaceous, Tertiary, and Quaternary times, *in* Wyoming Geol. Assoc. Guidebook 11th Ann. Field Conf., 1956: p. 140–150.

Love, J. D., and others, 1948, Stratigraphic sections of Jurassic and Cretaceous rocks in the Jackson Hole area, northwestern Wyoming: Wyoming Geol. Survey Bull. 40.

——— 1951, Geologic map of the Spread Creek-Gros Ventre River area, Teton County, Wyoming: U.S. Geol. Survey Oil and Gas Inv. Map OM 118.

Nelson, V. E., and Church, Victor, 1943, Critical structures in the Gros Ventre and northern Hoback Ranges, Wyoming: Jour. Geology, v. 51, no. 3, p. 143–166.

Richmond, G. M., 1945, Geology of the northwest end of the Wind River Mountains, Sublette County, Wyoming: U.S. Geol. Survey Oil and Gas Inv. Map 31.

Skinner, R. E., 1960, Tectonic elements of the northern Green River area of Wyoming, *in* Wyoming Geol. Assoc. Guidebook 15th Ann. Field Conf., 1960: p. 86–88.

Wanless, H. R., Belknap, R. L., and Foster, H. L., 1955, Paleozoic and Mesozoic rocks of Gros Ventre, Teton, Hoback, and Snake River Ranges, Wyoming: Geol. Soc. America Mem. 63.

742–652 O—64——3

PRE-FALL RIVER FOLDING IN THE SOUTHERN PART OF THE BLACK HILLS, SOUTH DAKOTA

By GARLAND B. GOTT, Denver, Colo.

Abstract.—Outcrop and drill-hole data show discordant relations between the Fall River Formation and the underlying Lakota Formation, both of Early Cretaceous age. This indicates that structural movement was contemporaneous with deposition of the Lakota Formation. Subsurface data indicate a pre-Fall River structural dome 7½ miles north of Edgemont, S. Dak.

A small quantity of petroleum produced from the Minnelusa Formation of Pennsylvanian and Permian age at the Barker dome, Custer County, S. Dak. (Gries, 1964) attracts attention to small structural traps in pre-Cretaceous rocks of the southern Black Hills. Some of these structures are concealed by discordant post-Jurassic rocks.

Along the southwest margin of the Black Hills uplift the regional dip averages about 3° SW. Small anticlinal folds, such as the Barker dome, occur in some places. Elsewhere the structural irregularities consist of a steplike series of terraces and monoclines of low relief. Locally, small faults exist that are probably related to subsidence.

Detailed studies (Gott and Schnabel, 1963, p. 170 and pl. 14) of the formations in the Lower Cretaceous Inyan Kara Group, consisting of the Fall River Formation and the underlying Lakota Formation, have brought out evidence that structural readjustments were in progress at the time that the Lakota Formation was being deposited. Although most of the folding occurred during post-Fall River time, discordance of the attitude of the Fall River Formation with all the major units of the underlying Cretaceous Lakota Formation indicates that some of the folding had occurred before the end of Lakota time. This folding resulted in the deposition of a relatively thick sequence of rocks in the structural troughs and a thin sequence of rocks on the structural highs. The thickness of the Lakota thus ranges from a minimum of about 325 feet to a maximum of about 650 feet.

Interpretation of subsurface data indicates a pre-Fall River structure located about 7½ miles north of Edgemont, S. Dak., in sec. 26, T. 7 S., R. 2 E. It is domal in shape and is concealed by discordant beds of the Lakota and Fall River Formations. The top of the Morrison Formation of Jurassic age has about 40 feet of closure (fig. 1*A*), while the base of the Fall River Formation of Cretaceous age has none (fig. 1*B*). One drill hole on a pre-Fall River anticline in the area penetrated the Lakota and Morrison Formations and the Redwater Shale Member of the Sundance Formation of Jurassic age. At that point the total maximum thickness of about 100 feet of Morrison Formation was present. This indicates that there was little, if any, post-Morrison and pre-Lakota erosion and, therefore, little, if any, folding prior to the beginning of Lakota time. Folding apparently continued through Lakota time, resulting in pronounced depositional and structural troughs.

It is possible that this pre-Fall River folding was part of the structural deformation accompanying the beginning of the Black Hills uplift. The post-Fall River Cretaceous marine invasion of the Black Hills, however, suggests that the area was more likely uplifted at the end of Cretaceous time. Folding accompanying the uplift was then superimposed on the earlier folding.

Outcrop data and logs of core holes supplied to the U.S. Geological Survey by the U.S. Atomic Energy Commission were the basis for the structural interpretation.

U.S. GEOL. SURVEY PROF. PAPER 501-D, PAGES D28–D29

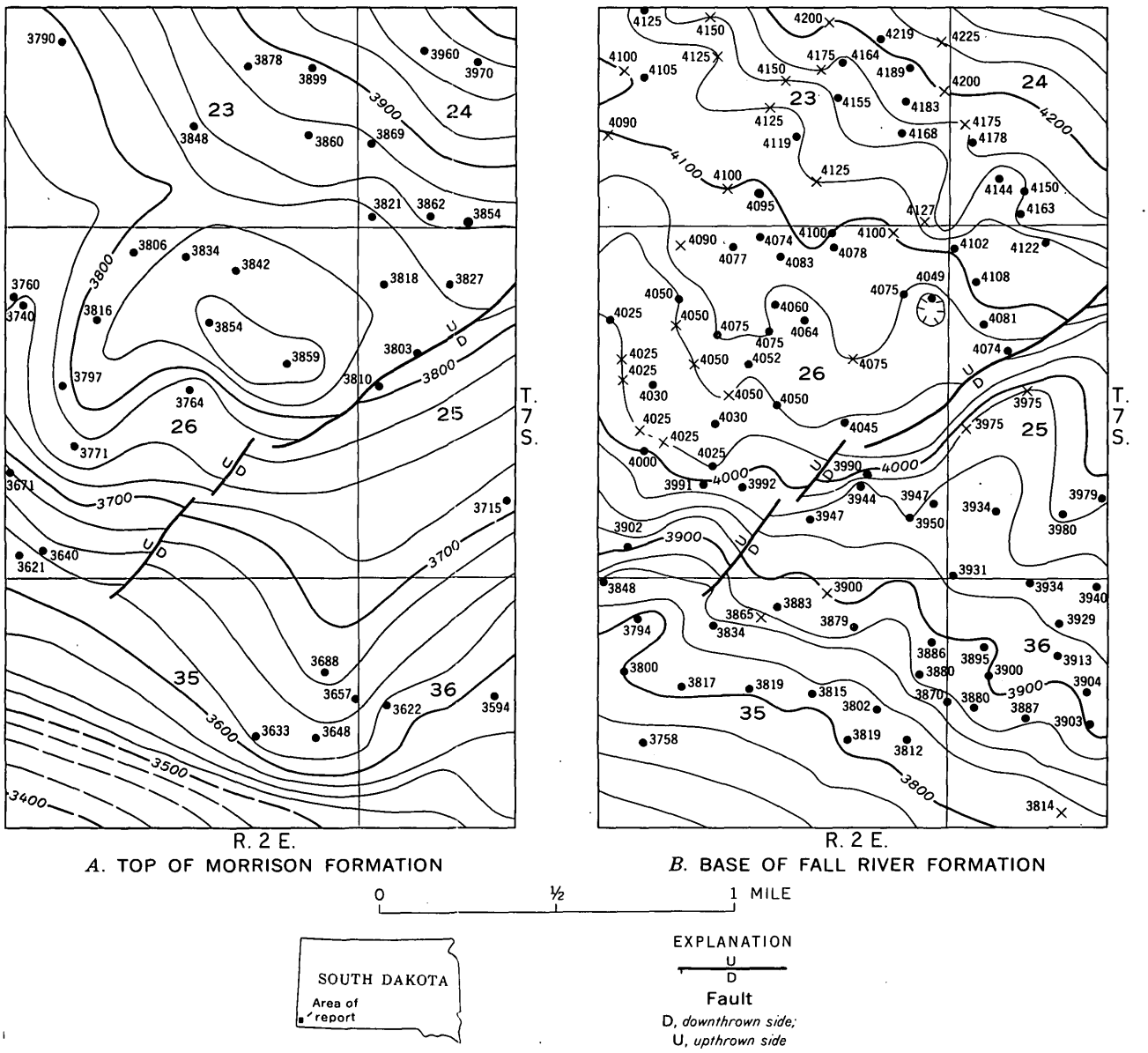

FIGURE 1.—Structure-contour maps of part of the Edgemont NE quadrangle, Fall River County, S. Dak. Dot, elevation of top of the Morrison Formation or base of the Fall River Formation in drill hole; ×, elevation of exposed base of the Fall River Formation. Contours dashed where inferred. Contour interval 25 feet; datum is mean sea level.

REFERENCES

Gott, G. B., and Schnabel, R. W., 1963, Geology of the Edgemont NE quadrangle, Fall River and Custer Counties, South Dakota: U.S. Geol. Survey Bull. 1063–E.

Gries, J. P., 1964, Barker dome oil field, Custer County, South Dakota: The Mountain Geologist, v. 1, no. 1, p. 43.

CHINLE FORMATION AND GLEN CANYON SANDSTONE IN NORTHEASTERN UTAH AND NORTHWESTERN COLORADO

By F. G. POOLE and J. H. STEWART,
Denver, Colo., Menlo Park, Calif.

Work done in cooperation with the U.S. Atomic Energy Commission

Abstract.—The Chinle Formation of Late Triassic age is composed of six lithologic units, in ascending order: (1) Gartra Member (new usage), (2) mottled member, (3) ocher siltstone member, (4) a local sandstone and conglomerate member, (5) red siltstone member, and (6) upper member. The ocher siltstone is correlated with the Popo Agie Member of the Chugwater Formation of Wyoming, and the red siltstone is correlated with the Church Rock Member of the Chinle of southeast Utah. A regional angular unconformity occurs at the base of the Chinle throughout the area and at the top of the Chinle in northwestern Colorado. The Glen Canyon Sandstone (new usage) of Late Triassic and Early Jurassic age overlies the Chinle in northeastern Utah and part of northwestern Colorado.

The Chinle Formation of Late Triassic age and the Glen Canyon Sandstone of Late Triassic and Early Jurassic age are widely exposed in northeastern Utah and northwestern Colorado. In northeastern Utah, exposures of the Chinle and the Glen Canyon are restricted to the flanks of the Uinta Mountains (fig. 1). In northwestern Colorado, the Chinle is exposed in the eastern part of the Uinta Mountains, along the margins of the Park and Gore Ranges, around the White River Plateau, along the southern extension of the Grand Hogback, and near State Bridge, Wolcott, East Brush Creek, Basalt, and Aspen (fig. 1). In northwestern Colorado, the Glen Canyon Sandstone is exposed in the eastern part of the Uinta Mountains and along the northern and western flanks of the White River Plateau.

Study of these exposures has led to the summary of the stratigraphic character and relations presented here, and is part of a regional investigation of the Chinle Formation and related strata of the Colorado Plateau region. Most of the information presented in this paper was collected during 1955–57, and concerns work done on behalf of the U.S. Atomic Energy Commission.

CHINLE FORMATION

The Chinle Formation unconformably overlies red beds of Early Triassic age in the Uinta Mountains; red beds of Early Triassic and(or) Permian age around the White River Plateau, along the southern extension of the Grand Hogback, and in the vicinity of State Bridge, Wolcott, and East Brush Creek; and red beds of Permian and possibly Pennsylvanian age along the margins of the Park, Gore, and Tenmile Ranges, and in the vicinity of Basalt and Aspen. In general, the Chinle rests on progressively older strata eastward from the Uinta Mountains to the Park, Gore, and Tenmile Ranges.

The Glen Canyon Sandstone appears to conformably overlie the Chinle Formation in the Uinta Mountains of northeastern Utah and northwestern Colorado, whereas in the vicinity of the White River Plateau, it overlies the Chinle with apparent unconformity. South and east of Meeker, Colo., beyond the wedge-edge of the Glen Canyon Sandstone, the Chinle is unconformably overlain by the Entrada Sandstone or equivalent strata of Late Jurassic age.

The Chinle Formation in northeastern Utah and northwestern Colorado is composed of six members (figs. 2, 3), in ascending order: (1) a unit of light-colored sandstone and conglomerate called the Gartra Member (new usage); (2) a unit of purple and red

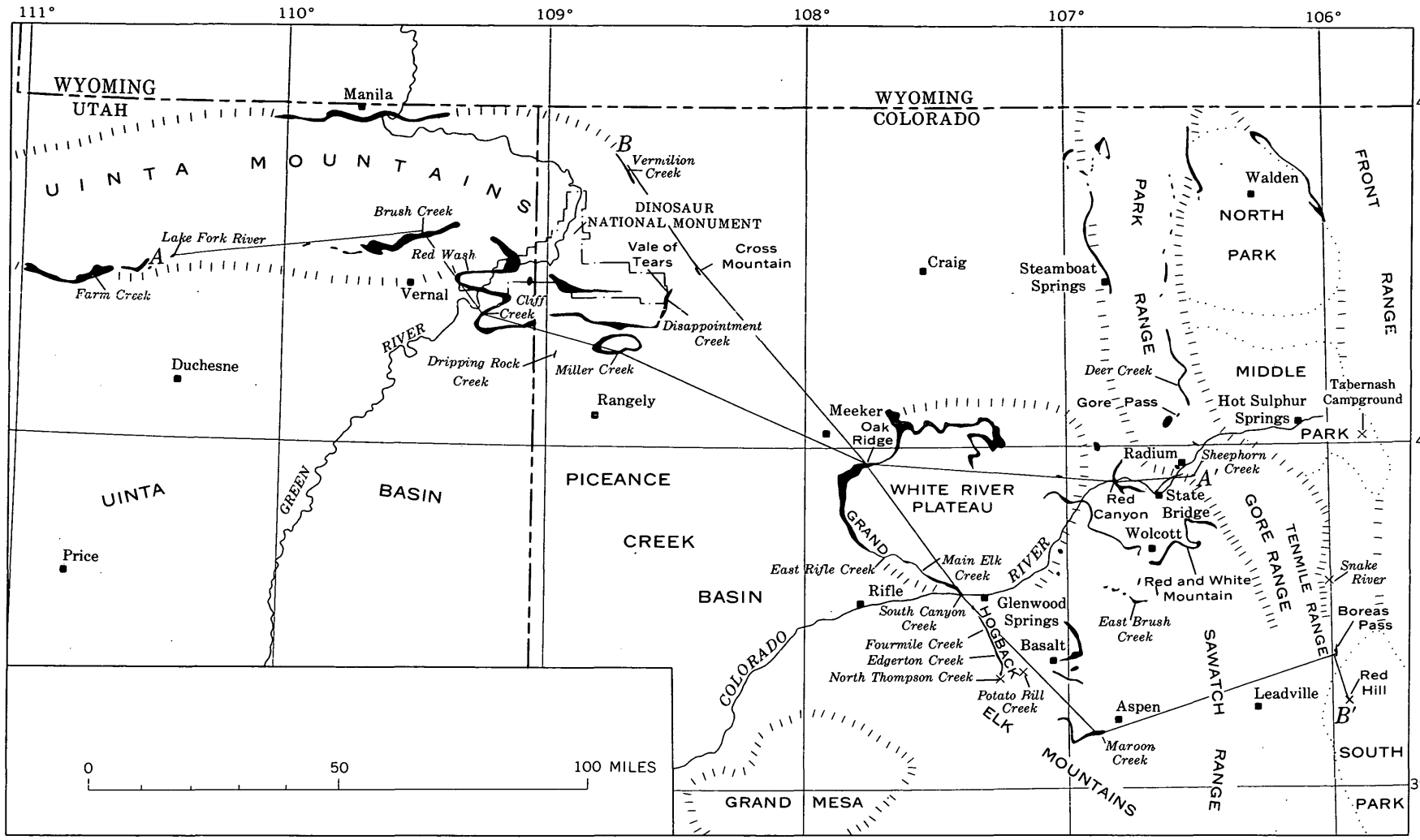

FIGURE 1.—Index map of northeastern Utah and northwestern Colorado, showing outcrops (black) of the Chinle Formation and related strata, and localities discussed in text.

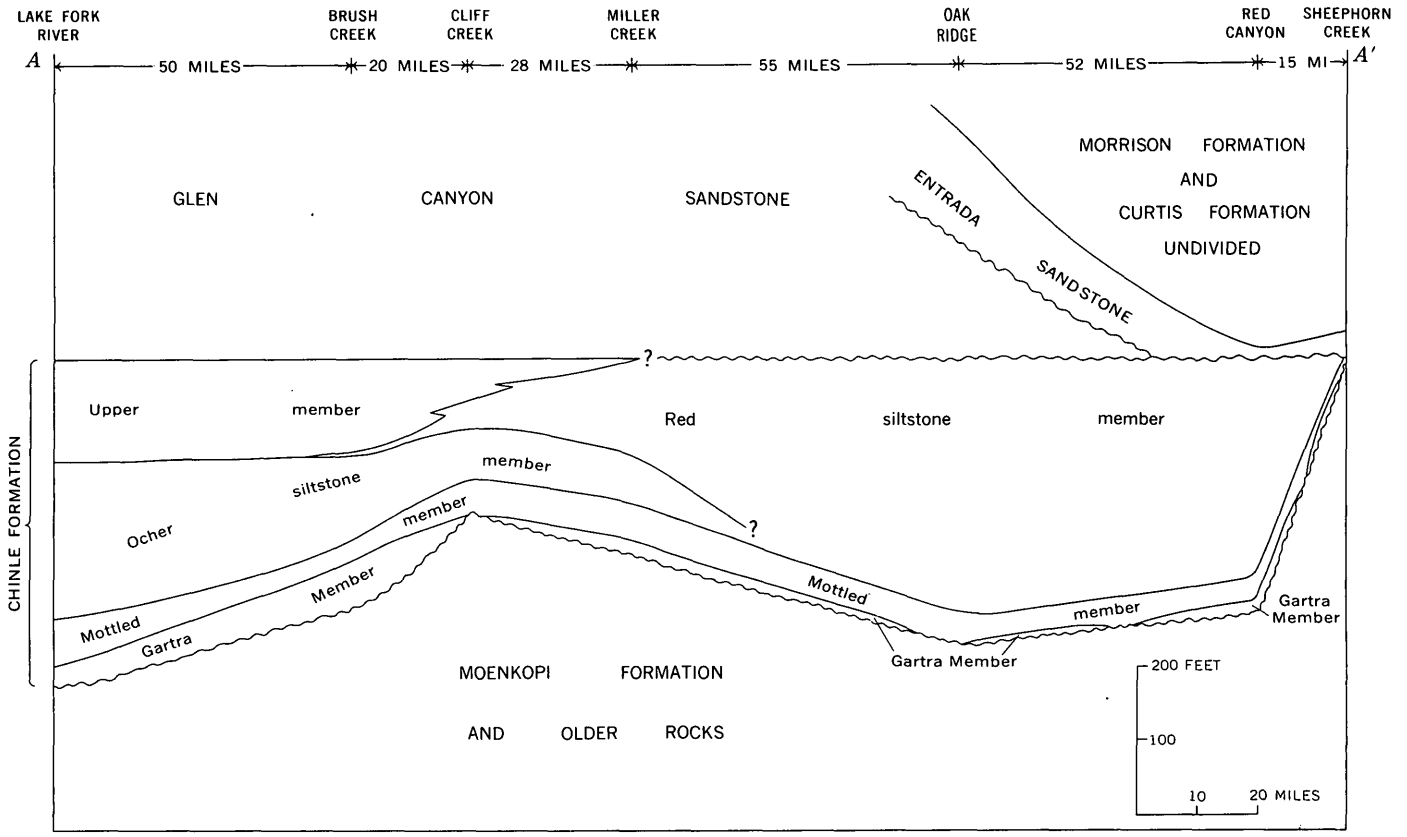

FIGURE 2.—Generalized west-to-east section, A–A', showing relation of members within the Chinle Formation. Location of section shown on figure 1. Vertical exaggeration ×660.

mudstone, mottled siltstone, and mottled sandstone referred to as the mottled member; (3) a unit of ocher siltstone, and some red siltstone, called the ocher siltstone member; (4) a local unit of gray, pink, and brown sandstone, mudstone, and mudstone-limestone pebble conglomerate referred to as the sandstone and conglomerate member; (5) a unit of red siltstone, and minor amounts of sandstone and siltstone-limestone pebble conglomerate, called the red siltstone member; and (6) a unit of orange, brown, and gray sandstone and red and green mudstone, called the upper member. Some of these units are local; others are widespread. The Gartra Member and mottled member are persistent throughout the region, whereas the other siltstone and upper members occur only in the Uinta Mountains, the red siltstone member in the eastern Uinta Mountains and throughout northwestern Colorado, and the sandstone and conglomerate member only locally in the easternmost Uinta Mountains.

Gartra Member

The Gartra Grit Member of the Stanaker Formation was named and described by H. D. Thomas and Krueger (1946) for a thin unit within Upper Triassic strata in the Vernal area of northeastern Utah. These names were not generally accepted because the well-established Colorado Plateau names Shinarump Conglomerate and Chinle Formation were already in use for these strata in northeastern Utah and northwestern Colorado (Powell, 1876; C. R. Thomas and others, 1945). Subsequent to Thomas and Krueger's work in the Uinta Mountains, geologists working there continued to use the names Shinarump Conglomerate and Chinle Formation (Huddle and McCann, 1947; Kinney and Rominger, 1947; Kinney, 1951, 1955; and Hansen, 1955). Regional stratigraphic work, however, has shown that the Shinarump is a member of the Chinle Formation that does not extend north of central Utah (Stewart, 1957) and that the Gartra is confined to the northern and northeastern parts of the Colorado Plateau (fig. 4). As the Gartra and Shinarump probably are not correlative and their relative age is uncertain, the name Gartra is preferred for the basal sandstone and conglomerate unit of the Chinle Formation in the area described in this paper. The lithologic term "grit" is not part of the formal name in the report area. The name Chinle Formation is retained for Upper Triassic strata as it is well estab-

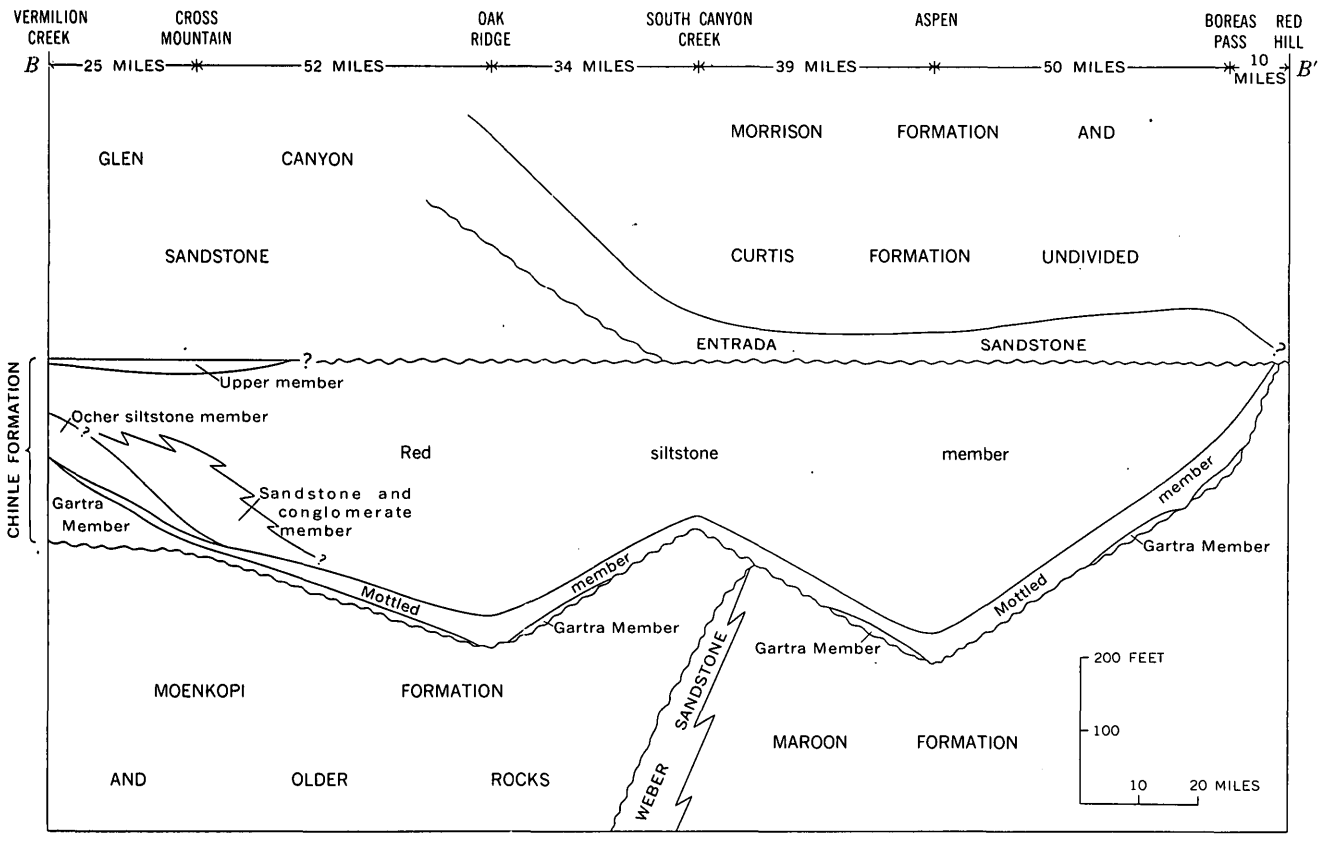

FIGURE 3.—Generalized northwest-to-southeast section, *B–B'*, showing relation of members within the Chinle Formation. Location of section shown on figure 1. Vertical exaggeration ×660.

lished and the Chinle Formation of northeastern Utah and northwestern Colorado can be demonstrated to be continuous with part of the Chinle Formation in the central part of the Colorado Plateau. Hence, the name Stanaker Formation is not used in this report. The Gartra Member is present throughout northeastern Utah and most of northwestern Colorado. Quartzose sandstone and conglomerate lenses within the Temple Mountain Member (Robeck, 1956) of the Chinle Formation in the San Rafael Swell, south of the Uinta Basin, are lithologically similar to the Gartra Member.

The Gartra Member consists mainly of light-colored sandstone, conglomeratic sandstone, and some conglomerate. Locally the member is stained purple and red. The sandstone is composed dominantly of subangular to well-rounded grains and granules of quartz, some feldspar, and sparse chert and quartzite; the matrix and cement consist of clay minerals, calcite, and locally silica (R. A. Cadigan, written communication, 1958). The gravels are subrounded to well-rounded pebbles and scattered cobbles composed of quartz, some chert and quartzite, and sparse feldspar, quartzose sandstone, and limestone. In general, the maximum gravel size increases eastward. The maximum measured diameter of quartz gravels ranges from about 1 inch at Farm Creek in Utah to about 3 inches at Red and White Mountain, East Brush Creek, Deer Creek, and Boreas Pass in Colorado. The Gartra is cross stratified in most areas, and contains silicified log fragments.

The Gartra Member varies widely in thickness, though in northeastern Utah the member is generally 20–50 feet thick. It is generally only 5–30 feet thick in northwestern Colorado (see accompanying table). Thickness is greatest where the member fills channels cut into the underlying rocks. The Gartra is discontinuous, especially in northwestern Colorado; where it is absent the mottled member is the basal unit of the Chinle.

In the exposures examined, a sharp erosional contact was noted between the light-colored Gartra Member and the underlying red beds. The contact is undulating and marked by small channels and scours. Beds above and below the contact appear concordant at all outcrops, and the contact is an apparent erosional disconformity; however, eastward the Gartra rests on older and older beds and the contact is clearly a regional angular unconformity.

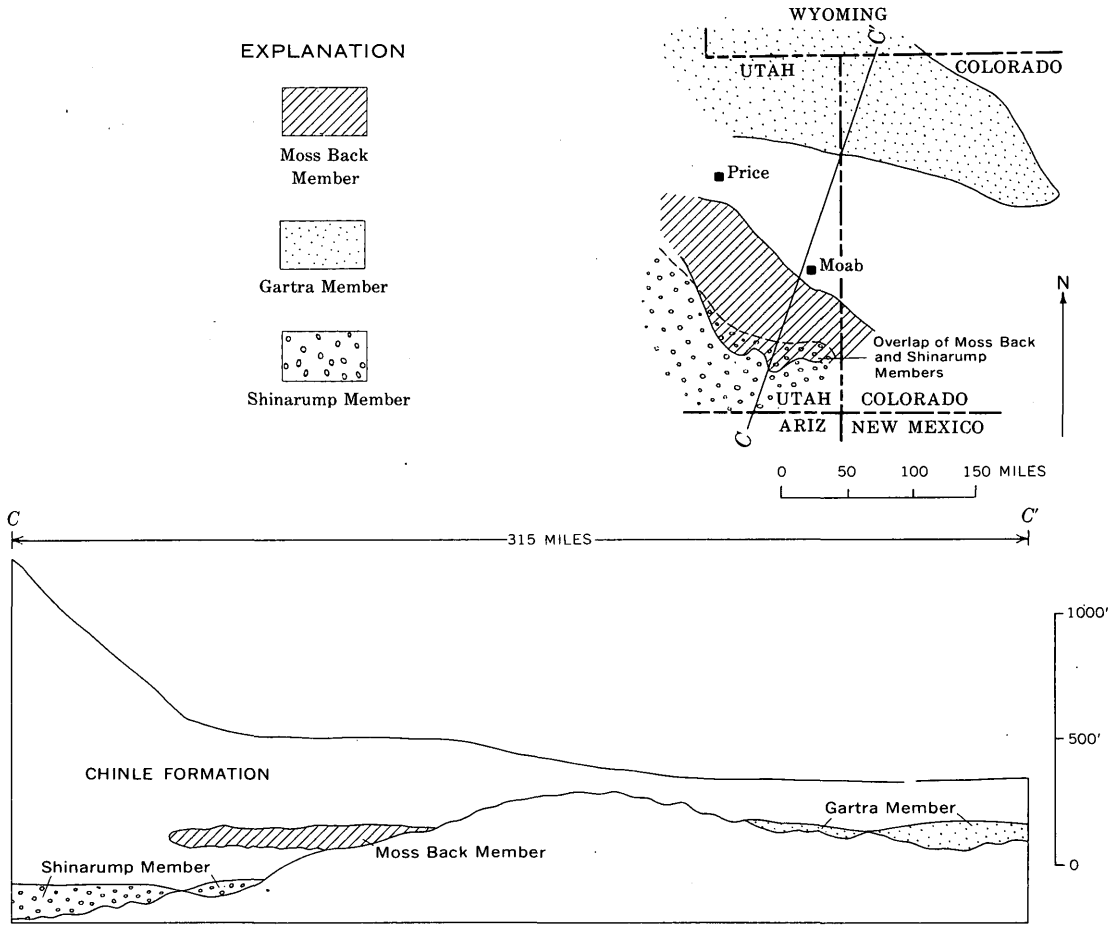

FIGURE 4.—Map and diagrammatic section showing inferred depositional limits and stratigraphic relations of Moss Back, Gartra, and Shinarump Members of the Chinle Formation. Vertical exaggeration ×416.

The mottled member is intimately related to the Gartra Member; the contact between them is placed at the top of the rather continuous light-colored sandstone and conglomerate that extends to the base of the Chinle Formation. The contact is gradational and intertonguing. Gartra-like sandstone and conglomerate occur as lenses within the mottled member, especially in northwestern Colorado, and tongues of mottled rock extend into the Gartra.

The general decrease in grain size toward the west and the westerly dip of cross strata indicate that the Gartra Member was deposited by westerly flowing streams (Poole, 1961). These streams probably originated in central and possibly west-central Colorado. The source rock was probably older red beds, such as the Maroon Formation, and exposed lower Paleozoic rocks and Precambrian igneous and metamorphic rocks in central and west-central Colorado.

Mottled member

The mottled member is persistent throughout northeastern Utah and northwestern Colorado. The mottled member north and east of the Uinta Basin may be equivalent to part or all of the Temple Mountain Member (Robeck, 1956) of the Chinle Formation in the San Rafael Swell (south of Price, Utah).

The mottled member is made up of purple and red mudstone and mottled siltstone and sandstone. The purple and red mudstone consists predominantly of silt and clay and variable amounts of sand. Dominant components of the mottled siltstone and sandstone are subangular to well-rounded grains of quartz, some feldspar, chert, quartzite, mica, and sparse tuff(?); the matrix and cement consist of silica, clay minerals, calcite, and iron oxide (R. A. Cadigan, written communication, 1958). Iridescent purple iron-oxide blebs, bedded chert, and jasper also are abundant. Many of

the sandstone layers are very coarse grained and conglomeratic. The gravels are composed of subrounded to rounded quartz and chert. Overall the member generally is crudely stratified, but the mottled siltstone and sandstone units locally are well bedded. A few of the silty and very fine to medium-grained sandstone beds are crossbedded. The member consists mainly of mottled sandstone at Boreas Pass in Colorado, whereas elsewhere it is mostly sandy mudstone.

The member is absent locally, as at Vermilion Creek and East Brush Creek. The mottled member is generally 30–50 feet thick in northeastern Utah and 20–40 feet thick in northwestern Colorado (see table).

The mottled member is overlain by the ocher siltstone member in the Uinta Mountains of northeastern Utah and northwestern Colorado, and by the red siltstone member in northwestern Colorado (fig. 2). The contact between the mottled member and ocher siltstone member is difficult to locate in many parts of the central Uinta Mountains where a thin reddish mudstone characteristic of the basal part of the ocher siltstone member is well developed and rests on similar rocks of the mottled member. The contact generally is marked by a subtle color change from purple and red strata of the mottled member to reddish strata of the basal part of the ocher siltstone member. The mottled member overlies the Gartra Member or pre-Chinle strata where the Gartra is missing.

Thickness of Chinle Formation and its members in northeastern Utah and northwestern Colorado

[*P*, present at section, but not measured. *PP*, probably present, but not differentiated; unit occurs either as a wedge edge or as thin tongues in adjacent unit. *A*, absent at section, but present nearby. *NP*, not present in area. *NE*, not exposed, but probably present in area]

County	Locality (fig. 1)	Thickness (feet)						
		Total formation	Members					
			Gartra	Mottled	Ocher siltstone	Sandstone and conglomerate	Red siltstone	Upper
Utah								
Duchesne	Lake Fork River	443±	23–100	68	215	NP	PP	137
Uintah	Vernal (Brush Creek)	340	65	19	122	NP	PP	135
	Red Wash	287	53	P	P	P	P	110
	Cliff Creek	212	A	50	68	PP	36	59
Colorado								
Moffat	Dripping Rock Creek	P	NE	NE	NE	NP	P	18
	Miller Creek	266	21	52	66	NP	127	A
	Disappointment Creek	259	A	42	21	53	143	1
	Vale of Tears	291	A	78	19	83	100	10
	Cross Mountain	244+	NE	NE	10+	115	100	20
	Vermilion Creek	246	110	A	64	NP	67	6
Rio Blanco	Oak Ridge	388	A	42	NP	NP	346	NP
Garfield	East Rifle Creek	P	6–15	P	NP	NP	P	NP
	Main Elk Creek	[1] 311	0–5	P	NP	NP	P	NP
	South Canyon Creek	226	NP	17	NP	NP	209	NP
	Fourmile Creek	100±	PP	20±	NP	NP	80±	NP
	Edgerton Creek	60±	PP	20±	NP	NP	40±	NP
Pitkin	North Thompson Creek [2]	NP?						
	Potato Bill Creek [2]	NP						
	Aspen (Maroon Creek)	413	A	35	NP	NP	378	NP
Eagle	Basalt	635	A	28	NP	NP	607	NP
Summit	Snake River [2]	NP						
	Boreas Pass	150	8	50	NP	NP	92	NP
Park	Red Hill [2]	NP						
Eagle	East Brush Creek	1, 083	70	A	NP	NP	1, 013	NP
	Wolcott	P	30	P	NP	NP	P	NP
	Red and White Mountain	250	25	25	NP	NP	200	NP
	Red Canyon	[3] 344	[3] 36	P	NP	NP	P	NP
	State Bridge	[4] 90	12–24	P	NP	NP	P	NP
	Sheephorn Creek	15	A	15	NP	NP	NP	NP
Grand	Radium	P	A	P	NP	NP	1	NP
	Gore Pass	P	10	10+	NP	NP	NE	NP
	Deer Creek	P	20	15+	NP	NP	NP	NP
	Tabernash Campground [2]	NP						

[1] Thomas and others (1945). [2] Just outside the limit of the Chinle; zero isopach nearby. [3] Sheridan (1950). [4] Donner (1949).

The clay mineralogy and mottled coloration of the mottled member suggest that it is derived from a residual weathered zone (Schultz, 1963). Coarse detritus and cross strata in some of the siltstone, sandstone, and conglomerate therein indicate that these sediments were reworked and transported by streams.

Ocher siltstone member

The informal name ocher siltstone member is assigned to a unit of ocher siltstone and minor amounts of red siltstone, which is present throughout the Uinta Mountains.

The member consists of structureless siltstone, clayey siltstone, and minor silty claystone. The ocher and reddish siltstone and claystone commonly contain oolites, carbonate nodules, and secondary gypsum veinlets. Many oolites and nodules contain analcite (Keller, 1953). The ocher color probably is due to goethite (L. G. Schultz, written communication, 1958).

Thickness increases from east to west in the Uinta Mountains (figs. 2, 3, and table). Range of thickness is 50 to 200 feet in the central and eastern Uinta Mountains.

The ocher siltstone member is overlain at Miller Creek and Cliff Creek by the red siltstone member, at Cross Mountain by the sandstone and conglomerate member, and at Vernal and Lake Fork River by the upper member (figs. 2, 3). The contact between the ocher siltstone member and overlying units is placed at the top of the distinctively colored siltstone.

The ocher siltstone member is lithologically identical to part of the Popo Agie Member of the Chugwater Formation in the Lander area, Wyoming, as was suggested originally by Keller (1953). South and east from the Uinta Mountains the ocher siltstone member apparently wedges out.

The composition of the ocher siltstone member suggests that it was deposited in a shallow water body, perhaps a marshy lake, in a broad basin or lowland (Keller, 1952).

Sandstone and conglomerate member

The sandstone and conglomerate member is composed of gray, pink, and brown siltstone, sandstone, and conglomerate. This member is restricted to outcrops in the easternmost Uinta Mountains at Cross Mountain, Vale of Tears, and Disappointment Creek. The sandstone and conglomerate member is considered a basal coarse facies of the red siltstone member.

The basal part of the member is mainly sandstone and subordinately siltstone and conglomerate. This basal part is composed of quartz, some feldspar, chert, and mica; the matrix and cement consist of calcite and clay minerals (R. A. Cadigan, written communication, 1958). The granules and pebbles are dominantly limy siltstone and sparse siliceous rock types. The remainder of the member consists of siltstone, sandstone, and mudstone pebble conglomerate. Phytosaur bone fragments and teeth (S. H. Mamay and G. E. Lewis, written communication, 1957) are numerous in this member and particularly abundant in the coarser parts. Stratification consists of horizontal laminae and thin beds with ripple laminae, current lineation, and cross strata.

The contact between the sandstone and conglomerate member and the overlying red siltstone member is generally placed at the base of the continuous or dominant red siltstone section.

A flood-plain environment is indicated by lithology, sedimentary structures, and phytosaur remains. Cusp ripples, current lineation, and cross strata indicate stream deposition. One study of orientation of cross strata in the top of the member at Cross Mountain indicates a southwesterly direction of sediment transport.

Red siltstone member

A unit of red siltstone and minor amounts of sandstone and conglomerate occurs in the eastern Uinta Mountains and in northwestern and west-central Colorado. This unit, referred to here informally as the red siltstone member, is correlated with the Church Rock Member of the Chinle, a member named and described by Witkind and Thaden (1963) in Monument Valley, Ariz. The name Church Rock is used widely in Utah south of the Uinta Basin (Stewart, 1957).

The siltstone, very fine grained sandstone, and the matrix of the conglomerate are composed dominantly of silt- and sand-sized grains of quartz, some feldspar, and sparse mica and tuff(?); the matrix and cement consist of iron oxide, calcite, and clay minerals (R. A. Cadigan, written communication, 1958). The red siltstone member is generally very calcareous. The conglomerate contains well-rounded elongate granules and pebbles of limy siltstone and silty limestone set in a siltstone matrix. The basal part of the red siltstone member at East Brush Creek contains lenses of subangular to rounded sand and locally conglomerate layers containing granules and pebbles, as well as a few cobbles composed of quartz, chert, feldspar, siltstone, and limestone. Quartz granules and pebbles occur in the basal part of the red siltstone member in many areas in northwestern and central Colorado. The basal siltstone at Cliff Creek contains gravel composed of material from the underlying ocher siltstone member.

From a distance the red siltstone member appears to be thin to thick bedded; however, close inspection shows that the member is either structureless or only crudely stratified. Locally it contains cross strata, mud cracks, and low-index ripple marks. Conspicuous purplish vertical cylindrical structures in red siltstone beds were noted in several areas. These structures appear to contain more lime than the adjacent siltstone and may have formed along vertical fracture intersections.

The only fossils found were sparse bone fragments at the base of the member at Cliff Creek and near the top of the member at Disappointment Creek.

The red siltstone member is generally absent in the vicinity of the Gore Range and is erratic in thickness in many parts of northwestern and west-central Colorado (see table), owing to pre-Late Jurassic erosion.

In the Uinta Mountains, the red siltstone member is underlain by the ocher siltstone member at Miller Creek, Cliff Creek, and Vermilion Creek; it is underlain by the sandstone and conglomerate member at Disappointment Creek and Cross Mountain. In northwestern Colorado, the red siltstone member is underlain by the mottled member in nearly all areas. At East Brush Creek it overlies the Gartra Member, which fills the stratigraphic position normally occupied by the mottled member.

The red siltstone interfingers laterally with the upper member between Cliff Creek and Vernal. The contact is generally placed between the highest structureless red siltstone and the lowest brown sandstone of the upper member. Where the upper member is absent, the Glen Canyon Sandstone overlies the red siltstone member of the Chinle.

In northwestern Colorado, beyond the eastern limit of the Glen Canyon Sandstone, the Entrada Sandstone or equivalent strata overlies the Chinle Formation (figs. 2, 3). Beds above and below the contact appear disconformable at nearly all outcrops; however, regional study indicates that from west to east younger and younger beds rest on the Chinle and that the contact is clearly a regional angular unconformity.

The red siltstone member is probably mainly a floodplain deposit but, in part, a deltaic and lake deposit. The source rock was probably mostly older red beds such as the Maroon Formation and Lower Triassic equivalents and, in part, exposed lower Paleozoic rocks and Precambrian igneous and metamorphic areas in central Colorado.

Upper member

The name upper member was applied by Kinney (1955) to a sequence of orange, brown, and gray sandstone; red, gray, and brown siltstone; and red, brown, gray, and green claystone. The member is at the top of the Chinle Formation and is best developed in the western and central Uinta Mountains. Many of the sandstone beds in the member resemble the overlying massive-weathering Glen Canyon Sandstone and may represent lenses or tongues of the Glen Canyon. The upper member may be transitional into the Glen Canyon Sandstone.

The sandstone layers are composed of subrounded to well-rounded very fine to medium grains of quartz, some feldspar, and sparse quartzite, chert, and tuff(?); the matrix and cement include calcite and clay minerals (R. A. Cadigan written communication, 1958). The layers are horizontally laminated to thick bedded. Ripple laminae and thin to thick planar and trough sets of small- and medium-scale cross laminae are present in the upper part of a few sandstone beds. Some cusp ripples, current lineation, and mud cracks were noted on a few stratification surfaces. Three studies of cross-strata orientation made of a lower sandstone (partly eolian) in the Vernal area indicate a wide range in direction of sediment transport from northeast to southwest, averaging southeasterly.

The siltstone is composed of quartz, some feldspar, and sparse mica; the matrix and cement consist of iron oxide, calcite, and clay minerals (R. A. Cadigan, written communication, 1958). The siltstone is horizontally thinly laminated to thick bedded; some parts are structureless. A few units contain ripple laminae, mud cracks, and clayey siltstone pellets. The claystone is generally silty and horizontally thinly laminated. A pale-red to grayish-red silty claystone unit 15–25 feet thick is at the top of the upper member throughout the central and most of the eastern Uinta Mountains.

The upper member at Vernal consists of about 72 percent sandstone, 20 percent siltstone, and 8 percent claystone. The proportion of sandstone decreases both to the east and to the west from Vernal. At Lake 30 percent claystone. At Cliff Creek, east of Vernal, Fork River, west of Vernal, the upper member consists of 19 percent sandstone, 51 percent siltstone, and the upper member intertongues with the red siltstone member and is thin. Here the upper member consists of 4 percent sandstone, 70 percent siltstone (which may be chiefly tongues of the red siltstone member), and 26 percent claystone.

The upper member overlies the ocher siltstone member west of the Green River. East of the Green River, the upper member overlies the red siltstone member (fig. 2). The contact between the upper member and red siltstone member is characterized by intertonguing, and the upper member wedges out eastward near Mil-

ler Creek above or at the top of the red siltstone member (fig. 2).

The upper member is overlain by the Glen Canyon Sandstone with apparent conformity. The contact between them in the central and eastern Uinta Mountains is at the top of a persistent grayish-red silty claystone which underlies a massive cliff-forming sandstone of the Glen Canyon Sandstone.

Sedimentary structures and lithology indicate that the upper member is mainly a flood-plain deposit but that it includes some wind deposits.

GLEN CANYON SANDSTONE

A thick sandstone overlying the Chinle Formation in the western Uinta Mountains has been generally called Nugget Sandstone, whereas in the eastern Uinta Mountains and in the vicinity of the White River Plateau it has generally been called Navajo Sandstone. Continuity and uniformity of this sandstone in the Uinta Mountains indicate the desirability of one name for this unit.

The available evidence indicates that the sandstone body is equivalent to part or all of the Glen Canyon Group of the Colorado Plateau province to the south. MacLachlan (1957) showed the Navajo Sandstone of the Uintas as being equivalent to the Wingate, Kayenta, and Navajo exposed south of the Uinta Basin. Later work by R. F. Wilson (written communication, 1962), however, indicates that in some areas the sandstone of the Uinta Mountains may be equivalent largely to the Wingate Sandstone. According to Wilson, drill-hole data north of the San Rafael Swell (east and southeast of Price, Utah) and along the Colorado-Utah State line (northwest of Grand Junction, Colo.), show the Wingate thickening northward and the Kayenta and Navajo thinning. If these trends continue northward, it seems likely that the Kayenta wedges out and that much of the sandstone of the Uinta Mountains is equivalent to strata older than Navajo. A widespread pre-San Rafael Group unconformity bevels older beds eastward in the eastern part of the Uinta Basin (Wright and Dickey, 1963), and the Navajo and Kayenta may have been partly or completely removed by erosion in the eastern Uinta Mountains and in northwestern Colorado. This evidence indicates that the name Navajo is undesirable for this sandstone unit. The name Nugget also is opposed by many geologists because of lithologic differences between the Nugget in the type area and that in the Uinta Mountains. As the existing evidence indicates that this sandstone body is equivalent to part or all of the Glen Canyon Group to the south, the name Glen Canyon is extended into this area and given formational rank. The Glen Canyon Sandstone is above the Chinle Formation and below rocks of the San Rafael Group in the Uinta Mountains and in the vicinity of the White River Plateau.

The Glen Canyon Sandstone is designated as Late Triassic and Early Jurassic in age in accordance with the current age assignment of the Glen Canyon Group in the southern part of the Colorado Plateau.

The Glen Canyon Sandstone extends throughout northeastern Utah and part of northwestern Colorado but wedges out southeastward in the vicinity of the White River Plateau. The Glen Canyon Sandstone is overlain by the Middle and Upper Jurassic rocks assigned to the Twin Creek Limestone in the western Uinta Mountains and to the Carmel Formation in the eastern Uinta Mountains. In the easternmost Uintas the Carmel wedges out to the east, and the Entrada Sandstone rests unconformably on the Glen Canyon Sandstone. The two sandstones, however, can usually be distinguished on the basis of type and orientation of cross strata and locally by the presence of scattered ventifacts or pebbles along the contact.

The Glen Canyon Sandstone consists of gray, orange, brown, yellow, pink, and white sandstone. It is composed of subrounded to well-rounded very fine to fine grains of quartz, some feldspar, and sparse chert and quartzite; the matrix and cement consist of calcite and clay minerals (R. A. Cadigan, written communication, 1958). The Glen Canyon contains varying amounts of flat-bedded strata in the lower 50–100 feet. Most of the Glen Canyon, however, contains thick wedge-planar, tabular-planar, and subordinate lenticular trough sets of large- and medium-scale cross strata. Parallel and cusp ripple marks, and mud cracks were noted in the basal part in some areas.

Sedimentary structures in the Glen Canyon Sandstone suggest that the basal 50 feet is mainly water laid but that the thick upper part is mainly eolian in origin. Cross-strata orientations indicate that the winds that deposited the eolian sandstone blew from the north and northeast (Poole, 1962).

REFERENCES

Donner, H. F., 1949, Geology of the McCoy area, Eagle and Routt Counties, Colorado: Geol. Soc. America Bull., v. 60, no. 8, p. 1215–1248.

Hansen, W. R., 1955, Geology of the Flaming Gorge quadrangle, Utah-Wyoming: U.S. Geol. Survey Geol. Quad. Map GQ–75.

Huddle, J. W., and McCann, F. T., 1947, Pre-Tertiary geology of the Duchesne River area, Duchesne and Wasatch Counties, Utah: U.S. Geol. Survey Oil and Gas Inv. Prelim. Map 75.

Keller, W. D., 1952, Analcime in the Popo Agie Member of the Chugwater Formation: Jour. Sed. Petrology, v. 22, no. 2, p. 70–82.

Keller, W. D., 1953, Analcime in the Chinle Formation of Utah correlative with the Popo Agie of Wyoming: Jour. Sed. Petrology, v. 23, no. 1, p. 10–12.

Kinney, D. M., 1951, Geology of the Uinta River and Brush Creek-Diamond Mountain areas, Duchesne and Uintah Counties, Utah: U.S. Geol. Survey Oil and Gas Inv. Map 123.

——— 1955, Geology of the Uinta River–Brush Creek area, Duchesne and Uintah Counties, Utah: U.S. Geol. Survey Bull. 1007, 185 p.

Kinney, D. M., and Rominger, J. F., 1947, Geology of the Whiterocks River–Ashley Creek area, Uintah County, Utah: U.S. Geol. Survey Oil and Gas Inv. Prelim. Map 82.

MacLachlan, M. E., 1957, Triassic stratigraphy in parts of Utah and Colorado, *in* Intermountain Assoc. of Petroleum Geologists Guidebook, Field conference in Uinta Basin, 1957: p. 82–91.

Poole, F. G., 1961, Stream directions in Triassic rocks of the Colorado Plateau: Art. 199 *in* U.S. Geol. Survey Prof. Paper 424–C, p. C139–C141.

——— 1962, Wind directions in late Paleozoic to middle Mesozoic time on the Colorado Plateau: Art. 163 *in* U.S. Geol. Survey Prof. Paper 450–D, p. D147–D151.

Powell, J. W., 1876, Report on the geology of the eastern portion of the Uinta Mountains: U.S. Geol. and Geog. Survey Terr., 2d div.

Robeck, R. C., 1956, Temple Mountain Member—new member of Chinle Formation in San Rafael Swell, Utah: Am. Assoc. Petroleum Geologists Bull., v. 40, no. 10, p. 2499–2506.

Schultz, L. G., 1963, Clay minerals in Triassic rocks of the Colorado Plateau: U.S. Geol. Survey Bull. 1147–C, p. C1–C71.

Sheridan, D. S., 1950, Permian(?), Triassic, and Jurassic stratigraphy of the McCoy area of west central Colorado: The Compass, v. 27, no. 3, p. 126–147.

Stewart, J. H., 1957, Proposed nomenclature of part of Upper Triassic strata in southeastern Utah: Am. Assoc. Petroleum Geologists Bull., v. 41, no. 3, p. 441–465.

Thomas, H. D., and Krueger, M. L., 1946, Late Paleozoic and early Mesozoic stratigraphy of Uinta Mountains, Utah: Am. Assoc. Petroleum Geologists Bull., v. 30, no. 8, p. 1255–1293.

Thomas, C. R., McCann, F. T., and Raman, N. D., 1945, Correlation of exposed rocks in northwestern Colorado and northeastern Utah, and logs of deep wells in northwestern Colorado: U.S. Geol. Survey Oil and Gas Inv. Prelim. Chart 16.

Witkind, I. J., and Thaden, R. E., 1963, Geology and uranium-vanadium deposits of the Monument Valley area, Apache and Navajo Counties, Arizona: U.S. Geol. Survey Bull. 1103, 171 p.

Wright, J. C., and Dickey, D. D., 1963, Block diagram of the San Rafael Group and underlying strata in Utah and part of Colorado: U.S. Geol. Survey Oil and Gas Inv. Chart 63.

SIGNIFICANCE OF TRIASSIC OSTRACODES FROM ALASKA AND NEVADA

By I. G. SOHN, Washington, D.C.

Abstract.—Marine ostracodes are recorded for the first time from sedimentary rocks assigned to the Upper Triassic of Alaska and Middle Triassic of Nevada. These occurrences extend the range of the Cytherellidae downward into the Middle Triassic and tentatively extend the ranges of the Paleozoic Beyrichicopina and Thlipsuracea into the Triassic.

Identifiable marine Triassic ostracodes have hitherto not been recorded in North America, although nonmarine forms have been known for more than a century in the continental Triassic beds of the Eastern United States (Jones, 1862). Jones described and illustrated *Candona? rogersii* and *C.? emmonsi* from the Triassic of North Carolina and Pennsylvania. These are probably decalcified films of ostracode shells, and are therefore unidentifiable (Sohn, 1958).

Marine ostracodes are present in limited numbers in samples collected for the U.S. Geological Survey by E. G. Sable in 1948 and C. L. Whittington in 1952 from the upper part of the Shublik Formation (Upper Triassic) of the Arctic slope of Alaska. The Foraminifera from this formation were described by Tappan (1951). Harlan Bergquist kindly segregated the ostracodes from the collections.

Silicified marine ostracodes from the Grantsville Formation of late Middle Triassic age (Silberling, 1959) in the Shoshone Mountains, Nev., were sent to me by Prof. David L. Clark, Department of Geology, University of Wisconsin. These specimens were extracted along with conodonts by Mr. Cameron Mosher, University of Wisconsin, from the insoluble residue of a limestone sample collected by N. J. Silberling of the Geological Survey.

Although the ostracodes from Alaska are pyritized and very poorly preserved, and those from Nevada are not perfectly silicified, several genera can be identified.

The samples from Alaska are from the Shublik Formation, on Dodo Creek 2 to 2.3 miles above the junction with the Sadlerochit River, in the foothills of the Sadlerochit Mountains, northern Alaska. The 30 collections made contain the following:

Hungarella sp. or spp.
Paracypris? sp. or spp.
Darwinula? sp.
Steinkerns unident.

The sample from Nevada is from USGS Mesozoic loc. M76, in the Grantsville Formation, in the Shoshone Mountains, and contains the following:

Acratia? sp.
Carinobairdia? sp.
Gen. indet. Bairdiidae
Cytherelloidea n. sp. 1
Cytherelloidea n. sp. 2
New genus Thlipsuracea?
Gen. indet. Cytheracea
Gen. indet. Healdiidae
Gen. undet. Beyrichicopina?

Prof. Clark informs me (written communication, 1964) that ostracodes are present in other Triassic samples from Nevada, so that additional collecting will doubtless increase the list. The available information, though meager, is of interest because it begins to fill the gap in the knowledge of Triassic ostracodes and the relation of Paleozoic to post-Paleozoic ostracode groups.

Figure 1 shows the current interpretation of the range and affinities of superfamilies and higher categories of the Ostracoda, upon which is superposed the information obtained from this study. Sylvester-Bradley (1962) discussed the classification and suggested alternate groupings. The stratigraphic ranges of the groups as illustrated by Scott and Sylvester-Bradley in Moore (1961) are indicated by dashed lines in the Triassic, with the exception of the family Cytherellidae which extends down to the Upper Triassic.

U.S. GEOL. SURVEY PROF. PAPER 501-D, PAGES D40-D42

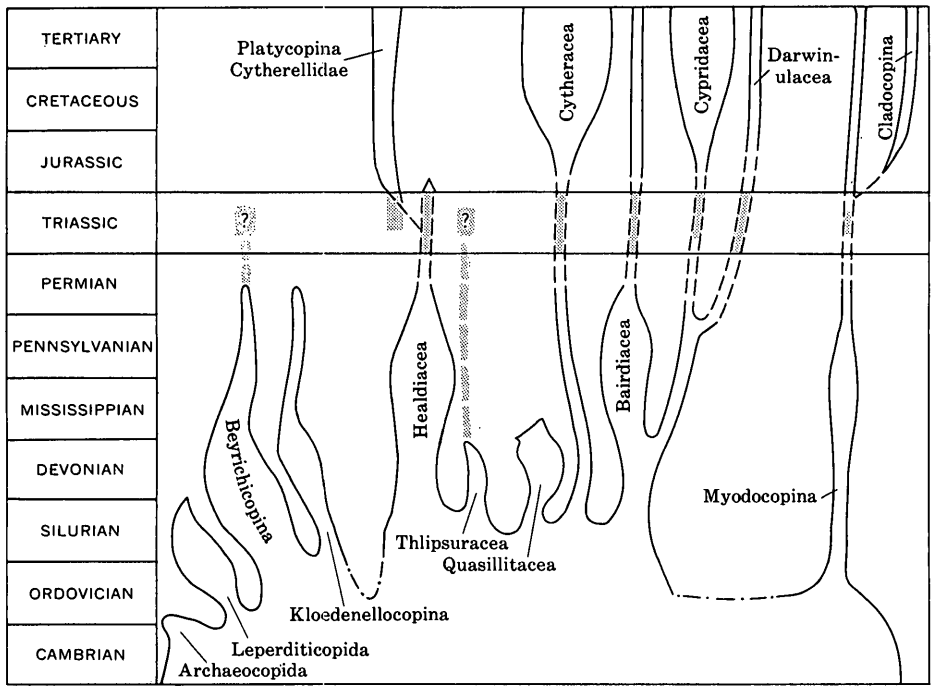

FIGURE 1.—Diagram showing stratigraphic distribution and inferred relations of the superfamilies and higher categories of Ostracoda, after Scott and Sylvester-Bradley, *in* Moore (1961, figs. 32 and 34). Stippled pattern shows age revisions discussed in text.

More recently, Hartmann discussed the phylogeny of Ostracoda and published a diagram (1963, p. 28, text fig. 8) in which the entire scheme is shown by dashed lines through the Triassic System.

The reasons for the revisions shown by the stippled pattern on figure 1 are given below:

Suborder Beyrichicopina

Kollmann (1963, p. 144–146) recorded Kirkbyidae? indet., a family that is included in the Byrichicopina, from the Upper Triassic of the Alps, and Hornibrook (1949) described the Recent family Punciidae that is tentatively placed in this suborder. The specimens from Nevada listed above as gen. undet. Beyrichicopina? substantiate the extension of the range of this suborder into the Middle Triassic.

Suborder Platycopina

The presence of *Cytherelloidea* in the assemblage from Nevada extends the range of this suborder into the Middle Triassic.

Superfamily Healdiacea

Hungarella in the Upper Triassic of Alaska, and gen. indet. Healdiidae in the Middle Triassic of Nevada are the basis for extending Healdiacea through the Triassic.

Superfamily Thlipsuracea

The new genus of Thlipsuracea? in the Middle Triassic of Nevada suggests that this taxon has a longer stratigraphic range than has been supposed.

Superfamily Cytheracea

The presence of an indeterminate genus of Cytheracea in the Middle Triassic of Nevada extends the range of this taxon into the Middle Triassic.

Superfamily Bairdiacea

Acratia?, *Carinobairdia*?, and Bairdiidae gen. indet. from Nevada document the presence of this group in the Triassic.

Superfamily Cypridacea

The Upper Triassic specimens from Alaska, identified is *Paracypris*? sp. or spp., are very poorly preserved. The fact that Styk (1962, p. 733) listed without illustrating *Paracypris* sp. from the Muschelkalk of Poland supports the extension of this superfamily into the Triassic.

Superfamily Darwinulacea

Although the identification of *Darwinula* in the Upper Triassic of Alaska is based on extremely poorly preserved specimens, the genus has been recorded many

times from the Triassic in Europe. Drawings of the diagnostic muscle scar of Darwinulacea by Beutler and Gründel (1963, pl. 7a, fig. 3) firmly establish the occurrence of this superfamily in the Triassic.

Suborder Myodocopina

Although several fragments in the assemblage from Nevada might possibly represent myodocopid ostracodes, they are inadequate for positive identification and are not mentioned in the faunal list. However, the description and illustration of *Cypridina balbersteinensis* Kittl *in* Trauth (1918) from the Middle Triassic, and *C. tonkinensis* Patte (1926) from Upper Triassic supports the inclusion of this taxon in the Triassic.

REFERENCES

Beutler, Gerhard, and Gründel, Joachim, 1963, Die Ostracoden des Unteren Keuper im Bereich des Thüringer Beckens: Freiberger Forschungshefte, C 164, p. 33–92, 9 pls.

Hartmann, Gerd, 1963, Zur Phylogenie und Systematik der Ostracoden: Zeitsch. zool. Syst. Evolutionsforsch. v. 1, 154 p., 35 figs.

Hornibrook, N. de B., 1949, A new family of living Ostracoda with striking resemblances to some Paleozoic Beyrichiidae: Royal Soc. New Zealand Trans., v. 77, pt. 4, p. 469–471, pls. 50, 51.

Jones, T. R., 1862, North American Lower Mesozoic Cypridae. Appendix *in* A monograph of fossil Estheriae: Palaeontogr. Soc. London, p. 123–127, pl. 5, text fig. 12.

Kollmann, Kurt, 1963, Ostracoden aus der alpinen Trias II. Weitere Bairdiidae: Jahrb. Geol. Bundensanst., Wien, v. 106, p. 121–203, pls. 1–11, 3 tables, 8 text figs.

Moore, R. C., ed., 1961, Treatise on invertebrate paleontology, pt. Q. Arthropoda, 3. Ostracoda: Geol. Soc. America and Univ. Kansas Press, 442 p., 334 figs.

Patte, Etienne, 1926, Etudes paléontologiques relatives a la géologie de l'Est du Tonkin (Paléozoïque et Trias): Service Géologique de l'Indochine, Bull., v. 15, fasc. 1, 240 p., 12 pls.

Silberling, N. J., 1959, Pre-Tertiary stratigraphy and Upper Triassic paleontology of the Union district, Shoshone Mountains, Nevada: U.S. Geol. Survey, Prof. Paper 322, 67 p., 9 pls., map [1960].

Sohn, I. G., 1958, Chemical constituents of ostracodes; some application to paleontology and paleoecology: Jour. Paleontology, v. 32, p. 730–736.

Styk, Olga, 1962, Triassic microfauna in borings of Sulechow and Ksiaz [abs.]: Poland Inst. Geol. Kwartalnik Geol., v. 6, no. 4, p. 732–733.

Sylvester-Bradley, P. C., 1962, The taxonomic treatment of phylogenetic patterns in time and space, with examples from the Ostracoda *in* David Nicols, ed., Taxonomy and geography: Systematic Assoc. Pub. 4, London, p. 119–133, 4 figs.

Tappan, Helen, 1951, Foraminifera from the Arctic slope of Alaska; General Introduction and pt. 1, Triassic Foraminifera: U.S. Geol. Survey Prof. Paper 236–A, 20 p., 5 pls.

Trauth, Friedrich, 1918, Uber einige Krustazeenreste aus der mediterranen Trias: Vienna Naturhistirisches Hofmuseums, Annalen, v. 32, p. 172–192, 1 pl.

MIDDLE DEVONIAN PLANT FOSSILS FROM NORTHERN MAINE

By JAMES M. SCHOPF, Columbus, Ohio

Abstract.—A new collection of plant fossils, including new species described as *Barrandeina*(?) *aroostookensis* and *Calamophyton forbesii*, is reported from the Mapleton Sandstone of northern Maine. *Calamophyton* is not previously recorded in North America. These fossils are allied with European fossils of the early Givetian, so the age of the Mapleton is probably equivalent. The Mapleton Sandstone is flat lying and was deposited in this region after Acadian folding.

Specimens of Mapleton Sandstone bearing spiny psilophytic remains were collected by Richard S. Naylor in the vicinity of Presque Isle in northern Maine and referred to me in February 1961 for paleobotanical study and age determination. Subsequently, additional specimens from the same area were sent by Mr. W. H. Forbes of Washburn, Maine. The psilophytic remains seemed to suggest an age not later than Middle Devonian for the Mapleton Sandstone. A later study of spores and other fragments from maceration residues suggested the possibility of an early Middle Devonian age and indicated that further collecting was needed. Shortly afterward, very characteristic spiny psilophytes were reported by Hueber and Grierson (July, 1961) in the lower part of the Upper Devonian deposits in New York State. This occurrence indicated that the spiny psilophytes were less restricted in age than had previously been supposed and reemphasized the need for additional collecting and study of collections from northern Maine. Last summer (1963) I was able to visit the Maine locality personally and obtain an ample collection of plant material.

These additional plant fossils are from Mapleton Sandstone at a quarry on the Winslow farm, about 3 miles west of Presque Isle. Shaly material rejected in quarrying the flat-lying and not highly indurated sandstone contains a variety of fossil plants. A protoarticulate member was recognizable in the field, in addition to both smooth and spiny representatives of psilophytes. Other elements have been recognized in subsequent study which show marked similarity with plants of the classical late Middle Devonian assemblages from Bohemia, the Rhineland, and Belgium that have been studied so thoroughly by Kräusel and Weyland, LeClercq, Høeg, and others (see references). A Middle Devonian age determination based on plant remains from the Mapleton Sandstone seems fully justified. The purpose of the present paper is to describe this new evidence and examine the possibility of more exact correlation.

The age of the flat-lying Mapleton Sandstone in northern Maine is of particular interest because the sandstone appears to be the oldest formation not affected by Acadian folding in that area. Beds of the Trout Valley Formation of Dorf and Rankin (1962) in the Traveler Mountain quadrangle, 60 miles southwest of the Presque Isle area, are only slightly inclined and may be a little older. The Chapman Sandstone, at Edmunds Hill, 3 miles southwest of the Winslow quarry, contains Early Devonian marine fossils and plant fragments and resembles the Mapleton Sandstone in general lithologic appearance, but the beds are strongly inclined and more indurated. Nematophycean propagula (see Schmidt, 1958) classified as *Pachytheca* sp. (see figs 1*a* and 1*e*) have been collected by W. H. Forbes and me at the Edmunds Hill exposure. These bodies were originally very readily disseminated, but I have found none in searching my more extensive collections of Mapleton Sandstone at the Winslow quarry locality. Such a locally restricted distribution would be unlikely if the two sandstones merely represented different aspects of the same deposit, so these plant remains add confirmation about the difference between Chapman and Mapleton Sandstones. The time interval between deposition of the two sandstones of the Presque Isle area thus seems to bracket a terminal point of the Acadian orogeny.

U.S. GEOL. SURVEY PROF. PAPER 501-D, PAGES D43-D49

742-652 O—64——4

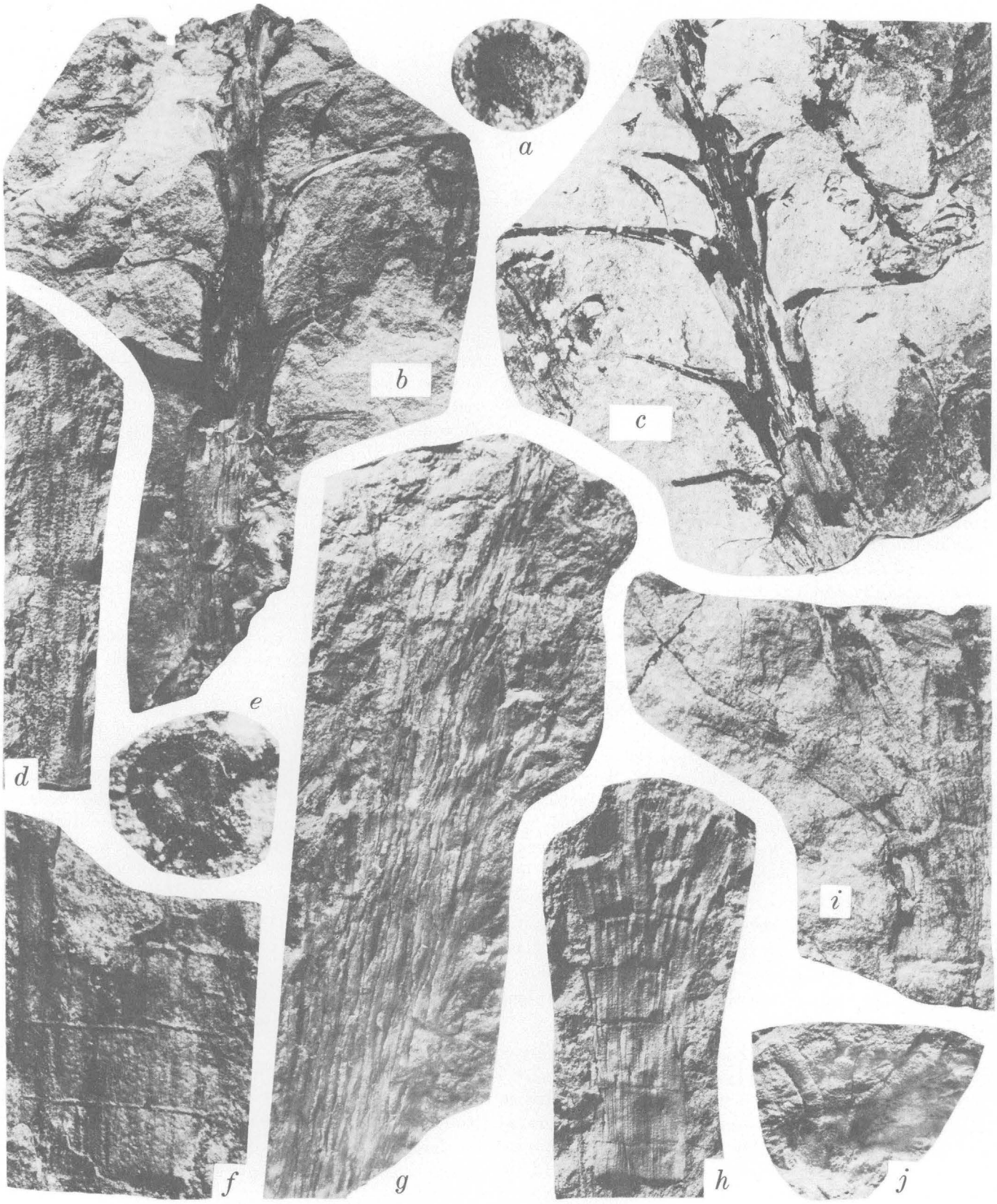

FIGURE 1

The plant assemblage from the Mapleton Sandstone at the Winslow quarry includes spiny psilophytes of the *Psilophyton princeps* var. *ornatum* type, and smooth psilophytes corresponding well with those Kräusel and Weyland (1923) have assigned as *Hostimella hostimensis*, and Dorf and Rankin assign as *Hostimella* sp. and *Aphyllopteris* sp. Larger smooth axes, some of them more than 20 mm in diameter, can perhaps be classed with *Taeniocrada*. Several specimens longitudinally grooved and striate and up to 8 cm broad are assigned tentatively and with considerable hesitation to the genus *Barrandeina* Stur (1882), and one unusually fine specimen with petioles attached is referable to a new species. These plants, if not directly congeneric with *Barrandeina*, seem to have a similar habit and structure and to be rather closely allied. A considerable number of fragments can be identified with *Calamophyton* as described below. Only brief descriptions of forms assigned to *Barrandeina*(?) and *Calamophyton* will be given at this time.

FIGURE 1*a*.—*Pachytheca* sp. Spheroidal mold of a nematophycean propagulum; ×10. Chapman Sandstone, Edmunds Hill, about 5 miles southwest of Presque Isle, Aroostook County, Maine. Specimen 3.
b, *Barrandeina*(?) *aroostookensis*, new species. Axis tip showing decurrent, phylloidal petioles; ×1. Inverted U-shaped petiolar scars appear on the caulome at points where petioles are lacking. Mapleton Sandstone, Winslow farm, 3 miles west of Presque Isle, Aroostook County, Maine. Specimen 44, holotype; repository U.S. National Museum (Cat. No. 42302).
c, Counterpart of specimen in *b*; ×1. Photographed under xylol. Recurved petiole second from the top on the right shows part of the foliated tip.
d, *Calamophyton* sp. Stem, ×1, showing coarse punctation, possibly owing to sclerotic nests in outer cortex, and longitudinal striation; nodal ridges obscure. Mapleton Sandstone, same location as *b*.
e, *Pachytheca* sp. Nematophycean propagulum; ×10, showing cortex and medulla along a median fracture plane. Chapman Sandstone, same location as *a*. Specimen 4.
f, *Calamophyton* sp. Stem segment, ×2.28, showing close-set nodal ridges and longitudinal striation. One leaf scar is directly on a nodal ridge, other similar scars (emergences?) are in the internodal zone. Mapleton Sandstone, same location as *b*, *c*, and *d*.
g, *Barrandeina*(?) sp. Axis, ×1, showing longitudinal ribs becoming diffuse toward the top. The specimen may be oriented basal end uppermost on the figure.
h, *Calamophyton* sp. Stem segment, ×1, with abrupt transverse fracture at the base (possibly an indication that the structural organization of the node continues within the axis) and broadening of distal end near point of digitate branching. Surface shows cortical punctation, linear striation, and nodal ridges. Only a few leaf or emergence scars are present. Mapleton Sandstone, same location as *b*.
i, *Calamophyton* sp. Asymmetric stem crown, ×2.6, showing successive bifurcations, punctate surface, and nodal grooves. Deep longitudinal fissures with intervening coaly layers suggest that an alternation of persistent tissues (coal) and softer structures were radially alined within the axis. Mapleton Sandstone, same location as *b*.
j, *Calamophyton* sp. Stem crown ×1, showing double bifurcation and punctate surface. Mapleton Sandstone, same location as *b*.

GENUS *BARRANDEINA* STUR (1882)

(see also: Pontonié and Bernard, 1903; Kräusel and Weyland, 1933).

Barrandeina(?) *aroostookensis* n. sp.

The specimen shown on figures 1*b* and 1*c* includes the distal part of a leafy[1] axis about 12½ cm long, nearly 15 mm broad at the base, and about half as wide at the top. The attached petioles are strongly reflexed away from the axis, tapering and with a median keel; they are strongly decurrent along the axis which appears deeply fluted and made up chiefly of the overlapping petioles. The leaves evidently are arranged spirally, although at the tip they appear to be sub-opposite and the arrangement may actually be irregular. Some petioles are missing, leaving a scar resembling an inverted U in which no simple vascular trace is apparent. Coalified films commonly show thin longitudinal bands on the scars and on the decurrent and excurrent parts of petioles which may reflect vascular organization or the presence of thin sclerotic strands in the cortex.

The smaller counterpart photographed under xylol on figure 1*c* appears to show a foliar continuation of the petiole at the right, second from the top. Several linear segments seem to be curled circinately as if not fully expanded. At the tip they appear with bifurcate digitation, not necessarily different from a *Psygmophyllum* or *Platyphyllum* type of megaphyllous leaf in juvenile condition (see Høeg, 1942, p. 98–113). Some cellular striation is visible parallel to the margin of the segments, but true venation is not apparent. Further details may become available when additional collections have been studied.

If actually referable to *Barrandeina*, this leafy specimen would seem to be the only one that has been found which clearly includes part of an axis adjacent to the stem tip. All others, including Krejci's type specimen of *B. dusliana*, the type species (see the excellent photographic illustration by Stur, 1882, pl. 5, fig. 8), provide very uncertain information about axis termination. In the Aroostook County specimen the reflexed petioles are more rapidly attenuate and sharply keeled than in other species. Some stubs of petioles seem persistent, generally strongly reflexed, and others are broken close to the axis, leaving a deep characteristic scar in specimens from Bohemia (Stur, 1882;

[1] Apparent similarity of lateral appendages on these axes with leaves may be more evident than real. The nature of leaves in Devonian time is not as definite as in later periods, yet the present examples could be prototypic megaphylls. Additional morphologic evidence will be sought. In the meantime, leaf and petiole terminology, discussed by Stur (1882) and followed both by Potonié and Bernard (1903) and by Kräusel and Weyland (1933), may readily be interpreted descriptively.

Potonié and Bernard, 1903; Kräusel and Weyland, 1933) and from western Norway (Høeg, 1931). Petioles of *Enigmophyton hoegii* Ananiev (1959) from central Siberia are somewhat similar to those of the Aroostook specimen, but other resemblances are much less evident. The leaves or lateral appendages in *Barrandeina* are notably decurrent and seem to be spiral in arrangement. The axis is grooved or fluted on this account and may have been a type of "false" stem consisting chiefly of adnate or adherent appendages. These plants grew erect and some of them must have been 1 or 2 meters tall. All these features accord well with the new material, but none of them provide any decisive indication of affinity.

The base of the new petiolate specimen, shown on figures 1*b* and 1*c*, is about the same size as the Bohemian specimens and shows the same type of pronounced cortical fluting. Other specimens without petioles from the Winslow quarry show a similar fluting and one of them is about 8 cm in diameter. The larger fluted specimens usually do not show petioles or clearly defined scars, so their identification is questionable. Commonly one end seems "feathered out," as at the top of the specimen shown on figure 1*g*. Some of the "feather" probably consists of sclerotic fibers, but in part it may be vascular. At the present time, it is problematic which end of this specimen is proximal. Rather similar cortical impressions have been described by Høeg (1942, p. 43–46) from the Middle Devonian of Wijdefjord, Spitzbergen.

Axes probably enlarged without aid of a cambium and growth may have been related to cortical roots. The origin and nature of the roots on these plants is an open question. However, an axis with structure similar to that shown at the bottom of figure 1*g* might easily correlate with that shown at the bottom of figure 1*b* below the stem tip. The nature of the vasculature of these stems is not yet known; however, a strong woody cylinder probably is lacking. A diffuse system of vascular strands similar to that described for *Duisbergia* by Kräusel and Weyland (1929) would appear consistent with what is now known from compression structures.

Diagnosis.—Plants erect, caulescent, probably as much as a meter high, axis distally tapering, fluted according to disposition of strongly decurrent lateral appendages, with coaly surface films striated to suggest separate strands of strengthening tissue. Foliation with bifurcate ultimate divisions, circinate in juvenile condition, possibly fairly large. Reproductive organs and organization and mode of substratal anchorage and growth, unknown.

The species is named for the county of its origin in northern Maine.

CALAMOPHYTON KRÄUSEL AND WEYLAND (1926)

Calamophyton sp.

Specimens consisting of axis segments like those illustrated on figures 1*d*, 1*f*, 1*h*, and 1*j* may be specifically indeterminable if taken out of the context of their occurrences in association with other specimens, but the habit unmistakably is that of the main stem of *Calamophyton* as described by Kräusel and Weyland (1926, 1929). Nodal ridges are clearly shown on figures 1*f*, 1*h*, and 1*i*. The sharp fracture line across the base of the stem shown on figure 1*h*, and shown less well on figure 1*f*, suggests natural articulation. Leaves or emergences are very similar in their distribution to those of *C. bicephalum* as described by Leclercq and Andrews (1960). The sandy matrix is well cemented, so it has not yet been possible to make preparations necessary for comparison of details of appendages, which in many instances are not preserved. The characteristically punctate outer cortex, best shown on figure 1*d*, is virtually identical to the *Calamophyton* cortex that has been illustrated by several authors for *C. primaevum*.

Probably the cortical punctation of *Calamophyton* is caused by the presence of sclerotic nests similar but more rounded than those Leclercq and Banks (1962) have demonstrated in *Pseudosporochnus*, another of the very characteristic elements of the Middle Devonian flora in Bohemia and Belgium. Cortical structures commonly are nearly duplicated in plants not very closely related. Nevertheless, the plants assigned to these two genera are very similar in size and habit. The presence of nodal ridges and longitudinal striation serves best to differentiate the main stems of plants belonging to the two groups. This difference may actually signify contrasting vascular arrangements more important than the superficial differences might seem to indicate. Those who have studied both genera concur in their taxonomic separation owing to verticillate tendency, separation of fertile and sterile parts, and the anatropous sporangia of *Calamophyton*. *Pseudosporochnus* commonly is regarded as a member of the Psilopsida and *Calamophyton* as a member of the Hyeniales assigned to the Sphenopsida. However, to some degree the implication of extreme systematic separation may well be synthetic owing to the fact that members of the major classes become more closely approximated toward their source. The Sphenopsida apparently originated from the psilopsids no later than the early part of the Middle Devonian (see Zimmermann, 1959).

The size, general conformation, nodal ridges, longitudinal striation, and branching of the stem specimens from the Winslow quarry all conform better with our present understanding of the genus *Calamophyton* than they do with *Pseudosporochnus*. Leclercq and Andrews (1960, p. 3, 17) emphasize the importance of general habit in distinguishing *Calamophyton*. It is entirely possible that additional study will show that all the specimens illustrated should be referred to the species based on a fertile frond described below.

Calamophyton forbesii, n. sp.

The specimen illustrated by figure 2 consists of an ascending system of fertile branches that is sufficiently distinctive to be specifically identified. The apparent irregularity in branching may chiefly be a result of dichotomy in alternating planes. Nodal ridges are lacking from fertile branches. The lower (sterile ?) appendages apparently are not arranged in any definite pattern.

The fine sandy matrix has preserved gross relations satisfactorily, but finer structure has been modified by compression. Pairs of compressed sporangia may be observed in position in relation to their rachis on the prepared counterpart fragment, but details of the connective sporangiophore have not been seen. As in other representatives of *Calamophyton*, the arrangement of sporangiophores on the rachis and the degree of separation of sterile and fertile appendages is not too clear. Many of the small flecks of carbonaceous material shown around the upper branches on figure 2 represent sporangia. From this, one might infer that fertile rachises were distal, but it would be premature to suggest that sterile appendages were always absent in these areas.

Along a line of longitudinal fracture showing a distal, fertile rachis 2–3 mm in diameter, sporangiophores probably were spaced at about 4-mm intervals. Judged by positions of sporangia, the sporangiophores were distally inclined at an angle of about 45°; bifurcation of the sporangiophore may have occurred 4 or 5 mm from the rachis. Paired sporangia, like those shown on figure 2, inset *A*, may be observed in several places in a symmetrical spacing to suggest that arms of the sporangiophore were recurved and to suggest that at least two sporangia may be borne on each of the arms. Such an arrangement has also been observed in *C. renieri* Leclercq (1940). However, a number of additional isolated sporangia also are present which are not easy to account for, and greater complexity may occur than can immediately be determined.

The sporangia, usually paired, are fusiform, about 2½-mm long, smoothly tapered distally and a little more obtusely rounded at the base; a dehiscence mechanism has not been detected. Spores, probably 128 in each sporangium, are thin walled, spheroidal,

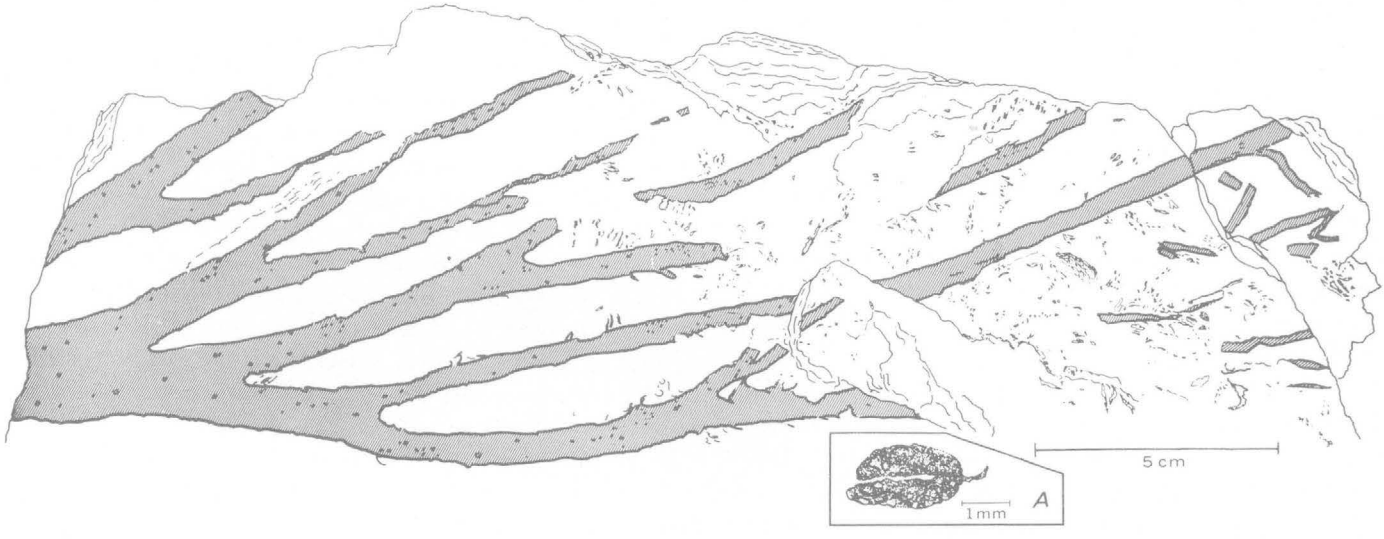

FIGURE 2.—*Calamophyton forbesii*, new species. Fertile shoot system, slightly reduced (scale indicated), showing apparent irregularity of bifurcation, irregular spiny emergences and numerous sporangia; most of the small flecks indicated in the distal area represent broken sporangia. *A*, paired sporangia, about × 10 (scale indicated), taken from a distal counterpart fragment. Mapleton Sandstone, Winslow farm quarry, about three miles west of Presque Isle, Aroostook County, Maine. All specimen 2 photoline drawings from holotype; repository U.S. National Museum (Cat. No. 42303).

about 80–110 μ in diameter, with ornamentation of tiny, well separated granules, and trilete rays about equal to half the normal radius. Sutures are probably straight and lips evidently are not prominent, but details are difficult to interpret in the preparations available. The demonstration of spores all of one kind in these sporangia suggests that *C. forbesii* may be an isosporous plant.

Diagnosis.—Plants shrubby, erect in habit, with fertile shoots branched dichotomously, commonly in alternating planes, very probably ascending from a digitately dichotomized caudex of which examples are in association, none attached. Mode of substratal growth and anchorage, unknown. Sterile appendages short, arranged irregularly on proximal parts of fertile shoots, probably mostly borne separately on vegetative branches. Numerous sporangiophores attach to stout distal rachises, probably inclined distally at about 45° on the rachis, as inferred from positions of sporangia. At least two pairs of closely paired sporangia are borne on delicate stalks in reflexed position on each dichotomized(?) sporangiophore. Sporangia elongate, about 2.6×0.7 mm maximum, probably containing about 128 spores per sporangium. Spores apparently all one kind (isosporous), trilete, originally spheroidal, 80–110 μ diameter, with thin, distinctly granulated coat, commissural rays extend about half the normal radius of the spore.

It is a pleasure to name this species for Mr. W. H. Forbes of Washburn, Maine, whose enthusiasm, knowledge, and interest in the geology of northern Maine is appreciated, and whose assistance in the field is gratefully acknowledged.

DISCUSSION

Very little new paleobotanical information on Devonian floras of Maine has been presented since David White's (1905) study of plant fossils from the Perry Basin along the seacoast in the southeastern part of the State. Dorf and Rankin (1962) recently discussed an assemblage of plant fossils from the Traveler Mountain area 60 miles southwest of Presque Isle, and Kräusel and Weyland (1941) have restudied much of Dawson's original material, some of which was obtained in the Perry Basin. Incidental occurrences of *Psilophyton* or other fragments of plants are mentioned in various geologic reports. Devonian terrigenous deposits in the Acadian highlands of eastern North America tend to occur in local or provincial intermontane basins which make stratigraphic correlation more difficult.

White's detailed consideration fully established the Late Devonian age of the Perry Formation, a matter upon which there had been long controversy. *Archaeopteris*, *Leptophloeum*, *Barinophyton*, and other plants are present in the Perry Formation that have not been found in the Mapleton Sandstone. Apart from similarities in the intermontane types of sediments, there is little to suggest that the Perry and Mapleton Formations are correlative. Dorf and Rankin have interpreted their Trout Valley psilophytic material as indicative of late Early Devonian age. The age differences between their *Psilophyton* flora and that of the Winslow quarry characterized by psilophytes and protoarticulates, is not nearly as clear as the distinction from the Late Devonian flora of the Perry Basin, in spite of a greater difference in sedimentary facies. It may be premature to think of the age relations of these deposits as well established.

Barrandeina is characteristic of the lower Givetian in Bohemia. It has not been widely identified elsewhere. Outside of the Bohemian area, Kräusel and Weyland (1933) admit that only Høeg's species from western Norway has been correctly identified with *Barrandeina*. They believe that all the American specimens White referred to this genus are unidentifiable, and suggest that stems of this type might also be confused with those of *Pseudobornia* (Kräusel and Weyland, 1933, 1941). I am not convinced that White's report of the genus from the Perry Formation is in error, although further evidence is badly needed. It is possible that the Perry Formation may be a little older than White believed (still well within the Upper Devonian, possibly "Portage" rather than "Chemung"); Jahn's (1903) and later studies apparently were not available to White and he did consider the plant remains from Barrande's H (h–i) stage, which he drew on for comparison, to represent a Late, rather than Middle, Devonian assemblage. Jahn showed that the Srbsko beds of Krejci occur below the zone of *Stringocephalus burtini*. Thus, if the occurrence of *Barrandeina* from the Perry Basin can be substantiated, it might represent the youngest record of the genus. The genus *Calamophyton* is particularly characteristic of the lower Givetian in the Rhineland and in Belgium. Marine fossils as well as other plants, such as *Pseudosporochnus* and numerous psilophytes, are in common within the Givetian of western Europe so that the similarity in age of these occurrences is fully authenticated.

Hueber and Grierson's report (1961) of *Psilophyton princeps* var. *ornatum* from early Upper Devonian beds appeared while Dorf and Rankin's paper was in press. More recently, Grierson and Banks (1963) show *Drepanophycus gaspianus* Dawson, also reported at Trout Brook, is present at least as high as the Tioughniogan stage of the Middle Devonian in New York. *Drepanophycus spinosus* is characteristically associated with the Middle Devonian Srbsko assemblage in Bohemia. Plants similar to *Taeniocrada*, *Aphyllopteris*, and *Hostimella* that Dorf and Rankin report at the Trout Brook localities also are present at the Winslow quarry and, in view of Grierson and

Banks report, the fact that *Drepanophycus* has not yet been found there cannot be assigned weight in age determination. It seems clear now that the traditional Early Devonian associations of *Psilophyton* and *Drepanophycus* may easily be given an undue prominence. At present the Early Devonian age assignment of the Trout Brook assemblage seems principally to depend on identification of one fragmentary specimen of *Sporogonites*. This positive evidence may be highly significant but it is undeniably scanty. Banks (1961) has pointed out that many of the Devonian genera "enjoyed a great vertical range," and Seward (1933, p. 130) expressed uncertainty as to whether Halle's original Röragen source for *Sporogonites* was "of Lower or possibly of Middle Devonian age." Under these circumstances the greater emphasis probably should be placed on presence of plants like *Barrandeina* and *Calamophyton* for interpretation of age relations.

Nevertheless, plants from the Mapleton Sandstone identified as *Barrandeina* (?) and *Calamophyton* are not identical with European plants, and not enough is known about them for the specific interpretation of evolutionary sequences. In comparison with plants of the western European assemblage, *B.* (?) *aroostookensis* might be slightly more specialized in foliar development, but *C. forbesii* seems to nearly duplicate some European material in arrangement of sporangiophores. Both types of plants are complexly organized and, taken altogether, they indicate a stage of evolutionary development in both groups which is very close to that shown by the genera in their European occurrences. They surely represent a very similar ecologic plant association. Within the limits imposed by possible inaccuracies of this paleontologic method, it seems most reasonable therefore to suppose that the age of the Mapleton Sandstone is also early Givetian, probably comparable to the Tioughniogan stage of the American standard section.

REFERENCES

Ananiev, A. R., 1959, Vazhneyshie mestonakhozhdeniya Devonskikh flor v sayano-altayskoy gornoy oblasti [The most important Devonian floral localities of Saian-Altai Mountains Oblast]: Izdatel'stvo Tomskogo Univ., Tomsk [Pub. Tomsk Univ.], 99 p., 25 pl., 22 figs., chart.

Banks, H. P., 1961, The stratigraphic occurrence of Devonian plants with application to phylogeny, *in* Phylogeny of Tracheophyta symposium *in* Recent advances in Botany: Univ. Toronto Press, p. 963–968.

Dorf, Erling, and Rankin, D. W., 1962, Early Devonian plants from the Traveler Mountain area, Maine: Jour. Paleontology, v. 36, p. 999–1004, 1 pl., 1 fig.

Grierson, J. D., and Banks, H. P., 1963, Lycopods of the Devonian of New York State: Palaeontographica Americana, v. 4, no. 31, p. 217–295, pl. 32–42, 9 tables.

Høeg, Ove Arbo, 1931, Notes on the Devonian flora of western Norway: Det Kgl. Norske Vidensk. Selsk. Skr., Trondheim, no. 6, p. 1–33, 8 pl., 2 figs.

——— 1942, The Downtonian and Devonian flora of Spitsbergen: Norges Svalbard- Og Ishavs-Undersøkelser Skr., no. 83, 228 p., 62 pl., 35 figs.

Hueber, F. M., and Grierson, J. D., 1961, On the occurrence of *Psilophyton princeps* in the early Upper Devonian of New York: Am. Jour. Botany, v. 48, no. 6, p. 473–479, 15 figs.

Jahn, J. J., 1903, Ueber die Etage H im mittel-böhmischen Devon: Verhandl. K. K. Geol. Reichsanstalt, Jahrg. 1903, p. 73–79.

Kräusel, R., and Weyland, H., 1923, Beiträge zur Kenntnis der Devonflora: Senckenbergiana, v. 5, no. 5/6, p. 154–184, pl. 6–9.

——— 1926, Beiträge zur Kenntnis der Devonflora II: Abh. senckenberg. naturf. Ges., v. 40, no. 2, p. 113–155, pl. 3–17, 46 fig.

——— 1929, Beiträge zur Kenntnis der Devonflora III: Abh. senckenberg. naturf. Ges., v. 41, no. 7, p. 315–360, 15 pl., 34 fig.

——— 1933, Die Flora des böhmischen Mitteldevons: Palaeontographica, v. 78, Abt. B, no. 1/2, p. 1–46, pl. 1–7, 39 fig.

——— 1941, Pflanzenreste aus dem Devon von Nord-Amerika: Palaeontographica, v. 86, Abt. B, no. 1/3, p. 1–78, pl. 1–15, 15 fig.

Leclercq, Suzanne, 1940, Contribution a l'etude de la flore da Devonien de Belgique: Acad. Roy. de Belgique Mem., v. 12, no. 3, p. 1–65, pl. 8, 10 fig.

Leclercq, Suzanne, and Andrews, H. N., Jr., 1960, *Calamophyton bicephalum*, a new species from the Middle Devonian of Belgium: Missouri Bot. Garden Annals, v. 47, no. 1, 23 p., 5 pl., 16 fig.

Leclercq, Suzanne, and Banks, H. P., 1962, *Pseudosporochnus nodosus* sp. nov., a Middle Devonian plant with cladoxylalean affinities: Palaeontographica, v. 110, Abt. B., no. 1–4, p. 1–34, pl. 1–10, 7 fig.

Potonié, H., and Bernard, Ch., 1903, Flore Dévonieene de l'etage H de Barrande: Leipzig, Raimund Gerhard and Wolfgang Gerhard, 68 p., 156 fig.

Schmidt, Wolfgang, 1958, Pflanzen-reste aus der Tonschiefer-Gruppe (unteres Siegen) des Siegerlandes. II *Pachytheca reticulata* Corsin aus den Betzdorfer Schichten nebst neuen Beobachtungen an *Pachytheca*: Palaeontographica, v. 104, Abt. B, no. 1–3, p. 1–38, pl. 1–5, 2 fig.

Seward, A. C., 1933, Plant life through the ages: Cambridge Univ. Press.

Stur, D. R. J., 1882, Die Silur-Flora der Etage H-h_1 in Böhmen: K. Akad. Wiss., Sitzungsb., math. naturw. Classe, [Wien], v. 84, Abt. 1, p. 330–391, 5 pl.

White, David, 1905, Paleontology, chap. III *of* Smith, G. O., and White, David, The geology of the Perry Basin in southeastern Maine: U.S. Geol. Survey Prof. Paper 35, p. 35–84, pl. 1–6.

Zimmermann, Walter, 1959, Die Phylogenie der Pflanzen: Stuttgart, Gustav Fischer Verlag, 777 p., 331 fig.

RADIOMETRIC AGES OF ZIRCON AND BIOTITE IN QUARTZ DIORITE, EIGHTS COAST, ANTARCTICA

By AVERY ALA DRAKE, JR., T. W. STERN, and H. H. THOMAS,
Washington, D.C.

Work supported by the National Science Foundation

Abstract.—Zircon and biotite separated from quartz diorite of the Eights Coast area, Antarctica, were found to have lead-alpha and potassium-argon ages of 150±200 m.y. and 97±5 m.y., respectively. This quartz diorite is both petrographically and chemically distinct from Andean plutonic rocks. The zircon age suggests that the Eights Coast-Thurston Island composite batholith is at least middle Mesozoic in age. If so, the younger biotite age possibly reflects later heating of the area during the Late Cretaceous Andean orogeny.

Plutonic rocks exposed on Thurston Island and along the Eights Coast of the Bellingshausen Sea, Antarctica (fig. 1), consist mostly of hornblende-biotite-quartz diorite (Craddock and Hubbard, 1961; Drake, 1962). These rocks are thought to belong to a composite batholith that is predominantly quartz diorite but which also has granodiorite, adamellite, and minor gabbro phases. The batholith is intrusive into metasedimentary rocks on Thurston Island and at places along the Eights Coast, and into leucocratic augite norite near lat 72°35′37″ S., long 95°07′00″ W. The batholithic rocks are cut by abundant mafic dikes (Craddock and Hubbard, 1961; Drake, 1962). In addition, the quartz diorite probably is intruded by fine- to medium-grained pink granitic rocks that range from granodiorite to granite and are characterized by abundant myrmekite. The intrusive relation is inferred from inclusions of white quartz diorite in pink granite seen only in float.

One sample of quartz diorite (table 1) sufficiently large for age determination was collected from the Eights Coast at a station informally known as "Peeler's Pinnacle," lat 72°34′56″ S., long 93°23′00″ W., in February 1961. A lead-alpha age of zircon concen-

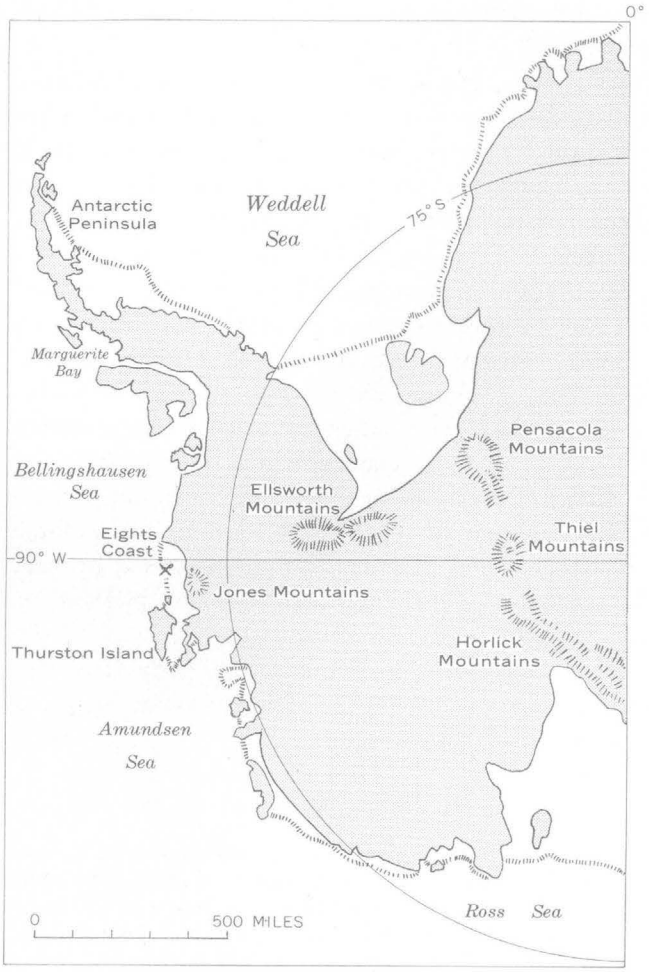

FIGURE 1.—Sketch map of West Antarctica, showing sample locality (×) on the Eights Coast.

TABLE 1.—*Chemical analysis, C.I.P.W. norm, and mode of quartz diorite from lat 72°34'56" S., long 93°23'00" W., Eights Coast, Antarctica*

Chemical analysis [1]		C.I.P.W. norm		Mode [2]	
Constituent	Weight percent	Mineral	Percent	Mineral	Volume percent
SiO_2	62.9	Quartz	17.8	Plagioclase [3]	60.6
Al_2O_3	17.2	Orthoclase	7.2	Quartz	22.5
Fe_2O_3	1.9	Albite	38.2	Biotite	7.1
FeO	2.4	Anorthite (Wo, 2.1).	23.4	Hornblende	6.1
MgO	1.8			Sphene	1.6
CaO	6.2	Diopside (En, 1.5) (Fs, 0.4)	4.0	Magnetite-ilmenite.	.8
Na_2O	4.5			Apatite	.8
K_2O	1.2			Zircon	Tr.
H_2O+	.60	Hypersthene	3.8	Sericite	Tr.
H_2O-	.05	Magnetite	2.8	Epidote	Tr.
TiO_2	.97	Ilmenite	1.8	Myrmekite	Tr.
P_2O_5	.44	Apatite	1.0		
MnO	.08				
		Total	100.0		
Total	100.24				

[1] By rapid methods; analysts: Paul Elmore, Samuel Botts, and Gillison Chloe.
[2] Based on 2,000 points counted by the Chayes method.
[3] Average composition is sodic andesine, about An_{32}, as determined optically.

trated from this sample (table 2) is the first of this type to be reported from this area. The zircon age of 150±20 million years suggests that the quartz diorite is at least as old as mid-Mesozoic (early Jurassic).

Biotite concentrated from the same sample was dated by the potassium method (table 3) at 97±5 m.y. This biotite age is considerably younger, and suggests another orogenic event in the early Late Cretaceous.

The rocks of the batholith are medium to coarse grained, and very light gray to white, although some plagioclase grains are tannish due to alteration. The rocks are fresh to slightly weathered; iron oxide coatings are fairly common on joint surfaces. Other joints are filled by white adamellite pegmatite. The quartz diorite of the dated sample has a well-developed foliation marked by alined biotite, hornblende, and plagioclase. In other exposures along the Eights Coast and on Thurston Island, related rocks are massive to well foliated. Float at the sample site includes a number of specimens of strongly mylonitic quartz diorite, suggesting that a shear zone is probably present at the locality.

Microscopic study shows that much of the plagioclase has oscillatory zoned andesine cores with calcic oligoclase rims. Many plagioclase crystals are broken, and zones of mortar structure are present. Quartz occurs both as large grains interlocking with plagioclase and in pockets of small grains interstitial to the feldspar and large quartz. Brown and green biotite form at the expense of hornblende. Many of the biotite flakes are kinked, suggesting deformation subsequent to crystallization. Trace amounts of myrmekite occur as interstitial patches. Small zircon crystals occur as separate grains in plagioclase, quartz, biotite, and hornblende. Relatively abundant quantities of sphene are spatially related to altered hornblende, as are minor quantities of magnetite-ilmenite.

The quartz diorite has been deformed locally, subsequent to its emplacement, as is shown by the broken plagioclase, areas of mortar structure, and kinked biotite. Late alteration and partial recrystallization is suggested by the formation of biotite at the expense of hornblende. The rock has not completely recrystallized, however, as the minerals interlock in a primary igneous fabric; the feldspars, though locally broken, are subhedral; and the delicate, euhedral oscillatory zonation is preserved in the plagioclases.

Little is known of the geologic age of the plutonic rocks of West Antarctica in general and of the Bellingshausen Sea area in particular. Granitic rocks of possible Tertiary age are present in the southern part of the Antarctic Peninsula (Knowles, 1945); they probably belong to the Antarctic Peninsula Andean intrusive suite which was assigned a Late Cretaceous or early Tertiary age by Adie (1955). Late Cretaceous to early Tertiary isotopic ages were reported by Halpern (1962) on minerals from intrusive rocks in the northern part of the Antarctic Peninsula that are petrographically similar to those farther south studied by Knowles and Adie. Older intrusive granites in the Marguerite Bay area were recognized by Adie (1954), who arbitrarily assigned them an early Paleozoic age. To the south of Eights Coast in the Thiel Mountains, Ford and others (1963) and Aaron and Ford (1963) report lead-alpha (zircon) and potassium-argon (biotite) ages that suggest Precambrian and early Paleozoic metamorphic events. In the absence of geologic data the Bellingshausen Sea area has been assumed to lie within a Mesozoic fold belt coextensive with the Antarctic Peninsula. Hamilton (1963) interpreted the batholith exposed along Eights Coast and on Thurston Island as being continuous with the Andean batholith

TABLE 2.—*Lead-alpha age of zircon from quartz diorite, Eights Coast, Antarctica*

Sample	Location	Alpha counts per milligram per hour	Lead [1] (ppm)	Calculated age [2] (m.y.)
361Z	Lat. 72°34'56" S., long. 93°23'00" W.	173	10.7	150±20

[1] Determination by Harold Westley. All values are averages of duplicate determinations.
[2] Age equation: $t=c\cdot Pb/alpha$, where
c=constant, 2,485 for Th/U=1,
Pb=lead in ppm, and
alpha=a/mg-hr.
Age is rounded to nearest 10 m.y.

TABLE 3.—*Analytical data and potassium-argon age of biotite from quartz diorite, Eights Coast, Antarctica*

[Analysts: H.H. Thomas, R. F. Marvin, P. L. D. Elmore, and H. Smith]

Sample	Location	K_2O (percent)	K^{40} (ppm)	$*Ar^{40}$ (ppm)	$*Ar^{40}$ (percent)	$*Ar^{40}/K^{40}$	Age (m.y.)
361B	Lat 72°34′56″ S., long 93°23′00″ W	9. 14	9. 26	0. 0539	88	0. 00582	97±5

Symbol: *Radiogenic.
Decay constants, K^{40}: 0.585×10^{-10}/yr (electron capture), 4.72×10^{-10}/yr (beta decay).
Abundance, K^{40}: 1.22×10^{-4} g/g K.

of the Antarctic Peninsula. The quartz diorite of the Eights Coast differs from the Andean quartz diorites of the Antarctic Peninsula in its distinctive white to very light gray color, its flow structure, and its lack of inclusions which are characteristic of the Andean quartz diorites. It is more quartzose and contains in general a more sodic andesine. The petrochemistry of the rocks is strikingly different as well (fig. 2).

In their study of the Jones Mountains, Craddock and others (1963) found that volcanic rocks unconformably overlie a basement terrane of pink to tan granite that is cut by both basaltic and felsic dikes. Muscovite in the granite has a potassium-argon age of 199±6 m.y. The felsic dike rock, a quartz latite porphyry, has a whole-rock potassium-argon age of 104±4 m.y.

Age relations of the basement granite and the felsic dikes to the Eights Coast quartz diorite are not known. Two of the geologic stations established during the 1961 Bellingshausen Sea expedition are near the Jones Mountains, but only typical Eights Coast quartz diorite and older gabbro are exposed.

Early or middle Mesozoic ages have rarely been reported from Antarctica, and most of those have been of diabase sills, principally from Victoria Land (McDougall, 1963). Miller (1960), however, reports potassium-argon ages of 176 to 199 m.y. on biotite and muscovite separated from quartz-mica schists from the South Orkney Islands. These ages suggest a metamorphic event in Late Triassic to Early Jurassic time. Craddock and others (1964) report a rubidium-strontium age (biotite) of 280 m.y. (late Carboniferous) for gneiss from Thurston Island. This gneiss is not the same unit as the quartz diorite described herein, as it is reported to be a granular garnet-bearing quartz diorite gneiss that is compositionally layered. This gneiss is interpreted as having a metamorphic origin (Craddock and others, 1964).

The age of the biotite agrees closely with the age of intrusive felsites, 104±4 m.y., reported by Craddock and others (1963) from the Jones Mountains. It seems reasonable to suggest that biotite formed, or recrystallized, as a result of Late Cretaceous Andean plutonism in the Eights Coast-Jones Mountains area. It is possible, also, that a single lead-alpha age can be completely erroneous, as old zircon ages have been reported from known young intrusive rocks. In the present case, however, it is felt that the Eights Coast batholith is indeed older than the Andean batholith of the Antarctic Peninsula, as the rocks are dissimilar, an Early Triassic potassium-argon age has been reported by Craddock and others (1963) from a nearby area, and older plutonic rocks have been reported from the Antarctic Peninsula itself. A substantial part of the crystalline rocks of the area, therefore, is not Late Cretaceous in age as has been assumed, but is probably at least as old as middle Mesozoic. The possibility cannot be eliminated that the Mesozoic zircon age reported herein reflects the age of a younger metamorphic event and that the quartz diorite is of late Paleozoic age.

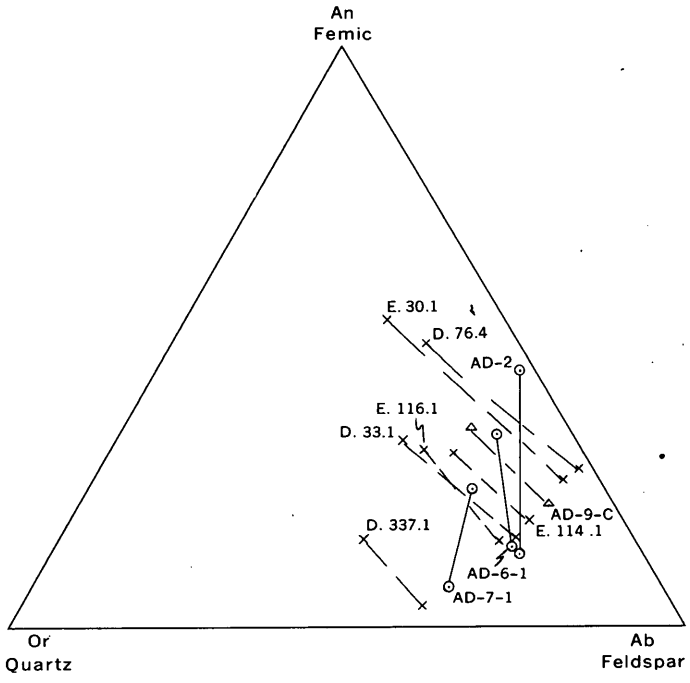

FIGURE 2.—Larsen plots showing normative comparison of rocks of the Eights Coast batholith (solid lines) with those of the Andean granite-gabbro intrusive suite (dashed lines). Symbols: ×, data from Adie (1955); ⊙, data from samples collected by Drake on the Eights Coast; and △, data from samples collected by Drake on the Antarctic Peninsula. Numbers on lines in triangle are sample numbers.

It appears that the Antarctic Peninsula orogenic belt does follow along the Eights Coast as far as Thurston Island, although events as young as Andean are apparently of minor importance in this area. More data are needed, of course, to better interpret the timing of orogenic events in this little known region.

REFERENCES

Aaron, J. M., and Ford, A. B., 1964, Isotope age determinations in the Thiel Mountains, Antarctica [abs.]: Geol. Soc. America Spec. Paper 76, p. 1.

Adie, R. J., 1954, The petrology of Graham Land, I. The basement complex; early Paleozoic plutonic and volcanic rocks: Falkland Islands Dependencies Survey, Sci. Rept. 11, 22 p.

——— 1955, The petrology of Graham Land, II. The Andean granite-gabbro intrusive suite: Falkland Island Dependencies Survey, Sci. Report 12, 39 p.

Craddock, Campbell, and Hubbard, H. A., 1961, Preliminary geologic report on the 1960 U.S. expedition to Bellingshausen Sea, Antarctica: Science, v. 133, no. 3456, p. 886–887.

Craddock, Campbell, Bastien, T. W., and Rutford, R. H., 1963, Geology of the Jones Mountains area, West Antarctica: Cape Town, Sci. Comm. for Antarctic Research–Internat. Union of Geol. Sciences Symposium on Antarctic Geology.

Craddock, Campbell, and others, 1964, Rubidium-strontium ages from Antarctica: Geol. Soc. America Bull., v. 75, p. 237–240.

Drake, A. A., Jr., 1962, Preliminary geologic report on the 1961 U.S. expedition to Bellingshausen Sea, Antarctica: Science, v. 135, no. 3504, p. 671–672.

Ford, A. B., Hubbard, H. A., and Stern, T. W., 1963, Lead-alpha ages of zircon in quartz monzonite porphyry, Thiel Mountains, Antarctica—a preliminary report: Art. 208 *in* U.S. Geol. Survey Prof. Paper 450–E, p. E105–E107.

Halpern, Martin, 1962, Potassium-argon dating of plutonic bodies in Palmer Peninsula and southern Chile: Science, v. 138, no. 3546, p. 1261–1262.

Hamilton, Warren, 1963, Tectonics of Antarctica, *in* Backbone of the Americas: Am. Assoc. Petroleum Geologists Mem. 2, p. 4–15.

Knowles, P. H., 1945, Geology of southern Palmer Peninsula, Antarctica: Am. Philos, Soc. Proc., v. 89, no. 1, p. 132–145.

McDougall, Ian, 1963, Potassium-argon age measurements on dolerites from Antarctica and South Africa: Jour. Geophys. Research, v. 68, no. 5, p. 1535–1545.

Miller, J. A., 1960, Potassium-argon ages of some rocks from the South Atlantic: Nature, v. 187, no. 4742, p. 1019–1020.

QUALITATIVE X-RAY EMISSION ANALYSIS STUDIES OF ENRICHMENT OF COMMON ELEMENTS IN WALLROCK ALTERATION IN THE UPPER MISSISSIPPI VALLEY ZINC-LEAD DISTRICT

By JOHN W. HOSTERMAN, ALLEN V. HEYL, and JANICE L. JOLLY,
Beltsville, Md.

Work done in cooperation with the Wisconsin Geological and Natural History Survey

Abstract.—Mineral alteration in a carbonaceous shale bed associated with a hydrothermal zinc-lead deposit in the Upper Mississippi Valley district is marked by the addition and migration of at least seven common elements (iron, manganese, titanium, potassium, silicon, aluminum, and magnesium) by ore-forming solutions. Calcium was leached from the ore body and moved to the edge of the alteration aureole. The suggestion is made that magmatically heated connate brines may have deposited the ore and altered the wallrocks.

Alteration of clay minerals associated with zinc-lead ore deposits in the Upper Mississippi Valley district was investigated by Heyl and others (1964) during 1960–63. This earlier study led to further investigations of the same suite of wallrock samples from the Thompson-Temperly mine in southwestern Wisconsin. Qualitative X-ray fluorescence analyses were made of samples to determine possible variations in relative quantities of the principal elements that are in the basal shale unit of the Quimbys Mill Member of the Platteville Formation in and adjacent to the Thompson ore body.

The Thompson-Temperly mine is at the southwest edge of New Diggings, Wis., a village about 10 miles north-northeast of Galena, Ill. It is in the highly productive south-central part of the Upper Mississippi Valley zinc-lead district of southwest Wisconsin, northwest Illinois, and northeast Iowa (fig. 1). The mine is opened by a truck incline that slopes to the northeast into the small Temperly ore body. From this body a truck haulage crosscut extends for about 1,500 feet into the large Thompson ore body (fig. 3).

FIGURE 1.—Index map showing location of the Thompson-Temperly mine.

The samples studied were taken from the Thompson ore body and alteration aureole, the barren wallrock zone between the two ore bodies, and the Temperly ore body and alteration aureole.

The Quimbys Mill Member of the Platteville Formation is a thin dolomite, limestone, and shale unit of distinctive lithology that can be traced for many tens of miles. At the Thompson-Temperly mine, where the member was studied, it passes from the Temperly ore body and its surrounding alteration aureole into a barren rock zone and then into the Thompson ore body and its alteration aureole. This study indicates that variations in the concentration of the elements in the

wallrock may be helpful in prospecting for ore in the mine and in exploratory drilling elsewhere in the Upper Mississippi Valley district.

GEOLOGY

The two zinc-lead ore bodies of the Thompson-Temperly mine, like many others in the Upper Mississippi Valley district, occur chiefly in the Quimbys Mill Member of the Platteville Formation, in the Decorah Formation, and in the lower part of the Galena Dolomite (fig. 2), all of which are of Middle Ordovician age. The Temperly ore body is a small irregular linear mass, whereas the Thompson ore body is an elliptical doughnut-shaped mass (fig. 3). Mining subsequent to preparation of figure 3 confirms that the shape inferred here is basically correct. The ore is in veins, replacements, and impregnations along small reverse and bedding-plane faults related to gentle folds. The main primary minerals in the ore bodies are quartz (mostly cherty jasperoid), dolomite, 2*M* illite, microcline, pyrite, marcasite, sphalerite, galena, cobaltite, chalcopyrite, barite, and calcite. Unlike galena in most deposits in the vicinity, galena in the Thompson-Temperly mine is common only locally in the ore bodies.

The Quimbys Mill Member (fig. 2) consists of dark-brown dolomite and limestone with thin carbonaceous shale partings and a carbonaceous shale bed at the base. The limestone is fine grained, dense, sublithographic, and has a conchoidal fracture. The basal dark-brown shale bed is a very persistent and uniform marker bed about 3 inches thick. Because it can be accurately traced throughout mineralized and barren areas, this shale bed was selected for detailed sampling in the Thompson-Temperly mine.

Ore solutions have produced alteration aureoles (fig. 3) in the host rock limestone, shale, and, to a lesser extent, in dolomite surrounding the deposits. The aureoles extend laterally as much as 200 feet from the sides of the ore bodies, and are known from drilling to extend out much shorter distances from the top and bottom of the bodies. The alteration aureoles result from a combination of six main processes (Heyl and others, 1959, p. 101–108; 1964): solution, dolomitization, silicification, development of sanded dolomite, clay- mineral alteration, and low-temperature feldspathization marked by the formation of microcline. Solution has considerably thinned the limestone of the Quimbys Mill Member as well as other carbonate beds above and below it (Reynolds, 1958, p. 157–159). The calcite in the carbonaceous shale bed at the base of the Quimbys Mill has been largely replaced by less soluble dolomite, thus preventing much thinning. Fossils and some shale beds have been silicified, but less markedly

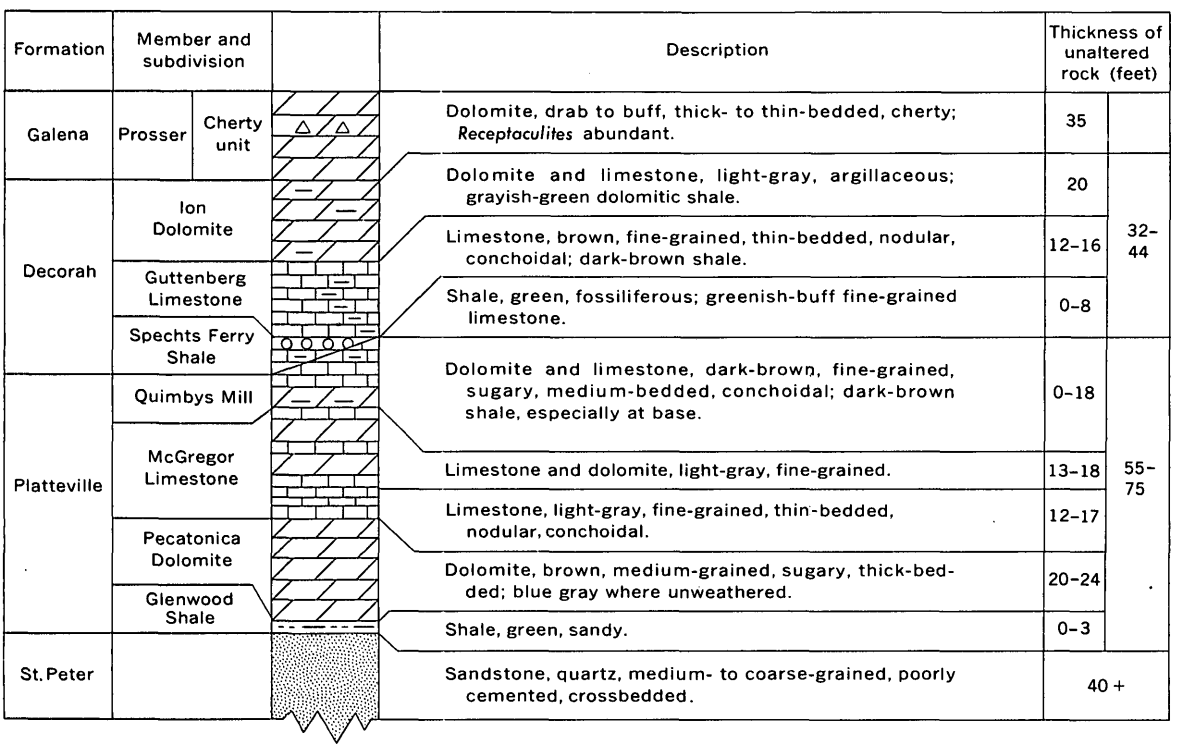

FIGURE 2.—Stratigraphic column of the Platteville and Decorah Formations and lower part of the Galena Dolomite in the Upper Mississippi Valley zinc-lead district.

in these two ore bodies than in some nearby ones, such as those in the Hoskins mine (Heyl and others, 1959, p. 105–107; Agnew, 1955, p. 792). Within the ore bodies the previously dolomitized limestones have been sanded, forming a friable or noncoherent mass of dolomite crystals in which the cementing bond between the crystals has been weakened or removed by intergranular solution. Wavy bands of brown shale, the residue of solution, separate the layers of sanded dolomite. The amount of shale relative to carbonate rocks increases within the aureoles, and shale becomes the major component within the ore bodies.

ALTERATION STUDIES

In 1960 the Quimbys Mill Member was first sampled at regular intervals in the long haulageway between the Thompson and Temperly ore bodies. The samples, though restricted to the Quimbys Mill Member, were

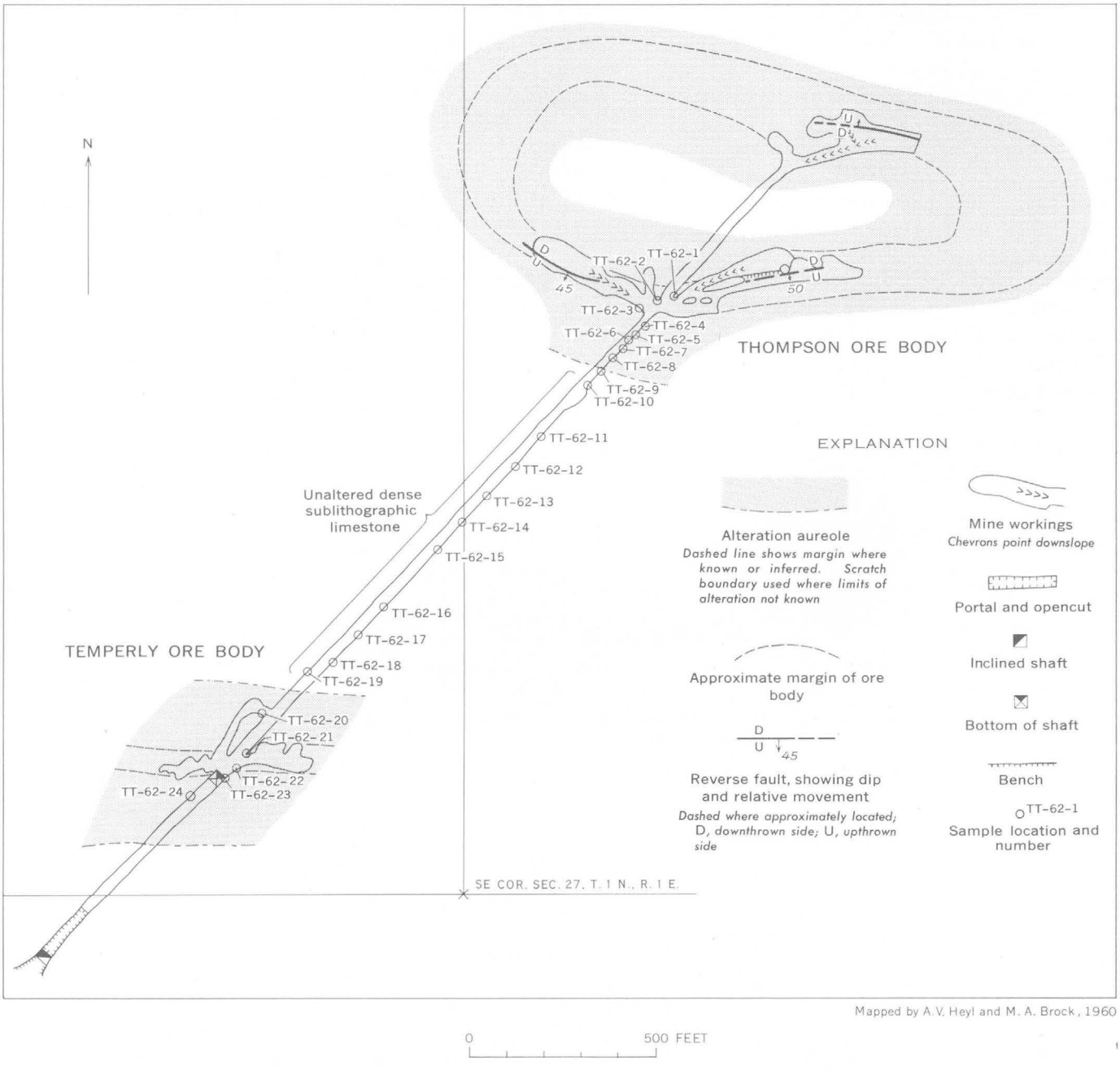

FIGURE 3.—Sketch of the Thompson-Temperly mine, showing approximate location of shale samples. Map is a horizontal section of the ore bodies at an elevation where they lie within the Quimbys Mill Member of the Platteville Formation of Middle Ordovician age.

scattered vertically throughout the member in both limestone and shale and in altered and unaltered rocks. The initial sampling showed that the basal shale bed was better than the limestone for clay-mineral alteration studies because of its more uniform lithology. Moreover, clay is very sparse in the limestone, and the acid treatment required to separate the clay from the limestone may alter the clay. In 1962 the basal shale bed was sampled at intervals of about 30 feet within the Thompson ore body and in the alteration aureole on the southwest side of the Thompson ore body, at intervals of 30 to 200 feet through the barren zone between the two ore bodies, and at a few places in the Temperly ore body and the alteration halo on either side of it (fig. 3).

All 24 samples were first studied by X-ray diffraction (Heyl and others, 1964), using CuKα radiation, to determine the whole mineral content (varieties and relative amount). A select few samples, which gave the complete range of variations between the unaltered rock and rock from the Thompson ore body, were treated to remove the calcite and dolomite from the carbonaceous shale. Six selected samples were further studied by X-ray emission, using a platinum-target tube as a primary source of X-rays, and lithium fluoride as a diffracting crystal. The samples were TT–62–1 from the center of the Thompson ore body; TT–62–4, TT–62–7, and TT–62–9 from the inner, center, and edge, respectively, of the alteration auerole surrounding the ore body; and TT–62–11 and TT–62–13 from the unaltered carbonaceous shale.

Normally, X-ray emission is used for determining the quantity of elements present in a given sample, and when compared with known chemical standards the elements are reported in percent oxide. Since only the relative amount rather than the calculated percentage of each element was necessary in the present study, no attempt was made to assign percentage values to the 8 elements (iron, manganese, titanium, calcium, potassium, silicon, aluminum, and magnesium) found in the 6 samples. These X-ray emission data are illustrated by a series of graphs for each element on figure 4. The ordinate is measured in counts per second, with the highest count obtained for each element arbitrarily given the maximum scale height; all other counts for the particular element are shown by bars proportional in length to that maximum. This procedure emphasizes the variation of each element from sample to sample but does not show the relative abundance of the different elements. Each shale sample

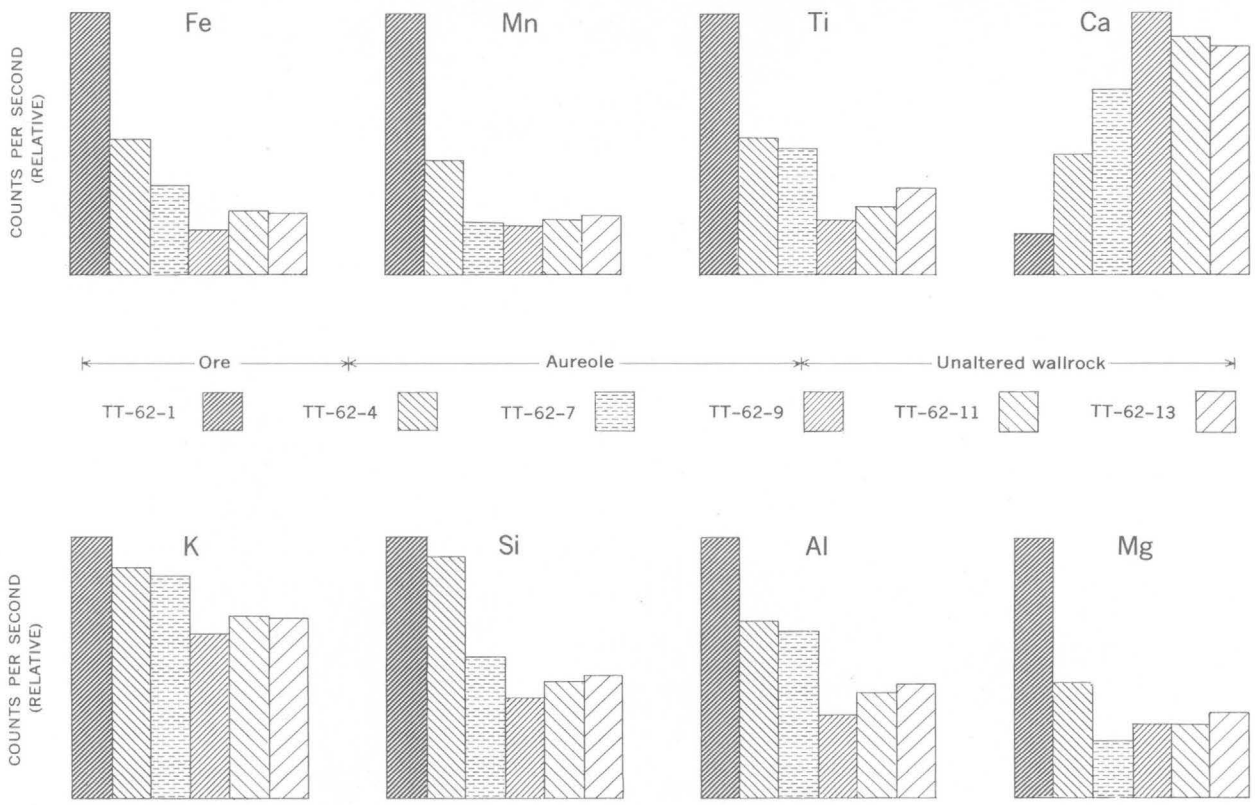

FIGURE 4.—Graphs showing relative amounts of 8 elements in 6 samples of shale from the Thompson-Temperly mine, as determined by X-ray emission analysis.

used in the X-ray emission analysis was ground and homogenized to pass through a 230-mesh sieve and pressed into a large pill. Several reruns of each sample were made and the results were found to be reproducible.

The graphs illustrate two outstanding features. All the elements, except calcium, give the highest count in sample TT–62–1, which is from the center of the Thompson ore body. Also, all the elements, except calcium and magnesium, give the lowest count in sample TT–62–9, which is from the outer edge of the alteration aureole. Calcium shows an inverse relation to all the other elements. The small variations of the elements in samples TT–62–11 and TT–62–13 from the unaltered host rock show the uniformity of the carbonaceous shale bed away from the ore bodies. Preliminary results of semiquantitative spectrographic analyses by Helen W. Worthing of many of these samples confirm the trends that are shown on figure 4. Figure 5 shows graphically the quantities of potassium and magnesium in 18 of the 24 samples of the carbonaceous shale. The amounts of potassium and magnesium in the shale bed within the ore bodies are larger than the amounts in the aureoles in the haulageway, and both elements are least abundant near the outer edges of the wallrock alteration zones. Figure 6 shows graphically the quantities of aluminum, iron, titanium, and manganese in some of the samples from the Thompson ore body only. The quantities of these elements shown by the additional analyses further confirm the variations obtained by qualitative X-ray emission analyses on the similar samples. Calcium and silicon contents were for the most part greater than 10 percent, and hence were too high for semiquantitative determination by the method used.

The X-ray diffraction information (Heyl and others, 1964, figs. 4 and 5) supports the data on figures 4 and 5. Calcite decreases with decrease in calcium from the outer edge of the alteration aureole toward the ore body, and the wallrock of the ore body contains only a trace of calcite. The only other calcite is in scattered crystals occurring as a late gangue mineral in the ores. Dolomite increases with increase in magnesium from the outer edge of the aureole to the ore body. Less quartz is present at the outer edge of the aureole than in the unaltered rock, but it becomes a

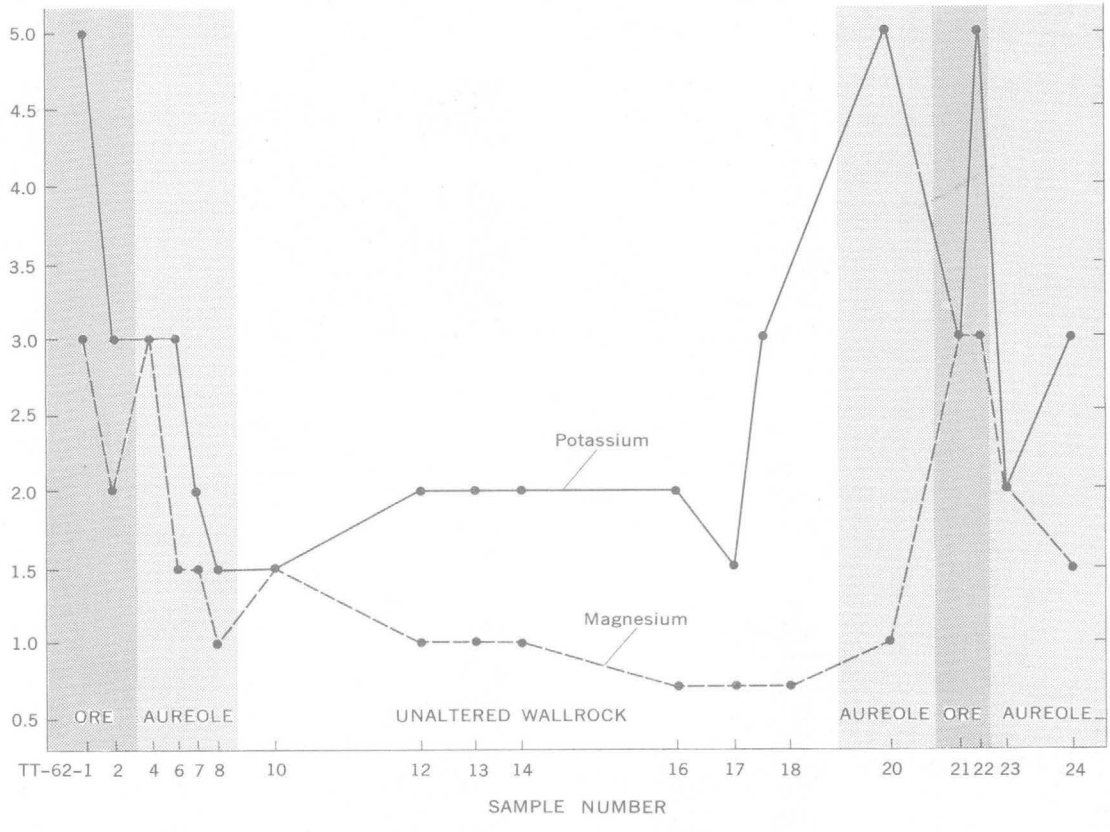

FIGURE 5.—Results of semiquantitative spectrographic analyses of potassium and magnesium from the Thompson-Temperly mine. Results are reported in percent to the nearest number in the series 1, 0.7, 0.5, 0.3, 0.2, 0.15, and 0.1, and so forth, which represent approximate midpoints of group data on a geometric scale. The assigned group for semiquantitative results will include the quantitative value about 30 percent of the time.

predominant constituent in the inner part of the aureole and in the ore body. Illite, a clay-size dioctahedral mica, is present in all samples. It occurs as an *Md* polymorph in the unaltered rock, a 1*M* polymorph in the alteration halo, and a 2*M* polymorph in the ore body. This change in polymorphic form is attributed to the potassium and aluminum added in the ore body (fig. 4), as well as to the decrease in water content in the ore body and alteration aureole (Heyl and others, 1964, p. 452).

Migration of elements can be postulated from the data presented on figure 4. The large counts for almost all elements, as shown by comparing the graphs of samples TT–62–1, TT–62–4, TT–62–7 with those of samples TT–62–11 and TT–62–13, indicated that iron, manganese, titanium, potassium, silicon, aluminum, and magnesium were, in part, epigenetic and were introduced with the ore-forming solutions. Samples TT–62–4 and TT–62–7 show that most of the introduced elements (iron, titanium, potassium, especially silicon, and aluminum) also diffused and migrated beyond the ore zone to the inner part of the alteration aureole. The low counts in sample TT–62–9 for most elements indicate a decrease in the amount present at the edge of the alteration aureole and show that along with the introduction and outward migration, some leaching occurred at the edge of the aureole, and inward migration of iron, titanium, potassium, silicon, and aluminum occurred from the outer edge of the aureole. Magnesium shows a similar but larger leached zone. Calcium increases to the outer margin of the alteration aureole and decreases in the unaltered rocks, indicating that the ore solutions leached calcite from the ore body plus the inner part of the aureole and concentrated it in the outer fringe of the aureole. The leached zone suggests the presence of a diffusion front between the mineralizing solutions and the normal ground water at the time of deposition. The elements leached from the wallrock aureole were transferred inward by lateral secretion to the ore bodies, contributing to the total amounts of the iron deposited in pyrite and marcasite, the manganese deposited in the sphalerite and calcite, the potassium and aluminum deposited in illite and microline, the silicon deposited in quartz, and the magnesium deposited in dolomite. The titanium may be in several of these minerals, as anatase, or in the clay minerals. In the final stage of deposition the calcium remaining in solution was deposited as calcite crystals in open spaces in the ore bodies.

Part of the wallrock alteration, especially some silicification, dolomitization, and minor wallrock leaching, probably occurred prior to sulfide deposition by the ore-bearing solutions in the initial stages of mineralization (Heyl and others, 1959, p. 97–98, 101–108). The main period of solution of the wallrock limestone and dolomite, however, probably began not too long before the start of sulfide mineralization, and continued during sulfide deposition. The process apparently continued all through the period of sulfide deposition and ceased simultaneously as the last marcasite was deposited during the middle of the period of calcite deposition.

The data available are not sufficient to clarify whether the bulk of the elements other than the sulfides that are found in the ore deposits and their aureoles were introduced by the heated connate waters possibly mixed with a smaller magmatic fraction, or whether they were hydrothermally leached from the wallrocks and redistributed in the ore deposits. Only a three-dimensional study backed by geologic mapping and detailed quantitative sampling, already in progress, will probably yield enough data to answer this question. It is known by drilling that the aureoles extend 50 or 100 feet above ore bodies and 5 to 30 feet

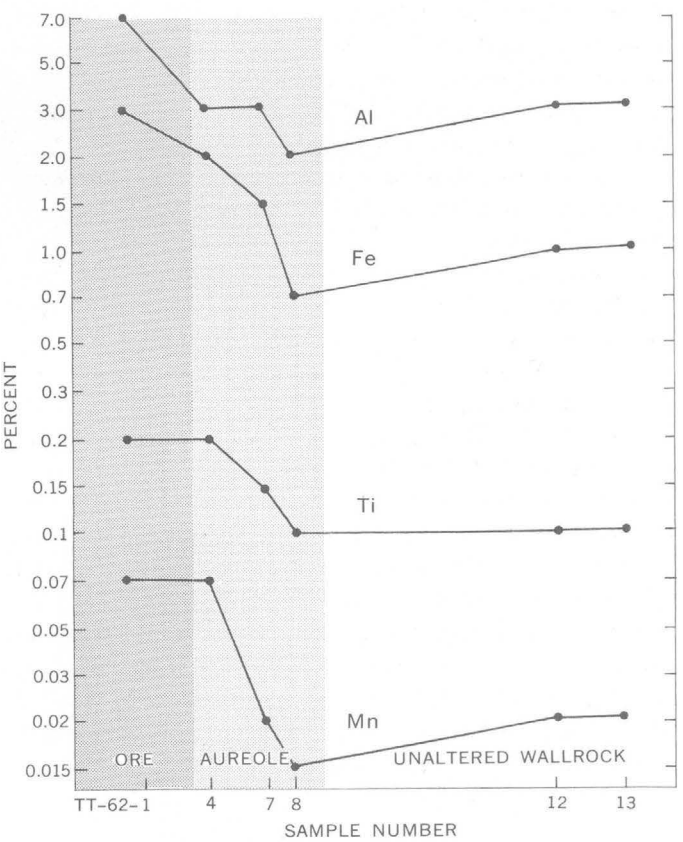

FIGURE 6.—Results of semiquantitative spectrographic analyses of aluminum, iron, titanium, and manganese from the Thompson ore body. Results are reported in percent to the nearest number in the series 1, 0.7, 0.5, 0.3, 0.2, 0.15, and 0.1, and so forth, which represent approximate midpoints of group data on a geometric scale. The assigned group for semiquantitative results will include the quantitative value about 30 percent of the time.

below; likewise, they do not extend far into the central core of elliptical ore bodies.

The almost-uniform composition of the unaltered Quimbys Mill wallrock in the long haulageway indicates quite clearly that the source of redistributed elements in the Platteville Formation is restricted to the wallrocks themselves within the alteration aureoles. The volume of the altered rock is far too small to provide more than a small proportion of the lead, zinc, and iron sulfides deposited in the ore bodies, but it is quite sufficient to provide for the increase in calcium in the narrow outer part of the aureoles (fig. 4), and in the calcite in the ore. The major increases in amount of all other elements in the ore bodies and in the wide inner part of the aureoles above the background in barren wallrock (figs. 4, 5, 6) and the narrow width of the outer leached part, suggest to the writers that the bulk of the elements were introduced by the ore-bearing solutions. A substantial lesser part of the elements was probably redistributed during mineralization and the accompanying alteration. Much of the added elements may have come from limestones, sandstones, and shales, through which the solutions passed; but also some may come from the heated connate waters themselves. In addition, further pre-ore mingling of connate and magmatic solutions may have provided some elements from the granitic basement rocks, and from the juvenile waters supplied by the igneous magma.

Magmatically heated connate brines derived from the Illinois or Forest City basins may have provided the main solutions from which the ore bodies were deposited. When heated the brines may have migrated updip through aquifers, deposited the ores, and altered the host rock when they were trapped beneath the cap of Upper Ordovician shale. Such concentrated heated brines may have formed diffusion fronts with dilute meteoric water already present in the wallrocks along fracture zones above the aquifers, and these diffusion fronts altered the host rocks and deposited the ores.

Hall and Friedman (1963) have shown that the liquid inclusions in galena, sphalerite, and calcite from the Upper Mississippi Valley mining district contain nearly saturated brines similar in composition to present-day deep-seated connate waters of the Illinois basin. These solutions are highly concentrated sodium-calcium chloride brines that have a relatively high deuterium concentration. Potassium and magnesium are fairly abundant in the liquid inclusions that formed during the main stages of sulfide deposition; the much more dilute solutions of the late calcite stages are relatively enriched in sulfate. Such concentrated brines, especially if heated magmatically, would have provided solutions that could be trapped, could readily alter the wallrocks, and could add potassium, magnesium, and other major elements to the deposits.

Bailey and Cameron (1951, p. 625, 626) found the filling temperatures (uncorrected for pressure) of fluid inclusions in the Upper Mississippi Valley district to range from 121°C to 75°C for sphalerite and 78°C to 50°C for stage-2 and stage-3 calcite. The lower filling temperature and the lower concentration of salts and deuterium in the inclusions in the calcite may be attributed to the dilution of heated brines by meteoric water during the late stages of mineralization. Such heated brines could well have provided the type of solutions that formed the alteration aureoles and the described changes in host-rock composition.

REFERENCES

Agnew, A. F., 1955, Application of geology to the discovery of zinc-lead ore in the Wisconsin-Illinois-Iowa district: Mining Eng., v. 7, no. 8, p. 781–795.

Bailey, S. W., and Cameron, E. N., 1951, Temperatures of mineral formation in bottom-run lead-zinc deposits of the Upper Mississippi Valley, as indicated by liquid inclusions: Econ. Geology, v. 46, p. 626–651.

Hall, W. E., and Friedman, Irving, 1963, Composition of fluid inclusions, Cave-In-Rock fluorite district, Illinois, and Upper Mississippi Valley zinc-lead district: Econ. Geology, v. 58, no. 6, p. 886–911.

Heyl, A. V., Agnew, A. F., Lyons, E. J., and Behre, C. H., Jr., 1959, The geology of the Upper Mississippi Valley zinc-lead district: U.S. Geol. Survey Prof. Paper 309, 310 p.

Heyl, A. V., Hosterman, J. W., and Brock, M. R., 1964, Clay-mineral alteration in the Upper Mississippi Valley zinc-lead district, *in* Clays and clay minerals: Proc. 12th Natl. Conf. on Clay and Clay Minerals, p. 445–453.

Reynolds, R. R., 1958, Factors controlling the localization of ore deposits in the Shullsburg area, Wisconsin-Illinois zinc-lead district: Econ. Geology, v. 53, no. 2, p. 141–163.

SUGGESTED EXPLORATION TARGET IN WEST-CENTRAL MAINE

By F. C. CANNEY and E. V. POST, Denver, Colo.

Abstract.—Stream-sediment sampling has suggested that the drainage basin of a stream tributary to Bean Brook in the Long Pond quadrangle, Somerset County, has a mineral potential distinctly above average for the region. Analysis of active stream sediment indicated lead and zinc contents as high as 2,500 ppm and 7,000 ppm, respectively. The lead anomaly is the highest so far revealed in Maine by the regional geochemical mapping program of the U.S. Geological Survey. The known exposures of quartz veins containing sparse bismuth- and silver-rich galena and pyrite appear to be inadequate to produce this intense anomaly.

Reconnaissance geochemical drainage surveys have located a stream in the southern part of the Long Pond quadrangle in Somerset County, Maine, in which the active stream sediment contains as much as 2,500 parts per million lead and 7,000 ppm zinc. Although a heavy-metal anomaly has been known here for some time (Post and Hite, 1963), its apparent significance has recently increased. Reappraisal of the anomalous pattern in the light of a large quantity of geochemical data obtained by a regional geochemical mapping program during the past 2 years has shown that this lead anomaly is by far the strongest one yet found by the U.S. Geological Survey in Maine. Galena- and pyrite-bearing quartz veins are present in the drainage basin of this stream, but the exposed veins are not believed to contain enough lead to be the principal cause of the geochemical anomaly. Accordingly, the drainage basin of this stream is believed to be above average in mineral potential.

The officially unnamed stream in which the lead and zinc anomalies occur, here named Pyrite Creek for convenience, is the northeastern branch of a major tributary to Bean Brook.

Figure 1 presents the data of the detailed geochemical survey along Pyrite Creek, reconnaissance geochemical data in the surrounding area, and the approximate distribution of the major rock types.

The rocks in the general vicinity of Pyrite Creek (fig. 1) are on the southeastern limb of the Boundary Mountain anticlinorium (Albee, 1961) and comprise quartz monzonite of probable Cambrian or Ordovician age, and metasedimentary rocks and diabase of Early Devonian age. The metasedimentary rocks are not exposed in the immediate vicinity of Pyrite Creek, but elsewhere in the area of figure 1 they include slate, metasiltstone, and fine-grained argillaceous sandstone of the Seboomook and Tarratine Formations (Boucot, 1961). These rocks are, in part, overlain conformably by a sheetlike body of altered diabase. The metasedimentary rocks rest unconformably on the quartz monzonite, and dip easterly at a moderate angle.

The quartz monzonite in this area is typically coarse grained, pinkish green, and consists of quartz, pink euhedral to subhedral phenocrysts of microcline, plagioclase, and a small amount of chloritized mafic minerals. In thin section, the plagioclase is moderately sericitized, the mafic minerals (probably principally biotite) are completely altered to chlorite, quartz is strained, and the rock is crisscrossed by an anastomosing network of tiny fractures healed with fine-grained granular quartz and sericite.

The quartz monzonite at several places in the area of figure 1 is extensively silicified so that in hand specimen it resembles a dense pinkish-green felsite. Remnant outlines of the original crystals of the coarse-grained quartz monzonite can be seen in thin section within a groundmass of fine-grained granular quartz and sericite. The reconnaissance nature of our geologic mapping does not permit us to outline the areas of silicified rock on figure 1.

A waterfall 20–25 feet high is present on Pyrite Creek about 700 feet upstream from the unpaved road in Parlin Pond Township. A 10- to 12-inch quartz vein, which strikes N. 70° W., and dips about 80° to the southwest is well exposed in a narrow gorge at the

U.S. GEOL. SURVEY PROF. PAPER 501–D, PAGES D61–D64

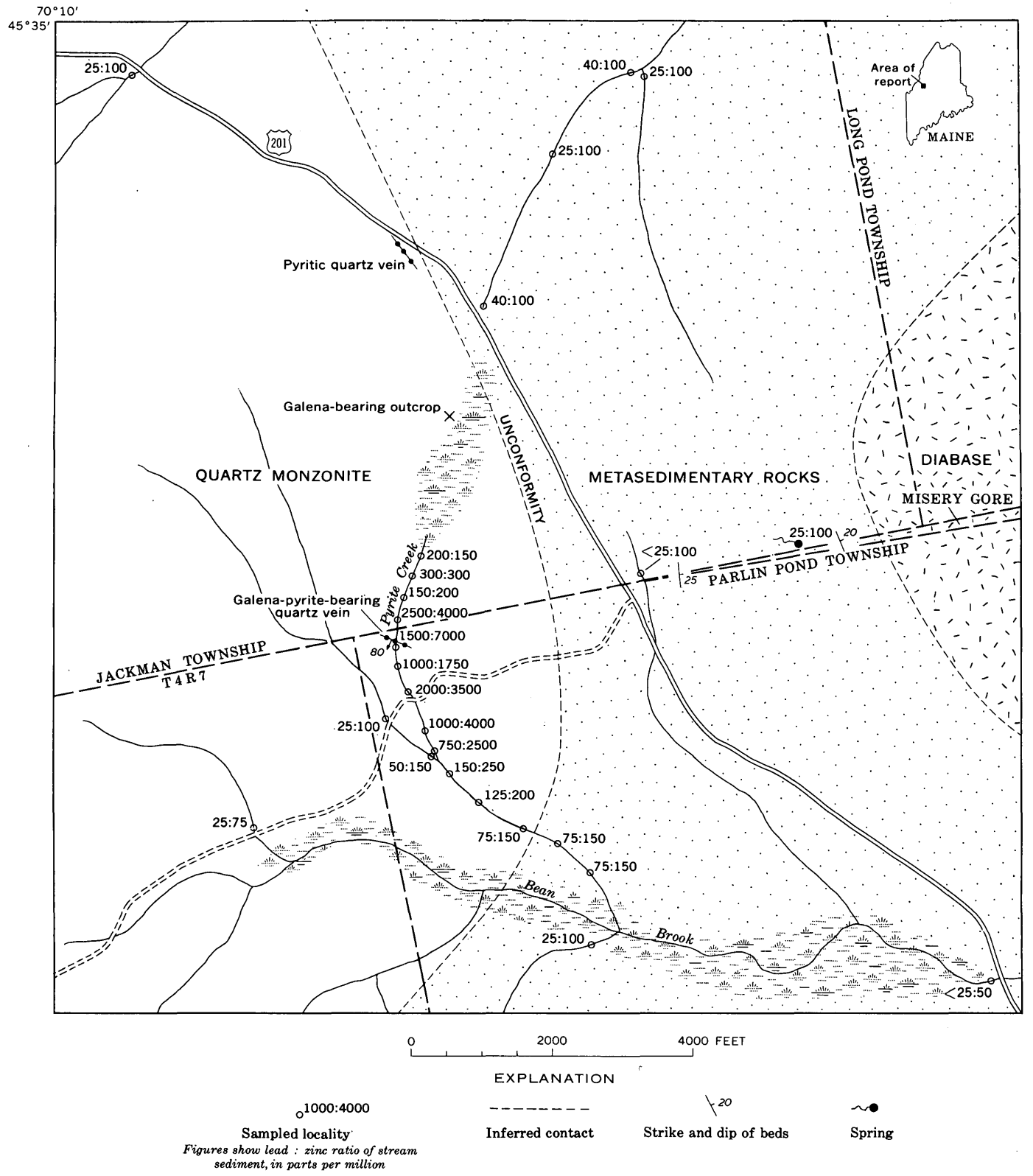

FIGURE 1.—Geochemical and geologic map of the Pyrite Creek area, southern part of the Long Pond quadrangle, Somerset County, Maine. Geology modified from Boucot (1961). Base from U.S. Geological Survey Long Pond 1 : 62,500 quadrangle, 1922.

foot of the falls. On strike and about 150 feet to the southeast, a quartz vein bordered by silicified and pyritized rock is exposed on a steep hillside. Presumably this is the same vein. The vein in the gorge at the foot of the falls appeared to be mostly barren quartz, but when broken open, it was found to contain small pockets of galena, pyrite, and very sparse chalcopyrite. The country rock adjacent to the vein is highly silicified and pyritized. This vein apparently does not extend far to the northwest, for a shallow, angled diamond drill hole collared near the edge of the stream at the top of the falls did not intersect the vein at its projected position.

The galena from the vein is rich in silver and bismuth. One sample containing selected pieces of galena-bearing quartz assayed 1.6 percent lead and 5.4 oz of silver per ton; no gold was detected. A semiquantitative spectrographic analysis of a sample of relatively pure galena showed the bismuth and silver contents to be about 2 percent and 0.7 percent respectively.

Approximately 3,300 feet north-northeast of the waterfall zone an outcrop of silicified quartz monzonite is cut by narrow stringers of galena-bearing quartz. A little more than a mile north of the waterfall, a highly pyritic quartz vein is present on the southwest side of U.S. Route 201 (fig. 1). It trends N. 37° W., and is surrounded by iron-stained and silicified quartz monzonite. No galena was seen, but its presence has been reported.

The quartz monzonite locally contains stringers and clots of specular hematite where the rock is extensively silicified and altered. Although the hematite is not known to be related to the sulfide minerals in the quartz veins, it does characteristically accompany extreme alteration of the quartz monzonite in this area.

The geochemical data were obtained by analyzing the fine-grained fraction (minus-250 micron) of samples of stream sediments collected from the active channels. Field methods of chemical analysis described by Ward and others (1963) were used.

The most striking feature of the geochemical pattern is the exceedingly high contents of lead and zinc in Pyrite Creek from a point just north of the Parlin Pond Township line to the junction of Pyrite Creek with the western branch of the tributary to Bean Brook. Although the heavy-metal content of the stream sediment is anomalous along the entire length of Pyrite Creek (lead background in this part of Maine is about 10–30 ppm and zinc background about 50–125 ppm), a marked decrease in the anomalous values occurs at the confluence of Pyrite Creek with the western branch of the tributary. This is due to the much greater load of fine sediment carried by the western branch.

The stream sediments of Pyrite Creek also have extremely high contents of manganese, with numerous samples containing between 1 and 15 percent manganese. Visible manganese in the form of black coatings on boulders in stream courses, and in many places as discrete nodules, is not uncommon in streams in Maine, especially in streams draining swampy areas. Pyrite Creek does drain a northeasterly trending swamp; nevertheless, the manganese content of the Pyrite Creek sediments appears to be unusually high when compared with the manganese content of sediments from other streams draining similar environments, and therefore these high manganese values are in themselves suggestive of a mineralized area.

Interpretation of the data of geochemical drainage surveys in Maine is complicated by the scavenging action of manganese coatings and nodules. Zinc, cobalt, molybdenum, and barium are among the elements we know to be concentrated by this material. Accordingly, the variability in the zinc pattern along Pyrite Creek is controlled partially by the varying manganese content of the stream sediment. Nevertheless, the ratio of zinc to manganese is considerably above average. This suggests that the zinc is derived from a mineral deposit, rather than being merely the product of manganese oxide scavening. The significance of the lead anomaly is also increased by the fact that much of our data on the lead and manganese content of stream sediments suggest that lead is not scavenged by manganese to any significant extent.

Appraisal of the possible economic significance of this anomaly is difficult. The known exposures of mineralized rock appear to be inadequate to produce this very intense anomaly. The galena-bearing vein exposed in the gorge at the foot of the waterfall appears to have little effect on the anomaly, for the highest lead content (2,500 ppm) was measured about 300 feet upstream from the vein. It is conceivable that a swarm of similar weakly mineralized zones is concealed beneath the extensive glacial cover and swamp upstream and that sufficient lead and zinc is being leached by circulating ground water to account for this anomaly. On the other hand, the possible presence of larger and richer zones cannot be ruled out on the basis of present knowledge. It is our opinion that the intensity of this anomaly justifies a more detailed exploration program of the upper Pyrite Creek area by geological, geophysical, and geochemical surveys.

REFERENCES

Albee, A. L., 1961, Boundary Mountain anticlinorium, west-central Maine and northern New Hampshire: Art. 168 *in* U.S. Geol. Survey Prof. Paper 424–C, p. C51–C54.

Boucot, A. J., 1961, Stratigraphy of the Moose River synclinorium, Maine: U.S. Geol. Survey Bull. 1111–E.

Post, E. V. and Hite, J. B., 1963, Heavy metals in stream sediment, west-central Maine: U.S. Geol. Survey Min. Inv. Field Studies Map MF–278.

Ward, F. N., Lakin, H. W., Canney, F. C., and others, 1963, Analytical methods used in geochemical exploration by the U.S. Geological Survey: U.S. Geol. Survey Bull. 1152.

RADIOACTIVITY- AND DENSITY-MEASURING DEVICES FOR OCEANOGRAPHIC STUDIES

By CARL M. BUNKER, Denver, Colo.

Abstract.—Field tests with modified gamma-ray logging equipment indicate that it is feasible to make continuous profiles of gamma radioactivity and relative bulk density on lake or ocean bottoms. Lack of adequate geologic control in the test area prevented correlation of the peaks and valleys in the profiles with specific changes in the lithology. On the basis of these experiments an underwater vehicle and sensing system were designed to make simultaneous measurements of radioactivity and relative bulk density for routine mapping programs.

Preliminary studies and equipment tests to determine the feasibility of measuring the gamma radioactivity and relative bulk density of recent lake-bottom sediments were made in Lake Superior (fig. 1) and in Burt Lake, Cheboygan County, Mich., during the summers of 1961 and 1962, respectively. Measurements of these types have been proposed for use in the U.S. Geological Survey oceanographic program and are expected to provide a method of mapping the upper few inches of the ocean bottom in conjunction with geologic and mineralogic studies.

When carried on together with an adequate bottom-sampling program to provide geologic control the technique makes possible inferences about the physical properties of the lithologic units exposed on the sea floor. Such inferences are of potential value in harbor construction and in related engineering problems. In addition, the submarine radioactivity measurements may permit (1) outlining underwater ore deposits when such deposits are associated with radioactive materials as, for example, the Florida phosphates, and (2) plotting the course of low-level radioactive wastes along the ocean bottom after waste-bearing waters have left the mouths of rivers into which they have been dumped.

The efficiency of the detection system is low because of the inherent insensitivity of the Geiger-Mueller

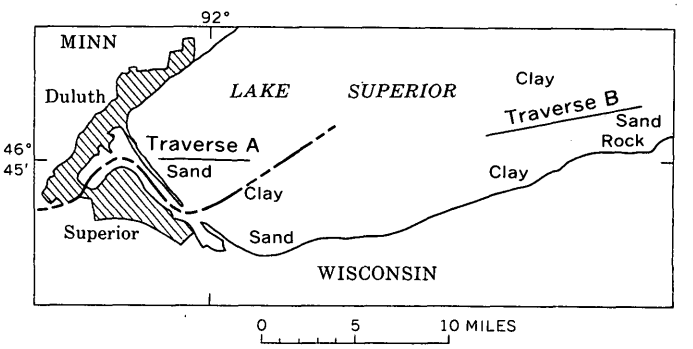

FIGURE 1.—Index map showing location of traverses made in western Lake Superior.

tubes, and the absorption of the radiation by the detector housing and the water layer between the sediments and the housing. The low counting rate which results from the low efficiency and low intensity radiation in the sediments precludes the possibility of obtaining gamma-ray spectral data from a small area while the detector is being towed across the sediments. Thus, only a gross measurement of the radiation intensity is obtained, from which isotope identification is impossible. The gross radiation intensity may be from natural radioisotopes of uranium, thorium, and potassium, from nuclear-explosion-produced fission products in fallout, or from a combination thereof. Semiquantitative data expressed in terms of equivalent uranium or milliroentgens per hour can be obtained from the gross radioactivity measurements. Disequilibrium of the natural radioisotopes and the presence of fission products may lead to erroneous conclusions concerning the radioisotope content of the sediment. A bottom-sampling program in areas of anomalously intense radioactivity in conjunction with the gross radioactivity measurements will permit isotope identification to determine the source of the radioactivity.

U.S. GEOL. SURVEY PROF. PAPER 501-D, PAGES D65–D69

The author gratefully acknowledges the cooperation of the U.S. Coast Guard and of Commander C. G. Porter and the crew of the USCG cutter *Woodrush* without which the Lake Superior measurements could not have been made. M. D. Shutler aided with the Lake Superior and Burt Lake studies; T. H. Cleveland also assisted at Burt Lake.

EQUIPMENT AND PROCEDURE

The equipment used is similar to that used by the U.S. Geological Survey for borehole logging in conjunction with geologic studies and uranium exploration (Vaughn and others, 1959; Bell and others, 1961). It consists of a probe containing a gamma-ray detector and an impedance matching circuit; a reel unit containing several hundred feet of coaxial cable for towing the probe, for transmitting power to the detection equipment, and for transmitting signals from the detectors to the monitoring equipment; a high-voltage power supply; a pulse amplifier which sometimes includes a pulse gating circuit; a ratemeter, and a recorder. The system operates on 115-volt a-c power.

Measurements of gamma radioactivity in Lake Superior were made with a single Geiger-Mueller tube or with a scintillation detector consisting of a sodium iodide crystal coupled to a photomultiplier tube. The monitoring circuitry is adjusted to accept gamma-ray energies greater than about 100 thousand electron volts to measure the gross radioactivity; no attempt was made to measure individual gamma-ray energies or to identify the gamma-emitting radioisotopes.

Measurements of relative bulk density were made with the above detectors separated by 0.6 foot of lead from a 1.0 millicurie source of cobalt-60. The radiation from the source penetrates the sediment, where it is scattered or absorbed. The amount reaching the detector depends on the bulk density of the material through which the photons pass. An increase in density results in a decrease in the path length of the photons, thereby causing less radioactivity to be measured at the detector. The measurement of this radioactivity therefore is a measure of the bulk density of material, including the water, adjacent to the space between the source and the detector.

The gamma radioactivity and relative bulk-density measurements were made independently. However, the measurements can be made simultaneously if the detector for measuring the radioactivity in the sediments is spaced at a sufficient distance from the radioactive source and shielded to prevent measuring the radiation from the radioactive source used for the density measurement.

Two traverse lines in Lake Superior near Duluth, Minn., were chosen on the basis of available, though sparse, data on the type of lake-bottom sediments indicated by hydrographic charts. Measurements were made from the USCG cutter *Woodrush*. The monitoring equipment was installed in the chart room, with direct communication lines to the bridge and to the winch operator on the quarterdeck. Power and signal cables also connected the winch and underwater equipment with the electronics and data-recording systems. The detector was towed at various speeds up to 10 miles per hour; the detector could not be held on bottom above this speed in water depths ranging from 40 to 150 feet. The ship's location along the traverse was determined at the instrument operator's request and at prearranged locations; the location was then indicated on the recording chart to provide a means of comparing several types of data at a given location. A traverse along the predetermined line was required for each type of data required and for each instrumentation change.

The measurements at Burt Lake were made similarly, except that the traverse lines were located between the shore and points in the lake. The monitoring equipment was located in a laboratory vehicle parked at the lake shore. Flag buoys were set about 900 feet from shore to establish the in-lake position from which repeated traverses were made. The sediments ranged from mud in the offshore locations to sand and gravel at the shore.

RESULTS AND PROBLEMS

The lack of geologic data with which the geophysical data might have been related confined the field studies to problems of instrumentation. Records from repeated measurements along the same traverse lines often showed similar configurations (fig. 2), suggesting that changes in the records were related to changes in the characteristics of the bottom sediment. Therefore, the field studies were directed toward increasing the sensitivity of the sensing systems to indicate these changes. The radiation intensity was greater in the areas indicated as sandy on the hydrographic charts than in the areas of clay. The records showing relative bulk density indicated changes along the traverses, but these could not be related to sediment type.

The sensitivity of the single Geiger-Mueller tube was generally insufficient for measuring gamma radioactivity, although some records obtained with this equipment could be related to others obtained with the more sensitive scintillation equipment. Use of the scintillation equipment resulted in records show-

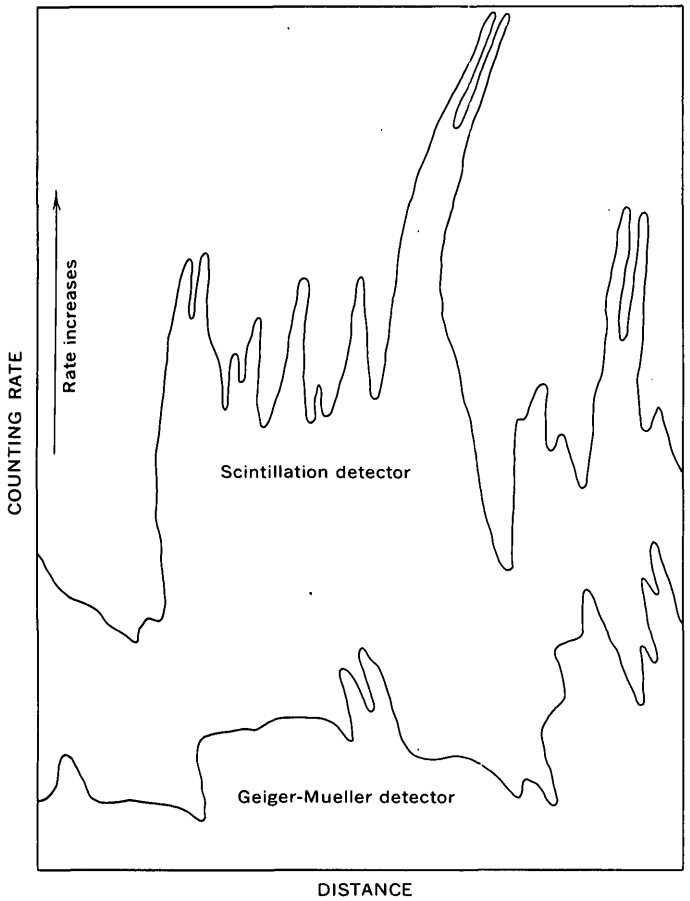

FIGURE 2.—Portion of gamma-ray logs of lake bottom of Lake Superior, near Duluth, Minn. Logs reproduced from curvilinear recording chart. Horizontal distance represents about ⅛ mile.

ing relatively large changes in counting rate. On the basis of sensitivity, the scintillation equipment gave the best results. However, experience with this equipment when used in other applications has shown that it is affected by temperature and voltage changes. Instability of this type would preclude its use for obtaining semiquantitative data. Therefore, a probe containing a bundle of seven Geiger-Mueller tubes was partially tested at Burt Lake to increase the sensitivity and to utilize the relatively high stability of the Geiger-Mueller detection system. Although the system requires further modifications, the sensitivity was improved with the tube bundle.

EQUIPMENT FOR FUTURE STUDIES

On the basis of field studies and the problems related thereto, an underwater vehicle and instrument package (fig. 3) was designed, and requirements for the monitoring system (fig. 4) were decided upon. The instrument package provides for two detection systems, which allows simultaneous measurements of gamma radioactivity and relative bulk density, thereby avoiding repeated measurements on each traverse line.

The instrument package is transported on a skid designed to hold the package on the bottom and to minimize the possibility of its snagging in weeds and rocks. Diving planes are included at the front of the unit to counteract the upward pull of the cable. The weight of the lead shielding in the package should be sufficient to keep the back of the vehicle against the sediment. A vertical plane on top of the vehicle is provided to prevent fishtailing. Based on previous experience, the detection package will easily withstand the pressure of 1,500 feet of water.

Two identical monitoring and recording systems are required for simultaneous measurements of natural radioactivity and density. Detailed requirements provide for a wide range of readouts and time constants. Discriminator circuits are included to provide for scintillation detectors, if required by special conditions.

The distance between the radiation detector and the radiation source (the lake or ocean bottom) must remain virtually constant because of the effects of source-to-detector geometry and radiation absorption by water. The half-thickness value of water is about 3.3 inches for the average gamma-ray energy (about 0.7 million electron volts) from uranium and its daughter products. This means that the radiation incident on the detector is reduced by about one half for each 3.3 inches of water between the detector and the radiation source. The value is related directly to gamma-ray energy. The effect of distance is greater than the effect of water because the radiation varies as a function of the square of the distance between the detector and the radiation source. Small changes in distance can cause large changes in the amount of radiation incident on the detector. Ideally, the detection system should be in constant contact with the sediment to eliminate the effects of distance and water absorption, and to keep the detector in the area of maximum radiation intensity. However, some finite distance is required between the sediments and the waterproof housing encasing the detector to provide protection against abrasion. Although maintaining the detector in constant contact with the sediments is extremely difficult in actual operation, the distance between the detector and the sediment can be kept to about 1 inch as the detector is dragged along the lake or ocean bottom.

A problem greater than reducing the sediment-to-detector spacing to a minimum is maintaining a constant distance while the measurements are being made at the relatively high speeds required to conduct a mapping program economically. During the Lake

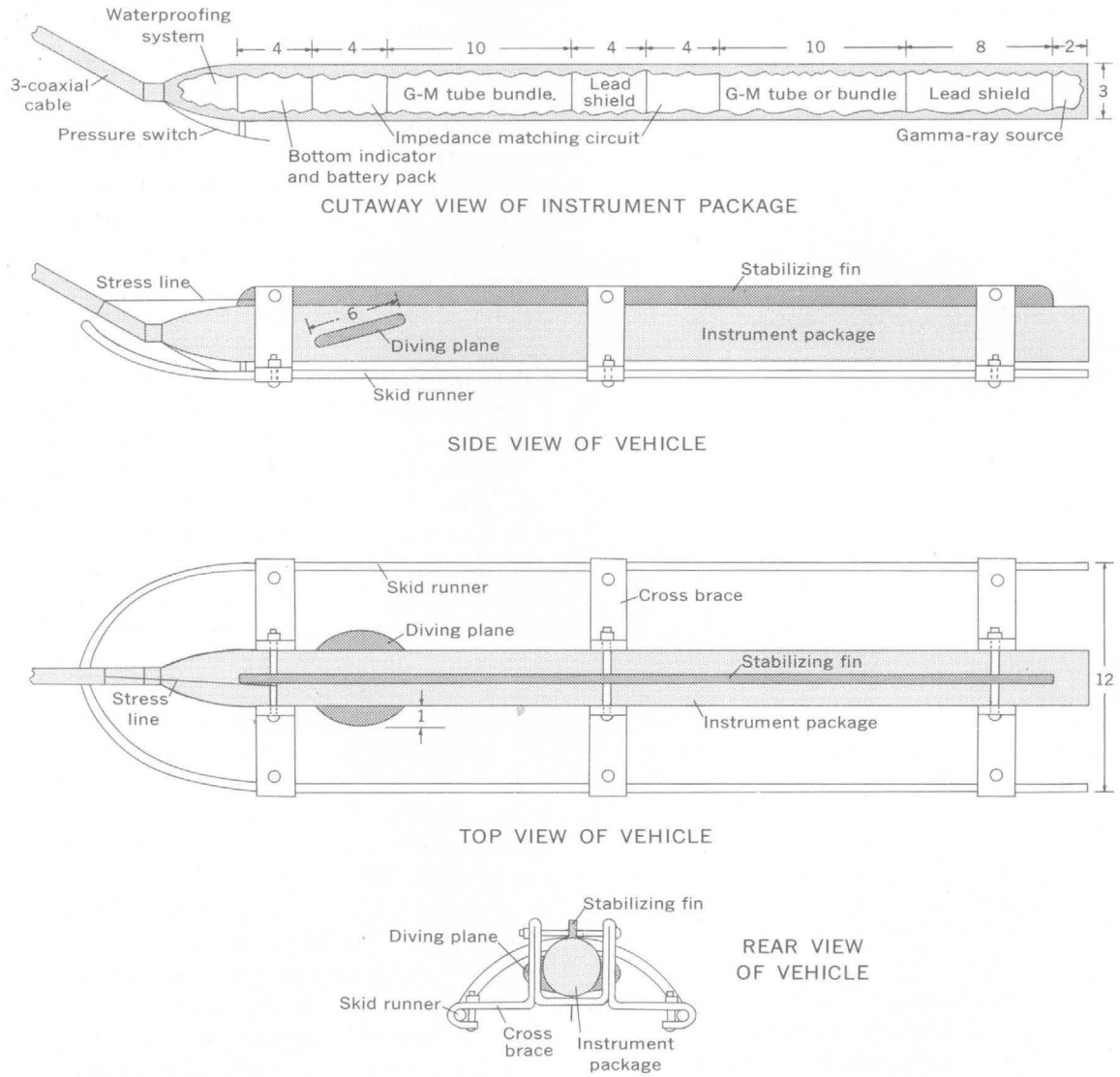

FIGURE 3.—Diagrammatic sketch showing preliminary design of vehicle for measuring radioactivity and density of underwater sediments. Dimensions are in inches.

Superior studies the winch operator could generally detect changes in the vibration or tension on the towline when the probe lifted from the lake bottom. The ship's speed was then reduced until the probe remained on bottom. A more reliable system to indicate automatically when the probe is in contact with the sediments is required for routine measurements to aid equipment operations and to provide a method for determining when the data are valid. A bottom indicator was designed to send a signal to a side-marker pen on the recording equipment to show when the vehicle is in contact with the lake or ocean bottom. The bottom indicator consists of a strip of spring steel which is depressed against a contact switch in the probe shell to close a battery-powered electrical circuit when the probe is on bottom.

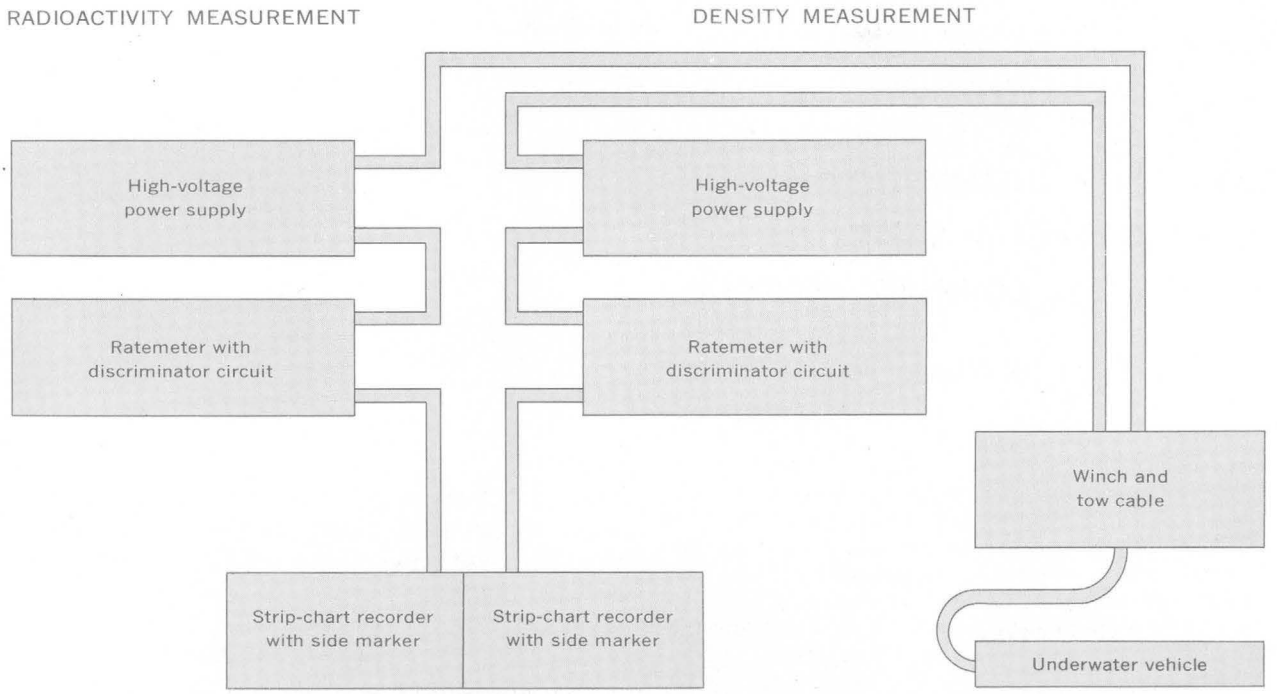

FIGURE 4.—Diagrammatic sketch of arrangement of instruments for measuring radioactivity and density of underwater sediments.

REFERENCES

Bell, K. G., Rhoden, V. C., McDonald, R. L., and Bunker, C. M., 1961, Utilization of gamma-ray logs by the U.S. Geological Survey, 1949–1953: U.S. Geol. Survey open-file report, 89 p.

Vaughn, W. W., Rhoden, V. C., Wilson, E. E., and Faul, Henry, 1959, Scintillation counters for geologic use: U.S. Geol. Survey Bull. 1052–F, p. 213–240.

AEROMAGNETIC INTERPRETATION OF THE GLOBE-MIAMI COPPER DISTRICT, GILA AND PINAL COUNTIES, ARIZONA

By ANNA JESPERSEN, Silver Spring, Md.

Abstract.—No correlation appears to exist between the magnetic highs and the known ore deposits in the Globe-Miami copper district, but the ore-bearing structures have a northeasterly trend that is reflected in the magnetic pattern. The large positive anomalies in the southern part of the mapped area are attributed to Madera Diorite. Irregular clusters of smaller anomalies are associated with diabase dikes.

The major part of the Globe 15-minute quadrangle, in Gila and Pinal Counties, southeast-central Arizona (fig. 1), covers a copper-mineralized belt that is about 6 miles wide. This belt extends east-northeastward across the middle part of the quadrangle (Peterson, 1962, fig. 14, p. 142) and includes the Globe-Miami copper-mining district. The terrain is rugged; altitudes range from 7,850 feet on Pinal Peak, in the southeastern part of the quadrangle, to 3,050 feet where Pinal Creek crosses the north boundary of the quadrangle. Prospecting in this area, which began as early as 1874, led to the discovery and development of the Globe-Miami, Castle Dome, and Copper Cities copper deposits. As about 60 percent of the mineralized belt is buried under volcanic sheets and surficial deposits, it was hoped that an airborne magnetic survey might delineate additional ground favorable for further copper prospecting. Such a survey was made in 1946.

Total-intensity aeromagnetic measurements were made with a continuously recording AN/ASQ–3A airborne magnetometer installed in a twin-engine aircraft. The distance from plane to ground was measured with a continuously recording radar altimeter. Traverses were flown north-south at quarter-mile intervals and about 1,000 feet above the ground. Because of the rugged terrain this altitude could not be continuously maintained; it ranged between 500 and 2,000 feet. Alternate flight lines were omitted in areas of broad magnetic features. A preliminary version of the contoured map (Dempsey and Hill, 1952) was released in 1952.

GENERAL GEOLOGY

The generalized geologic map (fig. 2) is adapted from Peterson (1962) and Ransome (1904). The oldest rocks are the lower Precambrian Pinal Schist and dioritic and granitic intrusions into this schist. Overlying the lower Precambrian rocks are the Apache Group of late Precambrian age, and Paleozoic sedimentary rocks. The younger rocks comprise intrusive and volcanic rocks, conglomerate, and surficial deposits. Intrusive rocks underlie about a fourth of the mapped area.

The region is strongly faulted along northeasterly and northwesterly trends. The earliest faulting preceded the intrusions of diabase, and the latest was later than the accumulation of Gila Conglomerate. The Globe Hills block, the Globe Valley graben, the Inspiration block, and the Castle Dome horst are all bounded by mapped or inferred fault zones. The Globe Hills block occupies the northeastern part of the map area, the Globe Valley graben coincides in general with the Pinal Creek drainage, and the Castle Dome horst forms Porphyry Mountain.

The ore deposits of the Miami-Inspiration, Castle Dome (now mined out), and Copper Cities mines are large tabular generally horizontal zones of disseminated copper sulfides. The host rocks for the Miami-Inspiration deposit are Pinal Schist and granite porphyry and for the Castle Dome and Copper Cities deposits are quartz monzonite and granite porphyry intruded by thin sills of thoroughly brecciated diabase. The copper mineralization of the district occurred

after the intrusions of Schultze Granite and granite porphyry and before the eruption of the dacite (Peterson, 1962, p. 67, 82, 89; Peterson and others, 1951, p. 103; Ransome, 1919, p. 169).

The principal ore minerals are pyrite, chalcopyrite, chalcocite, malachite, and chrysocolla. Although the original iron minerals of the host rocks were completely destroyed by hydrothermal alteration during mineralization, the iron content of the mineralized rock generally was greatly increased owing to introduction of pyrite and chalcopyrite. During oxidation and enrichment most of these minerals were altered to limonite (Peterson, written communication, March 6, 1964), which is nonmagnetic.

The deposits at Globe are vein deposits. The veins were formed by replacement of breccia and wallrock along faults and fissures that cut upper Precambrian and Paleozoic sedimentary rocks and bodies of diabase intruded into them (Peterson, 1962, p. 97). The ore is localized in west-pitching shoots and irregular masses, as replacement of the different types of wallrock. No magnetic minerals are present. The wallrocks are strongly altered adjacent to the veins, but the altered zones are generally only a few feet wide, rarely more than 10 feet. The veins commonly contain abundant specular hematite, earthy hematite, and limonite.

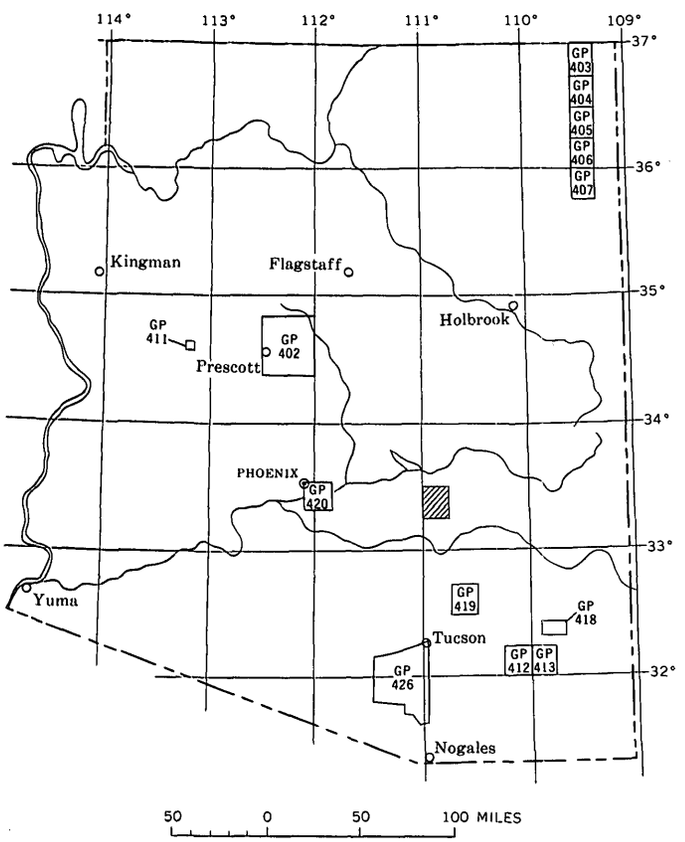

FIGURE 1.—Index map of Arizona, showing location of the Globe 15-minute quadrangle (cross hatched) and other areas covered by published aeromagnetic maps (in the Geophysical Investigations, GP, series) of the U.S. Geological Survey.

CORRELATION OF MAGNETIC DATA WITH GEOLOGY AND MINERAL DEPOSITS

The aeromagnetic map of the area (fig. 3) shows a general east-northeast magnetic trend, which correlates with the trend of the geologic structure and with the trend of the ore zone (see Peterson, 1962, fig. 14, p. 142). The overall magnetic pattern comprises northern and southern anomalous areas of steep gradient, divided by a broad middle east-west band of gentle gradients. Although many of the highs in the northern half of the area coincide roughly with topographic highs, the magnetic expression is believed to be due mainly to the character of the rock itself rather than to the relative nearness of the magnetometer to the mountain peaks.

Magnetic minerals seem to be rare or absent from the ore deposits in the Globe quadrangle, but the ore-bearing structures have a persistent northeasterly trend throughout the region, and that trend is reflected in the magnetic pattern. No correlation appears to exist between the magnetic highs and the known ore deposits. In fact, the principal mines are associated not with the maxima of the highs but with their flanks. In general, the magnetic anomalies appear to be associated with rock masses of varying magnetic properties rather than with known ore deposits.

The diabase sills show a characteristic pattern of small magnetic highs and lows, particularly in the northeastern and the northwestern parts of the area (figs. 2 and 3). According to Peterson (1962, p. 29), the diabase varies considerably in mineral composition even within relatively small outcrops. Some of the diabase contains as much as 10 percent olivine or its alteration products, and magnetite is abundant in all the diabase. The variation in magnetite content and in thickness of the sills, the irregularity in distribution, and the intense faulting and fracturing of the diabase contribute to the lack of uniformity in the magnetic pattern associated with the exposed and postulated buried bodies of this rock.

Some of the lows in the northern part of the mapped area may be due to reverse remanent magnetization of the dacite sheets. The two kidney-shaped magnetic lows, the one on the southwest and the other on the southeast flank of Webster Mountain, appear to be typical expressions of reverse magnetization.

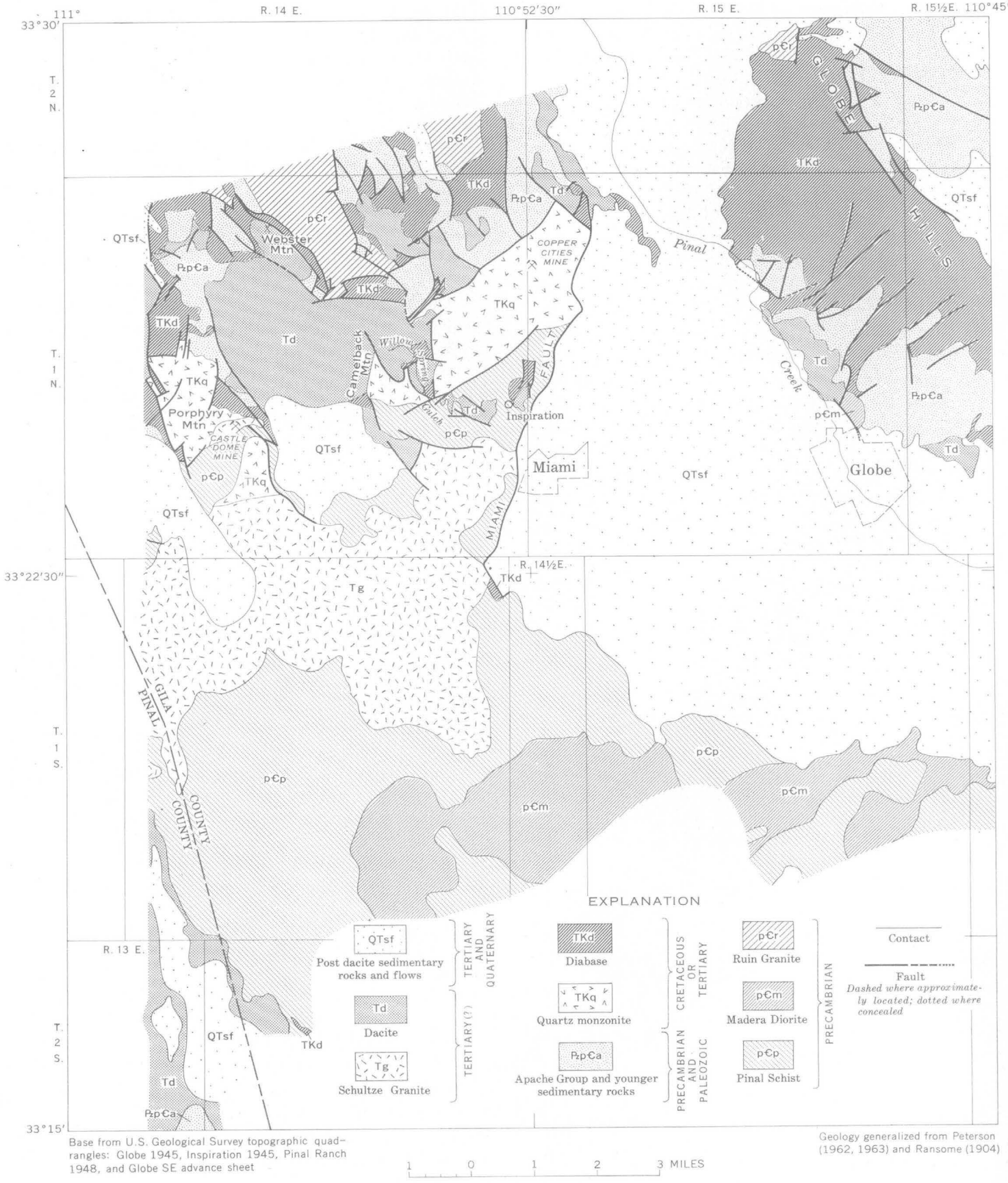

FIGURE 2.—Generalized geologic map of the Globe quadrangle, Arizona.

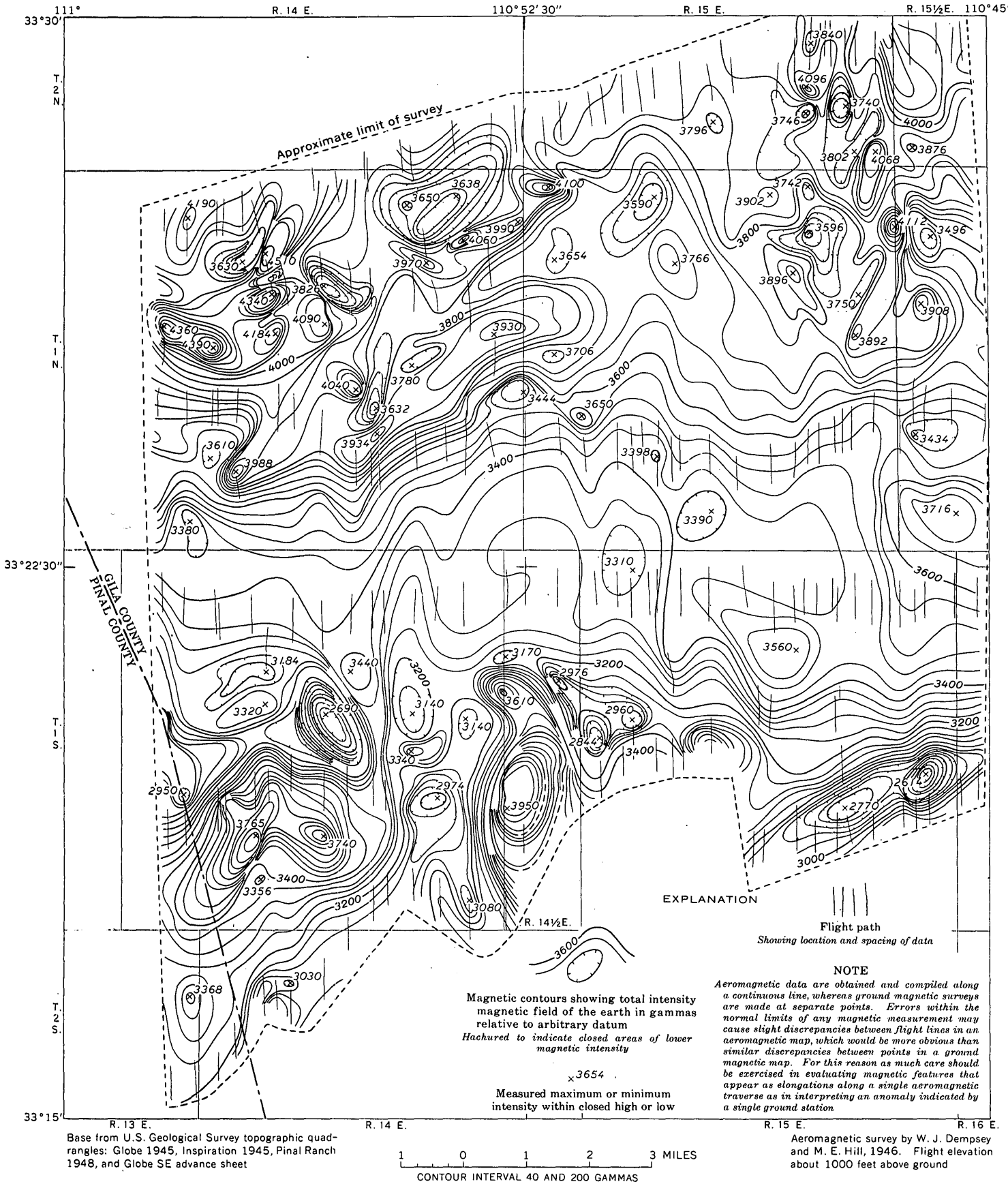

Base from U.S. Geological Survey topographic quadrangles: Globe 1945, Inspiration 1945, Pinal Ranch 1948, and Globe SE advance sheet

Aeromagnetic survey by W. J. Dempsey and M. E. Hill, 1946. Flight elevation about 1000 feet above ground

FIGURE 3.—Aeromagnetic map of the Globe quadrangle, Arizona.

A large magnetically flat pattern is associated with the Globe Valley graben. This flat pattern is due, at least in part, to the fact that here the magnetic rocks are not only at a relatively greater distance from the magnetometer, but are, in addition, buried by younger deposits of nonmagnetic material.

The various granitic rocks generalized on the map as quartz monzonite, the Ruin Granite, and the Schultze Granite are all associated with a distinctive magnetic pattern of low gradient. The pattern in places is somewhat complicated by the influence of buried diabase sills, as, for example, a 200-gamma gradient that crosses longitude 110°52′30″ W. in a northeasterly direction a mile south of the common corner of Ts. 1 and 2 N., Rs. 14 and 15 E. (see Ransome, 1904, structure section B–B).

The rather large anomaly just west of longitude 110°52′30″ W. in the southern half of the mapped area and the one 4 miles farther west are attributed to the mapped and concealed Madera Diorite. The concealed diorite is interpreted to lie a few hundred to 1,000 feet below the surface. The magnetic lows northeast of these highs indicate a vertical or steep northern face on the batholithic body of diorite (see Vacquier and others, 1951). The large elongated low at the southeast corner of the mapped area is believed to be due to a steep north face on the body of Madera Diorite that crops out there and to the south. If the aeromagnetic survey had been extended farther southward it would doubtless have shown a magnetic high to the south of this low, similar to the two highs farther west. The sharp linear gradient to the north of this low suggests a fault boundary at the south edge of the Globe Valley graben (see also Peterson, 1962, fig. 14, p. 142).

CONCLUSIONS AND RECOMMENDATIONS

This survey was made to determine the magnetic expression associated with ore-deposit host rocks and structures as a basis for interpreting similar expression over buried rock masses and thus possibly delineating favorable ground for further prospecting. In an area that has been prospected and mined for nearly a century, undiscovered ore deposits are likely to be few or nonexistent. It must also be emphasized that aeromagnetic mapping is a reconnaissance method and is not expected to pinpoint the spots best suited for drilling. Attention is called, however, to a few localities of possible buried rock masses and structures that are similar magnetically and in their geologic relations to exposed host rocks.

Contacts of diabase with Pinal Schist.—In past mining in the region, ore has been found at the contact of diabase with Pinal Schist and favorable granitic rocks. Several such contacts are shown on detailed geologic maps of various parts of the quadrangle (Peterson and others, 1951, p. 126; Peterson, 1962, p. 97). Other similar but buried contacts are suggested by comparable magnetic patterns; for example, the small lows that form an arc around the large anomaly in the southwestern half of T. 1 S., R. 14 E. The past history of prospecting in these areas, as in all other areas pointed out for possible future prospecting, should be kept in mind in any plans for further search for ore deposits here.

The area northeast of Willow Spring Gulch (fig. 2) marked by an elongated anomaly, has already been thoroughly prospected. However, the area southeast of that gulch, that is, the east flank of Camelback Mountain, may warrant further prospecting. This area is delineated by a paired magnetic high and low.

Dacite-covered anomalous areas.—Ransome (1919, p. 169–173) has shown that the hypogene copper deposits near Miami had been exposed and a chalcocite ore body produced by supergene enrichment before the dacite covered the area. Dacite-covered areas that coincide with magnetic lows could conceivably conceal oxidized and enriched deposits.

Only a few faults have been mapped in the large Tertiary dacite flow south of Webster Mountain. Peterson (1962, p. 141) has called attention to an occurrence of exotic copper in a fracture zone in the dacite body on the Empress claim, 2.2 miles east-northeast from Porphyry Mountain; a few shallow pits and a 40-foot shaft explored the fracture zone. From the magnetic pattern associated with this dacite flow it can be postulated that the diabase, Pinal Schist, and other concealed rocks are highly fractured. If this is the case, this area appears to have mineral possibilities; yet it is the least prospected part of the entire mineral belt. The magnetic pattern, the small fault and the small Tertiary-Quaternary and basalt flows mapped by Peterson (1962, pl. 1), and the drainage across the dacite-covered area all suggest that if prospecting is undertaken it should cross the area in a southeast-to-northwest direction close to and parallel to the fault, the basalt outcrops, and the streams, thus coinciding with the flanks of the anomalies.

REFERENCES

Dempsey, W. J., and Hill, M. E., 1952, Preliminary aeromagnetic map of Globe quadrangle, Arizona: U.S. Geol. Survey open-file report.

Peterson, N. P., 1962, Geology and ore deposits of the Globe-Miami district, Arizona: U.S. Geol. Survey Prof. Paper 342, 151 p.

——— 1963, Geology of the Pinal Ranch quadrangle, Arizona: U.S. Geol. Survey Bull. 1141–H, p. H1–H18.

Peterson, N. P., Gilbert, C. M., and Quick, G. L., 1951, Geology and ore deposits of the Castle Dome area, Gila County, Arizona: U.S. Geol. Survey Bull. 971, 134 p.

Ransome, F. L., 1904, Description of the Globe quadrangle, Arizona: U.S. Geol. Survey Geol. Folio 111, 17 p.

——— 1919, The copper deposits of Ray and Miami, Arizona: U.S. Geol. Survey Prof. Paper 115, 192 p.

Vacquier, Victor, Steenland, N. C., Henderson, R. G., and Zietz, Isidore, 1951, Interpretation of aeromagnetic maps: Geol. Soc. America Mem. 47, 151 p.

742–652 O—64——6

EPIGENETIC URANIUM DEPOSITS IN SANDSTONE

By WARREN I. FINCH, Paducah, Ky.

Work done in part in cooperation with the U.S. Atomic Energy Commission

Abstract.—Nearly all of the approximately 4,600 sandstone uranium deposits in the United States are in continental sediments that accumulated in shallow, poorly drained foreland or postorogenic basins. Data from these deposits suggest that the uranium was precipitated from alkaline connate-water solutions during and after diagenesis under reducing conditions at normal rock temperatures and pressures.

Some 4,600 epigenetic uranium deposits in sandstone constitute the Nation's chief source and reserve of uranium ore. About 95 percent of the deposits lie in two belts: a major belt extending northeasterly from Arizona and New Mexico through the Colorado Plateau and Wyoming into South Dakota, and a minor belt extending easterly through New Mexico into northern Texas and Oklahoma (fig. 1). This principal uranium region or province also contains other kinds of large uranium ore deposits (Butler and Schnabel, 1956; Klepper and Wyant, 1956) and has been related to tectonic elements in Precambrian rocks of the Cordilleran foreland by Osterwald (1956). Most of the remaining 5 percent of uranium deposits in sandstone are in California and Nevada, southeast Texas, and Pennsylvania. Most deposits have been described as peneconcordant (Finch, 1959) and the remainder as vein deposits. This paper summarizes the major conclusions from a longer report that describes the geology of the uranium deposits in sandstone formations in the conterminous United States.

Nearly all the sandstone in which the deposits lie is continental and formed in shallow, poorly drained basins either within foreland areas or between fault-block uplifts. Some of the sandstone is marine and formed in epicontinental seas along margins of the craton. None of the deposits are in geosynclinal sandstone.

Most of the Paleozoic host sandstone in the Western States formed on the Ouachita foreland; and in the Eastern States, on the Appalachian foreland (fig. 1). Most Mesozoic host sandstones in the West formed on the Cordilleran foreland; in the East, in rift valleys of New Jersey and Connecticut. Tertiary host sandstones in the principal uranium region and in California and Nevada formed in basins between fault-block uplifts; in southeast Texas, they formed on the coastal foreland. Exceptions to these generalizations include lower Mesozoic host sandstones that formed east of the Cordilleran foreland, mainly along the late Paleozoic Ouachita foreland, and Paleozoic sandstones that contain vein rather than peneconcordant deposits and formed in areas west of the Ouachita foreland.

Water within the basins of sandstone deposition was mostly fresh, but associated coal and saline rocks in many basins suggest that drainage was poor and internal, at least locally, especially in the last stages of deposition. Thus, concentrations of metals, salts, and humic acids in the water may have increased during deposition, with subsequent entrapment of this water in the rocks at the close of each sedimentary cycle.

The host sandstones are mainly stream-deposited lenses. They are chiefly quartzose, arkosic, or tuffaceous; most of the quartzose sandstones are closely associated with tuffaceous rocks. Carbonized plant remains are common in ore-bearing beds, and some sandstones are impregnated with epigenetic asphaltlike material that was probably derived from humic matter dissolved in connate water.

Deformation since the accumulation of the host sandstones has been slight to moderate and seems, in most areas, to have occurred after most of the uranium mineralization. Igneous activity is not evident in some areas of sandstone uranium deposits. In other areas, igneous activity bears little direct relation to the distribution and nature of deposits, except for two iso-

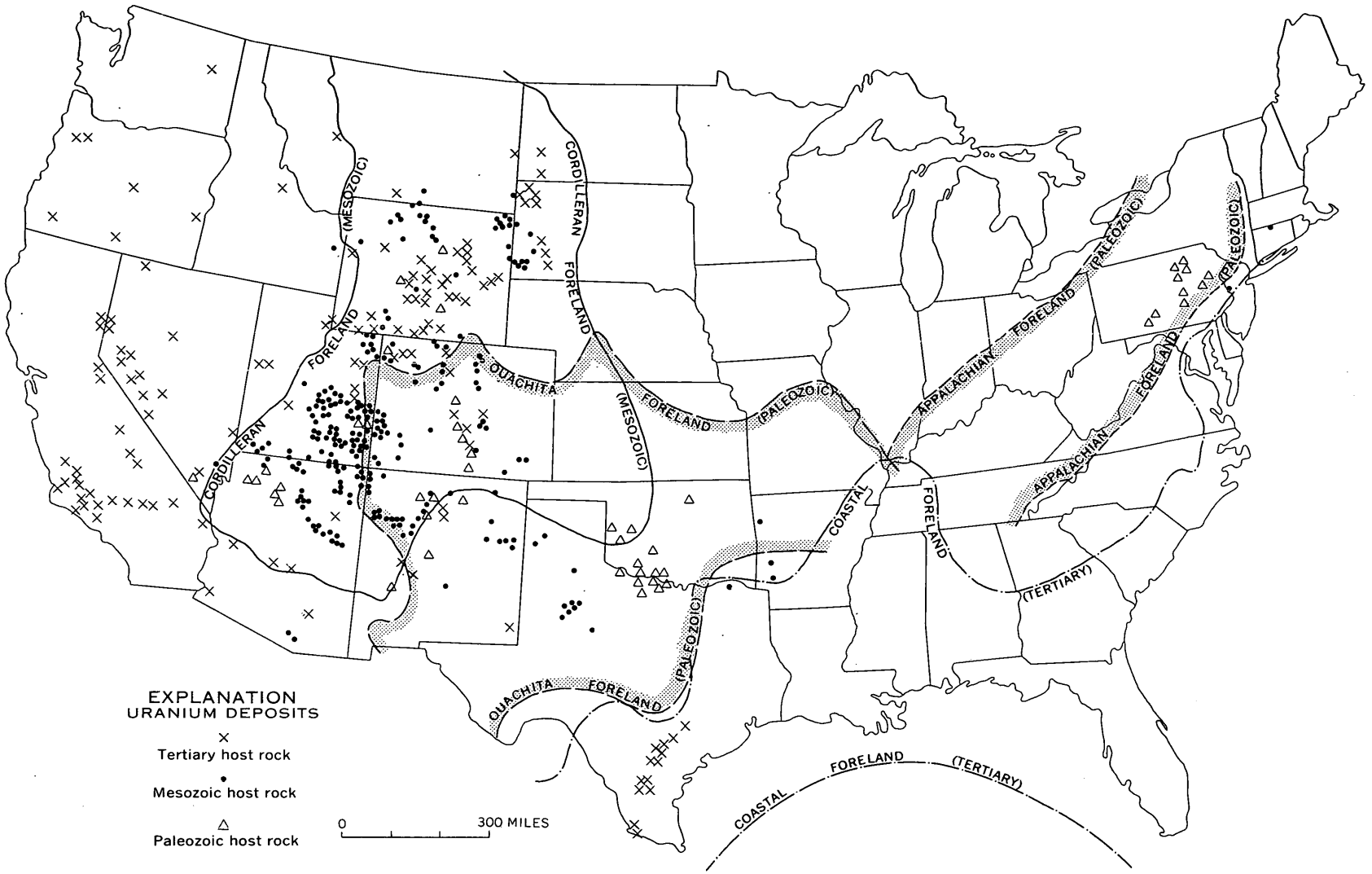

FIGURE 1.—Distribution of epigenetic uranium deposits in sandstone, and related foreland areas in the conterminous United States. Cordilleran foreland boundary after Osterwald (1961, fig. 1); other boundaries after Osterwald and G. W. Walker (written communication, 1957).

lated districts where vein deposits are inferred to have formed from magmatic differentiation or volcanic emanations (Neuerburg and Granger, 1960; Kern, 1959).

The ore bodies are chiefly tabular masses, but roll-like pods, concretionary masses, and mineralized fossil logs are common. In peneconcordant deposits the ore bodies virtually follow the bedding, but in vein deposits the ore bodies mostly follow faults and shear zones that cut sharply across bedding. The mineralization was not intense, and little or no gangue mineral matter was introduced. Ore solutions were nearly in equilibrium with the host rocks, which are altered but slightly. Bleaching is the principal alteration, but it can hardly be distinguished from diagenetic bleaching.

Primary minerals of the sandstone ores consist of low-valent uranium and vanadium oxides and silicates, and of common sulfide minerals of iron, copper, lead, and zinc. Uraninite and coffinite are the chief primary uranium minerals. Uraninite occurs chiefly as grains, either dense and structureless or with a microbotryoidal structure. Coffinite is mostly very fine grained and intergrown with other minerals. Some vanadium and uranium substitutes for other elements in certain sedimentary minerals. The chief ore-mineral textures include crystals partially filling open spaces, and replacements of fossil plant matter, sand grains, cementing materials, and earlier minerals. Paragenetic sequences of the ore minerals consist of numerous overlapping stages that cannot be clearly separated, particularly the early stages from the sequence of diagenetic minerals. The primary ores commonly oxidize to produce a wide variety of secondary minerals, the most common of which are carnotite and tyuyamunite.

Inferences regarding genesis must account for sources of the metals, for the transporting media, and for mineralization controls indigenous to the host rocks. Although a possible telethermal origin is by no means eliminated, mineralization by connate water is here regarded as more likely for most of the sandstone uranium deposits, particularly for those that are peneconcordant, and the following conclusions seem to best fit the field and laboratory observations.

Uranium and associated metals are believed to have been derived from the weathering of granite and related rocks, from the devitrification of volcanic glass during sandstone deposition and during diagenesis, and from the alteration of heavy minerals.

It is inferred that the metals were transported in moderately concentrated metallic and alkaline bicarbonate solutions (Hostetler and Garrels, 1962), of connate and (or) ground water at temperatures and pressures about the same as those of the enclosing rocks. Mineralization was protracted, and it began early during diagenesis. During compaction of the sediments, especially of the tuffaceous muds, the connate solutions moved into the permeable sandstone beds, particularly those beneath thick beds of volcanic material. Further movement was laterally along the beds. The ores were modified by changes in movement of the solution due to (1) ground-water recharge, (2) reactivation in response to tectonic and igneous activity, and (3) Recent erosion and weathering. Mineralization in most areas probably ceased when the mineral-bearing waters were flushed out and replaced by normal ground water, most likely at the time of major structural deformation.

Precipitation of the low-valent ore minerals was due chiefly to reduction by carbonized plant remains, asphaltlike material, hydrogen sulfide gas from decaying plant matter, and (or) diagenetic iron sulfide minerals. Colloidal deposition predominated, perhaps brought about by anerobic bacteria, but crystallization, ion-exchange, adsorption, and replacement were also prevalent. Concretionary growth of ore through diffusion seems to have been common. Deposits were localized mainly by sedimentary structures and also partly by deformational structures.

REFERENCES

Butler, A. P., Jr., and Schnabel, R. W., 1956, Distribution and general features of uranium occurrences in the United States, *in* Page, L. R., Stocking, H. E., and Smith, H. B. compilers, Contributions to the geology of uranium and thorium . . .: U.S. Geol. Survey Prof. Paper 300, p. 27–40.

Finch, W. I., 1959, Peneconcordant uranium deposit—a proposed term: Econ. Geology, v. 54, no. 5, p. 944–946.

Hostetler, P. B., and Garrels, R. M., 1962, Transportation and precipitation of uranium and vanadium at low temperatures, with special reference to sandstone-type uranium deposits: Econ. Geology, v. 57, no. 2, p. 137–167.

Kern, B. F., 1959, Geology of the uranium deposits near Stanley, Custer County, Idaho: Idaho Bur. Mines and Geology Pamph. 117, 40 p.

Klepper, M. R., and Wyant, D. G., 1956, Uranium provinces, *in* Page, L. R., Stocking, H. E., and Smith H. B., compilers, Contributions to the geology of uranium and thorium . . .: U.S. Geol. Survey Prof. Paper 300, p. 17–25.

Neuerburg, G. J., and Granger, H. C., 1960, A geochemical test of diabase as an ore source of uranium deposits of the Dripping Spring district, Arizona: Neues Jahrb. Mineralogie, Abh., v. 94, Festband Ramdohr, p. 759–797.

Osterwald, F. W., 1956, Relation of tectonic elements in Precambrian rocks to uranium deposits in the Cordilleran foreland of western United States, *in* Page, L. R., Stocking, H. E., and Smith, H. B., compilers, Contributions to the geology of uranium and thorium . . .: U.S. Geological Survey Prof. Paper 300, p. 329–335.

——— 1961, Critical review of some tectonic problems in Cordilleran foreland: Am. Assoc. Petroleum Geologists Bull., v. 45, no. 2, p. 219–237.

THE OCCURRENCE OF PHOSPHATE ROCK IN CALIFORNIA

By HOWARD D. GOWER and BETH M. MADSEN,
Menlo Park, Calif.

Abstract.—More than 60 occurrences of phosphate rock in California are located and briefly described. Most of the phosphate occurs in siliceous rocks of Miocene age in the southern Coast Ranges and along the west side of the San Joaquin Valley. Carbonate-fluorapatite is the principal phosphate mineral. Pelletal phosphorites of middle and late Miocene age appear to offer the most promise of containing commercial deposits.

The initial phase of a current U.S. Geological Survey study of the occurrence of phosphate in California included a search of the literature for references on phosphate in the State and a compilation of known but previously unpublished phosphate-bearing localities. Reconnaissance field examination was made of some of the more promising of these known localities, and in addition, nine new localities were found in areas where the geologic conditions seemed favorable for the occurrence of phosphate.

This paper gives the location of 67 localities in California that contain significant quantities of phosphate in sedimentary rocks (fig. 1), briefly describes each occurrence from north to south in the State (table 1), and summarizes the chemistry and mineralogy of the phosphate rock. Most of the occurrences are small and of little economic importance, but they offer a starting point for more detailed investigations and, because of the current interest in phosphate in California, they are presented here.

Most of the phosphate localities are in the southern Coast Ranges between San Francisco and Los Angeles and along the west side of the San Joaquin Valley. At nearly all these localities the phosphate is in rocks of Miocene age. West of the San Andreas fault, phosphate commonly occurs in rocks of middle and late Miocene age. East of the fault, phosphate appears to be most abundant in rocks of early Miocene age. The phosphate-bearing rocks are commonly thin bedded and closely associated with siliceous shale and bentonite. Bentonite laminae and thin beds make up as much as 10 percent of some phosphatic sections.

In this paper, phosphorite refers to rocks composed dominantly of phosphate. There are three principal types of California phosphorite: pelletal, nodular, and argillaceous laminar. Most phosphorites are composed dominantly of one type, but may contain minor amounts of others. Pelletal phosphorites are composed of light-gray to dark-brown spherical pellets 0.1 mm to 1 mm in diameter. The pellets are structureless and contain silt-sized inclusions of nonphosphatic material, chiefly quartz and feldspar. Pellets are usually concentrated in soft to moderately hard beds 1 to 4 inches thick. Phosphate nodules are dark brown to white, ellipsoidal or irregular in shape, and up to 8 inches in length. They usually contain chalcedony and abundant inclusions of nonphosphatic clastic material, microfossils, and fragments of bone. Argillaceous laminar phosphorites consist of finely divided phosphate and abundant silt-sized nonphosphatic clastic material in light-gray laminae. These laminae are often cemented with phosphate. Nodular and argillaceous laminar phosphorites usually contain appreciable amounts of calcium carbonate, chiefly in the form of Foraminifera tests, while most pelletal phosphorites contain little or no calcium carbonate. Dark-brown phosphatic mollusk shells are found in sandstone beds in several places. They usually occur with scattered phosphate pellets and nodules. In a few places phosphatic fossils are abundant enough to form a phosphorite.

The chemistry and mineralogy of the California phosphorites are poorly known. The only material examined in detail thus far in the current investigation was from the Indian Creek area of San Luis Obispo County (fig. 1, loc. 32). The deposit is in the Monterey Formation, here of middle Miocene age. The main phosphate-bearing zone is about 35 feet thick. This zone is composed of 75 percent siliceous

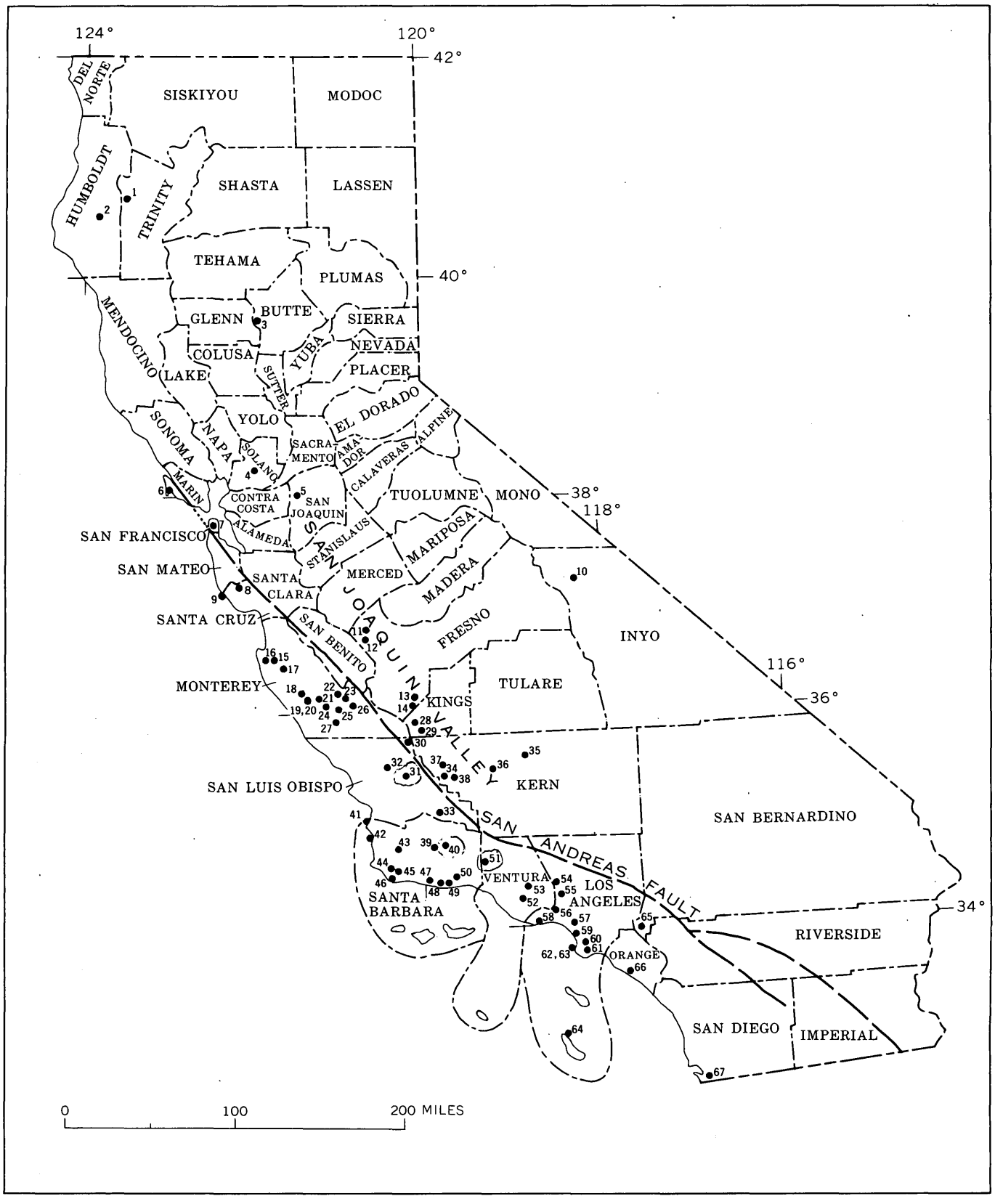

FIGURE 1.—Map showing phosphate-rock localities of California.

TABLE 1.—*Occurrence of phosphate rock in California*

[H. B. and M., Humboldt base line and meridian; M. D. B. and M., Mount Diablo base line and meridian; S. B. B. and M., San Bernardino base line and meridian]

Locality No.	Description	Location
	Trinity County	
1	Phosphate in nonmarine sedimentary rocks of Oligocene(?) age (P. H. Lydon, California Div. Mines and Geology, oral communication, 1963).	S½ sec. 13, T. 3 N., R. 6 E. (H. B. and M.).
	Humboldt County	
2	Small specimen of presumably sedimentary phosphorite in the mineral collection of the California Division of Mines. Stratigraphic position and detailed locality description are unknown (Rogers, 1944, p. 419).	Near Yager, probably in T. 2 N., R. 3 E. (H. B. and M.).
	Butte County	
3	Scattered phosphatic material in shales of Late Cretaceous age (Thomson, 1962, p. 27).	T. 20 N., R. 1 W. (M. D. B. and M.).
	Solano County	
4	Limonitic phosphatic interbeds in Eocene shales (Tolman, 1943, p. 596).	T. 4 N., R. 1 W. (M. D. B. and M.), Potrero Hills gas field.
	San Joaquin County	
5	Phosphatic nodules in shales of Paleocene and Eocene age (Knox, 1943, p. 590).	T. 2 N., R. 4 E. (M. D. B. and M.), McDonald Island gas field.
	Marin County	
6	Phosphatic nodules and mudstone interbeded with siliceous and calcareous shales, upper Miocene.	West side of Drakes Bay.
	San Francisco County	
7	Phosphatic nodules in highly sheared graywacke and black shale, Franciscan Formation, Mesozoic (J. G. Schlocker, oral communication, 1964).	South side of Clarendon Ave., 200 feet east of Seventh Ave., San Francisco.
	Santa Cruz County	
8	Phosphate pellets associated with a Tertiary glauconite, San Lorenzo Formation [1] (Cummings and others, 1962, p. 186–187).	SE¼, sec. 31, T. 8 S., R. 2 W. (M. D. B. and M.).
9	Phosphatic nodules and laminae in middle Miocene siliceous and calcareous shales.	T. 9 S., R. 4 W. (M. D. B. and M.), Año Nuevo Point.

See footnote on p. 83.

TABLE 1.—*Occurrence of phosphate rock in California*—Con.

[H. B. and M., Humboldt base line and meridian; M. D. B. and M., Mount Diablo base line and meridian; S. B. B. and M., San Bernardino base line and meridian]

Locality No.	Description	Location
	Inyo County	
10	Phosphate in Pleistocene sediments (Tucker, 1926, p. 520).	T. 9 S., R. 35 E. (M. D. B. and M.). 6 miles east of Big Pine on the Big Pine–Saline Valley road.
	Fresno County	
11	Scattered phosphate pellets in soft mudstone in lower part of the Eocene and Oligocene (?) Kreyenhagen Shale (Payne, 1951, p. 20).	Sec. 19, T. 14 S., R. 12 E. (M. D. B. and M.).
12	Nodules of apatitized wood and leucophosphite in lower part of the Upper Cretaceous and Paleocene(?) Moreno Formation (Gulbrandsen and others, 1963).	Secs. 6 and 7, T. 15 S., R. 12 E. (M. D. B. and M.).
13	Phosphate pellets in basal part of the upper Miocene McLure Shale Member of the Monterey Formation (Anderson, 1952, p. 187).	T. 20 S., R. 16 E. (M. D. B. and M.), Guijarral Hills oil field.
14	Phosphate pellets in Eocene and Oligocene(?) Kreyenhagen Shale (Woodring and others, 1940, p. 147).	T. 21 S., R. 16 E. (M. D. B. and M.), Kettleman Hills oil field.
	Monterey County	
15	Phosphate-pellet beds in siliceous shales of the Miocene Monterey Formation.	SE¼SW¼ sec. 16, T. 16 S., R 2 E. (M. D. B. and M.), exposed in roadcuts.
16	Phosphate-pellet beds as much as 1 foot thick in siliceous shales of the Miocene Monterey Formation (Galliher, 1931, p. 266; Rogers, 1944, p. 411).	SE¼ projected sec. 24, T. 16 S., R. 6 E. (M. D. B. and M.).
17	Three 2- to 6-inch phosphate-pellet beds in thin-bedded slightly phosphatic siliceous shale, of the Miocene(?) Monterey(?) Formation.	T. 17 S., R. 3 E. (M. D. B. and M.), roadcuts along Tularcitos Creek, about ½ mile NW of USGS bench mark 1153, Rana Creek quadrangle.
18	Pellet phosphate beds in the Miocene Monterey Formation.	450 feet W. of SE. cor. sec. 21, T. 19 S., R., 5 E. (M. D. B. and M.), roadcuts along Arroyo Seco road.
19	Abundant phosphate pellets in siltstone in the Miocene Vaqueros Formation (Thorup, 1943, p. 466).	T. 20 S., R. 6 E. (M. D. B. and M.), Vaqueros Creek.
20	Pellet phosphate beds 4 to 6 inches thick in the Miocene Monterey Formation (Reed, 1927).	T. 20 S., R. 6 E. (M. D. B. and M.), Vaqueros Creek.
21	Pellet phosphate beds in lower part of the Miocene Monterey Formation (D. L. Durham, oral communication, 1963; Kleinpell, 1938, fig. 4).	NW¼ sec. 13, T. 20 S., R. 6 E. (M. D. B. and M.), Reliz Canyon.

TABLE 1.—*Occurrence of phosphate rock in California*—Con.

[H. B. and M., Humboldt base line and meridian; M. D. B. and M., Mount Diablo base line and meridian; S. B. B. and M., San Bernardino base line and meridian]

Locality No.	Description	Location
	Monterey County—Continued	
22	Phosphatic mollusk shells, nodules and scattered pellets in the lower Pliocene Pancho Rico Formation (D. L. Durham, oral communication, 1963).	T. 20 S., R. 9 E. (M. D. B. and M.).
23	Phosphate pellets in the basal part of the Pliocene, Pancho Rico Formation (Bramlette and Daviess, 1945; Hughes, 1963, p. 94–95).	On east line of sec. 15, T. 21 S., R. 9 E. (M. D. B. and M.).
24	Phosphate pellets in the Miocene Monterey Formation (D. L. Durham, oral communication, 1964).	SE¼ sec. 9, T. 21 S., R. 7 E. (M. D. B. and M.).
25	Phosphate pellet beds in the Miocene Monterey Formation (Durham, 1964).	NW¼NW¼ sec. 32, T. 21 S., R. 9 E. (M. D. B. and M.).
26	Phosphate pellets and phosphatic mollusk shells in the lower Pliocene Pancho Rico Formation (D. L. Durham, oral communcation, 1964). Hughes (1963, p. 94–95) also mentions phosphate in the Pancho Rico Formation in the Salinas Valley.	T. 22 S., R. 10 E., sec. 5 (M. D. B. and M.).
27	Thin phosphate-pellet bed in the Miocene Monterey Formation (D. L. Durham, oral communication, 1963).	T. 23, S., R. 8 E. (M. D. B. and M.), west side of Tule Canyon.
	Kings County	
28	Phosphate pellets in lower part of the Miocene McLure Shale Member of the Monterey Formation (Woodring and others, 1940, p. 126; Galliher, 1931, p. 258; Galloway, 1943, p. 492; and Henny, 1930, p. 404).	T. 23 S., R. 17 E. (M. D. B. and M.), Kettleman Hills oil field.
29	Phosphate pellets in the Miocene Temblor Formation (Curtin, 1955, p. 28).	T. 24, S., R. 18 E. (M. D. B. and M.), Pyramid Hills oil field.
	San Luis Obispo County	
30	Five-inch nodular phosphate bed in middle Miocene shale.	NW¼SW¼ sec. 24, T. 25 S., R. 16 E. (M. D. B. and M.), roadcut east side U.S. Highway 466.
31	Phosphate pellet beds and scattered pellets through 75-foot section of siliceous shale and siltstone of the Miocene Santa Margarita(?) Formation.	NE¼NW¼ sec. 13, T. 29 S., R., 16 E. (M. D. B. and M.).
32	Abundant phosphate pellet beds in the upper part of the Miocene Monterey Formation (Reed, 1927, p. 195; Kleinpell, 1938, p. 121–122; and Bramlette, 1946, pl. 2).	Indian Creek area, sec. 20, T. 28 S., R. 15 E. (M. D. B. and M.).

TABLE 1.—*Occurrence of phosphate rock in California*—Con.

[H. B. and M. Humboldt base line and meridian; M. D. B. and M., Mount Diablo base line and meridian; S. B. B. and M., San Bernardino base line and meridian]

Locality No.	Description	Location
	San Luis Obispo County—Continued	
33	Minor pelletal phosphate in the Miocene Monterey Formation.	SE¼SE¼ sec. 14, T. 11 N., R. 28 W. (S. B. B. and M.).
	Kern County	
34	Phosphate pellets and pellet beds in the Miocene Temblor Formation (Woodring and others, 1940, p. 130).	NW¼SE¼ sec. 9, T. 29 S., R. 20 E. (M. D. B. and M.), Zemorra Creek.
35	Phosphatic nodules in the Kern River Series (Pliocene?) of Diepenbrock (1933, p. 12).	T. 27 S., R. 28 E. (M. D. B. and M.), Mount Pozo oil field.
36	Scattered phosphate streaks in shale of Miocene age (Kasline, 1941, p. 9).	T. 28 S., R. 25 E. (M. D. B. and M.), Rio Bravo oil field.
37	Considerable number of phosphate pellets in lower Miocene rocks (Wharton, 1943, p. 503; Galliher, 1931, p. 258).	T. 27 S., R. 20 E. (M. D. B. and M.), Belridge oil field.
38	Phosphate nodules and stringers in the Miocene Monterey Formation (Woodring and others, 1940, p. 125).	T. 29 S., R. 20 E (M. D. B. and M.), Chico-Martinez Creek.
	Santa Barbara County	
39	Pelletal phosphate in siliceous shale, lower part of the Miocene Santa Margarita Formation (J. G. Vedder, oral communication, 1963). Pellets not identified as phosphate mentioned by Hill and others (1958, p. 2,996).	1,482,000 ft. W., 509,600 ft. N., California plane coordinate system, east side of Branch Canyon.
40	Phosphate pellets and pellet beds in siltstone and siliceous shale, upper part of the Miocene Santa Margarita Formation. Phosphate zone is more than 80 feet thick (J. G. Vedder, oral communication, 1963).	T. 9N., R. 26 W., S. B. B. and M., exposed in roadcuts 1,491,000 ft. W., 509,600 ft. N., California plane coordinate system.
41	Phosphate nodules and laminae in siliceous and calcareous shales, lower member of the Miocene Monterey Formation (Woodring and Bramlette, 1950, p. 21.)	T. 10 N., R. 36 W. (S. B. B. and M.), on the coast near Mussel Rock.
42	Phosphatic nodules and laminae in siliceous and calcareous shales of the lower member of the Miocene Monterey Formation (Woodring and Bramlette, 1950, p. 18–20).	T. 9 N., R. 36 W. (S. B. B. and M.), on the coast near Lions Head.
43	Phosphatic pellets and nodules in the upper Miocene to lower Pliocene Sisquoc Formation (Woodring and Bramlette, 1950, p. 29).	T. 9 N., R. 32 W. (S. B. B. and M.), Gato Ridge, Foxen Canyon area.

TABLE 1.—*Occurrence of phosphate rock in California*—Con.

[H. B. and M., Humboldt base line and meridian; M. D. B. and M., Mount Diablo base line and meridian; S. B. B. and M., San Barnardino base line and meridian]

Locality No.	Description	Location
	Santa Barbara County—Continued	
44	Phosphatic nodules in upper Miocene to lower Pliocene Sisquoc Formation (T. W. Dibblee, Jr., oral communication, 1963).	T. 6 N., R. 33 W. (S. B. B. and M.), along Santa Ynez River.
45	Phosphate pellets in the lower Miocene Rincon Shale (T. W. Dibblee, Jr., oral communication, 1963).	West of Gaviota Pass on south side of Santa Ynez Mountains.
46	Phosphatic shale (probably not pelletal), in the Miocene Monterey Formation (Bramlette, 1946, pl. 2).	Along Bixby Canyon near Point Conception.
47	Phosphate pellets in rocks of early Miocene age (Kribbs, 1943, p. 375).	T. 5 N., R. 30 W. (S. B. B. and M.), Capitan oil field.
48	Phosphatic shales (probably nonpelletal), in the Miocene Monterey Formation (Bramlette, 1946, pl. 2).	T. 4 N., R. 29 W. (S. B. B. and M.), sea cliffs west of Naples.
49	Phosphate pellets in rocks of early Miocene age (Hill, 1943, p. 381).	T. 4 N., R. 29 W. (S. B. B. and M.), Elwood oil field.
50	Abundant phosphate pellets in lower Miocene rocks (Bandy and Kolpack, 1963, p. 136, 155).	T. 5 N., R. 27 W. (S. B. B. and M.), in Tecolote Tunnel.
	Ventura County	
51	Abundant phosphate pellets and pellet beds in upper Miocene shales (W. R. Dickinson, oral communication, 1964).	Sec. 1, T. 6 N., R. 24 W., and sec. 6, T. 6 N., R. 23 W. (S. B. B. and M.).
52	Phosphate reported by Tucker and Samson (1932, p. 270). May be in Pliocene sedimentary deposits.	T. 3 N., R. 21 W. (S. B. B. and M.).
53	Phosphatic shales in the Monterey Formation (Bramlette, 1946, pl. 2).	Sec. 31, T. 4 N., R. 19 W. (S. B. B. and M.), Grimes Canyon.
	Los Angeles County	
54	Phosphatic "material" in upper Miocene sedimentary rocks (Nelson, 1952, p. 60).	T. 4 N., R. 17 W. (S. B. B. and M.), Del Valle oil field.
55	Phosphatic shales in the Miocene Modelo Formation (Winterer and Durham, 1962, p. 287).	T. 3 N., R. 16 W. (S. B. B. and M.).
56	Phosphatic shales in the basal part of the Miocene Modelo Formation (Kleinpell, 1938, p. 47).	Sec. 35, T. 1 N., R. 17 W. (S. B. B. and M.).
57	Pelletal phosphate in the basal part of the Miocene Modelo Formation (Hoots, 1930, p. 105–106; Bramlette, 1946, pl. 2).	T. 1 S., R. 15 W. (S. B. B. and M.).

TABLE 1.—*Occurrence of phosphate rock in California*—Con.

[H. B. and M., Humboldt base line and meridian; M. D. B. and M. Mount Diablo base line and meridian; S. B. B. and M., San Barnardino base line and meridian]

Locality No.	Description	Location
	Los Angeles County—Continued	
58	Phosphatic nodules in siliceous shales of the Miocene Monterey Formation (R. F. Yerkes, oral communication, 1963).	T. 2 S., R. 18 W. (S. B. B. and M.), south side of Dume Cove.
59	Nodular phosphate in the upper Miocene Puente Formation (Hodges, 1944, p. 6).	T. 2 S., R. 15 W. (S. B. B. and M.), Playa del Ray oil field.
60	Phosphatic nodules in upper Miocene shale (Davis, 1943, p. 299).	T. 4 S., R. 14 W. (S. B. B. and M.), Torrance oil field.
61	Phosphate nodules in Pleistocene Lomita Marl (Tucker, 1927, p. 328; Dietz and others, 1942, p. 831; Rogers, 1944, p. 421; and Emery and Dietz, 1950, p. 12).	T. 4 S., R. 14 W. (S. B. B. and M.), Lomita quarry.
62	Phosphatic shale, Altamira Shale Member of the Miocene Monterey Formation (Woodring and others, 1936, p. 139).	T. 5 S., R. 15 W. (S. B. B. and M.), Lunada Bay.
63	Phosphatic laminae in Valmonte Diatomite Member of the Miocene Monterey Shale (Woodring and others, 1946, p. 34).	T. 4 S., R. 15 W. (S. B. B. and M.), Malaga Cove.
64	Phosphatized Foraminifera of early(?) Miocene age (Olmsted, 1958, p. 65).	Wilson Cove, San Clemente Island.
	San Bernardino County	
65	Phosphatic nodules in upper Miocene Yorba Member of the Puente Formation (Durham and Yerkes, 1964, p. B59).	Secs. 21 and 22, T. 3 S., R. 8 W. (S. B. B. and M.), in San Juan Tunnel.
	Orange County	
66	Phosphate nodules in the Miocene Monterey Formation (J. G. Vedder, oral communication, 1963). Emery and Dietz (1950, p. 12) report large phosphatic nodules in marine conglomerate overlying the Monterey Formation at Newport Bay.	4,200 ft. N., 700 ft. E. of SE cor. sec. 26, T. 6 S., R. 10 W. (S. B. B. and M.), Newport Bay.
	San Diego County	
67	White phosphatic calcareous bed (Merrill, 1916, p. 717). Probably in the Pliocene San Diego Formation.	T. 18 S., R. 2 W. (S. B. B. and M.), mesa east of Otay.

[1] E. E. Brabb, 1960, Geology of the Big Basin area, Santa Cruz Mountains, California: Stanford Univ., unpub. Ph.D. thesis, 192 p.

shale, 18 percent phosphate pellet beds, and 7 percent bentonite laminae and beds. The siliceous shale is laminated to very thin bedded and locally contains abundant fish remains, chiefly scales, and scattered phosphate pellets. The pellet beds range from a fraction of an inch to 10 inches in thickness. They have sharp irregular to planar bases and grade upward into the overlaying siliceous shale. Most pellet beds contain a few (less than 1 percent) coarse quartz grains. Foraminiferal studies by Patsy B. Smith (oral communication, 1963) indicate that the phosphatic zone contains a shallow-water fauna.

A chemical analysis of a pellet concentrate from Indian Creek is shown in table 2. The chemical analysis and the results of X-ray diffraction studies show that the phosphate mineral is carbonate-fluorapatite. X-ray studies of phosphorite samples from 20 other localities listed in table 1 have been made, and all but 2 had similar mineralogy. The two exceptions are the nonmarine phosphate of locality 1 and the leucophosphite of locality 12.

TABLE 2.—*Chemical analysis of a pelletal phosphate concentrate from locality 32, Indian Creek area, San Luis Obispo County* [1]

Constituent	*Percentage*
SiO_2	1.3
Al_2O_3	1.0
Fe_2O_3	.28
FeO	.08
MgO	.19
CaO	51.8
Na_2O	.43
K_2O	.07
H_2O-	1.5
H_2O+	2.2
TiO_2	.10
P_2O_5	35.7
MnO	0
CO_2	2.5
F	4.0
Deduct O_2 equivalent to F	(−1.7)
Total	99.45

[1] Collected by R. A. Gulbrandsen. Rapid rock analysis by P. Elmore, S. Botts, G. Chloe, and H. Smith.

Among the California occurrences, the pelletal phosphorites of middle and late Miocene age appear to offer the most promise of being commercially valuable. Particularly promising are deposits in the upper Miocene Santa Margarita Formation along the southeast-trending belt through localities 31, 40, and 51 (fig. 1) of San Luis Obispo, Santa Barbara, and Ventura Counties, and those in the middle and upper Miocene Monterey Formation in Monterey and San Luis Obispo Counties. The lower Miocene pelletal phosphorites along the west side of the San Joaquin Valley also deserve attention. Some of the nodular and argillaceous laminar phosphatic shales of western and southern Santa Barbara and western Los Angeles Counties are more than 200 feet thick and appear to contain large tongues of phosphate. They are of low grade, however, and their high calcium carbonate content would hinder their use by normal acid-treatment procedures.

REFERENCES

Anderson, J. Q., 1952, Guijarral Hills oil field, *in* Field trip routes, geology, oil fields: Am. Assoc. Petroleum Geologists, Soc. Econ. Paleontologists and Mineralogists, and Soc. Econ. Geologists Guidebook, Joint Ann. Mtg., Los Angeles, Calif., 1952, p. 184–188.

Bandy, O. L., and Kolpack, R. L., 1963, Foraminiferal and sedimentological trends in the Tertiary sections of the Telcolote Tunnel, California: Micropaleontology, v. 9, no. 2, p. 117–170.

Bramlette, M. N., 1946, The Monterey formation of California and the origin of its siliceous rocks: U.S. Geol. Survey Prof. Paper 212, 57 p.

Bramlette, M. N., and Daviess, S. N., 1945, Geology and oil possibilities of the Salinas Valley, California: U.S. Geol. Survey Oil and Gas Inv. Prelim. Map 24.

Cummings, J. C., Touring, R. M., and Brabb, E. E., 1962, Geology of the northern Santa Cruz Mountains, California: California Div. Mines Geol. Bull. 181, p. 179–220.

Curtin, George, 1955, Pyramid Hills oil field [California]: California Oil Fields, v. 41, no. 2, p. 25–33.

Davis, E. L., 1943, Torrance oil field, *in* Geologic formations and economic development of the oil and gas fields of California: California Div. Mines Bull. 118, p. 298–300.

Diepenbrock, Alex, 1933, Mt. Poso oil field: California Oil Fields, v. 19, no. 2, p. 4–35.

Dietz, R. S., Emery, K. O., and Shepard, F. P., 1942, Phosphorite deposits on the sea floor off southern California: Geol. Soc. America Bull., v. 53, no. 6, p. 815–848.

Durham, D. L., 1964, Geology of the Cosio Knob and Espinosa Canyon quadrangles, Monterey County, California: U.S. Geol. Survey Bull. 1161–H.

Durham, D. L., and Yerkes, R. F., 1964, Geology and oil resources of the eastern Puente Hills area, southern California: U.S. Geol. Survey Prof. Paper 420–B, p. B1–B62.

Emery, K. O., and Dietz, R. S., 1950, Submarine phosphorite deposits off California and Mexico: California Jour. Mines and Geol., v. 46, no. 1, p. 7–15.

Galliher, E. W., 1931, Collophane from Miocene brown shales of California: Am. Assoc. Petroleum Geologists Bull., v. 15, no. 3, p. 257–269.

Galloway, John, 1943, Kettleman Hills oil fields, *in* Geologic formations and economic development of the oil and gas fields of California: California Div. Mines Bull. 118, p. 491–493.

Gulbrandsen, R. A., Jones, D. L., Tagg, K. M., and Reeser, D. W., 1963, Apatitized wood and leucophosphite in nodules in the Moreno Formation, California: Art. 85 *in* U.S. Geol. Survey Prof. Paper 475–C, p. C100–C104.

Henny, Gerard, 1930, McLure shale of the Coalinga region, Fresno and Kings Counties, California: Am. Assoc. Petroleum Geologists Bull., v. 14, no. 4, p. 403–410.

Hill, M. L., 1943, Elwood oil field, *in* Geologic formations and economic development of the oil and gas fields of California: California Div. Mines Bull. 118, p. 380–383.

Hill, M. L., Carlson, S. H., and Dibblee, T. W., Jr., 1958, Stratigraphy of Cuyama Valley-Caliente Range area, California: Am. Assoc. Petroleum Geologists Bull., v. 42, no. 12, p. 2973–3000.

Hodges, F. C., 1944, Gas storage and recent developments in the Playa del Rey oil field [California]: California Oil Fields, v. 30, no. 2, p. 3–10.

Hoots, H. W., 1930, Geology of the eastern part of the Santa Monica Mountains, Los Angeles County, California: U.S. Geol. Survey Prof. Paper 165–C, p. 83–134.

Hughes, A. W., 1963, The two sides of Salinas, *in* Guidebook to the geology of Salinas Valley and the San Andreas fault: Am. Assoc. Petroleum Geologists, Pacific Sec., Ann. Mtg. 1963, p. 94–97.

Kasline, F. E., 1941, Rio Bravo oil field [California]: California Oil Fields, v. 27, p. 9–12.

Kleinpell, R. M., 1938, Miocene stratigraphy of California: Tulsa, Okla., Am. Assoc. Petroleum Geologists, 450 p.

Knox, G. L., 1943, McDonald Island gas field, *in* Geologic formations and economic development of the oil and gas fields of California: California Div. Mines Bull. 118, p. 588–590.

Kribbs, G. R., 1943, Capitan oil field, *in* Geologic formations and economic development of the oil and gas fields of California: California Div. Mines Bull. 118, p. 374–376.

Merrill, F. J. H., 1916, The counties of San Diego, Imperial: California Mining Bur., 14th Rept. State Mineralogist, pt. 5, p. 635–743.

Nelson, L. E., 1952, Del Valle and Ramona oil fields, *in* Field trip routes, geology, oil fields: Am. Assoc. Petroleum Geologists, Soc. Econ. Paleontologists and Mineralogists, and Soc. Econ. Geologists Guidebook, Joint Ann. Mtg., Los Angeles, Calif., 1952, p. 57–63.

Olmsted, F. H., 1958, Geologic reconnaissance of San Clemente Island, California: U.S. Geol. Survey Bull. 1071–B, p. 55–68.

Payne, M. B., 1951, Type Moreno formation and overlying Eocene strata on the west side of the San Joaquin Valley, Fresno and Merced Counties, California: California Div. Mines Spec. Rept. 9, 29 p.

Reed, R. D., 1927, Phosphate beds in the Monterey Shales [abs.]: Geol. Soc. America Bull., v. 38, no. 1, p. 195–196.

Rogers, A. F., 1944, Pellet phosphorite from Carmel Valley, Monterey County, California: California Jour. Mines and Geology, v. 40, no. 4, p. 411–421.

Thomson, J. N., 1962, Geology of the Kione Formation: San Joaquin Geol. Soc. Selected Papers, v. 1, p. 27–35.

Thorup, R. R., 1943, Type locality of the Vaqueros formation, *in* Geologic formations and economic development of the oil and gas fields of California: California Div. Mines Bull. 118, p. 463–466.

Tolman, F. B., 1943, Potrero Hills gas field *in* Geologic formations and economic development of the oil and gas fields of California: California Div. Mines Bull. 118, p. 595–598.

Tucker, W. B., 1926, Inyo County: California Mining Bur., 22d Rept. State Mineralogist, v. 22, no. 4, p. 453–530.

——— 1927, Los Angeles County: California Mining Bur., 23d Rept. State Mineralogist, no. 3, p. 287–345.

Tucker, W. B., and Sampson, R. J., 1932, California Mining Bur., 28th Rept. State Mineralogist, no. 3, p. 247–277.

Wharton, J. B., 1943, Belridge oilfield, *in* Geologic formations and economic development of the oil and gas fields of California: California Div. Mines Bull. 118, p. 502–504.

Winterer, E. L., and Durham, D. L., 1962, Geology of southeastern Ventura basin, Los Angeles County, California: U.S. Geol. Survey Prof. Paper 334–H, p. 275–366.

Woodring, W. P., and Bramlette, M. N., 1950, Geology and paleontology of the Santa Maria district, California: U.S. Geol. Survey Prof. Paper 222, 185 p.

Woodring, W. P., Bramlette, M. N., and Kew, W. S. W., 1946, Geology and paleontology of Palos Verdes Hills, California: U.S. Geol. Survey Prof. Paper 207, 145 p.

Woodring, W. P., Bramlette, M. N., and Kleinpell, R. M., 1936, Miocene stratigraphy and paleontology of Palos Verdes Hills, California: Am. Assoc. Petroleum Geologists Bull., v. 20, no. 2, p. 125–149.

Woodring, W. P., Stewart, Ralph, and Richards, R. W., 1940, Geology of the Kettleman Hills oil field, California; stratigraphy, paleontology, and structure: U.S. Geol. Survey Prof. Paper 195, 170 p.

THE DISTRIBUTION AND QUALITY OF OIL SHALE IN THE GREEN RIVER FORMATION OF THE UINTA BASIN, UTAH-COLORADO

By W. B. CASHION, Denver, Colo.

Abstract.—Oil-shale beds of the Green River Formation (Eocene) were deposited in an unusual lacustrine environment that preserved thick sequences of kerogenaceous material. These beds are an important potential source of liquid synthetic fuel. Incomplete oil-yield assay data indicate that in the Uinta Basin a sequence of kerogen-rich beds 15 feet or more thick with an average oil yield of 15 gallons per ton contain about 321 billion barrels of oil.

The extensive thick oil-shale beds of the Rocky Mountain region are of prime importance as a possible source of synthetic liquid fuel. The Green River Formation of Eocene age underlying parts of Utah, Colorado, and Wyoming contains much of the oil-shale resources of the United States. A large portion of the Green River oil-shale beds lies in the Uinta Basin of Utah and westernmost Colorado.

The physical and mineralogic characteristics of the oil-shale beds of the Green River Formation have been described in detail by Bradley (1931, p. 22–37, 39–40), and some of these characteristics are discussed below. The oil shales are dense magnesian marlstones with a high content of organic matter. The organic matter is of two types: (1) structureless, translucent, and lemon yellow to reddish brown material, and (2) complete or fragmentary remains of organisms such as algae, protozoa, and insects, and parts of higher plants —spores, pollen grains, or minute pieces of tissue. The predominant inorganic constituents of the shale are dolomite, calcite, and clay minerals.

Oil shale contains little or no free oil that can be removed by petroleum solvents, but the organic matter (kerogen) can be converted to oil by destructive distillation at high temperature, commonly known as retorting.

The Green River Formation is composed predominantly of lacustrine beds deposited for the most part in two large lakes. One of these lakes was north of the present Uinta Mountains and lay almost entirely in southwestern Wyoming and northwesternmost Colorado. The other was south of the Uinta Mountains in eastern Utah and western Colorado and lay principally in the area now occupied by the Uinta and Piceance Creek basins. Bradley (1930, p. 88) referred to the northern lake as Lake Gosiute and the southern lake as Lake Uinta. The precise age relation of the two Eocene lakes is not known, but they were, in part, contemporaneous. During part of Green River time these lakes may have been connected around the eastern end of the Uinta Mountains, but evidence of such a connection, if it ever existed, has been removed by erosion. The present-day Uinta and Piceance Creek basins are separated by a structurally high area, the Douglas Creek arch, but it is postulated that during much of Green River time these areas were covered by one body of water, for there is a remarkable similarity between the oil-shale sequences in the two basins. In many cases, precise correlation can be achieved by a comparison of oil-yield histograms representing assays of cored sections of the basin.

The strata of the Green River Formation can be divided roughly into three lithologic groups, each one representing a particular lacustrine environment. One group is characterized by beds of algal, ostracodal, and oolitic limestone, shale, siltstone, and sandstone, and contains negligible amounts of kerogenaceous matter. These beds were deposited in shallow water near the margins of the lake and are peripheral to, and interfinger basinward with, beds deposited in the other two environments. A second group contains beds of marlstone, siltstone, tuff, and minor amounts of oil shale. The environment of this group of beds was located far enough from shore to prevent the deposi-

tion of coarse clastic material and was in water deep enough to prevent disturbance by wave or current action. If abundant kerogenaceous matter was deposited in this environment it was not preserved. The third group of beds, composed of oil shale, marlstone, and tuff, was, for the most part, deposited along the trough of the lake near the axis of deposition. This environment was conducive to the accumulation and preservation of kerogenaceous matter and thus produced the thick oil-shale sequence of the Green River Formation. Bradley (1926, p. 127) postulated that the rich oil shale formed in water that was probably less than 100 feet deep, and apparently resulted from a periodic concentration of organic matter due to a very pronounced reduction in the volume of the lake. Chemical and thermal stratification of the lake waters played an important role in the deposition of oil-shale beds (Bradley, 1948, p. 644). Stratification must have been a more critical factor than depth of water, for numerous widespread continuous thin rich oil-shale beds can be correlated from the Uinta Basin to the Piceance Creek basin, and it is unlikely that the lake was of uniform depth over such a large area during the deposition of each bed. Also, in the areas where oil-shale sequences interfinger with nearshore sequences, some oil-shale beds show mud cracks or lie adjacent to algal limestone, denoting shallow-water deposition.

Many fluctuations in the size and depth of the lake produced complex interfingering and facies changes between the lithologic groups described above, as well as interfingering and facies changes involving nearshore lacustrine deposits and fluvial deposits. Above, below, and peripheral to the main body of the Green River Formation there are sandstone, conglomerate, and shale beds of fluvial formations that interfinger with it. Fluctuations of the lake, and the accompanying decrease or increase of the inflow of clastic material, enlarged or reduced the area in which oil-shale beds were being deposited but had little effect on these beds near the axis of deposition. The position of this axis did not change greatly during much of Green River time, and a thick sequence of organic-rich beds accumulated. The axis trends roughly east-west, and its position can be determined from the location of lines showing maximum thickness of oil-shale beds on figure 1. The position of the axis is obvious in the area east of the Green River, but is poorly defined in the area west of the river. Reliable assay data in the western area are scarce, so the reason for the poor delineation of the axis by oil-shale thickness is not known. Perhaps the environmental conditions of this area were not favorable for the accumulation of a thick oil-shale sequence or perhaps assay data from additional drill holes will show a more pronounced depositional trend.

The richest and thickest oil-shale bed in the Green River Formation is the Mahogany bed. This bed, deposited during a stage when Lake Uinta was widespread, is found over a very large area in the Piceance Creek and Uinta basins. Its outcrop in the Uinta Basin is shown on figure 1. The maximum outcrop thickness of the Mahogany bed in the Uinta Basin is about 8 feet, along the White River approximately 5 miles west of the Utah-Colorado boundary. Its maximum thickness is in the subsurface along the depositional axis of the basin, and it thins in all directions away from the depositional axis. The Mahogany bed and adjacent rich oil-shale beds form a prominent outcrop feature—the Mahogany ledge, the subsurface correlative of which is the Mahogany zone. The maximum thickness in outcrop of the ledge is about 60 feet at the White River locality mentioned above. The ledge thins more abruptly away from the depositional axis than does the Mahogany bed, and in much of the southern part of the Uinta Basin the Mahogany ledge is formed by only the Mahogany bed. Near the axis of deposition, stratigraphic sequences a few hundred feet thick above and below the Mahogany ledge contain many oil-shale beds. In the southwestern part of the Uinta Basin a significant lower oil-shale zone (fig. 1), below the Mahogany bed, was mapped by Bradley (1931, pl. 1). This zone is not present in the southernmost part of the basin and was not mapped in the easternmost part.

Estimates of oil-shale resources are based on the oil-yield assay data from groups of samples that, for the most part, represent continuous rock sequences. These sequences are represented by assays of cores, rotary-drill cuttings, and outcrop channel samples. Actual oil yields of stratigraphic sections are most accurately represented by assay data from cores. Rotary cuttings are less accurate than cores, owing to the possibility of contamination during drilling or human error during collection. Generally, surface samples are less reliable than subsurface samples, because of weathering. For example, a sample of weathered shale from the Mahogany bed assayed 12.8 gallons of oil per ton, whereas an unweathered sample of the bed taken 2 feet beneath the surface at the same locality assayed 45.5 gallons per ton (Guthrie, 1938, p. 99). Although assay oil yields of weathered samples are known to be low, a constant upgrading factor cannot be applied because of great variation in the weathering of oil-shale beds.

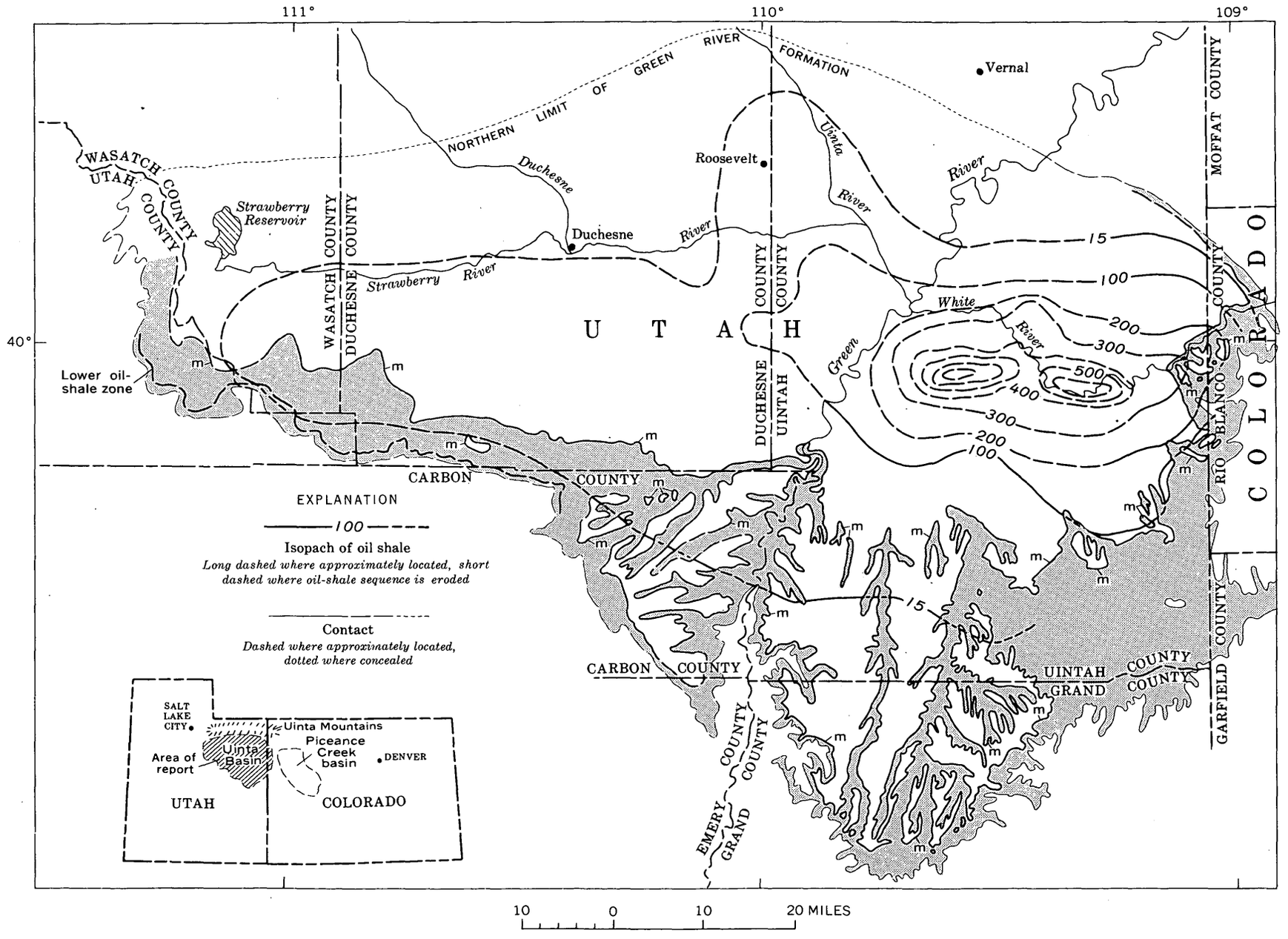

FIGURE 1.—Map of the Uinta Basin area, showing thickness, in feet, of oil-shale beds in the Green River Formation that will yield an average of 15 gallons of oil per ton. Thickness interval is 100 feet, with a 15-foot cutoff. Pattern shows outcrop area of the part of the Green River Formation underlying the Mahogany bed (m). Outcrop area west of the Green River modified from Bradley (1931, pl. 1).

Assays of groups of samples representing 40 core holes, 110 exploratory wells, and about 25 surface localities were used in the estimate of oil-shale resources given here.

Core-hole and exploratory-well assay data used to calculate resource figures for this report have been published by the U.S. Bureau of Mines (Stanfield and others, 1954; 1964). All the core holes are located in the southeastern part of the basin, and most of the exploratory wells are located in the eastern part of the basin. Thus, control points of any type are sparse in the western part of the basin, and there are no core-assay data to substantiate rotary-cuttings data from a critical part of the eastern Uinta Basin. In addition, assays of cuttings from some wells in the east-central part of the basin show anomalous thicknesses of rich oil shale. Therefore, oil-shale beds in the area of relatively closely spaced core holes are classed as indicated resources, and the remainder of the oil-shale beds are classed as inferred resources.

The estimate of oil-shale resources given in this report is for a sequence of rocks, including the Mahogany ledge and adjacent beds, 15 feet or more thick having an average oil yield of 15 gallons per ton. No allowances are made for losses in mining or retorting. It is estimated that oil-shale beds of the Uinta Basin contain indicated resources amounting to 31 billion barrels of oil, most of which is in an area east of the Green River and south of the latitude of the mouth of the White River; the beds contain inferred resources of 290 billion barrels. This 321 billion barrels of resources is in an area of approximately 3,000 square miles and is in a sequence that is believed to have a maximum thickness of more than 700 feet.

REFERENCES

Bradley, W. H., 1926, Shore phases of the Green River Formation in northern Sweetwater County, Wyoming: U.S. Geol. Survey Prof. Paper 140–D, p. 121–131.

——— 1930, The varves and climate of the Green River epoch: U.S. Geol. Survey Prof. Paper 158–E, p. 87–110.

——— 1931, Origin and microfossils of the Green River Formation of Colorado and Utah: U.S. Geol. Survey Prof. Paper 168, 58 p.

——— 1948, Limnology and the Eocene lakes of the Rocky Mountain region: Geol. Soc. America Bull., v. 59, no. 7, p. 635–648.

Guthrie, Boyd, 1938, Studies of certain properties of oil shale and shale oil: U.S. Bur. Mines Bull. 415, 159 p.

Stanfield, K. E., Rose, C. K., McAuley, W. S., and Tesch, W. J., Jr., 1954, Oil yields of sections of Green River oil shale in Colorado, Utah, and Wyoming, 1945–52: U.S. Bur. Mines Rept. Inv. 5081, 153 p.

Stanfield, K. E., Smith, J. W., and Trudell, L. G., 1964, Oil yield of sections of Green River oil shale in Utah, 1952–62: U.S. Bur. Mines Rept. Inv. 6420, 217 p.

BTU VALUES OF FRUITLAND FORMATION COAL DEPOSITS IN COLORADO AND NEW MEXICO, AS DETERMINED FROM ROTARY-DRILL CUTTINGS

By JIM S. HINDS, Farmington, N. Mex.

Abstract.—Btu values of coal obtained from wells show that coal from the Fruitland Formation of Late Cretaceous age is of highest quality in the northwest part of the San Juan basin when reported on an "as received" basis. On a "moisture and ash free" basis the Btu values show a steady increase from southwest to northeast.

A comprehensive study of the coal deposits of the Upper Cretaceous Fruitland Formation, which underlies the San Juan basin at depths of as much as 4,500 feet, was made to provide a basis for coal classification of public land remaining in outstanding coal-land withdrawals within the basin. To satisfy this objective it was necessary to determine the thickness, depth, and heating value of Fruitland coal deposits throughout the basin. As the Fruitland Formation crops out only in a narrow band on the north, west, and south sides of the basin (fig. 1), the study was necessarily a subsurface one and was conducted through examination of electric logs, drilling-rate logs, cores, and samples from rotary drill cuttings. This paper concerns the well sampling, which was undertaken primarily to obtain representative Btu values of Fruitland coal beds throughout the San Juan basin.

GEOLOGY

The Fruitland Formation of Late Cretaceous age consists of very irregularly bedded brackish- and fresh-water deposits of sandstone, siltstone, shale, and coal. It lies conformably above the regressive marine Pictured Cliffs Sandstone and grades into the overlying Kirtland Shale of fresh-water origin. The beds are lenticular throughout the formation, and few of the rock units are persistent for distances greater than 1 or 2 miles. The coal beds, however, are more persistent than the associated sandstone and shale beds; some coal beds may be traced in the outcrop and subsurface for 4 to 6 miles. In addition to its lenticularity, the Fruitland Formation is characterized in the subsurface throughout the basin by intertonguing with the underlying Pictured Cliffs Sandstone. The intertonguing indicates temporary pauses and minor transgressions in the general regression of the sea.

Because of their lenticularity, the coal beds of the Fruitland Formation must be studied collectively. Generally speaking, the coal beds are thickest and most numerous in the northwest quadrant of the basin, where many wells have penetrated coal beds 30 to 40 feet thick, as indicated by samples and electric logs. The quality of Fruitland coal is also better in the northwest quadrant, ranging usually between 12,000 and 13,000 Btu per pound on an "as received" basis as opposed to values elsewhere generally of 10,000 to 12,000 Btu. The coal beds become progressively fewer and thinner toward the southern and eastern margins of the basin. On the east side of the basin, from Dulce to Cuba, N. Mex., the Fruitland Formation is missing from the outcrop, its eroded edge being covered by younger sedimentary rocks.

Figure 2 shows a well section of the Fruitland Formation, the electric-log response to the coal beds, and an analysis of Fruitland coal. This particular well, about 10 miles northeast of Farmington, N. Mex., was chosen for illustration because it depicts very nearly the average lithic character of the Fruitland Formation. Coal beds occur at random throughout the vertical extent of the formation, although there is usually a concentration or zone of coal beds in the lowest part of the formation. The coal may be directly overlain, underlain, or interbedded with either sandstone, siltstone, shale, or carbonaceous shale. This sequence of

U.S. GEOL. SURVEY PROF. PAPER 501-D, PAGES D90-D94

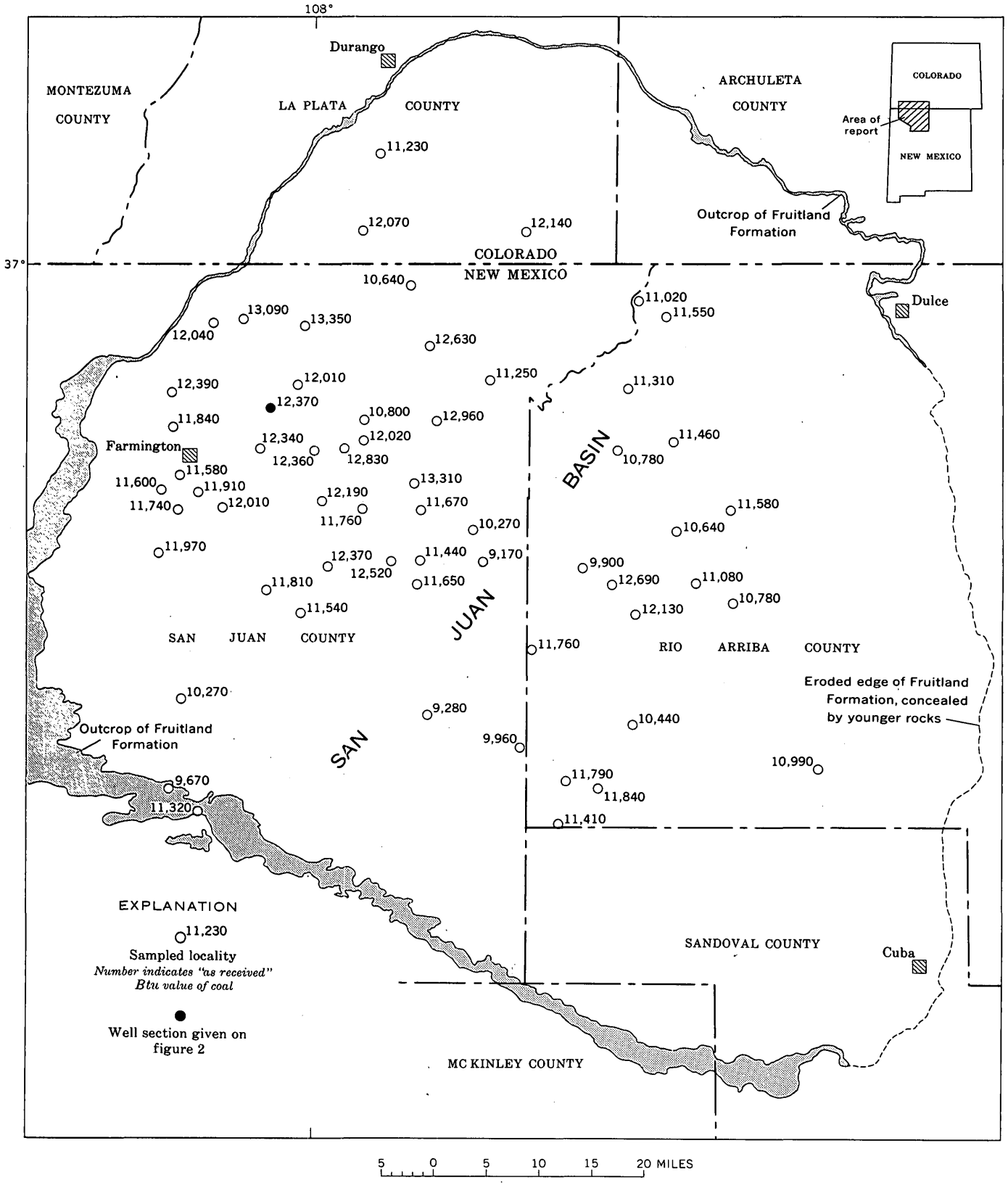

FIGURE 1.—Map showing outcrop of the Fruitland Formation, location of drill holes sampled, and "as received" Btu values of coal samples.

742-652 O—64——7

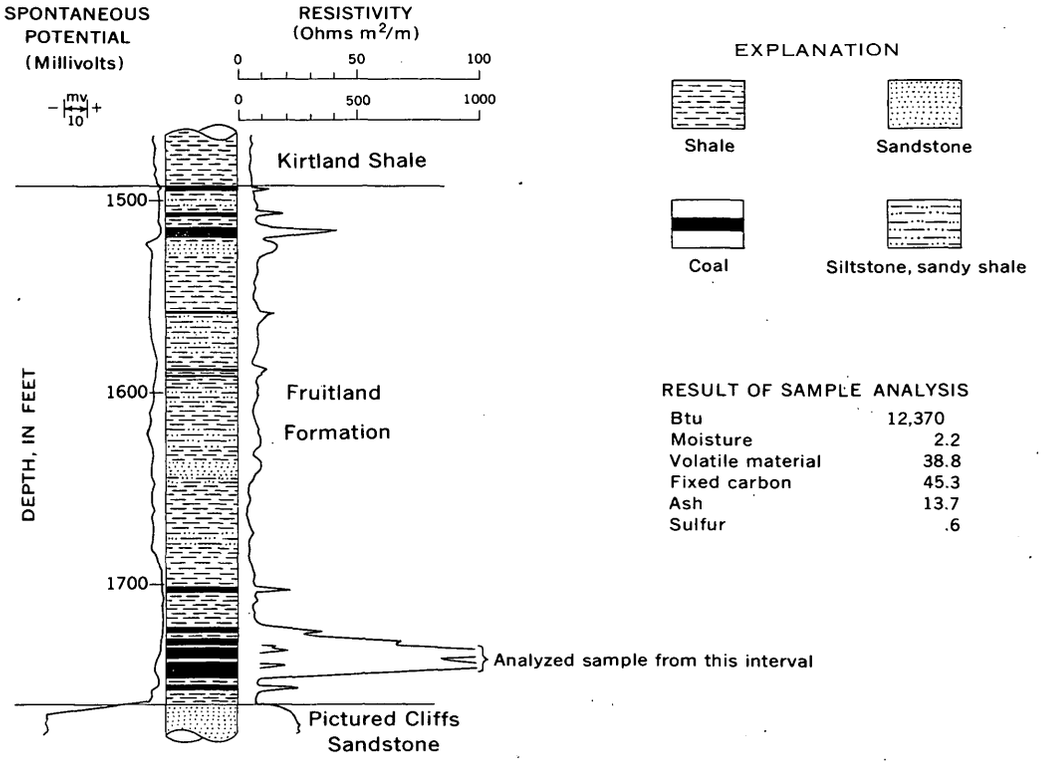

FIGURE 2.—Lithologic section and electric log of a well in the Fruitland Formation, showing typical occurrence of coal. Location of well shown on figure 1.

rocks definitely does not represent cyclic deposition, but rather a complex interbedding of coastal-swamp, flood-plain, and sluggish stream deposits which were laid down behind the shores of the Cretaceous sea as it withdrew to the northeast.

SAMPLING AND ANALYSIS

As of January 1964, various coal beds of the Fruitland Formation had been sampled at 64 separate well locations in the San Juan basin. The attempt was made at each locality to sample the lowest economically important coal bed or zone of the formation; later, one analysis per well was made of coal sampled. Sampling uncertainties prevented absolute consistency, but all samples were from the lower part of the formation if not the lowest coal bed. The samples were obtained by collection of cuttings from shale shakers as the cuttings from coal zones were discharged from the bore hole. After collection, the cuttings were thoroughly mixed to insure representative sampling, and then were washed at the well site to remove drilling mud. The samples then were dried by a cool forced-air current and floated in carbon tetrachloride (specific gravity 1.59) to remove rock cuttings and cavings picked up by the sample in the mud column during circulation (the specific gravity of coal ranges generally from 1.2 to 1.5). The lighter fraction from the floating process was then sent to the U.S. Bureau of Mines laboratory at Pittsburgh, Pa., for analysis. Because of the flotation, the resultant Btu values represent maximum figures for the heating values of the coals sampled. Any shale or sand partings and carbonaceous material with a specific gravity greater than 1.59 present in the sampled zone were removed through flotation. Hence, the reported values represent the heating value of the coal without partings. These samples would be comparable to regular channel mine samples from which all partings are excluded.

In addition to Btu data, information was obtained and recorded on moisture, volatile matter, fixed carbon, ash, and sulfur content of coal of the Fruitland Formation. These data are summarized in the accompanying table.

Major constituents of coal from the Fruitland Formation

Constituent	*Range (percent)*	*Average (percent)*
Moisture	0.8– 6.7	2.6
Volatile matter	20.6–41.7	35.8
Fixed carbon	33.3–56.4	43.2
Ash	9.8–30.5	18.4
Sulfur	0.5– 2.2	0.75

The location of sampled wells and the "as received" Btu values obtained at each location are shown on figure 1. The values range from 9,170 to 13,350. The distribution of the Btu values shows that the quality

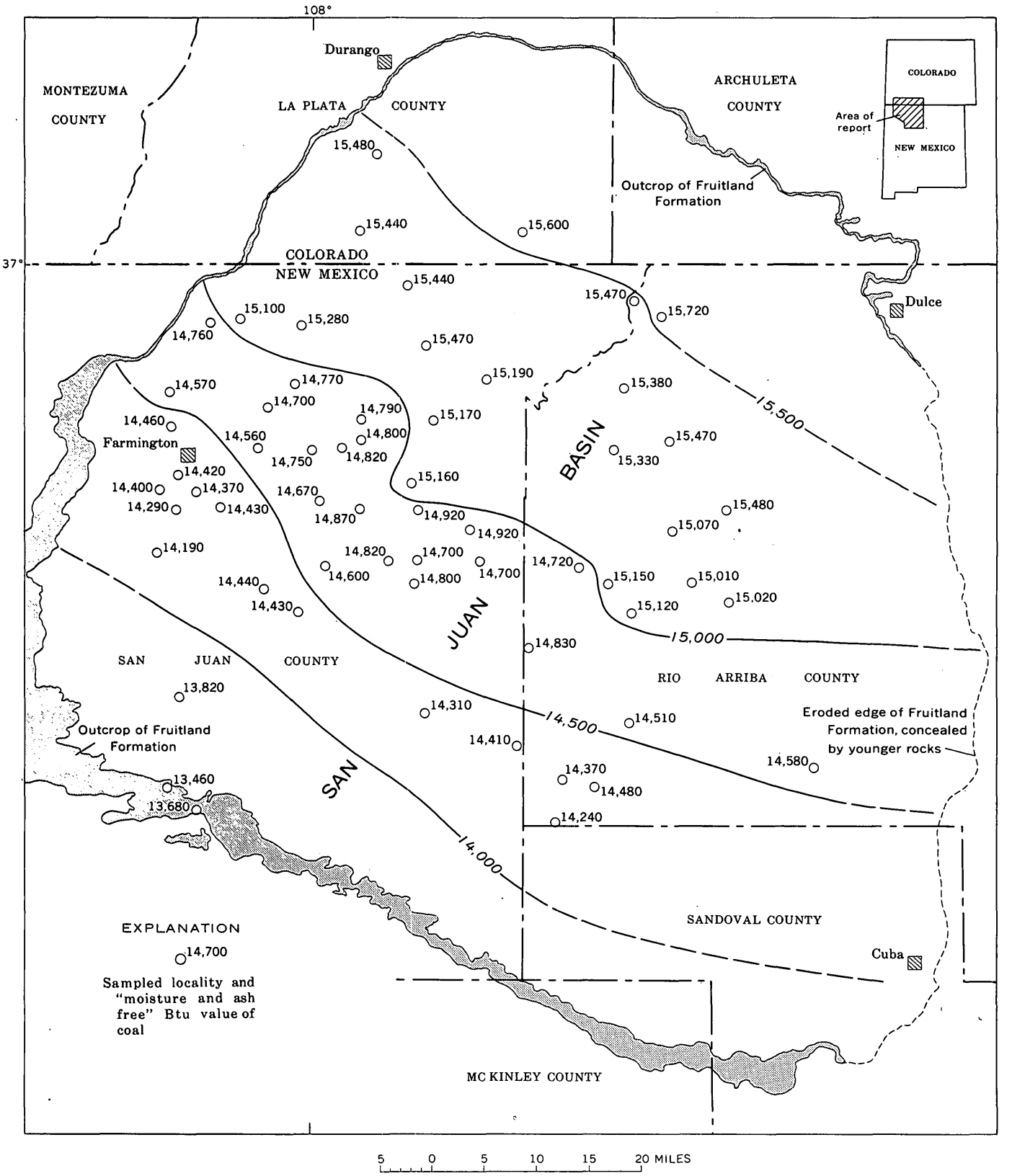

FIGURE 3.—Map showing "moisture and ash free" Btu values of coal samples from the Fruitland Formation.

of Fruitland coal, on an "as received" basis, is best in the northwest part of the San Juan basin, where most values exceed 12,000 Btu. In the rest of the basin most of the "as received" values are less than 12,000 Btu.

CONCLUSIONS

Figure 3 shows the "moisture and ash free" Btu values of the coal samples. In contrast to the "as received" values of figure 1, these values show a definite pattern, a regular increase from 13,460 in the southwest to 15,720 in the northeast. Zones characterized by about the same Btu values trend northwest across the basin. This direction nearly parallels the strandlines of the Pictured Cliffs and Fruitland Formations and is at right angles to the northeastward withdrawal of the sea. Thus the oldest coal deposits, those in the southwest part of the basin, have the lowest Btu values on a "moisture and ash-free" basis. The highest "moisture and ash-free" Btu values are found in the youngest coals in the northeast part of the basin. What this pattern of Btu values reflects is open to conjecture. It does not represent a pattern in the moisture and ash content, for these are random. The pattern could be due to differences in depth of burial, different types of original vegetation, slowly changing climatic conditions in Late Cretaceous time, thermal gradients affecting the buried coals, or possibly other factors as yet unrecognized.

GIANT SUBMARINE LANDSLIDES ON THE HAWAIIAN RIDGE

By J. G. MOORE, Menlo Park, Calif.

Abstract.—Topographic evidence indicates the presence of two large submarine landslides on the slope of the Hawaiian Ridge northeast of Oahu. One slide is more than 150 km long and moved on a slope with an overall gradient of about 2 degrees. A concave escarpment marks the head of the slides, and flat-topped tilted blocky seamounts occur on the middle and lower parts.

Several thousand square kilometers of irregular topography, quite distinct from surrounding regions, occurs northeast of the island of Oahu in Hawaii. The area is on the northeast slope of the Hawaiian Ridge, a volcanic ridge which extends 2,600 kilometers west-northwest from the island of Hawaii to Ocean Island. The irregular topography of the area is well shown on a U.S. Navy Oceanographic Office preliminary bathymetric map, part of which is reproduced on figure 1. The topography is characterized by elongate blocky seamounts with tilted relatively flat upper surfaces, as shown in the geologic section (fig. 2).

The topography and geologic setting of this area suggest that it represents the surface of two giant submarine landslides. The slides extend down the northeast slope of the Hawaiian Ridge and out on the adjacent ocean floor. They cross the axis of the Hawaiian Trench, an ocean deep flanking the ridge and presumably formed by downwarp of the crust due to the load of the volcanic pile which forms the ridge. Only the higher points on the surface of the lower end of the slides project above the level of the young sediments of the trench.

TOPOGRAPHY

The larger landslide, northeast of the island of Oahu, extends northeastward down the slope of the Hawaiian Ridge and is more than 160 km long and 50 km wide. The area of the slide is marked by a concave escarpment at its upper end and by a blocky welt in the middle and at the lower end. The blocky seamounts on the slide are commonly from 8 to 25 km long and 5 to 15 km wide. Almost all the seamounts are oriented with their long axes perpendicular to the long axis of the slide. Several of the blocks, including the largest one, are relatively flat on top, and this upper flat surface is tilted either toward or away from the Hawaiian Ridge. The majority of the blocks are tilted toward the ridge.

A geologic section through the axis of this slide (figs. 1 and 2) shows the rugged blocky relief of its upper surface. The individual blocks are commonly bounded by steep slopes up to 2,000 meters in height. The distance between crests of the blocky seamounts, or between the troughs of the intervening basins, is rather constant and averages about 15 km. Based on the surface topography, the geologic section was drawn to show the inferred subsurface structure of the slide (fig. 2). The sole of the slide is believed to be at a depth of about 6,000 m below sea level, and the slide averages 2,000 m in thickness.

The gradient of the upper part of the landslide, extending down to a depth of about 3,000 m, is approximately 6°. The average gradient of the surface of the slide from sea level to its lower end is about 2°. The sole of the slide is shown as being horizontal and at its lower end upward sloping, as is common with smaller landslides (Eckel, 1958, p. 24).

The second landslide extends northward down the slope from the north side of the island of Molokai. This feature is also about 50 km wide and is more than 80 km long; however, both slides coalesce at their lower ends, and the overall length of the second one is not known with certainty. Very likely it is older than the first one, because the lower part of it appears to be more deeply buried by deep-sea sediment near the axis of the Hawaiian Trench.

The upper end of this slide is also marked by a distinct concavity in the regional slope. The west-facing lateral scarp on the east side of this amphitheater is typical of such lateral scarps on many

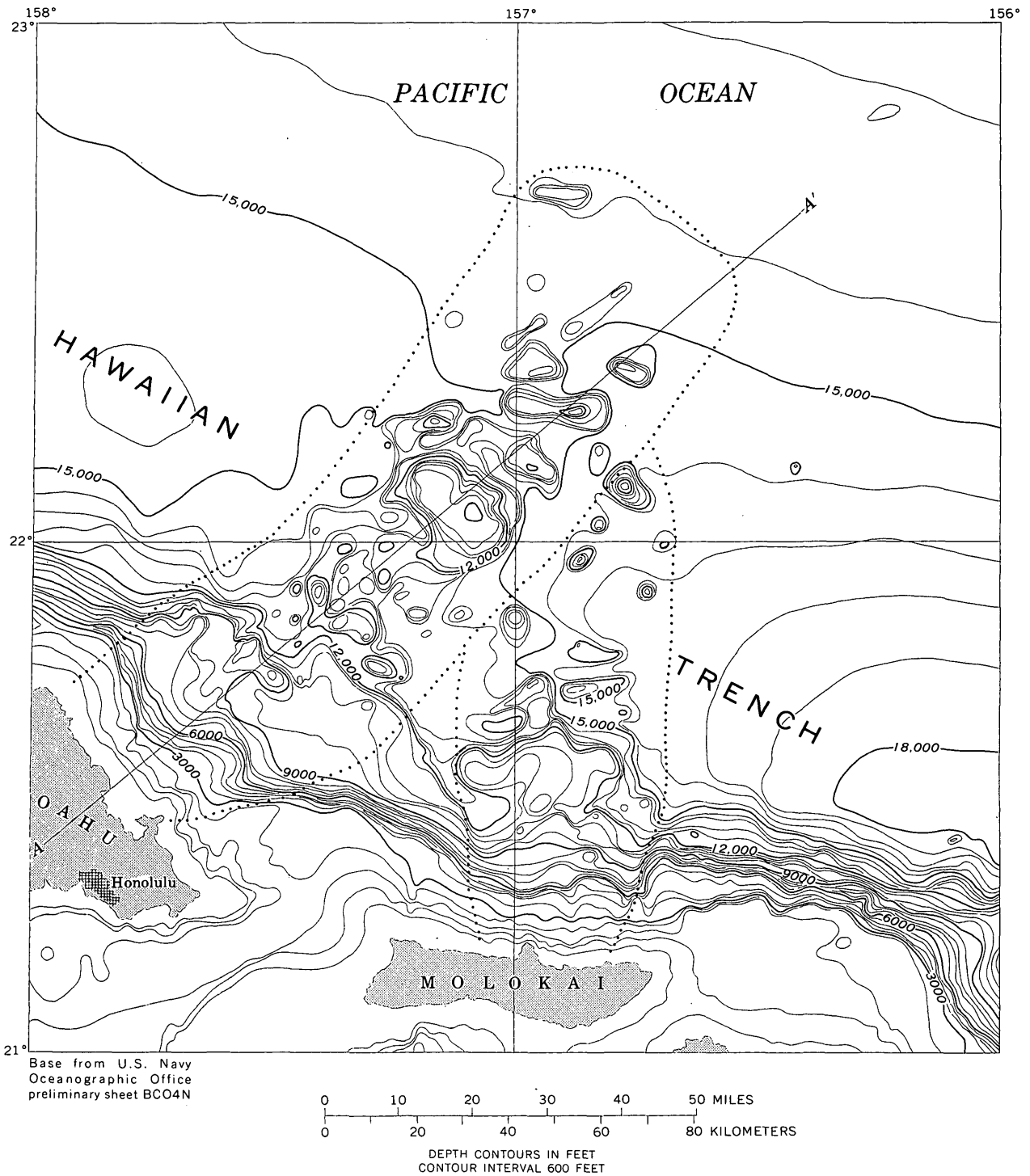

FIGURE 1.—Map of submarine topography adjacent to the islands of Oahu and Molokai. Inferred boundaries of landslides are shown by dotted lines. Geologic section *A–A'* is shown on figure 2.

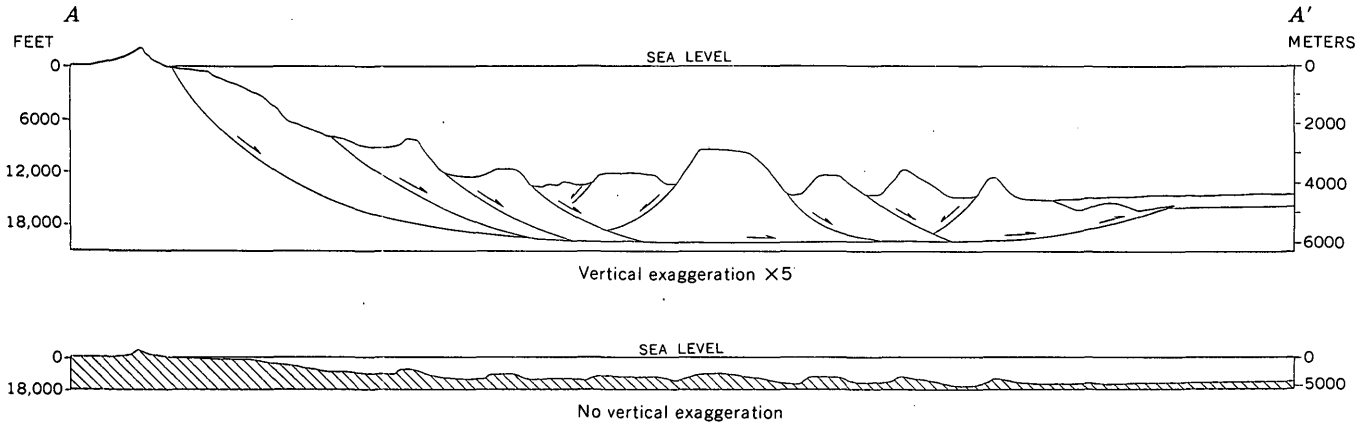

FIGURE 2.—Geologic section A–A' of the area adjacent to the islands of Oahu and Molokai. Location of section is shown on figure 1.

smaller landslides. The lower part of the slide is a tonguelike welt with tilted blocks of about the same dimensions as those of the other slide and arranged perpendicular to the long axis of the slide. Two of these blocks, each about 15 km long, are down-tilted toward the Hawaiian Ridge.

ORIGIN

Other than landsliding, a possible origin of the irregular topography northeast of Oahu is that constructional volcanic features were produced either by submarine eruption along a rift zone of one of the major volcanoes or by eruption from isolated volcanic vents.

The submarine extensions of rift zones on the island of Hawaii are quite unlike the topography described above. The submarine part of the east rift zone of Kilauea (Moore and Reed, 1963, p. B154) is a narrow steep-sided ridge with smooth crest and sides. It extends from a salient rather than from a reentrant on the regional slope, and is not marked by any prominent blocky or irregular topography. Moreover, the two supposed landslides are not on the extension of any known rift zones of either Oahu or Molokai (Stearns, 1946, pl. 1).

The form of the blocky seamounts in the region described is quite different from that of known submarine volcanic cones nearby. Bushnell Seamount off the southeast coast of the island of Hawaii is known to be a recently active volcano, because fresh lava flows were photographed on it (Moore and Reed, 1963, p. B155). It is a rather sharp-crested equidimensional cone with three summits, quite distinct from the elongate, flat-topped seamounts northeast of Oahu. The possibility of the flat-topped seamounts being formed by wave planation before a rise of sea level is rejected because of their greatly differing summit elevation and tilted upper surface.

Submarine landsliding is therefore the favored hypothesis for the origin of the topographic features northeast of Oahu. Not only does the general topographic form of the features strongly resemble that of subaerial landslides (Eckel, 1958, pl. 1), but the position on the steep slopes of the Hawaiian volcanoes is favorable to landsliding.

Large structures caused by downslope sliding of parts of the Hawaiian Ridge have been mapped on several of the volcanoes above sea level. These are best displayed on the island of Hawaii, to the southeast, where the volcanoes are young and have not been subject to the prolonged erosion of the western islands. Stearns and Macdonald (1946, p. 97 and 130) describe major faults on the west flank of Mauna Loa and the south flank of Kilauea which are "probably caused by the instability of the dome and landsliding on a huge scale." The faults are parallel to the coast, are downthrown on the seaward side, and show displacements up to several hundred meters; the zone of faulting on the south flank of Kilauea (Hilina fault system) is 40 km wide. There is also evidence that the east rift zone of Kilauea owes its form to seaward sliding of the south flank of the volcano (Moore and Krivoy, 1964).

The Hawaiian Ridge rises 5,000 meters from the ocean floor to sea level, and extends another 4,000 meters above sea level on the island of Hawaii. On the steeper submarine slopes of the ridge, the slope dips 13° through a vertical distance of 4,000 meters. Because the Hawaiian Ridge is one of the earth's steepest and youngest major topographic features, it is a region favorable to large-scale landsliding.

REFERENCES

Eckel, E. B. ed., 1958, Landslides and engineering practice: Highway Research Board, Spec. Rept. 29, 232 p.

Moore, J. G., and Krivoy, H. L., 1964, The 1962 flank eruption of Kilauea volcano and structure of the east rift zone: Jour. Geophys. Research, v. 69, p. 2033–2045.

Moore, J. G., and Reed, R. K., 1963, Pillow structures of submarine basalts east of Hawaii: U.S. Geol. Survey Prof. Paper 475–B, p. B153–B157.

Stearns, H. T., 1946, Geology of the Hawaiian Islands: Hawaii Div. Hydrography Bull. 8, 106 p.

Stearns, H. T., and Macdonald, G. A., 1946, Geology and ground-water resources of the Island of Hawaii: Hawaii Div. Hydrography Bull. 9, 363 p.

A ZONE OF MONTMORILLONITIC WEATHERED CLAY IN PLEISTOCENE DEPOSITS AT SEATTLE, WASHINGTON

By DONAL R. MULLINEAUX, THOMAS C. NICHOLS, and ROBERT A. SPEIRER, Denver, Colo.

Work done in cooperation with the Municipality of Metropolitan Seattle

Abstract.—On Capitol Hill in Seattle, previously unrecognized weathered clay occurs in a zone that includes the top of a pre-Vashon drift sheet and a thin overlying nonglacial deposit of the following interglaciation: The weathered clay contains more montmorillonite and produces higher swell pressures than does unweathered glacial clay of comparable grain size. The zone of weathered clay probably extends southward under downtown Seattle.

A zone of greenish weathered clayey deposits of Pleistocene age was temporarily exposed in numerous excavations in 1962 and 1963 during construction of a new freeway on Capitol Hill in Seattle (fig. 1). The clays in this zone contain a higher proportion of montmorillonite than do unweathered glacial clays in the Seattle area. Preliminary examination indicates that, under at least some conditions, the weathered clays produce higher swell pressures and may have lower shear strength than unweathered clays, yet the weathered clays do not show consistently higher Atterberg limits or activity values. The chief purposes of this paper are to direct attention to the existence of the zone of weathered clays, which has not been recognized previously, and to suggest that green or greenish-brown clays in Seattle should be suspected of being relatively rich in montmorillonite unless proved otherwise.

Field investigations of the weathered clays were made by Mullineaux, identification of the clay minerals by X-ray-diffraction methods was done by Nichols, and the other laboratory tests were made by Speirer. Some unusual properties of these weathered clays and their probable importance to engineers were first pointed out by E. R. McMaster, and one radiocarbon sample was collected by D. S. Tillson; both are members of the engineering firm serving the Municipality of Metropolitan Seattle under contract. Two other radiocarbon samples were collected by H. H. Waldron, of the U.S. Geological Survey, and the three samples were analyzed by the Radiocarbon Laboratory of the U.S. Geological Survey, Washington, D.C.

STRATIGRAPHY

The sequence of deposits exposed in freeway excavations along the western slope of Capitol Hill (fig. 1) consists of pre-Vashon drift, overlain successively by a nonglacial deposit and Vashon Drift (see accompanying table and fig. 2). The exposed part of the pre-Vashon drift includes a sequence of sand, till, gravel, and massive silt about 20 feet thick, and, at the top, varved silt and clay 20 feet or more thick. This drift and perhaps other older Pleistocene deposits make up an ancient hill that underlies the present Capitol Hill. The pre-Vashon drift apparently was deposited during the glaciation just preceding a widely recognized interglaciation that is yet to be named, but it cannot be dated definitely. The varved silt and clay in the upper part of the pre-Vashon drift contains a profile of weathering that apparently formed during the unnamed interglaciation.

The nonglacial deposit that overlies the pre-Vashon drift consists of thin interbeds of silty clay, stony clay, peat, sand, and gravel. It includes both fluvial and lacustrine beds, and probably also contains significant amounts of slopewash derived from weathered drift on older hills bordering the depositional basin. Along the side of Capitol Hill from Roanoke Street

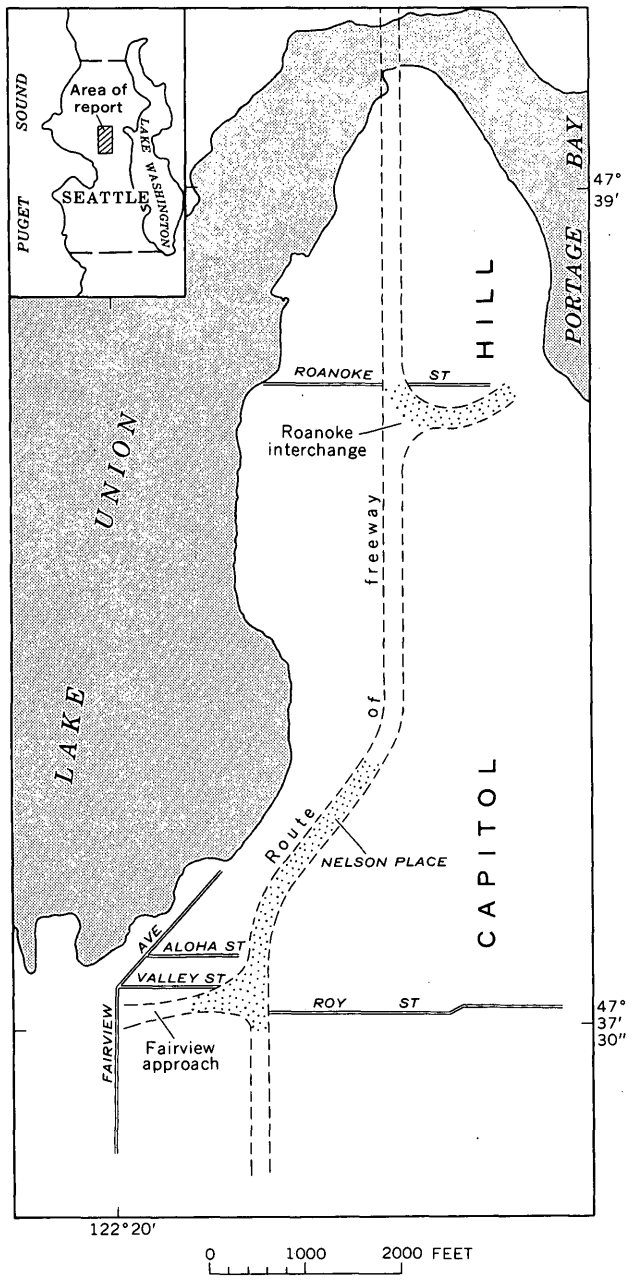

FIGURE 1.—Index map of the west flank of Capitol Hill in Seattle. Stipple pattern, areas where weathered clay was discontinuously exposed during freeway construction.

to Aloha Street, the nonglacial deposit decreases in altitude, and increases in thickness from about 5 to 25 feet or more (fig. 2).

Deposition of the nonglacial beds occurred during an unnamed interglaciation, which extended from more than 35,000 to about 15,000 years ago in this part of the Puget Sound lowland (Mullineaux and Waldron, unpublished data). Two wood samples from the nonglacial beds (fig. 3) were dated by the C^{14} method as 15,000±400 (W–1227) and 15,100±300

Age and stratigraphic position of deposits exposed along the west side of Capitol Hill in Seattle

Geologic-climate unit	Deposits	
Vashon Glaciation	Vashon Drift.	Till.
		Esperance Sand Member.
		Lawton Clay Member, glaciolacustrine clay and silt.
Unnamed interglaciation	Nonglacial deposits: silty clay, stony clay, peat, sand, and gravel. Includes some materials reworked from weathered older drift. Consists of fluvial, lacustrine, and slopewash deposits.	
Pre-Vashon glaciation	Glacial drift: sand, gravel, till, and silt and clay. Locally includes a strong profile of weathering in varved silt and clay at top.	

(W–1305) years old, respectively. In an excavation for the Fairview Avenue approach (figs. 1 and 3), fragments of a mammoth tooth and several fragments of mammoth tusks were found in interbedded green stony clay and iron-stained sand and gravel (V. S. Mallory, University of Washington, oral communication, 1963) that probably are also part of the nonglacial deposit of the same unnamed interglaciation.

Weathered clay occurs throughout the part of the nonglacial deposit exposed along the hill, although not in each bed. In general, nonglacial sediments containing weathered material can be distinguished from underlying weathered glacial clays only where the nonglacial sediments contain plant fragments or other fossils, or lie above other nonglacial sediments containing such fossils.

Overlying the nonglacial deposit is the Lawton Clay Member of the Vashon Drift, a glaciolacustrine clay and silt deposit formed during the advance of the Puget glacier lobe in Vashon time (see table) The maximum thickness of the Lawton Clay Member exposed along the freeway in the Capitol Hill area is about 80 feet. At the northern end of the hill it is overlain directly by Vashon till, but toward the south these two units are separated by the Esperance Sand Member of the Vashon Drift (fig. 2).

WEATHERING PROFILE IN PRE-VASHON DRIFT

A profile of weathering in the top of the pre-Vashon drift was temporarily exposed in excavations for the Roanoke Street interchange (fig. 1). There, weathering of the upper part of the varved silt and clay is represented by progressive changes upward in color, structures, and constituent clay minerals. Where newly exposed, the varved deposit shows a gradual

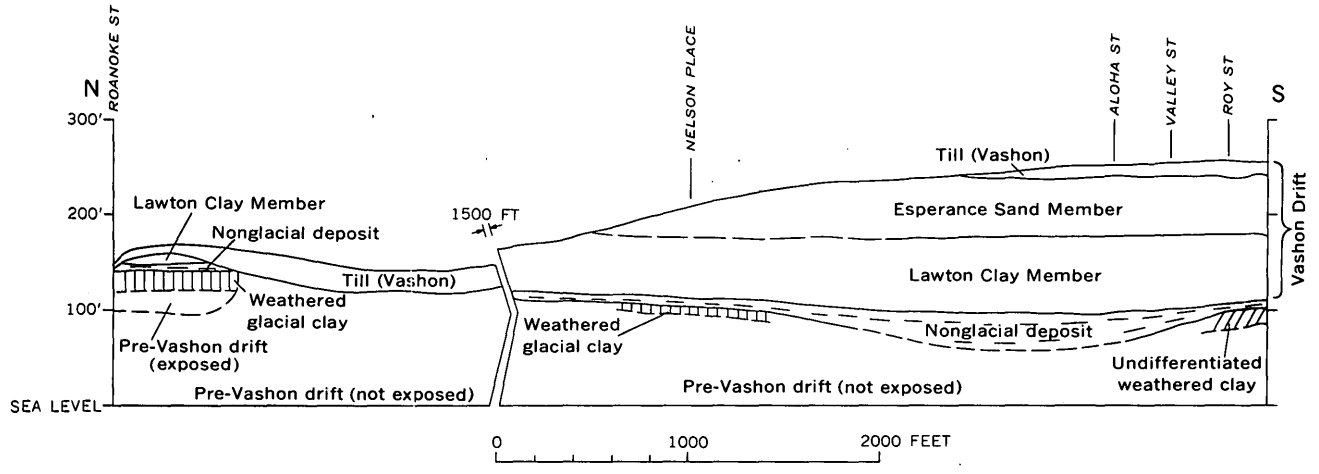

FIGURE 2.—Diagrammatic geologic section of deposits exposed in and above freeway excavations on Capitol Hill.

color change from gray unweathered material up through grayish-green and olive-green weathered material; with exposure, the green color generally changes to brown or brownish green. The upward color change is accompanied by progressive eradication of bedding structures and increase of deformation. In the upper, most weathered part of the deposit, the bedding is almost indistinguishable, and the clay is highly deformed and crossed by closely spaced, slickensided fractures of seemingly random orientation. The principal clay minerals identified in a sample of the unweathered varved silt and clay were chlorite, illite, and montmorillonite, in order of decreasing abundance. These same clay minerals are present in the same order of abundance in all unweathered glaciolacustrine clay samples from Seattle that have been analyzed during the current investigation.[1] In a sample from the lower part of the weathering profile, however, montmorillonite is as abundant as chlorite, illite is only a minor constituent, and some kaolinite was identified. In a sample from higher in the profile, a mixed-layer clay composed chiefly of montmorillonite was the most abundant constituent, kaolinite and chlorite were next most abundant, and illite was not found.

The alteration of clay minerals evident in the weathering profile, from chlorite and illite to montmorillonite, montmorillonitic mixed-layer clay minerals, and kaolinite, is apparently a common result of surficial weathering (Jackson and others, 1948; Harrison and Murray, 1959). The profile exposed at Roanoke Street indicates that the montmorillonite-rich clays there were formed by weathering, and their stratigraphic position immediately underlying the unweathered Lawton Clay Member indicates that the weathering occurred during the unnamed interglaciation that immediately preceded the Vashon Glaciation. Consequently, it is inferred that the mineralogically similar clays that directly underlie the Lawton Clay Member farther south along Capitol Hill are also weathering products formed during the same interglaciation.

Green silt and clay strata similar to those exposed at Roanoke Street were exposed in several excavations farther south along the freeway. A sample of indistinctly varved strongly deformed green clay exposed near Nelson Place (fig. 1) consisted chiefly of a mixed-layer clay composed mostly of montmorillonite; kaolinite was the only other clay mineral identified. Thus, composition as well as color and structure suggests that the clay sampled at Nelson Place had been strongly weathered.

WEATHERED MATERIAL IN THE NONGLACIAL DEPOSIT

No profile of weathering was seen in the nonglacial deposit, but the deposit contains interbeds of apparently strongly weathered material. Interbedding of weathered and unweathered material suggests that the nonglacial sediments were not weathered in place, but merely contain varying proportions of previously weathered clay. The weathered clay probably was derived from the slopes of adjacent hills of pre-Vashon drift by slopewash and creep.

The weathered clay in the nonglacial deposit occurs mostly in layers of green to brown silty clay as much as 3 feet thick, and in layers of massive green to brown stony clay 2 to 3 feet thick. Most of these clays are similar to weathered glaciolacustrine clay in color, but locally the silty clay is brown because of abundant organic matter and shows no evidence of weathered material. A sample of one such brown clay, however,

[1] Kaolinitic clay has been reported as the principal clay mineral in some clays interpreted as glacial or melt-water deposits in Seattle (McManus, 1963), but it has not been identified in our samples of unweathered glaciolacustrine clays.

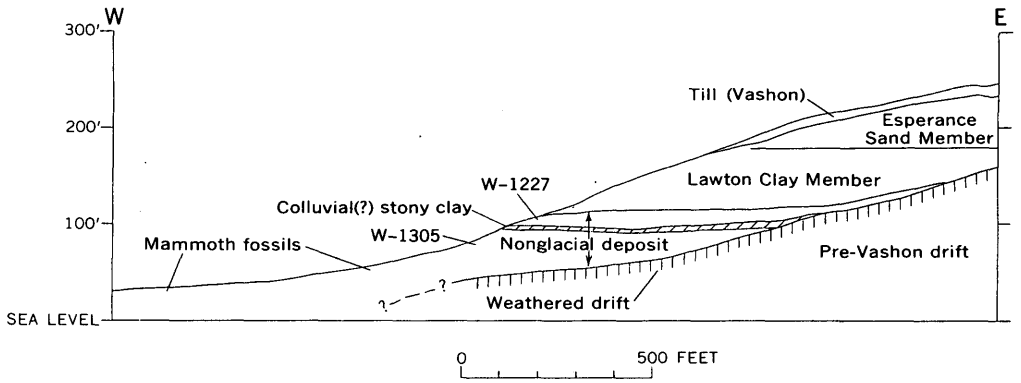

FIGURE 3.—Diagrammatic section in the vicinity of the Fairview Avenue approach, showing postulated relation of hill of pre-Vashon drift to the nonglacial deposit, the stratigraphic position of wood samples W–1227 and W–1305, and the position of mammoth fossils.

consisted almost entirely of a mixed-layer montmorillonitic clay mineral.

The beds of stony clay are sandy, unsorted, unstratified, and much more cohesive than other clays exposed along the freeway. The only structures noted in them were polygonal shrinkage cracks on exposed faces. One sample of stony clay consisted of a mixed-layer montmorillonitic clay, kaolinite, and chlorite, in decreasing order of abundance, suggesting a high proportion of weathered material. A sample of similar clay from another locality, however, consisted of chlorite, montmorillonite, illite, and perhaps a little kaolinite, indicating a lower proportion of weathered material.

ENGINEERING PROPERTIES

Clay deposits with a high content of montmorillonite commonly have unusual properties of special importance to engineers (Grim, 1962, p. 272; Lambe and Martin, 1957). The extreme properties sometimes associated with montmorillonite are not expected from the weathered clays on Capitol Hill because the principal mineral is calcium montmorillonite, which usually is less troublesome than sodium montmorillonite. However, both field and laboratory observations indicate that the weathered clays are significantly different in some engineering properties from the unweathered glacial clays that are far more common in the Seattle area. Relatively low shear strength, perhaps at high water content, is suggested because the weathered varved clays appear to be more susceptible to slope failure, and also to other deformation. For example, the strongly deformed, slickensided beds appear to be limited to the zone of weathered clays; it appears that the weathered clays were deformed selectively, between undeformed unweathered clays, perhaps during loading by sediments or ice during Vashon time. Furthermore, potentially higher swell pressures in the weathered clays were indicated by preliminary swell-index (Lambe, 1960) and confined swell-pressure tests of remolded samples, which were made on 4 samples of weathered glacial clay, 2 samples from nonglacial beds containing weathered material, and 8 samples of unweathered glacial clay. Although these tests are complicated by factors that are unknown or are difficult to control, the pressures measured for the weathered clay samples were consistently higher, averaging about twice as high as those for unweathered clay samples of comparable grain size.

The principal conclusion of this preliminary work is that these green to brown clays should be recognized as different from the common gray unweathered clays of the Seattle area, and, until proved otherwise, regarded as possibly unstable. Their mineralogy should be determined and their properties investigated to determine whether or not they will significantly affect engineering projects. Not all laboratory tests indicate that they will act differently from unweathered clays. Although measured swell pressures were higher for weathered clay samples, neither Atterberg limits nor activity values of the same samples were consistently higher. Besides laboratory tests, investigations should particularly include evaluation of the behavior of these green to brown clays when disturbed by construction activity; the properties of montmorillonite-rich clays may change markedly with changes of water content or chemical environment.

DISTRIBUTION OF THE WEATHERED ZONE

For clarity, the weathered glaciolacustrine clay has been described separately from the weathered material derived from drift and incorporated in the nonglacial deposit, yet the two deposits are commonly superposed along the freeway. For most engineering purposes, they can be considered as a single unit, because of their

proximity and apparent similarity. The entire zone of weathered clay near Roanoke Street lies between altitudes of about 145 and 120 feet (fig. 2). It thickens as it decreases in altitude to the south, and nowhere else has the base of the zone been seen. South of Roy Street, only one small outcrop of weathered clay was seen, but exploratory drilling for the freeway indicates that the weathered clay may continue at least half a mile farther south (D. E. Wegner, Washington State Highway Department, oral communication, 1963). The weathered zone appears to lie along the slope of an older hill that has been buried by younger deposits. The shape of the older hill cannot be determined at present, but it appears likely that the southward decrease in altitude of the exposed part of the zone results from the freeway alinement crossing the west-facing slope of the old hill at a slight angle.

Unfortunately, the distribution of weathered clays elsewhere in Seattle cannot be accurately predicted, for little is known about the weathered clay zone except on the west side of Capitol Hill. The problem is complicated because: (1) the topography during the unnamed interglaciation, and thus the shape and location of the zone as originally developed, is not well known; (2) erosion during and after weathering may have removed the weathered material in many places; and (3) some nonglacial sediments deposited in the Seattle area during the unnamed interglaciation do not contain abundant weathered clay. The fact that the zone has not been recognized previously suggests that it is not widespread as a well-developed zone in the city. Nevertheless, weathered clays should be anticipated in parts of the city that are underlain by older drift or by nonglacial deposits that lie near hills of older drift. Furthermore, it seems likely that the weathered clays will be best preserved where they have been buried and protected by the Lawton Clay Member, as along Capitol Hill.

The most important locality in which the zone of weathered clays might be encountered is downtown Seattle. Nonglacial deposits probably underlie a large part of the downtown district, where they are overlain by the Lawton Clay Member; older drift makes up much of the adjacent hills to the northeast (Capitol Hill) and to the south (south end of First Hill and Beacon Hill). Green clay associated with organic material dated as about 20,000 years old has been found in one excavation in downtown Seattle, at an altitude of about 125 feet (H. H. Waldron, oral communication, 1964). Thus the weathered clay zone probably is present there. However, not enough information is available now to determine whether or not the weathered zone is extensive or well developed in the downtown district.

REFERENCES

Grim, R. E., 1962, Applied clay mineralogy: New York, McGraw-Hill, 422 p.

Harrison, J. L., and Murray, H. H., 1959, Clay mineral stability and formation during weathering, *in* Swineford, A., ed., Clays and clay minerals, Sixth National Conference on clays and clay minerals, Proc.: Internat. Ser. Mons. Earth Sci., v. 2, p. 144–153.

Jackson, M. L., Tyler, S. A., Willis, A. L., Bourbeau, G. A., and Pennington, R. P., 1948, Weathering sequence of clay-size minerals in soils and sediments, I: Jour. Phys. and Colloid Chemistry, v. 52, no. 7, p. 1237–1260.

Lambe, T. W., 1960, The character and identification of expansive soils: Federal Housing Administration Tech. Studies Rept., FHA–701.

Lambe, T. W., and Martin, R. T., 1957, Composition and engineering properties of soil, V: Highway Research Board, 36th ann. mtg., Proc., p. 693–702.

McManus, D. A., 1963, Postglacial sediments in Union Bay, Lake Washington, Seattle, Washington: Northwest Sci., v. 37, no. 2, p. 61–73.

THREE PRE-BULL LAKE TILLS IN THE WIND RIVER MOUNTAINS, WYOMING— A REINTERPRETATION

By GERALD M. RICHMOND, Denver, Colo.

Abstract.—Detailed mapping at Bull Lake shows that the Dinwoody Lake Till is in fact the lower till of the Bull Lake Glaciation. The name Dinwoody Lake Till therefore is abandoned. Three pre-Bull Lake tills successively underlying the lower till of the Bull Lake Glaciation are: Sacagawea Ridge Till, Cedar Ridge Till, and a newly discovered till, here named the Washakie Point Till.

In a recent paper (Richmond, 1962) the author described a stratigraphic section at Bull Lake (fig. 1), on the northeast flank of the Wind River Mountains, Wyo., in which three tills and partly preserved intervening buried soils underlie undoubted till of the Bull Lake Glaciation.

The Bull Lake Glaciation is next older than the Pinedale Glaciation, the last major glaciation of the region. The Bull Lake Glaciation was defined from a sequence of broad mature end moraines that lie just beyond the rough bouldery end moraines of the Pinedale Glaciation at Bull Lake (Blackwelder, 1915). The end moraines of the Bull Lake Glaciation have been interpreted as representing at least two and possibly three major advances of the ice. They form two and locally three groups; outwash channels extend from younger groups through older groups. Downstream from the moraines, the outwash deposits rest on two and locally three sets of terraces. Where outwash deposits of the two older groups are superposed, they are commonly separated by a mature zonal soil so like the interglacial soil separating youngest Bull Lake and oldest Pinedale deposits that a considerable recession of the ice, if not deglaciation, is indicated. No soil has yet been found between deposits of the middle and younger groups at Bull Lake. Currently, the oldest group of moraines define the early stade of Bull Lake Glaciation, and the middle and youngest groups together define the late stade.

The stratigraphic section described in 1962 occurs in the precipitous bluff on the north side of Bull Lake, in the center of SW¼ sec. 28, T. 3 N., R. 3 W. (fig. 2). The three tills beneath undoubted Bull Lake Till at the top of the section were named, from oldest to youngest: Cedar Ridge Till, Sacagawea Ridge Till, and Dinwoody Lake Till. All were considered of pre-Bull Lake age because they differ in composition from the undoubted Bull Lake Till above, and because the Cca (lime enriched) horizons of partly preserved pedocal soils on the lower two tills are intensely impregnated with calcium carbonate, a characteristic common to pre-Bull Lake tills at lower altitudes in this region. Further study, detailed mapping, and

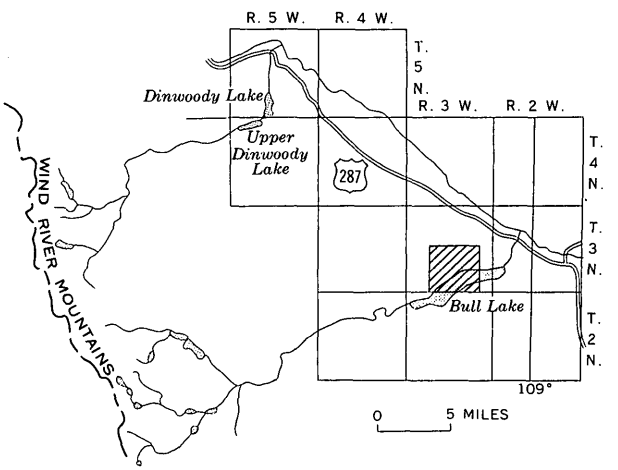

FIGURE 1.—Sketch map showing location of Bull Lake, on the northeast side of the Wind River Mountains, Wyo., and location of area shown on figure 2 (cross-hatched).

discovery of additional exposures of buried soils separating the tills have shown that the youngest till, the Dinwoody Lake Till, can be traced into, and actually forms the end moraine of the early stade of Bull Lake Glaciation. In addition, a previously unrecognized till and associated thick weathered zone were found beneath the Cedar Ridge Till. A revised interpretation and correlation of the deposits are therefore in order.

The undoubted Bull Lake Till at the top of the section in the bluff is a compact brown to light-brown stony silty sand, less pink than the underlying Dinwoody Lake Till. It forms two large mature end moraines that extend north from the rim of the bluff and represent the late stade of Bull Lake Glaciation (fig. 2).

The Dinwoody Lake Till is also a compact stony silty sand, but has a distinctly pinkish hue imparted by silt derived from Mesozoic red rocks. It is considered to represent the early stade of Bull Lake Glaciation for four reasons:

(1) The till can be traced westward from beneath the undoubted Bull Lake Till to the top of the bluff where it forms a large end moraine previously identified as that of the late stade of Bull Lake Glaciation. The moraine extends northward from the bluff rim outside moraines of the late stade.

(2) The moraine formed by the Dinwoody Lake Till is similar in form and surface characteristics to moraines of the Bull Lake Glaciation.

(3) A buried soil found on the Dinwoody Lake Till beneath the undoubted Bull Lake Till is similar to that on the undoubted Bull Lake Till and dissimilar to soils on pre-Dinwoody Lake tills. The Cca horizon of this soil is thinner and has a much lesser concentration of calcium carbonate than the thick intensely calicified soils on the older tills.

(4) Outwash gravel from the end moraine formed by the Dinwoody Lake Till, extends to the highest of three gravel-capped terraces, 80 to 200 feet above the Wind River, on all of which the soil is very similar to soils on moraines of the Bull Lake Glaciation.

The stratigraphic, physiographic, and pedologic features of the Dinwoody Lake Till thus are more closely related to the Bull Lake Glaciation than to older glaciations. The terms "Dinwoody Lake Till" and "Dinwoody Lake Glaciation" are therefore abandoned in favor of the informal terms "lower till" and "early stade" of Bull Lake Glaciation.

In the stratigraphic section described in 1962 the "Dinwoody Lake Till", now the lower till of the Bull Lake Glaciation, is underlain successively by the Sacagawea Ridge Till and the Cedar Ridge Till. These tills are lithologically distinct; the Sacagawea Ridge Till is buff and contains sedimentary and crystalline rocks in about equal proportions. The Cedar Ridge Till is gray and contains mainly crystalline rocks. More complete buried soil profiles than those described on these tills in 1962 have subsequently been found and are presented below. Their thick massive Cca horizons support the interpretation that the tills represent separate glaciations, each followed by a distinct interglaciation.

Discovery of an additional till and an associated very strongly developed soil beneath deposits of the Cedar Ridge Glaciation define still another, and earlier, glacial-interglacial cycle. The till is here named the Washakie Point Till for Washakie Point, an abrupt promontory along Cedar Ridge on the north side of Bull Lake (center, NE¼ sec. 32, T. 3 N., R. 3 W.). The point is not named on the 1952 edition of the Bull Lake West quadrangle, but its location on Cedar Ridge is marked by two large adjacent elongate glaciated boulders in upright position.

The type locality of the Washakie Point Till is in the bluff of Cedar Ridge below a small promontory 2,000 feet east of Washakie Point (SE¼ SE¼ sec. 29, T. 3 N., R. 3 W.) and about 2,000 feet west of the section described in 1962. The Washakie Point Till lies disconformably beneath varved lake silts subjacent to the Cedar Ridge Till and overlies lake beds that rest unconformably on a conglomerate of Tertiary age. It has a thick pedocal soil developed on it and is characterized by abundant material from the conglomerate.

The following stratigraphic section measured in the bluff at the type locality includes not only the Washakie Point Till but the entire column of overlying glacial deposits and soils to the top of the upper till of the Bull Lake Glaciation.

Section in escarpment of Cedar Ridge on the north side of Bull Lake, 2,000 feet northeast of Washakie Point (SE¼SE¼ sec. 29, T. 3 N., R. 3 W.). Measured by G. M. Richmond and J. F. Murphy.

	Thickness (feet)
Post-Bull Lake soil:	
B horizon (partly stripped); brown (7.5*YR* 4/4), loose stony silty fine sand	0.5–0.8
Cca horizon; light-brown (7.5*YR* 6/4) stony silty sand. Calcareous coatings on cobbles and boulders; matrix slightly sticky, slightly plastic, firm, hard	1–2

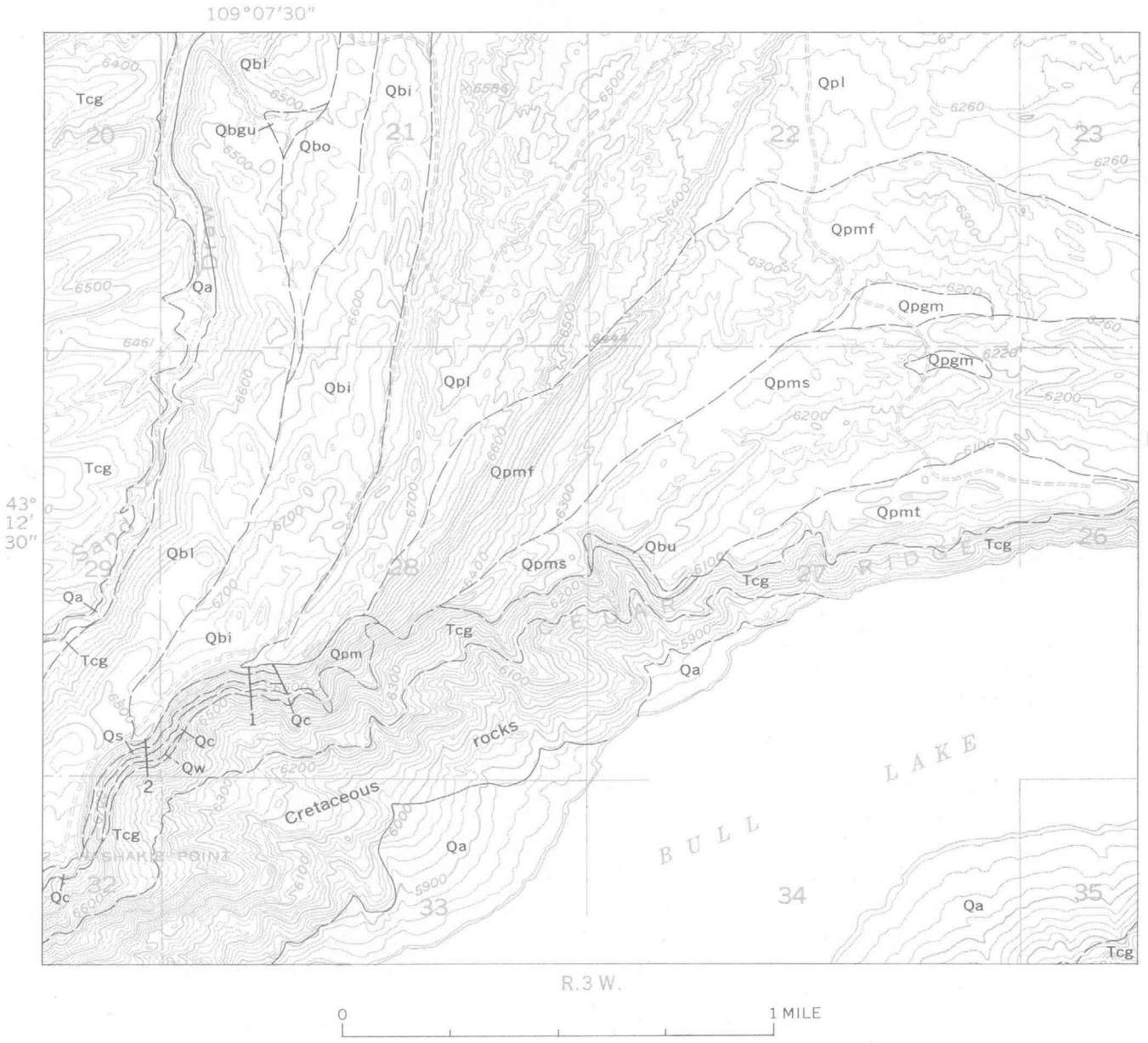

FIGURE 2.—Quaternary geology of part of the Bull Lake area, Bull Lake East and Bull Lake West quadrangles, Wind River Mountains, Wyo.

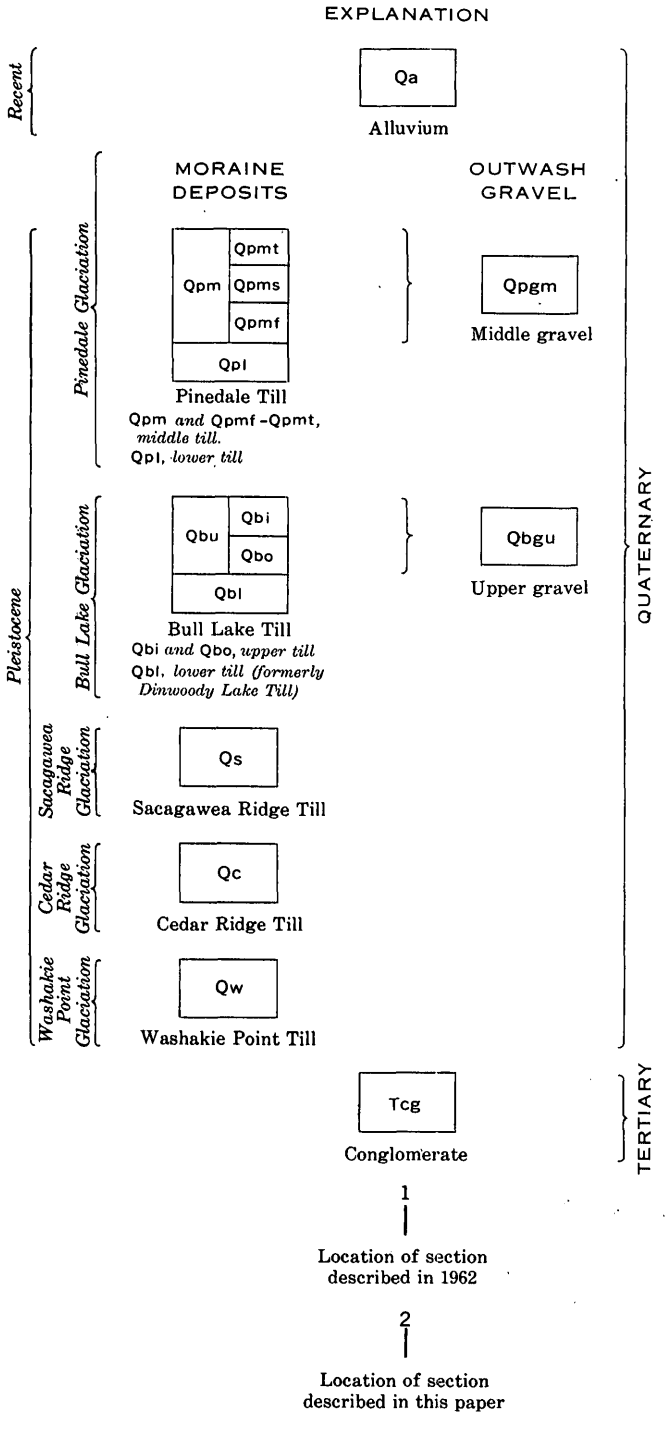

FIGURE 2.—Explanation.

Section in escarpment of Cedar Ridge on the north side of Bull Lake, 2,000 feet northeast of Washakie Point (SE¼SE¼ sec. 29, T. 3 N., R. 3 W). Measured by G. M. Richmond and J. F. Murphy—Continued

	Thickness (feet)
Bull Lake Till:	
Upper till, light-brown (7.5*YR* 4/4–6/4); locally light olive brown (2.5*YR* 5/4); compact friable silty sand and unsorted, unsized subangular to angular pebbles to boulders. Boulders numerous. Most stones of fresh crystalline rock but some of sedimentary rock, mostly limestone. A few stones decomposed; a few soled, faceted, or striated	46
Disconformity.	
Intra-Bull Lake soil:	
B horizon; light-reddish-brown (2.5*YR*–5*YR* 6/4 stony silty sand. Weak angular blocky structure; nonsticky, nonplastic, firm, friable	1. 8
Cca horizon, pink (7.5*YR* 7/4); stony silty sand; weak platy structure; moderately impregnated with calcium carbonate; slightly sticky, slightly plastic, firm, friable	2
Lower till; light-brown (7.5*YR* 6/4) to light-yellowish-brown (10*YR* 6/4) compact massive stony silty sand; very bouldery. Matrix has distinctive pinkish hue owing to silt derived from Mesozoic red beds. A few stones soled, faceted, or striated. About half of rock material is crystalline, about half sedimentary. Lenses of pinkish bedded silt throughout; local layers of angular gravel and silty sand at base	84
Disconformity	
Buried soil developed on colluvium:	
B horizon (partly stripped); light-brown (7.5 *YR* 6/4) to brown (7.5*YR* 5/4) oxidized partly leached pebbly sandy silt; coarse blocky structure; slightly sticky, slightly plastic, firm, crumbly	1. 5
Cca horizon; white (10*YR* 8/2) fine granular silt with local pebbles; coarse platy structure; sticky, plastic, firm, hard. Less calcareous and more friable in lower part	5. 5
Disconformity	
Deposits of Sacagawea Ridge Glaciation:	
Lake beds:	
Varved silt and clay, buff	8
Fine sand and pebbles, loose	4
Varved silt and clay, buff	6
Lake silt, white, fine-grained, well-sorted	0. 5

Section in escarpment of Cedar Ridge on the north side of Bull Lake, 2,000 feet northeast of Washakie Point (SE¼SE¼ sec. 29, T. 3 N., R. 3 W). Measured by G. M. Richmond and J. F. Murphy—Continued

	Thickness (feet)
Deposits of Sacagawea Ridge Glaciation—Continued	
Sacagawea Ridge Till, very pale brown (10*YR* 7/4), massive, calcareous, nonsorted, unsized. Sandy silt matrix is nonplastic, nonstocky, firm, hard, very compact; preserves casts of stones. About 50 percent of cobbles are of Paleozoic rock, mainly buff limestone and dolomite; very little Flathead Sandstone; about 50 percent are of crystalline rock. Practically no Mesozoic rock. Striated cobbles, mostly of limestone. Fewer boulders than in tills above or below; most are of crystalline rock. Deposit thickens to west	5–11
Disconformity	
Buried soil developed on Cedar Ridge Till:	
B horizon (mostly stripped); yellowish-brown (10*YR* 5/4) to pale-brown (10*YR* 6/3) compact stony silty sand. Stones mostly crystalline; many rotted. Wavy irregular bands and zones. Rotted biotite-gneiss cobbles smeared out as streaks. Matrix partly leached, nonsticky, nonplastic, firm, hard. Gradational boundary	0. 5–1. 0
Cca horizon; white (7.5*YR* 8/2) compact coarse to fine sandy silt and stones; strongly impregnated with calcium carbonate; streaky local material like B horizon along joints and as irregular streaks. Matrix slightly sticky, slightly plastic, firm, hard. Stones mostly crystalline, several rotted; gradational lower boundary	2. 5–3
Cedar Ridge Till; light-gray (2.5*YR* 7/2) to brownish-gray (10*YR* 6/2) stony silty sand; calcareous, nonsticky, nonplastic, loose to compact. Nonsorted, unsized. Cobbles and boulders subangular to subround, some soled and faceted, a very few striated, most are of crystalline rock—granite, biotite gneiss; sharp lower boundary	20
Lake beds of Cedar Ridge Glaciation:	
Sand and fine crystalline gravel, light-gray (2.5*YR* 7/2); gradational lower boundary	5
Sand, gray, clean, medium- to fine-grained, loose. Sharp lower boundary	15
Fine-grained sand and silt, light-gray (2.5*YR* 7/2); in 2- to 12-in. layers, not true varves. Gradational lower boundary	6
Varved silt and clay, pale-yellow (2.5*YR* 7/3), thin-bedded, well-sorted, nonsticky, plastic, smooth. Lenses of gravel and sand in lower part	12
Disconformity	
Soil developed on Washakie Point Till:	
B horizon, light-brown (7.5*YR* 6/4), bouldery; many broken and deeply weathered rocks, mostly crystalline, some of Paleozoic rock, many derived from conglomerate of Tertiary age. Silty sand matrix is compact, partly leached, slightly sticky, slightly plastic, firm, hard; coarse angular blocky structure. Gradational lower boundary with streaks extending into zone beneath	1–2

Section in escarpment of Cedar Ridge on the north side of Bull Lake, 2,000 feet northeast of Washakie Point (SE¼SE¼ sec. 29, T. 3 N., R. 3 W). Measured by G. M. Richmond and J. F. Murphy—Continued

	Thickness (feet)
Soil developed on Washakie Till—Continued	
Cca horizon; white (2.5*YR* 8/2) to pale-brown (10*YR* 6/3) bouldery till, as above, but strongly impregnated with calcium carbonate; boulders coated with carbonate. Till thickens to 11 feet immediately westward where fresh material beneath the soil has greenish cast (2.5*YR* 7/2) owing to its high content of material derived from conglomerate of Tertiary age	4–11
Cca horizon on lake beds; white (2.5*YR* 8/2) stony silty sand; slightly sticky, slightly plastic, firm, hard. Carbonate concentrated along joints and permeable zones	2
Deposits of Washakie Point Glaciation:	
Lake beds:	
Silt, pale brown (10*YR* 6/2), massive and thin-bedded, clayey	5. 5
Sand, pebbly, loose, clean, fine-grained. Rusty zone at top. Pebbles, angular to subangular, mostly of crystalline rock; some pebbles of Paleozoic rock and some derived from conglomerate of Tertiary age	8. 4
Silt, pale-brown (10*YR* 6/3), massive to banded; gravelly at base	9
Total thickness of Pleistocene deposits	254
Angular unconformity	
Conglomerate of Tertiary age:	
Boulders, cobbles, and pebbles, rounded to subrounded; all of crystalline rock in arkosic sandy matrix. Material stained brownish to greenish; many stones deeply weathered	150–200

The Washakie Point Till and underlying associated deposits extend in the wall of the bluff beneath the Cedar Ridge Till about 1,500 feet to the west and 1,000 feet to the east of the type section. Similar deposits occur beneath the Cedar Ridge Till in the bluff of a morainal reentrant in sec. 35, T. 3 N., R. 4 W., north of the west end of Bull Lake. There, the Washakie Point Till contains many huge blocks of Bighorn Dolomite and is separated from the Cedar Ridge Till by crudely stratified colluvium, derived largely from red Triassic rocks that form the canyon wall.

In my 1962 report, the "Dinwoody Lake," Sacagawea and Cedar Ridge Tills were correlated with a sequence of outwash terraces along the Wind River on the basis of extensions of the terrace deposits to moraines and deposits of till on the south side of Bull Lake. There, however, the moraine identified as "Dinwoody Lake" is in fact of pre-Bull Lake age, and is actually the equivalent of the Sacagawea Ridge Till at its type exposure. Similarly, tills on the south side of the lake and terrace deposits correlated in 1962 as Sacagawea Ridge and Cedar Ridge are here correlated with the

type exposures of the Cedar Ridge and Washakie Point Tills respectively. This revised correlation is tabulated as follows:

Glaciation or stade	Terrace height, in feet, above Wind River near Bull Lake
Pinedale Glaciation	40
Bull Lake Glaciation, late stade	50 and 100
Bull Lake Glaciation, early stade	200
Sacagawea Ridge Glaciation	380 and 500
Cedar Ridge Glaciation	660
Washakie Point Glaciation	760

A corresponding revision in regional correlation suggests that the respective counterparts of the Washakie Point, Cedar Ridge, and Sacagawea Ridge Tills are the three pre-Bull Lake or "pre-Wisconsin" tills of the La Sal Mountains and Glacier National Park (Richmond, 1957, 1960, 1961), the Rocky Flats Alluvium, Verdos Alluvium, and Slocum Alluvium of the Denver basin (Scott, 1960, 1963), and the Nebraskan, Kansan, and Illinoian Tills of the mid-continent region.

REFERENCES

Blackwelder, Eliot, 1915, Post-Cretaceous history of the mountains of central western Wyoming: Jour. Geology, v. 23, p. 97–117, 193–217, 307–340.

Richmond, G. M., 1957, Three pre-Wisconsin glacial stages in the Rocky Mountain region: Geol. Soc. America Bull., v. 68, p. 239–262.

——— 1960, Correlation of alpine and continental glacial deposits of Glacier National Park and adjacent High Plains, Montana: Art 98 *in* U.S. Geol. Survey Prof. Paper 400–B, p. B223–B224.

——— 1961, Quaternary stratigraphy of the La Sal Mountains, southeast Utah: U.S. Geol. Survey Prof. Paper 324, 135 p.

——— 1962, Three pre-Bull Lake tills in the Wind River Mountains, Wyoming: Art. 159 *in* U.S. Geological Survey Prof. Paper 450–D, p. D132–D136.

Scott, G. R., 1960, Subdivision of the Quaternary alluvium east of the Front Range near Denver, Colorado: Geol. Soc. America Bull., v. 71, p. 1541–1544.

——— 1963, Quaternary geology and geomorphic history of the Kassler quadrangle, Colorado: U.S. Geol. Survey Prof. Paper 421–A, 70 p.

POST-HYPSITHERMAL GLACIER ADVANCES AT MOUNT RAINIER, WASHINGTON

By DWIGHT R. CRANDELL and ROBERT D. MILLER,
Denver, Colo.

Abstract.—Presence or absence of distinctive dated layers of volcanic ash on moraines, in addition to ring counts of trees on moraines, provides chronologic evidence of a rebirth or reexpansion of glaciers on Mount Rainier between 3,500 and 2,000 years ago, and again at some time prior to 750 years ago. The two glacial episodes are here named the Burroughs Mountain Stade (older) and Garda Stade (younger) of the Winthrop Creek Glaciation.

The glaciers of Mount Rainier, Wash., have long been of interest because of their size, relative accessibility, and economic importance in providing melt water used for hydroelectric power. At times during the recent geologic past these glaciers have been substantially smaller than now, and at other times far larger. During part of the Fraser Glaciation, which lasted from about 25,000 to 10,000 years ago, ice and snowfields mantled the slopes of Mount Rainier volcano above an altitude of about 5,000 feet. Alpine glaciers fed by this source and by ice from cirques in the Cascade Range extended to distances of 15 to 40 miles down valleys that head on the volcano. This glaciation was followed by a period of relative warmth and dryness, the "hypsithermal interval," when glaciers on the volcano were smaller than now, and when many probably disappeared altogether (Matthes, 1942). Following this period of maximum warmth and dryness, a resumption of somewhat cooler and moister conditions permitted rebirth and reexpansion of glaciers within the last few millennia.

The purpose of this paper is to describe evidence of two post-hypsithermal episodes of glacier advance at Mount Rainier and to name these episodes. The paper is based on fieldwork undertaken as part of a broader program of mapping the surficial deposits of Mount Rainier National Park. Only the moraines on the north, east, and south sides of Mount Rainier have been studied to date.

The age of post-hypsithermal moraines at Mount Rainier has been determined by identification of several ash layers that overlie the moraines, and determination of the age of the oldest trees that grow on the moraines. The pyroclastic deposits that are most helpful in limiting the age of the moraines are layers called W, C, and Y by Crandell and others (1962), all of which have been deposited within the last 3,500 years (table 1). Ash layer W, the youngest, is probably between 400 and 500 years old. Organic matter above and below the ash layer yielded radiocarbon ages of about 300±200 years, indicating that an age of less than 500 years is likely. The layer probably

TABLE 1.—*Age and source of five distinctive layers of volcanic ash on the flanks of Mount Rainier*

[Modified after Crandell and others, 1962]

Pyroclastic layer	Source	Radiocarbon ages and sample numbers [1] of interbedded organic matter (years)
W [2]	Mount St. Helens	290 ± 200 (W–1120). 320 ± 200 (W–1119). 1,500 ± 200 (W–1397). 2,040 ± 200 (W–1393).
C	Mount Rainier	2,340 ± 200 (W–1396). 2,460 ± 200 (W–1394). 2,550 ± 200 (W–930). 2,980 ± 250 (W–1118).
Y	Mount St. Helens	3,500 ± 250 (W–1115). 4,000 ± 250 (W–1116).
O [3]	Mount Mazama	8,750 ± 280 (W–950).
R	Mount Rainier	

[1] Radiocarbon determination by U.S. Geological Survey Radiocarbon Laboratory, Washington, D.C.
[2] At least 400 years old, on the basis of tree-ring counts.
[3] Resulted from an eruption 6,500 years ago of Mount Mazama at present site of Crater Lake, Oreg.

is more than 400 years old, however, because the ash is not present on either a lateral moraine of Emmons Glacier or a terminal moraine of South Tahoma Glacier, both more than 400 years old as determined by tree-ring counts.

The age of the oldest trees that grow on a moraine provides a minimum age for the formation of the moraine (Sigafoos and Hendricks, 1961). However, several factors tend to make even the oldest trees examined substantially younger than formation of the moraine on which they grow. These factors are the possible lapse of time between stabilization of the moraine and germination of the first trees that survived on it, the possibility that the oldest tree on the moraine is no longer living or was not sampled, and the possibility that many years of stunted growth early in the life of the tree are not recorded in a core taken a foot or two above the base of the trunk. The net result of these combined factors is that a moraine may be older by at least several decades than the trees on it that were sampled. While this difference is substantial in a consideration of moraines formed within the past hundred years, it becomes proportionately less in the case of moraines several centuries old. On the other hand, with increasing age of moraines, there is a decrease in the chances of sampling a tree that started to grow soon after formation of the moraine, because of the possibility that many of the oldest trees are no longer living.

WINTHROP CREEK GLACIATION

Two episodes of glacier advance within the last 3,500 years are included in the Winthrop Creek Glaciation, which is here named for Winthrop Creek on the northern side of Mount Rainier (fig. 1). Moraines along Winthrop Creek form the type section of the glaciation. The two episodes are separated in time by at least 1,000 years, and thus constitute two separate stades. The older stade, represented by a lateral moraine on the northwestern slope of Burroughs Mountain, its type section, is here named the Burroughs Mountain Stade. The younger stade is here named the Garda Stade for lateral and terminal moraines near Garda Falls, which is also designated as the type section.

During the Winthrop Creek Glaciation, many cirques whose floors are at or above an altitude of 6,500 feet were occupied by glaciers. In contrast, cirques occupied by glaciers during the last Pleistocene glaciation have a lower limit of about 4,500 feet at Mount Rainier. According to Bender and Haines (1955) the snowline at Mount Rainier moved upward from about 5,900 feet in 1910 to nearly 7,600 feet in 1952. During the past decade, the firn line has generally been at altitudes between 6,900 and 8,600 feet (Mark F. Meier, written communication, 1963).

Burroughs Mountain Stade

Densely forested and well-stabilized lateral moraines on both the east and west sides of Winthrop Glacier are overlain by, and hence older than, ash layers C and W. The moraines are younger than ash layer Y, which is absent from the moraines, but present on the valley wall just beyond the lateral moraine east of Winthrop Glacier. The crest of this lateral moraine is about 300 feet higher than the oldest adjacent lateral moraine of Garda age in the vicinity of the Wonderland Trail. A terminal moraine of Burroughs Mountain age was not recognized in front of Winthrop Glacier, but the terminal moraine of Garda age lies on an outwash terrace that is mantled with ash layer C and is, presumably, of Burroughs Mountain age.

Moraines of Burroughs Mountain age have also been recognized along the east side of Carbon Glacier, near Fryingpan Glacier, and at a few other places (fig. 1). These moraines typically are only a few yards beyond the maximum extent of ice during the Garda Stade, and moraines of comparable age in most valleys and in most cirques may have been overridden by that ice.

Based on the limiting dates of ash layers, the Burroughs Mountain Stade occurred between 3,500 and 2,000 years ago. It is noteworthy that a glacial advance in the La Sal Mountains of eastern Utah (Richmond, 1962) and an advance of glaciers on the northern side of the Brooks Range in Alaska (Porter, 1964) are both thought to have occurred about 2,800 years ago.

Garda Stade

Drift of Garda age along the Wonderland Trail near Winthrop Glacier includes forested lateral moraines that probably were formed during the latter part of the 17th century and bare, unstable moraines formed within the last decade and still partly underlain by stagnant ice. The terminal moraine of Garda age north of Winthrop Glacier has trees as old as 140 years growing on it, suggesting that it was formed in the early part of the 19th century. The oldest terminal moraine of Garda age yet recognized in Mount Rainier National Park lies in front of Cowlitz Glacier; it was formed some time before 1363 A.D. The oldest lateral moraine of Garda age yet recognized is adjacent to Carbon Glacier at Moraine Park. It bears trees that started to grow early in the 13th century, and its topographic position indicates that

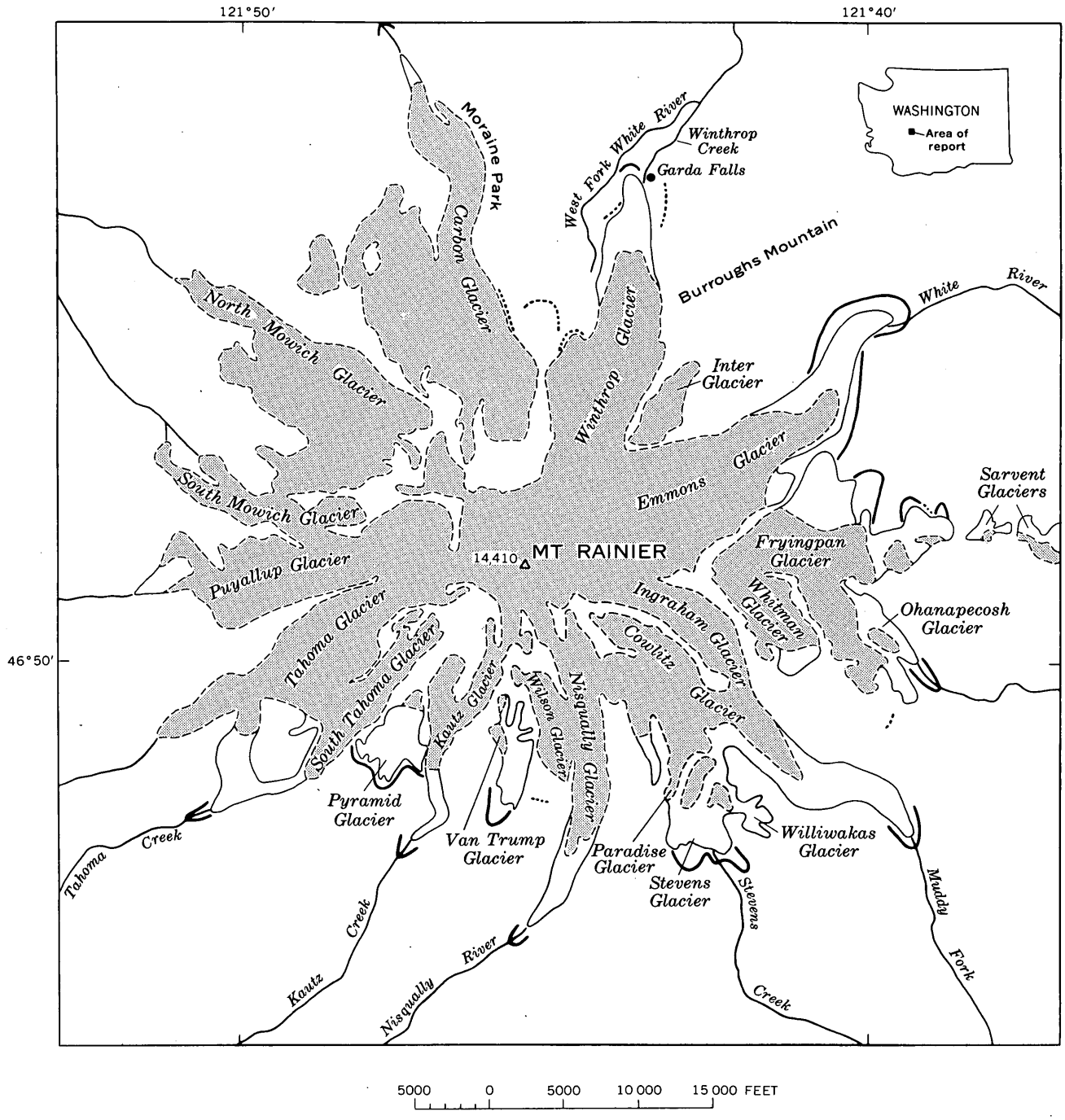

FIGURE 1.—Location map of glaciers on Mount Rainier. Heavy lines, maximum extent of glaciers during Garda Stade; light solid lines, portion of glacier margin surveyed in 1910–13 extending beyond present area (stippled pattern) of glacier; heavy dotted lines, moraines of Burroughs Mountain Stade.

Carbon Glacier was thicker at Moraine Park in the early part of the 13th century than it is today. Thus, the Garda Stade may have begun some time in the late 12th century or early 13th century. The episode of glacier expansion culminated in various valleys at different times ranging from the middle of the 14th century to the middle of the 19th century.

Moraines of Garda age can be differentiated from those of Burroughs Mountain age by the absence of pumice layer C. Some of the oldest moraines of Garda age are mantled with ash layer W, but most are ash free.

DESCRIPTION OF MORAINES OF SOME REPRESENTATIVE GLACIERS

A terminal moraine of South Tahoma Glacier is at the intersection of Tahoma Creek Trail and Wonderland Trail on the north side of Tahoma Creek. This moraine consists of a single narrow ridge of drift on which very large trees are growing, among which one, nearly 4 feet in diameter, started to grow some time before 1554 A.D. Ash layer W was not found on the moraine. Banked against the upvalley side of the terminal moraine is a younger moraine, on which trees as old as 110 years are growing. This younger moraine probably was formed shortly before 1850, and both moraines were formed during the Garda Stade. Apparent lack of moraines of Burroughs Mountain age may be due to the presence of a thick debris flow of post-Y, pre-W age on the floor and lower slopes of the Tahoma Creek valley.

Stevens and Williwakas Glaciers once were lobes of the larger Paradise Glacier, but recent glacier shrinkage has destroyed both lobes. The part of Paradise Glacier that remains includes two small isolated remnants and a higher and larger icefield from which they are separated by a cliff. End moraines of Garda age formed by Paradise and Stevens Glaciers are both older and younger than ash layer W. The pre-W terminal moraine of Paradise Glacier is a single low ridge of drift; immediately behind it is ash-free drift and in front of it is a Pleistocene moraine covered by layers of old volcanic ash. At its maximum extent during the Garda Stade, Stevens Glacier formed two small tongues near its terminus. The western tongue extended into the head of the canyon of Stevens Creek, and the eastern tongue formed a low terminal moraine now forested and covered with ash layer W. Within a distance of about 1,500 feet north of this terminal moraine, there are at least 15 bare, arcuate ridges that mark successive stands of the receding Stevens Glacier; all of these moraines are younger than ash layer W.

The outermost terminal moraine formed by Cowlitz Glacier during the Garda Stade lies only a few hundred yards beyond the ice terminus of 1910–13. The moraine consists of a single, sharp-crested ridge, about 100 feet wide at the base, which is mantled with ash layer W. Trees as old as 590 years were found on the moraine in 1963; trees are only as old as 190 years on the next-younger, ash-free moraine, whose crest is less than 100 feet away. In front of the older moraine is drift of late Pleistocene age which is mantled with ash layers W, C, Y, and O; no moraine of Burroughs Mountain age was recognized.

At its maximum extent during the Winthrop Creek Glaciation, Ohanapecosh Glacier was a large continuous body of ice, but its lower and upper parts are now separated by a cliff. A pre-W terminal moraine of Garda age is well preserved; it is flanked on the downvalley side by drift of late Pleistocene age which is mantled with ash layers as old as layer R.

The bulkiest terminal moraine of Garda age is that of Emmons Glacier, which is about 1,000 feet from the upstream side to the downstream toe. A tree that started to grow about 1700 A.D. was found on the downstream toe, and the topographic map of Mount Rainier National Park, surveyed in 1910–13, shows the front of Emmons Glacier in contact with the upstream side of the moraine. Some of the bulk of this terminal moraine might be due to superposition of a Garda moraine on a preexisting terminal moraine of Burroughs Mountain age. The terminal moraine includes three distinct morainal ridges formed at ice fronts in about A.D. 1745, 1850, and 1895, respectively (Sigafoos and Hendricks, 1961). Thus, the moraine apparently was formed at the front of a glacier that was characterized by a slow but persistent recession, punctuated by occasional stillstands or slight readvances over a period of about 200 years.

Segments of terminal moraine on both sides of the Carbon River valley record two successive stands of Carbon Glacier, the older in the early part of the 16th century and the younger near the end of the 18th century. Lateral moraines are particularly numerous at Moraine Park (altitude about 5,500 feet), located on the east side of the glacier about a mile upvalley from the present glacier terminus. Here at least 15 lateral-moraine segments range in age from less than 100 years to at least 750 years. The oldest dated moraine of Garda age bears trees that started to grow early in the 13th century, and is the oldest moraine thus far recognized from tree-ring counts. The absence of a terminal moraine of comparable age may be attributed either to destruction by stream erosion on the valley floor of the Carbon River or to over-

riding by ice represented by the 16th century terminal moraine. A lateral moraine of Burroughs Mountain age lies outside the moraines of Garda age south of Moraine Park.

CORRELATIONS BETWEEN GLACIERS DURING THE GARDA STADE

In order to show possible correlations from valley to valley, moraines of Garda age are listed below (table 2) with a limiting date for formation of the moraine provided by the oldest trees growing on them.

TABLE 2.—*Limiting dates of formation of moraines of Garda age at Mount Rainier*

[All dated trees are on end moraines except the oldest (1217), which is on a lateral moraine of Carbon Glacier. Year shown is the earliest known date of tree growth on moraine.]

Year	*Moraine of—*
1862	Ohanapecosh Glacier.
1853	Van Trump Glacier.
1851	South Tahoma Glacier.
1850 [1]	Emmons Glacier.
1840	Nisqually Glacier.
1835 [1]	Tahoma Glacier.
1823	Winthrop Glacier.
1800	Carbon Glacier.
1772	Cowlitz Glacier.
1745 [1]	Emmons Glacier.
1700	Emmons Glacier.
1635 [1]	Tahoma Glacier.
1554	South Tahoma Glacier.
1540	Carbon Glacier.
1363	Cowlitz Glacier.
1217	Carbon Glacier.

[1] Sigafoos and Hendricks (1961).

End moraines formed during the middle part of the 19th century have been recognized in front of six glaciers on Mount Rainier. Moraines of this age mark the maximum stand of Nisqually, Van Trump, and Ohanapecosh Glaciers during Winthrop Creek time. Older moraines seemingly do not fall into a consistent pattern from glacier to glacier. This may be a result of insufficient data, or may reflect different behavior patterns of various glaciers.

REFERENCES

Bender, V. R., and Haines, A. L., 1955, Forty-two years of recession of the Nisqually Glacier on Mount Rainier; Erdkunde, v. 9, p. 275–281.

Crandell, D. R., Mullineaux, D. R., Miller, R. D., and Rubin, Meyer, 1962, Pyroclastic deposits of Recent age at Mount Rainier, Washington: Art. 138 *in* U.S. Geol. Survey Prof. Paper 450–D, p. D64–D68.

Matthes, F. M., 1942, Report of committee on glaciers, 1941–42: Am. Geophys. Union Trans., pt. 2, p. 374–392.

Porter, S. C., 1964, Late Pleistocene glacial chronology of north-central Brooks Range, Alaska: Am. Jour. Sci., v. 262, p. 446–460.

Richmond, G. M., 1962, Quaternary stratigraphy of the La Sal Mountains, Utah: U.S. Geol. Survey Prof. Paper 324, 135 p.

Sigafoos, R. S., and Hendricks, E. L., 1961, Botanical evidence of the modern history of Nisqually Glacier, Washington: U.S. Geol. Survey Prof. Paper 387–A.

OCCURRENCE OF DISSOLVED SOLIDS IN SURFACE WATERS IN THE UNITED STATES

By W. B. LANGBEIN and D. R. DAWDY,
Washington, D.C., Menlo Park, Calif.

Abstract.—Records show that the load of dissolved solids carried by rivers increases directly with the amount of runoff only up to about 3 inches mean annual runoff. The load increases less rapidly in those rivers whose annual runoff exceeds 3 inches, and it attains a generalized maximum of 150 tons per square mile per year in rivers having a runoff in excess of 10 inches. Dissolved load carried by rivers is commonly less than the suspended load, but the proportion increases with the humidity of the climate. In dry climates, less than 10 percent of the total load may be carried in solution, whereas in humid climates the percentage may be 50 percent or more.

The quantity of dissolved solids and the chemistry of a flowing stream are commonly considered to depend primarily on the types of rocks or soils through, or over, which the water has passed in reaching the stream, and on the length of time the water has been in contact with the rocks and soils. However, it also is of interest to consider the effect of the quantity of water on the quantity of dissolved solids in surface waters.

In order to study the countrywide variation in quantity of dissolved solids in surface waters, records of chemical quality of water at 168 stations where water was sampled regularly were abstracted from U.S. Geological Survey water-supply papers. The mean annual runoff, in inches, the mean annual dissolved load, in tons, and the mean dissolved-solids concentration, in parts per million, at each station were listed. The annual dissolved load per unit of drainage of each stream was computed (annual runoff, in inches × concentration of dissolved solids, in parts per million × 0.072 = tons of dissolved solids per square mile per year). These data were then grouped by mean annual runoff, and median values for each group were determined for runoff, concentration of dissolved solids, and dissolved annual load. The results for concentration and annual load are shown in the accompanying table and are plotted on figure 1.

Dissolved solids in surface waters of the United States

Range in mean annual runoff (inches)	Number of stations in group	Median runoff (inches)	Dissolved solids	
			Median concentration (ppm)	Median annual load (tons per sq mi per year)
0–0.25	7	0.2	720	10
0.26–0.50	10	.355	950	25
0.51–1.00	19	.71	630	33
1.01–1.80	15	1.5	460	50
1.81–3.00	13	2.3	460	77
3.01–6.00	14	4.7	360	123
6.01–8.00	12	6.8	235	115
8.01–11.0	17	9.7	140	99
11.1–15.0	15	13.5	90	88
15.1–18.0	15	16.5	110	132
19.1–22.0	13	19.6	100	140
22.1–25.0	9	22.9	108	180
25.1–80.8	9	29.7	57	136
	168			

It should be emphasized that the data in the table and on figure 1 apply only to the generalized variation in concentration among streams with different rates of runoff. The data should not be used to predict the concentration in any given stream.

For dissolved load, the relation pictured is rather as one might hypothesize. With increased runoff the load increases until a point is reached at which the rate of dissolution becomes the controlling factor. Above this point, increased water is less and less effective in the weathering process and the amount of total dissolved solids approaches a constant. These are the characteristics of the load curve shown by figure 1. Dissolved load increases directly with runoff, up to about 3 inches of runoff, with a slope of approxi-

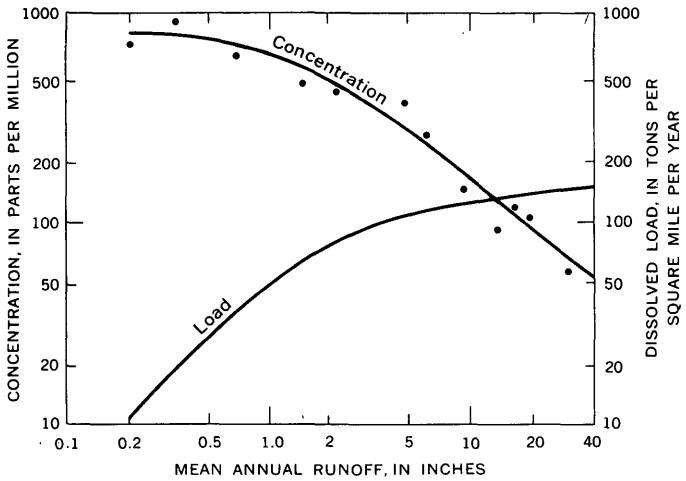

FIGURE 1.—Variation of dissolved-solids concentration and dissolved load in surface waters, with annual runoff.

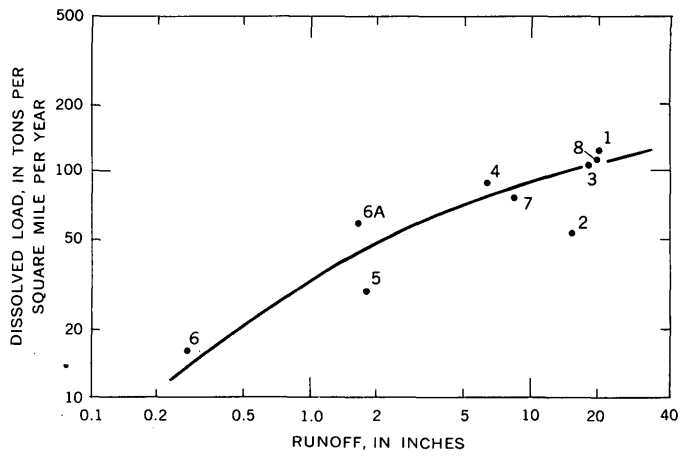

FIGURE 2.—Variation in dissolved load among major river basins in the United States. *1*, North Atlantic slope basins. *2*, South Atlantic slope basins. *3*, Eastern Gulf of Mexico basins. *4*, Mississippi River basin. *5*, Western Gulf of Mexico basins. *6*, Colorado River basin above Yuma, Ariz. *6A*, Colorado River basin above Grand Canyon. *7*, Pacific slope basins in California, and *8*, Columbia River and North Pacific slope basins.

mately unity. Beyond 3 inches of runoff, the dissolved load increases less rapidly, attaining a maximum of about 150 tons per sq mi per year.

Conversely, for concentration of dissolved solids the evidence indicates a decrease in concentration with increase in runoff. The concentration ranges downward from an average of 800 parts per million in arid climates, to as little as 50 ppm in humid climates (fig. 1), where mean annual runoff exceeds 10 inches. In humid climates, concentration is inversely related to runoff, representing a straight dilution effect.

All stations with less than 5 inches annual runoff are west of the Mississippi River, and most are from areas of widely varying climate. Part of the curvature of the graphs from these stations may be due to the fact that the major portion of the dissolved solids may originate in one part of a catchment area and the major part of the water in another, and that both are measured in a channel in the midst of a large noncontributing arid area where only water losses occur. This would reduce the runoff and the apparent load per unit area when computed over the entire area, so that neither statistic would have any simple meaning as computed. Even if a drainage area were composed of two regions, one of greater than 2.5 inches of runoff and the other of less than 2.5 inches, the resultant load would plot lower than the curve of figure 1, since the two regions would be on different sides of the break in the relation. Thus, if half the area had 0.2 inch and the other half had 20 inches of runoff, the combined area would have a runoff of 10.1 inches, and a load of 75 tons per sq mi per year rather than the 120 tons expected from the mean runoff.

Tonnages of dissolved solids per square mile for major drainages in the United States are given by Durum and others (1960). Their results, slightly modified and plotted on figure 2, define a graph with values somewhat lower than those of the corresponding graph for load shown on figure 1. The difference reflects in large part the effect of the nonlinear relation between load and runoff described above.

Inferences about the shape of the curves on figure 1 may be obtained from a consideration of Nernst's law, according to which, the rate of dissolution of rocks would be proportional to the saturation deficit, which in a general way is the same as evaporation. Thus

$$\frac{dL}{dt}=DA\left(\frac{S-C}{S}\right),$$

where L is dissolved load; D is the maximum rate of dissolution of a given kind of lithology per unit area; A, is area; S is the concentration at saturation; and C the concentration at time t.

Considering a rock being dissolved by a flow of water at rate Q, when the rate of dissolution equals the rate of removal, then

$$Q\,(C-C_o)=DA\left(\frac{S-C}{S}\right)$$

and

$$C=\frac{S(1+C_oQ/DA)}{1+QS/DA},$$

where C_o is the concentration of the influent water (rainfall) and the other terms are as before.

The concentration decreases with the ratio Q/DA from a value S for $Q=0$ to C_o, the concentration of rainfall as Q goes to infinity.

Interpreting the ratio Q/A as the runoff in inches, r, and if $C_o=0$, then

$$C=\frac{S}{1+0.073rS/D}.$$

Where concentrations are in parts per million, r is in inches of runoff per year, and D is in tons per sq mi per year.

Values of S and D can be estimated from the data shown on figure 1. The maximum concentration is about 1,000 ppm, and the maximum annual load is 150 tons per sq mi per year. These values are set equal to S and D, respectively.

Thus, $C=\frac{1000}{1+0.5r}$ is the equation of the graph shown on figure 1.

This analysis assumes that the rate of dissolution varies with the saturation deficit and assumes that ionic composition remains the same. However, composition varies with concentration. As might be expected, river records show that the percentage of highly soluble salts, called "lake constituents" by Langbein (1961, p. 13), increases with the concentration. (See fig. 3.)

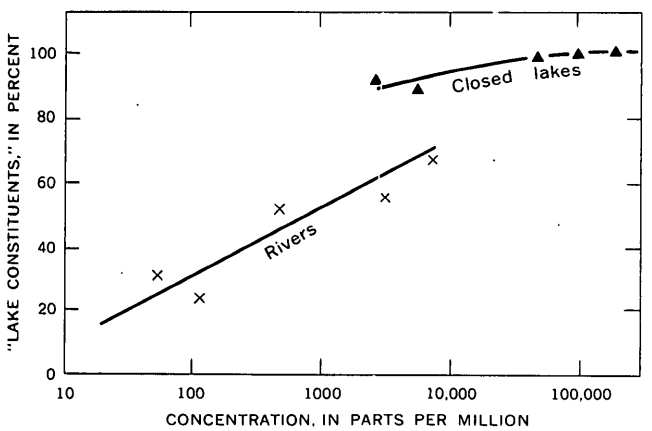

FIGURE 3.—Variation of highly soluble "lake constituents" in rivers, with total concentration of dissolved solids. All quantities computed in parts per million.

These comprise chiefly the sodium salts, magnesium sulfate and chloride, and calcium chloride.

Comparison of data on dissolved load with those of suspended load of rivers at gaging stations where both kinds of information are collected indicates that the dissolved load is commonly less than the suspended load (fig. 4), and that the proportion carried in solution tends to vary with the climate. The dashed

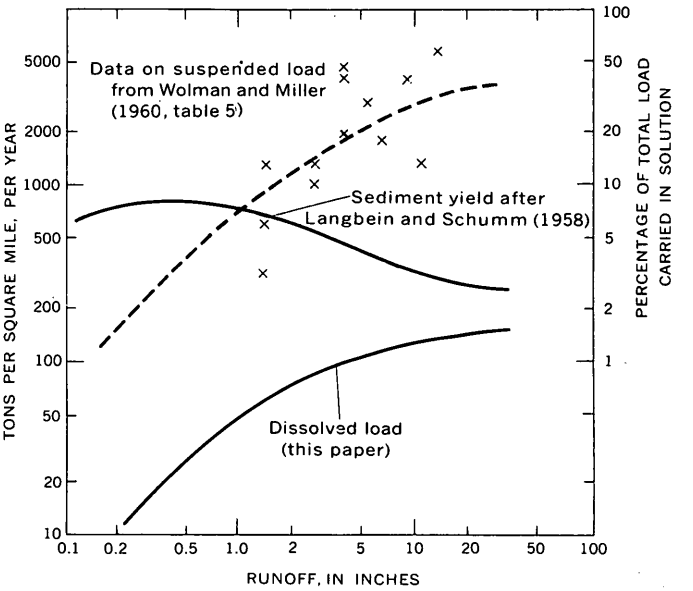

FIGURE 4.—Comparison between dissolved load, suspended load, and sediment yield of rivers. Solid-line curves refer to scale on left; dashed curve to scale on right.

line on figure 4 is the ratio, in percent, between dissolved load and total load (dissolved load plus suspended load). Also shown are data on this same ratio published by Wolman and Miller (1960, p. 63). Thus in dry climates, less than 10 percent of the total load may be carried in solution; in these regions the far greater part of the load consists of clastic sediments. In humid climates the inhibiting effect of vegetation on erosion and the abundance of water for weathering and solution tend to increase the percentage carried in solution. Thus, in humid regions, say where runoff exceeds 20 inches, 50 percent or more of the total load may be carried in solution, but generally the amount of dissolved load remains below that carried in suspension.

REFERENCES

Durum, W. H., Heidel, S. G., and Tison, L. J., 1960, Worldwide runoff of dissolved solids: Internat. Assoc. Sci. Hydrology, Comm. of Surface Waters, Pub. 51, p. 618–628.

Langbein, W. B., 1961, Salinity and hydrology of closed lakes: U.S. Geol. Survey Prof. Paper 412, 20 p.

Langbein, W. B., and Schumm, S. A., 1958, Yield of sediment in relation to mean annual precipitation: Am. Geophys. Union Trans., v. 39, no. 6.

Wolman, M. G., and Miller, J. P., 1960, Magnitude and frequency of forces in geomorphic processes: Jour. Geology, v. 68, no. 1, p. 54–74.

STATISTICAL PARAMETERS OF CAPE COD BEACH AND EOLIAN SANDS[1]

By JOHN SCHLEE, ELAZAR UCHUPI, and J. V. A. TRUMBULL,
Woods Hole, Mass.

Abstract.—Statistical parameters of size of 6 beach and 9 eolian sand samples, as determined by the sieving method and the settling-tube method, reveal no significant size difference between sand of the 2 environments. With the exception of skewness, values obtained by the two methods are similar. Plots of kurtosis versus skewness, standard deviation versus mean grain size, and skewness versus mean grain size show no parts of the fields restricted to a particular environment.

Size distribution of sediments has been used by many workers to infer something about the type of transporting medium and ultimately the environment of deposition. Behind this approach is the expectation that transport by wind, ice, or water uniquely affects the sediment size distribution through selective transport of certain grain sizes. As a test of this approach, a suite of beach and dune samples was collected from the outer arm of Cape Cod, Mass., and analyzed to determine whether sediments from the two environments could be distinguished by statistical parameters.

J. A. Udden (1914) first noted the manner in which grain size is related to the transporting medium—wind or water. He related the genesis of the deposit to certain descriptive features of the grain-size histogram. Later workers refined this use of grain-size analysis through visual examination of the size-distribution curve (Doeglas, 1946; van Andel and Postma, 1954) and through the use of statistical parameters that summarize the distribution (Folk and Ward, 1957; Friedman, 1961).

Results of previous investigations have not been consistent. Harris (1957, 1959), Mason and Folk (1958), Friedman (1961), and Mabesoone (1963) have reported that they could distinguish between the two environments by statistical parameters. Mason and Folk (1958) stated that the best means of differentiating between the two environments was by plotting skewness versus kurtosis, inasmuch as geologic processes seem to have their greatest effects on the tails of the size distribution. Friedman (1961) found that a scatter plot of mean grain size against skewness resulted in a complete separation of the fields representing dune and beach sands. Others, like Udden (1914) and more recently Shepard and Young (1961), found that statistical parameters are unreliable for distinguishing beach from dune sands. Folk (1962), in a review of Shepard and Young's article, stated that their failure to find any grain-size difference between their samples was because they used the settling tube for grain-size analysis of their samples rather than a set of calibrated sieves. Folk considered that the settling tube lacks the ability to detect the subtle differences in genetically important parts of the size distribution—the tails.

PROCEDURE

Six beach and nine dune samples were collected from the outer arm of Cape Cod (fig. 1). Beach sand was collected from the uppermost centimeter of sediment in the swash zone and in the first berm. Eolian sand was collected from the lee and windward sides of active dunes and from small ripplelike accumulations in the flats behind the berm.

Samples were washed, dried, and split for mechanical analysis. Before sieving, screens were calibrated by making 100 measurements of the mesh opening for each screen with a microscope and ocular micrometer. Results of screen calibration are shown in table 1. Maximum departure from the correct mesh opening was 0.05 phi units. A 15-gram split of each

[1] Contribution No. 1408 from the Woods Hole Oceanographic Institution.

U.S. GEOL. SURVEY PROF. PAPER 501-D, PAGES D118-D122

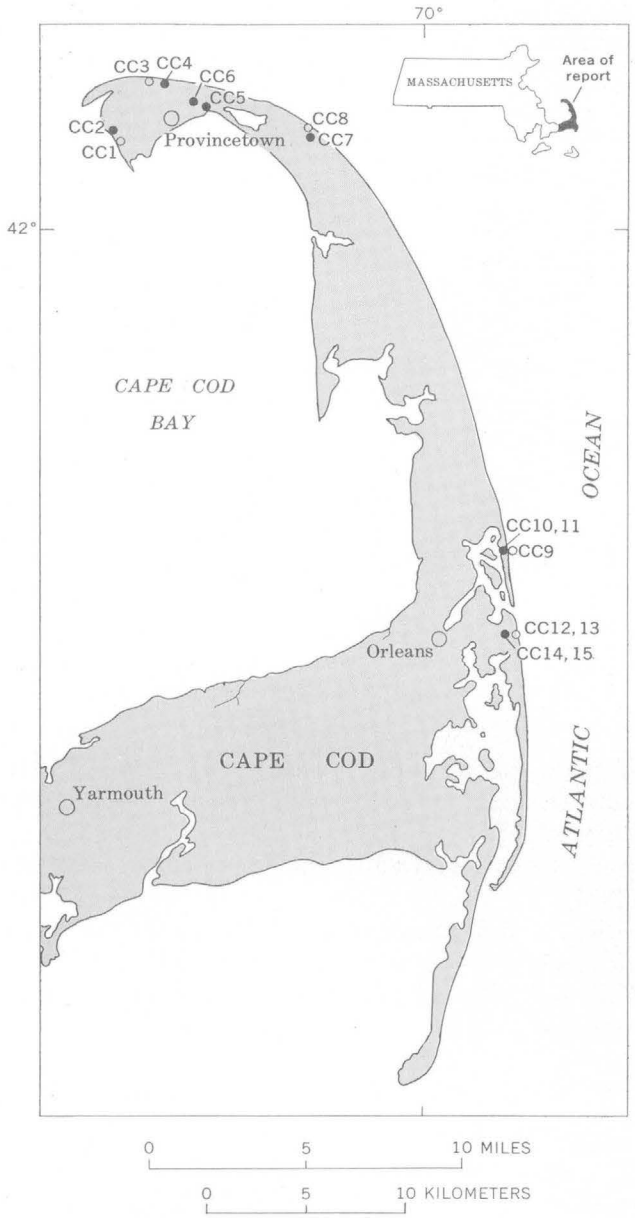

FIGURE 1.—Map showing sampled localities. Beach sand, open circles; eolian sand, dots.

sample was sieved for 15 minutes on a Rotap shaker using 8-inch screens at ¼-phi intervals. Fractions were weighed to the nearest milligram, and the results were plotted on probability paper. Clotted aggregates were not detected in finer fractions, though an examination was made under the binocular microscope.

Settling-tube analyses were made with a modified version of the Woods Hole rapid sediment analyzer (Zeigler and others, 1960). This analyzer measures pressure changes induced in a water column by sediment settling through a measured distance. Samples weighing between 10 and 15 g were used. Settling time was converted to equivalent phi size. On each record the 5, 16, 25, 50, 75, 84 and 95 percentiles were read.

TABLE 1.—*Results of screen calibration based on 100 measurements of the mesh of each screen*

Stated opening		*Mean of measured opening*		*Difference*	
μ	φ	μ	φ	μ	φ
63	3.98	62.4	3.99	−0.6	+.01
74	3.75	76	3.72	+2	−.03
88	3.50	91	3.46	+3	−.04
105	3.25	106	3.24	+1	−.01
125	3.00	129	2.97	+4	−.03
149	2.75	153	2.70	+4	−.05
177	2.50	182	2.45	+5	−.05
210	2.25	211	2.23	+1	−.02
250	2.00	256	1.96	+6	−.04
295	1.75	303	1.71	+8	−.04
350	1.50	359	1.48	+9	−.02
417	1.25	431	1.21	+14	−.04
500	1.00	504	.97	+4	−.03
589	.75	598	.74	+9	−.01
710	.50	703	.51	−7	+.01
840	.25	814	.28	−26	+.03
1,000	.00	1,013	−.02	+13	−.02
1,168	−.25	1,159	−.20	−9	+.05
1,410	−.50	1,383	−.46	−27	+.04
1,680	−.75	1,665	−.72	−15	+.03
2,000	−1.00	2,008	−1.00	+8	.00
2,380	−1.25	2,372	−1.25	−8	.00
2,830	−1.50	2,787	−1.48	−43	+.02
3,360	−1.75	3,290	−1.72	−70	+.03
4,000	−2.00	4,101	−2.01	+101	−.01

Previous workers have not used the same formulas to compute size parameters. Mason and Folk (1958) used formulas from an earlier report by Folk and Ward (1957) to summarize their analyses. Shepard and Young (1961) used formulas published by Inman (1952). Friedman (1961, table 1) used moment measures to calculate his statistical parameters. In an effort to present our data in a form comparable with most other workers, Folk and Ward's formulas have been used. According to Shepard and Young (1961), the values obtained with these formulas differ only slightly from those obtained with Inman's.

RESULTS

Results of the grain-size analyses are shown in table 2 and on figures 2 to 4. Wind-deposited sand (average mean size 0.75 phi) appears to be slightly finer grained than the beach sand (average mean size 0.46 phi), although the values show a considerable overlap (fig. 2). In order to determine whether the difference in mean values is significant, Student "t" tests were made separately on the sieve and tube analyses. Values of "t" at 1.64 for sieve analyses and 1.33 for tube analyses are both less than 2.16 and hence there is no difference at the 95-percent significance level (Hoel, 1954, p. 320) between the means of the samples from the beach and eolian environments. Settling-tube values

TABLE 2.—*Statistical parameters for grain-size distribution of Cape Cod sands*

Sample No.	Mean (φ)		Standard deviation (φ)		Skewness		Kurtosis	
	Sieve	Tube	Sieve	Tube	Sieve	Tube	Sieve	Tube
Beach sand								
CC1	−0.10	−0.37	0.37	0.36	−0.27	0.20	1.16	1.72
CC3	.64	.57	.20	.25	−.13	.31	1.12	1.00
CC8	.57	.55	.27	.28	.06	.47	.96	1.07
CC9	.67	.74	.43	.44	−.06	.29	1.08	.90
CC12	.35	.25	.29	.33	−.33	.38	1.32	1.10
CC13	.69	.70	.31	.34	.01	.34	1.05	.93
Mean	.46	.41	.31	.33	−.12	.33	1.12	1.12
Range	−.01 to .69	−.37 to .74	.20 to .43	.25 to .44	−.33 to .06	.20 to .47	.96 to 1.32	.90 to 1.72
Eolian sand								
CC2	0.29	0.17	0.31	0.29	−0.15	0.25	1.03	0.85
CC4	.50	.45	.31	.33	−.13	.40	.96	1.03
CC5	.69	.62	.36	.42	−.05	.28	1.03	1.02
CC6	.65	.44	.37	.42	−.03	.31	1.11	.85
CC7	.80	.59	.28	.32	0	.40	1.25	1.04
CC10	.97	.91	.46	.47	−.15	.03	1.15	1.16
CC11	1.26	1.37	.27	.37	.20	.19	1.10	.81
CC14	.83	.81	.35	.40	−.03	.27	1.17	.93
CC15	.79	.81	.35	.35	−.05	.30	1.05	.95
Mean	.75	.69	.34	.37	−.04	.27	1.10	.96
Range	.29 to 1.26	.17 to 1.37	.27 to .46	.29 to .47	−.15 to .20	.03 to .40	.96 to 1.25	.81 to 1.16

for mean grain size tend to be lower than the corresponding sieve measures, though the differences are minor.

Sands from Mustang Island, Tex., studied by Mason and Folk (1958), are much finer grained and have much less variation in grain size than the Cape Cod sands. Mean grain size ranges from 2.65 to 3.00 phi for the samples from Mustang Island and −0.31 to 1.37 phi for the samples from Cape Cod. Coarseness of grain size probably reflects the inclusion of glacial outwash and morainal material reworked from nearby deposits. The Cape Cod sands are also coarser than beach sands near Cadiz, Spain, studied by Mabesoone (1963).

Standard deviation of Cape Cod sand from both environments averages less than 0.35 phi, and hence by Folk and Ward's criterion the sand is well sorted.

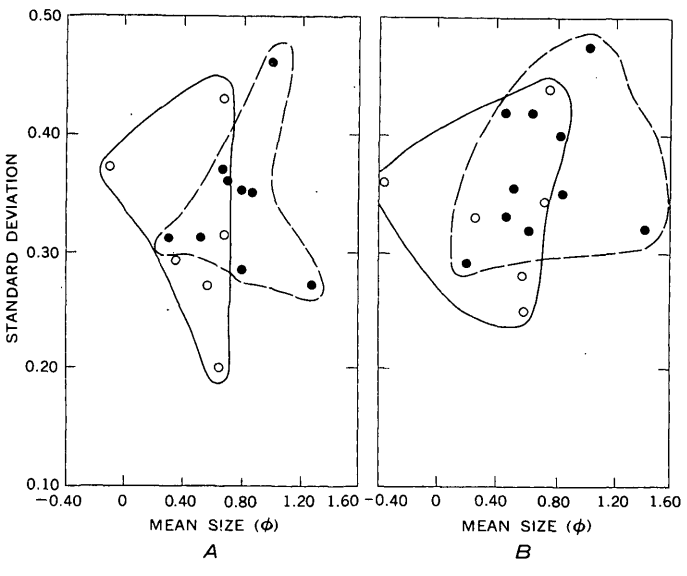

FIGURE 2.—Mean size versus standard deviation. *A*, sieve analysis; *B*, settling-tube analysis. Beach sands, open circles enclosed by solid line; eolian sands, dots enclosed by dashed line.

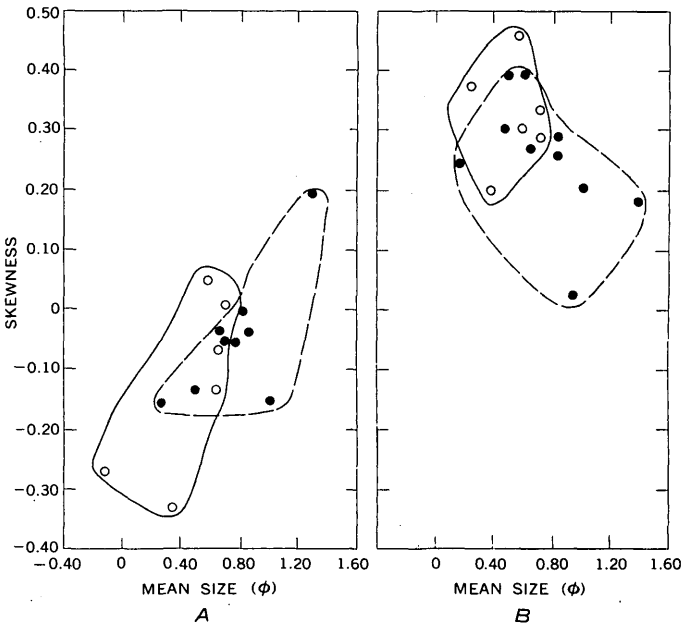

FIGURE 3.—Mean size versus skewness. *A*, sieve analysis; *B*, settling-tube analysis. Beach sands, open circles enclosed by solid line; eolian sands, dots enclosed by dashed line.

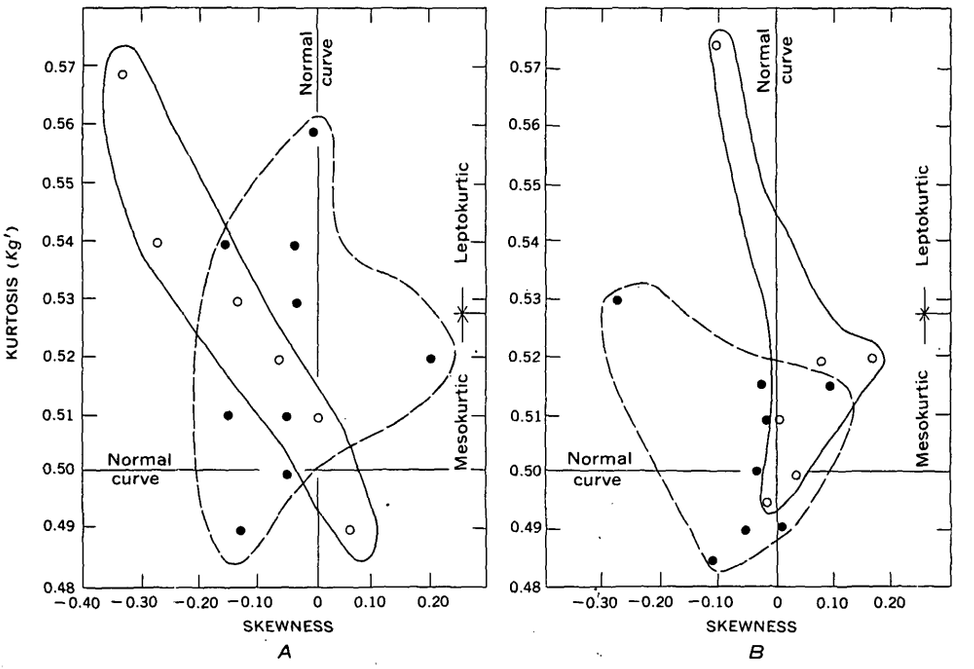

FIGURE 4.—Skewness versus kurtosis expressed as $K_{G'}$. *A*, sieve analysis; *B*, settling-tube analysis. Beach sands, open circles enclosed by solid line; eolian sands, dots enclosed by dashed line.

As with mean grain size, standard-deviation values from beach and eolian sands overlap almost completely (fig. 2). Mean sorting values tend to be slightly lower in the beach sands, in contrast to the results of Mason and Folk (1958) and Shepard and Young (1961), who report that dune sands are better sorted. Student "t" tests for the sorting values reveal no significant differences at the 95-percent level between the values of the two environments. Sieve and tube analyses of sand give similar results; mean sorting values differ by only 0.03 phi.

Skewness values from the two environments show considerable overlap (fig. 3), and Student "t" tests again indicate that there is no significant difference at the 95-percent level ($t_{sieve}=0.74$, $t_{tube}=1.76$, $t_{95\ percent}=2.16$). This contrasts with the results of Mason and Folk (1958, p. 218), Friedman (1961, p. 517), and Mabesoone (1963, p. 38), who found that dune sands tend to be positively skewed and beach sands tend to be negatively skewed. Shepard and Young (1961, p. 200–201) analyzed size by settling tube, and their results show a complete overlap of values from beach and eolian areas. However, almost all their values are negative, in contrast with the positive skewness obtained by settling-tube analysis in this study. As pointed out by Folk (1962, p. 146), some differences may result because Shepard and Young used a formula to estimate skewness that emphasizes the 95th and 5th percentiles with respect to the median, rather than comparing the 95th and 5th percentiles to the 84th and 16th percentiles as is done here.

Though our skewness values of sands from the two environments overlap, sieve and settling-tube values do not. Sieve values are mostly negative, whereas those obtained by the settling-tube analysis are all positive.

A plot of mean grain size versus skewness (fig. 3) shows a large degree of overlap for beach and eolian values. This is in contrast to Friedman's results (1961, fig. 2), which show a nearly complete separation of fields representing beach and dune sands. A partial explanation of the difference may be due to his use of moment measures rather than percentile measures or the coarseness of the Cape Cod sands.

As with the other parameters, a nearly complete overlap of beach and eolian kurtosis values occurs (fig.4). Student "t" tests reveal no significant difference in mean kurtosis values at the 95-percent level. Settling-tube values broadly overlap those obtained by sieving, although the latter tend to be smaller.

Kurtosis is one of those statistical measures for which the geologic significance has yet to be established. Folk and Ward (1957), Mason and Folk (1958), Shepard and Young (1961) and Friedman (1961) have had little or no success in using it to distinguish beach from dune sand. Folk and Ward (1957, p. 15) devised a normalized function:

$$K_{G'}=\frac{K_G}{K_G+1}.$$

With kurtosis values computed in this manner, Mason

and Folk (1958, fig. 4) could distinguish eolian-flat sediments from beach and dune deposits. In this study, though the ranges of $K_{G'}$ values were similar to those of Mason and Folk and overlapped in a similar way, a plot of $K_{G'}$ versus skewness (fig. 4) revealed no separation of eolian and beach sands.

CONCLUSIONS

Grain-size distribution appears to be reliable in distinguishing such deposits as glacial till from beach sands, but distinguishing beach and eolian deposits by this criterion is much more difficult. The present study indicates that none of the standard size parameters or combinations of them can be used to separate Cape Cod beach sands from dune sands. These sands differ from many of those described elsewhere in that they are coarser grained and they are derived mainly from glacial debris. Our results suggest that other factors such as source material may overshadow local sorting by the transporting medium and thus prevent distinguishing beach sands from eolian sands by statistical measures of the particle-size distribution.

Grain-size parameters computed from sieve and settling-tube analyses are very similar, with the exception of skewness. Sieve values for mean grain size tend to be slightly higher (finer grained) than settling-tube analyses of the same samples. Better sorting is indicated for sieved sands than for samples that were analyzed by settling velocity, though the difference is very slight. With a few exceptions, sieve analyses are negatively skewed and settling-tube values are positively skewed. Kurtosis values from both methods are similar and broadly overlap the kurtosis shown by a normal curve.

REFERENCES

Andel, T. H. van, and Postma, Hendrik, 1954, Recent sediments of the Gulf of Paria: Verh. Koninkl. Ned. Acad. Wetenschap., v. 20, no. 5.

Doeglas, D. J., 1946, Interpretation of the results of mechanical analysis: Jour. Sed. Petrology, v. 16, p. 19–40.

Folk, R. L., 1962, Of skewness and sands: Jour. Sed. Petrology, v. 32, p. 145–146.

Folk, R. L., and Ward, W. C., 1957, Brazos River bar: a study in the significance of grain size parameters: Jour. Sed. Petrology, v. 27, p. 3–26.

Friedman, G. M., 1961, Distinction between dune, beach, and river sands from their textural characteristics: Jour. Sed. Petrology, v. 31, p. 514–529.

Harris, S. A., 1957, Mechanical constitution of certain present-day Egyptian dune sands: Jour. Sed. Petrology, v. 27, p. 421–434.

———. 1959, The mechanical composition of some intertidal sands: Jour. Sed. Petrology, v. 29, p. 412–424.

Hoel, P. G., 1954, Introduction to mathematical statistics (2d ed.): New York, John Wiley and Sons, 331 p.

Inman, D. L., 1952, Measures for describing the size distribution of sediments: Jour. Sed. Petrology, v. 22, p. 125–145.

Mabesoone, J. M., 1963, Coastal sediments and coastal development near Cadiz (Spain): Geologic en Mijnbouw, no. 2, p. 29–44.

Mason, C. C., and Folk, R. L., 1958, Differentiation of beach, dune and eolian flat environment by size analysis, Mustang Island, Texas: Jour. Sed. Petrology, v. 28, p. 211–226.

Shepard, F. P., and Young, Ruth, 1961, Distinguishing between beach and dune sands: Jour. Sed. Petrology, v. 31, p. 196–214.

Udden, J. A., 1914, Mechanical composition of clastic sediments: Geol. Soc. America Bull., v. 25, p. 655–744.

Zeigler, J. M., Whitney, G. G., Jr., and Hayes, C. R., 1960, Woods Hole rapid sediment analyzer: Jour. Sed. Petrology, v. 30, p. 490–495.

AN INSTRUMENTAL TECHNIQUE FOR THE DETERMINATION OF SUBMICROGRAM CONCENTRATIONS OF MERCURY IN SOILS, ROCKS, AND GAS

By W. W. VAUGHN and J. H. McCARTHY, JR.,
Denver, Colo.

Abstract.—In the technique described and evaluated, detection of mercury is based on the principle of atomic absorption. An analog signal, produced when mercury vapor absorbs ultraviolet light, is converted to digital form and calibrated to mercury concentration. Interferences are eliminated by selectively trapping the mercury on gold. The lower limit of sensitivity, using a 1-gram sample, is 5 parts per billion. A model of the instrument mounted in a station wagon has been tested successfully in the field.

The high volatility of mercury and the association of small amounts of mercury with many sulfide deposits suggest that extensive mercury halos may exist around sulfide deposits. Several investigations appear to substantiate this hypothesis (Saukov, 1946; Hawkes and Williston, 1962; Williston, 1964). More extensive application of the technique of locating sulfide deposits by detecting the associated mercury halo has been limited, largely because an analytical method of adequate sensitivity has not been available. The methods currently used for the determination of trace amounts of mercury have been reported by Williston. The instrumental technique described here provides a reliable, rapid, and sensitive method for analyzing rocks, soils, and gases for mercury. The technique, with a sensitivity (5 parts per billion) well below the average abundance of mercury in rocks and soils, can be used to detect the small amounts of mercury that may indicate hidden ore deposits.

There are many ways of using the large-volume atomic absorption technique for vapor analysis, as demonstrated by various types of commercially available vapor detectors. These vapor detectors, however, are sensitive to several specific substances as well as to smoke and dust in general. When they are used it is therefore essential that the type of vapor be known if meaningful analyses are to be obtained. Our instrument, the heart of which is a plug-in type of absorption chamber, was designed for specific application to mercury determination on a wide range of geologic materials. A gold-foil trap is used to separate mercury from contaminating vapors prior to its determination.

INSTRUMENT DESIGN AND OPERATION

The apparatus (fig. 1) used with this technique of mercury determination consists basically of an upright quartz tube with necessary accessories, and an absorption chamber with associated electronic equipment. In operation, a sample holder is placed on an insulated rod and inserted by a revolving cam into the lower end of the tube. The holder and the sample are heated with 400-kilocycle radio-frequency energy for 2 minutes, reaching a temperature of approximately 500°C. All of the mercury is vaporized and carried up the tube by an air stream created by a fan. Smoke resulting from burned organic matter is also carried by the air stream. The mercury is trapped by amalgamation with gold contained in a mercury trap at a constriction higher in the tube, while smoke and gases pass on out the tube through the exhaust vent at the top. After the smoke and gases pass off, the air stream is diverted into an absorption chamber by changing a T-valve at the top of the tube. The mercury trapped on the gold is then volatilized by heating the gold with radio-frequency energy, and the resulting mercury vapor is carried up the tube and into the absorption chamber. Two water-cooled copper coils control the temperature of the parts of the tube in which the sample and the gold are heated.

U.S. GEOL. SURVEY PROF. PAPER 501-D, PAGES D123-D127

742-652 O—64——9

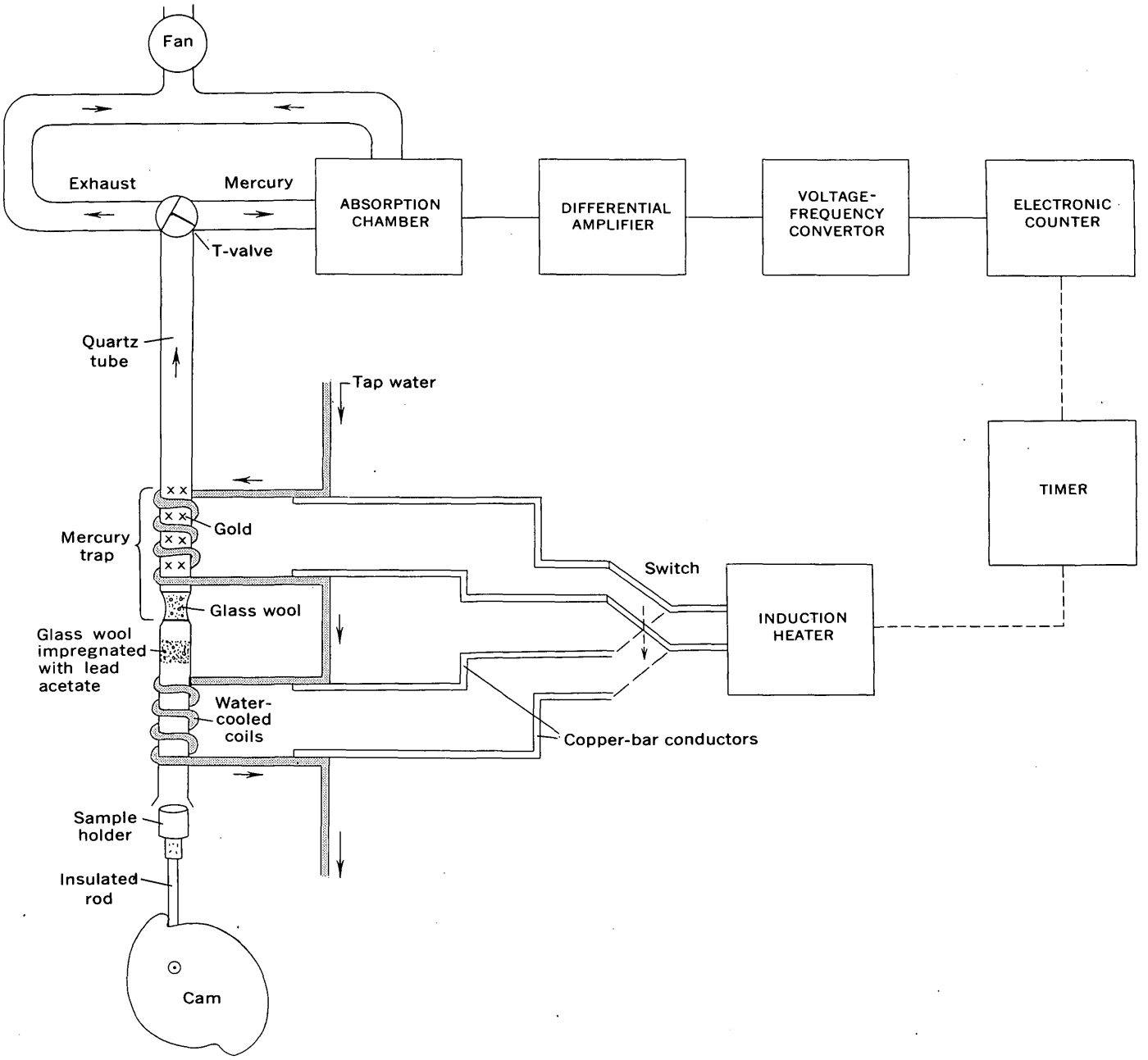

FIGURE 1.—Schematic diagram of mercury-vapor detector.

As a result of passage of the mercury vapor through the absorption chamber the count rate increases to a maximum, then slowly returns to zero. The integrated count is recorded numerically and converted to mercury concentration by use of a calibration curve. The gold is allowed to cool to ambient temperature and the cycle repeated with another sample. Approximately 8 minutes is required for the analysis of a sample; however, if it is known that the sample contains no organic matter the gold can be removed and the time for analysis cut in half.

Two interchangeable absorption chambers, each having a single-spot ultraviolet-light source and two photosensing devices, were constructed for our study (fig. 2). The chambers have different optical geometry but are approximately equal with respect to sensitivity and selectivity. Chamber operation is based on the fact that mercury vapor in an unexcited state will absorb its resonant energy (2,537 angstroms).

The single-cavity chamber (fig. 2*A*) has an optical filter (*f*) between one photocell (*a*) and the ultraviolet lamp (*d*). This photocell responds to all changes in

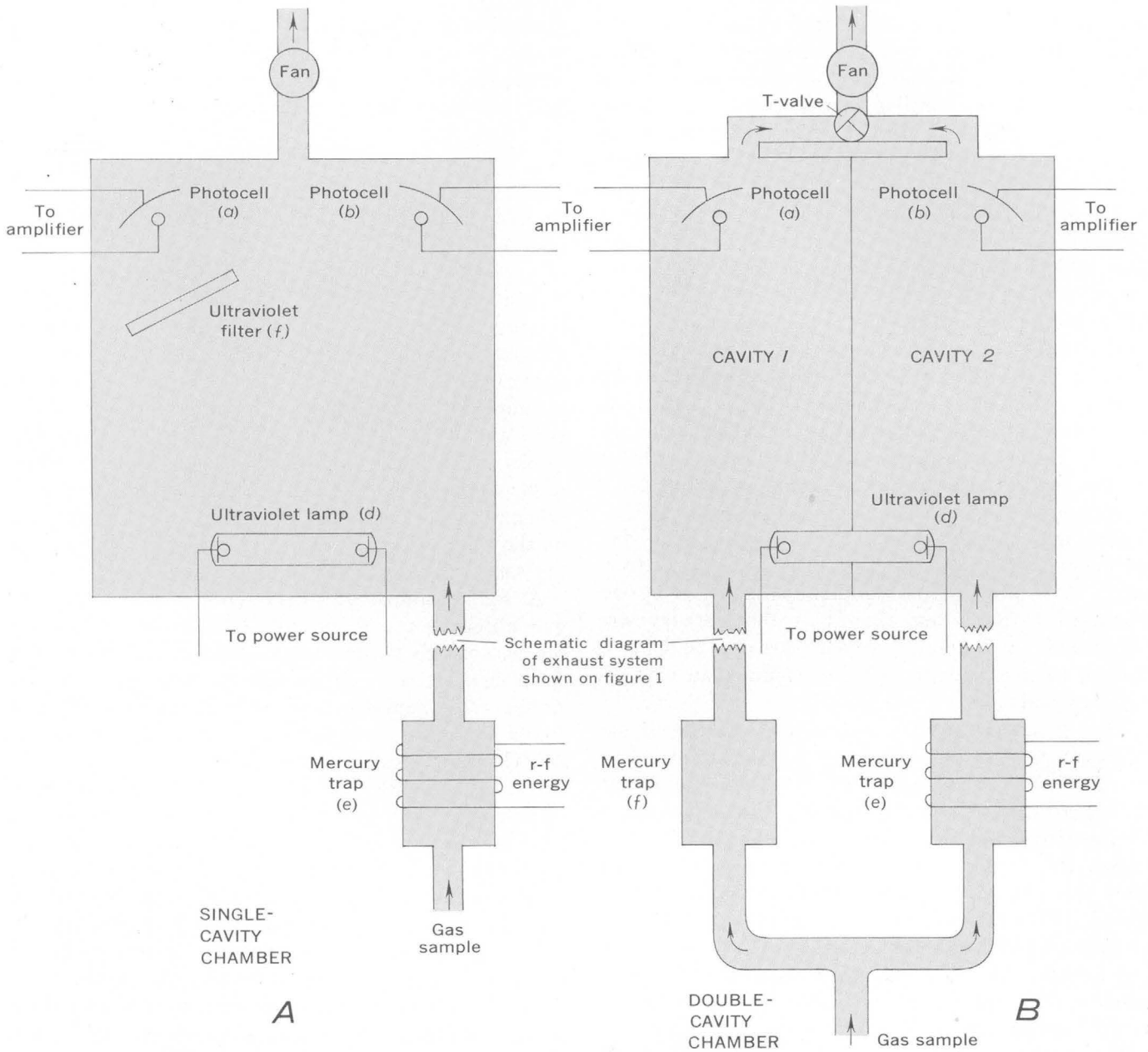

FIGURE 2.—Single-chamber (*A*) and double-chamber (*B*) absorption chambers for mercury-vapor detection.

light intensity except those changes caused by absorption of light in the effective range of the filter. The unfiltered photocell (*b*) responds to all changes in ultraviolet light intensity. The ratio of the electric current generated by the unfiltered photocell to the current generated by the filtered cell is proportional to the absorption of ultraviolet light by the filter and by mercury vapor, from the trap (*e*), passing through the chamber.

The double-cavity chamber (fig. 2*B*) has two mercury traps and two cavities, through each of which the air stream is drawn with equal velocity. One trap (*f*) removes all mercury from the air stream passing through cavity *1*. Consequently, this cavity has no resonant absorption and can be used as an optical blank or reference. The second trap (*e*) removes the mercury from the air stream entering cavity 2. After the two cavities have been nulled electronically the mercury in the second trap is released by heating and is drawn through cavity *2*. The amount of mercury drawn through cavity *2* is then determined from the ratio of photocell currents in the two cavities.

The ratio of photocell currents from either the single- or double-cavity chamber is converted to a

voltage, amplified by a differential amplifier, and fed into a 100-kilocycle voltage-to-frequency converter. The output from the converter is fed into an electronic counter capable of 1 billion counts total. The numerical indication is read directly from the counter and by means of a calibration curve is translated into mercury concentration.

Approximately 15 grams of gold squares 2 mm on a side and ½ mm thick were used for each mercury trap. The gold is supported by a plug of glass wool at the constriction of the quartz tube and is positioned in the center of the upper coil. Experiments conducted to determine the temperature at which the mercury is released from the gold showed that very little mercury is volatilized until a temperature of 400°C is attained, at which time a sharp evolution of mercury occurs. All the mercury is driven off when the temperature reaches 500°C. In practice the gold is heated for 2 minutes and attains a temperature of about 600°C.

Platinum metal is also a good mercury trap, but mercury is not released from it as readily as from gold. At the maximum temperature attained by the platinum (615°C) less than half the mercury was volatilized. Apparently a more stable amalgam is formed between mercury and platinum than between mercury and gold.

Two standard samples were used to determine the temperature at which mercury is volatilized. One standard sample was prepared by diluting cinnabar with quartz, and the other, mercuric oxide with quartz. The mercury began to volatilize at about 150°C, continued at a regular rate and was completely released from the sample when the temperature had reached 300°C. No difference in the temperature or rate of evolution of mercury was detected using either standard sample. A 1.0–g sample of rock was found to reach a temperature of 500°C in this time, allowing a comfortable margin for differences in heating.

The rate of flow of air, hence of mercury, through the absorption chamber has a pronounced effect on the count obtained. In general, the faster the mercury vapor passes through the chamber, the lower the total count. However, reproducibility is poorer at very low flow rates, and sensitivity poorer at rapid rates. Air flowing at the rate of 60 milliliters per minute was found to provide the desired balance between good reproducibility and good sensitivity.

The rapid flow of the mercury vapor past the gold of the mercury trap presented the possibility that some of the mercury might not be trapped. In a test to check this, sample aliquots containing as much as 40 micrograms of mercury were run through the apparatus, and all the mercury was found to be trapped. Gold thus proves to be a very efficient trap for mercury. This is particularly important in the analysis of air or soil gases, during which large volumes of gas must be rapidly passed around the gold.

INTERFERENCES

The principal interference encountered in this technique is from smoke from organic matter in the samples. Interference from this source has been largely overcome by selectively trapping the mercury on gold and allowing the smoke to pass by. Samples containing less than 10 percent organic matter can be analyzed reliably. With samples containing more organic matter, interference is met, presumably because incompletely burned organic matter condenses on the gold and burns when the gold is heated, producing smoke which passes into the absorption chamber along with the mercury. It is also possible that tars, and other products from the organic material, condensing on the gold lessen its effect as an amalgam, thus allowing some mercury to escape detection.

A second source of interference is sulfur dioxide gas which results when sulfide minerals are heated; the gas strongly absorbs ultraviolet light. Interference from this source is eliminated by covering with iron filings those samples that contain sulfides. It was found necessary to bake the iron filings in air at 600°C for several minutes to completely eliminate sulfur interference. A loose-fitting plug of glass wool impregnated with lead acetate is placed in the quartz tube between the upper and lower coils to absorb the small amounts of sulfur found in many rocks and soils.

It is believed that most interfering gases entering the chamber well below saturation diffuse very rapidly and upon reaching a homogeneous condition are nulled by equal response in the photocells. If on the other hand the interfering gases are concentrated and form striated patterns that screen only one photocell, the result prohibits valid mercury analysis.

SENSITIVITY, ACCURACY, AND PRECISION

A calibration curve was prepared by analyzing, in the manner described above, different weighed aliquots of a standard sample. Total counts versus nanograms of mercury were plotted on a rectilinear graph (fig. 3). The curve is linear and has a slope of one; thus a single standard sample analyzed at regular intervals serves to monitor variations in operating conditions, and the curve can be changed accordingly.

A sample aliquot containing 10 nanograms of mercury gives about 1,200 counts, 100 nanograms about 12,000, and so forth. Approximately two minutes are

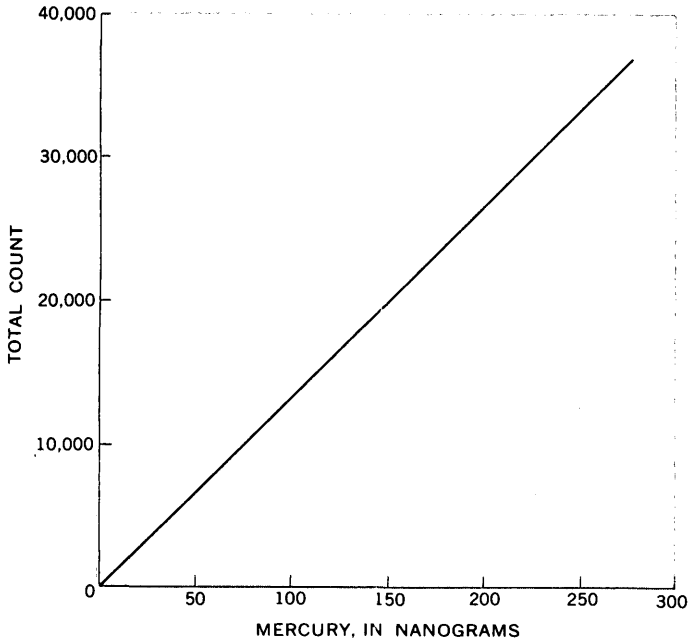

FIGURE 3.—Calibration curve for mercury determinations.

required to obtain a total count of 12,000. Because of circuit nonlinearity, counting efficiency decreases in excess of 50,000 counts; therefore, small aliquots should be taken. The lower limit of sensitivity can be extended by volatilizing mercury from a large sample and collecting it on the gold. A 1.0-g sample of most rocks is sufficient to give a detectable count. This is not unexpected, because present data indicate that the abundance of mercury in igneous rocks and in limestone is 80 and 30 parts per billion, respectively (Green, 1953).

The reproducibility of the method was determined by analyzing a standard sample 10 times (table 1). The standard sample used was that containing cinnabar diluted with quartz. The variation in results is attributed to voltage fluctuations that influence the stability of the instrument, the distribution of mercury in the sample, and the variable concentration of mercury in the air.

The accuracy of the method was assessed by comparing the mercury content determined by the mercury detector with the mercury content determined by a spectrographic method (Sergeev, 1961). Data from the spectrographic analyses are shown in table 2. The samples listed in table 2 are jasperoid and silicious limestone.

TABLE 1.—*Replicate analyses of a standard sample*

Mercury (nanograms)	*Total counts*
100	11, 603
100	11, 519
100	11, 425
100	11, 839
100	11, 826
100	11, 715
100	12, 042
100	12, 421
100	11, 568
100	11, 130
Mean	11, 709
Deviation from the mean, 11 percent	

TABLE 2.—*Comparison of data obtained by mercury detector and spectrographic method on standard sample*

[Analyst, Paul Barnett]

Sample No.	Mercury (ppm)	
	Detector	Spectrographic method
1	19. 5	18. 0
2	2. 1	2. 3
3	. 85	. 89
4	. 22	. 30
5	. 07	. 12

FIELD TRIAL

The instrument was installed in the back of a four-wheel-drive station wagon for field checking. Power for operation was supplied by a 110-v a–c generator of 4 kw capacity. The generator was mounted between the two front seats and operated by the power takeoff of the vehicle. Several hundred samples were analyzed in the field in 1963 to evaluate the usefulness and reliability of the instrument under field conditions. The instrument proved useful in the field to indicate the type of material to be sampled as well as the area to be sampled. Application of the instrument to geochemical exploration will be described at a later date.

REFERENCES

Green, Jack, 1953, Geochemical table of the elements for 1953: Geol. Soc. America Bull., v. 64, p. 1001–1012.

Hawkes, H. E., and Williston, S. H., 1962, Mercury vapor as a guide to lead-zinc-silver deposits: Mining Cong. Jour., v. 48, no. 12, p. 30–32.

Saukov, A. A., 1946, Geokhimiya rtuti [Geochemistry of mercury]: Tr. AN SSSR, Min. Geokh. ser., no. 17.

Sergeev, E. A., 1961, Methods of mercurometric investigations: Internat. Geol. Rev., v. 3, no. 2, p. 93–99.

Williston, S. H., 1964, The mercury halo method of exploration: Eng. Mining Jour., v. 165, no. 5, p. 98–101.

DETERMINATION OF MERCURY IN VEGETATION WITH DITHIZONE—A SINGLE EXTRACTION PROCEDURE

By F. N. WARD and JOHN B. McHUGH, Denver, Colo.

Abstract.—A spectrophotometric method for determining small amounts of mercury in vegetation is based on the reaction of mercury with dithizone after sample dissolution by wet ignition under reflux. Treatment of the sample solution with sulfur dioxide provides a reducing environment during the formation and extraction of the mercury dithizonate into n-hexane. Thus, a single extraction suffices to obviate side reactions, and double extractions or reversion steps are unnecessary. The method is useful for determining as little as 0.4 ppm of mercury in dry vegetation, and this range is enough to evaluate the usefulness of the mercury content of vegetation in prospecting.

The mercury content of vegetation may be a useful guide in biogeochemical prospecting, and in order to facilitate the evaluation of this parameter a sensitive method is needed to determine small amounts of mercury likely to be present in different vegetation samples.

The reaction between mercury and dithizone in an acidic medium to form an extractable orange mercuric dithizonate is the basis of a colorimetric procedure that appears to be suitable for vegetation. To date this reaction is the basis of several methods of determining mercury in biological materials such as urine, blood, kidney tissue, and various other kinds of human tissue (Cholak and Hubbard, 1946; Kozelka, 1947; Barrett, 1956), but it has not been applied extensively to the determination of mercury in vegetation except where the mercury resulted from pesticide applications (Hordynska and others, 1961) and the concentration was relatively large.

Sample dissolution of biological materials including vegetation is most often accomplished by a wet oxidation under reflux. A mixture of hot acids is used to oxidize the material, and the residual products of the decomposition often cause oxidation of the dithizone to another compound, diphenylthiocarbadiazone, which is yellow and also extractable into various immiscible solvents. This tendency is a serious drawback to dithizone procedures and often leads to difficulties, especially in the determination of mercury, because of the similarity in the color of mercuric dithizonate and diphenylthiocarbadiazone.

The difficulty is most often overcome by the use of a double extraction technique—similar to double precipitation—or to the reversion principle as suggested by Irving and others (1949) and modified by Simonsen (1953).

In the proposed procedure a single extraction of the acidic sample solution is made after bubbling sulfur dioxide gas through the solution prior to adjusting the pH to 4. This simple expedient nullifies the oxidative properties of the sample solution with respect to dithizone and no reduction of mercury(II) to mercury(I) occurs (Melles and De Bree, 1953), as shown by absorption measurements of mercury dithizonate formed in the presence and absence of sulfur dioxide.

At the pH used to extract the mercury dithizonate, bismuth, copper, and silver form extractable dithizonates, but copper and bismuth are complexed with EDTA (ethylenediamine tetraacetic acid, disodium salt), and silver is removed with thiocyanate.

The procedure as described has a useful range from 0.4 parts per million of mercury upward, depending on the aliquot size. The sample size may also be adjusted within limits to extend the range. The ratio of digesting mixture to sample has to be maintained, and the volumes of acids should be adjusted along with the sample size.

We wish to acknowledge the assistance of E. H. Bailey of the U.S. Geological Survey and Professor H. V. Warren of the University of British Columbia, who furnished the samples of vegetation included in this paper.

U.S. GEOL. SURVEY PROF. PAPER 501-D, PAGES D128–D130

REAGENTS AND APPARATUS

Ammonium hydroxide, concentrated, A.C.S.

Ammonium hydroxide, 0.4*M*, metal-free. Bubble ammonia into demineralized water.

Ammonium thiocyanate, 5-percent. Dissolve 5 grams of ammonium thiocyanate (NH_4SCN) in 100 milliliters of metal-free water.

Buffer. Mix 1 liter of 2*M* acetic acid with 500 ml of 2*M* sodium acetate. Prepare 2*M* acetic acid by mixing 114 ml of glacial acetic acid with water and adding water to 1 liter. Prepare 2*M* sodium acetate by dissolving 164 g of the anhydrous salt or 272 g of the trihydrate in water and adding water to 1 liter. Adjust pH of mixture to 4.0 ± 0.2 by adding 2*M* acetic acid or 2*M* sodium acetate solution.

Bromophenol blue. Grind 0.1 g in a mortar with 15 ml of 0.01*M* sodium hydroxide and dilute to 250 ml with water, or dissolve the commercially available sodium salt in water. Store in small dropping bottle.

Dithizone, 0.01-percent (w/v). Dissolve 0.01 g of purified reagent in 100 ml. of reagent grade chloroform ($CHCl_3$). Remove trace metals from the chloroform by shaking once with 10 ml of 0.5*M* sulfuric acid, and removing acid by shaking successively 3 times with 50-ml portions of metal-free water.

Dithizone, 0.0015-percent (w/v). Mix 15 ml of the 0.01-percent solution of dithizone in chloroform with 85 ml of n-hexane.

Ethylenediamine tetraacetic acid, disodium salt (EDTA).

n-Hexane, practical grade. Remove trace metals by the procedure suggested above for chloroform.

Hydrogen peroxide, 50-percent.

Hydroxylamine sulfate solution, 20-percent. Dissolve 20 g of hydroxylamine sulfate ($NH_2OH \cdot H_2SO_4$) in 100 ml of metal-free water.

Mercury standard A. 1,000 micrograms per ml. Dissolve 0.1354 g of reagent grade mercuric chloride ($HgCl_2$) in 100 ml of 0.5*M* sulfuric acid.

Mercury standard B. 10 μg per ml. Dilute 1 ml of standard A to 100 ml with 0.5*M* sulfuric acid. This standard is stable for at least 3 months at ordinary temperatures.

Nitric acid, concentrated, A.C.S.

Perchloric acid, 70-percent.

Sulfuric acid, concentrated, A.C.S.

Sulfur dioxide gas. Can be generated in situ or delivered from cylinder.

Water, metal-free. Purify by passing tap water through any of the several types of resin demineralizers now commercially available.

Condenser, 300-mm; with standard taper 24/40 male.

Flask, round-bottom, 300-ml capacity; with standard taper 24/40 female.

Flask, volumetric, 100-ml capacity.

Funnels, separatory, 125-ml.

Heating mantles with variacs for control.

Pipets.

PROCEDURE FOR MERCURY IN VEGETATION

Digestion of sample

To a 1- or 2-g sample of ground vegetation in a 300-ml round bottom flask add 2 ml of water and 5 ml each of perchloric acid, sulfuric acid, and nitric acid.

After addition of acids, connect flask to water-cooled condenser through standard taper 24/40. Set heating mantle at low heat (60°–70°C) at first and at higher settings as the oxidation proceeds. As the oxidation nears completion—reaction subsides—increase heat until moderate refluxing occurs and temperature reaches 140°–145°C. Maintain moderate refluxing for 1 hour.

Remove heating mantle and add 1 ml of 50-percent hydrogen peroxide through condenser. Allow flask to cool to about 80°–90°C and add four 10-ml portions of metal-free water through condenser to digestion mixture. Disassemble the apparatus and transfer contents of digestion flask to 100-ml volumetric flask. Wash digestion flask twice with 10-ml portions of metal-free wash water. Add 5 ml of 20-percent hydroxylamine sulfate to flask and make up to 100 ml with water. Mix.

Extraction

Transfer a 5- to 50-ml aliquot to a 125-ml separatory funnel and bubble sulfur dioxide through aliquot for 1 minute. Aliquots smaller than 50 ml should be made up to that volume with water prior to sulfur dioxide treatment. Add 3 drops of bromophenol blue, 0.5 g of disodium salt of ethylenediamine tetraacetic acid (EDTA) and concentrated ammonium hydroxide drop by drop until near color change. Cool contents of funnel to about 25°C and continue ammonia addition until the color change. Add 20 ml of acetate buffer, cool, and add 5 ml of 0.0015-percent dithizone in n-hexane and shake mixture for 2 minutes. Allow phases to separate and discard separated aqueous—lower—phase.

Estimation

To the hexane solution in the 125-ml separatory funnel add 10 ml of metal-free water and shake 5 seconds. Drain and discard separated aqueous phase. Repeat using 10 ml of ammonium thiocyanate reagent in place of water. After draining the separated aqueous phase, add 5 ml of 0.4 molar metal-free ammonium hydroxide and shake funnel for 10 seconds. Drain and discard the aqueous phase. Decant organic phase into cuvette and measure transmittance at 490 millimicrons. Ascertain the mercury content of the extract by referring to a standard curve established as follows:

To 5 round-bottom digestion flasks add incremental amounts of mercury from a 10 γ/ml standard solution as follows: none to first flask, 2 γ to second flask, 4 γ to third flask, and so forth. The highest standard will seldom need to be greater than 16 γ. Digest contents of flasks for usual time and treat digestates as described above. Take aliquots of 50 ml from each standard solution to obtain a standard series consisting of none, 1.0, 2.0, 4, and 8 γ of mercury. As little as 0.4 γ of mercury in 5 ml of n-hexane is easily detected and if one starts with a 2-g sample and takes a 50-ml aliquot—equivalent to 1 g of vegetation—he can measure as little as 0.4 ppm of mercury in the dry sample.

RESULTS

The repeatability of the proposed procedure was tested by making 5 separate determinations on 11 different plant samples ranging in mercury content from about 0.6 ppm to more than 90 ppm. The range of the repeat determinations, the relative standard deviation, and the confidence limits at the 95-percent level

are shown in table 1. As expected, the precision deteriorates as the lower limit of the method is approached. Other differences in the relative standard deviation can in certain samples be correlated with differences in grinding techniques. Some of the air-dried samples were ground to pass a sieve with holes 1 mm in diameter, and others were pulverized in a Waring blender with no special precaution to insure a maximum particle size or guarantee the fineness. All were hand mixed prior to analysis.

TABLE 1.—*Repeatability of mercury determinations*

[Five determination on each sample, except as noted. Confidence limits about mean at the 95-percent level]

Sample No.	Name of vegetation	Mercury found (ppm)			Relative standard deviation (percent)
		High	Low	Mean and confidence limit at 95-percent level	
Na–4	Chamise (*Adenostoma fasciculatum*).	1.0	0.4	0.6±0.2	[1] 28.3
Na–5	Baccharis	.7	.4	0.6±0.2	20.0
Na–2	do	1.3	1.2	1.2±0.1	5.8
Na–1	Chamise (*Adenostoma fasciculatum*).	2.2	1.6	1.8±0.3	13.3
63–201	*Shepherdia canadensis.*	2.4	2.3	2.4±0.1	2.9
Na–3	Baccharis	2.7	2.3	2.5±0.2	6.8
63–142	Lupine	4.7	3.8	4.3±0.5	9.5
63–197	*Shepherdia canadensis.*	13.5	9.0	11.8±2.3	14.4
63–195	*Populus trichocarpa*	22.0	19.0	21.0±1.2	4.8
63–191	*Betula papyrifera*	42.0	40.0	40.8±1.4	2.7
63–9	*Shepherdia canadensis.*	97.0	90.0	93.0±4.1	3.6

[1] 10 repeats.

The presence of relatively large amounts of salts resulting from the neutralization of the excess acid after sample dissolution has a depressive effect on the extraction of mercury dithizonate into n-hexane. The results obtained by taking different sized aliquots are given in table 2. Aliquots of 25 ml or less but adjusted volumetrically for valid comparison showed higher values than aliquots of 50 ml. Although our data are not sufficiently detailed to permit more than a qualitative interpretation, the behavior is one of inhibition of extraction by the presence of salts and not of enhancement such as observed in cases of salting out of an organic solvent. The effect is readily produced by the addition of a salt such as ammonium sulfate prior to the extraction. The danger of indiscriminate use of different aliquots is clear, especially when determining mercury contents of a few parts per million.

TABLE 2.—*Effect of aliquot size on determination of mercury in vegetation*

Sample No.	Name of vegetation	Mercury (ppm) found in aliquot of—			
		5 ml	10 ml	25 ml	50 ml
Na–2	Baccharis	------	1.0	1.6	1.3
Na–1	Chamise (*Adenostoma fasciculatum*).	------	1.5	2.4	1.9
63–201b	*Shepherdia canadensis.*	------	2.0	2.4	2.4
Na–3	Baccharis	------	3.0	3.0	2.3
63–142a	Lupine	6.0	6.0	5.6	3.8
63–142e	do	6.0	6.0	5.2	4.2
63–195	*Populus trichocarpa*	22.0	22.0	22.0	17.6
63–191a	*Betula papyrifera*	34.0	40.0	38.0	------

Like most analytical methods for plant materials, the proposed procedure is at a disadvantage in the time required for sample dissolution. However among dithizone procedures, it possesses several advantages, such as freedom from oxidation of the dithizone, single, in place of double extraction, and direct measurement of the mercury dithizone complex.

REFERENCES

Barrett, F. R., 1956, Microdetermination of mercury in biological materials: Analyst, v. 81, p. 294–298.

Cholak, Jacob, and Hubbard, D. M., 1946, Microdetermination of mercury in biological material: Indust. and Eng. Chemistry, Anal. Ed., v. 18, p. 149–151.

Hordynska, S., Legatowa, B., and Bernstein, I., 1961, Colorimetric determination of microgram quantities of mercury in grains and apples: Roczniki Panstwowege Zakladu Hig., v. 12, p. 105–108.

Irving, H., Andrew, G., and Risdon, E. J., 1949, Studies with dithizone, pt. I. The determination of traces of mercury: Jour. Chem. Soc., p. 541–547.

Kozelka, F. L., 1947, Determination of mercury in biological material: Indust. and Eng. Chemistry, Anal. Ed., v. 19, p. 494.

Melles, J. L., and De Bree, W., 1953, The determination of microgram quantities of mercury: Recueil des Travaux Chimiques des Pays-Bas, v. 72, p. 576–80.

Simonsen, D. J., 1953, Determination of mercury in biological materials: Am. Jour. Clinical Pathology, v. 23, p. 789–797.

ION-EXCHANGE SEPARATION OF TIN FROM SILICATE ROCKS

By CLAUDE HUFFMAN, JR., and ARDITH J. BARTEL,
Denver, Colo.

Abstract.—An ion-exchange, carbamate extraction method has been developed for the isolation of microgram amounts of tin in silicate rocks before fluorimetric determination with flavonol. The lower limit of detection is about 2 parts per million when a 2-gram sample is used.

Because of the low concentration of tin in rocks and the insensitivity of analytical reagents, tin must be isolated from a large sample and concentrated in a small volume of solution before quantitative determination. The familiar hydrobromic-hydrochloric acid distillation procedure, one modification of which is described by Onishi and Sandell (1956), is generally used to make the separation. Although this method provides a good separation of tin from most elements, it is time consuming, and a need exists for a more rapid separation having equal reliability. An ion-exchange, carbamate extraction method has been developed for the isolation of microgram amounts of tin. This procedure reduces the separating time by a factor of about four.

Few references are given in the literature as to the anion-exchange behavior of tin. Smith and Reynolds (1955) separated tracer quantities of Sn^{+4}, Sb^{+5}, and Te^{+4} from each other in 0.1 *M* oxalic acid on an oxalate-form, anion-exchange resin and eluted the Sn^{+4}, with 1 *M* H_2SO_4. This separation is not applicable to solutions of rock samples, because in oxalic acid solution many elements are insoluble and tin cannot be separated from common elements, such as iron. A hydrochloric–oxalic acid influent is used to solve these difficulties.

Tin is absorbed on an oxalate-form, anion-exchange resin from a hydrochloric-oxalic acid solution and is eluted with 1 *M* H_2SO_4. The tin in the eluted solution is then concentrated into a small volume by a carbamate-chloroform extraction. To oxidize tin and to bring it into water solution, the chloroform extract is wet ashed with HNO_3, H_2SO_4, and $HClO_4$. Tin, in the final solution, is determined fluorimetrically with flavonol, as described by Coyle and White (1957). If a 2.0-gram sample is used, the method has a lower limit of detection of about 2 parts per million.

The dithiol procedure (Onishi and Sandell, 1956) may be used to estimate tin directly in an aliquot of the [eluant] solution when the sample contains more than 20 micrograms of tin. This alternative procedure may be useful, following ion-exchange separation of the tin, for scanning samples for their tin content.

EXPERIMENTAL

Apparatus.—The fluorimeter used is described by Parshall and Rader (1957). This fluorimeter was adapted to measure the fluorescence of solutions by rotating the search head 90° and attaching it to a 5-centimeter cell compartment (Beckman, D.V. part). Light filters found satisfactory are Corning 2-inch polished squares, primary filter No. 5970 (ultraviolet transmitting) and secondary filters No. 5543 (blue) and No. 3389 (sharp-cut). Any fluorimeter may be used that has sufficient sensitivity to measure the blue fluorescence of the tin flavonol complex at about 470 mμ.

Reagents.—The resin column is 25 cm long, with an inside diameter of 0.8 cm. Convert Dowex 1 (X–8, 50 to 100 mesh, chloride form) to the oxalate form by allowing the resin to stand in a 1.0 *M* oxalic acid solution for several days. Prepare the resin column by adding the oxalic acid solution–resin slurry until the slurry is 10 cm in depth. No attempt was made to regenerate the used resin; it was discarded after each run.

Thioglycolic acid, 80 percent. Avoid use of old reagents.

N,N′-Dimethylformamide, C.P. grade, no purification necessary.

Flavonol (3-hydroxyflavone) solution, 0.05 percent (w/v) in redistilled 95-percent alcohol.

Diethyldithiocarbamic acid, diethylammonium salt solution, 1 percent (w/v) in water.

Sn^{+4} stock solution (1 milliliter=1 milligram). Dissolve 0.100 g of tin metal in 50 ml hot concentrated H_2SO_4. Heat to sulfuric acid fumes, cool, and make to 100-ml volume with water.

Standard Sn^{+4} solution (1 ml=100 μg). Transfer 10 ml of the tin stock solution to a 100-ml volumetric flask, add 3.3 ml H_2SO_4 and dilute to volume with water. Make appropriate

dilutions from the 100 μg/ml solution, keeping the acid concentration at 3 *N* H_2SO_4.

Procedure.—Transfer 2.0 g of the rock powder to a platinum dish. Process a reagent blank with the samples. Add 10 ml demineralized water, 10 ml HNO_3, 10 ml HF, cover, and let stand overnight. Add 10 ml $MClO_4$ and 5 ml H_2SO_4. Place dish on a steam bath and evaporate for about 1 hour, then place dish on a hot plate and fume off the acids until about 3 ml remain. Wash down the sides of the dish with water, add 5 ml $HClO_4$ and repeat the fuming until all the acid is evaporated. Do not bake the salts. Cool. Add 12 ml HCl and 25 ml water to the dish, cover and digest on the steam bath for 30 minutes. If an insoluble residue remains, filter the solution through a retentive filter paper into a 100-ml volumetric flask. Wash residue with water. Place filter paper in a zirconium crucible and ignite it at 500°C. in a muffle furnace. Cool. Fuse residue with 1.0 g NaOH and cool. Dissolve the melt in 10 ml water, add sufficient HCl to neutralize the NaOH and combine the solution with the reserved filtrate. Add 10 ml 0.5 *M* oxalic acid to the flask and dilute to volume with water.

Condition the resin column for use by passing 100 ml 0.1 *M* oxalic acid through it and leave about 1.0 ml above the resin. Quantitatively transfer the sample solution to the resin column. Regulate the flow rate of the solution through the column to about 2 ml per minute. When the flow stops, discard the solution that has passed through, wash the column with 25 ml 0.1 *M* oxalic acid solution and discard the wash solution. Elute the tin by passing 100 ml of 1 *M* H_2SO_4 through the resin column at a flow rate of 1 ml per minute and discard the first 25 ml. Catch the next 75 ml of 1*M* H_2SO_4 in a 100-ml volumetric flask and dilute to volume with water. The carbanate separation described below must be carried out within 48 hours.

Quantitatively transfer a 50-ml aliquot of the solution containing the tin to a 125-ml separatory funnel. Add 0.1 ml thioglycolic acid and mix. Immediately add and mix in 3 ml diethyldithiocarbamate solution. Add 10 ml redistilled chloroform, stopper the funnel, and shake to extract the tin-carbamate complex. Drain the chloroform layer into a clean 150-ml beaker. Repeat this operation twice more, starting with addition of diethyldithiocarbamate solution, and combine all the chloroform extracts in the 150-ml beaker. Discard the aqueous phase. Add 5 ml HNO_3, 4 ml H_2SO_4, and 5 ml $HClO_4$ to the beaker. Place the beaker on a steam bath and evaporate the solution to about 10 ml. Place beaker on a shaking hot plate and fume until about 0.5 ml H_2SO_4 remains. Cool. Add 10 ml water to the beaker, transfer the solution to a 25-ml volumetric flask and dilute to volume with water.

Transfer an appropriate aliquot (1 to 3 ml) of the solution, containing less than 4 μg of tin, to a 25-ml volumetric flask. Add 7.5 ml N,N′-dimethylformamide to the flask and mix. Add 2 ml flavonol solution, dilute the solution to 25-ml volume with water, and mix. Let stand 30 minutes and then measure the blue fluorescence of the solution in a 5-cm cell with a suitable fluorimeter. Use the 4-μg standard described below as the reference solution.

Standardization.—Add 0, 0.25, 0.50, 0.75, and 1.0 ml standard Sn^{+4} solution (1 ml=4 μg Sn^{+4}) respectively to separate 25 ml volumetric flasks. Add sufficient 3 *N* H_2SO_4 to each flask so that each will contain 1.0 ml of 3 *N* H_2SO_4. Process standards as directed in the preceding paragraph, starting with the addition of N,N′-dimethylformamide.

RESULTS AND DISCUSSION

Radioactive Sn 113 was used as a tracer to study the behavior of tin on the resin column. Tests with Sn 113 added to shale solutions and processed through the ion-exchange step of the procedure showed an average tin recovery of 97 percent. About 98 percent of the tin is absorbed on the resin and 96 percent or more of the total is eluted with 100 ml of 1*M* H_2SO_4. Experiments showed that the first 25 ml of 1*M* H_2SO_4 passed through the column contains little or no tin; therefore, this portion is discarded because it contains the major portion of any iron absorbed on the column.

The effect of other ions on the recovery of tin was studied, using the described procedure. Single test solutions containing 200 μg of tin and different amounts of diverse ions were processed, starting with ion-exchange separation. Tin determinations in these tests show a range from 95 to 110 percent recovery (table 1). With the exceptions of copper and bismuth, all these determinations are within the coefficient of variation of 5 percent determined for standard tin solutions processed with no interfering ions.

TABLE 1.—*Recovery of tin in the presence of other elements*

Element added	Amount of element added (micrograms)	Amount of tin added (micrograms)	Tin recovered (micrograms)
Bi	250	200	215
Cu	500	200	220
Ni	500	200	205
Co	200	200	210
Mo	100	200	200
Pb	100	200	210
Cd	100	200	195
As	100	200	210
Zn	200	200	210
Cr	500	200	190
Zr	200	200	205
P	90, 000	200	200
Sn	----------	200	200

The effect of other ions in diabase (standard sample W–1) and granite (standard sample G–1) on recovery of tin, in the procedure described here, was investigated. Solutions were prepared from 1.0-g samples of these rocks, spiked with 100 μg of tin, and then analyzed for tin. These recovery experiments were run on three different days. The recovery of tin added to the solution of granite G–1 was 98, 100, and 99 μg, and the tin recovery from diabase W–1 was 92, 95, and 90 μg. The small amount of tin, 2 to 3 ppm, reported in these

samples (Fleischer and Stevens, 1962) is not significant in figuring percent recovery. Analysis of granite G–1 in this laboratory, with no tin added, showed an average value of 2.7 ppm tin.

TABLE 2.—*Comparison of tin content of seven samples from Seward Peninsula, Alaska, determined by the method described in this paper and by the bromide distillation method*

[Samples collected by C. L. Sainsbury. Tin determined chemically by the authors and Dorothy Ferguson [1]]

Sample No.	Tin (percent)		Sample description
	Method described in this paper	Bromide distillation method [1]	
284632	0. 0015	0. 003	Stream sediment from Boulder Creek, Cape Mountain, containing principally grains of granite, dark dike rock, and limestone.
284648	. 0043	. 005	Stream sediment from south contact area of granite of Car Mountain. Contains grains of granite, tactite, marble, and tourmalinized granite.
284584	. 0082	. 008	Stream sediment from Tin Creek, west of granite in Lost River area.
284612	. 013	. 010	Stream sediment from east branch of Mint River that heads against west side of granite of Brooks Mountain. Contains grains of limestone, tactite, and granite.
284701	. 018	. 021	Fragment of mineralized rock from dump at Winfield shaft, Car Mountain.
284576	. 042	. 040	Do.
284668	. 12	. 11	Slope wash below tin-uranium prospects southwest side of Brooks Mountain.

[1] Method described by Onishi and Sandell (1956).

The blue fluorescence produced by the tin-flavonol complex is very stable. Over a 3-month period, the tin standards have not deviated more than ±1 scale division. This reproducibility is exceptionally good for a fluorimetric reagent. Optimum conditions for the flavonol determination, such as acid, N,N′-dimethylformamide, and flavonol concentrations, are described in detail by Coyle and White (1957).

Seven selected rock samples from the Seward Peninsula, Alaska, previously analyzed for tin by the bromide distillation separation and estimation by dithiol as described by Onishi and Sandell (1956), were analyzed by the new method. Results obtained are compared in table 2.

REFERENCES

Coyle, C. F., and White, C. E., 1957, Fluorimetric determination of tin with flavonol: Anal. Chemistry, v. 29, p. 1486–1488.

Fleischer, Michael, and Stevens, R. E., 1962, Summary of new data on rock samples G–1 and W–1: Geochim. et Cosmochim. Acta, v. 26, p. 525–543.

Onishi, Hiroshi, and Sandell, E. B., 1956, Colorimetric determination of traces of tin with dithiol: Anal. Chim. Acta, v. 14, p. 153–161.

Parshall, E. E., and Rader, L. F., Jr., 1957, Model '54 transmission and reflection fluorimeter for determination of uranium, with adaptation to field use: U.S. Geol. Survey Bull. 1036–M, p. 221–251.

Smith, W. S., and Reynolds, S. A., 1955, Anion exchange separation of tin, antimony, and tellurium: Anal. Chim. Acta, v. 12, p. 151–153.

DETERMINATION OF CARBONATE, BICARBONATE, AND TOTAL CO_2 IN CARBONATE BRINES

By S. L. RETTIG and B. F. JONES, Washington, D.C.

Abstract.—Samples of carbonate brines having a CO_2 content in the range from 0.5 to approximately 9 percent have been analyzed by potentiometric titration and manometric measurement of total CO_2 evolved upon acid treatment. A plot of the potentiometric data shows inflection points that indicate that the carbonate and bicarbonate end points may differ significantly from the pH values of 8.2 and 4.5 used in routine water analysis. The direction, source, and range of error in the potentiometric method is evaluated by comparative use of the manometric technique.

The following presents a preliminary study of a problem in the analysis of concentrated waters from lacustrine closed basins.

The western Great Basin has several intermontane areas of interior drainage which constitute completely closed hydrologic systems. The end points of drainage in most of these basins are saline lakes or playas containing brines high in carbonate content. These brines have been derived principally by evaporative concentration of waters draining igneous rocks. Such waters are dominantly of a sodium carbonate composition, because of precipitation of alkaline-earth carbonate, and lack of sources of appreciable sulfate or chloride; some waters contain, however, significant amounts of anions in addition to CO_3^{-2} and HCO_3^{-1}.

In most natural waters, carbonate and bicarbonate are assumed to account for nearly all the alkalinity determined by titration with a strong acid (for example, H_2SO_4) to end points at pH 8.2 and pH 4.5, respectively (Rainwater and Thatcher, 1960, p. 93). But in the particular samples studied by this method, other bases, such as those formed by silica, boron, and phosphorus, and certain soluble organic compounds are titrated also, as evidenced by the form of the titration curves, and are included erroneously in the values for carbonate and bicarbonate. The titration end points in such solutions may vary significantly from pH 8.2 and 4.5, at least partly because high concentrations of carbonate and the other weak bases tend to form a natural buffering system.

In the analysis of brines containing appreciable carbonate in the western Great Basin an attempt was made to assess the sources of error in the titration method. The distribution of carbonate and bicarbonate was obtained from potentiometric titration curves, and the sum of the two, calculated as total CO_2, was compared with total CO_2 values determined by an evolution method from a duplicate sample. Samples of brine were obtained from the Abert and Alkali Lake basins of south-central Oregon and from the Deep Springs and Honey Lake basins of eastern California. Carbonate plus bicarbonate ranged from 15 to 81 percent of the total anion equivalent content. Samples were collected and stored in polyethylene bottles. Most analyses were made within 3 months of the date of sample collection.

Abert Lake is a large body of saline water in south-central Oregon. It occupies an eastern arm of the composite graben that constitutes the Abert-Summer Lake basin (Donath, 1962, p. 1), and is a remnant of a large pluvial lake that at one time covered much of the combined basin. Although during historical time the water surface of Abert Lake has varied considerably, a total area of 45 square miles, a mean depth of 3 feet, and a maximum depth of about 6 feet are probably close to average dimensions (A. S. Van Denburgh, oral communication, 1964). The retreat of higher lake stages is marked by efflorescent crusts on the north side of the lake. One sample was obtained in this area adjacent to a brine pool maintained perennially by inflow from a small spring.

The Alkali Lake basin is about 19 miles north-northeast of Abert Lake. The intermittent Alkali Lake itself lies in the southern part of its basin and consists

U.S. GEOL. SURVEY PROF. PAPER 501-D, PAGES D134-D137

of a broad very shallow pond adjacent to several large circular depressions known as "potholes" (Van Winkle, 1914, p. 115). These "potholes" contain highly concentrated carbonate brines, apparently as a result of the rate of ground water discharge being approximately equal to the rate of evaporation in the area.

Honey Lake, the lowest part of a large basin of interior drainage in southeast Lassen County, Calif., covers an area of approximately 12 by 15 miles. The lake frequently dries up completely in late summer and even at highest stage has a maximum depth of only 4 or 5 feet. Surface waters of Honey Lake usually are dilute, but substantial salinity characterizes interstitial solutions of the sediments immediately beneath the present lake-bed surface.

Deep Springs Lake (Jones, 1961, 1963; Peterson and others, 1963) is a small intermittent saline lake at about 5,000 feet elevation in northern Inyo County, Calif., about 35 miles west of northern Death Valley. About a third of the lake area is covered with porous layered saline crusts containing perennial interstitial brine. Major normal faulting at the mountain base east of the lake has formed a distinct trough containing two sag ponds, one of which has no outlet at low stage. Carbonate spring waters from the fault zone feed the ponds and are also the principal source of flow into the lake. Carbonate species remain high in the ponds, whereas during periods of surface flow through marshes to the lake, total carbonate percentage of spring waters drops, owing to mixing of waters, precipitation of solids, and loss of CO_2. Actually, sulfate is the dominant anion in the intercrustal brines of the lake.

Alkalinity of brines from the western Great Basin areas was determined by both field and laboratory titrations. In most samples the field and laboratory values differed significantly, primarily because of temperature change with resulting CO_2 loss between time of collection and analysis. For example, the field determination of sample 3HL4 showed 6,470 parts per million total CO_2 compared with 5,940 ppm for the laboratory determination. For sample 3AK3 the field value was 77,300 ppm CO_2 and the laboratory value was 71,020. Only the laboratory titrations gave CO_2 results directly comparable to the values determined by the evolution method.

In the laboratory, titrations for total alkalinity were performed potentiometrically using a laboratory pH meter. The tip of the burette was kept beneath the surface of the sample, and the sample was constantly stirred in order to avoid high concentrations of acid in some parts of the beaker where free carbon dioxide might be released. Effervescence before the carbonate end point is reached indicates that carbonate is being converted to free carbon dioxide and lost. Therefore the calculated value of bicarbonate will be low, though the determination of total CO_2 species as CO_3^{-2} would still be valid. The strength of the titrant used was approximately $0.1N$; stronger acid proved too likely to cause effervescence.

Complete titration curves were prepared by plotting pH against milliliters of acid, as shown by the solid lines on figure 1. The points of maximum inflection were selected as the end points of the titration. Concentrations of carbonate and bicarbonate so obtained were converted to equivalent CO_2 for comparison with total CO_2 determined by the manometric evolution method.

Total carbon dioxide by evolution was determined manometrically using a modification of the apparatus described by Pro and others (1959). By this method, carbon dioxide is liberated with addition of an excess of $1N$ sulfuric acid to the sample, in an evacuated system. The resulting change in pressure on a mercury manometer can be substituted in the ideal gas law equation, $PV=\frac{g}{M}RT$, and the equation solved for g, the weight of carbon dioxide, in grams.

A modification of the evolution method was used to verify approximately the carbonate and bicarbonate values obtained by potentiometric titration. Sulfuric acid ($0.1N$) was added to the reaction flask in increments of 5.0 ml, and the resulting manometer readings, in millimeters of mercury, were plotted as functions of the amount of acid added. The results are shown by the dashed lines of figure 1. There is a close similarity in the amount of titrant required to reach the inflection points in each of the two methods. Lack of better agreement probably is the result of (1) the use of a more dilute acid ($0.1N$ instead of $1N$), which in the manometric determination requires a larger volume, thus changing the calibration of the system; (2) inability to read the inflection points accurately; and (3) local loss of CO_2 during the titration.

The carbonate and bicarbonate values derived from potentiometric titrations were compared with the total carbon dioxide, in parts per million, determined by the evolution method. The results are listed in the accompanying table on page D137.

As indicated in the table, the percentage difference between results of the two methtods ranges from less than 1 percent to nearly 6 percent. This is not much greater than the reproducibility range found for the manometric method alone. In 6 of the 9 samples, the carbon dioxide values from the evolution method are greater than those calculated from the potentiometric

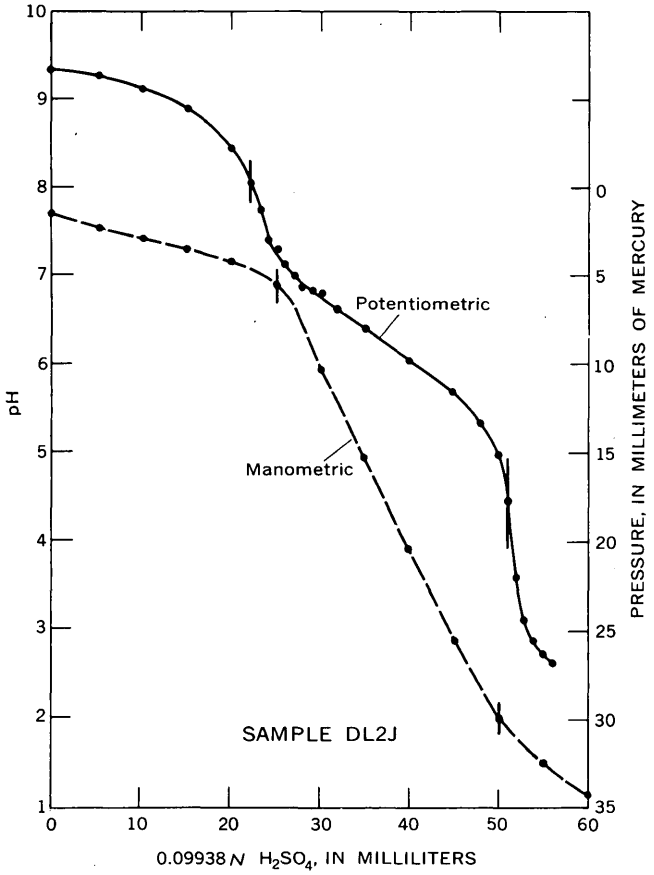

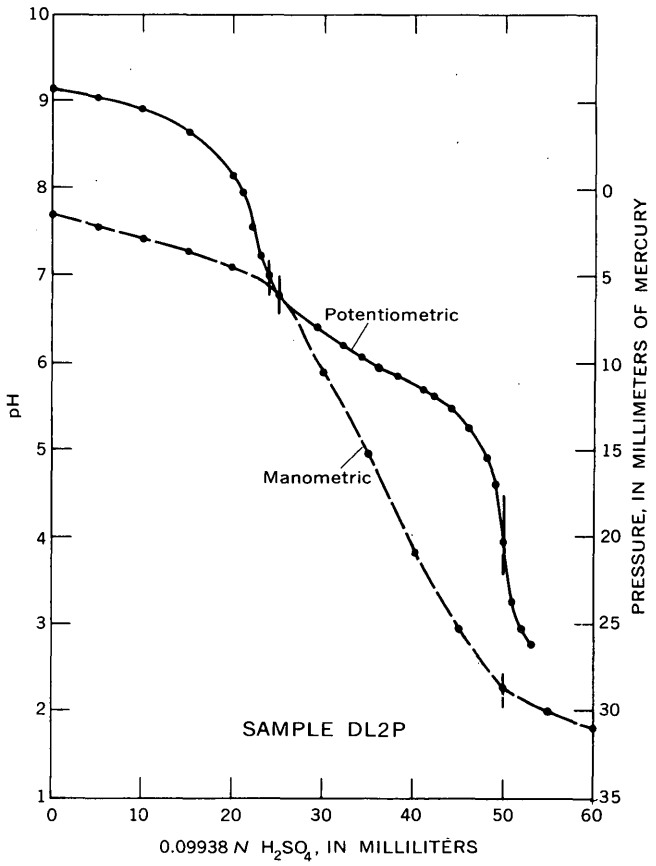

FIGURE 1.—Titration curves for three samples (DL2J, DL39H, and DL2P) of carbonate brines from the Deep Springs Valley, Calif. Dashed lines, results obtained by the manometric (CO_2 evolution) method; solid lines, results obtained by potentiometric titration.

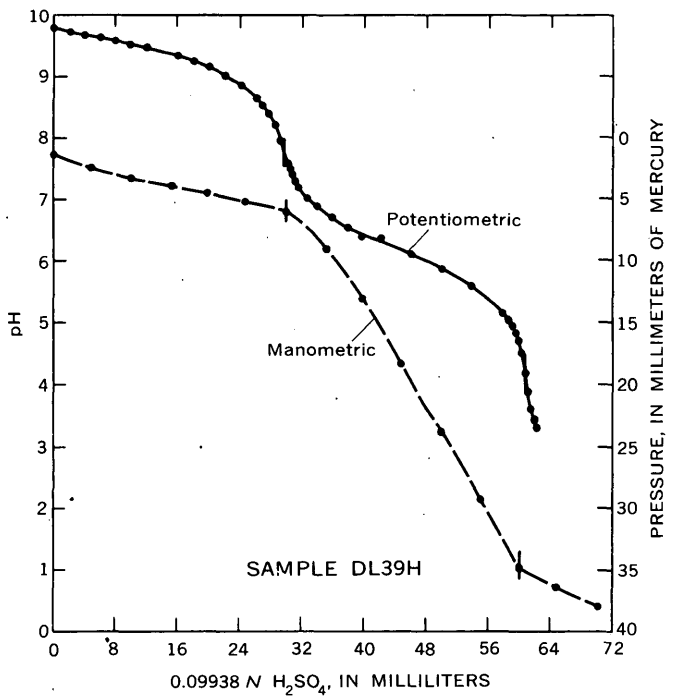

titration values. This suggests that interfering ions in these samples, at least, were not present in sufficient amounts to consume a significant quantity of titrant.

Several sources of error are recognized in the use of the manometric apparatus. For the most highly concentrated samples it was necessary to use a 2.0-ml sample in order to keep the manometer deflection within scale; to measure out a 2.0-ml sample accurately is very difficult, especially when the sample must be exposed to the atmosphere as little as possible. Duplicate determinations of sample 3AK2B (90,900 ppm CO_2) differed by 3.7 percent. In brines with relatively low total CO_2 content, errors may result from the inaccurate reading of very small deflections on the manometer. Duplicate determinations of sample 3HL4 (5,720 ppm CO_2) varied by only 0.5 percent, but in preliminary analyses of brines below 3,000 ppm in total CO_2, variation greater than 10 percent has been observed. The precision of the total CO_2 determination probably could be improved significantly by calibration of the apparatus with an optimum-size reaction flask for each concentration range.

Comparison of potentiometric titration and manometric (CO_2 evolution) methods for the determination of total CO_2 in brines of the western Great Basin

Sample	Dissolved solids (ppm)	Potentiometric titration			Manometric measurement	Percent deviation[1]
		CO_3^{-2} (ppm)	HCO_3^{-1} (ppm)	$CO_3^{-2}+HCO_3^{-1}$ (calc. as ppm CO_2)	Evolution (ppm total CO_2)	
Deep Springs Lake, Calif.:						
DL2J (intercrustal brine)	332, 000	20, 800	6, 580	20, 050	21, 000	−4. 5
DL2P (intercrustal brine)	316, 000	22, 400	2, 000	17, 840	18, 700	−4. 6
DL39H (sag pond)	337, 000	66, 100	3, 630	51, 120	54, 300	−5. 9
Alkali Lake basin, Oregon:						
3AK2B (pothole)	270, 000	113, 400	15, 400	94, 200	90, 900	+3. 6
3AK3 (Alkali Lake pond)	297, 000	94, 300	2, 520	71, 020	72, 000	−1. 4
Honey Lake, Calif.:						
3HL1 (pit in lake bed)	54, 300	8, 000	5, 470	9, 810	10, 400	−5. 7
3HL4 (pit in lake bed near Amedee Springs)	25, 100	5, 320	2, 830	5, 940	5, 720	+3. 8
Abert Lake, Oreg.:						
3AB5 (Albert Lake)	38, 400	6, 880	3, 640	7, 660	7, 640	+0. 3
3AB11–2 (brine pit, north end)	98, 300	16, 100	9, 680	18, 780	19, 000	−1. 2

[1] Percent deviation $= \frac{CO_2 \text{ titration} - CO_2 \text{ evolution}}{CO_2 \text{ evolution}} \times 100$.

In the potentiometric titration, a major possibility for error lies in the selection of the proper inflection points. The inflection points of the samples in the table were all quite sharp and could be determined with reasonable certainty within ±1 ml, which represents a percentage error of about ±2 percent. But in at least one sample (not reported here), the upper part of the titration curve was sufficiently flat that the choice of an inflection point involved considerable uncertainty. Presumably the bicarbonate+carbonate end points are obscured by the titration of other weak bases. In such samples the manometric method probably comes much closer to the determination of the true total carbon dioxide present. In the brines of the western Great Basin, the difference between total CO_2 values obtained by the two methods probably can be applied in large part to the correction of the carbonate end point, where weak base interference is most pronounced.

REFERENCES

Donath, F. A., 1962, Analysis of basin-range structure, south-central Oregon: Geol. Soc. America Bull., v. 73, no. 1, p. 1–16.

Jones, B. F., 1961, Zoning of saline minerals at Deep Spring Lake, California: Art. 83 *in* U.S. Geol. Survey Prof. Paper 424–B, p. B199–B202.

——— 1963, The hydrology and mineralogy of Deep Springs Lake, Inyo County, California: Johns Hopkins Univ., unpub. PhD. dissert., 238 p.

Peterson, M. N. A., Bien, G. S., and Berner, R. A., 1963, Radiocarbon studies of recent dolomite from Deep Spring Lake, Calif.: Jour. Geophys. Research, v. 68, no. 24, p. 6493–6505.

Pro, M. J., Etienne, Arthur, and Feeny, Frank, 1959, Determination of carbon dioxide in wines using a vacuum system: Jour. Assoc. Official Agr. Chemists, v. 42, p. 679–683.

Rainwater, F. H., and Thatcher, L. L., 1960, Methods for collection and analysis of water samples: U.S. Geol. Survey Water-Supply Paper 1454, 301 p.

Van Winkle, Walton, 1914, Quality of the surface waters of Oregon: U.S. Geol. Survey Water-Supply Paper 363, 137 p.

MAPMAKING APPLICATIONS OF ORTHOPHOTOGRAPHY

By MARVIN B. SCHER, Washington, D.C.

Abstract.—Orthophotographs, which present images in true planimetric position, are useful tools in planimetric and topographic mapping. They can be used to evaluate the horizontal accuracy of maps, to provide new data for revising existing topographic maps, and to serve as a source of information for compiling planimetric maps. Additionally, a map product suitable for publication may be prepared by proper cartographic treatment of mosaicked orthophotographs at a lower cost than for planimetric compilation.

Orthophotographs furnished to geologists, foresters, hydrologists, and engineers have proved to be of great value in alleviating field mapping problems caused by lack or inadequacy of map coverage. Orthophotographs are uniform-scale photographs prepared from conventional perspective aerial photographs by means of an Orthophotoscope. All features in such photographs are shown in their correct relative positions and at correct relative distances from one another. The Orthophotoscope may be described as photogrammetric restituting enlarger that corrects distortion by magnifying the different images on a perspective photograph inversely as their scale differences (Scher, 1962). Orthophotographs retain detail, such as individual trees appearing on the conventional perspective photographs from which they are prepared, thereby simplifying the problem of recording scientific field observations in their correct orthographic positions.

Methods for effectively applying orthophotography in a planimetric or topographic-mapping program are being investigated. Though incomplete, these studies disclosed several practical uses of this type of product in mapmaking operations and have indicated that, with proper cartographic treatment, a photographic type of map prepared directly from the orthophotographs may be acceptable to the map-using public.

EXPERIMENTAL APPLICATIONS

Because the geometrically faithful stereoscopic model is already available to the mapmaker, the geometric qualities of orthophotographs do not present a unique advantage to him. However, other characteristics of orthophotographs are decidedly different from those of stereoscopic models formed in precise plotters. For example, an orthophotograph is a permanent record that can be reproduced on a variety of materials, and it is readily portable and easily stored. Certain mapping procedures and operations may benefit from these distinguishing characteristics of orthophotographs.

Orthophotographs have been applied in map-revision experiments to evaluate maps of doubtful horizontal accuracy and to determine whether the existing map is sufficiently reliable to serve as a base for adding new map data. Orthophotographs have also served as a source of new map data and as a guide to positioning of the data.

The feasibility of compiling the planimetry (the plan details) of an urban area from a 1:24,000-scale orthophotomosaic was the objective of a recent research project. For this experiment, a continuous-tone diazo orthophotomosaic was printed on a white scribe-coated scale-stable plastic. This research project demonstrated that the direct scribing of the planimetric information on this kind of base is entirely feasible. The accuracy and completeness of the planimetry scribed on the orthophotomosaic compared favorably with the accuracy and completeness of that compiled by stereophotogrammetric procedures. The total time for the experimental compilation was about 10 percent greater than for standard compilation. However, the Orthophotoscope operating time was less than one fourth that of the stereoplotter operating time. It may be concluded, therefore, that orthophotography offers a significant advantage in compiling the planimetry for areas of dense cultural detail by permitting more efficient use of expensive instruments.

In another experiment, the mapworthy planimetry on a similar diazo print of the same orthophotomosaic

U.S. GEOL. SURVEY PROF. PAPER 501-D, PAGES D138-D140

79°57′30″ 55′

37°17′30″

1 0 1 MILE

A part of the experimental orthophotomap of the Roanoke, Va., 7½-minute quadrangle; scale 1:24,000.

was compiled in the field. The objective of this study was to determine what advantages accrue when a source of accurately positioned planimetric data, formerly available only in an accurate stereoplotter, is made portable and readily available to a fieldman. In domestic mapping operations, field inspection and surveying are usually needed to complete and correct planimetric information compiled in the office by stereophotogrammetric methods. In searching for the errors and omissions of a photogrammetric compilation, considerable time and effort must be spent in reviewing features that have already been plotted and portrayed correctly.

To reduce the time spent in the field to a minimum, the planimetric detail that could be photoidentified with certainty was scribed in the office before the manuscript copy was sent to the field. Using the orthophotomosaic and working without an assistant, the field engineer combined the field review and the compilation of the more obscure planimetry into one efficient operation. The fruitless effort involved in checking complete and correct information was eliminated.

THE ORTHOPHOTOMAP—A FINAL MAP PRODUCT

Studies to ascertain the cartographic treatment of orthophotographs necessary to provide a map suitable for publication have led to the preparation of an experimental orthophotomap. This orthophotomap is an orthophotomosaic prepared in quadrangle-map format, with a limited amount of added cartographic symbolization and marginal information, and lithographed in several colors. The recent development of the photoline-phototone photographic printing technique by the U.S. Army Map Service (Wickland, 1964) was most timely for this purpose. In this technique, two negative transparencies are prepared from a continuous-tone negative of the orthophotomosaic. One of these, the photoline negative, is printed in a manner that enhances all image edges and suppresses the remaining detail (Clarke, 1962). A positive prepared from this negative approaches a line drawing in appearance (fig. 1, right). The other transparency, the phototone negative, retains the continuous-tone appearance but actually contains patterns of randomly spaced and irregularly shaped dots. These negatives are both suitable for preparing lithographic press-plates.

The orthophotomap of the Roanoke, Va., 7½-minute quadrangle was the first to be prepared (pl. 1). The density of planimetric features and the considerable relief in the area were appropriate for the purposes of this research. Color-separation plates were prepared for the limited amount of cartographic symbolization to be included in the orthophotomap. From these plates and the photoline and phototone transparencies, 28 different 6-color lithographic renditions of the orthophotomap were printed. In the rendition

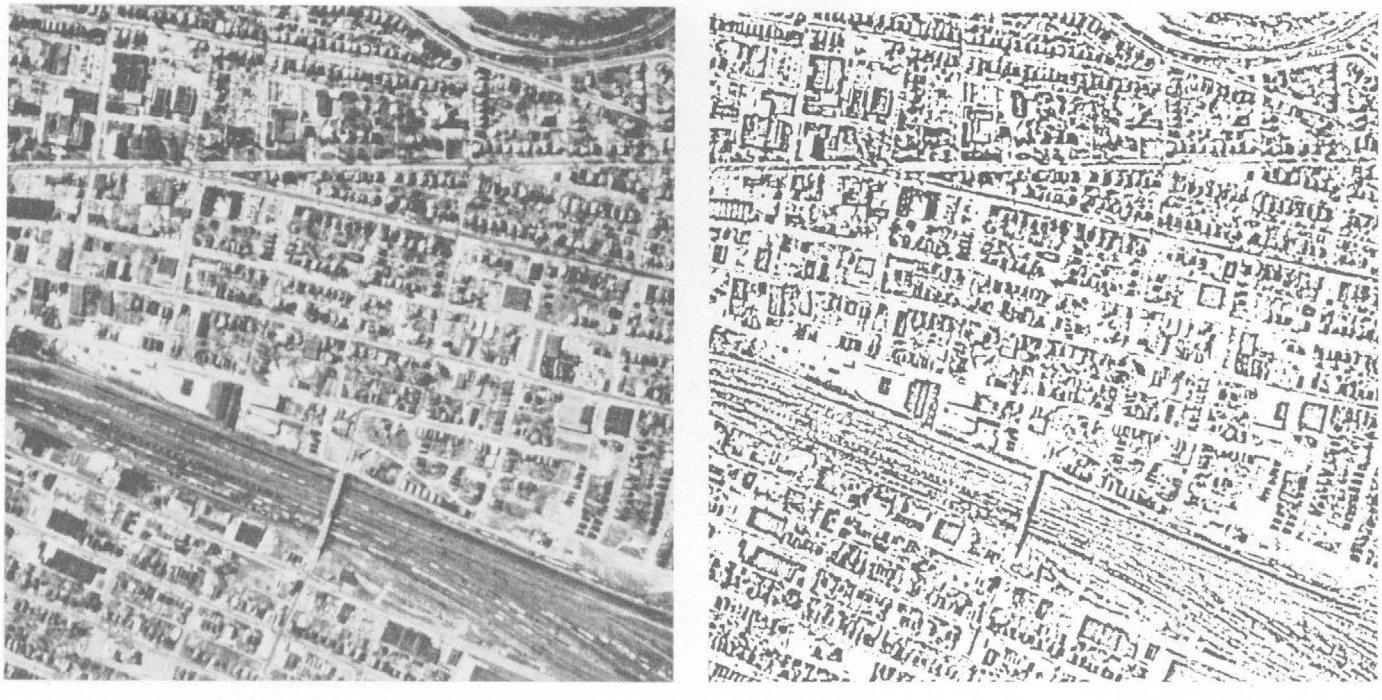

FIGURE 1.—A portion of an orthophotomosaic, left, of Roanoke, Va., and a photoline positive, right, of the same area, prepared from the same orthophoto negative. The scale of both is about 1:12,000.

742-652 O—64——10

considered most effective, the photoline images were printed in dark gray, the phototone images in gray green, the principal roads and their numbers in red, the major hydrographic features in blue, the wooded areas in green, and the names data and marginal information in black.

This form of map presentation is particularly advantageous in densely settled areas and, conversely, in areas of very sparse cultural detail. In urban areas the orthophotomap minimizes the need to delineate and scribe the congested planimetric detail, thereby offering savings in cost as compared with the standard planimetric compilation. In areas where little planimetric information would be shown on the standard line map, such features as lone trees or bushes and cattle trails, generally ignored as mapworthy features, are readily identifiable on the orthophotomap and are usable as landmarks. An experimental orthophotomap of such an area in Arizona is now being prepared.

Public acceptance of the orthophotomap will be influenced by the map user's willingness to assume the task and responsibility of photointerpretation required in using this product. It is quite possible that map users have become too accustomed to the simplicity of line drawings and the clarity of cartographic symbols. The amount of cartographic symbolization that should be added to an orthophotomap to satisfy public needs has not been finally determined. It is expected, however, that the cost of this additional cartographic work will not significantly reduce the advantages of orthophotomaps.

REFERENCES

Clarke, A. B., 1962, Edge isolation in photogrammetry and geologic photography: Art. 166 *in* U.S. Geol. Survey Prof. Paper 450–D, p. D160–D163.

Scher, M. B., 1962, Research activity with the U–60 orthophotoscope: Art. 57 *in* U.S. Geol. Survey Prof. Paper 450–B, p. B135–B137.

Wickland, L. R., 1964, Map substitute products: Am. Cong. on Surveying and Mapping Mtg., Washington, D.C., March 16–19.

GROUND-WATER CONDUITS IN THE ASHLAND MICA SCHIST, NORTHERN GEORGIA

By CHARLES W. SEVER, Quitman, Ga.

Work done in cooperation with the U.S. Atomic Energy Commission

Abstract.—Although joints in the rocks govern the course of streams that drain outcrops of the Ashland Mica Schist, they are not the principal conduits through which ground water moves toward the streams. Instead, ground water moves mainly through planar openings parallel to the bedding, schistosity, and axial-plane cleavage of the schist.

The Ashland Mica Schist of Precambrian age crops out within the Georgia Nuclear Laboratory (GNL) site in Dawson County, Ga., about 50 miles north of Atlanta. This formation, a thick sequence of biotite schist interbedded with biotite gneiss, is complexly folded into tight overturned isoclinal folds in which the bedding, schistosity, and axial-plane cleavage are parallel, or nearly so. These structural features cannot be distinguished one from another except locally on the nose of folds. They strike about N. 60°E. and dip about 60° SE. except where bedding and schistosity are wrapped around the nose of folds. Two conspicuous sets of high-angle joints trend N. 30° W. and N. 54° W. and intersect the strike of the schist at angles of about 90° and 66°.

The crystalline rocks are deeply weathered and are mantled by a thick saprolite zone. On hills the saprolite generally is about 50 feet thick, although in one well it exceeded 137 feet in thickness. Fresh rock crops out in valleys, drains, and deep road cuts, and a few small streams are steeply incised in the bedrock. Bedding, schistosity, jointing, and at many places cleavage, are preserved in the saprolite beneath the soil zone. The land surface is deeply dissected; ridge crests are sharp, and slopes are steep. Slopes on the southeast sides of valleys generally are steeper than slopes on the northwest sides.

During a hydrologic investigation at the GNL site Stewart and others (1964) found the average porosity of saprolite to be much greater than the average porosity of fresh crystalline rock and indicated that the transition zone between saprolite and fresh rock was the most permeable zone. Inasmuch as all the water percolating downward through the saprolite cannot flow into the few openings available in the fresh rock, most of it accumulates in the transition zone. Accumulation of the water steepens the hydraulic gradient, causing the water to be shunted laterally toward discharge points along surface drainage courses.

Laboratory tests show that the permeability due to interstitial voids is too small to account for the amount of water transmitted by the Ashland Mica Schist; thus the principal conduits for ground-water movement must be of either the tubular or planar type. Tubular openings, such as are common in some limestone, generally are the result of solution activity and are unlikely in schist; furthermore, none were observed to intersect exposed rock surfaces in the area. On the other hand, the Ashland Mica Schist has abundant planar openings that have resulted from the development of jointing, schistosity, and axial-plane cleavage during metamorphism and orogenic deformation of the original sedimentary rocks. Moreover, unloading and weathering have widened these openings to a probable depth of several hundred feet.

In the hydrologic investigation of the GNL site, R. F. Carter (Stewart and others, 1964) observed that the base flow of streams varied considerably with their orientation (fig. 1). As the pattern of surface drainage reflects the systems of high-angle joints in the

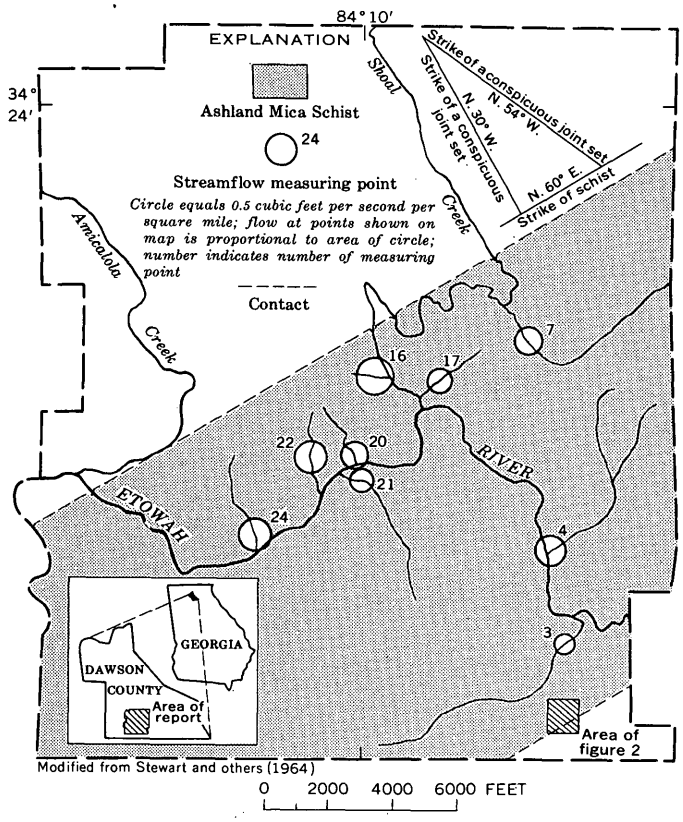

FIGURE 1.—Map of the Georgia Nuclear Laboratory site, showing amount of base flow per square mile of drainage area for streams draining outcrops of the Ashland Mica Schist.

Ashland Mica Schist, Carter postulated that joints in the rocks are the principal conduits through which ground water moves.

A cone of depression that develops around a pumped well tapping steeply dipping planar openings should be elliptical with the long axis parallel to the strike of the planar openings. It should have a steeper gradient along the dip of these openings. On the updip side of the cone the hydraulic gradient would be more nearly parallel to the planar openings and water could move along the planar openings toward the pumped well. But on the downdip side of the cone the hydraulic gradient would be nearly normal to the planar openings and the water would have to move by an indirect path to reach the pumped well. A steeper hydraulic gradient would be required to move the water normal to the planar openings than would be required to move water along (through) the planar openings.

If the high-angle joints were the principal conduits for ground-water movement, the cone of depression around a pumped well that taps the Ashland Mica Schist necessarily would be elliptical in plan view and the longer axis of the ellipse would trend N. 30° W. to N. 54° W. in line with the strike of the joints. However, as observed when a well was pumped during aquifer tests at the GNL site, the water-level drawdown in the more than 40 observation wells indicated that the longer axis of the elliptical cone of depression was in line with the strike of the schist, roughly normal to the strike of the principal joint sets (fig. 2). The cone of depression had a steeper gradient southeast of the pumped well than northwest, indicating that the well was draining water from rocks northwest of the well faster than from rocks southeast of the well. A hydraulic barrier located immediately southeast of the pumped well could cause this effect, but a geologic investigation disclosed no such barrier. When infiltration tests were made on the GNL site (Stewart and others, 1964) the resulting ground-water mound, or cone of impression, also was found to be elliptical in plan view and to have its longer axis in line with the strike of the schist. The shape and orientation of the cones of depression and impression indicate that openings along schistosity, cleavage, and bedding planes and not joints are the principal conduits through which ground water moves toward discharge points.

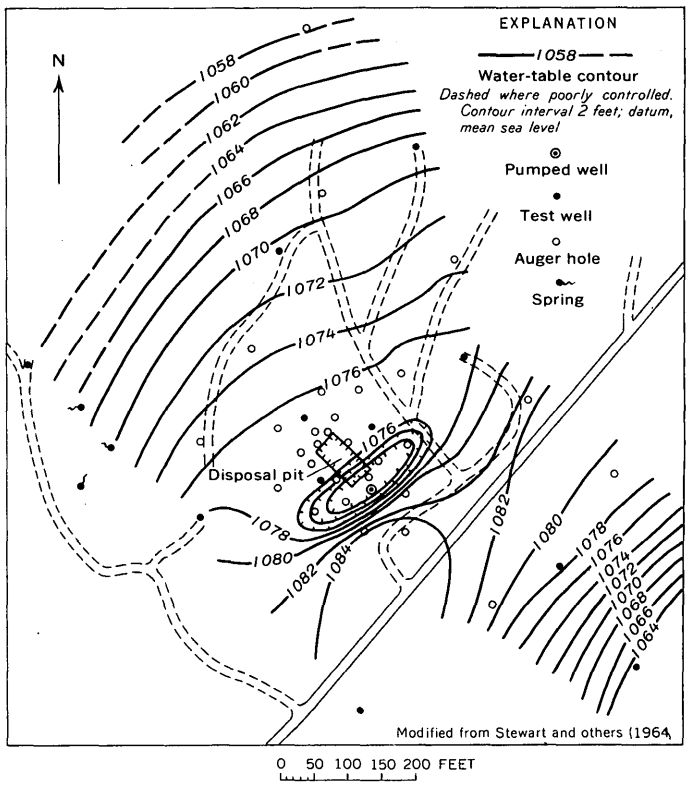

FIGURE 2.—Water-table contour map at end of 30-hour pumping test, June 19, 1958, Georgia Nuclear Laboratory, Dawson County, Ga.

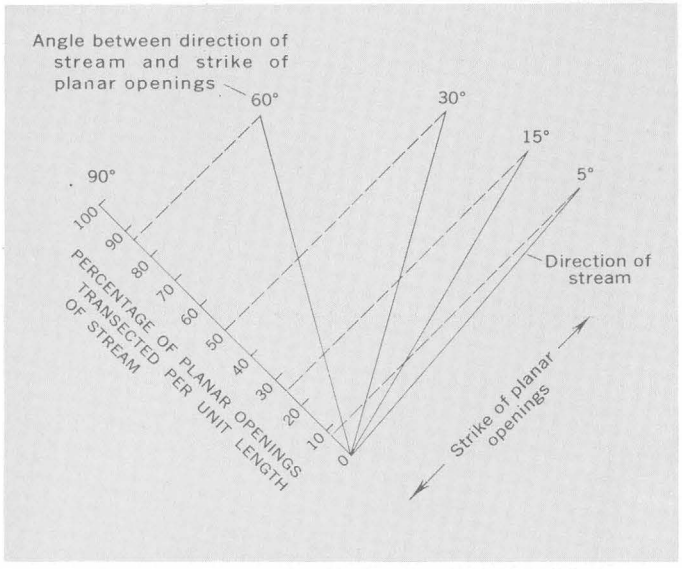

FIGURE 3.—Relation between direction of streamflow and the percentage of planar openings transected per unit length of stream.

If the planar openings are assumed to be parallel, or nearly so, and are distributed uniformly throughout the schist, the amount of ground water discharged into a given reach of a stream would be related directly to the angle between the direction of streamflow and the strike of the planar openings. As shown on figure 3, the greater the angle between them, the greater the percentage of openings transected per unit length of stream.

The relation of ground-water discharge to the strike and dip of the schist and the strike of the principal joints is illustrated on figure 4. Ground-water discharge is greatest to streams flowing normal to the strike of the schist and least to streams flowing normal to the strike of the joints. This is precisely the relation that should be expected if the principal ground-water conduits are planar openings oriented parallel to schistosity and cleavage in the schist. Further studies will be needed to determine which type of planar opening—schistosity, axial-plane cleavage, or bedding plane—forms the principal conduit.

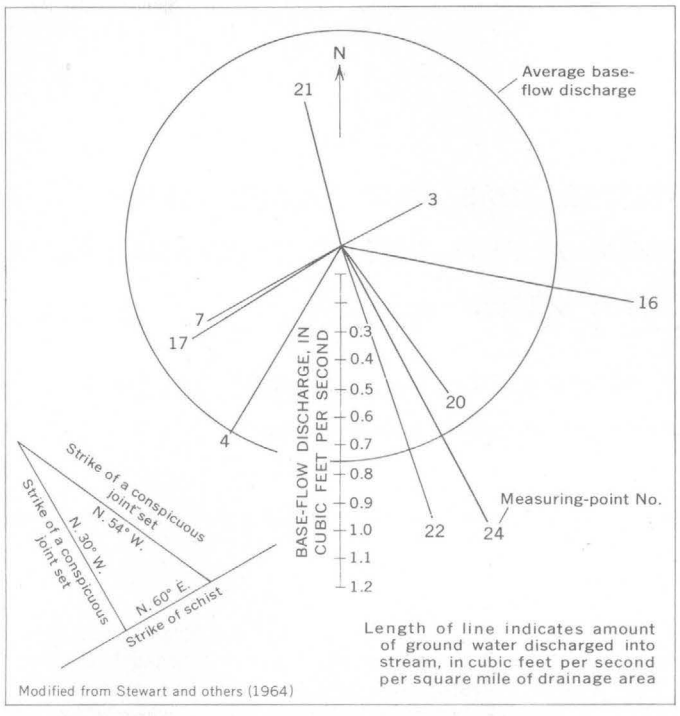

FIGURE 4.—Relation between base-flow discharge to streams and direction of the major axis of stream basins at the Georgia Nuclear Laboratory, Dawson County, Ga.

REFERENCE

Stewart, J. W., Callahan, J. T., Carter, R. F., and others, 1964, Geologic and hydrologic investigation at the site of the Georgia Nuclear Laboratory, Dawson County, Ga.: U.S. Geol. Survey Bull. 1133-F. [In press]

TEMPERATURE AND CHEMICAL QUALITY OF WATER FROM A WELL DRILLED THROUGH PERMAFROST NEAR BETHEL, ALASKA

By ALVIN J. FEULNER and ROBERT G. SCHUPP,
Anchorage, Alaska, Palmer, Alaska

Work done in cooperation with the U.S. Air Force, Alaskan Air Command

Abstract.—A water well drilled on the Kuskokwim delta near Bethel, Alaska, obtained potable water beneath 603 feet of permafrost. Temperature of the subpermafrost water was 33.2°F. Chemical similarity of well water to water from the Kuskokwim and Yukon Rivers suggests recharge from either of these rivers through unfrozen zones in the delta deposits.

A water well, 622 feet deep, drilled in delta deposits of the Kuskokwim River at a military installation near Bethel (fig. 1) produced water from beneath permafrost 603 feet thick. Located on the older part of the delta, which has been trenched by modern streams, the well site (well 2) is about 175 feet above mean sea level (fig. 2). According to Waller (1957, p. 4) the area is underlain by clay, silt, sand, and some gravel, and the deposits generally are coarser with depth. Waller (1957) also reports that the deposits of coarse sand and fine gravel penetrated in the drilling of wells in and near Bethel are lenticular and cannot be correlated from one well to another.

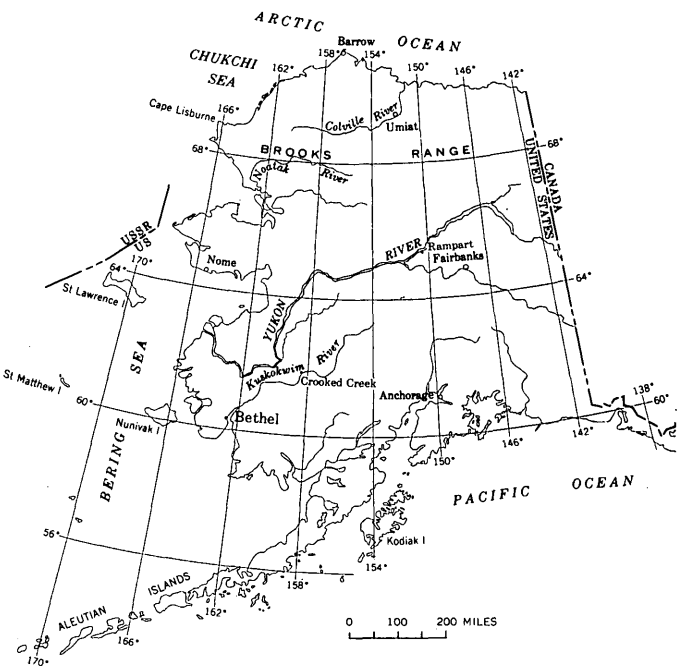

FIGURE 1.—Map of Alaska, showing areas referred to in text.

WELL DRILLING AND TESTING

The materials penetrated in drilling well 2, as reported by the U.S. Army Engineers, Alaska District, consist of interbedded sandy silt, silty fine sand, fine sand, and pebbly sand (fig. 3). All these materials are believed to be of deltaic origin. The depth to which the deltaic deposits extend at the well site is not known, but in the general vicinity of the well the total thickness of the deltaic deposits ranges from 450 to nearly 1,000 feet (T. L. Péwé, oral communication, 1963). Permafrost at well 2 extends to a depth of 603 feet. When the drill reached the base of permafrost, a slurry of water, sand, and wood fragments surged up the hole, filling it to within about 350 feet of the surface. One fragment of wood, believed to have come from just below the base of permafrost, has been dated by the carbon-14 method as older than 34,000 years (Ives and others, 1964, sample W–1287).

After well 2 had been drilled to a depth of 662 feet, the interval between 626 and 651 was screened, the hole was plugged back to the bottom of the screen,

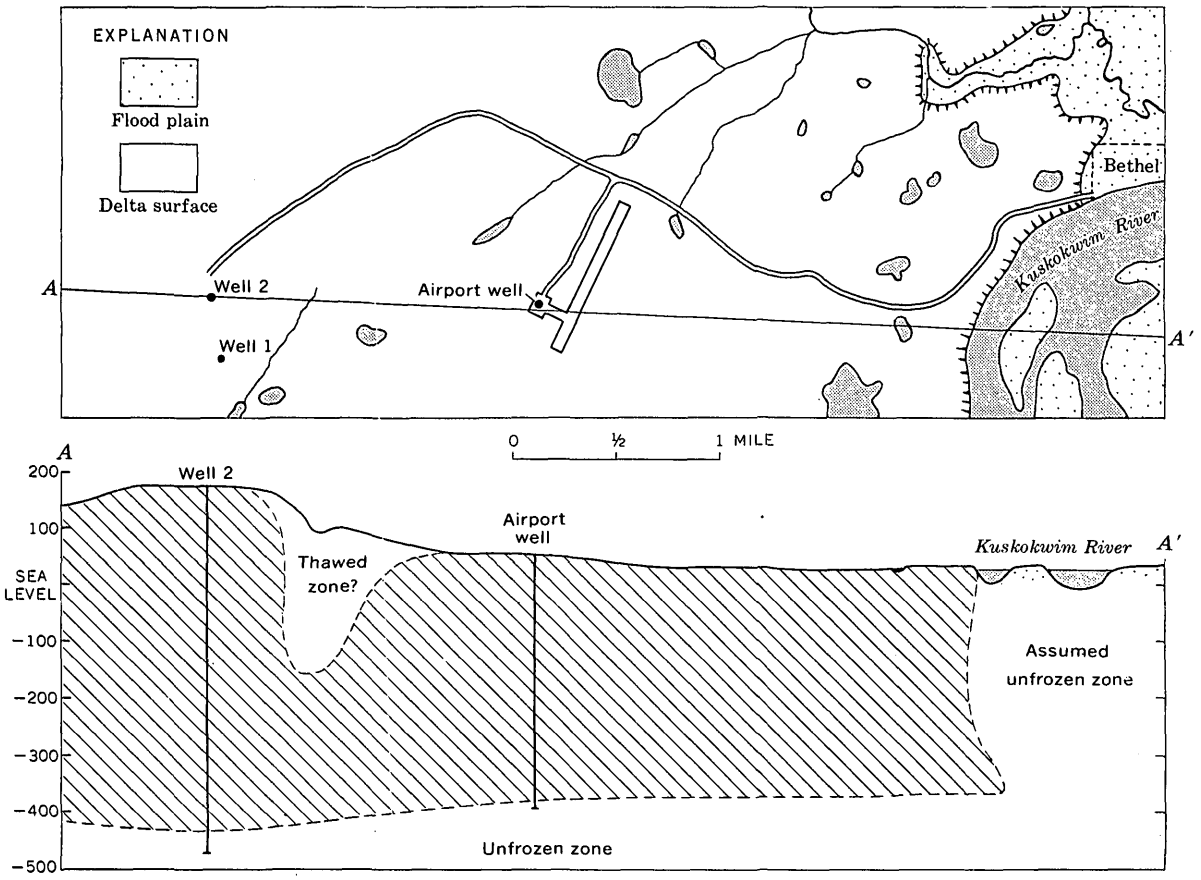

FIGURE 2.—Map showing location of wells near Bethel, and cross section showing thickness of permafrost (diagonal lines) in the area.

and the well was developed by surging and bailing. Following the development of the well, the static water level stood 136 feet below land surface. Because the water level stood so high in the permafrost (more than 450 feet), it was necessary to introduce about 1½ gallons per minute of warmed water into the well to prevent freezing. In early January a pump having a capacity of 12 gpm was installed, and by continuous pumping the water in the well was kept from freezing.

Although the capacity of the pump was small, the pump was used in making a preliminary test. After the well had been pumped continuously for 64 hours at a rate of 12 gpm, the water level stood at 146.7 feet below land surface, or 10.7 feet below static level, indicating a specific capacity of about 1 gpm per foot of drawdown.

At intervals of 12, 24, and 36 hours after completion of the preliminary test, the temperature of the water in the well was measured at increments of depth from the water surface to the base of the screen. A Whitney underwater thermometer, rated accurate to within 0.1°F, was used to make the measurements. The three sets of water temperatures were averaged and are presented on figure 3. The greatest deviation from the average of the three temperature determinations at any given depth was 0.1°F. The average temperature of water opposite the permafrost zone was 31.8°F, but the average of the three readings at the different depths within this zone ranged from 31.8° to 31.9°F. All temperatures below a depth of 605 feet were the same on all three readings. The maximum water temperature recorded was 33.2°F at a depth of 620 feet. The presence of a solid casing rather than a screen at this depth is not believed to have had any significant effect in the temperature determinations.

The temperature at which water in the well would freeze inward opposite the permafrost zone was not determined. However, during construction of the well, the water froze inward from the casing during the night when drilling was not in progress. Collars of ice, more than an inch thick, formed in the casing at a depth of about 300 feet during the period between midnight and 8 o'clock in the morning. After completion of drilling and development of the well, convection currents between warmer water at the base

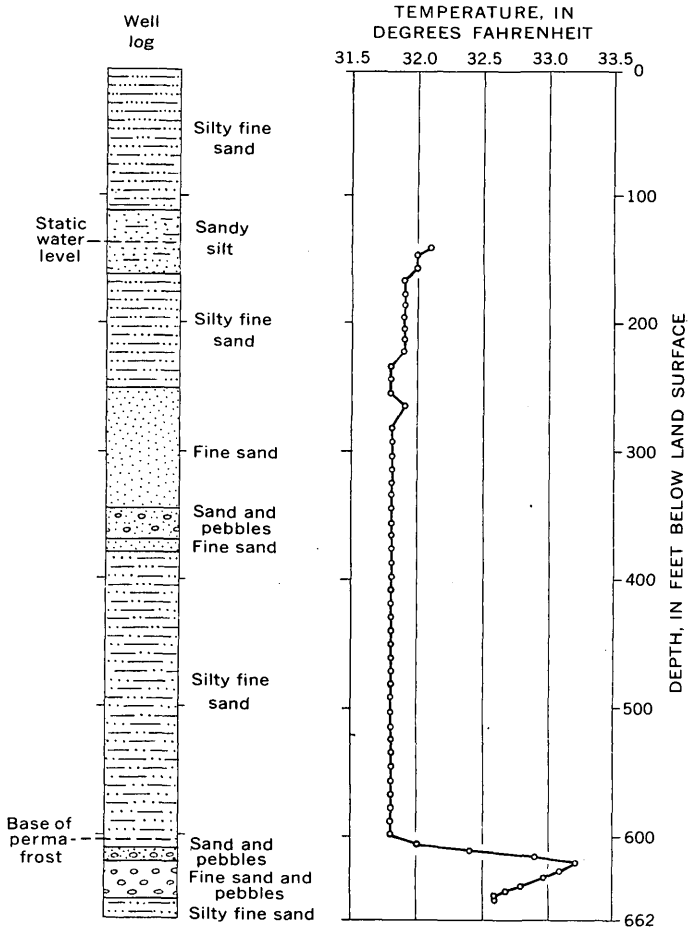

FIGURE 3.—Generalized lithologic log and water-temperature log of deep well near Bethel, Alaska. Temperature measurements made on January 21 and 22, 1963. Each circle on the water-temperature log indicates a separate temperature measurement.

of permafrost and the cold water above may have kept the water from freezing inward during the period in which the temperature measurements were made. After the last set of temperature measurements were made, warm water from storage was again introduced into the well to prevent freezing.

About a week after the conclusion of the preliminary pumping test a larger pump was installed and a second pumping test made. This test lasted only 10 hours because the electric water-level tape, used to measure depth to water, became entangled in the pump column. A third and final test was begun 2 days later, and pumping continued for 33 hours. During this test the average rate of pumping was about 45 gpm and the drawdown was about 40 feet, again indicating a specific capacity of about 1 gpm per foot of drawdown.

PERMAFROST

In the immediate vicinity of Bethel the base of permafrost is about 350 below sea level (Waller, 1957, fig. 3). The greater thickness of the permafrost in the vicinity of well 2 is probably due to the fact that the ground surface at the site is about 150 feet higher than at Bethel. Beneath rivers and old meanders, and in areas where tributaries have flowed in comparatively recent times, the permafrost has partly thawed from the surface downward, or has been removed entirely by downward thawing. At the site of well 1, about 1,500 feet south of well 2, permafrost was reported at depths of from 22 to 42 feet and from 280 to at least 378 feet, where drilling was stopped. The well was backfilled to 202 feet, and the zone between 192 and 202 feet was screened and developed. According to Waller (1957, p. 5), the report of permafrost from 22 to 42 feet is questionable. Well 1 is in a depression that is believed to have been the channel of a fairly sizable stream which fed the Kuskokwim River within comparatively recent times. This thawed zone is shown on figure 1 between well 2 and the airport well. Elsewhere in the vicinity, permafrost extends from near ground surface to 350 to 425 feet below sea level (fig. 2).

WATER QUALITY

Three water samples were collected from well 2 for chemical analysis (see accompanying table). The first of these samples was a bailer sample taken when water and sand first entered the hole from a depth of 603 feet. The second was a bailer sample collected about 8 hours after the conclusion of the preliminary pumping test. The third sample was collected about 1 hour before the conclusion of the final pumping test. The analyses show that the well yields a bicarbonate water in which calcium and magnesium are the predominant cations. The dissolved-solids content ranges from 123 to 172 ppm.

Also included in the table are analyses of water from well 1, from a 436-foot well at the Bethel airport (fig. 2), from the Kuskokwim River upstream from Bethel, and from the Yukon River. The analysis reported for the Kuskokwim River represents an average of 11 samples taken during 1962 at Crooked Creek, about 145 miles northeast of Bethel, and the analysis for the Yukon River represents an average of 12 samples taken during 1962 at Rampart, about 480 miles northeast of Bethel.

Chemical analyses of water from wells near Bethel and from the Yukon and Kuskokwim Rivers

[Mineral constituents in parts per million. Analyses by the Quality of Water Branch, U.S. Geological Survey, Palmer, Alaska]

Source of water sample	Date of collection	Silica (SiO_2)	Iron (Fe)	Manganese (M)	Calcium (Ca)	Magnesium (Mg)	Sodium (Na)	Potassium (K)	Bicarbonate (HCO_3)	Sulfate (SO_4)	Chloride (Cl)	Fluoride (F)	Nitrate (NO_3)	Dissolved solids (residue on evaporation at 180°C)	Hardness as $CaCO_3$		Specific conductance (micromhos at 25°C)	pH	Color
															Carbonate	Noncarbonate			
Well 2, 651 feet deep: Bailer sample from depth of 603 feet, before completion of well	11/27/62	21. 0	0. 03	----	23	15. 0	12. 0	5. 3	157	7. 0	11. 0	0. 0	0. 3	172	118	----	273	8. 0	----
Bailer sample 8 hours after end of first pumping test	1/21/63	9. 8	. 05	0. 33	23	8. 3	4. 0	2. 2	128	3. 0	4. 0	. 1	. 3	123	105	----	206	7. 8	10
Pump sample near end of third pumping test	1/31/63	24. 0	. 05	----	19	13. 0	3. 7	2. 2	123	1. 0	4. 0	. 0	. 3	127	100	----	189	8. 0	----
Well 1, 202 feet deep, 1,500 feet south of well 2	12/29/60	34. 0	. 87	. 35	35	4. 8	3. 8	1. 1	138	4. 0	4. 0	. 0	. 0	155	108	----	216	7. 1	20
Airport well, 436 feet deep, 2.8 miles west of Bethel	6/ 9/58	25. 0	. 31	. 02	25	7. 4	4. 4	1. 2	116	3. 5	3. 5	. 0	. 0	127	98	----	204	6. 0	----
Yukon River at Rampart, average of 12 analyses	1962	6. 7	. 03	----	32	8. 6	2. 6	1. 7	105	28. 0	1. 3	. 1	1. 1	132	111	25	219	8. 0	25
Kuskokwim River at Crooked Creek, average of 11 analyses	1962	8. 5	. 07	----	25	5. 2	1. 8	1. 1	89	17. 0	. 6	. 2	. 5	103	85	12	181	7. 8	15

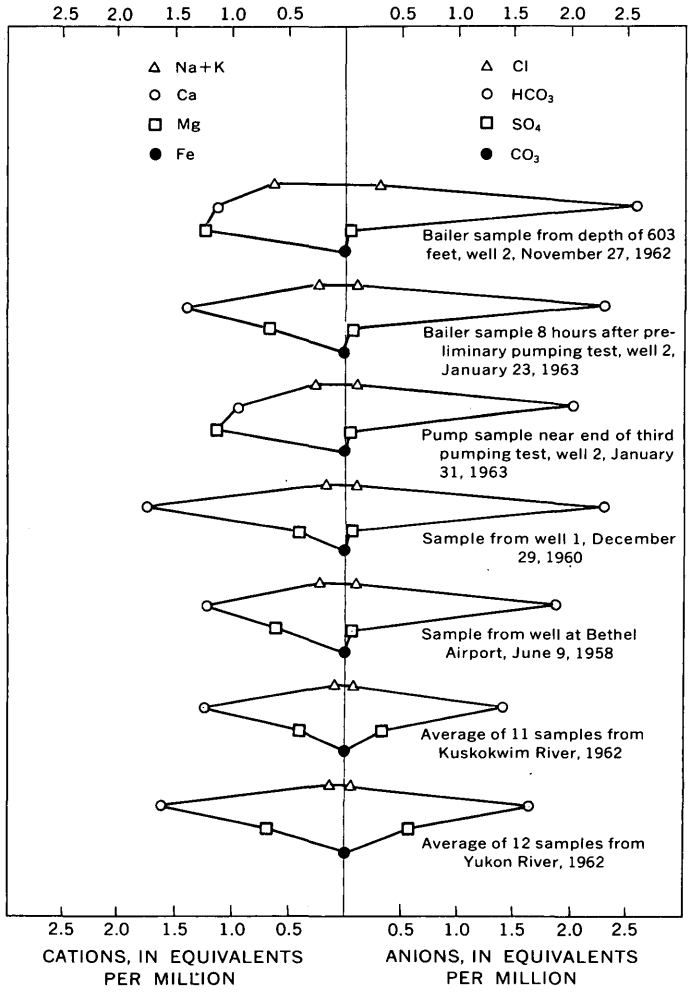

FIGURE 4.—Chemical quality of ground water in the Bethel area, Kuskokwim River water at Crooked Creek, and Yukon River water at Rampart.

Diagramatic representations of the water analyses (fig. 4) show that 8 hours after completion of the preliminary pumping test, water from well 2 was generally similar to that from other wells in the area and to average water from the Kuskokwim and Yukon Rivers. The possibility of recharge from either river through unfrozen zones upstream from the Bethel area has been postulated by Waller (1957, p. 7).

Analyses of water from well 2 suggest that the sample taken immediately after drilling may be water concentrated by freezing. Similar, more pronounced, changes have been noted elsewhere in Alaska (Feulner and Schupp, 1963). The water from well 2 is of good quality and generally is suitable for domestic or industrial use.

REFERENCES

Feulner, A. J., and Schupp, R. G., 1963, Seasonal changes in the chemical quality of shallow ground water in northwestern Alaska: Art. 52 *in* U.S. Geol. Survey Prof. Paper 475–B, p. B189–B191.

Ives, P. C., Levin, Betsy, Robinson, R. D., and Rubin, Meyer, 1964, U.S. Geological Survey radiocarbon dates VII: Am. Jour. Sci., Radiocarbon Supp., v. 6. [In press]

U.S. Geological Survey, 1963, Quantity and quality of surface waters of Alaska, 1962: U.S. Geol. Survey, Water Resources Div., Basic Data Release, 138 p.

Waller, R. M., 1957, Ground water and permafrost at Bethel, Alaska: Alaska Dept. Health, Section of Sanitation and Engineering, Water Hydrological Data Rept. 2, 11 p.

HYDROGEOLOGIC RECONNAISSANCE OF THE REPUBLIC OF KOREA

By W. W. DOYEL and R. J. DINGMAN,
Washington, D.C., Lawrence, Kans.

Work done under the auspices of the Agency for International Development, U.S. Department of State

Abstract.—The Republic of Korea is underlain largely by metamorphic and intrusive igneous rocks which generally yield only small amounts of water from the weathered zone. Present ground-water supplies, mostly from unconsolidated deposits in the river valleys and coastal flatlands, can be expanded considerably.

The Republic of Korea[1] (fig. 1) is a country in which approximately 25,000,000 persons are subsisting on a land area (96,929 square kilometers) about the same size as that of the State of Indiana. Their major occupation is the cultivation of rice with which to feed the rapidly increasing population. Rice is grown in small plots, or paddies, which are flooded during the growing season principally with water diverted from streams. A severe drought during the spring of 1962 resulted in poor crops and stimulated interest in the possibility of developing ground water for supplemental irrigation. At that time no organization in South Korea was carrying on systematic ground-water investigations nor were there personnel, either local or foreign, qualified to undertake the work. As a result, the Agency for International Development, U.S. Department of State, requested the U.S. Geological Survey to make a ground-water reconnaissance and evaluate current water-supply problems. The work was done during January–March 1963.

The study revealed that ground water is used for domestic, municipal, and industrial supplies and, to a lesser extent, for irrigation but that development of this resource has proceeded with very little scientific guidance or direction. Recognizing the importance of ground-water resources and the need for their proper management, the Japanese initiated in the late 1930's a comprehensive investigation of the ground-water resources, but the program was halted abruptly by World War II and was not resumed after the war. Since World War II, water wells have been drilled by the U.S. Army, U.S. Operations Mission to Korea, drilling contractors, and Republic of Korea agencies, but largely for exploitation rather than for investigation. Although many satisfactory supplies have been developed, very little information has been obtained regarding the overall availability and the quantitative limits of the ground-water resources.

The Republic of Korea is mountainous and is cut by steep-walled river valleys and some wider rift-type structural valleys. Most of the country has an average annual rainfall of more than 1,000 millimeters; the annual precipitation at Seoul and Pusan averages 1,254 and 1,403 mm, respectively. Rainfall is heaviest during the summer months.

Igneous and metamorphic rocks are exposed throughout most of the country (fig. 2). Metamorphism has largely destroyed the primary porosity in the sedimentary rocks and, in general, no important secondary porosity has developed. The thick layer of weathered material that mantles these rocks through much of the country has sufficient permeability to sustain dug wells for domestic and rural farm use. Jointing and faulting, although present, have not resulted in any effective porosity. Small springs are found in the higher areas but usually flow only during, and for a short time following, the rainy season. Most of the springs occur at the contact of the weathered and unweathered rock.

[1] The official designation, Republic of Korea, is used interchangeably with ROK, South Korea, and Korea in accordance with common usage. All refer to that part of the Korean Peninsula south of the demilitarized zone separating the Republic of Korea from the northern, communist-controlled Peoples Republic of Korea or North Korea.

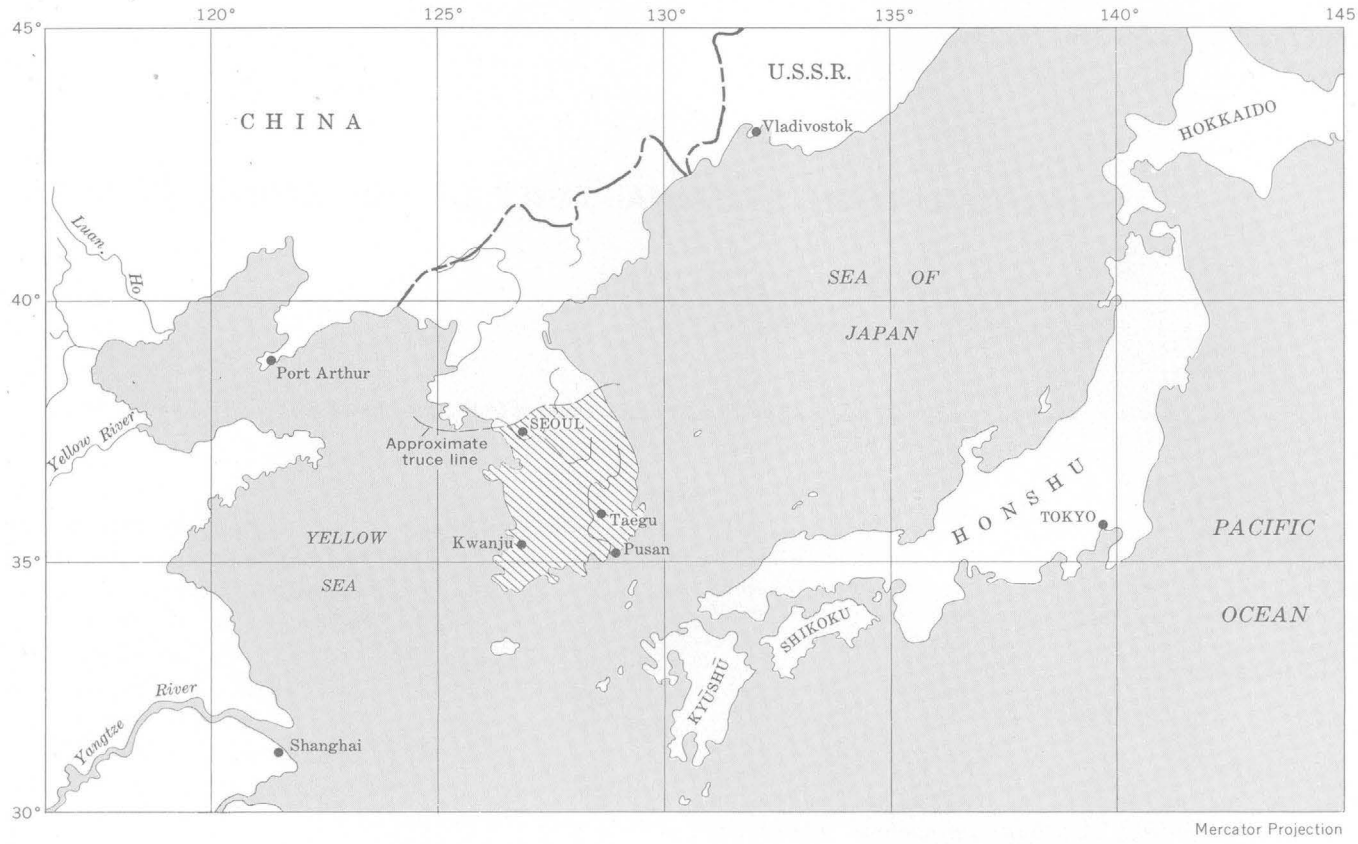

FIGURE 1.—Map showing location of the Republic of Korea (diagonal lines).

Mesozoic rocks consisting of shale, sandstone, and siltstone are present in the southeastern part of the country. They have a reported maximum thickness of 20,500 meters in the Taegu area (Kobayashi, 1953, p. 233) and are gently folded. The axes of the folds are oriented in a general northwest direction, and the rocks are cut by faults trending in the same direction. The nature of the rocks and the structural features in the Taegu area suggest that the rocks contain ground water under artesian conditions (fig. 2). However, exploratory drilling would be required to determine the availability of artesian water supplies.

Unconsolidated Pleistocene and Recent alluvial deposits resting on bedrock underlie the floors of the steep-walled flat-bottomed valleys. The broad flatlands along the west coast of the country also are underlain by unconsolidated sediments that rest on bedrock. Hills of intrusive and metamorphic rocks projecting upward through the coastal unconsolidated sediments indicate that the bedrock surface is irregular and probably was produced by erosion. The alluvial and coastal deposits are not only the current source of most of the large ground-water supplies but also the best potential source; their areal distribution is shown on figure 2.

Present-day deposits in stream valleys consist mostly of sand and silt. Gravel is being deposited by streams

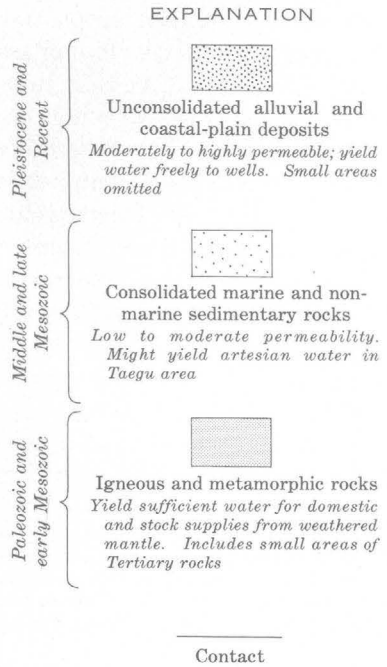

FIGURE 2.—Explanation.

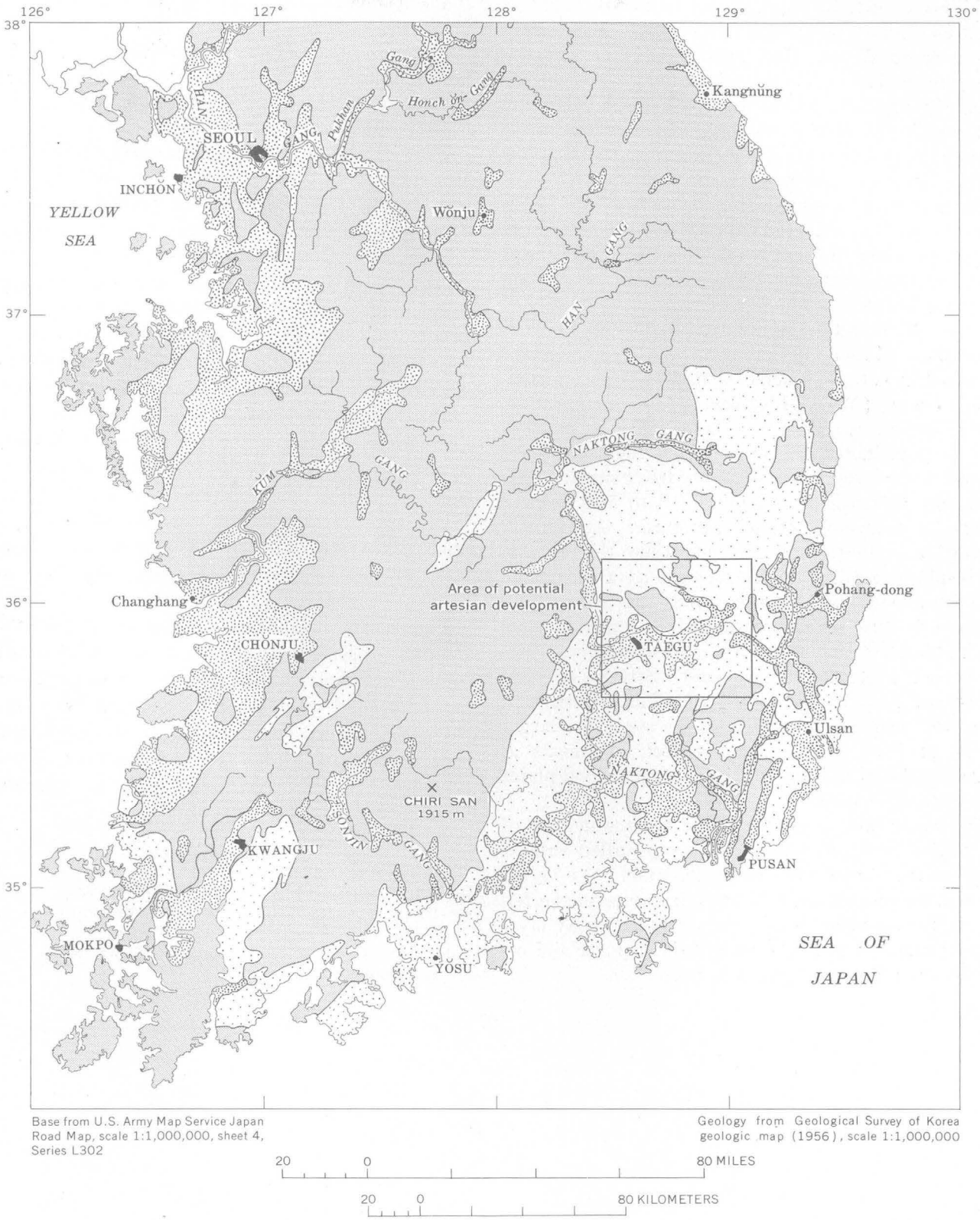

FIGURE 2.—Geologic map showing areas of ground-water availability in the Republic of Korea south of the 38th parallel.

at higher elevations only, mostly in and adjacent to the high chain of mountains that extends southeasterly across South Korea. The streams carry heavy loads of sediment during floods, and the major streams are gradually aggrading their lower reaches. Deltas are being built by streams discharging into the Pacific Ocean along the south coast and into the shallow Yellow Sea along the west coast.

Some information regarding the nature and thickness of the unconsolidated deposits and the occurrence of ground water in them has been obtained as a result of the various development programs. In the drilling of wells, bedrock commonly is reached at depths of less than 35 m, although one well drilled by the U.S. Operations Mission to Korea near Changhang was bottomed in valley-fill deposits at a depth of approximately 75 m (M. K. Fletcher, oral communication, 1963), and several wells have been drilled 45 to 60 m into unconsolidated sediments along the west coast. Owing to the irregularity of the bedrock surface, bedrock may be reached at depths of 3 to 5 m even in places far from any bedrock exposures. Apparently during or following Pleistocene time the Korean Peninsula was tilted southwestward as a block and the old erosion surface was partly buried by predominantly fine sediments carried by streams from the highlands to the east. Widespread tidal mudflats are present along the western coast. Streams crossing the coastal plain carry heavy loads of suspended sediment and meander sluggishly to the sea. The larger rivers, at flood stage, transport rock fragments as large as pebbles and deposit them on their flood plains and in their channels.

The water table is near the land surface in most of the coastal flatlands and in the steep-walled valleys. Some of the deeper wells in the flatlands tap both the water-table aquifer and an underlying artesian aquifer. The artesian aquifer is confined above by a clay layer that separates it from the water-table aquifer and below by the bedrock on which it rests.

The yields of wells tapping the unconsolidated deposits range from 1 to 25 liters per second. However, the permeability, extent, and thickness of these deposits indicate that with proper construction and careful development, wells yielding 50 to 100 l per second could be drilled in many places.

Most of the nonmountainous parts of the country are covered by rice paddies. Constructed so that seepage losses are minimal, the paddies have a floor of impermeable clay. Therefore, even though they are kept flooded much of the year, the paddies are not considered to be a significant source of recharge to underlying aquifers. Most of the recharge probably results from influent seepage through river beds and from infiltration of flood waters and precipitation on uncultivated flood plains. Because artificial withdrawal of ground water is on such a small scale, fluctuations of the water table are due largely to natural causes. Extensive development of the ground water in unconsolidated deposits along stream courses would probably induce recharge by influent seepage from the streams and thereby lessen the amount of fresh water discharged into the sea. The effect would be more pronounced during the times of low flow.

Population increase and industrial growth in the Republic of Korea will require fuller utilization of the country's water resources. Moderate to large quantities of ground water can be developed from the unconsolidated deposits and possibly from sedimentary bedrock aquifers. Any such development should be preceded by, and based on, the results of detailed hydrogeologic studies.

REFERENCES

Geological Survey of Korea, 1956, Geologic map of Korea: Prepared jointly with the Geol. Soc. Korea, scale 1:1,000,000.

Kobayashi, Teuchi, 1953, Geology of South Korea: Tokyo Univ. pub., 293 p.

SOURCE OF HEAT IN A DEEP ARTESIAN AQUIFER, BAHÍA BLANCA, ARGENTINA

By STUART L. SCHOFF, JORGE H. SALSO, and JOSÉ GARCÍA,
Recife, Brazil; Buenos Aires, Argentina

Work done in cooperation with the Dirección Nacional de Geología y Minería of Argentina under the auspices of the Agency for International Development, U.S. Department of State

Abstract.—Artesian water from wells more than 500 meters deep in the Bahía Blanca area discharges at temperatures 12° to 26°C above expectable normal. The extra heat may be related to a fault through which deep-seated waters could rise or by which intrusive rocks could have been introduced at depth.

Part of the public water supply of the city of Bahía Blanca, southern Buenos Aires province, Argentina, is obtained by artesian flow from an aquifer 500 meters or more below the land surface. The temperature of the water discharged from 9 wells in and north of the city ranges from 55° to 59°C and average 56.6°C. This average is about 17°C higher than the expectable temperature calculated from the normal geothermal gradient for the region, 1°C per 28 m. Yet volcanic activity or other obvious sources of heat are unknown for hundreds of kilometers in any direction.

The authors present the principal know facts regarding the artesian water supply and postulate that the extra heat is related to a fault. This paper is based chiefly on the records of 19 wells drilled by the Dirección Nacional de Geología y Minería and its predecessor agencies, as reported by Salso and García (1958), and also on observations made in 1959 by the senior author, and Dr. García and Señor Amílcar F. Galván, of the Dirección Nacional de Geología y Minería of Argentina.

The city of Bahía Blanca is near the head of the bay of the same name on the Atlantic coast, about 560 kilometers southwest of Buenos Aires. It is near the seaward edge of a vast gently sloping plain where rocks are poorly exposed. The outcrop of the principal artesian aquifer has not been identified, but rocks probably equivalent to those of the underlying basement crop out in the Sierra de la Ventana, 50 km northeast of Bahía Blanca. These rocks are intricately folded quartzite and schist of Paleozoic age (Harrington, 1947). The basement rocks have been penetrated at depths of 291 to 812 in wells at Pelicurá, Algarrobo, Anzoategui, and at a well 21 km south of General San Martín (fig. 1). The aquifer that yields thermal water at Bahía Blanca has not been identified in these wells, however. Still farther northwest the basement rocks probably are within 50 to 200 of the land surface (fig. 1).

Although several aquifers underlie the coastal plain, only the principal aquifer, described in this paper, yields large supplies of water. The discovery well, drilled at Argerich in 1913 by the Dirección de Minería, was 711 m deep and initially flowed 348 cubic meters per hour. This well was damaged and was replaced in 1915 by a second well, 705 m deep, which initially flowed 500 cu m per hour and in 1959 was still flowing about 20 cu m per hour. More than 30 wells tap the highly productive aquifer in an area extending about 60 km west and 25 km southeast of Bahía Blanca. Northwest of Argerich, the aquifer terminates against a fault, which has been mapped on the basis of physiographic relations, seismic evidence, and test drilling: The proved and probable extent of the principal aquifer is shown on figure 1. The wells considered in this paper are at Bahía Blanca, near Grümbein, at Puerto Belgrano, at Argerich, and near Lake Chasicó (well Chasicó 1).

U.S. GEOL. SURVEY PROF. PAPER 501-D, PAGES D153-D157

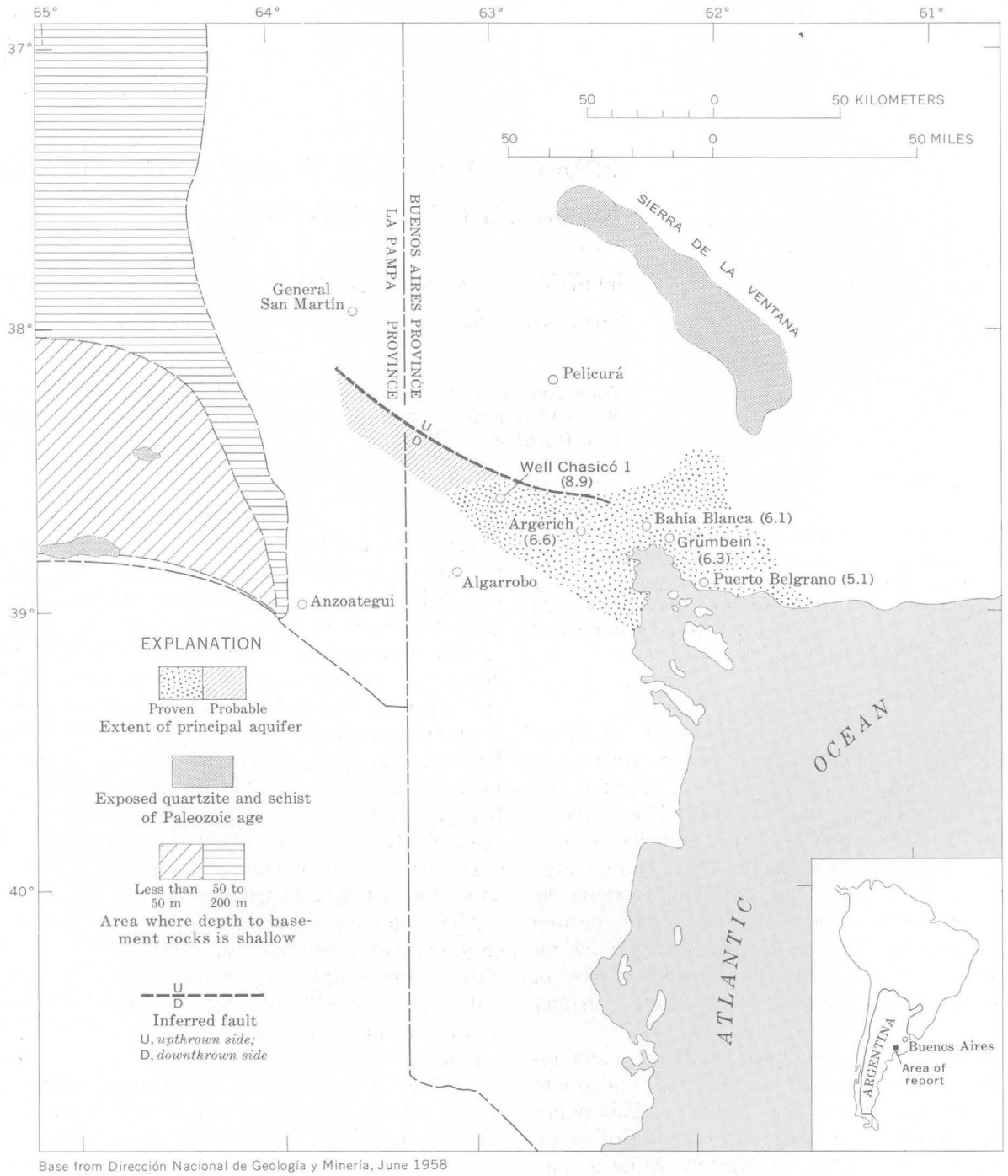

Base from Dirección Nacional de Geología y Minería, June 1958

FIGURE 1.—Map of the Bahía Blanca area, Argentina, showing geothermal gradient in degrees centigrade per 100 m depth (in parentheses), extent of thermal artesian aquifer, and distribution of basement rocks.

The principal aquifer consists of fine- to medium-grained sand, gravel, and conglomerate derived from quartzitic rocks, together with lenticular beds of red clay. It probably is of Miocene age. Known only in wells more than about 500 m deep, it has been penetrated completely in only two wells, where it is 283 and 382.5 m thick. Most other wells considered in this paper penetrate not more than 40 m of the aquifer. The top of the aquifer descends southeastward (seaward) about 0.8 m per km, and the deepest producing wells are at Puerto Belgrano.

Initial yields of wells that tap the principal aquifer range from 50 to 1,000 cu m per hour. The yields generally have declined progressively, in part, no doubt, because discharge causes reduction of head, but also because of encrustation of the well casing; most wells have not been cleaned out. Yields also decline as a result of competing discharge. The yield of one of the wells in Bahía Blanca declined when another 1.2 kilometers away, began to flow, and increased when the flow of the other was stopped.

CHEMICAL CHARACTER OF THERMAL WATER

At best, the chemical quality of the water is acceptable for drinking, but the quality is not uniform from well to well. The dissolved-solids content (residue at 180°C) in 17 samples ranged from about 300 to about 1,760 milligrams per liter. Large differences in the dissolved-solids content and in some individual constituents have been recorded in waters of adjacent wells and also in wells of almost equal depth (Salso and García, 1958, p. 23). The water from wells in the Bahía Blanca–Grümbein area on the whole contains less dissolved solids than the water at Argerich, to the west, or at Puerto Belgrano, to the southeast. Water from 3 of 13 wells sampled in the Bahía Blanca–Grümbein area contained more than 1,000 mg per 1 of dissolved solids. No analysis is available for the water from the westernmost well (Chasicó 1).

Thirteen analyses are complete enough to permit chemical classification of the waters. All are sodium waters containing substantial proportions of chloride and bicarbonate. Two waters can be classed as sodium bicarbonate, 2 as sodium chloride, and 9 as sodium chloride-bicarbonate waters. Sodium ranges from 56 to 98 percent of the total cations (in equivalents per million), as illustrated for the Bahía Blanca–Puerto Belgrano area on figure 2*A*. The "knot" in the upper part of the figure is due to abnormally low sodium content (offset by abnormally high calcium content) at one well. The distribution of chloride, in percent of total anions, is illustrated on figure 2*B*. The proportions of both sodium and chloride increase eastward and northward away from the sea. This suggests an independent source of sodium chloride inland; however, the water from most of the wells is not highly mineralized.

WATER TEMPERATURE AND GEOTHERMAL GRADIENT

The water temperatures generally were measured upon completion of each well and occasionally thereafter; they probably are comparable although spread over a period of years, for the temperature of water coming from depths greater than 500 m is not likely to vary greatly. The warmest water (68°C) comes from a well at Puerto Belgrano, the deepest of those for which records are available. The shallowest well, however, yields the highest temperature water in relation to depth (well Chasicó 1, fig. 1).

The water temperatures have been studied in terms of excess temperature above expectable normal temperature, and also in terms of geothermal gradient. The estimated excesses of temperature serve chiefly to show that the water is unusually warm, but they cannot be precise because they involve (a) an assumed "normal" geothermal gradient for the locality, and (b) an assumed mean annual air temperature of 15.5°C over the entire area. The same assumption as to mean annual air temperature is used in estimating the geothermal gradients, but no assumption as to "normal" geothermal gradient enters into this calculation. The calculations of geothermal gradient ignore the fact that the temperature of the rocks at moderate depth is likely to be a degree or two above mean annual air temperature (Van Orstrand, 1935, p. 88) and the fact that the lowest temperature in a well generally is not at the land surface but at a depth of about 30 m (McCutchin, 1930, p. 20).

The observed water temperatures probably represent somewhat different intervals within the aquifer, but in the absence of information as to permeability or other differences within the aquifer, all temperatures are assumed to represent that of water from the top of the aquifer. No obvious relation of water temperature to depth of aquifer, to thickness of aquifer penetrated, or to depth of well was noted; nor is there a simple relation between excess temperatures or geothermal gradients and these factors. When either excess temperatures or geothermal gradients are plotted on a map, they differ sufficiently within small areas to make the drawing of contours both difficult and dubious. Yet, for the area as a whole, certain major distinctions are apparent, as indicated by average gradients computed for Bahía Blanca, Grümbein, and Puerto Belgrano (fig. 1).

742-652 O—64——11

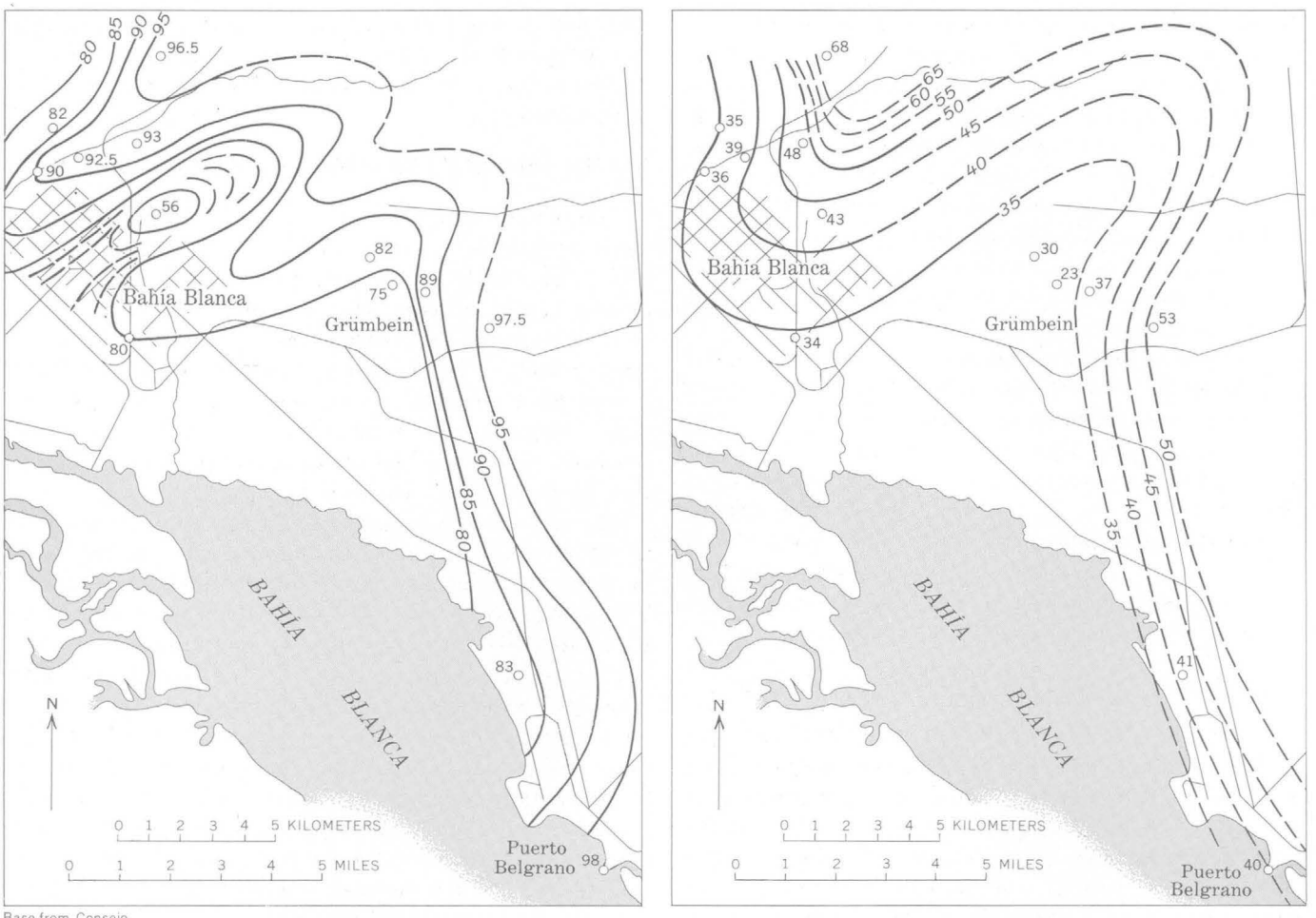

Base from Consejo Federal de Inversiones 1962, vol. 1, p. 139

FIGURE 2.—Map of the Bahía Blanca–Puerto Belgrano area, Argentina, showing relative concentration of sodium and chloride in water from deep wells. *A*, lines of equal sodium concentration, as percent of total cations; *B*, lines of equal chloride concentration, as percent of total anions; computed from equivalents per million.

A computation of excess temperature at well Chasicó 1 follows. An assumed normal geothermal gradient of 1 °C per 28 m of depth was computed on the basis of observations of temperature in different strata in the region. Dividing the depth to the aquifer, 507 m, by 28 gives 18 °C, the expected temperature increment due to depth. Adding the mean annual air temperature for the locality, 15 °C, gives 33.5 °C, the temperature expected at a depth of 507 meters; and subtracting this from the observed water temperature, 60° gives 27 °C, the excess at well Chasicó 1. Similar computations indicate that the excess at Argerich is about 21.7 °C; at Bahía Blanca, 15.8° to 19.5 °C; at Grümbein, 15.6° to 20.6 °C; and at Puerto Belgrano, 12.1° to 15.1 °C.

The computation of the temperature gradient for well Chasicó 1 starts with the observed discharge temperature, 60 °C. From this is subtracted the mean annual air temperature, 15 °C, to get the temperature increment due to depth, 45 °C. This divided by depth to top of aquifer, 507 m, gives the geothermal gradient, 0.089 °C per meter, or 8.9 °C per 100 m depth.

Arranged in order from northwest to southeast, the average computed gradients are as follows:

Location	*Geothermal gradient (degrees Centigrade per 100 m depth)*
Chasicó well 1	8. 9
Argerich (2 wells)	6. 6
Bahía Blanca (9 wells)	6. 1
Grümbein (3 wells)	6. 3
Puerto Belgrano (3 wells)	5. 1

Averaging the geothermal gradients does not conceal overlap of gradient ranges. None of the wells at Bahía Blanca has a gradient as high as those at Argerich or Chasicó 1, or as low as those at Puerto Belgrano. However, at Grümbein, the group nearest to Bahía Blanca, some of the wells have geothermal gradients in

the upper range of those at Bahía Blanca, but none of them exceed this range.

The highest geothermal gradient is nearest a fault that marks the boundary of the principal aquifer northwest of Argerich (fig. 1). Admittedly, this may not be the only fault in the region, but it is the only one now recognized with reasonable certainty. The fault may be a conduit through which deep-seated thermal waters rise into the aquifer, or through which intrusives have invaded either the basement rocks or the lower part of the sedimentary section. Whether deep-seated waters or an intrusive body provide the heat in the Bahía Blanca area is a matter for speculation. The following points, however, are pertinent.

(1) A fault at great depth is more likely to be closed than open and more likely to allow the passage of a trickle than a flood of water. The passage of enough thermal water to raise the temperature in the aquifer substantially at Bahía Blanca therefore may be questioned.

(2) Thermal water from great depth is more likely to be mineralized than fresh. If entering the aquifer in quantities sufficient to raise the temperature as much as indicated, such water conceivably could make the water in the aquifer too mineralized for use.

(3) An intrusive could introduce a large amount of heat, perhaps accompanied by only a relatively small amount of fluid. It could heat the aquifer and the water in it without greatly contaminating the water.

(4) Volcanic glass found in strata of Miocene age above the principal aquifer in well Chasicó 1 (Salso and García, 1958, p. 18) suggests that intrusion could have occurred somewhere in the region, but it is hardly proof that it occurred near Bahía Blanca. Volcanic ash in rocks of Tertiary and Quaternary age in the region generally has been attributed to volcanism in the Andes Mountains to the west. Volcanic ash from an eruption that occurred only a few years ago in the Andes was identified at Buenos Aires.

REFERENCES

Harrington, H. J., 1947, Explicacion de las hojas 33 m y 34 m, Sierras de Curamalal y de la Ventaria, prov. de Buenos Aires: Argentina, Direc. Minas y Geol. Bull. 61, 43 p., 2 pls.

McCutchin, J. A., 1930, Determination of geothermal gradients in oil fields located in anticlinal structures in Oklahoma: Am. Petroleum Inst., Production Bull. 205, pt. 3, p. 19–61.

Salso, J. H., and García, José, 1958, Estado actual del conocimiento hidrogeológico de la cuenca artesiana de Bahía Blanca: Direc. Nac. Geol. y Min. Bol. Inf. año 2, no. 9 p. 15–26.

Van Orstrand, C. E., 1935, Normal geothermal gradients in the United States: Am. Assoc. Petroleum Geologists Bull., v. 19, p. 78–115.

THE CARRIZO SAND, A POTENTIAL AQUIFER IN SOUTH-CENTRAL ARKANSAS

By R. L. HOSMAN, Little Rock, Ark.

Abstract.—Electric-log interpretations made as part of a water-resources study of the Mississippi embayment indicate that the Carrizo Sand of Eocene age is a potential aquifer in an area of about 5,000 square miles in south-central Arkansas. The dissolved-solids content of water from a recently drilled 2,050-foot test hole was less than 1,000 parts per million, confirming these interpretations.

The Carrizo Sand is the basal formation of the Claiborne Group of Eocene age throughout most of the Coastal Plain area in Arkansas, Louisiana, and Texas. According to electric-log interpretations made for the water-resources study of the Mississippi embayment, water in the Carrizo contains less than 1,000 parts per million of dissolved solids in an area of about 5,000 square miles in south-central Arkansas. However, substantiating water-quality data were not available until late in 1963, when a deep exploratory test hole near Pine Bluff was drilled into this formation.

In south-central Arkansas the Carrizo Sand is tapped by very few wells. It crops out in a narrow northeast-trending belt that in places is concealed by a thin cover of Quaternary deposits, and it dips to the southeast (fig. 1). The Carrizo consists generally of clean subangular to subrounded fine to medium sand, and in the subsurface it ranges in thickness from less than 25 feet to slightly more than 300 feet (fig. 2). It overlies the Wilcox Group and is overlain by the Cane River Formation of the Claiborne Group. In the subsurface south of lat 35° N., the Cane River is predominantly a marine clay, but north of there it grades into sand, which together with the underlying Carrizo and the overlying Sparta Sand, forms a massive sand hundreds of feet thick.

The area in which the Carrizo contains fresh water (dissolved-solids content less than 1,000 ppm) ranges in width from 8 to 55 miles, and within this area the depth to the formation ranges from 0 to a little more than 2,000 feet. In almost all of this area the Carrizo has not been developed as an aquifer because sufficient water could be obtained from the highly productive Sparta Sand and other shallower aquifers. The only withdrawals from the Carrizo are from a few shallow wells at and near the outcrop of this sand.

In the vicinity of Pine Bluff, because the water level in the Sparta Sand has declined and because the water from the shallower aquifers generally requires treatment for industrial use, supplemental supplies are being sought for industries. Consulting engineers visiting the U.S. Geological Survey office in Little Rock were informed that the Carrizo Sand in the Pine Bluff vicinity probably contains fresh water, and on the engineers' recommendation, an industry drilled a test hole to the base of the Carrizo. The test hole penetrated the top of the formation at a depth of 1,900 feet and the base at 2,050 feet. The hole was cased and a short screen was set in the Carrizo section, but the well was not developed, as the primary interest was in the quality of the water rather than in the quantity available. Analysis of a sample of the water from the test hole showed the water to have a dissolved-solids content of 650 ppm. However, the chloride content was 280 ppm, which is marginal for many uses without treatment or dilution of the water (dissolved-solids content and chloride content should decrease updip). The hardness of the water was 11 ppm, and pH was 7.7. The static water level was less than 15 feet below land surface and the bottom-hole temperature, recorded at the time the electric log of the well was made, was 103°F. The sand as observed in the drill cuttings was somewhat coarser than that in the Sparta. This fact coupled with the shallow

U.S. GEOL. SURVEY PROF. PAPER 501–D, PAGES D158–D160

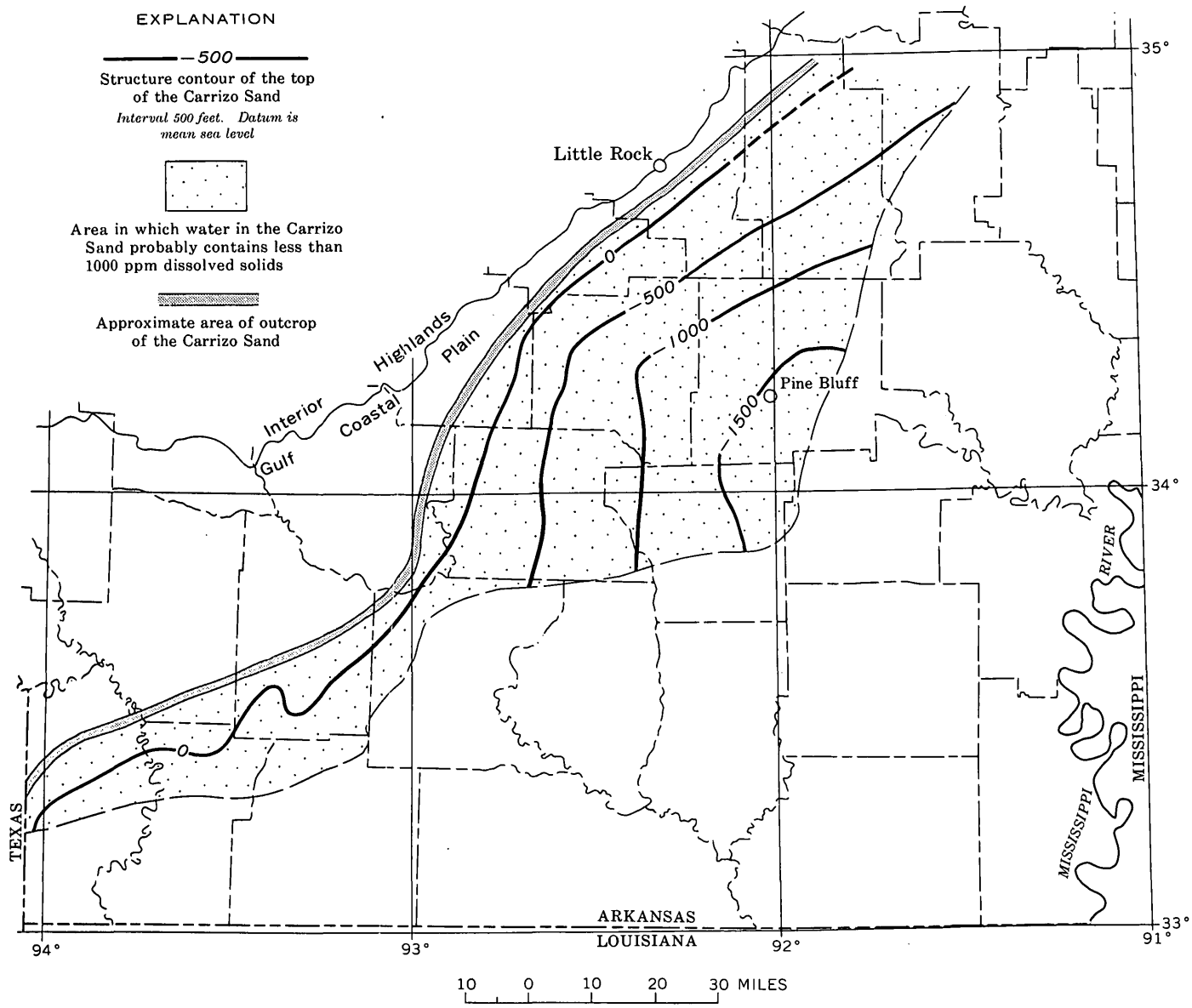

FIGURE 1.—Configuration of the top of the Carrizo Sand.

static water level, suggests that large yields probably would be available at low lifts from the Carrizo and that the sand probably will be an important source of water in the future.

The test hole, located near the estimated downdip limit of fresh water in the Carrizo, proved a sizable area in which the Carrizo Sand is a potential aquifer containing a large reserve of ground water. Delineation of the area, which is virtually that shown on figures 1 and 2, is based entirely on interpretation of electric logs of oil tests. More exact limits of the aquifer capabilities of the Carrizo can be determined as supplies are developed from this sand and as water-quality and pumpage data become available.

As ground-water supplies are developed from the Carrizo Sand, it would be advisable to monitor the quality of the water pumped from wells near the downdip limit of fresh water, in order to detect changes that might occur as a result of large withdrawals. Prolonged pumping in this area might cause updip encroachment of saline water. Changes in salinity should be detected as soon as possible so that remedial measures can be taken if the changes should be detrimental to the quality of the water. Systematic sampling and analyzing of water from observation wells located downdip from production wells would be the best method for the early detection of changes in water quality.

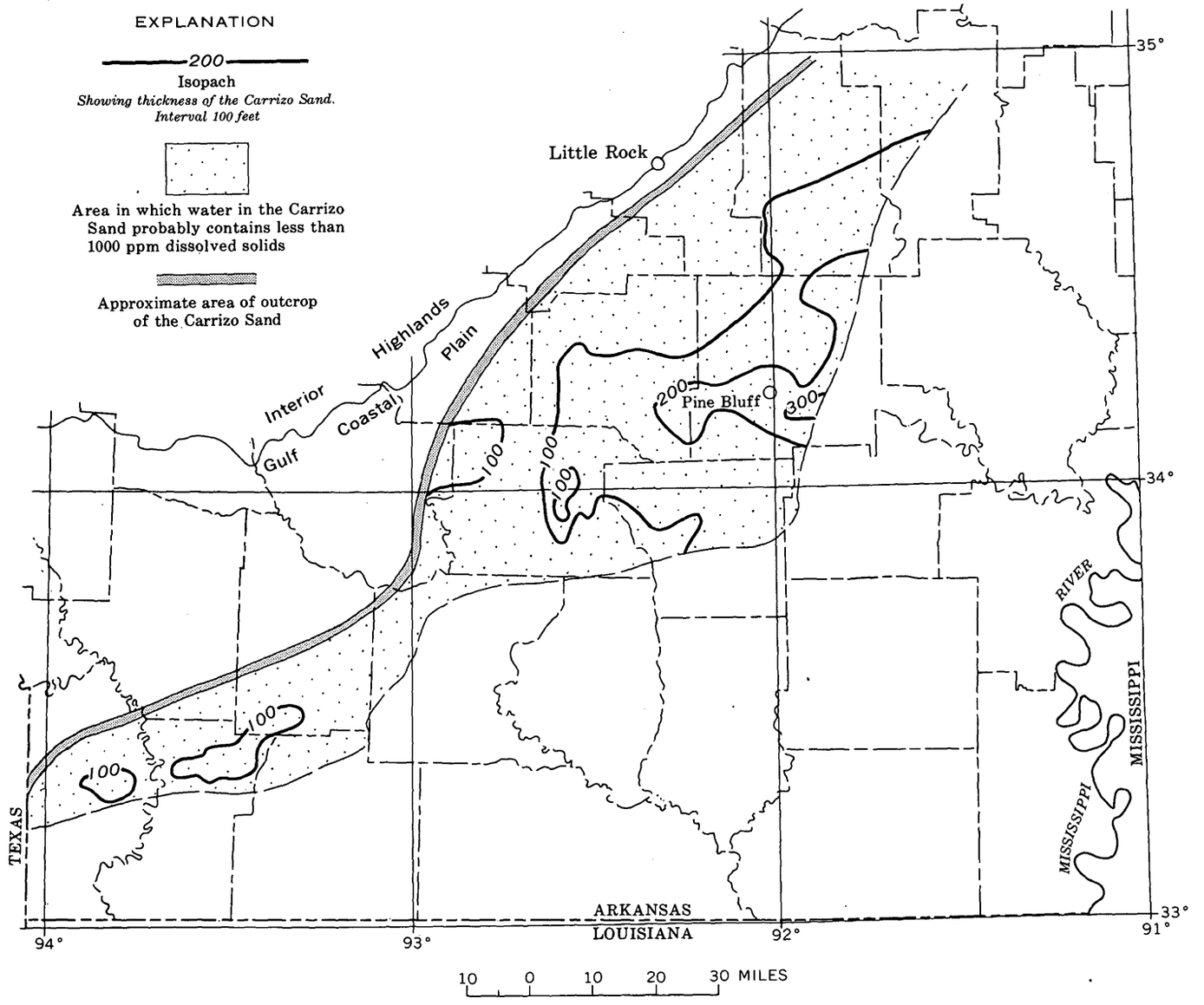

FIGURE 2.—Thickness of the Carrizo Sand.

GEOHYDROLOGY OF THE SPIRITWOOD AQUIFER, STUTSMAN AND BARNES COUNTIES, NORTH DAKOTA

By T. E. KELLY, Grand Forks, N. Dak.

Work done in cooperation with the North Dakota State Water Conservation Commission and the North Dakota Geological Survey

Abstract.—The Spiritwood artesian aquifer is a buried bedrock channel deposit composed of sand and gravel averaging 50 feet in thickness and exceeding 320 square miles in areal extent. Aquifer tests indicate a coefficient of transmissibility of 92,000 gallons per day per foot and a coefficient of storage of 0.0016. The water is of the sodium bicarbonate type.

A large buried bedrock valley, which is occupied by the Spiritwood aquifer, was discovered in 1958 during reconnaissance test drilling in eastern Stutsman County, N. Dak. Subsequent test drilling in conjunction with a ground-water study of Barnes County has further delineated the aquifer (fig. 1). Although preliminary study (Huxel, 1961) indicated that the bedrock valley was part of a preglacial drainage system occupied by a northward-flowing stream, subsequent test drilling has shown that the valley has functioned also as a southward-draining outwash channel. This is indicated by the valley gradient, which is toward the south, and by the presence of thick deposits of glacial outwash in the channel.

The Spiritwood valley has a relatively uniform width of 5 miles, except in Townships 142 and 143 N., where the apparent width increases abruptly to more than 12 miles (fig. 1). The valley was eroded more than 250 feet into the Pierre Shale of Late Cretaceous age. On the basis of test-drilling information, Huxel (1961, fig. 350.3) and Winters (1963, p. 35) reported the depth of the bedrock valley to be substantially greater. However, according to W. A. Cobban (oral communication, 1963) and Gill and Cobban (1961, p. D185), a reevaluation of the test-drilling information indicates that the samples previously classified as lacustrine silt and clay of Pleistocene age actually are calcareous shale and marlstone from near the base of the Pierre Shale.

The Spiritwood channel is bordered on the east by an elongate ridge that separates the main channel from a northeast-trending depression in Tps. 141 and 142 N. Test drilling indicates that the depression locally is deeper than the main channel but contains no deposits of sand and gravel. The depth of the depression, its lack of water-deposited coarse clastic material, and its parallelism with the main channel seem to preclude its being a tributary valley. The depression does not seem to be related genetically to the Spiritwood channel; because it is parallel to the direction of major ice advances across the area, it may be a feature caused by glacial scour.

At least two ice sheets have overridden the Spiritwood valley and deposited thick accumulations of till and associated glaciofluvial sediments (Lemke and Colton, 1958, fig. 3). These deposits range in thickness from 75 feet to more than 200 feet and completely obscure the bedrock valley at the surface.

The Spiritwood aquifer occupies the lower part of the bedrock valley. Its thickness differs appreciably from place to place but in general decreases from north to south (fig. 2). The average thickness of the aquifer is about 50 feet; however, 162 feet of sand and gravel was penetrated in the drilling of a test hole in sec. 31, T. 140 N., R. 61 W. The aquifer underlies an area of at least 320 square miles in Stutsman and Barnes Counties, and recent test drilling indicates that it extends at least 10 miles farther north.

U.S. GEOL. SURVEY PROF. PAPER 501-D, PAGES D161-D165

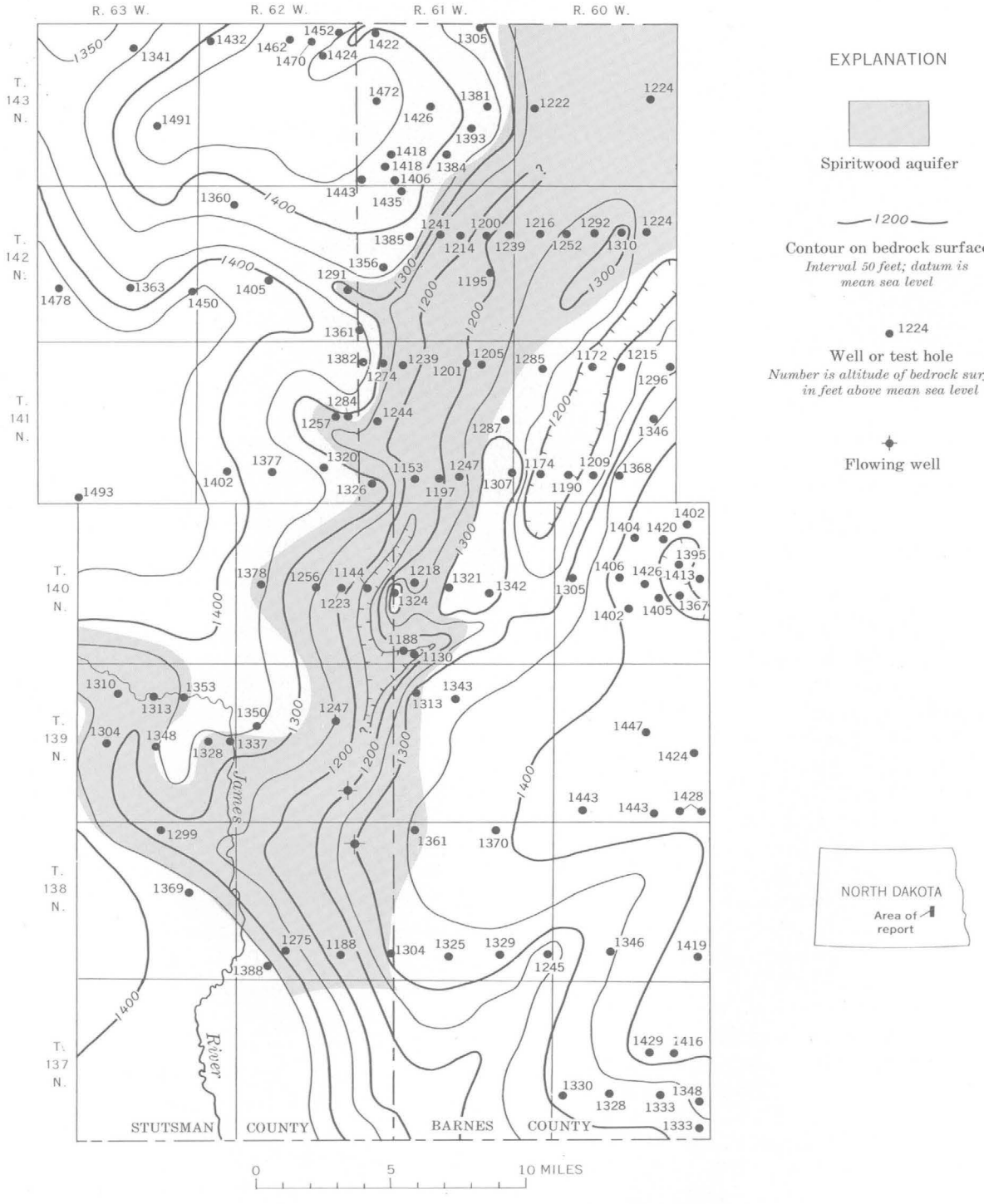

FIGURE 1.—Bedrock contour map of the Spiritwood channel in Stutsman and Barnes Counties, N. Dak.

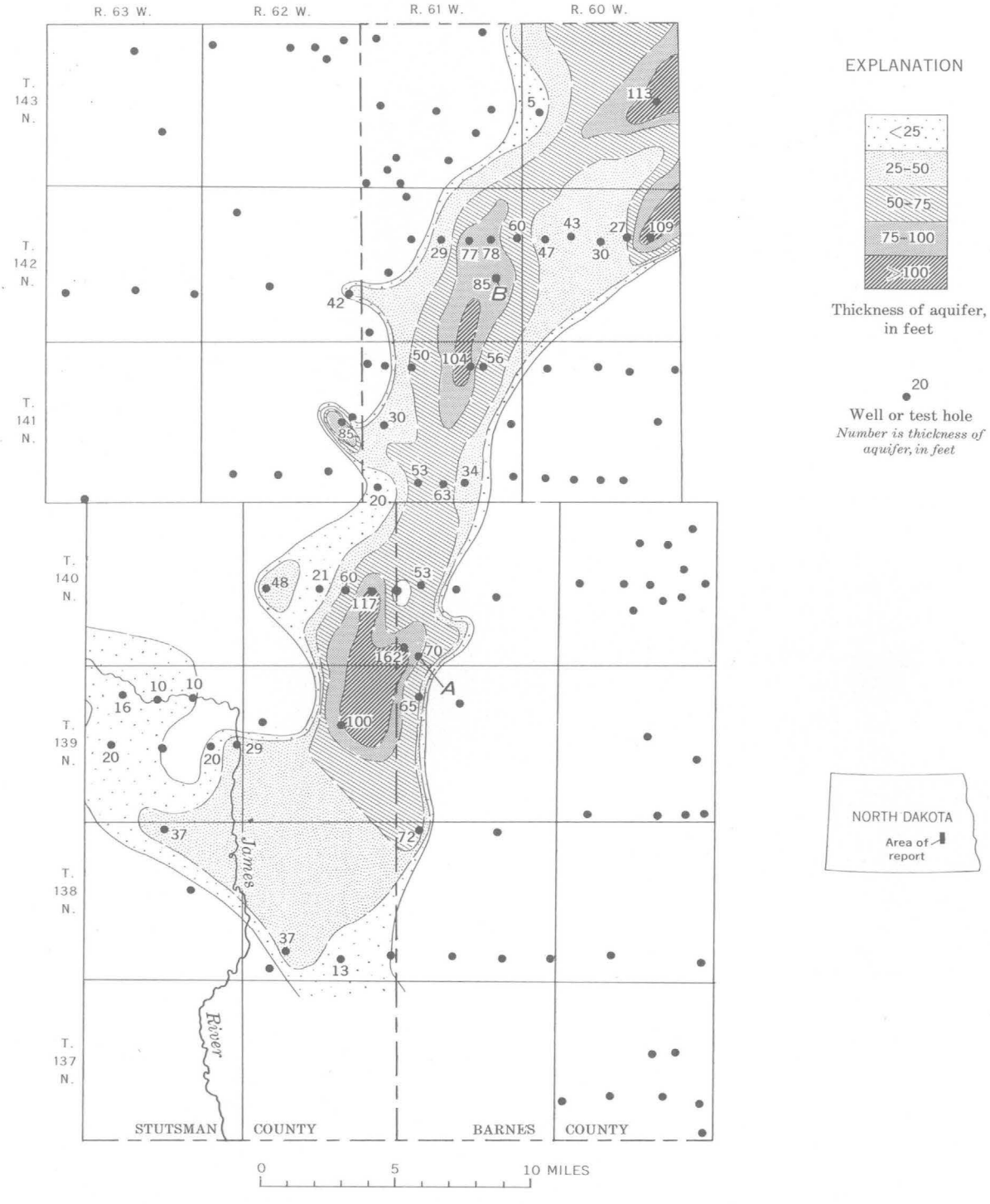

FIGURE 2.—Isopach map of the Spiritwood aquifer, Stutsman and Barnes Counties, N. Dak. *A*, *B*, sites of aquifer tests.

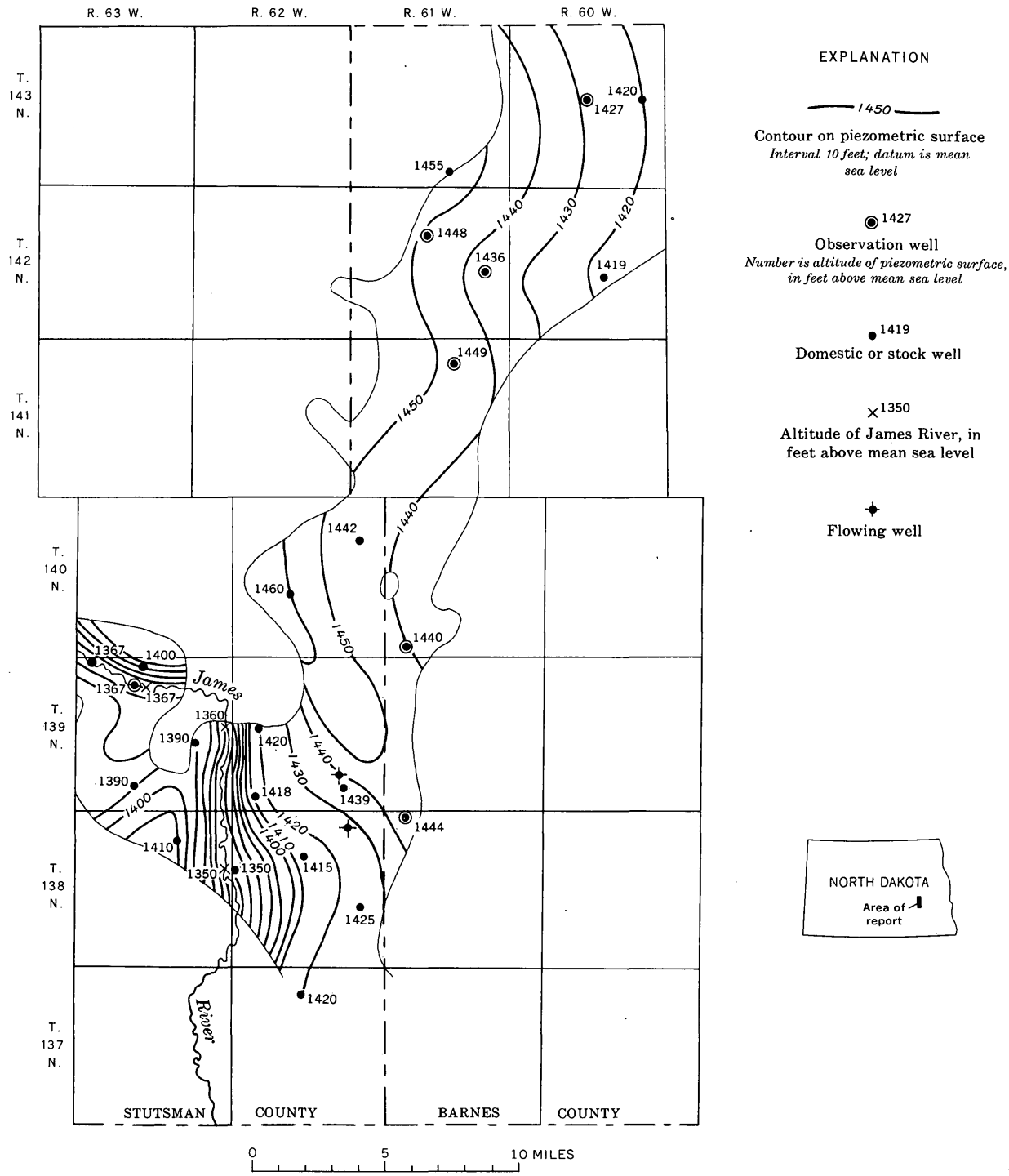

FIGURE 3.—Contour map of the piezometric surface of the Spiritwood aquifer, Stutsman and Barnes Counties, N. Dak.

The gravel in the aquifer consists primarily of subangular to subrounded fragments of shale and limestone, although fragments of igneous and metamorphic rocks constitute as much as 20 percent of the total. The shale fragments were derived locally; however, the other rock fragments are typical of those in the Canadian Shield or lower Paleozoic sequence which borders the shield on the southwest. The sand grains range in size from very fine to very coarse and are angular to subangular. In areas of detailed test drilling, such as at sites A and B (fig. 2), the aquifer was found to differ lithologically both vertically and horizontally. In general, the lithologic characteristics of the sand and gravel indicate that these deposits were transported relatively short distances by large volumes of water. Silt and clay are only minor constituents of the aquifer and occur in thin, discontinuous beds.

In Tps. 138 and 139 N., R. 63 W., the Spiritwood aquifer underlies the James River valley, the floor of which is 150 feet below the bordering plains (Paulson, 1962, p. 2; Winters, 1963, p. 74). Here the river flows on glacial outwash that partly fills the valley. The slope of the piezometric surface in the vicinity of the river (fig. 3) indicates that a natural discharge area exists where the outwash deposits in the James River valley are hydraulically continuous with the Spiritwood aquifer. However, data are insufficient to estimate the rate at which ground water is discharged to the river.

Two flowing wells tap the aquifer, one of which is reported to flow 150 gallons per minute. These wells were drilled through relatively thin sequences of confining drift in Tps. 138 and 139 N., R. 62 W. (figs. 1, 3).

Aquifer tests at sites A and B (fig. 2) indicate that the Spiritwood aquifer will yield large quantities of water. The well pumped for the test at site A taps fine to medium gravel and coarse sand. Before the test the static water level was 127 feet above the top of the aquifer and 25 feet below the land surface. The coefficients of transmissibility and storage were computed, from the Theis nonequilibrium formula (Theis, 1935), to be 92,000 gallons per day per foot and 0.0016, respectively. In addition to indicating the impermeable barrier on the east (known also from test-hole data) this test indicated the presence of several indistinct boundaries which may be due to differences in permeability within the aquifer. The test at site B gave slightly lower coefficients of transmissibility and storage and did not indicate any aquifer boundaries. If the porosity is assumed to be 30 percent, the amount of water in transient storage is computed to be about 3 million acre-feet.

Chemical analyses of water samples collected during aquifer tests and from test holes drilled elsewhere in the Spiritwood aquifer indicate that the water is of the sodium bicarbonate type. The total dissolved-solids content ranges from 680 to 1,370 parts per million and averages about 900 ppm. Differences in water quality from place to place in the aquifer are probably due to inflow of water from the underlying Pierre Shale and overlying glacial till. The total dissolved-solids content of water from the shale averages approximately 6,000 ppm and is as high as 8,110 ppm, whereas the total dissolved-solids content of water from the till ranges from 300 ppm to more than 4,000 ppm and averages about 2,500 ppm.

As of early 1964, relatively few wells tapped the aquifer, and all of these were used for stock and domestic purposes. However, several irrigation operations are planned and large-scale development of the aquifer is anticipated in the near future. Because of its broad areal extent, large storage volume, high permeability, and high hydrostatic pressure, the Spiritwood aquifer is expected to become one of the more important confined aquifers in North Dakota.

REFERENCES

Gill, J. R., and Cobban, W. A., 1961, Stratigraphy of lower and middle parts of the Pierre Shale, northern Great Plains: U.S. Geol. Survey Prof. Paper 424–D, p. D185–D191.

Huxel, C. J., Jr., 1961, Artesian water in the Spiritwood buried valley complex, North Dakota: U.S. Geol. Survey Prof. Paper 424–D, p. D179–D181.

Lemke, R. W., and Colton, R. B., 1958, Summary of the Pleistocene geology of North Dakota: North Dakota Geol. Survey, Midwestern Friends of the Pleistocene 9th Ann. Field Conf. Guidebook, p. 41–57.

Paulson, Q. F., 1962, Report on results of test drilling and pumping test in wildlife research project area, James River valley, Stutsman County, North Dakota: U.S. Geol. Survey open-file report, 18 p., 2 figs.

Theis, C. V., 1935, The relation between the lowering of the piezometric surface and the rate and duration of discharge of a well using ground-water storage: Am. Geophys. Union Trans., v. 16, pt. 2, p. 519–524.

Winters, H. A., 1963, Geology and ground-water resources of Stutsman County, North Dakota, pt. I, Geology: North Dakota Geol. Survey Bull. 41, 84 p.

VARIATION OF PERMEABILITY IN THE TENSLEEP SANDSTONE IN THE BIGHORN BASIN, WYOMING, AS INTERPRETED FROM CORE ANALYSES AND GEOPHYSICAL LOGS

By JOHN D. BREDEHOEFT, Washington, D.C.

Abstract.—An empirical relation of porosity versus permeability was developed for the Tensleep Sandstone within the Bighorn Basin, Wyo., from laboratory core-analysis data. Coefficients of permeability were estimated using this empirical relation and porosity values interpreted from sonic and neutron logs. A wide but systematic variation in permeability from very high values in the outcrop area to low values in the center of the basin, which is consistent with geologic knowledge, was observed.

In the analysis of large aquifer systems, hydrologists must rely on data already available from petroleum exploration for information on the deep parts of sedimentary basins. Commonly the only applicable data are porosity and permeability determinations from laboratory analyses of drill cores and from geophysical logs made in the course of exploratory drilling for petroleum. In an effort to determine the areal distribution of permeability in the Tensleep Sandstone of Pennsylvanian age in the Bighorn Basin, Wyo., the relation between porosity and permeability of the Tensleep Sandstone was determined and used in interpreting the permeability from the porosity of the formation throughout the basin.

At the time of this study, approximately 750 laboratory core analyses were available from 17 wells from which porosity and permeability of the Tensleep Sandstone in the Bighorn Basin had been determined from small plugs. Although the plugs represent a good sampling of vertical sections of the formation, they provided only limited knowledge about areal variations in permeability. Several of the 17 wells from which information was available were closely spaced; on a regional scale, data were available for 9 localities in the basin.

The laboratory porosity and permeability data provide a basis for determining an empirical relation between permeability and porosity, making possible the extrapolation of permeability data on the basis of porosity values interpreted from standard geophysical borehole logs. Fortunately, many problems of fluid movement require only that estimates of transmissibility be within the proper order of magnitude. Other investigators have made similar studies of porosity versus permeability, as for example, Law (1944) and Archie (1950), who published semilog plots of this relation for several formations in the Gulf Coastal Plain.

EMPIRICAL RELATION OF POROSITY TO PERMEABILITY

Porosity values from laboratory analyses of drill cores of the Tensleep Sandstone were plotted against the logarithm of permeability (fig. 1). A best-fit trend line then was drawn by eye through the Tensleep data (fig. 1), and a digital computer was used in an attempt to derive the best least-squares polynomial fit for the data. Polynomials up to and including degree five were calculated; however, the best fit appears to be the line drawn by eye (fig. 1). At lower values this curve agrees rather well with the slope that Archie (1950) found for Gulf Coast sediments (one log-cycle change in permeability per 3-percent change in porosity).

Except for differences in thickness and degree of cementation, the Tensleep Sandstone is lithologically similar throughout the Bighorn Basin; presumably it was deposited as a uniform sand across the entire basin. The size and sorting of the sand grains making up the sandstone are reasonably uniform over the basin, and differences in porosity as well as in permeability appear to be primarily the result of secondary cementation and recrystallization of the sand grains. This results in an increasingly interlocking fabric of

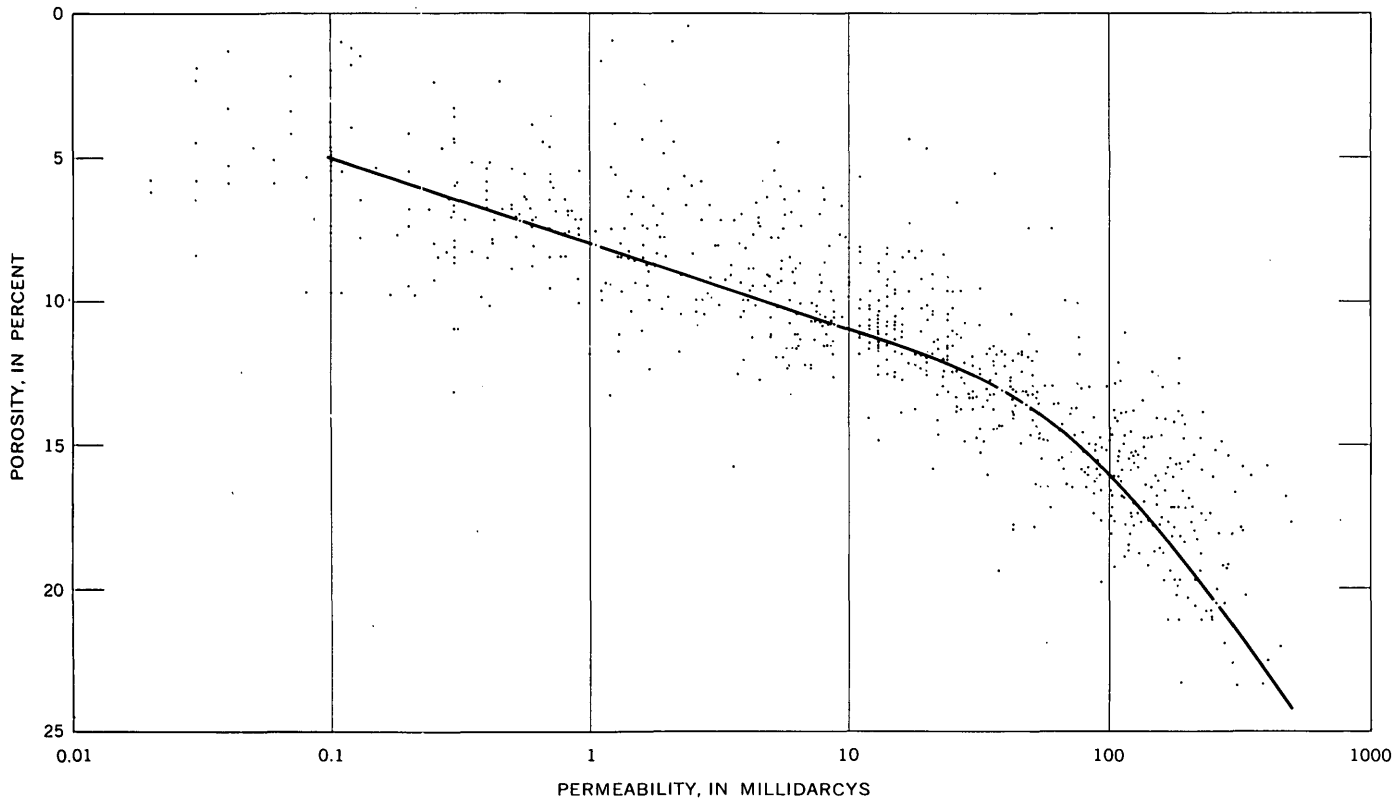

FIGURE 1.—Semilog plot of porosity versus permeability, based on data from the analyses of cores of the Tensleep Sandstone in the Bighorn Basin, Wyo.

sand grains with increased depth of burial. Because both porosity and permeability differences are mainly the result of secondary cementation, it is reasonable to conclude that permeability relates directly to porosity, as figure 1 indicates.

COMPUTATION OF POROSITY AND PERMEABILITY

Both the sonic log and the neutron log can be used to determine formation porosity, in place. Procedures using these logs are in general use in the petroleum industry. A theoretical method is used to determine formation porosity from the sonic log (Wyllie, 1963, p. 130–133); an empirical method is used to determine porosity from the neutron log (Wyllie, 1963, p. 118–119). Figure 2*A* shows a comparison of porosity determined from cores with porosity determined from a sonic log in one well, and figure 2*B*, a comparison of porosity determined from cores with porosity determined from a neutron log in a second well. Core analyses were not available for a well with both a sonic log and a neutron log, and hence no direct comparison of the use of both methods together for estimating permeability is possible.

It is not expected that the coefficient of permeability based upon laboratory determination from a small plug would compare in detail with the coefficient of permeability based upon calculations from a continuous log of rocks in place. The sample analysed in the laboratory represents only a small fraction of even the total sample taken in a single foot of core. In the geophysical log the logging device is continuously recording a signal that represents an integration of a particular physical property of the rock and of borehole fluid within the radius of influence of the device. Hence, although both the laboratory and log data are plotted as foot-by-foot determinations on figure 2, it is not to be expected that each pair of plots would agree in detail. Nevertheless, overall there is a clear general correspondence.

There is some question as to whether laboratory core analysis of permeability is applicable to field conditions. However, Johnson and Greenkorn (1960) found that permeabilities derived from laboratory determinations from cores showed good agreement with permeabilities determined by conventional aquifer tests in the field. For the purposes of this paper it is assumed that the laboratory data are representative of field conditions.

Thirty-three neutron logs and 15 sonic logs, which included all the logs of these types available from wildcat holes in the Bighorn Basin, were used to estimate the permeability to the Tensleep Sandstone.

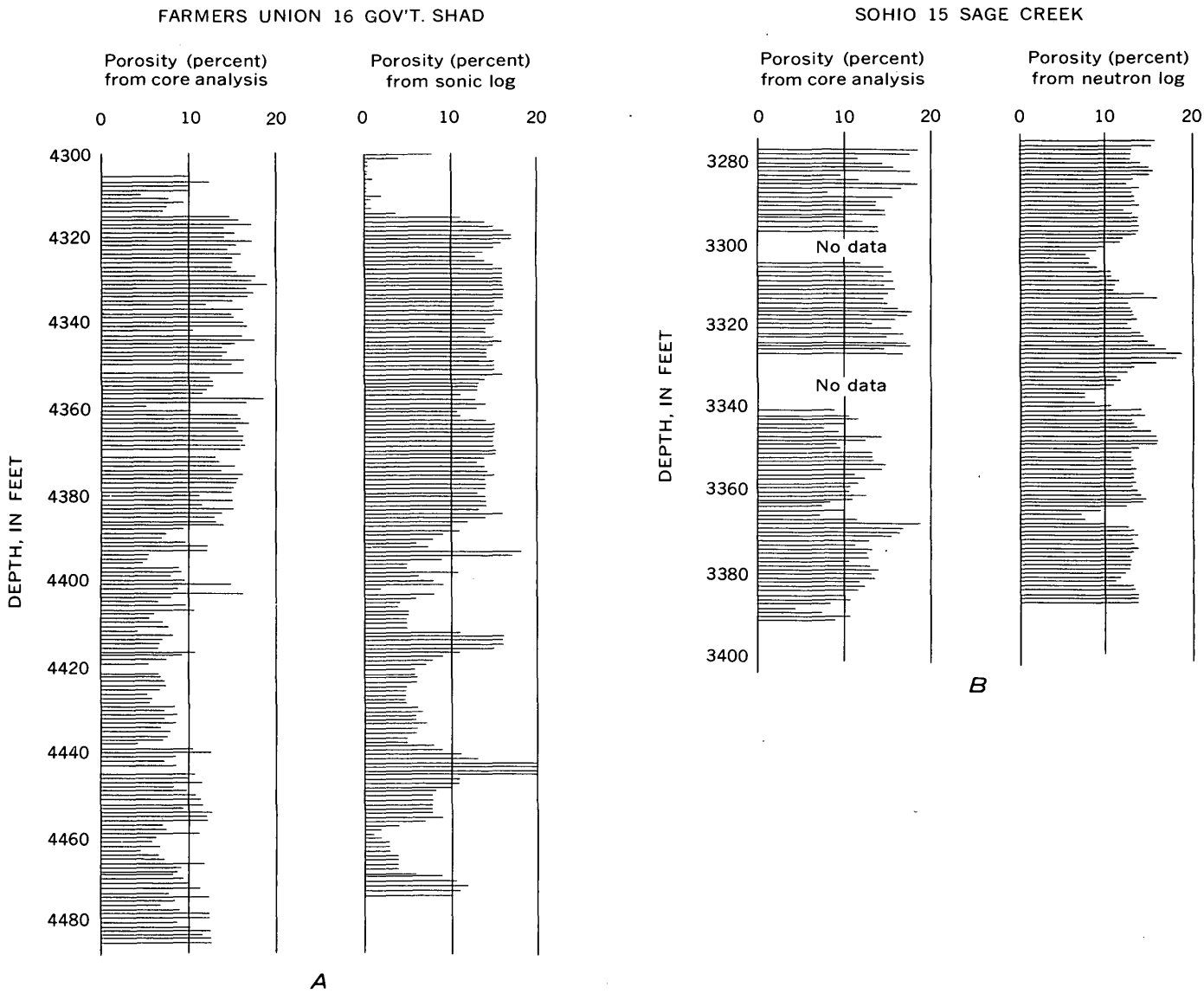

FIGURE 2.—Comparison of porosity of the Tensleep Sandstone as determined by three methods. *A*, comparison of porosity determined from core samples with porosity computed from a sonic log. *B*, comparison of porosity determined from core samples with porosity computed from a neutron log.

The interval of formation logged was divided into categories on the basis of the computed porosity, as follows: less than 8 percent porosity, 8 to 11 percent porosity, 11 to 16 percent porosity, and greater than 16 percent porosity. These categories were selected from the curve of porosity versus permeability (fig. 1) to correspond to successive log cycles of permeability on the porosity-permeability curve.

The transmissibility of an aquifer may be defined as:

$$T=\Sigma K_i m_i,$$

where

$i=1, 2, 3 \ldots n$,
T=transmissibility,
K_i=permeability of the i layer,
m_i=thickness of the i layer, and
n=number of layers of differing permeability.

In estimating the transmissibility from the logs the following relation was applied to the data 1:

$$T=\Sigma\overline{K}_1 m_1+\Sigma\overline{K}_2 m_2+\Sigma\overline{K}_3 m_3+\Sigma\overline{K}_4 m_4,$$

where

m_1=footage logged of <8 percent porosity,
m_2=footage logged of 8–11 percent porosity,
m_3=footage logged of 11–16 percent porosity,
m_4=footage logged of >16 percent porosity,
$\overline{K}_1$=mean permeability of <8 percent porosity interval,

$\overline{K}_2$=mean permeability of 8–11 percent porosity interval,
$\overline{K}_3$=mean permeability of 11–16 percent porosity interval, and
$\overline{K}_4$=mean permeability of >16 percent porosity interval.

Because of the great spread in permeability values the intervals with high porosity and permeability determine the effective transmissibility of the formation. From calculations based on figure 1 it can be seen that 1 foot of Tensleep Sandstone with 13 percent porosity has the equivalent transmissibility of approximately 8 feet with 10 percent porosity. Most intervals of less than 11 percent porosity contribute only a small fraction of the ability of the Tensleep Formation to transmit fluids.

Transmissibilities computed from the logs by the procedure described represent standard laboratory conditions, not field conditions. Accordingly, the effects of changes of temperature under field conditions on viscosity were corrected for in translating the computed coefficient of transmissibility to field conditions at depth. Many wells penetrate only part of the Tensleep Sandstone, and the data were extrapolated on the assumption that the interval logged was representative of the entire formation.

Because of the wide variation in the coefficients of transmissibility in the Bighorn Basin (in excess of three orders of magnitude) it is most convenient for statistical manipulation to express coefficients of transmissibility in terms of their logarithms.

Table 1 lists the logarithms of the values for the coefficient of transmissibility (expressed in millidarcy-feet) determined from laboratory measurement and as computed from the sonic and neutron logs of the same well. Values computed from two or more closely spaced wells, generally less than 2 miles apart, are compared in table 2. Statistical analysis of these results from limited areas was made to evaluate the reliability of the data. The geometric mean of all the transmissibility values for a limited area was assumed to represent the most probable value for the area (table 2). The geometric mean was used because it is less affected by the extreme variability of the transmissibility data than is the arithmetic mean. A normal distribution plot of the deviations from this mean value was made to obtain a measure of the scatter of the data. The standard deviation of the data was approximately 0.2 log cycle. Results of various methods were grouped and analyzed statistically; the analysis shows reasonable agreement between the different methods (fig. 3).

TABLE 1.—*Comparison of coefficient of transmissibility of the Tensleep Sandstone in the Bighorn Basin computed from different source data from single wells.*

Location [1]			Well	Core analysis (log md-ft) [2]	Neutron log (log md-ft) [2]	Sonic log (log md-ft) [2]
Township (north)	Range (west)	Section				
43	91	6	Farmers Union 16 Gov't. Shad.	4. 123	------	4. 024
44	95	24	Continental 38 Gebo.	------	3. 577	3. 995
45	92	23	California Co. 11 Unit.	2. 788	3. 416	------
46	98	19	Ohio 6 Pre-Tensleep.	------	3. 602	3. 562
51	93	12	Kirk Oil 10 Lamb	4. 395	3. 810	------
57	97	18	Sohio 15 Sage Creek.	4. 279	4. 106	------

[1] Referred to 6th principal meridian and base line.
[2] 1 millidarcy-foot=0.01824 gallons per day per foot (see Wenzel, 1942).

TABLE 2.—*Comparison of coefficient of transmissibility of the Tensleep Sandstone in the Bighorn Basin computed from different source data in closely spaced wells*

Location [1]			Core analysis (log md-ft)	Neutron log (log md-ft)	Sonic log (log md-ft)	Geometric mean value (log md-ft)
Township (north)	Range (west)	Section				
43	91	6	4. 123	--------	4. 024	4. 039
43	92	1	4. 168	--------	--------	----------
43	92	1	3. 843	--------	--------	----------
44	95	23	--------	3. 978	--------	3. 852
44	95	24	--------	3. 577	3. 995	----------
44	98	12	--------	--------	3. 662	3. 972
44	98	13	--------	4. 151	--------	----------
44	98	15	3. 668	4. 408	--------	----------
45	92	23	2. 788	3. 416	--------	3. 102
46	98	19	3. 602	3. 562	--------	3. 582
48	102	11	4. 394	3. 839	--------	4. 026
48	102	14	--------	4. 114	3. 758	----------
48	103	20	3. 686	3. 407	--------	3. 529
48	103	29	--------	--------	3. 494	----------
51	93	12	4. 395	3. 810	--------	4. 102
55	95	19	3. 608	--------	--------	3. 411
55	55	29	3. 308	--------	--------	----------
55	95	32	3. 317	--------	--------	----------
56	97	14	4. 270	--------	--------	4. 142
56	97	14	4. 014	--------	--------	----------
56	101	16	2. 902	2. 128	--------	2. 565
57	97	18	4. 279	4. 106	--------	4. 345
57	97	18	4. 653	--------	--------	----------

[1] Referred to 6th principal meridian and base line.

CONCLUSIONS

Use of an empirical porosity-permeability relation proved applicable in mapping differences in transmissibility of the Tensleep Sandstone within the confines of the Bighorn Basin. Data interpreted from the sonic and neutron logs were combined with data from core analyses and from drill-stem tests and were plotted on a map (not shown) showing the regional transmissibility of the Tensleep Sandstone. Although the plots indicate considerable variation in any small

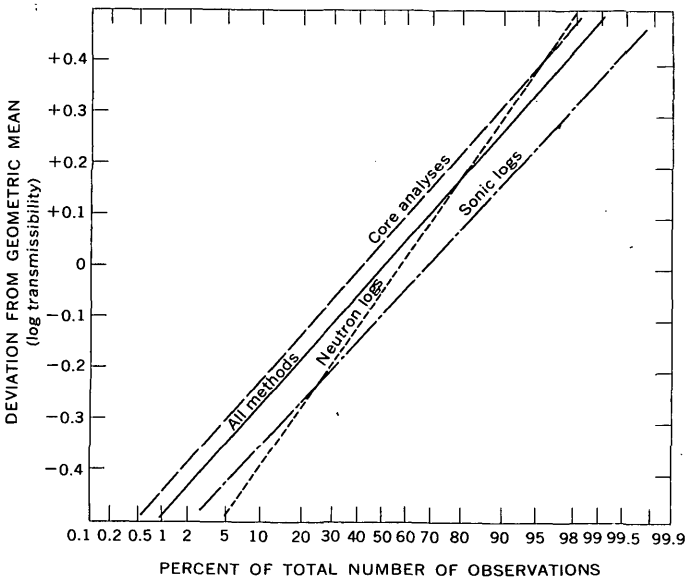

FIGURE 3.—Probability graph of deviation of the coefficient of transmissibility (log millidarcy-feet) from the "most probable" value—geometric mean of observations in a limited area—versus cumulative percent of the total number of observations.

area, areal plotting indicates a systematic regional decrease in transmissibility from the outcrop toward the structural center of the basin. The average permeability ranges from approximately 1 millidarcy in the structurally deeper parts of the Bighorn Basin to more than 800 millidarcies near the outcrop. This variation is reflected in a range in coefficient of transmissibility from several hundred millidarcy-feet in the deeper parts of the basin to values greater than 100,000 millidarcy-feet near the outcrop. This systematic regional pattern of transmissibility change, which agrees well with the known geology, lends support to the usefulness of the empirical method in this area.

REFERENCES

Archie, G. E., 1950, Introduction to the petrophysics of reservoir rocks: Am. Assoc. Petroleum Geologists Bull., v. 34, no. 5, p. 943–961.

Johnson, C. R., and Greenkorn, R. A., 1960, Comparison of core analysis and drawdown test results from a water-bearing upper Pennsylvanian sandstone of central Oklahoma [abs.]: Geol. Soc. America Bull., v. 71, no. 12, pt. 2, p. 1898.

Law, Jan, 1944, A statistical approach to the interstitial heterogeneity of sand reservoirs: Am. Inst. Mining Metall. Engineers Trans., Petroleum Div., v. 155, p. 202–222.

Wenzel, L. K., 1942, Methods for determing permeability of water-bearing materials with special reference to discharging-well methods: U.S. Geol. Survey Water-Supply Paper 887.

Wyllie, M. R. J., 1963, The fundamentals of well log interpretation: New York, Academic Press, 238 p.

UNIFORMITY OF DISCHARGE OF MUDDY RIVER SPRINGS, SOUTHEASTERN NEVADA, AND RELATION TO INTERBASIN MOVEMENT OF GROUND WATER

By THOMAS E. EAKIN and DONALD O. MOORE,
Carson City, Nev.

Work done in cooperation with the
Nevada Department of Conservation and Natural Resources

Abstract.—Flow measurements show that Muddy River Springs had uniform discharge during a period from September 1963 to April 1964; adjustments of the discharge record of Muddy River for local runoff and evapotranspiration show a long-term uniformity of springflow. Preliminary analysis of minor long-term variations suggests a 15- to 20-year lag in response to recharge from precipitation.

The Muddy River in southeastern Nevada is supplied principally by springs in the northwestern part of upper Moapa Valley. The ground water supplying the springs is inferred to be part of a regional groundwater system in Paleozoic carbonate rocks lying upgradient, or northward, from the Muddy River Springs. The area of the regional system provisionally is estimated to be roughly 7,700 square miles and includes 13 valleys in eastern and southeastern Nevada. Reconnaissance ground-water investigations for the specific valleys have been reported previously (Eakin 1961, 1962, 1963a, b, c, and 1964; Maxey and Eakin, 1949).

The inference that the Muddy River Springs are supplied from a large and complex regional groundwater system suggests that the discharge of the springs should tend to have a relatively uniform flow.

The flow of the Muddy River is gaged a short distance below the spring area. To utilize this record as a measure of the actual discharge of the springs, the record must be corrected for overland runoff resulting from local precipitation and losses of spring flow by evapotranspiration or diversion upstream from the gaging station.

DESCRIPTION AND RECORDS OF THE SPRINGS

The Muddy River Springs are at the head of the Muddy River, in upper Moapa Valley in southeastern Nevada (fig. 1). The springs issue from several groups of orifices and seep areas within the area shown on figure 2. Groups of orifices from which localized discharge occurs, such as the Iverson and Pederson groups, generally are along the margin of the flood plain. Others, such as Warm Spring and the group east of Warm Spring near U.S. Highway 93, however, issue from gravel ridges that extend into the general area of the flood plain. The seep areas are in the flood plain, downstream from the spring groups and along the natural and artificial channels. Along the main channel, flow derived from the spring area increases from zero near point 7 (fig. 2) to about 47 cubic feet per second at the gaging station, in a straight-line distance of 2 miles. Between the spring orifices and seep areas and the gaging station, evaporation and transpiration dissipate some of the spring discharge. Thus the flow of the river at the gaging station is less than the actual spring discharge. Evaporation and transpiration result from both natural effects and irrigation activities. The overall area in which evapotranspiration may have an effect on the flow at the gaging station probably is on the order of 750 acres.

U.S. GEOL. SURVEY PROF. PAPER 501-D, PAGES D171-D176

742-652 O—64——12

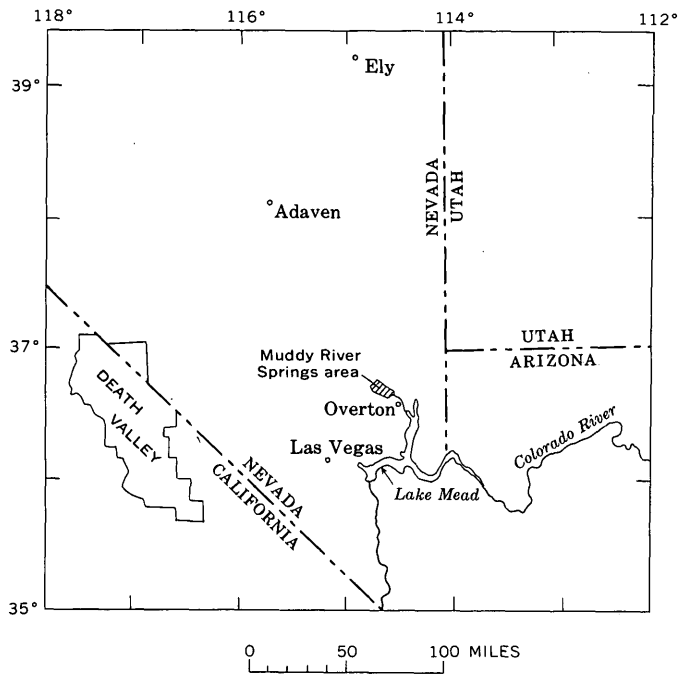

FIGURE 1.—Index map of southeastern Nevada, showing the Muddy River Springs area.

Although the springs issue from Recent alluvium in the flood plain and from conglomerate of the Muddy Creek (?) Formation in slopes bordering the flood plain, most of the water probably is transmitted to the spring area through Paleozoic carbonate rocks, which crop out close to some of the springs along the southwest side of the flood plain and which comprise most of the adjacent Arrow Canyon Range.

The records used in this analysis are for the flow of the Muddy River at U.S. Geological Survey gaging station 9–4160, Muddy River near Moapa, Nev., in the SE¼SE¼ sec. 15, T. 14 S., R. 65 E., Mt. Diablo base line and meridian. Long-term records have been published in Geological Survey water-supply papers.

As a part of a reconnaissance ground-water study of the area in September 1963 (Eakin, 1964), measurements or estimates of flow were made at 40 sites upstream from the gaging station to provide data on the relation of springflow to the gaging record. These sites included several springs and seep areas, main diversions, tributary confluences, and points along the main channel. Subsequently, measurements were made at the same sites in January 1964. Of these sites, 14 were selected and were measured again in March, April, and May 1964. Several sites of the 40 original sites, some the same as the present 14 sites, were measured in October and December 1963 and February 1964 for interim control. The present sites are sufficient to demonstrate the relative uniformity of spring discharge as compared to the seasonal fluctuations recorded at the gaging station.

RELATION OF SPRINGFLOW TO DISCHARGE OF THE MUDDY RIVER

The relation of the spring discharge to the flow of the Muddy River at the gaging station is illustrated for part of 1 year on figure 3, which shows a graph of measured discharge for 6 intervals of time between September 1963 and April 1964. The upper graph is a plot of the flow measured at the gaging station; the lower is a plot of the sum of the discharge at 6 points of measurement (points 1 to 6 on fig. 2) for the 6 intervals. The sum of spring-discharge measurements shows very little variation; the minimum is about 97 percent of the maximum. Measuring points 1 to 4 are close to spring orifices and are little affected by intermediate evapotranspiration. Measurements at points 5 and 6 show localized spring discharge and seepage gain along channel sections and may vary to a minor extent because of seasonal evapotranspiration. Together the discharge measured at the 6 points represents about 60 percent of the total spring discharge of the area and is considered to be reliable index of the uniformity of the total spring discharge. This is supported by the data obtained for the 2 series of measurements at the 40 sites upstream from the gaging station.

To reconstruct the spring discharge from the records of flow of the Muddy River at the gaging station, adjustments have been made for (1) streamflow at the gage resulting from local precipitation and runoff, (2) evapotranspiration between the springs and gaging station, (3) the effects of diversions that temporarily may bypass the gaging station and, (4) within-area changes of diversions which result in temporary modifications of the flow pattern. Ground-water underflow past the cross section of alluvium normal to the river at the gaging site is believed to be uniform and does not represent a significant accretion to streamflow downstream from the gaging station.

In large part the analysis concerns mean monthly and annual flow. Accordingly, item 4 above tends to be averaged out for present purposes, and item 3 probably was a minor factor during most of the period of record. Although past data are not available, the present diversion includes perhaps 1 cfs now carried in a pipeline to the town of Overton from one of the springs. Also, an irrigation well in the spring area north of the gaging station, which pumps about 3 cfs, is used for irrigation north and southeast of the gaging station. Although quantitative data are not available, the pattern of pumping of the well and the area

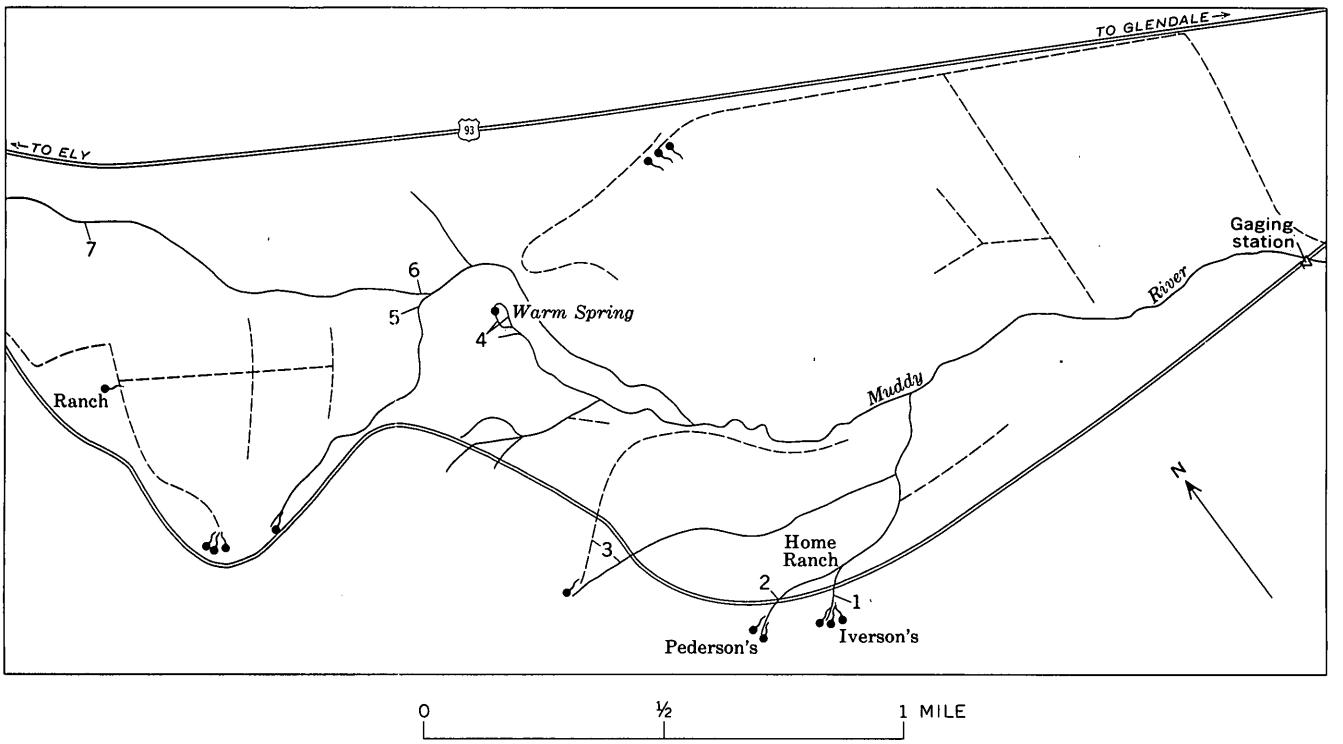

FIGURE 2.—Sketch map of the Muddy River Springs area, showing location of principal springs, stream channels (solid lines), and principal irrigation ditches (dashed lines). Numbers refer to selected measuring points.

irrigated suggest that, in effect, most of the water is evaporated or transpired from the area; however, a small amount may reach the main channel upstream from the gage from adjacent fields after periodic watering during the year. Evapotranspiration, both natural and from irrigation, between the springs and the gaging station is the principal factor resulting in differences between the total spring discharge and the flow of the river as measured at the gaging station.

Although streamflow generated from local runoff occasionally results in a very high peak discharge, the long-term effect on the flow of the Muddy River is small.

A simple correction for the effects of local precipitation on most of the streamflow was made for the 18-year period 1945–62. The adjustment was made by reducing the high flow shown for short intervals of storm runoff to values consistent with the immediately preceding and succeeding daily streamflow. The number of adjustments in mean monthly discharge is given in the accompanying table, together with the mean and median discharge. The distribution, by month, of the 24 adjustments shows 6 adjustments each for July and August, the principal months in which summer thundershowers occur.

As shown, the adjustment of streamflow to account for local precipitation has a minor effect on the record of annual flow of the Muddy River. However, the adjustment results in a month-to-month change in the record for the Muddy River at the gaging station that is more consistent with the expected pattern of the month-to-month change resulting from seasonal effects of temperature and evapotranspiration.

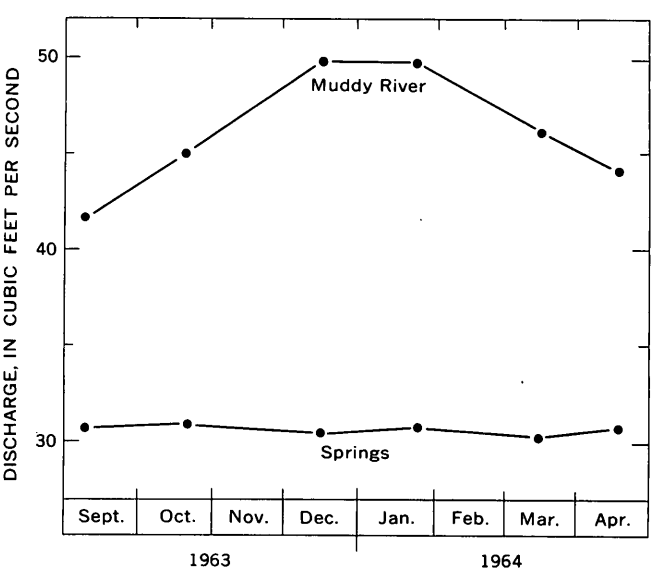

FIGURE 3.—Measured discharge at the gaging station, Muddy River near Moapa, and the sum of measurements of springs at 6 sites, numbers 1 to 6 inclusive on figure 2, for 6 time intervals during the period September 1963 to April 1964.

Long-term mean, median, and adjusted monthly discharge of Muddy River near Moapa for the period of water years 1945–62

Months	18-year mean discharge (cfs)	18-year median discharge (cfs)	18-year adjusted mean discharge [1] (cfs)	Number of adjustments, by month
October	46. 5	46. 5	46. 4	1
November	49. 5	48. 2	48. 8	3
December	50. 2	50. 1	50. 1	2
January	50. 2	49. 5	50. 2	0
February	49. 4	49. 6	49. 1	2
March	48. 3	47. 8	48. 2	1
April	46. 6	46. 6	46. 6	0
May	45. 3	45. 6	45. 2	1
June	43. 4	43. 7	43. 3	2
July	43. 4	43. 6	42. 9	6
August	44. 7	43. 3	43. 7	6
September	44. 4	44. 4	44. 4	0
Year	46. 8	46. 9	46. 6	24

[1] Adjusted to eliminate the amount of runoff derived from local precipitation from the gage record.

Adjustment for evapotranspiration

Diurnal and seasonal fluctuations in streamflow occur in response to evapotranspiration, which in turn is related mainly to the seasonal variations in temperature.

Figure 4 shows daily fluctuations in the water-stage record for August 12 and 13, 1963, resulting from the diurnal variation in the rate of evapotranspiration. The graph for January 29 and 30, 1964, shows no such fluctuation. The two periods shown by the graphs are during maximum (June–August) and minimum (December–January) periods of evapotranspiration. The range in fluctuation of the August graph represents about 2 cfs, and is considered to be due primarily to the diurnal effect of evapotranspiration along the main and the principal tributary channels of the stream.

Seasonal variations in evapotranspiration in the area between the gaging station and the springs also affect the flow of the river. The adjusted mean monthly discharge (from the table), plotted on figure 5, shows that the minimum mean discharge occurs in July and the maximum in January, with moderately large changes in the intervening months. The mean monthly temperature at Overton is plotted for comparison. It, too, shows a change from month to month, but as might be expected, in an inverse pattern—the months of highest temperature correspond to the time of greatest stream loss through evapotranspiration.

Figure 6 shows an excellent correlation of discharge of the Muddy River at the gage with air temperature. The high degree of correlation, even though the adjusted mean monthly discharge of the river ranged from 42.9 to 50.2 cfs, clearly indicates that the input, or spring discharge, supplying the river is highly uniform from month to month. Thus, because the spring discharge is uniform, it is represented closely by the gaging record of the river during January, the month of minimum evapotranspiration. The adjusted mean January discharge is 50.2 cfs. Furthermore, if this is representative of the mean annual discharge of the springs, then the amount of spring discharge dissipated by evapotranspiration can be estimated by subtracting the adjusted mean annual discharge (46.6 cfs) of the Muddy River. Thus 3.6 cfs represents the part of the mean annual springflow that discharges at the land surface and is consumed by evapotranspiration between the springs and gaging station.

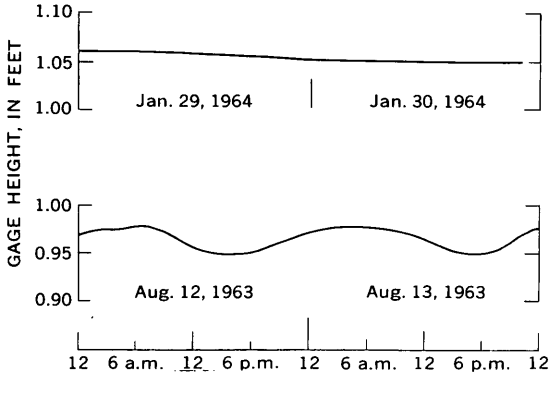

FIGURE 4.—Stage of the Muddy River for the 2-day periods January 29 and 30, 1964, and August 12 and 13, 1963, illustrating diurnal effect of evapotranspiration during the summer.

Long-term uniformity of discharge

Some variation in annual mean discharge of Muddy River Springs is evident from the published records of Muddy River streamflow. As noted in the table,

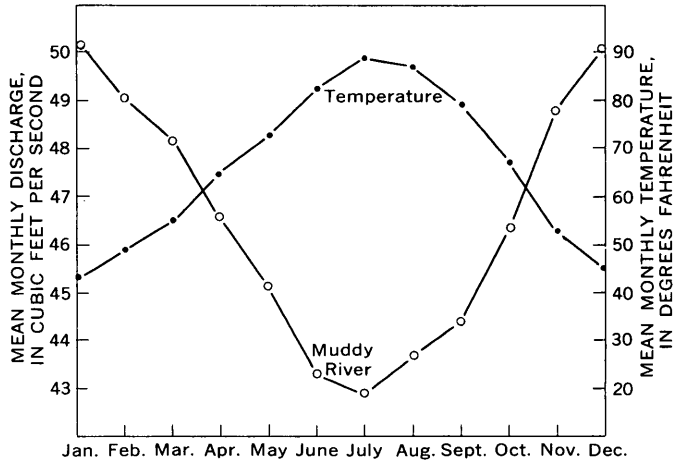

FIGURE 5.—Comparison of mean monthly discharge of Muddy River at the gaging station and mean monthly temperature at Overton, Nev., 1945–62.

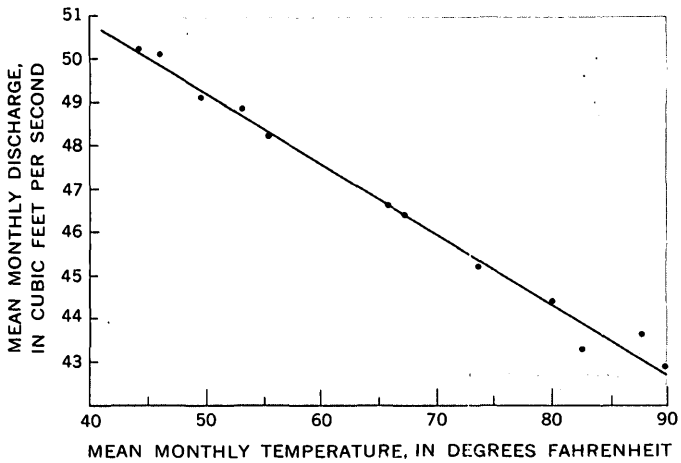

FIGURE 6.—Plot of the mean monthly discharge of Muddy River at the gaging station versus mean monthly temperature at Overton, Nev., without respect to time.

the mean annual discharge of Muddy River for the 1945 to 1962 period is 46.8 cfs, the median is 46.9, and the record adjusted for overland flow from local precipitation is 46.6. The minimum annual mean during the 18-year period was 44.5 cfs, in 1962, and the maximum was 49.6 cfs, in 1958. The small range in fluctuation is indicated by the fact that the discharge in the minimum year was about 90 percent of the maximum annual mean discharge uncorrected for locally derived streamflow. Thus, although some long-term variation occurs, the very small range of variation actually indicates a highly uniform long-term discharge characteristic of the Muddy River Springs.

Long-term variation of discharge

Although the Muddy River Springs have a highly uniform discharge, the small range of variation has long-time significance. Eakin (1964, fig. 4) compared a graph of cumulative departure from average annual precipitation at Adaven, Nev., for the period 1919–62 with a graph of cumulative departure from mean annual discharge of the Muddy River for the period 1945–62. A rising trend of discharge during the period 1957 to 1960 seemingly was related best to a noticeable rising trend of precipitation in the period 1937–41. Within these two periods, 1941 commonly was a year of much above normal precipitation in much of the Great Basin. The greatest increase in annual mean discharge over the prior year shown by the Muddy River record was in 1958. This suggests a possible timelag response of spring discharge to regional precipitation and consequent recharge of perhaps 15 to 20 years.

Additional simple tests of correlation between precipitation and spring discharge seem to support further a timelag response of the order indicated above. However, further analysis of the gaging record and of regional precipitation conditions is required and is in progress to evaluate this feature.

SUMMARY AND CONCLUSIONS

Several sets of measurements of the discharge of springs that supply the principal flow of the Muddy River in southeastern Nevada indicate that the spring discharge was much more uniform than was the flow of the Muddy River at the gage during the period September 1963 to April 1964. During the interval the flow of the river at the gaging station increased from a measured discharge of 42.8 cfs in September to 49.8 cfs in January and declined to 44.0 cfs in April, whereas the measured spring discharge was nearly constant. Comparison of mean monthly discharge at the gage for the period 1945–62 with mean monthly temperature for Overton, as a measure of evapotranspiration, shows a high correlation and indicates that, for practical purposes, the variation in mean monthly discharge is a function of evapotranspiration. From this it is inferred that the spring discharge supplying the Muddy River must be highly uniform or the correlation of discharge and temperature would not be so close. If this is the case, then the annual mean discharge of the springs in a given year should be approximately equal to the January mean discharge of the Muddy River for that year, as January is the month of minimum evapotranspiration. The adjusted mean January discharge of the river is 50.2 cfs for the period 1945 to 1962. The difference between the 50.2 cfs and 46.6 cfs, the adjusted mean annual discharge at the gaging station, is 3.6 cfs and approximately represents the mean annual evapotranspiration between the springs and the gaging station.

The long-term uniformity of spring discharge is suggested even by the uniformity of unadjusted mean annual discharge of the Muddy River. The minimum annual mean discharge for the period 1945–62 of gaging record is 90 percent of the maximum annual mean discharge.

Although long-term discharge of the springs is nearly uniform, some variation from year to year does occur. Preliminary tests suggest that spring discharge responds to pronounced variations in precipitation and consequent recharge with a timelag on the order of 15 to 20 years. These tests, though simple, are promising, and further studies are in progress.

REFERENCES

Eakin, T. E., 1961, Ground-water appraisal of Long Valley, White Pine and Elko Counties, Nevada: Nevada Dept. Conserv. Nat. Resources, Ground-Water Resources Reconn. Ser. Rept. 3, 35 p.

——— 1962, Ground-water appraisal of Cave Valley in Lincoln and White Pine Counties, Nevada: Nevada Dept. Conserv. Nat. Resources, Ground-Water Resources Reconn. Ser. Rept. 13, 19 p.

——— 1963a, Ground-water appraisal of Dry Lake and Delamar Valleys, Lincoln County, Nevada: Nevada Dept. Conserv. Nat. Resources, Ground-Water Resources Reconn. Ser. Rept. 16, 26 p.

——— 1963b, Ground-water appraisal of Garden and Coal Valleys, Lincoln and Nye Counties, Nevada: Nevada Dept. Conserv. Nat. Resources, Ground-Water Resources Reconn. Ser. Rept. 18, 29 p.

Eakin, T. E., 1963c, Ground-water appraisal of Pahranagat and Pahroc Valleys, Lincoln County, Nevada: Nevada Dept. Conserv. Nat. Resources, Ground-Water Resources Reconn. Ser. Rept. 21, 36 p.

——— 1964, Ground-water appraisal of Coyote Spring and Kane Spring Valleys and Muddy River Springs area, Lincoln and Clark Counties, Nevada: Nevada Dept. Conserv. Nat. Resources, Ground-Water Resources Reconn. Ser. Rept. 25, 40 p.

Maxey, G. B., and Eakin, T. E., 1949, Ground water in White River Valley, White Pine, Nye, and Lincoln Counties, Nevada: Nevada State Engineer Water Resources Bull. 8, 59 p.

GEOLOGIC FACTORS AFFECTING DISCHARGE OF THE SHEYENNE RIVER IN SOUTHEASTERN NORTH DAKOTA

By Q. F. PAULSON, Grand Forks, N. Dak.

Work done in cooperation with the North Dakota State Water Conservation Commission

Abstract.—Throughout much of its length the Sheyenne River is fed almost wholly by overland runoff from glacial till. However, in the reach 75 to 145 miles upstream from its junction with the Red River of the north, the Sheyenne drains ground water from sand deposits in the Sheyenne delta, into which its valley is deeply incised. Discharge measurements made in the fall of 1963 indicated an average gain of 28.8 cfs in this reach.

The Sheyenne River drains about 9,300 square miles in eastern North Dakota; about 4,000 square miles lies in the closed Devils Lake basin. The entire drainage area is underlain by glacial drift of late Wisconsin age. In most places the drift consists of till or lake sediments of relatively low permeability, but in a few places it consists of deltaic or outwash deposits having moderate to high permeability.

About 10 miles southeast of Lisbon the Sheyenne enters a broad area of mainly sand deposits that have been described by Upham (1895, p. 315–317) and others as deltaic in origin. Upham named the feature the Sheyenne delta (fig. 1) and estimated that it had an area of about 800 square miles. The delta is nearly flat in some parts but strongly rolling in others, where the sand has been heaped into dunes by wind action. Surface drainage is poorly developed—the only streams crossing the delta are the Sheyenne, Maple, and Wild Rice Rivers.

Logs of test holes and wells show that the deltaic deposits grade from gravel and very coarse sand in the western part of the Sheyenne delta to silt and clay in the eastern part. Recent study of the surface geology indicates that part of the coarser materials may be outwash rather than deltaic deposits. However, most of the deposits are sand and probably are of deltaic origin. The thickness commonly exceeds 50 feet and in a few places is known to be greater than 100 feet.

On reaching the delta the Sheyenne River turns northward and flows approximately along the contact between the east edge of the drift prairie and the west edge of the delta. Where it leaves the drift prairie, the river swings eastward across the delta. Compared to the channel along the contact with the drift prairie, the channel across the delta is much more sinuous. The distance measured along a straight line between stations *E* (fig. 1) at the west edge of the delta and *M* at the east edge is about 23 miles. The distance along the river, however, is about 52 miles.

Leaving the delta the Sheyenne flows mainly northward across the nearly flat Lake Agassiz plain and joins the Red River of the North about 10 miles north of West Fargo.

SUMMARY OF RIVER DISCHARGE

The discharge of the Sheyenne River has been measured continuously since March 1938 at Valley City, since September 1956 at Lisbon, since July 1949 near Kindred, and since September 1929 at West Fargo. At various times during the period 1938–41, the Sheyenne has had no flow at Valley City; the minimum flow of record at West Fargo was 2.0 cfs, on December 14, 1936. Since 1949, when Lake Ashtabula was created by completion of Baldhill Dam (13 miles upstream from Valley City), the flow of the river below the dam has been regulated by releases from the lake. Although during extended periods of little or no overland runoff the flow of the river is greater than it was before the dam was built, regulation of the flow does not diminish radically the value of the discharge data for comparative purposes.

U.S. GEOL. SURVEY PROF. PAPER 501-D, PAGES D177–D181

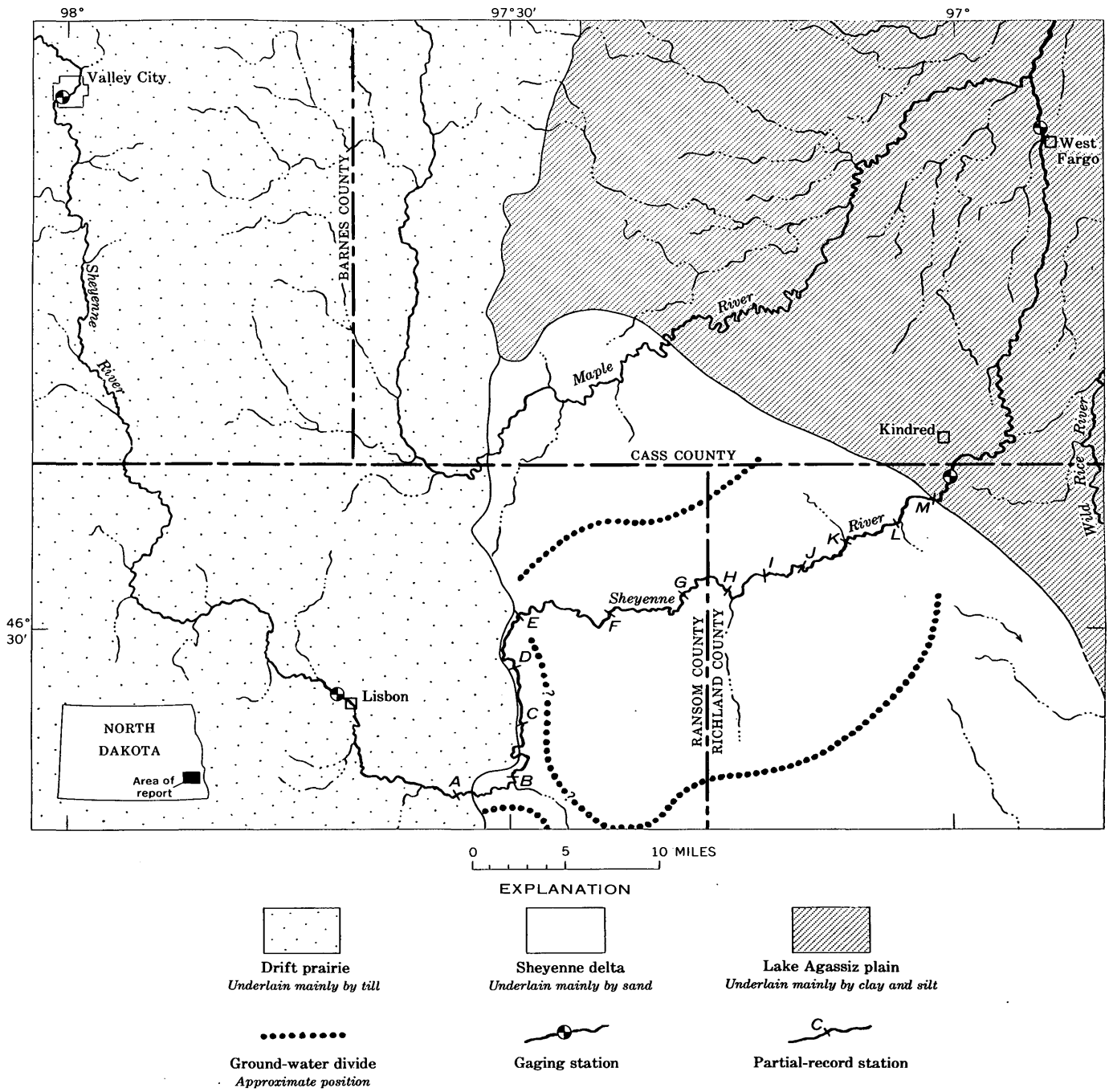

FIGURE 1.—Map showing generalized geomorphic subdivisions of southeastern North Dakota and observation stations along the Sheyenne River.

Table 1 gives the mean monthly discharge in cubic feet per second at discharge stations on the Sheyenne River at Valley City, Lisbon, Kindred, and West Fargo during the period October through February, 1957–62. The months of October through February were chosen for comparative purposes because, generally, little or no overland runoff occurs during this period. Although the discharge at Valley City includes releases from Lake Ashtabula, the changes in discharge recorded at stations below Valley City mainly reflect changes in ground-water inflow and evapotranspiration rates.

It may be seen from the table that the mean monthly discharge of the Sheyenne River from October through February for the period 1957–62 increased by 15.1 cfs between Lisbon and Kindred. As late fall and early winter is a time of little or no runoff, the increase is attributed mainly to ground-water inflow. In addition,

an estimated 1.7 cfs probably was held in storage as ice during this period (H. M. Erskine, 1963, written communication). Comparison of the data given in table 1 shows that the increase in discharge per mile length of channel between Lisbon and Kindred was about 20 times greater than between Valley City and Lisbon and about 6 times greater than between Kindred and West Fargo.

TABLE 1.—*Mean monthly discharge of Sheyenne River, October through February, 1957–62, in cubic feet per second*

[Numbers in parenthesis indicate river miles above mouth]

	Valley City (253)	Lisbon (162)	Kindred (68)	West Fargo (24)
October	28. 0	31. 7	50. 7	52. 6
November	41. 5	42. 9	62. 0	61. 0
December	43. 5	41. 9	56. 5	59. 3
January	41. 6	38. 8	52. 7	54. 4
February	40. 1	42. 5	51. 5	52. 6
Average for 5-month period	38. 9	39. 6	54. 7	55. 9
Average gain between stations	0. 7	15. 1		1. 2
Average gain per mile of river	. 008	. 160		. 027

In order to determine more precisely the nature and magnitude of the increase in discharge, a series of 13 partial-record stations (*A* through *M*, fig. 1) were established between Lisbon and Kindred. Five series of current-meter measurements were made at approximate 2-week intervals during the period from September 13 to November 19, 1963 (table 2). Each series of measurements was obtained in as short a period as possible (generally less than 24 hours) to minimize the effects of changing stage. However, a changing stage caused by releases from Lake Ashtabula affected the November 19 measurements made at Valley City, Lisbon, and West Fargo and at stations A and B. The averages of the discharge measurements, except those affected by releases from Lake Ashtabula, made at each of the partial-record stations, as well as at the stations at Valley City, Lisbon, near Kindred, and at West Fargo are plotted on the hydrograph shown on figure 2. The data in table 2 and on figure 2 show an average increase of 28.8 cfs in the discharge between the stations at Lisbon and Kindred. This is substantially more than the average increase of 15.1 cfs for the October through February, 1957–62, period (table 1). Precipitation and ground-water records indicate that the recharge received annually by the delta deposits was considerably larger in 1962 and 1963 than during the 3 years prior to 1962. The increased recharge resulted in a higher water table, steeper gradients toward the Sheyenne River, and increased rate of ground-water movement toward the river.

RELATION OF RIVER DISCHARGE TO GEOLOGY

The data in tables 1 and 2 and the graph on figure 2 indicate very little ground-water inflow between Valley City and Lisbon, a river distance of 91 miles. The surface and near-surface deposits draining into this stretch of the river consist mainly of till underlain

TABLE 2.—*Measurements of discharge of Sheyenne River between Valley City and West Fargo, N. Dak., 1963*

Gaging station	River mile	Discharge (cubic feet per second)					Average of discharge measurements made Sept. 13–Nov. 19
		Sept. 13	Oct. 1	Oct. 15	Oct. 29	Nov. 19	
Valley City (discharge computed from gage-height record)	253. 0	11. 0	7. 9	6. 9	5. 7	[1] 33. 0	7. 87
Lisbon	162. 0	6. 98	6. 22	11. 4	13. 7	[1] 25. 0	9. 57
Stations:							
A	147. 5	8. 60	8. 02	11. 0	17. 0	[1] 21. 4	11. 1
B	141. 6	10. 3	8. 96	13. 2	19. 3	[1] 18. 6	12. 9
C	134. 9	11. 1	9. 31	11. 4	21. 3	16. 2	13. 9
D	131. 5	11. 7	9. 20	13. 9	21. 8	19. 2	15. 2
E	125. 9	11. 6	8. 56	15. 0	21. 1	18. 2	14. 9
F	114. 0	16. 6	12. 5	18. 6	27. 9	24. 5	20. 0
G	104. 0	21. 9	18. 8	24. 1	28. 7	30. 8	24. 9
H	97. 4	24. 1	21. 1	28. 3	33. 1	27. 5	26. 9
I	91. 8	29. 8	26. 2	32. 9	35. 0	33. 0	31. 4
J	87. 6	31. 5	25. 8	34. 9	39. 5	38. 3	34. 0
K	81. 1	34. 2	29. 5	37. 8	46. 2	39. 1	37. 4
L	77. 3	36. 6	26. 6	35. 9	43. 4	39. 4	36. 4
M	73. 6	34. 5	28. 8	37. 2	41. 4	42. 0	36. 8
Near Kindred	68. 1	33. 5	31. 0	37. 8	46. 1	43. 8	38. 4
West Fargo (discharge computed from gage-height record)	24. 5	36	26	33	45	[1] 54	35. 0

[1] Discharge affected by releases from Lake Ashtabula. Not used in computing averages.

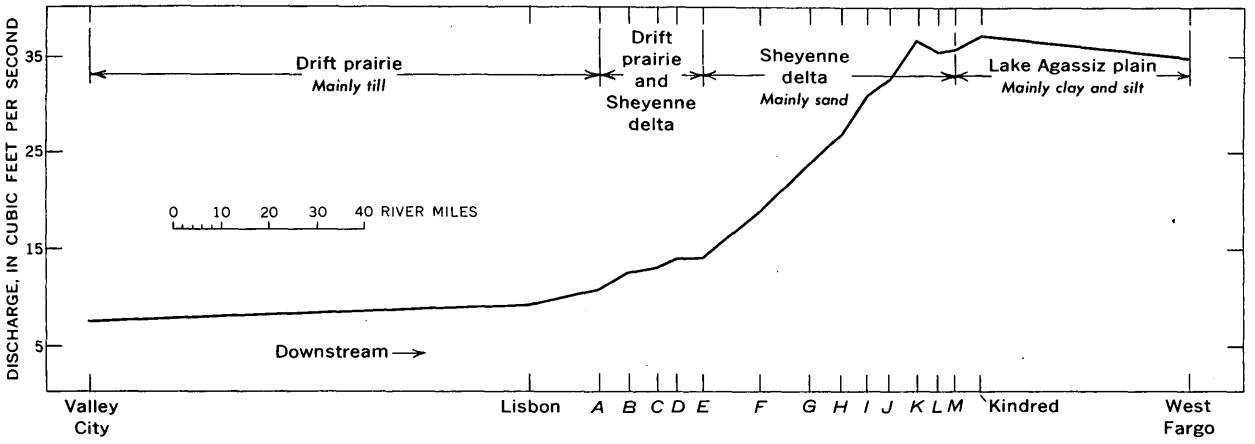

FIGURE 2.—Average discharge of the Sheyenne River, Valley City to West Fargo, September 13–November 19, 1963. Letters refer to partial-record stations shown on figure 1 and referred to in text.

by shale. Regionally these deposits have a low permeability and generally yield small quantities of ground water. However, the valley of the Sheyenne River is a half to three quarters of a mile wide in this reach and has been thought to be underlain by permeable deposits of outwash and alluvium that would yield substantial amounts of ground water. The lack of substantial increases in streamflow between Valley City and Lisbon during periods of low flow suggests either the absence of permeable deposits in the channel or, if such deposits are present, a lack of hydraulic connection between them and the river channel.

Between Lisbon and station A, 14.5 miles downstream, the flow in the Sheyenne River increased an average of 1.53 cfs. Here the valley is bordered on both sides by till, but the valley floor may be underlain by somewhat coarser and more permeable materials that discharge ground water into the river.

Between stations A and E, a river distance of 21.6 miles, the river flows along the west edge of the Sheyenne delta. The average increase in the discharge measurements in this reach was 3.8 cfs. Here the river is bordered on the west by till and on the east by delta(?) deposits consisting of coarse sand and gravel. Except where modified by sand dunes, the surface of the deltaic deposits slopes generally eastward. Probably the ground-water drainage divide (fig. 1), as well as the surface-water divide, is relatively near the Sheyenne River in the region between stations A and E. Consequently, although the river is deeply incised along the west margin of the delta, only a relatively small amount of ground water drains westward to the river.

From station E the river flows east-northeast across the Sheyenne delta and separates it into two segments, a smaller northern segment and a much larger southern one. The river flows in a meandering channel, in contrast to the relatively straight channel between stations A and E. The valley floor, which is commonly less than half a mile wide, is from 50 to 100 feet below the main level of the upland on either side, and the river channel is incised from 15 to 25 feet below the valley floor.

Test drilling indicates that the deposits on either side of the river valley in the region between stations E and K consist of sand grading eastward from coarse to fine. The deposits are generally more than 50 feet thick. Although a thorough discussion of the origin and stratigraphy of these deposits is beyond the scope of this paper, current geologic studies support Upham's theory of deltaic origin.

The deltaic deposits form a productive aquifer extending over several hundred square miles south of the Sheyenne River and, to a much lesser extent, north of the river. From station E to station K, a river length of 44.8 miles, the average increase in the discharge measurement was 22.5 cfs, which represents a gain of nearly 0.5 cfs per mile of river channel. This increase in flow, which is the largest known for any stream segment of comparable length along the entire course of the river, is produced by ground-water discharge from the deltaic deposits adjacent to both sides of the valley.

A significant part of the increase in the discharge measurements between stations E and K is due to inflow from short tributaries which head on the Sheyenne delta and whose base flow consists wholly of ground-water discharge from the deltaic deposits. Examination of U.S. Geological Survey 7½-minute topographic quadrangle maps reveals several tributaries extending back into the deltaic deposits from both sides of the Sheyenne River valley between sta-

tions E and K and, also, east of station K. The largest of these enters the valley from the south, a short distance east of the west boundary of Richland County (fig. 1). Five measurements of the discharge at the mouth of this tributary during the period September 13 to November 20, 1963, averaged 2.2 cfs.

Between stations K and M, 7.5 river miles apart, the average of the five discharge measurements decreased 0.6 cfs. Station M is a short distance east of the scarp that marks the northeastern edge of the delta. Test drilling and surface reconnaissance indicate that the deltaic deposits bordering this stretch are composed mainly of silt and very fine sand that yield only small amounts of ground water. Sandpoint wells, which are common throughout much of the delta, are not a successful means for obtaining water in this part of the area. Also, considerable ground water is diverted eastward or northeastward toward the edges of the scarp rather than into the Sheyenne River valley.

Between station M and Kindred, 5.5 miles apart, the average of the discharge measurements increased 1.6 cfs. It is not known whether ground-water inflow is distributed evenly along this segment or is restricted largely to one main locality. Probably most of the inflow occurs a relatively short distance below station M. Earlier workers apparently considered the scarp as the northeastern edge of the delta. However, detailed surface mapping indicates a body of sand extending about a mile beyond the scarp and grading eastward or northeastward into silt and clay. Test drilling in the vicinity of Kindred (Dennis and others, 1950, p. 75) indicates that the sand is at least 12 feet thick in places. It is reasonable to assume that most of the inflow is derived from this sand and from springs issuing from the delta scarp.

From Kindred to West Fargo the Sheyenne River meanders across the nearly flat surface of the Lake Agassiz plain. The river length between the two stations is 43.6 miles, but the average of the 5 measurements made between September 13 and November 19 showed a loss of 3.4 cfs. The lack of ground-water inflow is not surprising inasmuch as the surface deposits in this region consist of clay and silt having a low permeability.

CONCLUSION

The substantial increase in discharge of the Sheyenne River along its course across the Sheyenne delta has considerable significance in the appraisal of the hydrologic regimen of this region. The increase in mean monthly discharge for the months of October–February, 1957–62, of 15.1 cfs between the stations at Lisbon and Kindred and the average increase in discharge of 28.8 cfs for the five daily measurements made from September 13 to November 19, 1963, is due almost wholly to ground-water discharges from the delta deposits. However, this amount is only part of the total natural discharge of ground water, as substantial quantities are discharged during the warmer months of the year by evapotranspiration in areas where the water table is shallow. Also, ground water is discharged at springs along the scarp of the delta and, probably, as underflow to adjacent permeable bodies.

Full utilization of the ground water in the delta deposits depends, of course, both on physical and economic factors. Large ground-water yields over sustained periods can be developed only where the physical characteristics of the water-bearing deposits are favorable, such as in the western and central parts of the delta. Although large withdrawals of ground water in areas near the river would reduce inflow to the river and thus cause a decrease in streamflow at downstream points, the problem could likely be alleviated by appropriate releases from Lake Ashtabula.

REFERENCES

Dennis, P. E., Akin, P. D., and Jones, S. L., 1950, Ground water in the Kindred area, Cass and Richland Counties, North Dakota: North Dakota Ground-Water Studies, No. 14.

U.S. Geological Survey, 1957–60, Surface-water supply of the United States, pt. 5, Hudson Bay and Upper Mississippi River Basins, U.S. Geol. Survey Water-Supply Papers 1508, 1558, 1628, 1708.

U.S. Geological Survey, 1961, 1962, Surface-water records of North Dakota and South Dakota: Open-file reports.

Upham, Warren, 1895, The glacial Lake Agassiz: U.S. Geol. Survey Mon. 25, [1896].

MAGNITUDE AND FREQUENCY OF STORM RUNOFF IN SOUTHEASTERN LOUISIANA AND SOUTHWESTERN MISSISSIPPI

By V. B. SAUER, Baton Rouge, La.

Work done in cooperation with the Louisiana Department of Public Works

Abstract.—The relation between magnitude and frequency of individual storm runoff has been determined for streams in southeastern Louisiana and southwestern Mississippi. Graphical correlations indicate that the mean annual, or 2.33-year, storm runoff for any site in the area is 64 second-foot-days per square mile, which is equivalent to a uniform depth of 2.38 inches. It was also demonstrated that the recurrence interval of an individual storm runoff will, in many instances, be significantly different from the recurrence interval of the peak discharge resulting from the same storm.

The relation between individual storm runoff and frequency of occurrence has been established for streams in southeastern Louisiana and southwestern Mississippi. Storm runoff is defined, for this report, as the rainfall excess resulting from individual storms and is analyzed as an independent event. Coincident with the problem of relating storm runoff to frequency of occurrence, a study was also made to determine whether the recurrence interval of a given storm runoff is the same, or nearly the same, as the recurrence interval of the peak discharge resulting from the same storm.

The study area (fig. 1) includes what is known as the "Florida Parishes" in southeastern Louisiana and about eight counties to the north of the Florida Parishes in southwestern Mississippi. It is bounded on the east by the Pearl River and on the west by the Mississippi River. Topography of the 7,500-square-mile area is varied, ranging from rolling hills to flat, swampy lands. Average annual rainfall ranges from about 56 inches in southwestern Mississippi to 66 inches in southeastern Louisiana.

The total runoff, or volume, was computed for every storm that had a peak above a base so selected as to give an average of 3 to 5 floods a year at each of 17 gaging stations in the area. These stations, with drainage areas ranging from 0.73 to 1,330 square miles, were selected for this frequency study on the basis of length of record; all have 8 or more years of record. The base period for the study was 1940–61. Although the total runoff for several storms was computed for each year, only the maximum storm runoff for each year was used. Correlations with nearby stations were used to extend the records of maximum annual storm runoff of some stations so that it was possible to compute all records for the same base period.

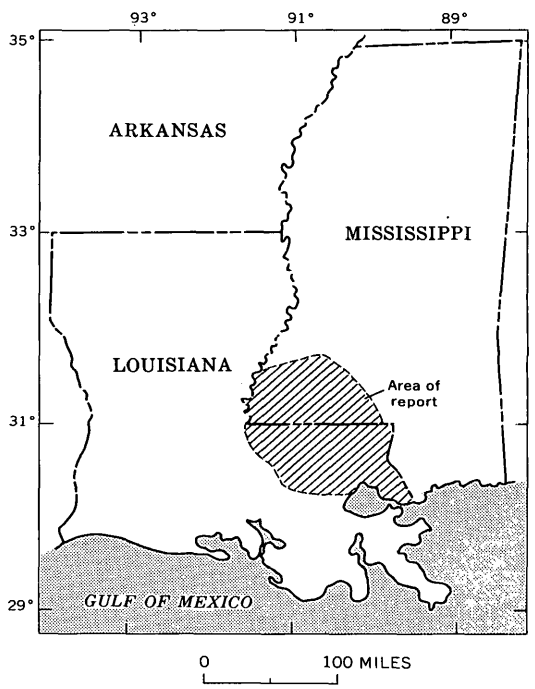

FIGURE 1.—Index map showing area of study.

Storm runoff is direct runoff only, and this is computed as the total runoff minus base flow. Recession curves were developed for each station and were used to separate the overlapping runoff from two or more storms. Before separation of runoffs that apparently overlapped, the hydrograph and rainfall records were carefully inspected to ensure that double peaks were not the effect of tributary timing. This procedure evaluates the runoff from each storm independently.

An annual-series frequency analysis was prepared for each station according to the procedures described by Dalrymple (1960). The mean annual storm runoff, in second-foot-days, was determined from each frequency curve at the 2.33-year recurrence interval. These values were then related to drainage area as shown on figure 2. The ratio of storm runoff (at other recurrence intervals up to 25 years) to mean annual storm runoff was computed for each station. The median of these ratios, for selected recurrence intervals, was plotted to obtain the regionalized frequency curve shown on figure 3. The comparable curve for annual peak discharges (Sauer, 1964) is also shown on figure 3.

The mean annual storm runoff, as determined from figure 2, is equal to 64 second-foot-days per square mile for any basin in the study area. Converted to a uniform depth over the area, this is equal to 2.38 inches. This value multiplied by the values from the frequency curve on figure 3 results in the curve shown on figure 4.

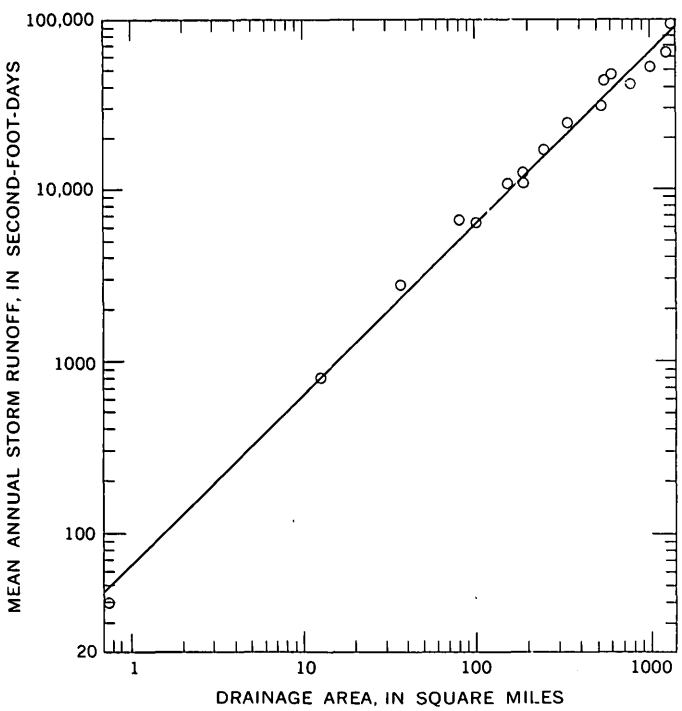

FIGURE 2.—Relation of drainage area to mean annual storm runoff.

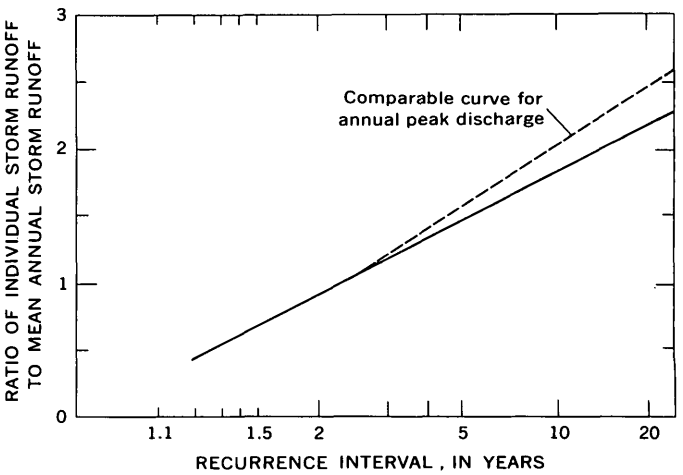

FIGURE 3.—Regional frequency curve of annual storm runoff.

Based on the data and analysis of this study, the standard deviation of the mean annual storm runoff is 13 percent, and the standard deviation of the 25-year frequency storm runoff is 17 percent.

Further investigations were made to determine whether the recurrence interval of the runoff of a given storm was the same, or nearly the same, as the recurrence interval of the instantaneous peak discharge resulting from the same storm. The recurrence intervals of storm runoffs were determined from the frequency curves presented in this report; those of instantaneous peak discharge were determined from flood reports by Sauer (1964) and by Wilson and Trotter (1961).

Eight stations, selected randomly from the 17 stations used in the analysis, were used to compare the recurrence intervals of storm runoff and peak discharge for each of 87 storms having runoff recurrence intervals greater than 1.7 years. It is evident from this comparison, shown graphically on figure 5, that

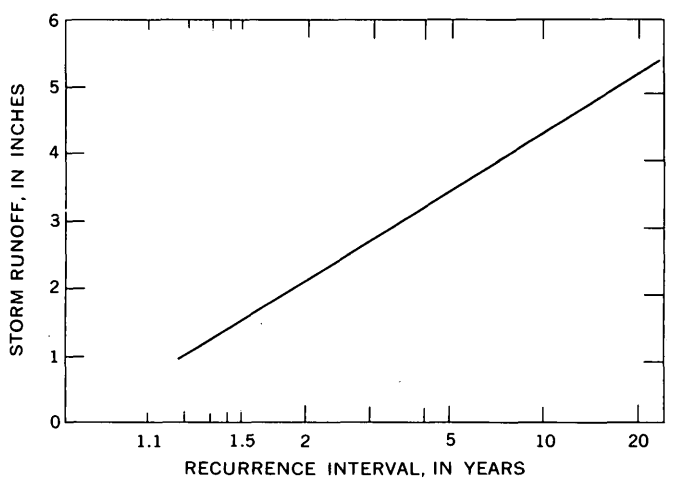

FIGURE 4.—Relation of individual storm runoff, in inches, to recurrence interval.

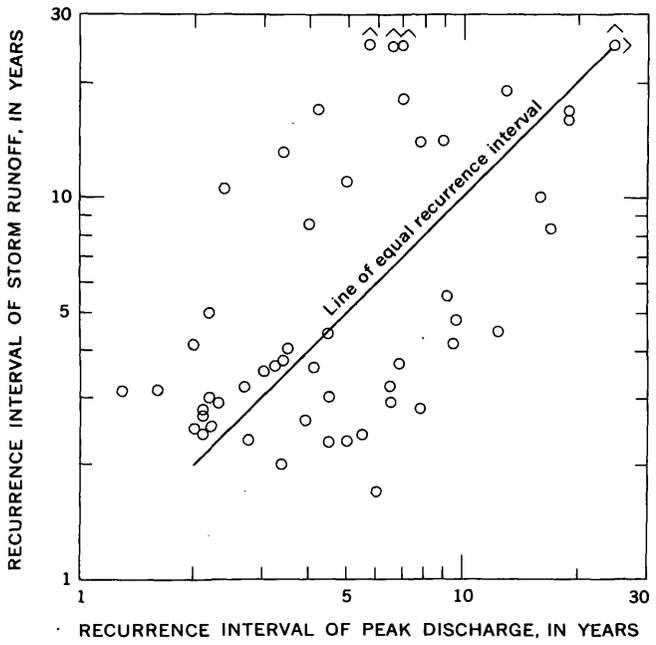

FIGURE 5.—Variation between the recurrence intervals of peak discharge and the corresponding storm runoff. V's above and to the right of points at the top of the graph indicate that these points have a recurrence interval of greater than 25 years in the direction of the V.

a wide variation exists between the recurrence intervals computed for storm runoff and corresponding peak discharge. This variation can be explained by several factors that affect the relation between storm runoff and peak discharge. Two storms having identical total runoff at a station may have considerably different peaks because of different storm durations or different distribution of rainfall over the basin. Direction of storm travel will cause variations in the relation between peak and runoff. Another significant factor is the rate of flow in the channel at the time of storm runoff, which may include only base flow or base flow plus flow from the recession of a previous storm. There are probably other factors of lesser significance that also affect this relation. It follows, therefore, that recurrence intervals of peak discharge cannot be determined with any reliability from recurrence intervals of storm runoff. Although no direct proof resulted from this study, it is evident that rainfall-frequency relations cannot be used to determine the recurrence intervals of peak discharge.

In conclusion, this report shows that the recurrence intervals for a storm runoff of a particular magnitude (within the limits defined) can be determined reliably for any site in the study area by using curves presented in this report. It is also demonstrated that the recurrence interval of a storm runoff will, in many instances, be greatly different from the recurrence interval of the peak discharge resulting from the same storm.

REFERENCES

Dalrymple, Tate, 1960, Flood-frequency analysis: U.S. Geol. Survey Water-Supply Paper 1543–A, 80 p.

Sauer, V. B., 1964, Floods in Louisiana, magnitude and frequency, 2d ed.: Louisiana Dept. Highways, 402 p. [In press]

Wilson, K. V., and Trotter, I. L., Jr., 1961, Floods in Mississippi, magnitude and frequency: Mississippi State Highway Dept., Traffic and Planning Div., 326 p.

CORRELATION AND ANALYSIS OF WATER-TEMPERATURE DATA FOR OREGON STREAMS

By ALBERT M. MOORE, Portland, Oreg.

Work done in cooperation with the Oregon State Water Resources Board, U.S. Public Health Service, U.S. Bureau of Reclamation, U.S. Soil Conservation Service, and Corps of Engineers, Department of the Army

Abstract.—For most Oregon streams, spot observations of water temperature can be correlated with continuous thermograph records of water temperature in another stream to obtain reasonably accurate figures of monthly maximum, minimum, and mean water temperature at the spot-observation site. Many of these correlations vary seasonally, and some of the variations apparently are caused by differences in the orientation of the stream courses. The correlations can be a useful tool in assessing the effect of reservoir operations on downstream water temperature.

In a study of the temperature of water in Oregon streams, spot observations of water temperature were correlated with continuous thermograph records. The spot observations, obtained as part of the regular stream-gaging program, have been made at more than 200 sites during periods ranging from 4 to 16 years, and at the rate of one measurement every 5 or 6 weeks at each site. The thermograph records used in the correlations are 8 to 12 years in length and may be on another stream or on the same stream as the spot-observation records.

INTERSTREAM TEMPERATURE CORRELATIONS

The correlations are developed by plotting observed temperatures at a spot-observation site against the temperature recorded for the same date and hour at a site where a continuous thermograph recorder is operated. This procedure allows for the diurnal fluctuations of stream temperatures. This type of correlation results in a curve or curves of relation between water temperature at the two sites. These curves are utilized to estimate for the spot-observation site monthly water temperatures corresponding to the known monthly water temperatures for the thermograph site.

Another type of correlation developed for this study relates monthly records of water temperature for the thermograph site to those for another thermograph site; the resulting curve or curves are used to fill gaps in the record at one or both sites.

The standard error for both types of correlation generally ranged from 1° to 2°F. These correlations, although in themselves accomplishing significant purposes, are described largely to provide background material for findings that resulted from their use.

EFFECT OF STREAM ORIENTATION ON WATER TEMPERATURE

The second type of correlation, that of water temperature of two thermograph sites, when used to fill a gap in the short thermograph record for Five Rivers near Fisher, drew attention to the fact that orientation of the stream can affect water temperatures. Correlation was made with the equally short record for Fall Creek near Alsea, and the curve of relation was found to change seasonally, as shown by figure 1. During the winter the two streams are at about the same temperature, but in the summer Five Rivers is substantially warmer than Fall Creek. The two streams drain areas that are culturally and geologically similar, and neither has significantly large spring-flow contributions. When possible reasons for this divergence were sought, it was found that Fall Creek has heavily wooded banks and runs nearly north-south, while Five Rivers flows generally east to west and is not so heavily wooded along the banks. Furthermore, even in those reaches of Five Rivers where the general direction is north-south, there are wide sweeping curves that result in most of the stream having an

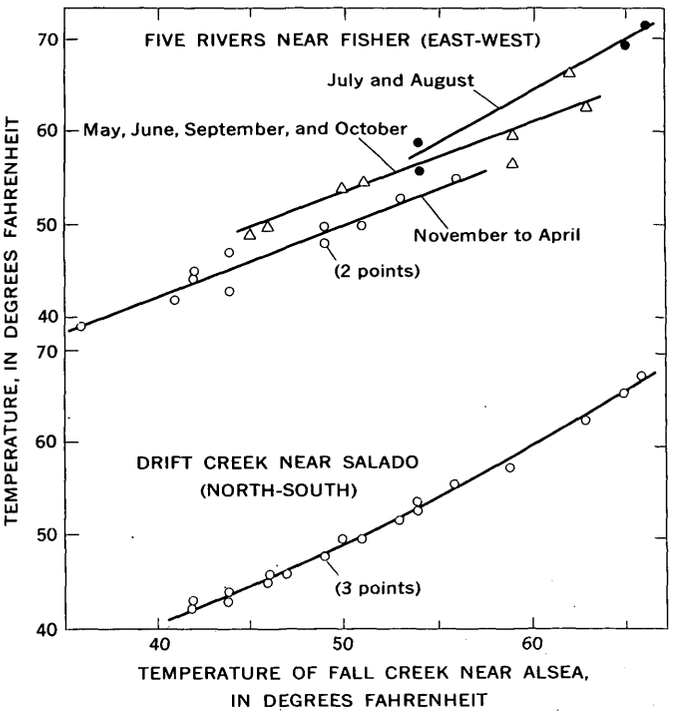

FIGURE 1.—Correlation of monthly extremes of water temperature of Fall Creek near Alsea (a north-south stream) with corresponding water temperatures of Drift Creek near Salado (north-south) and Five Rivers near Fisher (east-west).

east-west orientation. As a further check on the effect of shading provided by north-south orientation, another north-south stream (Drift Creek near Salado) was selected for correlation with Fall Creek near Alsea. Excellent correlation, with no seasonal variation, was found for these two north-south streams (fig. 1).

Another example of the effect of stream orientation was observed during the summer of 1963 when the U.S. Geological Survey obtained water-temperature records on both North and South Forks of the Trask River. At the time the records were begun, a local resident pointed out that North Fork was preferred over South Fork as a "swimming hole" because it was warmer. The first records in July showed that North Fork was indeed 4° to 8°F warmer than South Fork. The latter was tested with a hand thermometer for several miles upstream to see if there was evidence of any cool spring-flow contributions, and none was found. Evidently the difference was due to the north-south orientation of South Fork and the east-west orientation of North Fork. This conclusion was further supported when cloudy days resulted in closer agreement between the temperatures of the two streams. In fact, when cloudy weather continued for 2 or 3 consecutive days, the temperatures of the two streams became practically identical. Furthermore, a comparison of monthly mean temperatures for the two streams showed that North Fork was 4° to 5°F warmer than South Fork during the sunny months of July and August, but that this difference decreased to 3° and 2°F, respectively, for September and October, when more cloudy weather prevailed.

Other examples of the effect of stream orientation were found when the temperature of Oregon streams was compared with air temperature for the summer months. Mangan (1946 p. 9, 10) in discussing water temperature in Pennsylvania streams states, ". . . the mean monthly temperature of the water from May through November, will slightly exceed the monthly air temperature of the region."

This general statement does not hold for Oregon streams, however. Generally, those streams that are much exposed to direct sunlight do tend to have monthly mean temperatures that exceed monthly mean air temperature during the summer months. Streams with large spring-flow contributions have monthly mean temperature lower than monthly mean air temperature in the summer, as have those streams with a north-south orientation and steep canyon walls or wooded banks such that exposure to direct sunlight is minimized. Figures 2 and 3 compare monthly water temperatures for selected years at nine thermograph sites with corresponding air temperature at nearby U.S. Weather Bureau stations. The same year could not be used for all nine thermograph records shown on figures 2 and 3 because there was no single year when all were in operation. At four sites (fig. 2) the monthly mean water temperature during the summer is higher than the monthly mean air temperature; each of these four streams has a general east-west orientation upstream from the thermograph station. The other five sites (fig. 3) have summer temperatures that are lower than air temperature. Breitenbush River near Detroit, although having an east-west orientation, is colder than air temperature during the spring and summer because of large spring-flow contributions. A similar relation between water and air is found for North Umpqua River at Winchester, not only because of large amounts of spring flow but also because of snowmelt contributions extending into the summer months. South Fork John Day River near Dayville, Clatskanie River near Clatskanie, and Grande Ronde River at La Grande do not have large amounts of spring flow but are colder than air temperature during the summer, largely because of shading provided by north-south orientation and wooded banks.

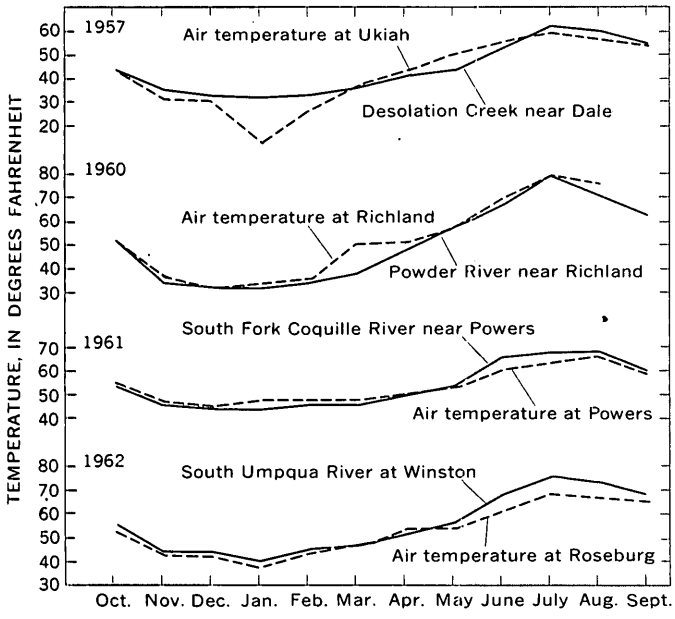

FIGURE 2.—Comparison of air temperature with monthly mean water temperature of east-west streams.

EFFECT OF RESERVOIRS ON DOWNSTREAM WATER TEMPERATURES

Correlation of spot observations of water temperature with a thermograph record provides a useful tool for assessing the effect of a reservoir on downstream water temperatures . A good example of the use of such a correlation is the study made of the effect of the Detroit Reservoir. This reservoir, on the North Santiam River, is used for flood control, power generation, and recreation; it was first used for storage in 1953. Its maximum depth is 290 feet, and its operating range is 144 feet. Water from well below the surface is released during summer, but in the autumn, when the reservoir is drawn down for flood control, warmer water from nearer the surface is released. From July to September there is little increase in flow in the reach of the river 50 miles or more below Detroit Dam, because tributary inflow is small and, below Mahama, diversions tend to offset inflow.

Inflow and outflow thermograph records are available for the reservoir, but farther downstream, at Mehama (North Santiam River) and at Jefferson (Santiam River), only spot-observation records are available for 1947 to 1962. These sites are, respectively, about 22 and 51 miles below Detroit Dam (fig. 4). The correlation procedures followed for Mehama were also used for Jefferson, but only those for Mehama are discussed here. The thermograph record for Breitenbush River, one of the streams flowing into Detroit Reservoir, extends from 1951 to 1962. Separate correlations with the Breitenbush thermo-

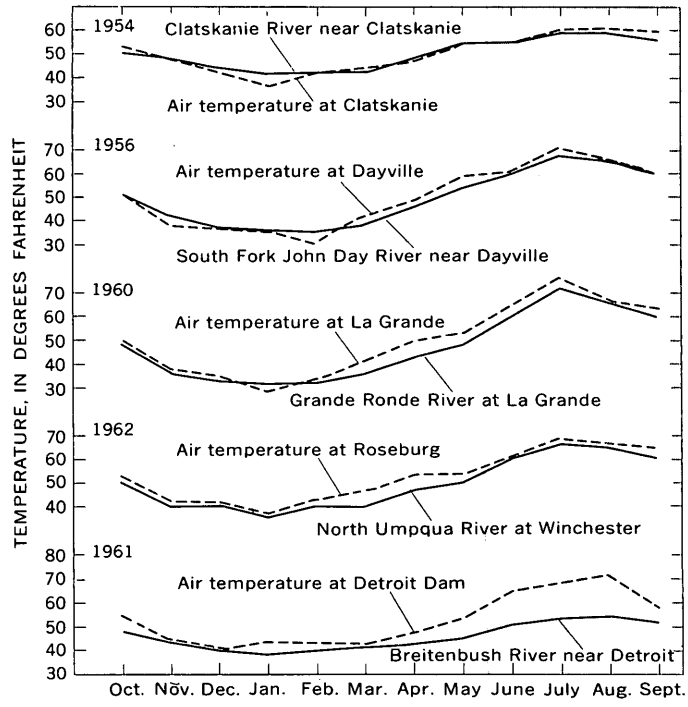

FIGURE 3.—Comparison of air temperature with monthly mean water temperature in spring-fed or in north-south streams.

graph record were made for spot observations of water temperature at Mehama prior to and subsequent to the filling of Detroit Reservoir. That is, the 1951–52 spot observations at Mehama were correlated with the 1951–52 thermograph record for Breitenbush River. By entering this correlation with known period-of-record (1951–62) mean monthly temperatures for Breitenbush River, the corresponding mean monthly water temperatures at Mehama for the same period (1951–62) were estimated. These are the mean monthly temperatures that would have occurred at Mehama if Detroit Reservoir had not been built. A similar correlation for the period 1953–62, when entered with the same 1951–62 mean monthly temperatures for Breitenbush River, yielded the mean monthly temperatures that would have existed at Mehama for 1951–62 if Detroit Reservoir had been in operation for the entire period.

In other words, the 2-year and the 10-year correlations both resulted in estimates of mean monthly temperature at Mehama for the 12-year period 1951–62, but the first excluded and the second included the effect of Detroit Reservoir. Subtraction of one set of mean monthly temperatures from the other shows the effect of Detroit Reservoir at Mehama. The accompanying table lists only the effect of the reservoir, not the water temperatures themselves.

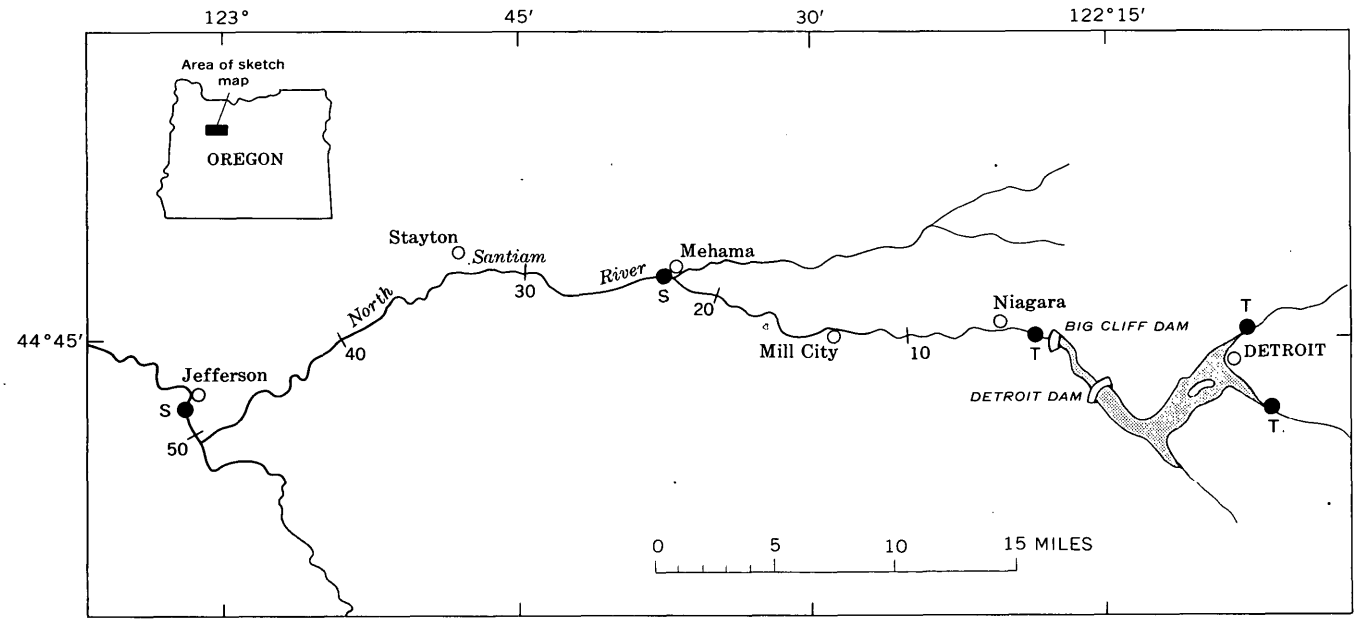

FIGURE 4.—Sketch of North Santiam River, showing location of various thermographs (T) and spot-observation sites (S) used in computing the effect of Detroit Reservoir on downstream water temperatures. Figures indicate river mileage below Detroit Dam.

Effect of Detroit Reservoir on monthly mean water temperature downstream

Site	Drainage area (sq mi)	Distance below Detroit Dam (miles)	Change in monthly mean water temperature, in degrees Fahrenheit, caused by operation of Detroit Reservoir											
			Oct.	Nov.	Dec.	Jan.	Feb.	Mar.	Apr.	May	June	July	Aug.	Sept.
Niagara	453	3. 6	+4	+5	+3	+1	0	−1	−1	−1	−4	−8	−7	−4
Mehama	665	22. 2	−1	+1	+2	+1	+1	+1	0	−1	−4	−6	−8	−7
Jefferson	1,790	51. 3	−3	−3	−1	0	0	−1	0	0	−1	−2	−3	−5

Release of reservoir water of relatively constant temperature should result in poor correlation between spot observations of water temperature immediately below the reservoir and a thermograph record on an unregulated stream. However, if the spot observations are made at a site several miles below the reservoir, good correlation with a thermograph record is usually found because in those few miles the water is subjected to the same natural conditions of solar radiation, air temperature, and so forth, that are affecting water temperature at the thermograph site. The correlations between the thermograph record for Breitenbush River and spot obsrvations both at Mehama and at Jefferson are reasonably good.

The following conclusions can be drawn from the data shown in the accompanying table:

1. Maintaining a nearly full reservoir during the summer and drawing the reservoir down in the autumn results in cooler than natural water temperatures at Niagara during the summer, and warmer than natural in the fall.
2. The cooling during the summer continues undiminished at Mehama, more than 20 miles downstream, and to a lesser extent at Jefferson, more than 50 miles downstream.
3. The cooling effect of the reservoir extends later into the summer and fall at the downstream sites.

The effect noted in item 3 above is believed to be accounted for by the changed water-temperature gradient between Niagara and the downstream sites, resulting from reservoir regulation that not only has lowered the water temperature but has changed the flow pattern. For example, the natural temperature difference between Niagara and Mehama for July is +5°F (56° to 61°F), but with Detroit Reservoir in operation the difference is +7°F (48° to 55°F). The regulated July flow is about the same as the natural flow, but, with water temperature at Niagara 8°F

cooler than under natural conditions, evaporation is reduced and the heat that would have been required for evaporation is available for warming the water. This same effect is present in August and September, also, but is more than offset by the fact that regulated flows are well in excess of natural flows. With more water to be warmed, the natural gradients between Niagara and Mehama of +5°F and +4°F for August and September are cut to +4°F and +1°F, respectively.

REFERENCE

Mangan, J. W., 1946, Temperatures of natural waters in Pennsylvania: Pennsylvania Dept. of Forests and Waters.

ELIMINATION OF THERMAL STRATIFICATION BY AN AIR-BUBBLING TECHNIQUE IN LAKE WOHLFORD, CALIFORNIA

By GORDON E. KOBERG, Denver, Colo.

Work done in cooperation with the Escondido Mutual Water Co.

Abstract.—Use of an experimental air-bubbling system at Lake Wohlford, Calif., resulted in the elimination of thermal stratification, definite improvement in taste and odor of the water, and a net reduction in evaporation of 35 acre-feet (5 percent) in 1962.

A study was made in 1962, in collaboration with the Escondido Mutual Water Co., of the effect of an air-bubbling system on the artificial mixing of thermally stratified water in Lake Wohlford, Calif. The air-bubbling system caused a marked improvement in the quality of water and a reduction in seasonal evaporation rates.

Lake Wohlford is a canyon-type reservoir formed by an earth-fill dam on Escondido Creek, 7 miles northeast of Escondido, Calif., and about 30 miles north of San Diego. The lake has a capacity of 7,000 acre-feet at full pool with a corresponding surface area of 222 acres. During the period of study the contents of the reservoir averaged 2,500 acre-feet with a surface area of 130 acres. The climate at Lake Wohlford is such that the temperature of the water always exceeds 4°C, the temperature of maximum density of water. The lake is used for storage of water for irrigation and domestic supply and as a recreational facility.

The seasonal changes in climate at Lake Wohlford are accompanied by a change in the distribution of temperature in the lake. During the spring and summer, the distribution of temperature is such that the hypolimnion or lower stratum of water is heated at a much slower rate than the epilimnion or upper stratum. Consequently, the hypolimnion is almost stagnant because cold water, being denser, remains on the bottom. During the period of stagnation, the processes tending to produce a uniform distribution of dissolved substances are very slow, and certain undesirable substances such as hydrogen sulfide increase in concentration until they reach an undesirable level, while other substances such as oxygen are depleted.

Changes in the distribution of lake temperature have an effect on the life cycle of the various organisms in the water, such as plankton and algae. These organisms tend to proliferate at certain levels in the lake, depending on the temperature peculiar to each genus, and then to die and fall to the bottom. As the organic matter accumulates on the bottom, the decaying process increases the demand for oxygen in the hypolimnion until oxygen is almost or completely depleted.

In the summer of 1959, most varieties of fish in Lake Wohlford died, probably because of the lack of dissolved oxygen in the water. In the summer of 1960, measurements indicated that the concentration of dissolved oxygen in the hypolimnion was reduced to 1 part per million, and in the epilimnion, to 6 ppm. During these two periods, the water delivered to the city of Escondido had an unpleasant taste and odor.

Because of the problems of water quality, experiments were undertaken in 1961 to determine the feasibility of bubbling air from the bottom of the reservoir to mix the lower and upper strata of water. The results of these experiments indicated a definite improvement in the dissolved-oxygen concentration, and a permanent air-bubbling system was installed.

U.S. GEOL. SURVEY PROF. PAPER 501-D, PAGES D190-D192

This system consists of a 210-cubic-foot-per-minute (free air) compressor powered by a 50-horsepower electric motor. Air is conducted from the compressor through a 2-inch galvanized pipe which extends into the lake a sufficient distance to cool the air. Attached to the end of the pipe is 1½-inch polyvinyl-chloride plastic tubing that conducts the air to the area where it is forced into the bottom water, approximately 40 feet below the surface. The last 60 feet of the plastic tubing is perforated with 90 holes, $\frac{9}{64}$ inches in diameter, spirally located to equalize the thrust of the escaping air.

The permanent-air-bubbling system was placed in operation on April 18, 1962. At first the system was operated only during approximately 9 daylight hours each day. The operational plan was based on the hypothesis that as the bottom water was brought to the surface by the bubbles, it would be heated by solar radiation and then remain at the surface. Experimental tests late in the summer of 1962 indicated that the water did not remain at the surface but sank almost immediately and that the rate of maximum mixing of the water in the lake was not achieved until after approximately 24 hours of continuous operation. Therefore, the plan of operation was changed so that the system is operated continuously until the lake is thoroughly mixed or isothermal. The time required for complete mixing ranges from 24 to 48 hours. Approximately 3 days after the air-bubbling operation, thermal stratification begins to form in the lake and the cycle is repeated.

In 1962, the air-bubbling system was operated intermittently from April 18 to September 5. During this period, the concentration of dissolved oxygen was maintained above 5 ppm throughout the lake with the exception of a 1-week period in August when it dropped to 4 ppm. The dissolved-oxygen concentration of 5 ppm is considered the safe limit for trout production. During the remainder of the year, the natural mixing motion of the wind maintained the concentration of oxygen above 5 ppm.

Water delivered to the city of Escondido for domestic purposes in 1960 required a maximum dosage rate of chlorine of 12 ppm. During 1962, while the bubbler system was in operation, the maximum dosage rate was reduced to 7 ppm. The decrease in dosage rate is attributed to the removal of hydrogen sulfide in the hypolimnion by the air-bubbling system. The removal of the hydrogen sulfide would result in a lower chlorine requirement to meet health standards because less chlorine would be needed to oxidize H_2S, and free available residual chlorine would be obtained at a lower dosage rate (Laubush, 1958). The reduction in the rate of chlorine dosage for 1962 resulted in monetary saving that was enough to pay for the power required for the operation of the compressor.

The improvement in taste and odor of the water delivered to the city of Escondido during 1962 is difficult to evaluate quantitatively. However, the citizens of Escondido must have noted a definite change in taste and odor of the water, because in 1963, complaints were received by the water company only when thermal stratification began to develop in the lake and the dissolved oxygen concentration in the hypolimnion was reduced.

During the spring and summer of 1962, the mixing of the cold water in the hypolimnion with the warm water in the epilimnion reduced the temperature of the water surface, which in turn reduced the evaporation rate. Measurements of evaporation were made by the energy-budget and mass-transfer methods (Harbeck and others, 1958).

Before changes in the evaporation rates could be determined, a comparison of the temperatures of the water surface was made between the monthly means determined for the period 1959–61 and the monthly means for 1962. The comparison indicated that the air-bubbling system reduced the temperature of the water surface 0.5°C, 2.2°C, and 1.3°C in May, June, and July, respectively, and increased the temperature 0.9°C, 1.4°C, and 0.3°C in October, November, and December, respectively. During the period when the temperature of the water surface was lower in 1962, more energy than normal was stored in the lake by the decrease in the evaporation rate and by net gains in radiation and conduction because of the lower temperatures of the water surface. In August and September, the temperature of the water surface was nearly normal, and during the fall was higher than normal because of the time required to dissipate the additional energy by increasing evaporation, radiation, and conduction.

The changes in the evaporation rates attributed to the air-bubbling system were computed by the mass-transfer method. A comparison of the monthly evaporation rates between 1962 and the period 1959–61 for the months of May, June, and July indicated that evaporation was reduced a total of 3.3 inches and for the months of October, November, and December evaporation was increased 1.3 inches. Because of the limited data available, it is difficult to explain why the increase in evaporation during the fall months did not equal the decrease in the summer months.

The regulation of stage for Lake Wohlford is such that the volume of water saved by the changes in evaporation rates is greater than that which would

result from a constant stage throughout the year. During the winter and spring, inflow is stored in the lake and is maintained at the spring level for recreational purposes throughout the summer. In the fall, the stage is lowered in anticipation of winter and spring runoff. With this type of operation of net decrease in evaporation of 35 acre-feet or 5 percent was attributed to the air-bubbling system in 1962.

The mixing of thermally stratified water in lakes and reservoirs by the use of an air-bubbling system has been successfully tried by other investigators such as Reddick (1957) and Heath (1961). Although their systems are different in design, the purpose of each system is the same. The efficiency of each design in mixing the water is unknown, mainly because the cold water brought to the surface immediately sinks to the bottom. Criteria for design of systems for other reservoirs and lakes is not available because the artificial mixing of thermally stratified water is not thoroughly understood.

REFERENCES

Harbeck, G. E., Kohler, M. A., Koberg, G. E., and others, 1958, Water-loss investigations—Lake Mead studies: U.S. Geol. Survey Prof. Paper 298, 100 p.

Heath, W. A., 1961, Compressed air revives polluted Swedish lakes: Water and Sewage Works, v. 108, p. 200.

Laubush, E. J., 1958, Chlorination of water: Water and Sewage Works, v. 105, p. 411.

Reddick, R. M., 1957, Forced circulation of reservoir water yields multiple benefits at Ossining, N.Y.: Water and Sewage Works, v. 104, no. 6, p. 231–237.

FIELD METHODS FOR DETERMINING VERTICAL PERMEABILITY AND AQUIFER ANISOTROPY

By EDWIN P. WEEKS, Madison, Wis.

Work done in cooperation with the University of Wisconsin Geological and Natural History Survey and the Wisconsin Conservation Department

Abstract.—The ratio of horizontal to vertical permeability in stratified sediments can be found by either a finite-difference solution of the differential equation for flow near a pumped well or a type-curve solution of a modified form of the analytical equation for drawdowns near a partially penetrating well. Applied to data from an aquifer test of glacial outwash in central Wisconsin, the type-curve solution provided more reliable values for coefficients of transmissibility (T) and storage (S) than those obtained from the nonequilibrium formula.

A knowledge of vertical permeability and aquifer anisotropy is necessary for solving various problems concerning three-dimensional ground-water flow. For example, vertical permeability must be known if the maximum infiltration rate in a recharge area is to be determined, and the ratio of horizontal to vertical permeability is needed for computation of seepage under dams and for analysis of the drawdown effects of partially penetrating wells.

The permeability across beds of clastic sedimentary rocks generally is much less than the permeability parallel to the bedding planes. For the methods of analysis described in this paper, it is assumed that the beds are horizontal and that the horizontal and vertical permeabilities are measured parallel and normal, respectively, to the bedding planes.

Anistotropic permeability in clastic sediments is due in part to the orientation of the constituent grains. Plate-shaped grains within the sediments tend to be oriented with their flat surfaces approximately parallel to the bedding plane. Such orientation minimizes the vertical cross-sectional area and, by increasing the tortuousity of the vertically interconnected pores, reduces the vertical permeability.

Anisotropic permeability in sediments is due in part also to intercalation of coarser and finer materials. The horizontal movement of water under a given head loss is affected only slightly by the presence of thin beds of fine-grained material of relatively low permeability within sediments of higher permeability, because most of the water is transmitted through the beds of coarser material. On the other hand, vertical movement of water under a given head loss is much less in interlayered coarser and finer materials than in an isotropic aquifer, because the water must pass through each fine-grained bed with a relatively sharp decline in head. Thus the head decline with depth accompanying vertical movement of water in stratified sediments is quite nonuniform. For many problems involving vertical flow of ground water in relatively thick aquifers, the nonuniform head declines may be averaged by considering the aquifer to be a homogeneous bed with low vertical permeability.

This report is one of several resulting from an investigation of the interrelationship of ground water and surface water in the Little Plover River basin, Portage County, Wis. It describes two field methods for determining the rates of horizontal to vertical permeability from data on changes in head due to pumping a nearby well. One method is based on a finite-difference technique, the other on a type-curve solution. Both methods may be used with data on water-level drawdown in piezometers (observation wells open only at the bottom) near partially penetrating wells that tap either artesian or water-table aquifers. Only the finite-difference method may be used with drawdown data from piezometers near a

U.S. GEOL. SURVEY PROF. PAPER 501-D, PAGES D193–D198

fully penetrating well in a water-table aquifer. For both methods, the data used must be obtained from a relatively large sample of the aquifer. The values for the permeability ratio computed by either of these methods include factors for anisotropy due both to grain orientation and to intercalation of fine- and coarse-grained materials within the aquifer.

THE FINITE-DIFFERENCE METHOD

The finite-difference method of determining aquifer anisotropy was suggested to the author by R. W. Stallman of the U.S. Geological Survey. This method is based on a finite-difference solution of the modified basic differential equation for radial flow with vertical flow components (Stallman, 1963, p. 208):

$$P_r\left[\frac{\partial^2 s}{\partial r^2}+\frac{1}{r}\frac{\partial s}{\partial r}\right]+P_z\frac{\partial^2 s}{\partial z^2}=0 \qquad (1)$$

where

P_r=horizontal permeability radially from the pumped well,
P_z=vertical permeability,
s=drawdown, or change in head due to pumping,
r=radial distance from pumped well to point at which s is observed,
z=vertical distance from base of aquifer to point at which s is observed,

Letting $\xi=\log r$, equation 1 may be written in finite-difference form for any point (p, n) corresponding to (ξ, z) (Stallman, 1963, p. 210) as:

$$s_{n-1}-2s_n+s_{n+1}+\frac{P_z}{P_r}\left(\frac{r_n\Delta\xi}{\Delta z}\right)^2(s_{p-1}-2s_p+s_{p+1})\approx 0, \qquad (2)$$

where

$$\Delta\xi=\log\frac{r_{n+1}}{r_n}=\log\frac{r_n}{r_{n-1}}, \text{ and} \qquad (3)$$

Δz=vertical spacing of piezometers.

As these equations were derived for artesian flow, they are not strictly applicable to flow in unconfined aquifers. However, for water-table aquifers in which the drawdowns due to pumping are small in comparison to the initial saturated thickness of the aquifer, the equations should yield results that are approximately correct.

Data for solving equation 2 were obtained by installing an array of piezometers in a vertical plane through the pumped well (Pt–279 or Pt–340) (fig. 1). Two piezometer arrays were installed for this study, one near well Pt–279, with r_n at this site equal to 150 feet, and the other near well Pt–340, with r_n equal to 80 feet. Drawdowns in the piezometers were measured periodically while the well was being pumped, and graphs of s versus time were plotted. From the data plots, values for s_{p-1}, s_p, s_{p+1}, s_{n-1}, s_n, and s_{n+1} were determined for a given time, and the resulting values were used in equation 2 to determine the P_r/P_z ratio.

The computed ratio of horizontal to vertical permeability at well Pt–279 was about 20:1 and at well Pt–340 was about 25:1. However, if the accuracy of head measurement is assumed to have been ± 0.005 foot, the ratio could range from 10:1 to 40:1 at well Pt–279 and from 13:1 to 50:1 at well Pt–340. Furthermore, an error in the measured value of $s_{n,p}$ of ± 0.01 foot would cause the ratio to range from 5:1 to ∞:1 at well Pt–279 and from 7:1 to ∞:1 at well Pt–340. These figures indicate that a high degree of accuracy is required of the data and, hence, that the finite-difference method is of limited usefulness in determining anisotropic permeability. Furthermore, minor variations in the piezometric head due to local nonhomogeneities of the aquifer would make the computed ratios meaningless. The method might prove much more precise if r_n were smaller, for if the piezometer array is located near the pumped well, vertical flow components are more pronounced and the head summation is more accurate than if the piezometer array is located far from the pumped well. Also, the method might be more applicable to data from other aquifers.

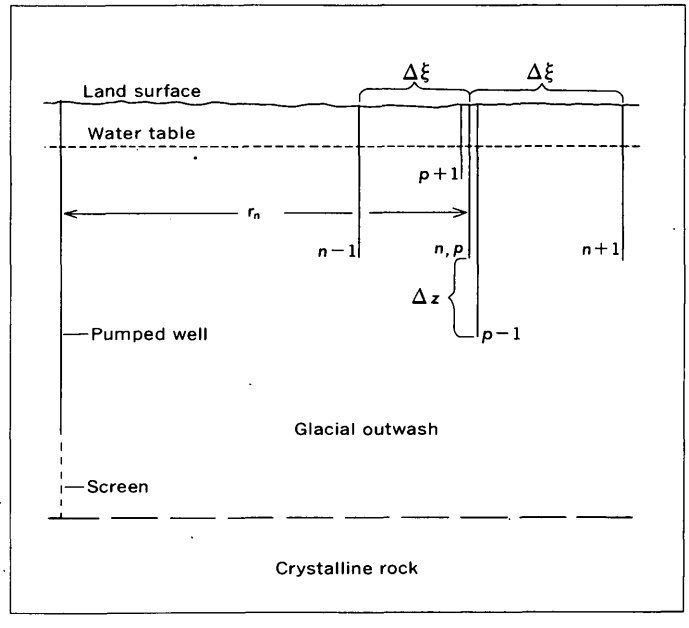

FIGURE 1.—Sketch showing the array of piezometers used to determine the ratio of horizontal to vertical permeability by the finite-difference method. Sketch is orthogonal, and the $\Delta\xi$'s, which are logarithmic functions of r (see text), consequently are unequal.

TYPE-CURVE METHOD

The type-curve method of determining aquifer anisotropy is based on a modification of an analytical equation derived by Hantush (1961a, p. 90, eq. 8a) for the drawdown distribution indicated by piezometers located near a partially penetrating well that discharges at a constant rate. The equation derived for isotropic aquifers is:

$$s=\frac{114.6Q}{T}\left[W(u)+f_s\left(\frac{r}{m},\frac{l}{m},\frac{d}{m},\frac{z}{m}\right)\right], \quad (4)$$

where

s=drawdown, in feet;
Q=discharge, in gallons per minute;
T=coefficient of transmissibility, in gallons per day per foot;
$u=\frac{1.87r^2S}{Tt}$,

in which

r=distance, in feet, from pumped well to piezometer;
S=coefficient of storage; and
t=time, in days, since pumping began;

$W(u)$=exponential integral (Ferris and others, 1962, p. 96–97);

and

$$f_s\left(\frac{r}{m},\frac{l}{m},\frac{d}{m},\frac{z}{m}\right)=\frac{4m}{\pi(l-d)}\sum_{n=1}^{\infty}\frac{1}{n}K_0\left(\frac{n\pi r}{m}\right)\left(\sin\frac{n\pi l}{m}-\sin\frac{n\pi d}{m}\right)\cos\frac{n\pi z}{m}, \quad (5)$$

in which

m=aquifer thickness, in feet;
l=depth from top of aquifer (or water table) to bottom of screen in pumped well;
d=depth from top of aquifer (or water table) to top of screen in pumped well;
z=depth from top of aquifer (or water table) to bottom of piezometer;
K_0=modified Bessel function of the second kind and zero order (Ferris and others, 1962, p. 115).

Equation 4 may be modified to account for anisotropic permeability conditions by multiplying the term r/m by $(P_z/P_r)^{1/2}$. A similar modification was used by Muskat (1937, p. 279) to determine the steady-state drawdown in a partially penetrating well tapping an anisotropic aquifer. Equation 4 thus modified becomes:

$$s=\left\{\frac{114.6Q}{T}W(u)+\frac{4m}{\pi(l-d)}\sum_{n=1}^{\infty}\frac{1}{n}K_0\left[\left(\frac{n\pi r}{m}\right)\left(\frac{P_z}{P_r}\right)^{1/2}\right]\left(\sin\frac{n\pi l}{m}-\frac{n\pi d}{m}\right)\cos\frac{n\pi z}{m}\right\}. \quad (6)$$

Equation 6 is valid for isotropic artesian aquifers if $t>\frac{mS}{2P}$ (Hantush, 1961a, p. 90), where P is the permeability of the aquifer. For anisotropic artesian aquifers, t would be limited by the vertical permeability and the equation would be valid when $t>\frac{mS}{2P_z}$. Although equation 6 was derived specifically for artesian flow, it is applicable to the response of water-table aquifers after vertical flow components resulting from changes in the position of the water table become negligible, that is, when $t>5\frac{mS}{P_z}$ (Boulton, 1954, p. 565).

The type-curve solution is a convenient method for using equation 6 to analyze aquifer-test data. If assumed values of P_z/P_r are used, values of

$$\frac{4m}{\pi(l-d)}\sum_{n=1}^{\infty}\frac{1}{n}K_0\left[\left(\frac{n\pi r}{m}\right)\left(\frac{P_z}{P_r}\right)^{1/2}\right]\left(\sin\frac{n\pi l}{m}-\sin\frac{n\pi d}{m}\right)\cos\frac{n\pi z}{m}$$

may be computed for each observation well from the appropriate values of m, r, l, d, and z. Values of

$$K_0\left[\left(\frac{n\pi r}{m}\right)\left(\frac{P_z}{P_r}\right)^{1/2}\right]$$

may be obtained by computing

$$\left(\frac{n\pi r}{m}\right)\left(\frac{P_z}{P_r}\right)^{1/2}$$

and looking up the corresponding $K_0(x)$ value from a table of the modified Bessel function of the second kind and zero order (Ferris and others, 1962, p. 115). Values of the term

$$\left(\sin\frac{n\pi l}{m}-\sin\frac{n\pi d}{d}\right)\cos\frac{n\pi z}{m}$$

may be computed quickly to 1 percent accuracy. Individual terms of the summation approach zero as n becomes large; for values of

$$\frac{r}{m}\left(\frac{P_z}{P_r}\right)^{1/2}=0.1,$$

the value of the summation may be determined to the necessary degree of accuracy from about 20 terms, and for values of

$$\frac{r}{m}\left(\frac{P_z}{P_r}\right)^{1/2}=5$$

or greater, the value may be computed from 3 or 4 terms.

In order to use the type-curve solution, the computed values of

$$f_s\left[\frac{r}{m}\left(\frac{P_z}{P_r}\right)^{1/2},\frac{l}{m},\frac{d}{m},\frac{z}{m}\right]$$

should be added to the various values of $W(u)$, and plots of u versus

$$W(u)+f_s\left[\frac{r}{m}\left(\frac{P_z}{P_r}\right)^{1/2},\frac{l}{m},\frac{d}{m},\frac{z}{m}\right]$$

for each piezometer should be prepared on logarithmic paper. The type curves computed for each piezometer for a given value of P_z/P_r should be plotted on the same graph to form a family of curves. Several families of type curves should be prepared, one for each of several assumed values of P_z/P_r.

Type curves prepared by this method were used to analyze data obtained from an aquifer test on well Pt–279 tapping glacial outwash in the Little Plover River basin, Portage County, Wis. The well was pumped at a rate of 1,060 gallons per minute for 74 hours, and measurements were made of the drawdown in 21 piezometers installed along 4 lines radiating from the pumped well (fig. 2). Each piezometer consisted of a 1¼-inch ID pipe fitted with an 18-inch well point.

The drawdown data obtained during the test were prepared for analysis by plotting, on logarithmic paper, values of s versus r^2/t for each piezometer. As the data for all the piezometers along one line were plotted as a single graph, four families of curves resulted. Each family of data curves was compared to the type-curve families of u versus

$$W(u)+f_s\left[\frac{r}{m}\left(\frac{P_z}{P_r}\right)^{1/2},\frac{l}{m},\frac{d}{m},\frac{z}{m}\right].$$

Then the data-curve family was superimposed on the best fitting type-curve family, and a match point for the two curve families was determined as shown on figure 3. Values for the terms u,

$$W(u)+f_s\left[\frac{r}{m}\left(\frac{P_z}{P_r}\right)^{1/2},\frac{l}{m},\frac{d}{m},\frac{z}{m}\right],$$

s, and r^2/t were determined at the match point and these values, along with the measured discharge from the well, were used to solve for T and S in the equations

$$T=\frac{114.6Q}{s}\left\{W(u)+f_s\left[\frac{r}{m}\left(\frac{P_z}{P_r}\right)^{1/2},\frac{l}{m},\frac{d}{m},\frac{z}{m}\right]\right\}$$

and

$$S=\frac{Tu}{1.87}\left(\frac{t}{r^2}\right).$$

The ratio P_r/P_z was determined from the value for the best fitting type-curve family, and the vertical permeability was computed from the identity

$$P_z=\frac{T}{m}\frac{P_z}{P_r}.$$

The results of the analysis indicated that the ratio P_r/P_z of the sediments in the vicinity of the test well ranges from 15:1 to 25:1 and averages about 20:1. Variations in the permeability ratio are probably due to discontinuous beds of low permeability erratically distributed through the aquifer.

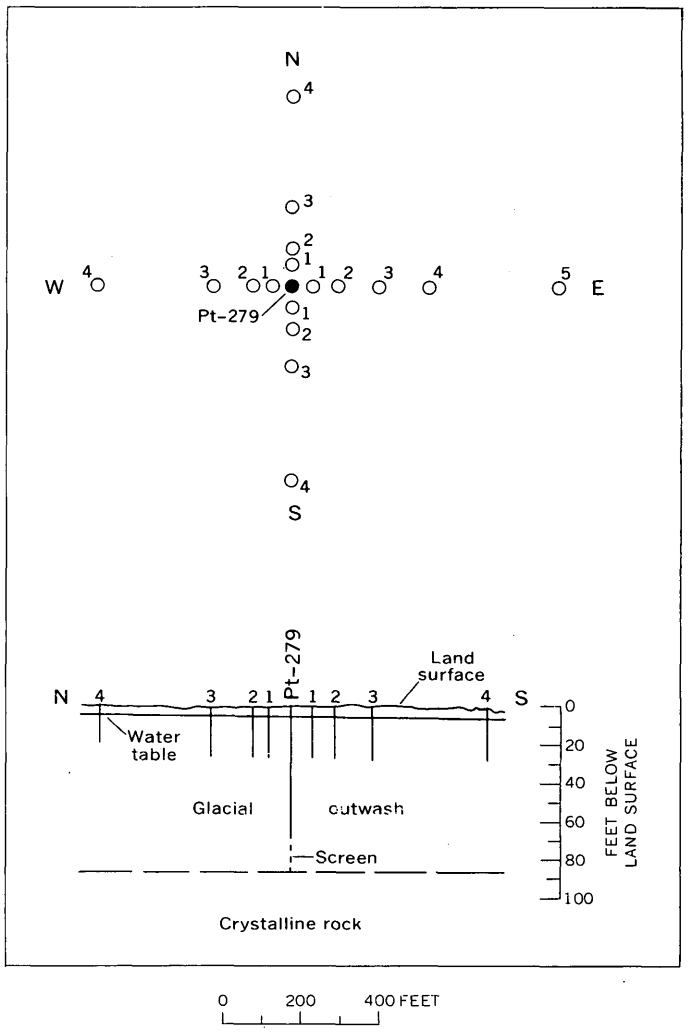

FIGURE 2.—Sketch showing locations of observation wells for aquifer test on well Pt–279.

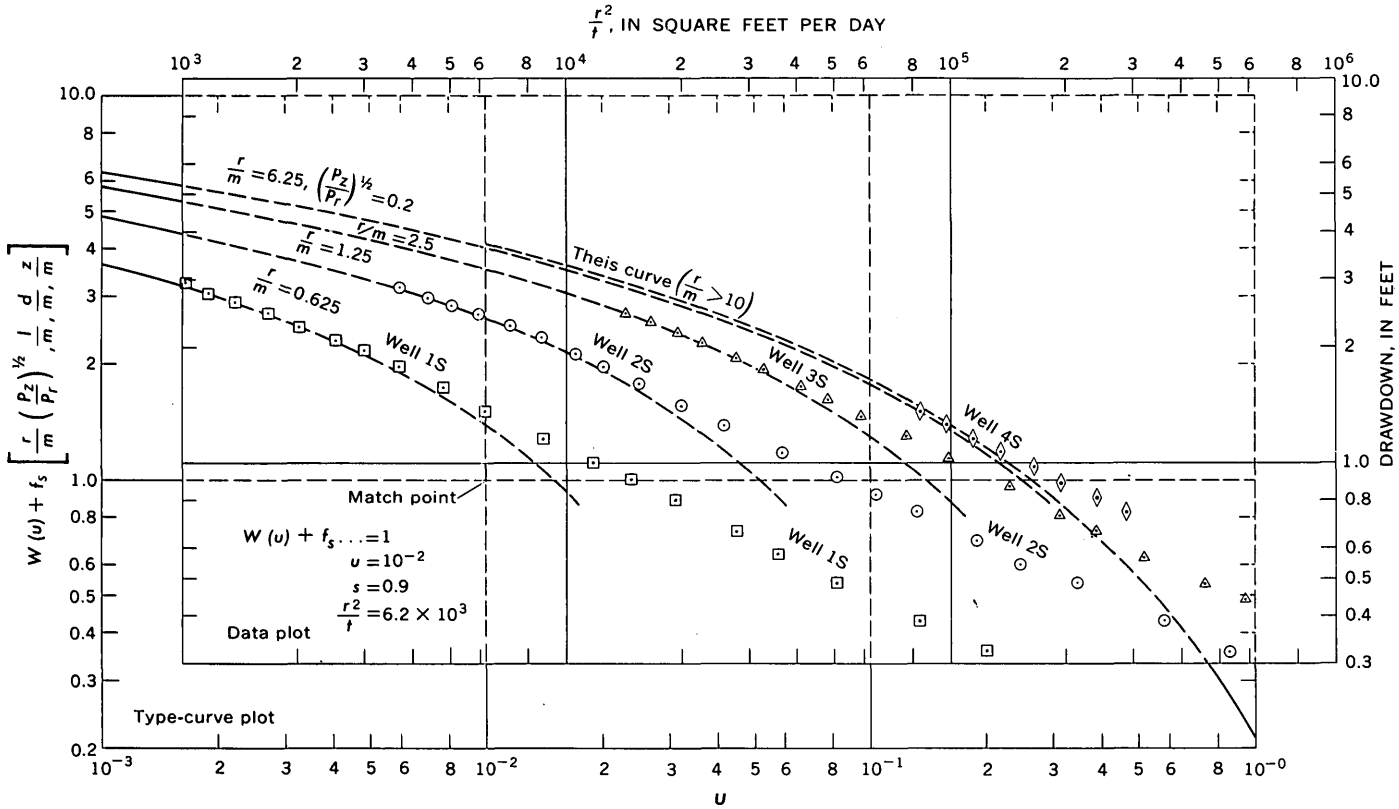

FIGURE 3.—Graph showing the match of data from observation wells 1S, 2S, 3S, and 4S to the type curves computed from equation 6.

The type-curve solution should be useful for determining ratios of horizontal to vertical permeability for many tests on partially penetrating wells. The method could be used with almost any variety of piezometer spacings and penetration depths if at least one of the piezometers is somewhat nearer than

$$r=1.5m\left(\frac{P_r}{P_z}\right)^{1/2}$$

to the pumped well. Vertical flow components due to partial penetration of the pumped well are negligible beyond that distance.

This method also would be useful for obtaining values for the aquifer coefficients T and S from tests on partially penetrating wells. The nonequilibrium equation developed by Theis (1935), which frequently is used to analyze data from partially penetrating wells, is strictly applicable only to fully penetrating wells. A comparison of values obtained by analysis of the data from the test on well Pt–279 by the two methods indicates that values for T check fairly closely. The nonequilibrium formula gave values of T ranging from 125,000 to 130,000 gallons per day per foot for piezometers near the pumped well to 140,000 gpd per foot for the more distant piezometers. These values are consistent with the value of 140,000 gpd per foot determined by the method described above. However, values of S determined by the nonequilibrium formula were completely unreliable, ranging from 0.2 to 2.56, whereas those determined by equation 6 range from 0.12 to 0.16 and are well within the range that might be expected for the glacial outwash.

As the permeability of most stratified sediments is anisotropic, the modification made in this report of the equation for drawdowns near a partially penetrating well also should be more useful than the original equation for analyzing aquifer tests in stratified sediments. In the case of the test on well Pt–279, the use of the original equation developed by Hantush gave values for T and S about equal to those determined by the nonequilibrium formula developed by Theis.

REFERENCES

Boulton, N. S., 1954, The drawdown of the water table under nonsteady conditions near a pumped well in an unconfined formation: London, Inst. Civil Engineers Proc., pt. III, p. 564–579.

Ferris, J. G., Knowles, D. B., Brown, R. H., and Stallman, R. W., 1962, Theory of aquifer tests: U.S. Geol. Survey Water-Supply Paper 1536–E.

Hantush, M. S., 1961a, Drawdowns around a partially penetrating well: Am. Soc. Civil Engineers Proc., v. 87, no. HY4, p. 83–98.

——— 1961b, Aquifer tests on partially penetrating wells: Am. Soc. Civil Engineers Proc., v. 87, no. HY5, p. 171–195.

Muskat, Morris, 1937, The flow of homogeneous fluids through porous media: New York, McGraw-Hill Book Co.

Stallman, R. W., 1963, Electric analog of three-dimensional flow to wells and its application to unconfined aquifers: U.S. Geol. Survey Water-Supply Paper 1536–H.

Theis, C. V., 1935, The relation between the lowering of the piezometric surface and the rate and duration of discharge of a well using ground-water storage: Am. Geophys. Union Trans., 16th Ann. Mtg., pt. 2, p. 519–524.

TWO-VARIABLE LINEAR CORRELATION ANALYSES OF WATER-LEVEL FLUCTUATIONS IN ARTESIAN WELLS IN FLORIDA

By HENRY G. HEALY, Tallahassee, Fla.

Abstract.—The statistical method of linear regression and correlation analysis is applied to the problem of estimating ground-water stages in one or more wells from the stages in another well. The method provides acceptable results in wells as far as 17.2 miles apart and may be used to evaluate individual water-level measurements, to estimate water-level positions during periods of missing record, and to identify wells in which the water-level fluctuations are representative of areal trends.

This paper describes the application and results of the statistical method of linear regression and correlation analysis to the problems of (1) estimating the ground-water stage in one artesian well from the ground-water stage in another artesian well and (2) determining the accuracy of individual estimates. The method is applied to water-level fluctuations in two artesian wells in the Floridan aquifer in Madison County in northern Florida and to 15 artesian wells in the Floridan aquifer in the heavy pumped Jacksonville area, about 100 miles to the east.

The Floridan aquifer, which consists of porous limestone formations having an aggregate thickness of several hundred feet, is the most widely tapped artesian aquifer in the State. The top of this aquifer is at or near the land surface in the central and northwestern part of the Florida peninsula and dips to more than 1,000 feet below the surface in the extreme southern part. In Madison County, where the Floridan aquifer is overlain by 30 to 100 feet of clay and clayey sand that is perforated by many sand-filled sinkholes, the water level in wells fluctuates primarily in response to seasonal and long-term trends in precipitation. In the Jacksonville area, where the aquifer is overlain by 450 to 500 feet of clay, marl, and clayey sand, the water level in wells responds primarily to seasonal changes in withdrawal rates. In both areas, earth tides and changes in barometric pressure cause minor water-level fluctuations.

One of the wells in Madison County, well Madison 18, was equipped with a water-level recording gage, and each time the chart on the gage was changed the water level in the other well, well Madison 17, was measured also. Water-level measurements made on the same date in both wells were used in constructing the hydrographs on figure 1. Shown in the same figure is a plot of the water-level measurement in well Madison 17 against the same-date measurements in well Madison 18; the line of "best fit" through the plot of paired measurements was determined mathematically by the method of least squares. A diagrammatic geologic log of both wells also is shown on figure 1.

The relation between fluctuations of artesian groundwater levels in wells Madison 17 and 18 may be expressed mathematically by the two-variable linear regression[1] equation $Y_c=a+bX$, in which Y_c is the estimated water level in well Madison 17 and X is the measured water level in Madison 18. The constants a and b are determined mathematically by the method of least squares. Although the data were not tested statistically for linearity, it is doubtful that a curvilinear regression line could be fitted that would produce a smaller sum of squares over most of the range of values. There is, however, some indication of increase in slope in the region of 17 to 20 feet on the abscissa, but only 6 points are involved.

The number of paired measurements that fell within one standard error of estimate ($\pm S_{y\cdot x}$) was 87.0 per-

[1] The term "regression" refers to the tendency to revert to a common type or average as originally used by Dalton in studying biological regression. Because correlation analysis is applied to many types of problems, the term "estimating equation" is more appropriate.

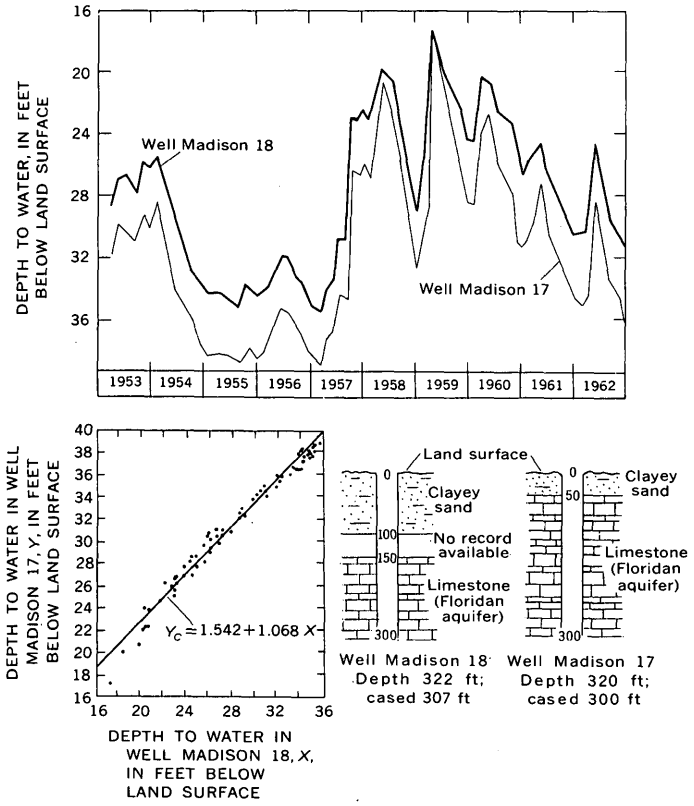

FIGURE 1.—Hydrographs of measured water levels, graph of paired water-level measurements, and diagrammatic logs of wells Madison 17 and 18.

cent of the total number of measurements for the sample size $N=69$.

Two groups of samples of water-level measurements were analyzed. One, sample size $N=69$, consisted of the water-level measurements made during the 9-year period March 1953 through December 1961. This period of record includes the maximum known range of fluctuations, which was 21.58 feet in well Madison 17 and 18.44 feet in well Madison 18. The observed extreme and estimated values of water levels in well Madison 17 indicated that the maximum deviations from the regression occurred during periods of high stage for the group having sample size $N=69$. This difference between observed and estimated water levels during times of high stage may be attributed to differences in the rate of recharge through the sinkholes in the vicinities of these two wells during times of heavy rainfall.

The second group analyzed, sample size $N=10$, included water-level measurements made from October 1960 through December 1961 in the same two wells. The results of the analyses of sample sizes 69 and 10 and the estimating equations for computing water level (Y_c) in well Madison 17 from observed water levels (X) in well Madison 18 are shown in table 1.

TABLE 1.—*Statistical data for wells Madison 17 and 18*

[Standard error of estimate ($S_{y.x}$) and correlation coefficient (r) are adjusted for the universe]

Sample size N	$S_{y.x}$ (feet)	r	Extimating equation for computing water-level records for well Madison 17 [1]
69	0.88	0.986	$Y_c=1.542+1.068X$
10	.21	.994	$Y_c=7.981+0.858X$

[1] Y_c=Computed water level in well Madison 17, in feet.
X=Observed water level in well Madison 18, in feet.

The estimating equations computed from the two sample sizes ($N=69$, $N=10$) were used in constructing estimated hydrographs for well Madison 17 (fig. 2). Although both estimated hydrographs correspond rather closely to the actual hydrograph, the one constructed by use of the equation computed from sample size $N=69$ matches significantly better at times of high stage. It is concluded, therefore, that the validity of an estimating equation increases with greater range of values in the sample from which the equation is computed. This conclusion is supported by the data in table 2.

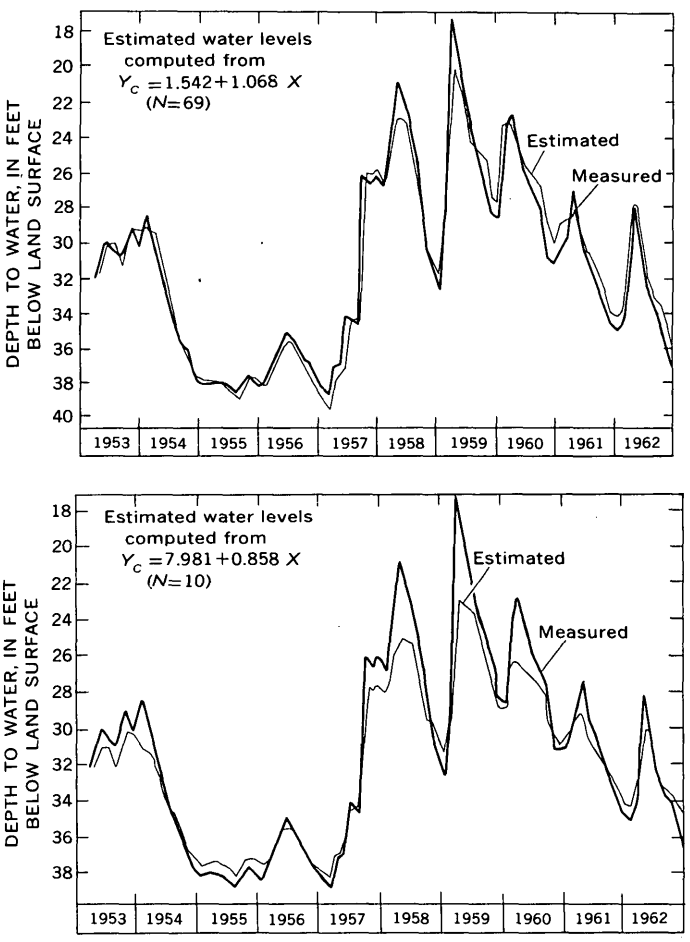

FIGURE 2.—Hydrographs of measured and estimated water levels in well Madison 17.

TABLE 2.—*Comparison of measured and estimated highest, lowest, and average water levels in well Madison 17*

Period of record and sample size	Water level (feet)		
	Highest	Lowest	Average
March 1953 through December 1961:			
Determined by actual measurement (Y)	17. 22	38. 80	30. 94
Estimated by equation computed from sample size $N=69$ (Y_{c69})	19. 95	39. 65	31. 24
Deviation ($Y-Y_{c69}$)	−2. 73	−. 85	−. 30
Estimated by equation computed from sample size $N=10$ (Y_{c10})	22. 76	38. 58	31. 84
Deviation ($Y-Y_{c10}$)	−5. 54	+. 22	−. 90
October 1960 through December 1961:			
Determined by actual measurement (Y)	27. 74	34. 70	31. 05
Estimated by equation computed from sample size $N=10$ (Y_{c10})	28. 26	34. 11	30. 86
Deviation ($Y-Y_{c10}$)	−. 52	+. 59	+. 19

The method of analysis was tested by applying it to 15 artesian wells in the Jacksonville area.

Observation wells were arranged into three groups on the basis of the similarity of their patterns of fluctuations of water levels in individual wells. Water-level measurements for one well (the control well) in each group were paired with the same-date measurements for each of the other wells in the same group. Estimating equations were then computed from paired water-level measurements made over a 5-year period in each pair of wells except control well Duval 122 and well Nassau 51. The estimating equation for well Nassau 51 was determined from 21 years of paired water-level measurements in wells Duval 122 and Nassau 51.

The results of the application of the method are summarized in table 3. The estimated water levels (Y_c), together with the measured water levels (Y) in the same well are listed. The maximum difference

TABLE 3.—*Comparison of measured and estimated water levels on July 11, 1961, in 15 wells in and near Jacksonville, Fla.*

[Standard error of estimate ($Sy.x$) and correlation coefficient (r) are adjusted for the universe]

Well	Distance from control well (miles)	$Sy.x$ (feet)	r	Estimating equation ($Y_r=a+bX$)	Water level (feet above land surface)		$Y-Y_c$ (feet)
					Measured Y	Estimated Y_c	
Control well Duval 115 [Measured water level (X)=20.3 ft.]							
Duval 12	4. 3	1. 50	0. 881	−2.461+1.185X	22. 9	21. 6	+1. 3
Duval 18	3. 8	1. 14	. 931	3.398+1.236X	30. 1	28. 5	+1. 6
Duval 129	. 4	. 76	. 960	4.293+1.100X	26. 6	26. 6	0
Control well Duval 122 [Measured water level (X)=29.3 ft.]							
Duval 123	4. 8	0. 74	0. 907	−14.639+1.215X	21. 9	20. 9	+1. 0
Duval 145	5. 5	. 54	. 874	−13.722+ .780X	8. 8	9. 1	−. 3
Duval 149	2. 9	. 66	. 892	−18.861+1.076X	13. 1	12. 7	+. 4
Duval 154	8. 8	1. 08	. 806	−16.634+1.126X	16. 4	16. 4	0
Nassau 51	17. 2	. 81	. 985	.742+ .929X	28. 2	27. 9	+. 3
Control well Duval 262 [Measured water level (X)=26.8 ft.]							
Duval 118	11. 3	0. 97	0. 854	−12.944+1.167X	19. 2	18. 3	+0. 9
Duval 151	4. 1	. 84	. 867	7.058+1.076X	36. 0	35. 9	+. 1
Duval 152	3. 0	1. 13	. 763	−1.010+ .895X	22. 9	22. 9	0
Duval 164	10. 5	. 83	. 840	4.709+ .961X	30. 5	30. 5	0
Duval 206	16. 3	. 57	−. 848	31.659+ .667X	[1] 14. 4	[1] 13. 8	+. 6
Duval 263	[2] 19. 0	. 25	. 983	.960+ .984X	27. 5	27. 5	0
Duval 264	[2] 39. 0	. 37	. 956	3.363+ .869X	26. 7	26. 7	0

[1] Feet below land surface.
[2] Feet.

$(Y-Y_c)$ between an estimated and corresponding measured water level was 1.6 feet, and the average difference was between 0.4 and 0.5 feet. The distances between the 3 control wells and the wells for which the water level was estimated range from 19 feet to 17.2 miles.

The method of analysis has practical application in evaluating trends and fluctuations of artesian water levels. In addition to the evaluation of control wells in areas where observation wells are numerous, the method of analysis has the following uses:

(1) Recognition of those measurements that may be considered to be inaccurate either because of instrumental or observational error. In general, such errors may be identified by comparison of the deviation between the observed water level (Y) and the computed water level (Y_c) with the standard error of estimate for the particular well.

(2) Estimation, with a known degree of accuracy, of missing record. If an individual measurement or series of measurements are to be estimated, the standard error of estimate for the particular pair of wells would determine the range of the estimated levels.

(3) Identification of changes in the pattern of fluctuations caused by physical factors affecting either, or both, the geologic or hydrologic environment. Factors such as change in pumping rate in a nearby well or in a well which has become plugged would result in a departure from the established relation between observed and estimated water levels.

A PERISCOPE FOR THE STUDY OF BOREHOLE WALLS, AND ITS USE IN GROUND-WATER STUDIES IN NIAGARA COUNTY, NEW YORK

By FRANK W. TRAINER and JAMES E. EDDY,
Washington, D.C.

Abstract.—A periscope made of aluminum tubing with a mirror and light at one end and a telescope at the other was used to study fractures in dolomite in shallow drill holes in western New York. Correlation of fractures observed with the periscope with inflections in temperature profiles in a well where downward flow occurs during periods of no pumping confirmed that the inflections coincide with water-bearing fractures in the rock. The periscope has also been used for examining well casings, well screens, and pump columns, and, in some places, for determining the texture and composition of the wallrock.

Study of the subsurface geology of rocks penetrated by wells has in the past generally been limited to indirect methods, such as geophysical logging and examination of well cuttings. Exceptions to this are the lowering of a geologist down a large-diameter drill hole for firsthand inspection of the zone above the water table, or the observing of wallrock with expensive and generally heavy photographic or television cameras lowered into a drill hole.

This paper describes a lightweight portable periscope assembly that has proved very useful in examining the casing and wallrock in wells up to 42 feet deep and which should be useful in examining crevices and shafts as well. The periscope was tested in conjunction with a field study of movement of ground water through fractures in the Lockport Dolomite in Niagara County, N.Y. Use of the periscope confirmed the presence of open-fracture conduits suggested by temperature logs in uncased wells.

Most of the observations made with the periscope, and all those described in this paper, pertain to fractures in the rock. However, other tests have shown that the periscope is well suited for the examination of well casings, well screens, and pump columns, and, in some places, for the determination of the texture and composition of wallrock. In general, a feature expressed by a difference in color or by sufficient relief to cast a shadow can be seen. For example, filamentous deposits of iron on pump columns, and white spots on the wall which probably represent masses of gypsum in the dolomite, were seen clearly because of their color.

PERISCOPE

The periscope column consists of aluminum tubing, in 5-foot segments with threaded ends, with a maximum outside diameter of 2 inches (fig. 1). At the lower end of the column a threaded clear plastic housing contains a mirror set 45° to the vertical, and two lamp bulbs. At the upper end, a telescope from a surveying alidade is set in a threaded fitting. This optical system is adequate for the purpose of the instrument and is much simpler than one in which a series of lenses is spaced along the length of the column. Two 7½-volt lantern batteries at the land surface provide current for the lamps, to which they are connected by plastic-covered cable fastened along the outside of the column. A clamp which rests on the top of the well casing supports the instrument in the well. Because the lower end of the column is closed, the periscope is rather buoyant and easy to manipulate when submerged.

We have used this periscope as much as 42 feet below the land surface. At that depth the wall of the well was seen clearly, and presumably the optical system is adequate for work to somewhat greater depths. The chief difficulty in the operation of the periscope is in controlling the position of the lower end of the column with respect to the wall of the well, to give a

U.S. GEOL. SURVEY PROF. PAPER 501-D, PAGES D203-D207

742-652 O—64——14

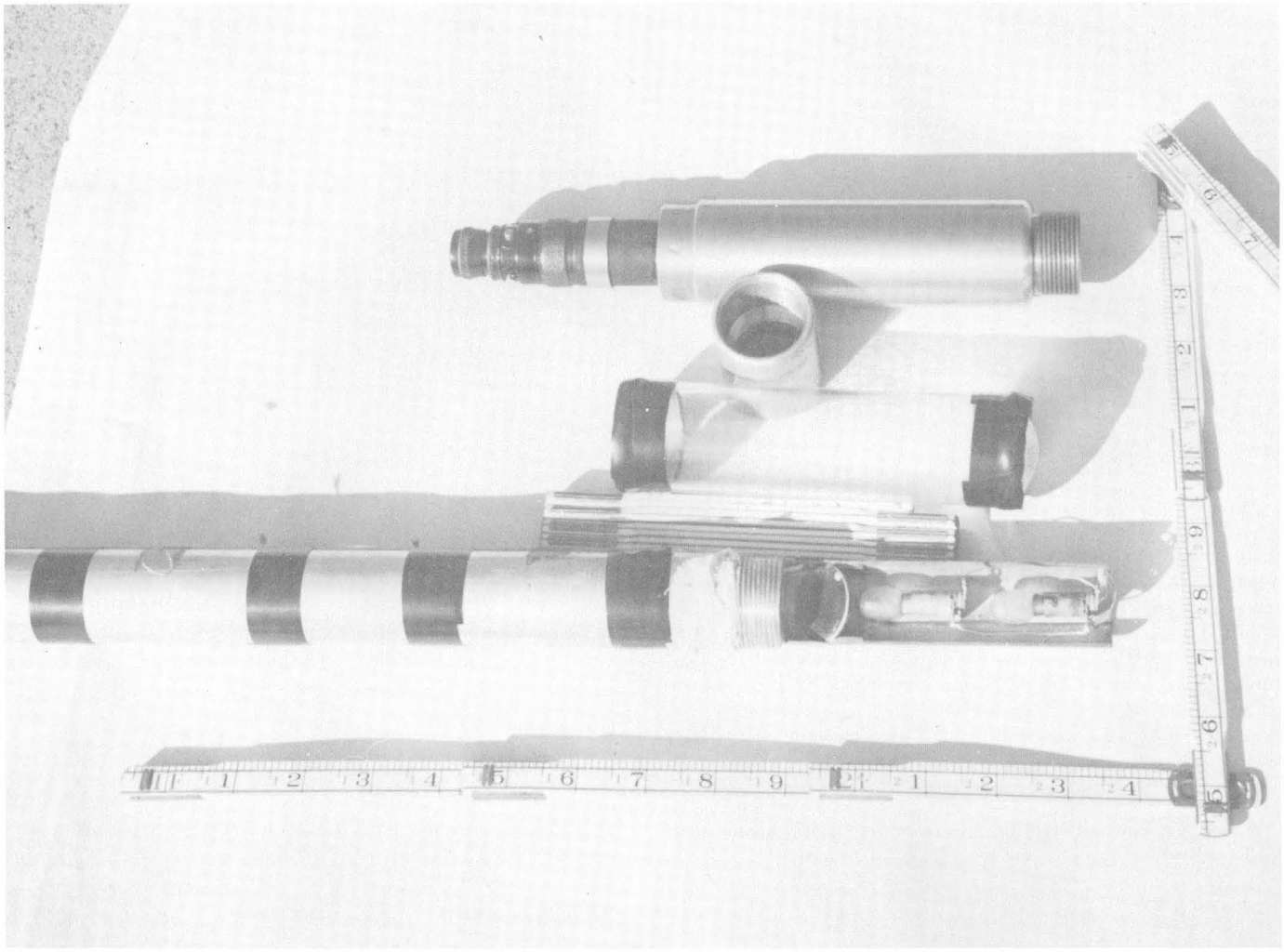

FIGURE 1.—Well periscope. Mirror-lamp unit (bottom), plastic mirror housing (center), and telescope (top). Scale is in tenths of feet.

clear and brightly lighted image. We plan to construct a larger mirror unit, which will permit study of a larger field, and to add a tripod, which should steady the instrument sufficiently to permit taking photographs of the walls of wells.

GROUND WATER IN THE LOCKPORT DOLOMITE NEAR SANBORN, NEW YORK

Occurrence

The Lockport Dolomite at Sanborn, Niagara County, is about 120 feet thick and dips gently (less than 1°) south. The occurrence of ground water is believed to be similar to that in the Niagara Falls area, about 10 miles to the west. There, Johnston (1962, 1964) found that openings in the Lockport Dolomite consist of bedding joints, vertical joints, and irregular cavities left by the solution of gypsum, all of which occur in the upper 10 to 15 feet of the rock. The ground water in them is either confined or unconfined, depending on local conditions. The remainder of the formation contains permeable zones of bedding joints, separated by relatively impermeable rock; each permeable zone acts as a confined aquifer.

During an earlier study of ground-water conditions at Sanborn, water was found running down the walls of several wells, above the static water level but below the casing; in a few wells water spurted from what evidently were fractures in the rock. During the present study, water was seen running into one of the wells studied with the periscope. Part of it was trickling from a single fracture, and part was inferred to come from several closely spaced fractures because the quantity of water flowing down the wall increased with depth over a distance of about 4 feet.

Distribution of fractures

Counts made with the periscope in 5 wells in the Sanborn area suggest that fractures are more abundant in the upper 25 feet of the dolomite than at greater depth. On the average, about 1 fracture per foot in the upper 15 feet was observed, but less than half as many were found between 25 and 35 feet. Most of the fractures were horizontal or nearly so, but a few were vertical or appeared to curve, and therefore to dip at intermediate angles. One fracture about an inch wide was found, but the widths of the other openings could not be estimated accurately; probably most of the fractures were less than an eighth of an inch wide except where a chip of rock had broken out during the drilling. Some openings had rounded edges which may have been produced by solution. The apparent length of the fractures ranged from 1 inch to several inches, as represented by the parts of the fractures wide enough to cast shadows.

Considerable differences in the abundance of these fractures in wells successively farther downdip are thought to reflect local structural differences. Additional data are needed to define better the depth-frequency relations of fractures in the Lockport Dolomite.

Temperature logs as indicators of water-bearing fractures

Temperature profiles of a well in the Sanborn area were measured in the spring and fall, and theoretical profiles were computed for the same days. A log of the fractures in the well was also made, by means of the periscope. (See fig. 2).

The measured profiles reflect undisturbed conditions because the well had not been pumped for periods of 1 month to several months before the temperature surveys. The theoretical profiles for the same days were computed according to a method given by Ingersoll and others (1948, p. 47, equation q), and are based on the assumption that the transfer of heat through the rocks is entirely by conduction. However, where water is moving through the rocks, as it is known to do in the Sanborn area, the water warms or cools a given part of the rock at a rate greater than would occur by conduction alone, and measured profiles deviate from computed profiles.

The form of measured profiles in the Sanborn area departs markedly from that of the theoretical curves, with localization of the departures above certain levels in the wells. On figure 2, for example, note the inflection at 32 to 33 feet in the April profile. Other conspicuous departures are associated with the inflections at 23 to 24 feet in the April profile and 28 to 29 feet in the November profile.

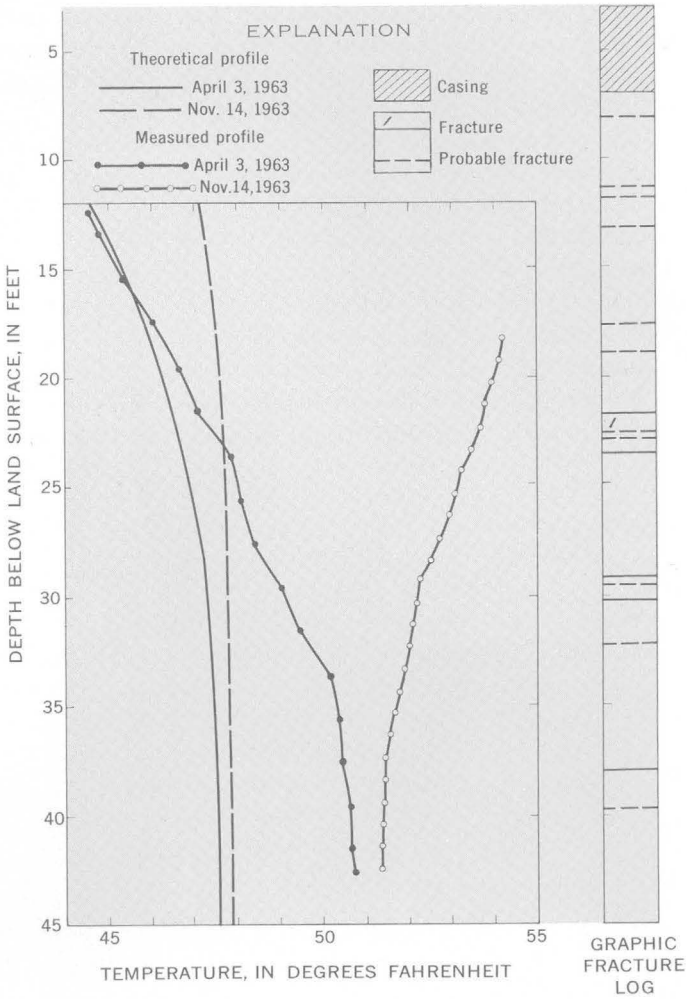

FIGURE 2.—Water-temperature profiles, and fracture log based on periscope observations.

Comparison of the measured temperature profiles and the log of fractures shows that each conspicuous temperature inflection is at the level of a fracture or group of fractures. The inflections evidently indicate the levels at which water flows out from the well bore into fractures. According to this interpretation the inflection at 32 to 33 feet in the April profile reflects the flow of relatively cold water down the well, during the winter and spring, and out into the fracture at about 32 feet. The wall of the well above 32 feet lost heat to the downward-flowing water much more rapidly than it could have done by conduction of heat through the rock. On the other hand, the sharp inflection in the November profile is believed to reflect the flow of relatively warm water down the well and out into fractures at about 29 feet. Temperature profiles for deeper wells near Sanborn show that the temperature of ground water below the zone of seasonal fluctuation is 50° to 51°F. Because temperatures below the level of the deepest inflections in the ob-

served profiles are about 50° to 51°F, and because the lower parts of the observed and computed profiles are of similar form, heat transfer below the inflections is believed to be largely by conduction.

The positions of the inflections on the two measured profiles are different because the head associated with each fracture or group of fractures changes with the seasons. (These changes are particularly significant where shallow fractures are completely drained in late summer.) As a result of these changes in relation of head among the fracture zones, the chief outward flow occurs at different levels at different times of the year.

It appears that with downward flow such as occurs under nonpumping conditions in many wells in the Sanborn area, temperature profiles may be used to locate water-bearing fractures in wells where the periscope cannot be used.

REFERENCES

Ingersoll, L. R., Zobel, O. J., and Ingersoll, A. C., 1948, Heat conduction with engineering and geological applications: New York, McGraw-Hill Book Co., Inc., 278 p.

Johnston, R. H., 1962, Water-bearing characteristics of the Lockport Dolomite near Niagara Falls, New York: Art. 110 *in* U.S. Geol. Survey Prof. Paper 450–C, p. C123–C125.

——— 1964, Ground water in the Niagara Falls area, New York, with emphasis on the water-bearing characteristics of the bedrock: New York Water Res. Comm. Bull. [In press]

SUBJECT INDEX

[For major headings such as "Economic geology," "Geophysics," "Structural geology," see under State names or refer to table of contents]

AUTHOR INDEX

U.S. GOVERNMENT PRINTING OFFICE : 1964 O—742-652